DISSERTATION / DOCTORAL THESIS

Titel der Dissertation /Title of the Doctoral Thesis
„QCD Resummation for Jets with Massive Quarks"

verfasst von / submitted by
Daniel Samitz, BSc MSc

angestrebter akademischer Grad / in partial fulfilment of the requirements for the degree of
Doktor der Naturwissenschaften (Dr. rer. nat.)

Wien, 2021 / Vienna 2021

Studienkennzahl lt. Studienblatt / degree programme code as it appears on the student record sheet:	A 796 605 411
Dissertationsgebiet lt. Studienblatt / field of study as it appears on the student record sheet	Physik
Betreut von / Supervisor:	Univ.-Prof. Dr. Andrè H. Hoang

Abstract

This thesis studies the resummation of logarithmic corrections in differential cross sections in the presence of QCD jets with massive quarks, using effective field theory methods based on factorization and renormalization group running, and parton shower algorithms. The main focus is on how the mass of a heavy quark affects the resummation properties and how on the other hand the resummation using parton shower algorithms affects the quark mass measurements in collider experiments. The thesis consists of two parts.

The first part presents two different ways of systematically including quark mass effects in the resummation of differential distributions in the jet limit in hadronic collisions, where large logarithmic contributions of ratios of different energy scales spoil the fixed-order perturbative expansion and need to be resummed to all orders. We call these two frameworks, that are based on slightly different approaches but are shown to give consistent results, the *universal factorization* (UF) scheme and the *mass mode factorization* (MMF) scheme. We study the Drell-Yan process, where we focus on the transverse momentum of the produced lepton pair and beam thrust as two observables that exhibit different resummation properties, and deep-inelastic scattering in the endpoint region. Within the UF and the MMF frameworks, factorization theorems based on Soft-Collinear Effective Theory (SCET) are constructed that provide variable flavor number schemes that are capable of correctly resumming all mass related logarithms for any given hierarchy of the quark mass with respect to the other physical scales in the process. The contributions from massive flavors to the beam and soft functions required for NNLL′ resummation (combining evolution with next-to-next-to-leading logarithmic accuracy (NNLL) with next-to-next-to-leading order (NNLO) boundary conditions) are calculated and the effects of the quark mass on the resummation concerning renormalization group (RG) evolution in both virtuality and rapidity are discussed.

The second part studies the interpretation of the top quark mass parameter in an angular order parton shower based on the coherent branching formalism. Parton showers as part of multipurpose Monte Carlo (MC) event generators are an essential tool in modern collider physics. The most precise measurements of the top quark mass, based on direct reconstruction, rely on the comparison of MC predictions to the experimental data. However, as of today the exact relation of the mass parameter in the MC event generator, generically called the "Monte Carlo mass", to a well defined mass scheme is still unclear. This results in uncertainties on how to interpret the top quark mass extracted in these measurements that are of the same order as current experimental uncertainties, which are about 0.5 GeV. We study the effect of the parton shower cutoff on the mass parameter for the angular ordered parton shower as implemented in the Herwig 7 MC event generator. For this we compare analytic calculations for the 2-jettiness distribution in the peak region in e^+e^- collisions in the coherent branching formalism with a transverse momentum cutoff, with results from the QCD factorization theorem based on SCET and boosted Heavy Quark Effective theory (bHQET). We show that in the presence of a shower cutoff the quark mass parameter cannot be interpreted as the pole mass. The main result of this work is to establish instead a cutoff dependent *coherent branching mass* as the mass scheme that is effectively implemented in the parton shower. All findings are directly compared to the Herwig 7 event generator, where a very good agreement with our predictions is found.

Zusammenfassung

Diese Dissertation behandelt die Resummierung logarithmischer Korrekturen zu differentiellen Wirkungsquerschnitten für Prozesse in denen QCD Jets mit massiven Quarks auftreten. Dazu werden Methoden der effektiven Feldtheorien sowie Parton Shower Algorithmen benutzt. Der Fokus liegt dabei einerseits darauf zu untersuchen wie die Masse eines schweren Quarks die Eigenschaften der Resummierung der logarithmischen Korrekturen ändert, und andererseits wie die Resummierung mithilfe von Parton Shower Algorithmen die Messungen der Quarkmasse an Teilchenbeschleunigern beeinflusst. Diese Dissertation besteht aus zwei Teilen.

Im ersten Teil werden zwei Methoden vorgestellt, wie man auf eine systematische Art und Weise die Masseneffekte eines schweren Quarks in die Resummierung differentieller Wirkungsquerschnitte in hadronischen Kollisionen inkludieren kann. Dabei beschränken wir uns auf den Fall von Jets im Endzustand. In diesem Fall treten große Logarithmen von Verhältnissen der verschiedenen Energieskalen in dem Prozess auf, welche zu allen Ordnungen der Störungstheorie resummiert werden müssen. Wir nennen diese beiden Methoden, welche auf leicht unterschiedlichen Prinzipien beruhen allerdings konsistente Resultate geben, das *universal factorization* (UF) Schema und das *mass mode factorization* (MMF) Schema. Wir erklären diese Methoden am Beispiel des Drell-Yan Prozesses, wobei als Observablen der Transversalimpuls des produzierten Leptonpaares sowie Beamthrust gewählt werden, da diese beiden Observablen unterschiedliche Eigenschaften bezüglich der Resummierung aufweisen. Als ein weiteres Beispiel wird tief-inelastische Streuung in der Endpunkt Region besprochen. Mit dem UF und dem MMF Schema können im Rahmen der Soft-Collinear Effective Theory (SCET) Faktorisierungstheoreme mit variabler Anzahl der aktiven Quarkflavors (variable flavor number scheme) konstruiert werden, welche es erlauben, alle Logarithmen, welche von der Quarkmasse abhängen, zu resummieren, und zwar für jedes beliebige Verhältnis der Quarkmasse zu den anderen Energieskalen in dem Prozess. Die Beiträge eines massiven Quarkflavors zu den Soft- und Beamfunctions, welche für eine NNLL′ Resummierung (d.h. Evolution mit "next-to-next-to-leading" logarithmischer (NNLL) Genauigkeit und Anfangsbedingungen bis zur "next-to-next-to-leading" Ordnung (NNLO)) nötig sind, werden berechnet. Außerdem wird der Einfluss der Quarkmasse auf die Evolution der Renormierungsgruppe sowohl in Virtualität als auch in Rapidität untersucht.

Der zweite Teil der Dissertation beschäftigt sich mit der Interpretation des Parameters der Top-Quark Masse in einem winkelgeordneten Parton Shower, welcher auf dem coherent branching Formalismus beruht. Parton Shower sind Teil von Monte Carlo (MC) Event Generatoren und damit wichtige Werkzeuge für die Beschreibung der Physik an Teilchenbeschleunigern. Die genauesten Messungen der Top-Quark Masse aus der Rekonstruktion der Zerfallsprodukte des Top-Quarks basieren auf dem Vergleich von experimentellen Daten mit Vorhersagen, die mit einem MC Event Generator gemacht wurden. Allerdings ist bis heute das exakte Verhältnis des Massenparameters von MC Event Generatoren - oft generisch als "Monte Carlo Masse" bezeichnet - zu feldtheoretisch wohldefinierten, renormierten Massendefinitionen unklar. Dies führt zu zusätzlichen Unsicherheiten in den Messungen der Top-Quark Masse, welche von der selben Größenordnung wie die derzeitigen experimentellen Messunsicherheiten sind, welche ungefähr 0.5 GeV betragen. In dieser Arbeit wird der Effekt eines Parton Shower Cutoffs auf den Massenparameter in einem winkelgeordneten Parton Shower, wie er im Herwig 7 MC Event Generator implementiert ist, untersucht. Dazu berechnen wir analytisch die 2-Jettiness Verteilung in der Peak-Region für e^+e^--Kollisionen im coherent branching Formalismus mit einem Cutoff, der auf den Transversalimpuls wirkt. Die Ergebnisse werden verglichen mit analogen Berechnungen im Rahmen von SCET und boosted Heavy Quark Effective Theory (bHQET). Es wird gezeigt, dass im Falle eines endlichen Shower Cutoffs der Massenparameter des Quarks nicht als die Pol-Masse interpretiert werden kann. Das wichtigste Resultat dieser Arbeit ist die Identifizierung einer Cutoff-abhängigen *coherent branching Masse* als jenes Massenschema, das durch den Parton Shower effektiv implementiert wird. Alle Resultate werden direkt mit dem Herwig 7 Event Generator verglichen, wobei wir eine sehr gute Übereinstimmung mit unseren Vorhersagen finden.

Danksagung

Ein Dissertationsprojekt über einen Zeitraum von mehreren Jahren zu verwirklichen ist nur möglich mithilfe der Unterstützung vieler Personen auf vielen verschiedenen Ebenen. Mein Dank gilt daher allen Personen die mich in irgendeiner Form in dieser Zeit unterstützt haben oder mir beigestanden sind, auch wenn hier nur einige davon aufgezählt werden können.

Mein aufrichtiger Dank gilt Prof. André Hoang für seine langjährige Unterstützung in allen Belangen des wissenschaftlichen Arbeitens und dafür dass er mir die Möglichkeit gab nach Abschluss meiner Masterarbeit meine Doktoratsstelle in der Teilchenphysikgruppe der Universität Wien anzutreten und meine Forschung in diesem Bereich weiterzuführen.

Sehr wichtig für mich waren natürlich jene Personen mit denen ich täglich arbeitete, allen voran meine Kollegen Piotr Pietrulewicz und Simon Plätzer. Sie waren eine wichtige Unterstützung für mich, und es war eine Freude mit ihnen zu arbeiten ich konnte unglaublich viel von ihnen lernen.

Eine große Hilfe waren auf jeden Fall alle meine lieben Kollegen der Teilchenphysikgruppe der Universität Wien sowie am DESY, sowohl durch ein gutes Klima und viele unvergessene fröhliche und lustige Momente als auch durch fachliche Diskussionen und Hilfestellungen. Besonders hervorheben möchte ich an dieser Stelle Moritz und Chris, die über Jahre äußerst sympathische sowie kompetente Bürokollegen waren, und speziell ohne die Hilfe des „Computer Gottes" wäre manches Projekt bereits an der Installation der Software gescheitert.

Auch die Institutionen abseits der Universität Wien die mich in dieser Zeit unterstützt haben seien hier erwähnt, das DKPI und das DESY Hamburg. An dieser Stelle gebührt Frank Tackmann großer Dank dafür dass sich dank seiner Unterstützung mein Aufenthalt am DESY so unkompliziert und erfreulich sowie im wissenschaftlichen Sinne fruchtbar gestaltet hat.

Danken möchte ich hier speziell auch meinen Eltern und meinem Bruder, die bereits mein ganzes Leben eine wichtige Stütze für mich darstellen.

Vorrei infine ringraziare Elisa per il suo amore e per rendere più felice ogni aspetto della mia vita.

Contents

Preface and Outline

In the era of precision measurements at hadron colliders a precise understanding of strong interactions in a collider environment is crucial for the measurement of fundamental parameters of the Standard Model from experimental data. Many different theoretical tools are used with the aim to provide theoretical predictions at the same level of accuracy as the experimental results, that are nowadays often at the percent level or below. This can be a challenging task. In regions of phase space where initial or final state particles are collimated into jets, large logarithmic corrections to the cross sections frequently spoil the perturbative expansion and thus need to be resummed to all orders in perturbation theory. This requires to disentangle the physics at the very different energy scales that are involved in a typical process at a hadron collider like the Large Hadron Collider (LHC), a task that can be tackled through the use of effective field theory (EFT) methods. Factorized cross sections, where each term depends only on a single energy scale, can then be resummed by using renormalization group running between them. Another widely used tool, essential for a wide range of studies at the LHC, are multipurpose Monte Carlo (MC) event generators, that are used to simulate the physics from the hard partonic interactions to the hadronization of the observable final state particles. An essential part of these MC event generators are parton showers, simulating the perturbative radiation of collinear and soft particles from a boosted progenitor, from the hard scale down to an infrared shower cutoff where the emissions would become non-perturbative. At this stage the parton shower terminates and the particles produced up to this point are handed over to a hadronization model. Both these methods, resummation based on EFT methods on the one side, and parton showers on the other, will be extensively used and studied in this thesis.

While these methods are often well understood for a variety of different observables involving massless quarks, the systematic generalization to also account for massive quark effects for computing resummed cross sections is usually not as clear. Not only are results for fixed-order calculations in the massive case usually only available at lower orders in perturbation theory compared to the massless case, because the calculations become much harder, but also the factorization and resummation setup can become more complex with the mass providing an additional energy scale in the problem, which can lead to new structures in the factorization theorems. Correctly including the effects of massive quarks in the resummed cross sections and on the other hand understanding effects that might affect the measurements of the quark masses themselves, especially when using tools like parton showers that are not so easily accessible analytically, is becoming increasingly important to keep up with better statistics and more precise measurements by the experimental collaborations. This thesis consists of two parts that both deal with massive quarks in QCD jets, but focus on different questions.

Part I is called *Variable Flavor Number Schemes for Jet Processes at Hadron Colliders*. This part deals with massive quark effects for initial and final state radiation in differential cross sections for Drell-Yan and deep-inelastic scattering in the regime where the hadronic final state is collimated into jets. It deals with both "primary" mass effects, where the heavy flavor is directly entering the hard interaction, and "secondary" mass effects, where light quarks enter the hard interaction and heavy quarks appear via virtual or real radiation from gluon splitting. Our analyses are based on Soft-Collinear Effective Theory and provide variable flavor number schemes, i.e. factorization theorems

involving flavor number dependent matching functions and matrix elements and also flavor number dependent RG evolution, for all possible hierarchies of the quark mass with respect to the other scales. Also the previously unknown massive quark corrections necessary for resummation up to NNLL′ accuracy for the observables studied here are calculated. Part of the content presented in this part of the thesis is published in Refs. [1] and [2].

Part II has the the title *On the Cutoff Dependence of the Quark Mass Parameter in Angular Ordered Parton Showers*. It studies the effects of an infrared transverse momentum cutoff in the coherent branching formalism, that is the basis of the angular ordered parton shower as implemented in the Herwig 7 event generator, and the QCD factorization theorem based on Soft-Collinear Effective Theory, on the thrust distribution in e^+e^- collisions for boosted stable top quarks. In this analysis it is shown that by introducing the infrared cutoff, the mass scheme that is effectively implemented by the parton shower is not the pole mass scheme, but instead a cutoff dependent short-distance mass scheme, called the "coherent branching mass". This is an important step for a better understanding of the so-called "Monte Carlo mass" that is measured in the most precise top quark mass measurements at the LHC, based on direct reconstruction of the top decay products. This part of the thesis is also published in Ref. [3].

Several appendices are provided that contain a collection of known results that were used in the body of the thesis, new results obtained for massive quark corrections and corrections arising from introducing a transverse momentum cutoff and details of some of the calculations.

Part I

Variable Flavor Number Schemes for Jet Processes at Hadron Colliders

Chapter 1

Introduction

For many high-precision studies at the LHC a thorough understanding of quark mass effects is necessary to achieve an accuracy in the theoretical predictions that matches experimental uncertainties. Often predictions for processes involving heavy flavors are known to lower precision than the corresponding predictions for massless quarks. Besides driving the calculations to higher orders in fixed-order perturbation theory and in the logarithmic counting for resummed predictions, it is therefore also necessary to provide results for massive quark effects to sufficiently high order and to understand how to correctly include them when resumming logarithmic terms to all orders in perturbation theory. Mass effects from charm and bottom quarks have been discussed extensively for inclusive heavy quark induced cross sections, leading to the development of several variable flavor number schemes (VFNS) (see e.g. Refs. [4–10]). On the other hand, heavy quark mass effects have received less attention so far in the context of resummed exclusive (differential) cross sections, i.e. where the measurement of additional observables restricts the QCD radiation into the soft-collinear regime, requiring the resummation of the associated logarithms.

When the mass of the heavy flavor is well below any physical dynamical scale μ_X, i.e. $m \ll \mu_X$, that is associated with the measurement of the differential observable at hadron collisions, which can be for example the transverse momentum of the electroweak boson $\mu_X \sim q_T$ in the Drell-Yan (DY) process or the invariant mass of the hadronic final state $\mu_X \sim Q\sqrt{1-x}$ for deep-inelastic scattering (DIS), the mass effects in the distributions are simply encoded by the matching between the parton distribution functions (PDF) across a flavor threshold (e.g. matching four-flavor PDFs onto five-flavor PDFs including a b-quark PDF at the scale m_b, for $m_b \ll \mu_X$). In the partonic cross section (which only involves dynamical scales much larger than the quark mass) the heavy quark can then be treated as an additional massless flavor. But this description it not suitable for $\mu_X \sim m$ or $\mu_X \ll m$, because the expansion in m^2/μ_X^2, that is performed when treating the heavy flavor as a massless degree of freedom in the partonic cross section, is breaking down. In this case the mass effects have to be included in the resummed partonic cross section in a way that keeps the relevant (power) corrections associated with the mass, but also allows for resummation of massive quark contributions in the limits where the mass is widely separated from other relevant dynamical scales.

In general, one can distinguish two types of mass effects, illustrated in Fig. 1.1, which have different characteristics: Contributions where the heavy quark enters the hard interaction process, see Fig. 1.1a, are called *primary* mass effects. Contributions from a gluon splitting into a massive quark-antiquark pair with light quarks entering the hard interaction, see Fig. 1.1b, are called *secondary*. The systematic description of secondary mass corrections for differential spectra in the various relevant hierarchies between the mass and other physical scales has been established for final state jets in the context of event shapes in e^+e^- collisions in Refs. [11, 12]. Here we will extend this approach to differential distributions in hadron collisions for jets from initial and final state radiation. We will focus on the DY process, a typical benchmark process for measurements at hadron-hadron colliders, and DIS at
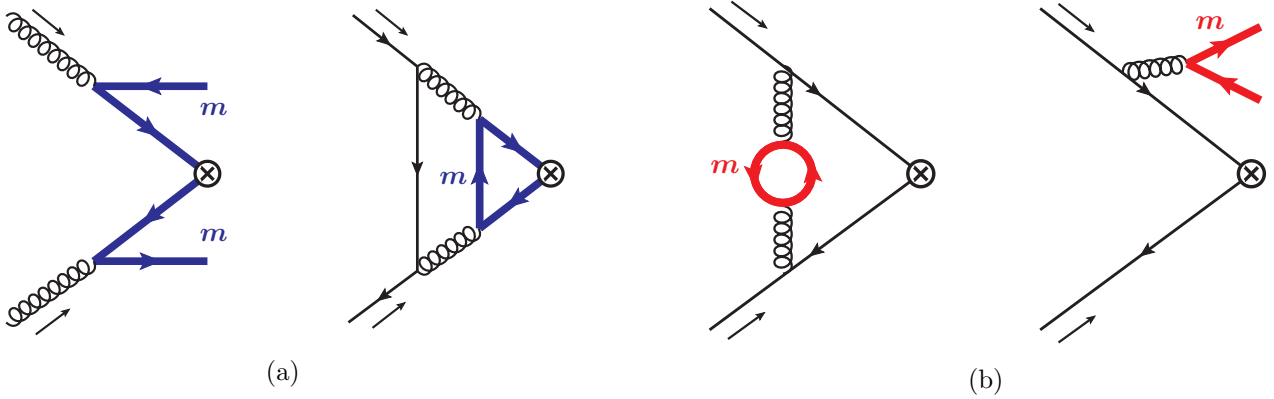
Figure 1.1: Primary (a) and secondary (b) heavy-quark mass effects for Z-boson production. Diagrams for mass effects in gluon-initiated processes are not shown.

hadron-electron colliders. Both processes are studied in the exclusive region where the measured observable is constrained in such a way that the hadronic final state is restricted to soft and collinear particle kinematic, i.e. the final state involves the formation of jets. For DY we will consider two different observables to restrict the final state to the exclusive region, the transverse momentum of the produced lepton pair q_T and beam thrust $\mathcal{T}$ [13]. The variable flavor number schemes presented here are based on factorization theorems in Soft-Collinear Effective Theory (SCET) [14–17] and include both secondary and primary massive quark corrections for initial state radiation, and only secondary massive quark correction to final state jets. Primary mass effects in final state jets will not be discussed in this work. In DIS in the endpoint region one would encounter this scenario only when considering intrinsic (non-perturbative) heavy flavors in the proton, because flavor mixing in the evolution of the PDFs is suppressed in this kinematic region. In $e^+e^- \to$ jets, primary mass effects can play a role and one may encounter a region that requires also boosted Heavy Quark Effective Theory (bHQET) [18, 19], but this is beyond the scope of the work presented in this part.

We will provide two different frameworks for constructing variable flavor number schemes for re-summed differential cross sections for different observables for an arbitrary scaling of the quark mass with respect to the other scales (always assuming that the quark mass can be treated as a perturbative scale). The *universal factorization* (UF) scheme was first described in Refs. [11, 12] and is discussed in detail also in Ref. [20]. The basic idea is that by applying appropriate renormalization conditions for the contributions from a heavy flavor, which means including it as an active degree of freedom in the renormalization group running above the mass scale and excluding it below, the mass related logarithms can be resummed while at the same time it is ensured that all functions in the factorization theorem have the correct massless and decoupling limits. Because the heavy flavor is never literally integrated out from the theory and all mass corrections are kept in the calculations, this results in a smooth transition between the different hierarchies that can arise between the mass and the other physical scales.

Another way of setting up the factorization theorems for the VFNS is what we will refer to as the *mass mode factorizatoin* (MMF) scheme. It strictly follows the EFT philosophy to always impose an expansion whenever there is a large scale hierarchy. In this way one can separate and identify all the relevant EFT modes that appear for a given scaling of the mass of the heavy flavor with respect to the other scales in the process. In regimes where the mass is parametrically smaller than the other typical scales involved in a collinear or soft sector of the theory, the heavy quark is strictly treated like an additional massless flavor. When crossing the flavor threshold the heavy flavor is integrated out from the theory. In this way one can identify certain building blocks in the factorization theorems that arise from integrating out the heavy flavor in the different collinear and soft sectors, that provide a systematic way of resumming rapidity logarithms related to secondary massive quark effects, that

can be shown to be universal for the different observables and processes studied here.

One of the results of this work is to explain how these two approach are related to each other, showing that they give equivalent results for the resummation of logarithms associated with massive quark corrections. The work presented here provides results that can be used in phenomenological studies at the LHC that rely on a precise understanding of differential distributions in the endpoint, where resummation of large logarithmic corrections and including charm and bottom mass effects can both be of importance.

The outline of this part of the thesis is as follows. In chapter 2 we will discuss the factorization and resummation for massive quark effects in exclusive Drell-Yan. We discuss in detail the effective field theory setup for the different parametric regimes in the MMF approach for the case of q_T in Sec. 2.1. Here, we elaborate on the relevant mode setup in SCET, the resulting factorization formulae, and all-order consistency relations between the factorization ingredients in the different regimes. In Sec. 2.1.7, we discuss the consequences of the secondary mass effects on the rapidity evolution for the q_T distribution in the regime $q_T \sim m_b$. As an outlook we provide in Sec. 2.1.8 an estimate of the potential size of the bottom quark effects for low-q_T Drell-Yan measurements. We proceed in Sec. 2.2 by discussing the mode setup, the factorization theorems and resummation properties in all possible different regimes for massive quark effects in DY for beam thrust $\mathcal{T}$, using again the MMF approach. In chapter 3 we discuss the factorization and resummation of secondary massive quark effects DIS in the endpoint region in a similar manner as for the case of DY. The UF scheme is reviewed and discussed in chapter 4. A short summary of the UF scheme and how it is implemented for the various functions in the factorization theorems is given in Sec. 4.1, and in Sec. 4.2 we compare the universal factorization and the mass mode factorization approach for the example of DIS in the endpoint region. In chapter 5 we conclude this part of the thesis. In appendix A we give a brief summary of how the factorization theorems in the different hierarchies based on the mass mode factorization theorem look like for thrust in $e^+e^- \rightarrow 2$ jets. In appendices B and C we give a collection of all massless and massive results relevant for including mass effects at NNLL$'$ order for the various functions in the factorization theorems. Further details on all calculations are provided in appendix D. In appendix E we also give the analytic fixed-order results for the massive quark effects for DY in the q_T and $\mathcal{T}$ distributions in the singular limit $q_T, \mathcal{T} \ll Q$ at $\mathcal{O}(\alpha_s^2)$.

Chapter 2

Variable Flavor Number Scheme for Exclusive Drell-Yan

Differential cross sections for the production of color-singlet states (e.g. electroweak vector bosons or the Higgs boson) in pp collisions represent benchmark observables at the LHC. For the Drell-Yan process, the measurements of the transverse momentum (q_T) spectrum of the vector boson have reached uncertainties below the percent level [21–26], allowing for stringent tests of theoretical predictions from both analytic resummed calculations and parton-shower Monte-Carlo programs. An accurate description of the q_T spectrum is also a key ingredient for a precise measurement of the W-boson mass at the LHC, which requires a thorough understanding of the W-boson and Z-boson spectra and in particular their ratio [27–30]. The associated uncertainties are one of the dominant theoretical uncertainties in the recent m_W determination by the ATLAS collaboration [31].

This chapter deals with the treatment of primary and secondary massive quark effects in the resummed cross sections for Drell-Yan in the exclusive region where the hadronic final state is restricted into two beam jets plus additional soft radiation, using the scheme for including massive quark effects that we refer to as the mass mode factorization (MMF) approach. We will consider two different types of observables that resolve the QCD radiation and are used to constrain the process to the exclusive region, namely the transverse momentum q_T of the gauge boson and beam thrust $\mathcal{T}$ [13]. Constraining the process to the exclusive region as mentioned above corresponds to the limits $q_T, \mathcal{T}\mathrm{e}^{|Y|} \ll Q$, where Q and Y are the invariant mass and rapidity of the color-singlet state. These two observables restrict the allowed QCD radiation into the collinear and soft regime in different ways, leading to different effective-theory setups with distinct factorization and resummation properties in the small q_T and $\mathcal{T}$ limits, which are well-known in the massless limit up to high orders in the logarithmic counting (see e.g. Refs. [32–42] and Refs. [13, 43, 44]). These two cases provide simple prototypical examples, which cover the essential features of the factorization with massive quarks that will also be relevant for including massive quark effects for other more complicated jet resolution variables whose factorization is known in the massless limit. Throughout this chapter we always consider the limit $\Lambda_{\mathrm{QCD}} \ll q_T, \mathcal{T}$ allowing for a perturbative description of the physics at these kinematic scales. For the q_T spectrum, earlier treatments of the heavy-quark initiated primary contributions for $m \lesssim q_T$ have been given in Refs. [45–47], essentially combining the ACOT scheme [4,5] with the standard CSS q_T resummation [34]. Here we give the complete treatment for primary and secondary massive quarks contributions over the whole range of possible hierarchies between the heavy-quark mass m and the kinematic scales, both for q_T and $\mathcal{T}$, using the framework of SCET and the mass mode factorization approach for including the massive quark effects in the factorization theorems.

We give results for all required ingredients for incorporating m_b effects at NNLL$'$ order, which combines NNLL evolution with the full NNLO singular boundary conditions (hard, beam, and soft functions). For Z-boson production at NNLL$'$, primary effects contribute via $\mathcal{O}(\alpha_s) \times \mathcal{O}(\alpha_s)$ (i.e. one real radi-
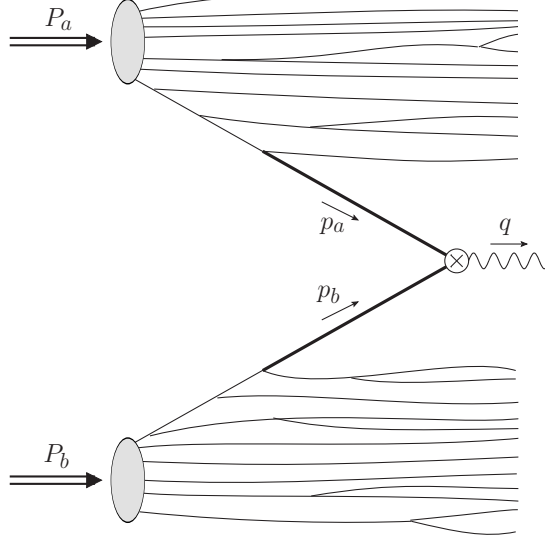
Figure 2.1: Schematic picture of the Drell-Yan process.

ation at $\mathcal{O}(\alpha_s)$ in each incoming beam) heavy-quark initiated contributions, illustrated in Fig. 1.1a. Secondary effects contribute as $\mathcal{O}(\alpha_s^2)$ corrections to light-quark initiated hard interactions, illustrated in Fig. 1.1b. Due to the strong CKM suppression primary m_b-effects do not play any significant role for W-production, which represents a key difference to Z-boson production. Primary m_c-effects enter W-production in the cs-channel, where they start already at NLL$'$ via $\mathcal{O}(\alpha_s) \times \mathcal{O}(1)$ corrections (i.e. one real radiation of a charm quark in one beam, and a non-perturbative (intrinsic) strange quark from the proton in the other beam). For this case, our explicit results for the regime $q_T \sim m_c$ allows for up to NNLL resummation. (Here, the resummation at NNLL$'$ would require the $\mathcal{O}(\alpha_s^2)$ primary massive contributions.)

Large parts of this chapter of the thesis and corresponding appendices were taken from Ref. [1]. Some remarks for further clarifications on the role of the csoft matrix elements and their relation to zero-bin subtractions have been added following the discussion after Eq. (2.76), and section 2.2.6 was added to discuss the implications of large rapidities for the massive factorization theorems for beam thrust. Smaller changes have been made throughout the rest of the text, clarifying some smaller issues and relating to other chapters of the thesis.

Before we set up the variable flavor number schemes for q_T and $\mathcal{T}$ in Secs. 2.1 and 2.2 , we will first briefly discuss the kinematics of the Drell-Yan process and set up the notation for the kinematic variables. The Drell-Yan process is sketched in Fig. 2.1, where two incoming protons with momenta P_a and P_b collide, and in a hard collision-process between two partons a color-singlet state is formed that will then decay into two leptons. We denote the momenta of the partons when they couple to the color-singlet as p_a and p_b, such that the momentum of the color-singlet is $q = p_a + p_b$. Throughout this chapter we will use the decomposition of a four-momentum p^μ into its light-cone components and transverse momentum components with respect to the beam axis as

$$p^\mu = n_a \cdot p \, \frac{n_b^\mu}{2} + n_b \cdot p \, \frac{n_a^\mu}{2} + p_\perp^\mu \equiv (n_a \cdot p, n_b \cdot p, p_\perp) \equiv (p^+, p^-, p_\perp)\,, \qquad (2.1)$$

where n_a and n_b are light-like four vectors along the beam axis

$$n_a = (1, 0, 0. - 1)\,, \qquad\qquad n_b = (1, 0, 0, 1)\,. \qquad (2.2)$$

and $n_a \cdot p_\perp = n_b \cdot p_\perp = 0$, such that the momenta of the incoming protons in the lab frame can be

written as (using the approximation of a massless proton)

$$P_a^\mu = E_{\mathrm{cm}} \frac{n_a^\mu}{2}\,, \qquad\qquad P_b^\mu = E_{\mathrm{cm}} \frac{n_b^\mu}{2}\,. \qquad\qquad (2.3)$$

The four-momentum of the color-singlet state that is produced, which we will denote as q^μ, is the sum of the momenta of the colliding partons

$$q^\mu = p_a^\mu + p_b^\mu = \omega_a \frac{n_a^\mu}{2} + \omega_b \frac{n_b^\mu}{2} + q_\perp^\mu\,. \qquad\qquad (2.4)$$

The invariant mass Q of the color-singlet and its rapidity Y can be written as

$$Q = \sqrt{q^2} = \sqrt{\omega_a \omega_b - q_T^2}\,, \qquad\qquad (2.5)$$

$$Y = \frac{1}{2} \ln\!\left(\frac{n_b \cdot q}{n_a \cdot q}\right) = \frac{1}{2} \ln\!\left(\frac{\omega_a}{\omega_b}\right), \qquad\qquad (2.6)$$

with $q_T^2 = -q_\perp^2 > 0$. If the transverse momentum is much smaller than the invariant mass, i.e. $q_T \ll Q$, we can perform the expansion

$$Q \approx \sqrt{\omega_a \omega_b} \times \left(1 + \mathcal{O}\!\left(\frac{q_T^2}{Q^2}\right)\right) \qquad\qquad (2.7)$$

such that we can define the kinematic variables as

$$\omega_a \approx Q e^Y\,, \quad \omega_b \approx Q e^{-Y}\,, \quad x_{a,b} = \frac{\omega_{a,b}}{E_{\mathrm{cm}}}\,. \qquad\qquad (2.8)$$

This is the approximation that we will use in the rest of the chapter. The expansion in q_T/Q will always be justified when restricting the final state to exclusive region according to the two different observables transverse momentum q_T and beam thrust $\mathcal{T}$. This is clear in the case of q_T, where the exclusive region is just defined by the condition that $q_T \ll Q$, and also holds the case of beam thrust $\mathcal{T}$, where the exclusive region is defined by $\mathcal{T} \ll Q \mathrm{e}^{-|Y|}$, as will be explained in the beginning of Sec. 2.2.1.

In the case where $(1 - x_{a,b}) \ll 1$ one would encounter large logarithms of the form $\sim \ln(1 - x_{a,b})$. In this chapter we will not deal with the resummation of these logarithms, so to ensure that $(1 - x_{a,b}) \sim 1$ we restrict ourselves to the kinematic region $Q \ll E_{\mathrm{cm}}\, \mathrm{e}^{-|Y|}$, in addition to any restrictions coming from constraining the final state to the exclusive region defined by the observables q_T and $\mathcal{T}$.

2.1 Variable flavor number scheme for the q_T spectrum in Drell-Yan

The first observable we consider for the Drell-Yan process is the transverse momentum q_T of the gauge boson

$$q_T = |\vec{q}_T| = |\vec{p}_{T\ell} + \vec{p}_{T\bar{\ell}}| = \left|\sum_i \vec{p}_{Ti}\right|. \qquad\qquad (2.9)$$

Here p_i are all hadronic final-state momenta (i.e. excluding the color-singlet final state). Due to transverse momentum conservation q_T measures the total transverse momentum of the final state hadronic radiation. The exclusive regime we are interested in corresponds to $q_T \ll Q$, where $Q = \sqrt{q^2}$ is the dilepton invariant mass that sets the hard scale of the process. We always assume $\Lambda_{\mathrm{QCD}} \ll q_T$ allowing for a perturbative description of the physics at this kinematic scale. The factorization and resummation properties of this observable are well known in the massless case up to high orders in the logarithmic counting, see e.g. Refs [32–42].

2.1.1 Factorization for massless quarks

Before discussing the massive quark corrections, we first briefly summarize the EFT setup and factorization for massless quarks. The relevant modes for the measurement of q_T in the limit $q_T \ll Q$ are n_a-collinear, n_b-collinear, and soft modes with the scaling[1]

$$
\begin{aligned}
n_a\text{-collinear:} \quad & p_{n_a}^\mu \sim \left(\frac{q_T^2}{Q}, Q, q_T \right), \\
n_b\text{-collinear:} \quad & p_{n_b}^\mu \sim \left(Q, \frac{q_T^2}{Q}, q_T \right), \\
\text{soft:} \quad & p_s^\mu \sim (q_T, q_T, q_T),
\end{aligned}
\tag{2.10}
$$

which we have written in terms of light-cone coordinates along the beam axis as in Eqs (2.1) and (2.2). Besides these perturbative modes there are also nonperturbative collinear modes with the scaling $(\Lambda_{\text{QCD}}^2/Q, Q, \Lambda_{\text{QCD}})$ and $(Q, \Lambda_{\text{QCD}}^2/Q, \Lambda_{\text{QCD}})$, which describe the initial-state protons at the scale $\mu \sim \Lambda_{\text{QCD}}$, and which are unrelated to the specific jet resolution measurement. The typical invariant mass of the soft modes is parametrically the same as for the collinear modes, $p_{n_a}^2 \sim p_{n_b}^2 \sim p_s^2 \sim q_T^2$, which is the characteristic feature of a SCET$_{\text{II}}$ theory. The soft and collinear modes are only separated in rapidity leading to the emergence of rapidity divergences and associated rapidity logarithms. The traditional approach for their resummation in QCD relies on the work by Collins, Soper, and Sterman [32–34]. In SCET the factorization and resummation were devised in Refs. [39–42].

Here we will use the rapidity renormalization approach of Refs. [40,41], where the rapidity divergences are regularized by a symmetric regulator and are renormalized by appropriate counterterms (by a $\overline{\text{MS}}$-type subtraction). We will refer to this regulator as the symmetric η-regulator, and it will be used throughout the whole part of this thesis. It acts on the Wilson lines as

$$
S_n = \sum_{\text{perms}} \exp\left[\frac{-g}{n \cdot \mathcal{P}} \, n \cdot A_s \right] \to \sum_{\text{perms}} \exp\left[\frac{-g}{n \cdot \mathcal{P}} \frac{\nu^{\eta/2}}{|2\mathcal{P}_3|^{\eta/2}} \, n \cdot A_s \right],
\tag{2.11}
$$

where $\mathcal{P}_3$ denotes the third component of the momentum operator and the light-like vector n can stand for either vector n_a or n_b. In Eq. (2.11) it is shown for the example of a soft Wilson line S_n as it appears in the soft function, but the replacement is analogous for the collinear Wilson lines, where one can further make the expansion $|2\mathcal{P}_3| = |n_a \cdot \mathcal{P} + n_b \cdot \mathcal{P}| \to |n_b \cdot \mathcal{P}|$ for the collinear scaling $n_b \cdot \mathcal{P} \gg n_a \cdot \mathcal{P}$ in the n_a-direction (and analogous for the collinear scaling in the n_b direction with $a \leftrightarrow b$). The dimension-1 "rapidity" scale ν takes a similar role as the dimension-1 scale μ in dimensional regularization. The rapidity logarithms are then resummed by solving the associated rapidity renormalization group equations in ν. Within this framework the factorized differential cross section with n_f massless quarks reads[2]

$$
\begin{aligned}
\frac{d\sigma}{dq_T^2 \, dQ^2 \, dY} = \sum_{i,j \in \{q,\bar{q}\}} H_{ij}^{(n_f)}(Q, \mu) \int d^2 p_{Ta} \, d^2 p_{Tb} \, d^2 p_{Ts} \, \delta(q_T^2 - |\vec{p}_{Ta} + \vec{p}_{Tb} + \vec{p}_{Ts}|^2) \\
\times B_i^{(n_f)}\!\left(\vec{p}_{Ta}, x_a, \mu, \frac{\nu}{\omega_a} \right) B_j^{(n_f)}\!\left(\vec{p}_{Tb}, x_b, \mu, \frac{\nu}{\omega_b} \right) S^{(n_f)}(\vec{p}_{Ts}, \mu, \nu) \left[1 + \mathcal{O}\!\left(\frac{q_T}{Q} \right) \right],
\end{aligned}
\tag{2.12}
$$

where $\omega_{a,b}$ and $x_{a,b}$ are defined as in Eq. (2.8) and are functions of Q, Y and the fixed E_{cm}. Here the RG evolution factors for the various functions to run them from their respective natural scale

---

[1]If the color-singlet state has a large boost along the beam axis, i.e. for example $\omega_b \sim Q e^{-Y} \ll Q \ll \omega_a \sim Q e^Y$, also these modes would be boosted with rapidity Y. But since the transverse momentum q_T is invariant under boosts along the beam axis, we can always boost back to the partonic center of mass frame, where the modes exhibit the symmetric scaling shown in Eq. (2.10). This means that the factorization theorem based on the scaling of the modes as in Eq. (2.10) can be used also for larger rapidities $Y \not\approx 0$, as long as we are not in the region where $(1 - x_{a,b}) \ll 1$.

[2]In principle there is also a corresponding contribution for a gluon initiated hard interaction. However, these contributions vanish for real Z-boson production $gg \to Z$ due to the Landau-Yang theorem [48,49], and are also subleading for off-shell Z-bosons in $gg \to Z^* \to \bar{\ell}\ell$, as discussed in App. F.

to the common renormalization scale μ are not shown explicitly for simplicity, but always implied. The same for the evolution factors in rapidity. Note that the particular form of the factorization theorem in Eq. (2.12), where the beam functions B_i and B_j for the two incoming beam jets take the same form, only arises when a rapidity regulator that is symmetric under $p^+ \leftrightarrow p^-$ is applied. Other choices of regulating the rapidity divergences that arise in the beam and soft functions can lead to two beam functions that do not take the same form in the a- and b-direction (and also change the results for the soft function). The full convolution of both beam and the soft function is, however, always independent of the rapidity regulator.

The superscript (n_f) on all functions indicates that the associated EFT operators and the strong coupling constant in these functions are renormalized with n_f active quark flavors. H_{ij} denotes the process-dependent (but measurement-independent) hard function. It encodes the tree-level result and hard virtual corrections of the partonic process $ij \to Z/W/\gamma^*$ at the scale $\mu \sim Q$ and can be calculated as the square of the Wilson coefficent of the matching of the full QCD to the SCET current. The transverse-momentum dependent (TMD) beam functions B_i [39,50–53] can be written as proton matrix elements of SCET operators

$$B_i\Big(\vec{p}_T, x = \frac{\omega}{P^-}, \mu, \frac{\nu}{\omega}\Big) = \langle p_n(P^-)|\theta(\omega)\mathcal{O}_i(\vec{p}_T, \omega, \mu, \frac{\nu}{\omega})|p_n(P^-)\rangle \tag{2.13}$$

where the light-like vector n is either n_a or n_b, depending on whether we deal with the n_a- or n_b-collinear beam function, and $\bar{n}$ is then the respective other light-like vector. The state $|p_n(P^-) >$ is the incoming proton state with momentum $P^\mu = P^- \frac{n^\mu}{2}$ and $\mathcal{O}_i$ a renormalized operator of collinear SCET jet fields

$$\mathcal{O}_i^{\mathrm{bare}}(\vec{p}_T, \omega) = \bar{\chi}_n^{(i)}(0)\delta^{(2)}(\vec{p}_T - \mathcal{P}_\perp)\frac{\slashed{\bar{n}}}{2}\Big[\delta(\omega - \bar{n} \cdot \mathcal{P})\chi_n^{(i)}(0)\Big] \tag{2.14}$$

with the momentum operator $\mathcal{P}$ acting always to the right. The renormalized TMD beam functions B_i can be matched onto PDFs as

$$B_i^{(n_f)}\Big(\vec{p}_T, x, \mu, \frac{\nu}{\omega}\Big) = \sum_k \mathcal{I}_{ik}^{(n_f)}(\vec{p}_T, x, \mu, \frac{\nu}{\omega}) \otimes_x f_k^{(n_f)}(x, \mu)\Big[1 + \mathcal{O}\Big(\frac{\Lambda_{\mathrm{QCD}}^2}{|\vec{p}_T|^2}\Big)\Big], \tag{2.15}$$

where the Mellin-type convolution denoted by $\otimes_x$ is defined as

$$g(x) \otimes_x h(x) = \int_x^1 \frac{\mathrm{d}z}{z}\, g\Big(\frac{x}{z}\Big)h(z)\,. \tag{2.16}$$

We will use this notation throughout the rest of this work. The perturbative matching coefficients $\mathcal{I}_{ik}$ describe the collinear initial-state radiation at the invariant mass scale $\mu \sim q_T$ and rapidity scale $\nu \sim \omega$, and the nonperturbative parton distribution functions (PDFs) are denoted by f_k. Finally, the soft function S (see Eq. (D.36) for the definiton in terms of a vacuum matrix element of soft Wilson lines) describes the wide-angle soft radiation at the invariant mass and rapidity scale $\mu \sim \nu \sim q_T$. The matching coefficients $\mathcal{I}_{ik}$ and the soft function are process-independent and have been computed to $\mathcal{O}(\alpha_s^2)$ in Refs. [54–57], and togehter with the three-loop noncusp anomalous dimension [58–60] allow for a full N^{3}LL analysis of Drell-Yan for massless quarks [61–64]. The results for the massless hard, beam and soft functions at order $\mathcal{O}(\alpha_s)$ and $\mathcal{O}(\alpha_s^2 C_F T_F)$ are collected in appendix B for the convenience of the reader. These are the only terms relevant for NNLL$'$ that will depend on the mass of the heavy flavor once we go to the massive quark case, while all other color structures at $\mathcal{O}(\alpha_s^2)$ are contributions from diagrams with only massless quarks (remember that primary massive quark effects enter only via two separate $\mathcal{O}(\alpha_s)$ real radiation contributions in the beam functions in the two beams as $\mathcal{O}(\alpha_s) \times \mathcal{O}(\alpha_s)$, while the secondary massive quark corrections from the splitting of a radiated gluon contribute to the $\mathcal{O}(\alpha_s^2 C_F T_F)$ terms in the hard, beam and soft function).

In Eq. (2.12), the logarithms of q_T/Q are resummed by evaluating all functions at their characteristic renormalization scales and evolving them to common final scales μ and ν by solving the set of coupled evolution equations

$$\mu \frac{\mathrm{d}}{\mathrm{d}\mu} H_{ij}^{(n_f)}(Q,\mu) = \gamma_H^{(n_f)}(Q,\mu) \, H_{ij}^{(n_f)}(Q,\mu) \,,$$

$$\mu \frac{\mathrm{d}}{\mathrm{d}\mu} B_i^{(n_f)}\Big(\vec{p}_T, x, \mu, \frac{\nu}{\omega}\Big) = \gamma_B^{(n_f)}\Big(\mu, \frac{\nu}{\omega}\Big) \, B_i^{(n_f)}\Big(\vec{p}_T, x, \mu, \frac{\nu}{\omega}\Big) \,,$$

$$\mu \frac{\mathrm{d}}{\mathrm{d}\mu} S^{(n_f)}(\vec{p}_T, \mu, \nu) = \gamma_S^{(n_f)}(\mu, \nu) \, S^{(n_f)}(\vec{p}_T, \mu, \nu) \,,$$

$$\mu \frac{\mathrm{d}}{\mathrm{d}\mu} f_i^{(n_f)}(x, \mu) = \sum_k \gamma_{f,ik}^{(n_f)}(x, \mu) \otimes_x f_k^{(n_f)}(x, \mu) \,,$$

$$\nu \frac{\mathrm{d}}{\mathrm{d}\nu} B_i^{(n_f)}\Big(\vec{p}_T, x, \mu, \frac{\nu}{\omega}\Big) = \int \mathrm{d}^2 k_T \, \gamma_{\nu,B}^{(n_f)}(\vec{p}_T - \vec{k}_T, \mu) \, B_i^{(n_f)}\Big(\vec{k}_T, x, \mu, \frac{\nu}{\omega}\Big) \,,$$

$$\nu \frac{\mathrm{d}}{\mathrm{d}\nu} S^{(n_f)}(\vec{p}_T, \mu, \nu) = \int \mathrm{d}^2 k_T \, \gamma_{\nu,S}^{(n_f)}(\vec{p}_T - \vec{k}_T, \mu) \, S^{(n_f)}(\vec{k}_T, \mu, \nu) \,. \tag{2.17}$$

The massless results for the anomalous dimension at order $\mathcal{O}(\alpha_s)$ and $\mathcal{O}(\alpha_s^2 C_F T_F)$, that will be relevant when discussing the massive quark case at NNLL′ (all other color structures at that order are left unchanged with respect to the purely massless case), are given in appendix B. Only the evolution of the PDF leads to flavor mixing. Consistency of RG running implies that

$$\gamma_H^{(n_f)}(Q,\mu) + \gamma_B^{(n_f)}\Big(\mu, \frac{\nu}{\omega_a}\Big) + \gamma_B^{(n_f)}\Big(\mu, \frac{\nu}{\omega_b}\Big) + \gamma_S^{(n_f)}(\mu, \nu) = 0 \,,$$

$$2\gamma_{\nu,B}^{(n_f)}(\vec{p}_T, \mu) + \gamma_{\nu,S}^{(n_f)}(\vec{p}_T, \mu) = 0 \,,$$

$$\mu \frac{\mathrm{d}}{\mathrm{d}\mu} \gamma_{\nu,S}^{(n_f)}(\vec{p}_T, \mu) = \nu \frac{\mathrm{d}}{\mathrm{d}\nu} \gamma_S^{(n_f)}(\mu, \nu) \, \delta^{(2)}(\vec{p}_T) = -4\Gamma_{\mathrm{cusp}}^{(n_f)}[\alpha_s(\mu)] \, \delta^{(2)}(\vec{p}_T) \,. \tag{2.18}$$

Note that in practice, the evolution is usually performed in Fourier space after performing a two-dimensional Fourier transform defined as

$$\tilde{g}(\vec{b}_T) = \int \mathrm{d}^2 p_T \, e^{i\,\vec{b}_T \cdot \vec{p}_T} g(\vec{p}_T) \tag{2.19}$$

for a generic function $g(\vec{p}_T)$, such that one actually resums the conjugate logarithms $\ln(b\mu)$ where $b = |\vec{b}_T| \sim 1/q_T$ is the Fourier-conjugate variable to q_T. The q_T spectrum is then obtained as the inverse Fourier transform of the resummed b-spectrum. The exact solution and evolution in q_T space, which directly resums the (distributional) logarithms in q_T, has been recently discussed in [65] (see also Ref. [66]).

In the following subsections, we discuss how the mode and factorization setup changes when massive quark flavors are involved, using the mass mode factorization approach. Including massive quarks leads to the appearance of additional modes related to fluctuations around the mass shell of the heavy flavor as discussed extensively in Refs. [11,12]. For the different hierarchies between the mass scale m and the scales Q and q_T the relevant modes are illustrated in Fig. 2.2. In the first case, $q_T \ll m \sim Q$, the massive flavor is integrated out at the hard scale. This leads to the case with n_l massless flavors in the beam and soft functions and mass corrections only in the hard function, as discussed in Sec. 2.1.2. The second case, $q_T \ll m \ll Q$, where the quark mass is larger than the jet resolution variable but smaller than the hard scale Q, is analogous to the corresponding case for thrust in $e^+e^- \to$ dijets in Refs. [11,12] and DIS in the $x \to 1$ limit [2]. We refer to these papers for details and only summarize briefly the main features for this regime in Sec. 2.1.3. Our main focus is on the hierarchies $q_T \sim m \ll Q$ and $m \ll q_T \ll Q$, which are important for bottom and charm quark mass effects at the LHC, and which are discussed in Secs. 2.1.4 and 2.1.5.

(a) $q_T \ll m \sim Q$

(b) $q_T \ll m \ll Q$

(c) $q_T \sim m \ll Q$

(d) $m \ll q_T \ll Q$
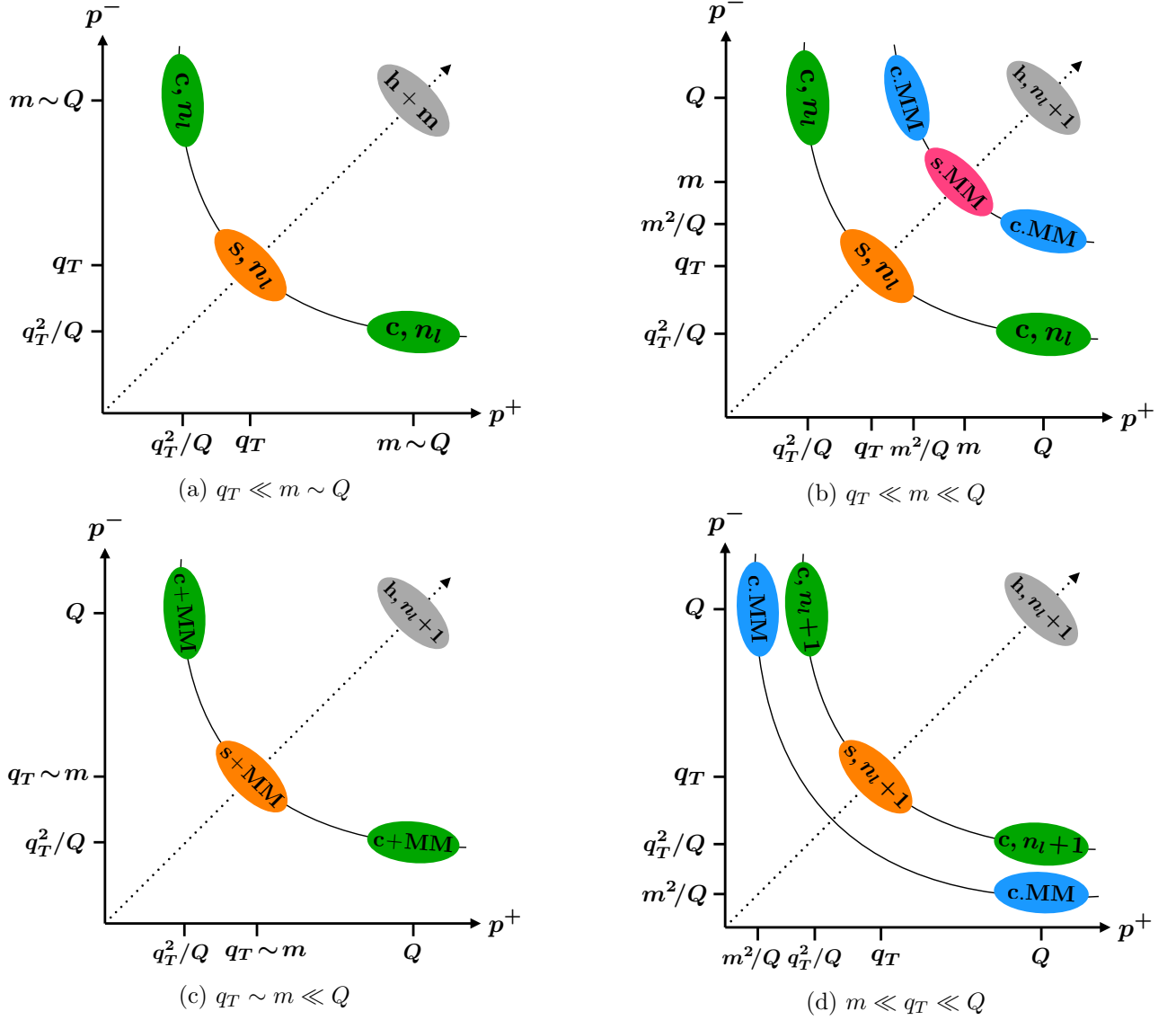
Figure 2.2: Effective theory modes for the q_T spectrum with massive quarks for $q_T \ll Q$ and $m \gg \Lambda_{\rm QCD}$.

2.1.2 Quark mass effects for $m \sim Q$

If the quark mass represents a large scale $\sim Q$ (which concerns the top quark at the LHC), this quark flavor does not play a dynamic role in the low-energy effective theory and is integrated out at the hard scale in the matching from QCD to SCET. The relevant modes are shown in Fig. 2.2a. The massive quark only contributes via mass-dependent contributions to the hard function. This yields the factorization theorem

$$\frac{{\rm d}\sigma}{{\rm d}q_T^2\,{\rm d}Q^2\,{\rm d}Y} = \sum_{i,j\in\{q,\bar q\}} H_{ij}(Q,m,\mu) \int {\rm d}^2 p_{Ta}\,{\rm d}^2 p_{Tb}\,{\rm d}^2 p_{Ts}\,\delta(q_T^2 - |\vec p_{Ta} + \vec p_{Tb} + \vec p_{Ts}|^2) \qquad (2.20)$$

$$\times B_i^{(n_l)}\!\left(\vec p_{Ta}, x_a, \mu, \frac{\nu}{\omega_a}\right) B_j^{(n_l)}\!\left(\vec p_{Tb}, x_b, \mu, \frac{\nu}{\omega_b}\right) S^{(n_l)}(\vec p_{Ts}, \mu, \nu)\left[1 + \mathcal{O}\!\left(\frac{q_T^2}{m^2}, \frac{q_T}{Q}\right)\right],$$

which is essentially equivalent to the massless case in the previous subsection with n_l massless flavors. The hard function $H_{ij}(Q,m,\mu)$ can be evaluated either in the $(n_f = n_l)$ or the $(n_f = n_l + 1)$ flavor scheme for α_s, where n_l is the number of light (massless) quark flavors. The contributions from the heavy flavor at $\mathcal{O}(\alpha_s^2 C_F T_F)$ are given in Sec. C.1.1. In general both primary and secondary

15

massive quark corrections contribute for initial (massless) quarks, shown in the virtual diagrams in Fig. 1.1a and Fig. 1.1b, repsectivley, at $\mathcal{O}(\alpha_s^2)$. Using the (n_l) flavor scheme for α_s these vanish as $\mathcal{O}(Q^2/m^2)$ in the decoupling limit $m \gg Q$ for the conserved vector current. For the axial-vector current, contributing to Z-boson production, there are in addition also anomaly corrections starting at $\mathcal{O}(\alpha_s^2)$ from the massive quark triangle in Fig. 1.1a that do not decouple [67–69].[3] Since the massive quark does not appear as a dynamic flavor in the EFT below the hard scale Q, the entire RG evolution to sum the logarithms of q_T is performed with n_l massless flavors as in Eq. (2.12).

2.1.3 Quark mass effects for $q_T \ll m \ll Q$

Next, we consider the hierarchies where the quark mass is parametrically smaller than the hard scale, $m \ll Q$. These require a different factorization setup than $m \sim Q$ since fluctuations around the mass-shell are now parametrically separated from hard fluctuations, which would lead to large unresummed logarithms inside the hard function $H_{ij}(Q, m, \mu)$. In this subsection, we start with the case where the transverse momentum is much smaller than the mass, $q_T \ll m \ll Q$, while $q_T \sim m \ll Q$ and $m \ll q_T \ll Q$ are considered in the following subsections.

In a first step the QCD current is matched onto the SCET current with $n_l + 1$ dynamic quark flavors at the scale $\mu \sim Q$. Since $m \ll Q$ this matching can be performed (at leading order in the expansion parameter m/Q) only with massless quarks (i.e. treating the heavy flavor as an additional massless quark), leading to the hard function with $n_l + 1$ massless flavors, $H_{ij}^{(n_l+1)}$ as in Eq. (2.12) with $n_f = n_l + 1$, where also the strong coupling is renormalized with $n_l + 1$ flavors.

At this point SCET contains not only the n_l massless collinear and soft modes, but also n_a-collinear, n_b-collinear, and soft mass modes (that could be treated like massless modes in the matching of QCD onto SCET at the scale $\mu \sim Q \gg m$) with the scaling

$$
\begin{aligned}
n_a\text{-collinear MM:} \quad & p_{m,n_a}^\mu \sim \left(\frac{m^2}{Q}, Q, m \right), \\
n_b\text{-collinear MM:} \quad & p_{m,n_b}^\mu \sim \left(Q, \frac{m^2}{Q}, m \right), \\
\text{soft MM:} \quad & p_{m,s}^\mu \sim (m, m, m),
\end{aligned}
\tag{2.21}
$$

as illustrated in Fig. 2.2b. These mass-shell fluctuations arise here purely from secondary virtual contributions.

In a second step at the scale $\mu \sim m$, the mass modes are integrated out and SCET with n_l massless and one massive flavor is matched onto SCET with n_l massless flavors with the usual scaling as in the massless case in Eq. (2.10). Since the soft and collinear mass modes have the same invariant mass set by the quark mass and are only separated in rapidity, there are rapidity divergences in their (unrenormalized) collinear and soft contributions. Their renormalization and the resummation of the associated logarithms can be again handled using the rapidity RG approach in Refs. [40, 41], which has been explicitly carried out in Ref. [70].[4] In addition, all renormalized parameters like the strong coupling constant are matched at the mass scale from $n_l + 1$ to n_l flavors taking into account that the massive flavor is removed as a dynamic degree of freedom.

After these steps, the factorization at the low scale $\sim q_T$ proceeds as in the massless case with all

---

[3]Instead, for $m \gg Q$ the heavy quark can be integrated out around its mass scale and the axial current can be evolved between m and Q to resum the associated logarithms $\ln(m/Q)$.

[4]The matching in Ref. [70] was performed with massive primary quarks yielding the matching functions denoted as $H_{m,n}$, $H_{m,\bar{n}}$ and $H_{m,s}$ there. However, this does not affect the structure of the rapidity logarithms arising from the secondary mass effects, which are independent of the primary quarks being massive or massless.

operator matrix elements depending on the n_l massless flavors, which yields the factorization theorem

$$\frac{\mathrm{d}\sigma}{\mathrm{d}q_T^2\,\mathrm{d}Q^2\,\mathrm{d}Y} = \sum_{i,j\in\{q,\bar{q}\}} H_{ij}^{(n_l+1)}(Q,\mu)\,H_c\Big(m,\mu,\frac{\nu}{\omega_a}\Big)H_c\Big(m,\mu,\frac{\nu}{\omega_b}\Big)H_s(m,\mu,\nu)$$
$$\times \int \mathrm{d}^2 p_{Ta}\,\mathrm{d}^2 p_{Tb}\,\mathrm{d}^2 p_{Ts}\,\delta(q_T^2 - |\vec{p}_{Ta}+\vec{p}_{Tb}+\vec{p}_{Ts}|^2)\,B_i^{(n_l)}\Big(\vec{p}_{Ta}, x_a, \mu, \frac{\nu}{\omega_a}\Big)$$
$$\times B_j^{(n_l)}\Big(\vec{p}_{Tb}, x_b, \mu, \frac{\nu}{\omega_b}\Big) S^{(n_l)}(\vec{p}_{Ts}, \mu, \nu)\left[1 + \mathcal{O}\Big(\frac{q_T}{Q}, \frac{q_T^2}{m^2}, \frac{m^2}{Q^2}\Big)\right]. \tag{2.22}$$

Here H_c and H_s denote the mass mode matching functions that arise from the matching at the mass scale $\mu \sim m$. Their exact form depends on the choice of the rapidity regulator, only the product of all three of them is independent of the choice of the regulator. The form given here, with the matching function for the two different collinear directions being identical and denoted here as H_c, arises when using the symmetric η-regulator. In this case their natural rapidity scales are $\nu \sim \omega_{a,b}$ for the collinear contributions and $\nu \sim m$ for the soft ones. They can be evaluated in either the (n_l) or $(n_l + 1)$ scheme for α_s. We will give their expressions at $\mathcal{O}(\alpha_s^2)$ in Sec. C.1.3. The resummation of all logarithms of ratios of q_T, m, and Q is achieved by performing the evolution in μ and ν of all functions appearing in Eq. (2.22) from their natural scales.

In principle, the μ evolution can be performed by evolving all functions with their respective number of quark flavors without switching the flavor scheme, i.e. with $n_l + 1$ flavors for H, n_l flavors for B and S and an additional evolution for the collinear and soft matching functions H_c and H_s. The consistency of RG running for the factorization theorems in Eqs. (2.22) and (2.20), and Eq. (2.18) with n_l massless flavors, implies that the μ-dependence of the product of the mass mode matching functions H_c and H_s is precisely given by the difference between n_l and $n_l + 1$ active quark flavors in the evolution of the hard function H_{ij},

$$\gamma_{H_c}\Big(m,\mu,\frac{\nu}{\omega_a}\Big) + \gamma_{H_c}\Big(m,\mu,\frac{\nu}{\omega_b}\Big) + \gamma_{H_s}(m,\mu,\nu) = \gamma_H^{(n_l)}(Q,\mu) - \gamma_H^{(n_l+1)}(Q,\mu), \tag{2.23}$$

where $\gamma_H^{(n_f)}$ is defined in Eq. (2.17), and γ_{H_c} and γ_{H_s} are defined analogously. At two loops this relation can be checked explicitly using the results in Eqs. (C.9), (C.11) and (B.3). As a result, the μ evolution for the hard, beam and soft functions can be conveniently implemented as illustrated in Fig. 2.3a, by carrying out the μ evolution with n_l active quark flavors below the matching scale $\mu_m \sim m$ and with $n_l + 1$ flavors above μ_m, providing in this sense a "variable-flavor number scheme" [2, 12]. (This effectively corresponds to using operator running for the hard scattering current, which is renormalized with $n_l + 1$ flavors above the mass scale and with n_l flavors below the mass scale.) If, for example, the global renormalization scale μ_{global}, to which all functions are evolved to, is chosen to be at $q_T < \mu_{\mathrm{global}} < m$, as in Fig. 2.3a, the hard function is evolved from $\mu_H \sim Q$ to $\mu_m \sim m$ with $n_l + 1$ active flavors, and from μ_m down to μ_{global} with n_l active flavors, while the beam and soft functions are both evolved with n_l active flavors from $\mu_B \sim q_T$ up to μ_{global}. In addition there is also a rapidity evolution (vertical), which is carried out at $\mu_m \sim m$, i.e. at the border between the $(n_l + 1)$ and (n_l)-flavor theories (see Ref. [70]), which is governed by the mass-dependent rapidity anomalous dimensions for H_s and H_c,

$$\gamma_{\nu,H_s}(m,\mu) = -2\gamma_{\nu,H_c}(m,\mu) = \frac{\mathrm{d}}{\mathrm{d}\ln\nu}\ln H_s(m,\mu,\nu). \tag{2.24}$$

2.1.4 Quark mass effects for $q_T \sim m \ll Q$

If the q_T scale is of the order of the quark mass, $q_T \sim m$, the massive quark becomes a dynamic degree of freedom, which contributes to the q_T spectrum via real radiation effects. The mass modes
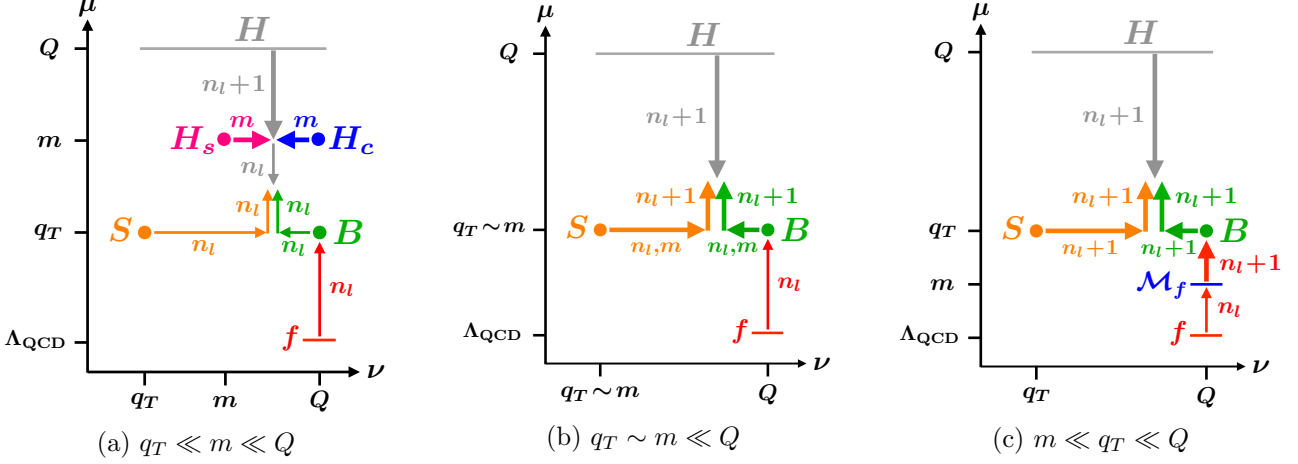
Figure 2.3: Illustration of the renormalization group evolution for q_T of the hard, beam, soft, and parton distribution functions in virtuality μ (vertical) and rapidity ν (horizontal). The anomalous dimensions for each evolution step involve the displayed number of active quark flavors. The label m indicates that the corresponding evolution is mass dependent. Here the global renormalization scale μ_{global}, to which all functions are evolved, was chosen to be between the scales Q and q_T. Any other choice of μ_{global} is possible and does not lead to different results, due to consistency of RG running of the various functions.

in Eq. (2.21) now coincide with the usual massless SCET_{II} modes for the q_T measurement in Eq. (2.10), since they have the same parametrically scaling for $q_T \sim m$, as illustrated in Fig. 2.2c. In this case, there is only a single matching at the hard scale $\mu \sim Q$ from QCD onto SCET with these common soft and collinear modes. This hard matching gives again rise to the (mass-independent) hard function $H_{ij}^{(n_l+1)}$ for $n_l + 1$ massless flavors. The SCET operator matrix elements at the scale $\mu \sim q_T$, i.e. the beam and soft functions, now encode the effects of the massive quark. They are now renormalized with $n_l + 1$ quark flavors and contain an explicit dependence on the quark mass. When integrating out the modes with the virtuality q_T also the massive quark is integrated out and the collinear matching functions $\mathcal{I}_{ik}$ between the beam functions and the PDFs thus also contain the effect from changing from $n_l + 1$ to n_l flavors, i.e.

$$B_i^{(n_l+1)}\left(\vec{p}_T, m, x, \mu, \frac{\nu}{\omega}\right) = \sum_{k\in\{q,\bar{q},g\}} \mathcal{I}_{ik}\left(\vec{p}_T, m, x, \mu, \frac{\nu}{\omega}\right) \otimes_x f_k^{(n_l)}(x,\mu)\left[1 + \mathcal{O}\left(\frac{\Lambda_{\text{QCD}}^2}{m^2}, \frac{\Lambda_{\text{QCD}}^2}{q_T^2}\right)\right].$$
(2.25)

Written out explicitly, the factorization theorem reads

$$\frac{\mathrm{d}\sigma}{\mathrm{d}q_T^2\,\mathrm{d}Q^2\,\mathrm{d}Y} = \sum_{i,j\in\{q,\bar{q},Q,\bar{Q}\}} H_{ij}^{(n_l+1)}(Q,\mu) \int \mathrm{d}^2 p_{Ta}\,\mathrm{d}^2 p_{Tb}\,\mathrm{d}^2 p_{Ts}\,\delta(q_T^2 - |\vec{p}_{Ta} + \vec{p}_{Tb} + \vec{p}_{Ts}|^2)$$

$$\times \left[\sum_{k\in\{q,\bar{q},g\}} \mathcal{I}_{ik}\left(\vec{p}_{Ta}, m, x_a, \mu, \frac{\nu}{\omega_a}\right) \otimes_x f_k^{(n_l)}(x_a,\mu)\right]$$

$$\times \left[\sum_{k\in\{q,\bar{q},g\}} \mathcal{I}_{jk}\left(\vec{p}_{Tb}, m, x_b, \mu, \frac{\nu}{\omega_b}\right) \otimes_x f_k^{(n_l)}(x_b,\mu)\right]$$

$$\times S^{(n_l+1)}(\vec{p}_{Ts}, m, \mu, \nu)\left[1 + \mathcal{O}\left(\frac{q_T}{Q}, \frac{m^2}{Q^2}, \frac{\Lambda_{\text{QCD}}^2}{m^2}, \frac{\Lambda_{\text{QCD}}^2}{q_T^2}\right)\right],$$
(2.26)

where $i, j = Q, \bar{Q}$ denotes the massive quark flavor in the sum over flavors. We stress that the renormalization of the bare soft and beam function with n_l massless and one massive flavor is carried

out in the $n_l + 1$ flavor scheme for α_s, while the strong coupling in the PDFs (which are defined in the lower theory with n_l massless flavors) is renormalized with n_l flavors. The *renormalized* soft function and beam function coefficients $\mathcal{I}_{ik}$ can then be expressed in terms of either the $(n_l + 1)$ or the (n_l) flavor scheme for α_s without introducing large logarithms.

In this hierarchy quark mass effects enter in Eq. (2.26) at $\mathcal{O}(\alpha_s^2)$ in two ways: There are secondary radiation effects appearing in the two-loop soft function $S^{(2)}$ and the flavor-diagonal beam function matching coefficients $\mathcal{I}_{qq}^{(2)}$. In addition, there are primary mass effects arising from a massive-quark initiated hard process. For Z/γ^* production, this requires the production of the massive quarks via gluon splitting in both collinear sectors, which manifests itself in two one-loop collinear matching coefficients $\mathcal{I}_{Qg}^{(1)} \times \mathcal{I}_{\bar{Q}g}^{(1)}$. For W-boson production, primary charm quark effects enter already at $\mathcal{O}(\alpha_s)$ from a single $\mathcal{I}_{Qg}^{(1)}$ with $Q = c$. We have for the first time calculated these previously unkown contributions from massive quarks to the TMD beam and soft functions, some details on the calculations can be found in appendix D. The primary massive quark beam function matching coefficient $\mathcal{I}_{Qg}$ at $\mathcal{O}(\alpha_s)$ and the secondary massive quark corrections to $\mathcal{I}_{qq}$ at $\mathcal{O}(\alpha_s^2 C_F T_F)$ are given in Sec. C.2.1, the secondary massive quark corrections to S in Sec. C.4.1.

The resummation of logarithms $\ln(q_T/Q)$ and $\ln(m/Q)$ is again obtained by performing the RG evolution for Eq. (2.26), which is illustrated in Fig. 2.3b. While the evolution of the PDFs proceeds in n_l flavors, the μ-evolution for the hard, beam, and soft functions above the scale m is now carried out purely with $n_l + 1$ flavors, and with n_l flavors below the scale m. If the global renormalization scale is chosen to be above the mass scale as in Fig. 2.3b, the beam, soft and hard functions are always evolved with $n_l + 1$ active flavors. Consistency of RG running for Eq. (2.25) implies that the matching coefficients $\mathcal{I}_{ik}$ satisfy the RG equality

$$\mu \frac{\mathrm{d}}{\mathrm{d}\mu} \mathcal{I}_{ik}\left(\vec{p}_T, m, z, \mu, \frac{\nu}{\omega}\right) = \left[\gamma_{B_i}^{(n_l+1)} \times \mathcal{I}_{ik}\right]\left(\vec{p}_T, m, z, \mu, \frac{\nu}{\omega}\right) - \sum_{j \in q, \bar{q}, g} \left[\mathcal{I}_{ij} \otimes_z \gamma_{f,jk}^{(n_l)}\right]\left(\vec{p}_T, m, z, \mu, \frac{\nu}{\omega}\right). \tag{2.27}$$

Here $\gamma_{B_i}^{(n_l+1)}$ and $\gamma_{f,jk}^{(n_l)}$ are the massless μ-anomalous dimensions of the beam function and the PDF as in Eq. (2.17), with $n_l + 1$ and n_l massless flavors, respectively.

Since the renormalization of the beam functions does not involve parton mixing, the one-loop primary mass contributions to $\mathcal{I}_{Qg}^{(1)}$ cannot give rise to rapidity divergences and associated logarithms. On the other hand, the secondary mass effects change the rapidity evolution. In particular, the beam and soft ν-anomalous dimensions become mass dependent[5],

$$\nu \frac{\mathrm{d}}{\mathrm{d}\nu} B_i^{(n_l+1)}\left(\vec{p}_T, m, \mu, \frac{\nu}{\omega}\right) = \int \mathrm{d}^2 k_T \, \gamma_{\nu,B}^{(n_l+1)}(\vec{p}_T - \vec{k}_T, m, \mu) \, B_i^{(n_l+1)}\left(\vec{k}_T, m, \mu, \frac{\nu}{\omega}\right),$$

$$\nu \frac{\mathrm{d}}{\mathrm{d}\nu} S^{(n_l+1)}(\vec{p}_T, m, \mu, \nu) = \int \mathrm{d}^2 k_T \, \gamma_{\nu,S}^{(n_l+1)}(\vec{p}_T - \vec{k}_T, m, \mu) \, S^{(n_l+1)}(\vec{k}_T, m, \mu, \nu). \tag{2.28}$$

The mass dependent ν-anomalous dimensions at $\mathcal{O}(\alpha_s^2 C_F T_F)$ are given in Eqs. (C.18) and (C.31) . We discuss the implications of the mass dependence for the rapidity evolution in Sec. 2.1.7.

2.1.5 Quark mass effects for $m \ll q_T \ll Q$

If q_T is much larger than the mass, the fluctuations around the mass-shell take place at a much lower scale than the jet resolution measurement. There are no relevant soft fluctuations scaling like $p_{m,s}^\mu \sim (m, m, m)$, since the measurement of q_T is IR safe and is thus insensitive to the scale $m \ll q_T$. This means that the heavy flavor contributes in the soft sector just like another massless flavor, i.e.

---

[5]The fact that quark masses can affect the evolution was already pointed out in Ref. [34].

the soft modes are described by a soft function with $n_l + 1$ massless flavors at the scale $\mu \sim q_T$. Due to the collinear sensitivity of the initial-state radiation there are still relevant collinear mass modes scaling like $p_{m,n_a}^\mu \sim (m^2/Q, Q, m)$ and $p_{m,n_b}^\mu \sim (Q, m^2/Q, m)$, as illustrated in Fig. 2.2d. Thus there are collinear modes in SCET at different invariant mass scales, which can be disentangled by a multistage matching. First, the beam functions are matched onto the PDFs with $n_l + 1$ massless flavors, i.e. the heavy flavor treated as massless at tha scale $\mu_B \sim q_T \gg m$. This gives just the matching coefficients $\mathcal{I}_{ik}$ for $n_l + 1$ massless flavors,

$$
B_i^{(n_l+1)}\Big(\vec{p}_T, m, x, \mu, \frac{\nu}{\omega}\Big) = \sum_{k \in \{q, \bar{q}, Q, \bar{Q}, g\}} \mathcal{I}_{ik}^{(n_l+1)}\Big(\vec{p}_T, x, \mu, \frac{\nu}{\omega}\Big) \otimes_x f_k^{(n_l+1)}(x, m, \mu)\Big[1 + \mathcal{O}\Big(\frac{m^2}{q_T^2}\Big)\Big].
$$
(2.29)

In a second step, at the mass scale $\mu_m \sim m$, the PDFs including the massive quark effects are matched onto PDFs with n_l massless quarks, and with α_s in the (n_l) flavor scheme,

$$
f_i^{(n_l+1)}(x, m, \mu) = \sum_{k \in \{q, \bar{q}, g\}} \mathcal{M}_{ik}(x, m, \mu) \otimes_x f_k^{(n_l)}(x, \mu)\Big[1 + \mathcal{O}\Big(\frac{\Lambda_{\text{QCD}}^2}{m^2}\Big)\Big].
$$
(2.30)

The PDF matching functions $\mathcal{M}_{ik}$ can be expressed in either the (n_l) or the $(n_l + 1)$ flavor scheme for α_s, the results for $\mathcal{M}_{ik}$ at $\mathcal{O}(\alpha_s)$ and $\mathcal{O}(\alpha_s^2 C_F T_F)$ are given in Sec. C.2.3.

In total, the factorization theorem reads

$$
\frac{\mathrm{d}\sigma}{\mathrm{d}q_T^2 \, \mathrm{d}Q^2 \, \mathrm{d}Y} = \sum_{i,j \in \{q, \bar{q}, Q, \bar{Q}\}} H_{ij}^{(n_l+1)}(Q, \mu) \int \mathrm{d}^2 p_{Ta} \, \mathrm{d}^2 p_{Tb} \, \mathrm{d}^2 p_{Ts} \, \delta(q_T^2 - |\vec{p}_{Ta} + \vec{p}_{Tb} + \vec{p}_{Ts}|^2)
$$

$$
\times \Bigg[\sum_{k \in \{q, \bar{q}, Q, \bar{Q}, g\}} \sum_{l \in \{q, \bar{q}, g\}} \mathcal{I}_{ik}^{(n_l+1)}\Big(\vec{p}_{Ta}, x_a, \mu, \frac{\nu}{\omega_a}\Big) \otimes_x \mathcal{M}_{kl}(x_a, m, \mu) \otimes_x f_l^{(n_l)}(x_a, \mu) \Bigg]
$$

$$
\times \Bigg[\sum_{k \in \{q, \bar{q}, Q, \bar{Q}, g\}} \sum_{l \in \{q, \bar{q}, g\}} \mathcal{I}_{jk}^{(n_l+1)}\Big(\vec{p}_{Tb}, x_b, \mu, \frac{\nu}{\omega_b}\Big) \otimes_x \mathcal{M}_{kl}(x_b, m, \mu) \otimes_x f_l^{(n_l)}(x_b, \mu) \Bigg]
$$

$$
\times S^{(n_l+1)}(\vec{p}_{Ts}, \mu, \nu)\Big[1 + \mathcal{O}\Big(\frac{q_T}{Q}, \frac{m^2}{q_T^2}, \frac{\Lambda_{\text{QCD}}^2}{m^2}\Big)\Big].
$$
(2.31)

As in Sec. 2.1.4, massive quark corrections can arise at $\mathcal{O}(\alpha_s^2)$ either via primary mass effects involving the product of two one-loop PDF matching corrections $\mathcal{M}_{Qg}^{(1)}$ (for Z/γ^*) generating a massive quark-antiquark pair that initiates the hard interaction, or via secondary mass effects involving one two-loop contribution $\mathcal{M}_{qq}^{(2)}$. Note that also the running of the light quark and gluon PDFs above μ_m generates an effective massive quark PDF via flavor mixing, i.e. in the evolution factors $U_{f,Qk}^{(n_l+1)}(\mu_B, \mu_m)$, which for large hierarchies $m \ll q_T$ can give $\mathcal{O}(1)$ contributions.

The evolution of the hard, beam, and soft functions can be performed purely with $n_l + 1$ massless flavors as long as the renormalization scale is above m, while the PDFs are evolved with n_l flavor below $\mu_m \sim m$ and with $n_l + 1$ flavors above $\mu_m \sim m$, see Fig. 2.3c, as usual in any variable-flavor number scheme. The μ_m dependence is canceled order-by-order by the matching factors $\mathcal{M}_{ij}$, which satisfy the consistency relation

$$
\mu \frac{\mathrm{d}}{\mathrm{d}\mu_m} \mathcal{M}_{ik}(m, z, \mu_m) = \sum_{j \in \{q, \bar{q}, Q, \bar{Q}, g\}} \Big[\gamma_{f,ij}^{(n_l+1)} \otimes_z \mathcal{M}_{jk}\Big](m, z, \mu_m) - \sum_{j \in \{q, \bar{q}, g\}} \Big[\mathcal{M}_{ij} \otimes_z \gamma_{f,jk}^{(n_l)}\Big](m, z, \mu_m).
$$
(2.32)

The absence of soft mass modes in this regime implies there is no rapidity evolution at the mass scale (and no associated rapidity divergences), while the rapidity evolution between beam and soft

functions is the same as for $n_l + 1$ massless flavors. In this regime, the mass dependence is thus fully contained in the collinear sectors and is treated as in standard variable-flavor number schemes for PDFs [4–10].

2.1.6 Relations between hierarchies

After having discussed all hierarchies separately, we now show how the ingredients in each of the associated factorization theorems are related to each other. These relation may be used to combine mass-dependent power corrections that are kept in one hierarchy but are dropped in another with the resummation of logarithms to obtain a systematic inclusion of the mass effects smoothly over the whole q_T spectrum. A straightforward way of doing that is presented in Sec. 4.2.1 for the example of DIS in the endpoint region (see also chapter 3), but it can be done for the factorization theorems for exclusive Drell-Yan in an analogous way. An alternative approach of constructing variable flavor number schemes, where these corrections are never dropped but included directly in all the structures in the factorization theorems, based on the "universal factorization" approach [2,12,71] where different renormalization schemes for the massive quark contributions to the EFT operators above and below the mass scale are applied, will be presented in chapter 4. We stress that different specific ways of how to incorporate the various power corrections are formally equivalent as long as the correct fixed-order expansion and the correct resummation is reproduced in each limit. Any differences then amount to resummation effects at the power-suppressed level and are thus beyond the formal (leading-power) resummation accuracy. A particular scheme (called "S-ACOT") to merge the $m \ll q_T$ and $q_T \sim m$ regimes was discussed in Ref. [45] for the primary massive quark corrections. In practice, for the numerical study of b-quark mass effects at low $q_T \ll m_b \ll Q$ the effective b-quark PDF at the scale q_T is still quite small, so that one may effectively count $f_b(\mu_B) \sim \mathcal{O}(\alpha_s)$, where μ_B is the scale where the matching between the PDFs and the beam functions takes place. In particular, this counting facilitates the seamless combination with the nonsingular corrections for $m \sim q_T$ encoded in the beam function matching coefficients in Eq. (2.26). This was discussed in Ref. [10] in the context of the inclusive $b\bar{b}H$ production cross section, and the analogous discussion applies here as well.

In this section we will discuss the massive power corrections, that arise in the MMF approach of deriving the variable flavor number schemes when completely integrating out the heavy flavor from the theory at its mass scale, and their numerical impact. The relations between the modes and their contributions between the different regimes are summarized in Fig. 2.4.

We will first set up the notation for the coefficients in the perturbation series that we will use for the rest of this part of the thesis. For any generic function F we define the coefficients $F^{(n)}$ at a given order in perturbation theory as

$$F = \sum_{n=0}^{\infty} \left(\frac{\alpha_s^{(n_f)}(\mu)}{4\pi} \right)^n F^{(n)} \tag{2.33}$$

where $\alpha_s^{(n_f)}$ is the strong coupling renormalized with n_f active flavors. When F does not receive mass dependent contributions, i.e. there is no heavy flavor contributing (when the heavy flavor is decoupled for $\mu \ll m$) or the heavy flavor is treated as massless (when $m \ll \mu$), this is equal to the total number of active flavors contributing in that function, i.e. $n_f = n_l$ for $\mu \ll m$ and $n_f = n_l + 1$ for $m \ll \mu$. For a matching function at the scale $\mu \sim m$, when the full mass dependence is kept in $F(m)$, the expansion in Eq (2.33) can in principle be done in either the (n_l) or the $(n_l + 1)$ flavor scheme for α_s. For definiteness we will use the convention that for such a case we will always use the $(n_l + 1)$ flavor scheme when giving explicit results at a given order in perturbation theory, such that $n_f = n_l + 1$ in Eq (2.33), i.e. doing an expansion in $\alpha_s^{(n_l+1)}$. The expansion in terms of $\alpha_s^{(n_l)}$ can be
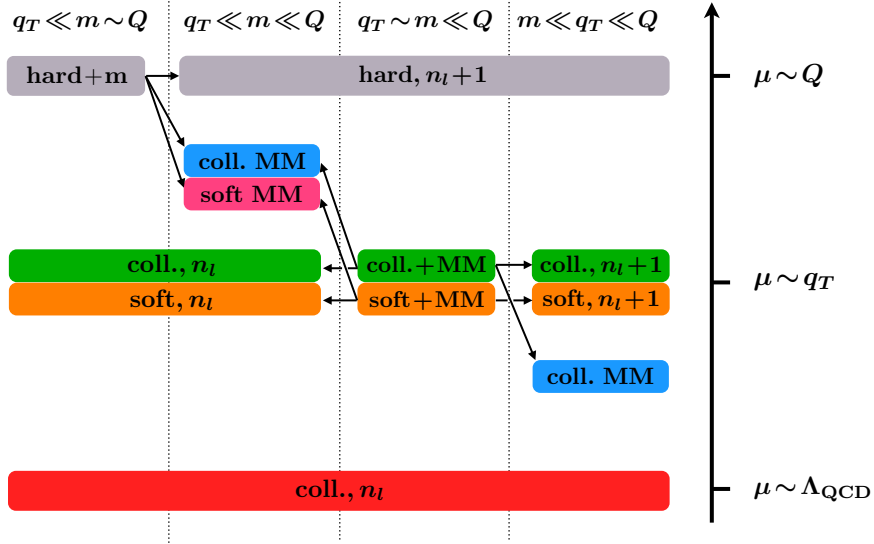
Figure 2.4: Relevant modes for the q_T spectrum with $q_T \ll Q$ for different hierarchies between the quark mass m and the scales q_T and Q. The directions of the arrows indicate how a particular mode contribution is separated when the expansion of another hierarchy is used.

easily obtained from this by using the matching relation for α_s

$$
\begin{aligned}
\alpha_s^{(n_l+1)}(\mu) &= \alpha_s^{(n_l)}(\mu)\left[1 + \frac{\alpha_s^{(n_l)}(\mu)T_F}{4\pi}\frac{4}{3}\left(\Gamma(\epsilon)\left(\frac{\mu^2 e^{\gamma_E}}{m^2}\right)^\epsilon - \frac{1}{\epsilon}\right) + \mathcal{O}(\alpha_s^2)\right] \\
&= \alpha_s^{(n_l)}(\mu)\left[1 - \frac{\alpha_s^{(n_l)}(\mu)T_F}{4\pi}\frac{4}{3}L_m + \mathcal{O}(\alpha_s^2) + \mathcal{O}(\epsilon)\right],
\end{aligned}
\tag{2.34}
$$

where here and in the following we abbreviate

$$
L_m \equiv \ln\frac{m^2}{\mu^2}.
\tag{2.35}
$$

We write the $\mathcal{O}(\alpha_s^2)$ coefficients $F^{(2)}$ as

$$
\begin{aligned}
F^{(2)} &= T_F n_l F^{(2,l)} + \dots, \\
F^{(2)}(m) &= T_F n_l F^{(2,l)} + T_F F^{(2,h)}(m) + \dots,
\end{aligned}
\tag{2.36}
$$

for the case where all quarks are treated as massless and the case with mass dependent corrections, respectively, such that $F^{(2,h)}$ contains all mass dependent two-loop corrections and $F^{(2,l)}$ the associated contributions from massless flavors. The ellipsis stands for all other color structures, which we omit here because they do not get contributions from massive quarks. We are considering primary massive quark effects only to $\mathcal{O}(\alpha_s)$, which means that all mass dependent corrections at two-loop are from secondary massive quarks, which are of the form $\mathcal{O}(\alpha_s^2 T_F C_F)$. These superscripts introduced above should not be confused with the superscripts of the form $F^{(n_l+1)}$ or $F^{(n_l)}$, which indicate how many flavors contribute to F. That means that for example $F^{(2,l)}$ stands only for a coefficient in the expansion of F in the strong coupling, in this case the coefficient at order $\mathcal{O}(\alpha_s^2 T_F)$, while $F^{(n_l)}$ is the full function, the superscript (n_l) only telling us that it depends on n_l massless flavors.

The mass mode matching functions H_c and H_s appearing in the hierarchy $q_T \ll m \ll Q$ in Eq. (2.22)

in Sec. 2.1.3 are related to the hard function for $q_T \ll m \sim Q$ in Sec. 2.1.2 as follows[6]

$$H_{ij}(Q, m, \mu) \stackrel{m \ll Q}{=} H_{ij}^{(n_l+1)}(Q, \mu) \, H_c\Big(m, \mu, \frac{\nu}{\omega_a}\Big) H_c\Big(m, \mu, \frac{\nu}{\omega_b}\Big) H_s(m, \mu, \nu) \Big[1 + \mathcal{O}\Big(\frac{m^2}{Q^2}\Big)\Big]. \qquad (2.37)$$

In the product of functions on the right-hand side, which appear in Eq. (2.22), the logarithms $\ln(m/Q)$ can be resummed to all orders. One can construct a smooth description of the cross section for $q_T \ll m$ that resums these logarithms and also includes the associated mass-dependent $\mathcal{O}(m^2/Q^2)$ power corrections by simply adding the power corrections to the hard function $H^{(n_l+1)}(Q, \mu)$ at the scale $\mu \sim Q$.

The fixed-order contributions to the operator matrix elements appearing in the hierarchy $q_T \ll m$ in are already encoded in the ones for $q_T \sim m$ in Sec. 2.1.4. The mass-dependent beam function matching coefficients for $q_T \sim m$ are related to those for $q_T \ll m$ and the collinear mass-mode function H_c by

$$\mathcal{I}_{ik}\Big(\vec{p}_T, x, m, \mu, \frac{\nu}{\omega}\Big) \stackrel{p_T \ll m}{=} H_c\Big(m, \mu, \frac{\nu}{\omega}\Big) \mathcal{I}_{ik}^{(n_l)}\Big(\vec{p}_T, x, \mu, \frac{\nu}{\omega}\Big) \Big[1 + \mathcal{O}\Big(\frac{p_T^2}{m^2}\Big)\Big]. \qquad (2.38)$$

Similarly, the mass-dependent soft function for $q_T \sim m$ is related to the one for $q_T \ll m$ and the soft mass-mode function H_s by

$$S^{(n_l+1)}(\vec{p}_T, m, \mu, \nu) \stackrel{p_T \ll m}{=} H_s(m, \mu, \nu) \, S^{(n_l)}(\vec{p}_T, \mu, \nu) \Big[1 + \mathcal{O}\Big(\frac{p_T^2}{m^2}\Big)\Big]. \qquad (2.39)$$

In the products on the right-hand side, which appear in Eq. (2.22), logarithms $\ln(q_T/m)$ can be resummed to all orders in the limit $q_T \ll m$. One can include the associated $\mathcal{O}(q_T^2/m^2)$ power corrections that are important for $q_T \sim m$, by obtaining them from the fixed-order expansions of Eqs. (2.38) and (2.39) and adding them to the (n_l)-flavor beam function coefficients and soft function at the scale $\mu \sim q_T$.

Finally, the fixed-order contributions for the operator matrix elements appearing in the hierarchy $m \ll q_T$ are also encoded already in the corresponding ones for $q_T \sim m$. Hence, the mass-dependent beam function matching coefficients are related to those for $m \ll q_T$ and the PDF matching functions by

$$\mathcal{I}_{ik}\Big(\vec{p}_T, m, x, \mu, \frac{\nu}{\omega}\Big) \stackrel{m \ll p_T}{=} \sum_{j=q,\bar{q},g} \mathcal{I}_{ij}^{(n_l+1)}\Big(\vec{p}_T, x, \mu, \frac{\nu}{\omega}\Big) \otimes_x \mathcal{M}_{jk}(m, x, \mu) \Big[1 + \mathcal{O}\Big(\frac{m^2}{p_T^2}\Big)\Big]. \qquad (2.40)$$

Similarly, the mass-dependent and massless soft function are related by

$$S^{(n_l+1)}(\vec{p}_T, m, \mu, \nu) \stackrel{m \ll p_T}{=} S^{(n_l+1)}(\vec{p}_T, \mu, \nu) \Big[1 + \mathcal{O}\Big(\frac{m^2}{p_T^2}\Big)\Big], \qquad (2.41)$$

since there are no relevant soft IR fluctuations below the mass scale. In the functions on the right-hand sides, which appear in Eq. (2.31), logarithms $\ln(m/q_T)$ can be resummed to all orders in the limit $m \ll q_T$. This can be combined with the associated $\mathcal{O}(m^2/q_T^2)$ power corrections relevant for $q_T \sim m$, by obtaining them from the fixed-order expansions of Eqs. (2.40) and (2.41) and adding them to the $(n_l + 1)$-flavor beam function matching coefficients and soft function at the scale $\mu \sim q_T$.

In the following we will verify the relations between the different hierarchies discussed above for the beam and soft functions up to $\mathcal{O}(\alpha_s^2)$. We also scrutinize the numerical impact of the power corrections

---

[6]Here and in the following it is implied that at a specific fixed order the functions on both sides have to be expanded in the same renormalization scheme for α_s. Since $H_{ij}^{(n_l+1)}$ is generically written with $n_l + 1$ (massless) flavors, the $(n_l + 1)$-flavor scheme is most convenient here and also to extract the $\mathcal{O}(m^2/Q^2)$ power corrections on the right-hand side of Eq. (2.37) from its fixed-order expansion.
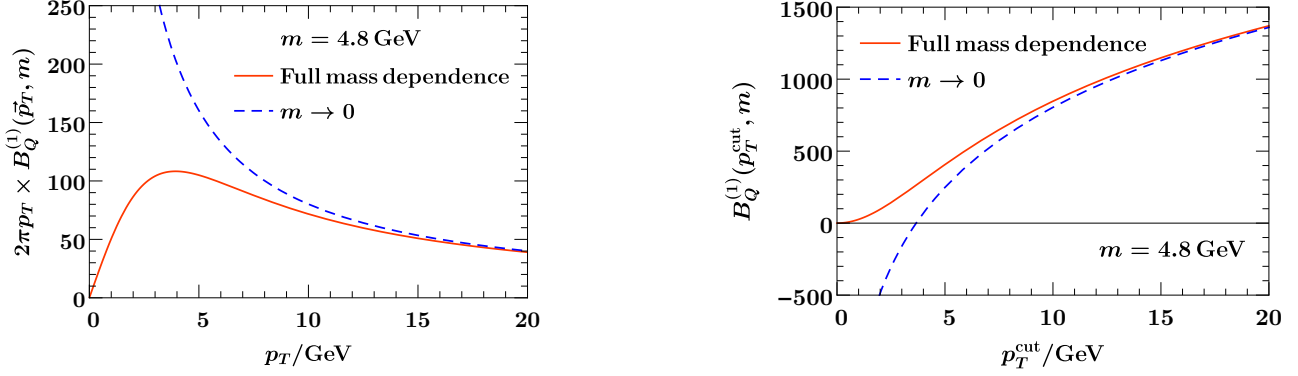
Figure 2.5: Massive b-quark beam function (left panel) and its cumulant (right panel) together with its $m \to 0$ limit. The input parameters are described in the text.

for these functions. We focus in particular on the $\mathcal{O}(m^2/q_T^2)$ corrections for the q_T spectrum for b quarks, which are contained in the factorization theorem Eq. (2.26) for $q_T \sim m$ but not in the massless limit for $m \ll q_T$ in Eq. (2.31), as these are phenomenologically important hierarchies for b-quark mass effects at the LHC.

For the numerical results we use the MMHT2014 NNLO PDFs [72] and evaluate the contributions for $\mu = m_b = 4.8$ GeV, $\omega = m_Z$, and $E_{\mathrm{cm}} = 13$ TeV. The main qualitative features of the results do not depend on these specific input parameters. We also do not explicitly specify the renormalization scheme for the quark mass, since all differences are beyond the order we are working here.

We first consider the primary mass effects at one loop, which are encoded in the TMD beam function matching coefficient $\mathcal{I}_{Qg}^{(1)}$ in Eq. (C.13). In the limit $p_T \ll m$ the primary massive quarks decouple, which is manifest in the result,

$$\mathcal{I}_{Qg}^{(1)}(\vec{p}_T, m, z) \overset{p_T \ll m}{=} \mathcal{O}\left(\frac{p_T^2}{m^2}\right). \tag{2.42}$$

On the other hand, in the opposite limit $m \ll p_T$ it becomes

$$\mathcal{I}_{Qg}^{(1)}(\vec{p}_T, m, z)$$

$$\overset{m \ll p_T}{=} T_F \, \theta(1-z)\theta(z) \left\{ 2 P_{qg}(z) \mathcal{L}_0(\vec{p}_T, \mu) + \delta^{(2)}(\vec{p}_T) \left[-2 P_{qg}(z) L_m + 4z(1-z) \right] + \mathcal{O}\left(\frac{m^2}{p_T^2}\right) \right\}$$

$$= \mathcal{I}_{qg}^{(1)}(\vec{p}_T, z, \mu) + \delta^{(2)}(\vec{p}_T) \mathcal{M}_{Qg}^{(1)}(m, z, \mu) + \mathcal{O}\left(\frac{m^2}{p_T^2}\right), \tag{2.43}$$

confirming that the relation in Eq. (2.40) is satisfied at $\mathcal{O}(\alpha_s)$. The massless one-loop matching coefficient $\mathcal{I}_{qg}^{(1)}$ can be found in Eq. (B.4) and the PDF matching coefficient $\mathcal{M}_{Qg}^{(1)}$ in Eq. (C.24). To account for the correct distributive structure in $\vec{p}_T$ that emerges in the massless limit, one can integrate the expressions with massive quarks and identify the distributions at the cumulant level.

In Fig. 2.5 we show the result for the massive quark beam function $B_Q^{(1)} = \mathcal{I}_{Qg}^{(1)} \otimes_x f_g$ at $\mathcal{O}(\alpha_s)$ as function of p_T using the full massive matching coefficient $\mathcal{I}_{Qg}^{(1)}$ (solid orange) and its small mass limit in Eq. (2.43) (dashed blue). In the right panel we show the corresponding results for the cumulant

$$B_Q(p_T^{\mathrm{cut}}, m) \equiv \int_{|\vec{p}_T| < p_T^{\mathrm{cut}}} \mathrm{d}^2 p_T \, B_Q(\vec{p}_T, m), \tag{2.44}$$

which also includes the $\delta^{(2)}(\vec{p}_T)$ constant contribution. We can see that in both cases the small mass limit is correctly approached for $p_T^{(\mathrm{cut})} \gg m_b$, while for $p_T^{(\mathrm{cut})} \ll m_b$ the primary mass effects decouple
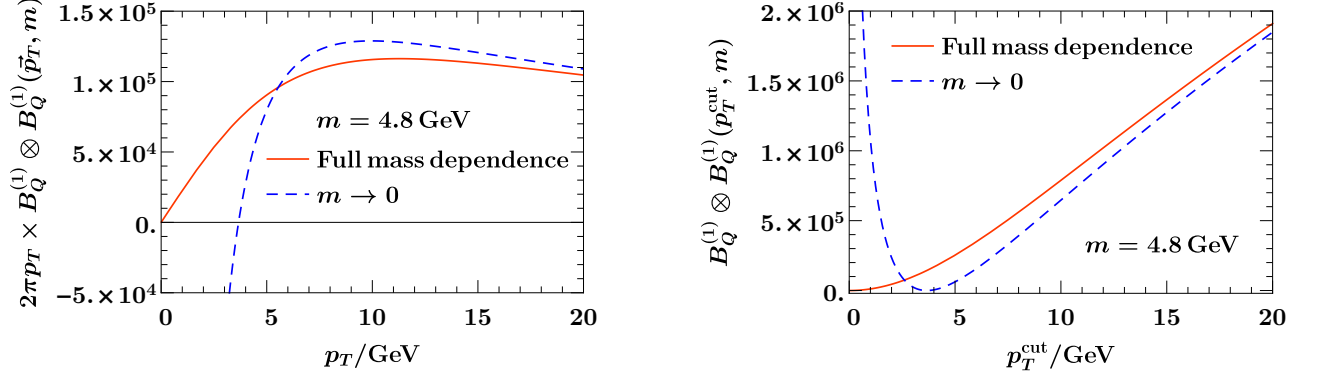
Figure 2.6: Convolution of two massive b-quark beam functions together with the result in the $m \to 0$ limit differential in the total $p_T \equiv |\vec{p}_T|$ (left panel) and the corresponding cumulant (right panel). This is proportional to the primary massive quark correction to the Z-boson spectrum at $\mathcal{O}(\alpha_s^2)$.

with the result going to zero. The corrections to the small mass limit become sizeable for $p_T \sim m_b$ and vanish quite fast for larger p_T.

In Fig. 2.6 we show the result for the convolution between two massive quark beam functions,

$$\left(B_Q^{(1)} \otimes B_Q^{(1)}\right)(\vec{p}_T, m) \equiv \int \mathrm{d}^2 p_T' \, B_Q^{(1)}(\vec{p}_T - \vec{p}_T', m) \, B_Q^{(1)}(\vec{p}_T', m) \,, \qquad (2.45)$$

which enters the result for Z-boson production at $\mathcal{O}(\alpha_s^2 T_F^2)$ and NNLL′. The analytic expression for the convolution between the two one-loop mass-dependent coefficients is given in Eq. (E.6). We see that now the corrections to the small-mass limit remain nonnegligible even for larger values of p_T. This is due to the fact that the $\vec{p}_T$-convolution generates a logarithmic dependence in the spectrum, such that the power corrections of $\mathcal{O}(m_b^2/p_T^2)$ become enhanced by logarithms $\ln(p_T^2/m_b^2)$. This can be seen directly by convoluting two one-loop primary massive beam function matching coefficients $\mathcal{I}_{Qg}^{(1)}$ given in Eq. (C.13), and expanding for $p_T^2 \gg m_b^2$.

Next, we consider the secondary massive quark corrections at $\mathcal{O}(\alpha_s^2 C_F T_F)$. The result for the secondary massive quark contributions to the massless quark TMD beam function coefficient $\mathcal{I}_{qq}^{(2,h)}(\vec{p}_T, m, z)$ is given in Eq. (C.15). In the decoupling limit $p_T \ll m$ all its terms without distributions in $\vec{p}_T$ give $\mathcal{O}(p_T^2/m^2)$ power-suppressed contributions. Combining its remaining distributional terms with the contributions arising from changing the α_s scheme from $n_l + 1$ (which is our default scheme for writing $\mathcal{I}_{qq}^{(2,h)}$) to n_l flavors yields

$$T_F \mathcal{I}_{qq}^{(2,h)}\left(\vec{p}_T, m, z, \mu, \frac{\nu}{\omega}\right) - \frac{4}{3} T_F L_m \mathcal{I}_{qq}^{(1)}\left(\vec{p}_T, z, \mu, \frac{\nu}{\omega}\right) \overset{p_T \ll m}{=} \delta^{(2)}(\vec{p}_T) \, \delta(1-z) \, H_c^{(2)}\left(m, \mu, \frac{\nu}{\omega}\right) + \mathcal{O}\left(\frac{p_T^2}{m^2}\right),$$
$$(2.46)$$

confirming the relation in Eq. (2.38) at this order. The massless one-loop coefficient $\mathcal{I}_{qq}^{(1)}$ and the collinear mass-mode function $H_c^{(2)}$ can be found in Eqs. (B.5) and (C.10), respectively. On the other hand, in the limit $m \ll p_T$ we get

$$T_F \mathcal{I}_{qq}^{(2,h)}\left(\vec{p}_T, m, z, \mu, \frac{\nu}{\omega}\right) \overset{m \ll p_T}{=} T_F \mathcal{I}_{qq}^{(2,l)}\left(\vec{p}_T, z, \mu, \frac{\nu}{\omega}\right) + \delta^{(2)}(\vec{p}_T) \, \mathcal{M}_{qq}^{(2)}(m, z, \mu) + \mathcal{O}\left(\frac{m^2}{p_T^2}\right), \quad (2.47)$$

consistent with the fact that all infrared mass dependence is given by the PDF matching, as required by the relation in Eq. (2.40). The results for the massless coefficient and the PDF matching coefficient are given in eqs. (B.7) and (C.25), respectively.
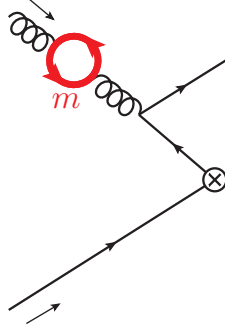
Figure 2.7: Secondary massive quark corrections to Compton-type gluon initiated Drell-Yan.

There are also secondary massive quark corrections at $\mathcal{O}(\alpha_s^2 T_F^2)$ to the Compton-type gluon initiated process shown in Fig. 2.7, encoded in the coefficient $\mathcal{I}_{qg}^{(2,h)}(\vec{p}_T, m, z)$. Since they arise only from virtual corrections to an external gluon line, the limiting behavior for this coefficient is trivial, since it vanishes identically in the (n_l)-flavor scheme for α_s, and in the $(n_l + 1)$-flavor scheme for α_s it is exactly

$$T_F \, \mathcal{I}_{qg}^{(2,h)}(\vec{p}_T, m, z, \mu) = \mathcal{I}_{qg}^{(1)}(\vec{p}_T, z, \mu) \otimes_z \mathcal{M}_{gg}^{(1)}(m, z, \mu) \,. \tag{2.48}$$

The contribution from secondary massive quarks to the TMD soft function is given in Eq. (C.30). In the limit $p_T \ll m$ all terms without distributions in $\vec{p}_T$ become $\mathcal{O}(p_T^2/m^2)$ power suppressed, just as for the beam function. Combining its remaining distributional terms with the contributions arising from changing the scheme of the strong coupling from $n_l + 1$ to n_l flavors yields

$$T_F S^{(2,h)}(\vec{p}_T, m, \mu, \nu) - \frac{4}{3} T_F L_m S^{(1)}(\vec{p}_T, \mu, \nu) \overset{p_T \ll m}{=} \delta^{(2)}(\vec{p}_T) \, H_s^{(2)}(m, \mu, \nu) + \mathcal{O}\left(\frac{p_T^2}{m^2}\right), \tag{2.49}$$

confirming the relation in Eq. (2.39). The massless one-loop TMD soft function $S^{(1)}$ and the softmass-mode function $H_s^{(2)}$ are given in Eqs. (B.13) and (C.8), respectively. Since the soft function is free of IR singularities, the limit $m \ll p_T$ just yields the massless soft function in Eq. (B.14),

$$S^{(2,h)}(\vec{p}_T, m, \mu, \nu) \overset{m \ll p_T}{=} S^{(2,l)}(\vec{p}_T, \mu, \nu) + \mathcal{O}\left(\frac{m^2}{p_T^2}\right). \tag{2.50}$$

We now discuss the numerical impact of the $\mathcal{O}(m^2/p_T^2)$ terms from secondary mass effects. Since the individual results for the beam and soft functions depend on the specific regularization scheme, we consider the combination[7]

$$\tilde{B}_q(\vec{p}_T, m, \omega, x, \mu) = \int \mathrm{d}^2 p_T' \, B_q\left(\vec{p}_T - \vec{p}_T', m, x, \mu, \frac{\nu}{\omega}\right) \sqrt{S(\vec{p}_T', m, \mu, \nu)} \,, \tag{2.51}$$

which is independent of ν. Here the root is defined as

$$\int \mathrm{d}^2 p_T' \, \sqrt{S(\vec{p}_T - \vec{p}_T', m, \mu, \nu)} \, \sqrt{S(\vec{p}_T', m, \mu, \nu)} = S(\vec{p}_T, m, \mu, \nu) \,. \tag{2.52}$$

The $\mathcal{O}(\alpha_s^2 C_F T_F)$ corrections explicitly depend on μ and the flavor-number scheme, but the difference between the full result and the small mass limits given in Eqs. (2.47) and (2.50) do not. In Fig. 2.8

---

[7]This combination is sometimes used as definition of a TMD PDF. $\tilde{B}_q$ contains large rapidity logarithms, which are resummed once the soft and beam functions are evaluated at their natural rapidity scales and evolved to a common scale ν. For demonstrating the size of the power corrections here, we evaluate it at fixed order.
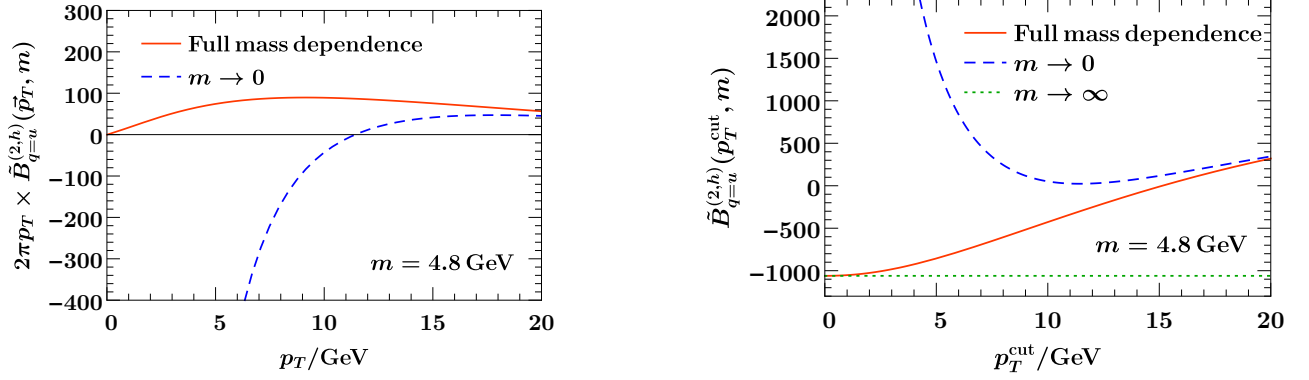
Figure 2.8: Secondary massive bottom quark corrections to the u-quark beam function (left panel) and its cumulant (right panel) at $\mathcal{O}(\alpha_s^2 C_F T_F)$ (including the square-root of the soft function here) for $\mu = m_b$ as a function of q_T.

we show the result for the $\mathcal{O}(\alpha_s^2 C_F T_F)$ corrections (with $\alpha_s = \alpha_s^{(n_l+1)}$) to the u-quark beam function, both differential in p_T and the corresponding cumulant. We see that the full mass dependent results correctly reproduce the small and large mass limits. The difference between the full mass dependent results and the massless case is much larger for secondary massive quarks in Fig. 2.8 than for the primary massive effects in Fig. 2.6. In particular, they are still of $\mathcal{O}(100\%)$ for $p_T^{(\mathrm{cut})} \sim 10$ GeV. This clearly indicates that for secondary radiation involving two massive quarks in the final state the corrections are rather of $\mathcal{O}(4m^2/p_T^2)$, as one might expect.

2.1.7 Rapidity evolution

Here, we discuss the solutions of the rapidity RGEs in Eq. (2.24), or equivalently Eqs. (2.92) and (2.100), and in particular the rapidity evolution for the mass-dependent soft function in Eq. (2.28) for $q_T \sim m$, where the massive quark corrections give rise to a different running than for massless flavors. Our primary aim here is to highlight the different features with respect to the massless case, while leaving the practical implementation for future work.

The rapidity evolution for the mass-mode matching functions H_s and H_c according to Eq. (2.24) has been discussed in Ref. [70]. The evolution for the beam thrust beam function and collinear-soft function that will be discussed in Sec.2.2 is completely analogous (see Eqs. (2.92) and (2.100)). For example, the ν-evolved soft matching function H_s is given by

$$H_s(m, \mu, \nu) = V(m, \mu, \nu, \nu_0)\, H_s(m, \mu, \nu_0)\,, \tag{2.53}$$

$$V(m, \mu, \nu, \nu_0) = \exp\left[\gamma_{\nu,H_s}(m, \mu) \ln \frac{\nu}{\nu_0}\right],$$

where $\gamma_{\nu,H_s}(m, \mu)$ is the ν-anomalous dimension of H_s defined in Eq. (2.24) and is given at $\mathcal{O}(\alpha_s^2)$ in Eq. (C.9). To satisfy path independence in the μ-ν-space, potentially large logarithms of μ need to be resummed in the anomalous dimension $\gamma_{\nu,H_s}(m, \mu)$, which can be done by solving its RGE in virtuality [41]

$$\mu \frac{\mathrm{d}}{\mathrm{d}\mu}\, \gamma_{\nu,H_s}(m, \mu) = -4\left(\Gamma_{\mathrm{cusp}}^{(n_l+1)}[\alpha_s^{(n_l+1)}(\mu)] - \Gamma_{\mathrm{cusp}}^{(n_l)}[\alpha_s^{(n_l)}(\mu)]\right)\,, \tag{2.54}$$

which leads to the resummed form

$$\gamma_{\nu,H_s}(m, \mu) = 4\eta_\Gamma^{(n_l)}(\mu_0(m), \mu) - 4\eta_\Gamma^{(n_l+1)}(\mu_0(m), \mu) + \gamma_{\nu,H_s}(m, \mu_0(m))\,, \tag{2.55}$$

27

where the evolution function η_Γ is defined by

$$\eta_\Gamma^{(n_f)}(\mu_0, \mu) = \int_{\mu_0}^{\mu} \frac{\mathrm{d}\mu'}{\mu'} \, \Gamma_{\mathrm{cusp}}^{(n_f)}[\alpha_s^{(n_f)}(\mu')] \,. \tag{2.56}$$

With the canonical scale choice

$$\mu_0(m) = m \,, \tag{2.57}$$

all logarithmic terms in $\gamma_{\nu, H_s}(m, \mu_0(m))$ are minimized.

The solution of the rapidity RGE for the soft function is more involved due to its two-dimensional convolution structure on $\vec{p}_T$. The formal solution of the rapidity RGE for massless quarks in Eq. (2.17) is most conveniently found in Fourier space using the two-dimensional Fourier transform as in Eq. (2.19), where the rapidity RGE becomes multiplicative

$$\nu \frac{\mathrm{d}}{\mathrm{d}\nu} \, \tilde{S}^{(n_f)}(b, \mu, \nu) = \tilde{\gamma}_{\nu, S}^{(n_f)}(b, \mu) \, \tilde{S}^{(n_f)}(b, \mu, \nu) \,. \tag{2.58}$$

where the impact parameter $b = |\vec{b}_T|$ is Fourier conjugate variable of the transverse momentum. The consistency (path independence) between μ and ν evolution requires the rapidity anomalous dimension in Fourier space to satisfy the RGE in virtuality

$$\mu \frac{\mathrm{d}}{\mathrm{d}\mu} \, \tilde{\gamma}_{\nu, S}^{(n_f)}(b, \mu) = -4 \, \Gamma_{\mathrm{cusp}}^{(n_f)}[\alpha_s^{(n_f)}(\mu)] \,. \tag{2.59}$$

Its solution is given by

$$\tilde{\gamma}_{\nu, S}^{(n_f)}(b, \mu) = -4\eta_\Gamma^{(n_f)}(\mu_0(b), \mu) + \tilde{\gamma}_{\nu, S}^{(n_f)}(b, \mu_0(b)) \,. \tag{2.60}$$

This equation can be used to chose an appropriate scale $\mu_0(b)$ where there are no large logarithms in the second term on the RHS, and evolve the rapidity anomalous dimension to the scale μ where the rapidity resummation is carried out. The canonical scale choice to eliminate the logarithms of $\ln(\mu \, b \, e^{\gamma_E}/2)$ in the second term on the RHS of Eq. (2.60) is

$$\mu_0^{(l)}(b) = \frac{2 \, e^{-\gamma_E}}{b} \,. \tag{2.61}$$

The superscript (l) should indicate that this is the scale choice for light (massless) quarks. Then the ν evolution of the soft function in Fourier space at any given scale μ is given by

$$\tilde{S}(b, \mu, \nu) = \tilde{S}(b, \mu, \nu_0) \exp\left[\tilde{\gamma}_{\nu, S}^{(n_f)}(b, \mu) \ln \frac{\nu}{\nu_0} \right] \,. \tag{2.62}$$

As is well known, the rapidity evolution kernel becomes intrinsically nonperturbative at $1/b \ll \Lambda_{\mathrm{QCD}}$ [32–34]. This nonperturbative sensitivity appears through the resummed rapidity anomalous dimension, which with the canonical scale choice in Eq. (2.61) gets evaluated at $\alpha_s(1/b)$. It is important to note that this is not an artefact of performing the evolution in Fourier space. Rather this is a physical effect, which also happens when the ν evolution is consistently performed in momentum space. As shown in Ref. [65], in this case the appropriate resummed result for $\gamma_{\nu, S}(\vec{p}_T, \mu)$ explicitly depends on $\alpha_s(p_T)$, which means it becomes nonperturbative for $p_T \lesssim \Lambda_{\mathrm{QCD}}$, introducing nonperturbative effects in the convolution between the soft function an the rapidity evolution kernel even when $q_T \gg \Lambda_{\mathrm{QCD}}$.

For the ν anomalous dimension including secondary massive quark corrections in the regime $q_T \sim m$ the μ dependence of the full rapidity anomalous dimension is the same as for $n_l + 1$ massless quarks, i.e. Eq. (2.59) with $n_f = n_l + 1$. This implies that

$$\tilde{\gamma}_{\nu, S}^{(h)}(b, m, \mu) = 4\eta_\Gamma^{(n_l)}(\mu_0(b, m), \mu) - 4\eta_\Gamma^{(n_l+1)}(\mu_0(b, m), \mu) + \tilde{\gamma}_{\nu, S}^{(h)}(b, m, \mu_0(b, m)) \,, \tag{2.63}$$

where $\tilde{\gamma}_{\nu,S}^{(h)}$ denotes only the contributions from the massive flavor to the full anomalous dimension. The explicit mass dependence here arises in the boundary contribution, which depends on both b and m. From the relations in Eqs. (2.41) and (2.39) we can directly infer the limiting behavior to the anomalous dimension,

$$\tilde{\gamma}_{\nu,S}(b,m,\mu) = \tilde{\gamma}_{\nu,S}^{(n_l+1)}(b,\mu) + \mathcal{O}(m^2 b^2)\,,$$

$$\tilde{\gamma}_{\nu,S}(b,m,\mu) = \tilde{\gamma}_{\nu,S}^{(n_l)}(b,\mu) + \gamma_{\nu,H_s}(m,\mu) + \mathcal{O}\Big(\frac{1}{m^2 b^2}\Big)\,. \tag{2.64}$$

This means that the massive quark corrections $\tilde{\gamma}_{\nu,S}^{(h)}$ are the same as for a massless flavor in the limit $m \ll 1/b$ and are the same as the rapidity anomalous dimension of the soft mass mode matching function H_s in the limit $1/b \ll m$, provided one uses the $(n_l + 1)$ and (n_l)-flavor scheme for α_s, respectively. To eliminate the logarithms inside $\tilde{\gamma}_{\nu,S}^{(h)}$, the canonical scale choice $\mu_0(b,m)$ should behave like the massless case for $m \ll 1/b$ and like the choice for the mass-mode matching functions for $m \gg 1/b$,

$$\mu_0^{(h)}(b,m) \sim \mu_0^{(l)}(b) = \frac{2\,\mathrm{e}^{-\gamma_E}}{b} \qquad \text{for} \quad 1/b \to \infty\,,$$

$$\mu_0^{(h)}(b,m) \sim m \qquad \text{for} \quad 1/b \to 0\,. \tag{2.65}$$

Since $\mu_0^{(h)}(b,m)$ freezes out naturally at the perturbative mass scale for $1/b \to 0$, the nonperturbative sensitivity in the ν evolution gets regulated by the quark mass for the massive quark contributions.

We first illustrate this behavior in a simple one-loop toy example: We consider the radiation of a massive gluon (with mass M) having the same couplings as a (massless) gluon in QCD, which exhibits the main features of the full results for secondary massive quarks. The associated corrections are obtained in the calculations of Sec. D.4.1 as intermediate results for the $\mathcal{O}(\alpha_s^2 C_F T_F)$ massive contributions. In b-space the one-loop rapidity anomalous dimensions for massless and massive gluons are given by

$$\tilde{\gamma}_{\nu,S}^{(1)}(b,\mu) = -C_F\,8 L_b\,,$$

$$\tilde{\gamma}_{\nu,S}^{(1)}(b,M,\mu) = C_F\left[8 L_M + 16 K_0(bM)\right]\,, \tag{2.66}$$

where K_0 denotes the modified Bessel function of the second kind and

$$L_b \equiv \ln\frac{b^2\mu^2 \mathrm{e}^{2\gamma_E}}{4}\,, \qquad L_M \equiv \ln\frac{M^2}{\mu^2}\,. \tag{2.67}$$

The mass-dependent result has the limiting behavior

$$\tilde{\gamma}_{\nu,S}^{(1)}(b,M,\mu) = -C_F\,8 L_b + \mathcal{O}(M^2 b^2)\,,$$

$$\tilde{\gamma}_{\nu,S}^{(1)}(b,M,\mu) = C_F\,8 L_M + \mathcal{O}\Big(\frac{1}{M^2 b^2}\Big)\,, \tag{2.68}$$

in close analogy to Eq. (2.64). A natural choice to eliminate any large terms in Eq. (2.66) in both limits is

$$\mu_0^{(h)}(b,M) = M\,e^{K_0(bM)}\,. \tag{2.69}$$

for which $\tilde{\gamma}_{\nu,S}^{(1)}(b,M,\mu_0^{(h)}(b,M))$ just vanishes. The behavior of this choice as a function of b compared to the massless result is shown in Fig. 2.9.
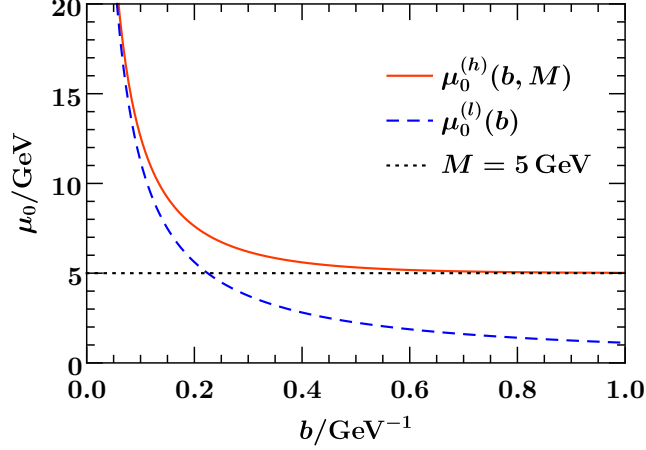
Figure 2.9: The canonical scales $\mu_0^{(h)}(b, M)$ for the massive case (red, solid) and $\mu_0^{(l)}(b) = \mu_0(b, M = 0)$ for the massless case (blue, dashed) with $M = 5\,\text{GeV}$.

For the secondary massive quark corrections at $\mathcal{O}(\alpha_s^2)$ the Fourier transform of Eq. (C.31) reads (expanded in terms of $\alpha_s^{(n_l+1)}$ as in Eq. (2.33))

$$\tilde{\gamma}_{\nu,S}^{(2,h)}(b, m, \mu) = C_F \left\{ -\frac{32}{3} L_b L_m - \frac{16}{3} L_m^2 - \frac{160}{9} L_m - \frac{448}{27} \right.$$
$$\left. + \frac{8\sqrt{\pi}}{3} \left[2\, G_{1,3}^{3,0}\left(\left. \begin{smallmatrix} \frac{3}{2} \\ 0,0,0 \end{smallmatrix} \right| m^2 b^2 \right) + G_{1,3}^{3,0}\left(\left. \begin{smallmatrix} \frac{5}{2} \\ 0,0,1 \end{smallmatrix} \right| m^2 b^2 \right) \right] \right\}, \tag{2.70}$$

where G denotes a Meijer G function. This result has the limiting behavior

$$\tilde{\gamma}_{\nu,S}^{(2,h)}(b, m, \mu) = C_F \left(\frac{16}{3} L_b^2 + \frac{160}{9} L_b + \frac{448}{27} \right) + \mathcal{O}(m^2 b^2) \,,$$
$$\tilde{\gamma}_{\nu,S}^{(2,h)}(b, m, \mu) - \frac{4}{3} L_m \tilde{\gamma}_{\nu,S}^{(1)}(b, \mu) = C_F \left(-\frac{16}{3} L_m^2 - \frac{160}{9} L_m - \frac{448}{27} \right) + \mathcal{O}\left(\frac{1}{m^2 b^2} \right) , \tag{2.71}$$

in the small and large mass limit, respectively. Hence, the correct massless limit is recovered (Fourier transform of the last line of Eq. (B.15)), while in the large-mass limit one obtains the ν-anomalous dimension of H_s in Eq. (C.9). Note that in Eq. (2.71) one needs to perform a change for the strong coupling between the $n_l + 1$ and n_l flavor schemes to obtain both limits correctly. To minimize the logarithms for any regime one should thus adopt a canonical scale choice that satisfies Eq. (2.65), as for example in Eq. (2.69).

2.1.8 Outlook: Phenomenological impact for Drell-Yan

Our results can be applied to properly take into account bottom quark mass effects for the Drell-Yan q_T spectrum at NNLL$'$. While a full resummation analysis is beyond the scope of this work, we can estimate the potential size of the quark-mass effects by looking at the fixed-order q_T spectrum. The full results for the mass dependent singular contributions to the q_T spectrum at fixed order at $\mathcal{O}(\alpha_s^2)$ for secondary massive quarks and $\mathcal{O}(\alpha_s) \times \mathcal{O}(\alpha_s)$ for primary massive quarks, that can be inferred from our calculations of the mass effects to the beam and soft functions, are given in Sec. E.1.

In Fig. 2.10, we show separately the contributions from primary and secondary massive quarks to the singular cross section at $\mathcal{O}(\alpha_s^2)$, normalized to the $\mathcal{O}(\alpha_s)$ spectrum $d\sigma^{(1)}$ including all flavors (treating the charm as a massless flavor). We utilize the MMHT2014 NNLO PDFs [72] and evaluate
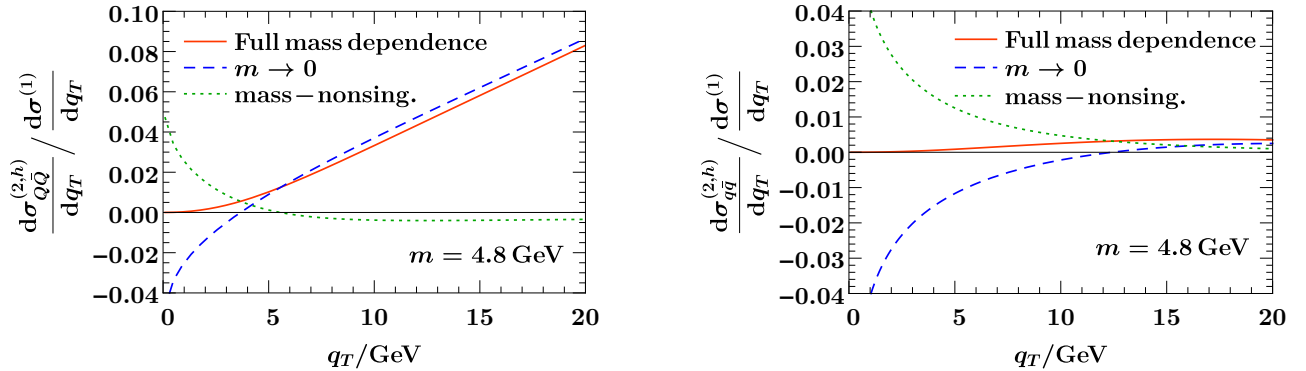
Figure 2.10: Primary (left panel) and secondary (right panel) massive bottom quark contributions for the Z-boson q_T spectrum at fixed $\mathcal{O}(\alpha_s^2 T_F^2)$ and $\mathcal{O}(\alpha_s^2 C_F T_F)$, respectively. The results are given relative to the full $\mathcal{O}(\alpha_s)$ result including all flavors.

the contributions for $\mu = m_b = 4.8$ GeV, $Q = m_Z$, $Y = 0$, and $E_{\text{cm}} = 13$ TeV. As can be seen, the relative contribution of the (primary) $b\bar{b}$-initiated channel in the left panel of Fig. 2.10 grows with larger q_T, while the impact of the secondary contributions in the right panel including the full mass dependence is at the sub-percent level throughout the spectrum. As expected, the difference between the full mass dependent results and the massless limit (called mass-nonsingular in the plot) are very small for $m_b \ll q_T$, but can reach the order of percent for $q_T \sim m_b$, which roughly corresponds to the peak region of the distribution where the cross section is largest.

The same can also be seen in Fig. 2.11, where we show the mass-nonsingular corrections at fixed order (as difference between full mass dependence and massless limit) for primary and secondary contributions as well as their sum. They are shown for $\mu = m_b$ in the left panel and for $\mu = q_T$ in the right panel. Comparing the two plots we see that these corrections are indeed only weakly dependent on the choice of μ (for $q_T \gtrsim 2$ GeV). At $q_T \sim 5$ GeV, where the peak of the Z-boson q_T-spectrum is located, the bottom quark mass can have a relevant effect for high precision prediction at the order of percent. Below the peak of the distribution the fixed-order result is of course not expected to give a reliable quantitative result, and furthermore nonperturbative effects become important in this regime. Nevertheless, we expect the qualitative features like the sign and order of magnitude of the mass effects to provide an indication for the behavior of the full resummed result.

For W production sizable corrections from bottom quark effects arise only through secondary contributions (due to the strong CKM suppression of the primary contributions), which have a similar impact as for Z-production. On the other hand, charm-initiated production plays an important role and enters already at $\mathcal{O}(\alpha_s)$. Estimating the nonsingular mass corrections for $q_T \sim m_c$ is more subtle, since higher-order corrections in the strong coupling and nonperturbative effects are likely to dominate the effect from the known beam function at $\mathcal{O}(\alpha_s)$ at these low scales. Thus, we do not attempt to determine their characteristic size here and leave this to future work. An analysis based on the leading-order matrix element and its potential impact on the determination of m_W can be found in Ref. [46].

31
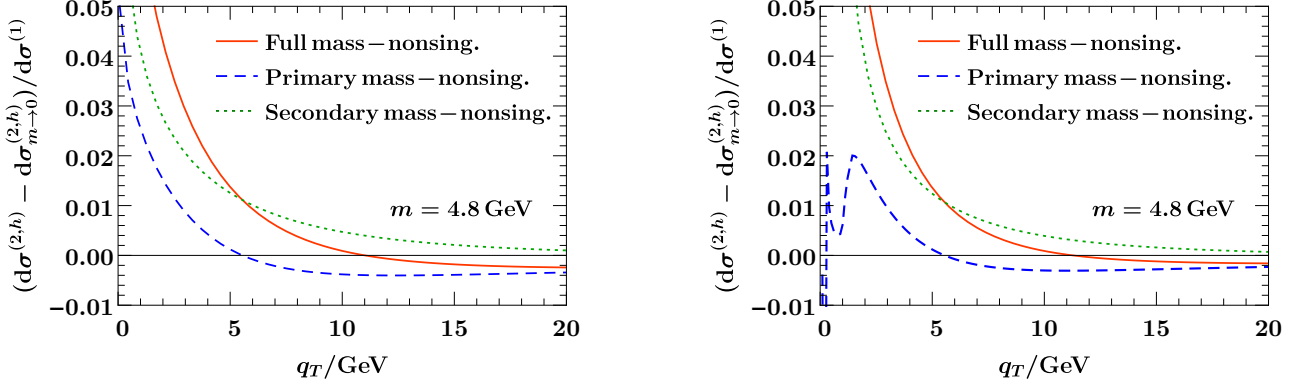
Figure 2.11: Different types of mass nonsingular corrections for Z-boson production at $\mu = m_b$ (left panel) and $\mu = q_T$ (right panel).

2.2 Variable flavor number scheme for beam thrust in Drell-Yan

As a second observable that restricts the final state in a different way and therefore leads to different structures of the resulting factorization theorems, we consider beam thrust[8] [13], using the definition in the hadronic center of mass frame as in Ref. [44]

$$\mathcal{T} = \sum_i \min\{n_a \cdot p_i, n_b \cdot p_i\} = \sum_i \mathrm{e}^{-|y_i|} \sqrt{|\vec{p}_{\perp,i}|^2 + m_i^2}\,. \tag{2.72}$$

Here, p_i are all hadronic final-state momenta (i.e. excluding the color-singlet final state), $n_{a,b}^\mu = (1, \pm \hat{z})$ are lightlike vectors along the beam axes, $\vec{p}_{\perp,i}$ and y_i the transverse momentum with respect to the beam axis and the rapidity of the hadronic final state particles, and m_i their masses. This definition of beam thrust, with all momenta and rapidities defined in the hadronic center of mass frame, is often referred to as "hadronic beam thrust". We will also briefly discuss the factorization theorems for "partonic beam thrust" in Sec. 2.2.6.

The exclusive regime we are interested in corresponds to $\mathcal{T} \ll Q\mathrm{e}^{-|Y|}$, where $Q = \sqrt{q^2}$ is the invariant mass and Y the rapidity of the color-singlet state produced in th hard interaction. We always assume $\Lambda_{\mathrm{QCD}} \ll \mathcal{T}$ allowing for a perturbative description of the physics at this kinematic scale. The factorization and resummation properties of this observable are well known in the massless case, see e.g. Refs [13, 43, 44].

2.2.1 Factorization for massless quarks

For the measurement of beam thrust with $\mathcal{T} \ll Q\mathrm{e}^{-|Y|}$ the relevant EFT modes are n_a-collinear, n_b–collinear and usoft modes with the scaling

$$\begin{aligned}
n_a\text{-collinear:} & \quad p_{n_a}^\mu \sim (\mathcal{T}, \omega_a, \sqrt{\omega_a \mathcal{T}})\,, \\
n_b\text{-collinear:} & \quad p_{n_b}^\mu \sim (\omega_b, \mathcal{T}, \sqrt{\omega_b \mathcal{T}})\,, \\
\text{usoft:} & \quad p_{us}^\mu \sim (\mathcal{T}, \mathcal{T}, \mathcal{T})\,,
\end{aligned} \tag{2.73}$$

with $\omega_{a,b} = Q\mathrm{e}^{\pm Y}$ as in Eq. (2.8). The scaling of the larger of the transverse momentum components of the collinear modes sets the scaling of the transverse momentum of the dilepton pair

$$q_T^2 \sim Q\mathcal{T}\mathrm{e}^{|Y|}\,, \tag{2.74}$$

---

[8]Sometimes beam thrust is defined with an additional factor of $1/Q$, i.e. $\tau_B = \mathcal{T}/Q$.

which implies that the condition $\mathcal{T} \ll Q\mathrm{e}^{-|Y|}$ ensures that all contributions that are leading in the SCET power counting also respect the scaling $q_T \ll Q$, that was assumed to perform the expansion in Eq. (2.7).

The usoft and collinear modes are now separated in invariant mass, $p_{us}^2 \ll p_{n_{a/b}}^2$, which is the characteristic feature of a $\mathrm{SCET_I}$ theory. In this case, there are no rapidity logarithms and the renormalization and evolution is solely in invariant mass. The resulting factorization formula for massless quarks reads [13]

$$\frac{\mathrm{d}\sigma}{\mathrm{d}Q^2 \, \mathrm{d}Y \, \mathrm{d}\mathcal{T}} = \sum_{i,j \in \{q,\bar{q}\}} H_{ij}^{(n_f)}(Q,\mu) \int \mathrm{d}t_a \, \mathrm{d}t_b \, B_i^{(n_f)}(t_a, x_a, \mu) \, B_j^{(n_f)}(t_b, x_b, \mu)$$
$$\times \, S^{(n_f)}\Big(\mathcal{T} - \frac{t_a}{\omega_a} - \frac{t_b}{\omega_b}, \mu\Big) \left[1 + \mathcal{O}\Big(\frac{\mathcal{T}\mathrm{e}^{|Y|}}{Q}\Big)\right], \tag{2.75}$$

with $\omega_{a,b}$ and $x_{a,b}$ as in Eq. (2.8) and Y the rapidity of color-singlet state. This as well as the expressions including mass effects in the subsequent subsections are valid for the primary hard scattering, and do not account for spectator forward (multiparton) scattering effects, since the Glauber Lagrangian of Ref. [73] has been neglected. (There are also corrections from perturbative Glauber effects starting at $\mathcal{O}(\alpha_s^4)$ [74, 75], which are well beyond the order we are interested in, but can be calculated and included using the Glauber operator framework of Ref. [73].) This is sufficient for our purposes for discussing the mass effects in a prototypical $\mathrm{SCET_I}$ scenario. Our results are also directly relevant to include massive quark effects in the Geneva Monte-Carlo program [76, 77], which employs $\mathcal{T}$ as the jet resolution variable for the primary interaction and where multiparton effects are included [78] via the combination with Pythia8 and its MPI model [79–81].

In contrast to the factorization theorems for the q_T spectrum discussed in Sec. 2.1, where there was always only one beam scale $\mu_B \sim q_T$ independent of the rapidity of the color-singlet state, the factorization theorem in Eq. (2.75) introduces two separate beam scales $\mu_{B_{a,b}} = \sqrt{\omega_{a,b}\mathcal{T}}$, that coincide only in the case $\omega_a \sim \omega_b \sim Q$, i.e. when $\mathrm{e}^Y \sim 1$. It is valid as long as both beam scales are clearly separated from the hard scale, i.e. $\mu_{B_{a,b}} \ll Q$. This implies that $\mathcal{T}\mathrm{e}^{|Y|} \ll Q$. This means that in the case of a large rapidity of the color-singlet state, i.e. when the leptonic center of mass frame is strongly boosted with respect to the hadronic center of mass frame, power corrections to the factorization theorem are increasing. The resulting separation of the two beam scales when $\mathrm{e}^{|Y|} \gg 1$ does not change the structure and the resummation properties of the factorization theorem in the massless case, as long as both are still much smaller than the hard scale, but can lead to different scalings of the mass of a heavy flavor with respect to the left and the right beam in the massive case. To avoid these kind of complications, we will for the moment constrain ourselves to more central rapidities and consider only the case $\omega_a \sim \omega_b \sim Q$ in the following sections, such that there is only one global beam scale $\mu_B = \sqrt{Q\mathcal{T}}$. We will discuss the implications of a large hierarchy between the two beam scales and the differences with respect of using the definition of beam thrust in the partonic instead of the hadronic center of mass frame, where these asymmetries do not arise, in Sec 2.2.6.

The hard function H_{ij} in Eq. (2.75) is measurement independent and the same as in Eq. (2.12). The beam and soft functions depend on the measurement and are different from those in Eq. (2.12). The soft function at the scale $\mu \sim \mathcal{T}$ is equivalent to the thrust soft function [82], which is known to $\mathcal{O}(\alpha_s^2)$ [83, 84]. The virtuality-dependent beam functions B_i can be factorized into perturbative matching coefficients $\mathcal{I}_{ik}$ at the scale $\mu \sim t \sim \sqrt{Q\mathcal{T}}$ and the standard nonperturbative PDFs [13, 85]

$$B_i^{(n_f)}(t, x, \mu) = \sum_k \mathcal{I}_{ik}^{(n_f)}(t, x, \mu) \otimes_x f_k^{(n_f)}(x, \mu) \left[1 + \mathcal{O}\Big(\frac{\Lambda_{\mathrm{QCD}}^2}{t}\Big)\right]. \tag{2.76}$$

The symbol $\otimes_x$ denotes the Mellin-type convolution defined in Eq. (2.16). The matching coefficients $\mathcal{I}_{ik}$ have been calculated to $\mathcal{O}(\alpha_s^2)$ [86, 87]. The noncusp anomalous dimensions required at $\mathrm{N^3LL}$ are

available from existing results [85]. The results for the massless beam and soft functions at order $\mathcal{O}(\alpha_s)$ and $\mathcal{O}(\alpha_s^2 C_F T_F)$ are collected in appendix B. In Eq. (2.76) the beam function B is understood to be defined with zero-bin subtractions [88] to eliminate any overlap with regions of lower virtuality.

We will now discuss the meaning of the zero-bin subtraction and compare it to an alternative approach where this overlap is eliminated by a matching on so-called collinear-soft matrix elements, as shown below. We denote with $\mathscr{B}$ the unsubtracted collinear matrix element

$$\mathscr{B}_i\left(t, x = \frac{\omega}{P^-}, \mu\right) = \langle p_n(P^-)|\theta(\omega)\mathcal{O}_i(t, \omega, \mu)|p_n(P^-)\rangle \tag{2.77}$$

where the light-like vector n is either n_a or n_b, depending on whether we deal with the n_a- or n_b-collinear beam function, and $\bar{n}$ is then the respective other light-like vector. The state $|p_n(P^-)>$ is the incoming proton state with momentum $P^\mu = P^- \frac{n^\mu}{2}$ and $\mathcal{O}_i$ a renormalized operator of collinear SCET jet fields

$$\mathcal{O}_i^{\text{bare}}(|\omega|b^+, \omega) = \frac{1}{\omega}\bar{\chi}_n^{(i)}(0)\delta(b^+ - n \cdot \mathcal{P})\frac{\slashed{\bar{n}}}{2}\left[\delta(\omega - \bar{n} \cdot \mathcal{P})\chi_n^{(i)}(0)\right] \tag{2.78}$$

with momentum operator $\mathcal{P}$ acting always to the right (see Ref. [85] for details of the derivation and notation). Then the beam function in Eq. (2.76) is defined as

$$B_i^{(n_f)}(t, x, \mu) = \mathscr{B}_i^{(n_f)}(t, x, \mu) - \text{zero-bin}. \tag{2.79}$$

These zero-bins are all scaleless in the massless case (i.e. zero in dimensional regularization), but are conceptually necessary to render the full beam function matching coefficient IR finite, by exchanging IR for UV divergences through the scaleless integrals. The matching of the beam function onto the PDF in Eq. (2.76) cancels any IR divergences coming from collinear regions of lower virtuality, but the zero-bin subtractions are still necessary to take care of the remaining IR divergences coming from soft regions, such that the matching coefficient $\mathcal{I}_{ij}(t, x, \mu)$ is IR finite.

An alternative way, that makes these cancellations of IR divergences in the soft region more explicit, is to match the unsubtracted collinear matrix elements $\mathscr{B}$ on a theory with all the hard-collinear modes integrated out. In this effective theory below the matching scale we do not only have the collinear modes at a lower virtuality, i.e. the PDFs as in Eq. (2.76), but also "collinear-soft" (csoft) modes, that encode contributions from fluctuations from virtualities between the collinear and the usoft scale. The scaling of the momenta of the collinear-soft modes is

$$\begin{aligned} n_a\text{-csoft:} \qquad p_{\text{cs}}^\mu &\sim \left(\mathcal{T}, k^2/\mathcal{T}, \sqrt{k^2}\right), \\ n_b\text{-csoft:} \qquad p_{\text{cs}}^\mu &\sim \left(k^2/\mathcal{T}, \mathcal{T}, \sqrt{k^2}\right), \end{aligned} \tag{2.80}$$

where k^2 is some virtuality between the collinear and the usoft scale, i.e. $\mathcal{T}^2 < k^2 < Q\mathcal{T}$. We refer to these intermediate modes as collinear-soft, because they are boosted but are softer than the standard collinear modes, thus coupling to the latter via Wilson lines and leading to a SCET$_+$ theory [89]. This type of intermediate SCET$_+$ modes have appeared in various contexts [89–92]. Note that also the scaling of the PDFs is collinear with a lower virtuality than the hard-collinear modes, with momenta $p^\mu \sim (Q, \Lambda_{\text{QCD}}^2/Q, \Lambda_{\text{QCD}})$, but with the large light-cone component having the same scaling as the one of the beam function $\sim Q$, while the collinear-soft modes are less boosted. Their momentum scaling in Eq. (2.80) is defined such that they can in principle contribute to the beam thrust measurement via their smaller light-cone component that is of order $\sim \mathcal{T}$. The matching relation between the two theories when integrating out the hard-collinear modes at the beam scale is

$$\mathscr{B}_i^{(n_f)}(t, x, \mu) = \sum_k \int \mathrm{d}\ell \, \mathcal{I}_{ik}^{(n_f)}(t - \omega\ell, x, \mu) \otimes_x f_k^{(n_f)}(x, \mu)\mathscr{S}_c^{(n_f)}(\ell, \mu)\left[1 + \mathcal{O}\left(\frac{\Lambda_{\text{QCD}}^2}{t}\right)\right]. \tag{2.81}$$

The csoft matrix elements $\mathscr{S}_c$ are defined as

$$\mathscr{S}_c(\ell, \mu) = \frac{1}{N_c} \text{tr} \left\langle 0 \left| \overline{\text{T}} \left[X_n^\dagger(0) V_n(0) \right] \delta(\ell - n \cdot \mathcal{P}) \text{T} \left[V_n^\dagger(0) X_n(0) \right] \right| 0 \right\rangle , \qquad (2.82)$$

with the csoft Wilson lines given by (see e.g. Refs. [89, 90])

$$X_n = \sum_{\text{perms}} \exp\left[-\frac{g}{n \cdot \mathcal{P}} \frac{\nu^{\eta/2}}{(\bar{n} \cdot \mathcal{P})^{\eta/2}} \, n \cdot A_{cs} \right], \quad V_n = \sum_{\text{perms}} \exp\left[-\frac{g}{\bar{n} \cdot \mathcal{P}} \frac{\nu^{\eta/2}}{(\bar{n} \cdot \mathcal{P})^{\eta/2}} \, \bar{n} \cdot A_{cs} \right], \qquad (2.83)$$

where the light-like vector n can again stand for either n_a or n_b for the n_a and n_b-collinear-soft matrix element, respectively, and $\bar{n}$ for the respective other light-like vector. The gluon fields A_{cs} in the Wilson lines are collinear-soft fields with the momentum scaling defined in Eq. (2.80). Here we have used again the η regulator on the Wilson lines to regulate rapidity divergences, and have already performed an expansion according to the collinear-soft scaling $\bar{n} \cdot \mathcal{P} \gg n \cdot \mathcal{P}$. The rapidity regulator is not necessary in the purely massless theory, where in fact all contributions to the csoft matrix elements beyond tree-level are scaleless, but we already introduced it here since it will be important once dealing with massive quark effects in the csoft matrix elements. Note that for the symmetric η regulator the csoft matrix elements are symmetric under changing the directions $n_a \leftrightarrow n_b$, which will in general not be the case for a different choice for the rapidity regulator. The collinear matrix elements $\mathscr{B}_i$ are the same as in Eq. (2.79) and f_k are the standard PDFs. The beam function matching coefficient $\mathcal{I}_{ik}$ is a Wilson coefficient of a matching of two effective theories and is therefore always IR finite because the IR divergences are the same in both theories.

For massless quarks the csoft matrix elements only lead to scaleless integrals beyond tree-level and thereby convert exactly the same IR to UV divergences as the zero-bins of the collinear matrix element. Because they appear on the right-hand side of the matching equation Eq. (2.81), they are also subtracted from the partonic beam function matrix element $\mathscr{B}$ when calculating the matching coefficient $\mathcal{I}$, and therefore lead to the same results as using the beam function defined with zero-bin subtractions. The massless csoft modes do not manifest themselves in any non-trivial matching function between the beam and the soft scale, since there is no perturbative scale that would give rise to non-scaleless integrals. Therefore these modes eventually contribute only to the soft-function when their virtuality reaches $k^2 \sim \mathcal{T}^2$, where they become identical to the soft modes. This is also the reason why they need to be subtracted from the collinear matrix elements in order to avoid double counting. The beam functions B_i how they appear in the factorization theorem are then defined via the collinear matrix elements after subtracting the overlap with the soft region (given by the collinear-soft matrix elements)

$$\begin{aligned} B_i^{(n_f)}(t, x, \mu) &= \int \mathrm{d}\ell \, \mathscr{B}_i^{(n_f)}(t - \omega\ell, x, \mu) \left(\mathscr{S}_c^{(n_f)}(\ell, \mu) \right)^{-1} \\ &= \sum_{k \in \{q, \bar{q}, g\}} \mathcal{I}_{ik}^{(n_f)}(t, x, \mu) \otimes_x f_k^{(n_f)}(x, \mu) . \end{aligned} \qquad (2.84)$$

Since the scaleless collinear-soft matrix elements cancel the same IR divergences as the zero-bin subtraction in $\mathscr{B}$, the definitions of the beam function B in Eq. (2.84) and in Eq. (2.79) are equivalent in the massless case. In the factorization theorem we are then left only with the soft function S, that already contains the massless csoft modes, and the beam function as in Eq. (2.84).

The definition of the beam function in Eq. (2.84) provides an alternative way of defining the subtraction of the soft region from collinear matrix elements, compared to the definition with zero-bins in Eq. (2.79), as a subtraction of collinear-soft matrix elements. The idea to associate the subtractions of soft regions from collinear functions like the beam function to collinear-soft matrix elements was already discussed in different contexts in Refs. [93, 94]. It was used in Ref. [1] to define infrared finite matching coefficients for virtuality-dependent beam functions and recently also discussed in

more detail in the context of the SCET quark jet function in Ref. [71]. This way of defining the subtractions from regions of lower virtuality in the beam function as a csoft matrix element will be of particular importance when dealing with massive quark effects in Sec. 2.2.3, where the virtuality of the csoft modes related to the heavy flavor is fixed to $k^2 \sim m^2$ and the corresponding massive csoft matrix element gives non-trivial contributions at two-loops, leading to a so called csoft function as an additional structure in the factorization theorem when integrating out the massive flavor.

The resummation of logarithms $\ln(\mathcal{T}/Q)$ is performed by evaluating all functions at their characteristic scales and evolving them to a common final scale μ using the solutions of the RGEs

$$\mu \frac{\mathrm{d}}{\mathrm{d}\mu} B_i^{(n_f)}(t, x, \mu) = \int \mathrm{d}t'\, \gamma_B^{(n_f)}(t - t', \mu)\, B_i^{(n_f)}(t', x, \mu)\,,$$
$$\mu \frac{\mathrm{d}}{\mathrm{d}\mu} S^{(n_f)}(\ell, \mu) = \int \mathrm{d}\ell'\, \gamma_S^{(n_f)}(\ell - \ell', \mu)\, S^{(n_f)}(\ell', \mu)\,. \tag{2.85}$$

In contrast to Eq. (2.12), there is no rapidity evolution in SCET_I for massless quarks. Consistency of the RG evolution implies that

$$\omega_a \gamma_B^{(n_f)}(\omega_a \ell, \mu) + \omega_b \gamma_B^{(n_f)}(\omega_b \ell, \mu) + \gamma_S^{(n_f)}(\ell, \mu) = \gamma_H^{(n_f)}(Q, \mu)\, \delta(\ell)\,. \tag{2.86}$$

Here and in the following, when we talk about RG evolution of the beam function, it will always be that of the subtracted beam function B, as it appears in the factorization theorem as $B_i = \mathscr{B}_i \otimes \mathscr{S}_c^{-1} = \sum_k \mathcal{I}_{ik} \otimes_x f_k$ as in Eq. (2.84). The anomalous dimension governing this evolution is given by

$$\gamma_B^{(n_f)}(t, \mu) = \gamma_{\mathscr{B}}^{(n_f)}(t, \mu) - \frac{1}{\omega} \gamma_{\mathscr{S}_c}^{(n_f)}(t/\omega, \mu)\,, \tag{2.87}$$

where by $\gamma_{\mathscr{B}}$ and $\gamma_{\mathscr{S}_c}$ we denote the anomalous dimensions of the collinear operator in Eq. (2.78) and the csoft matrix elements in Eq. (2.82), respectively. We do not provide the individual results for $\gamma_{\mathscr{B}}$ and $\gamma_{\mathscr{S}_c}$ as they are not infrared finite, in contrast to γ_B where the infrared divergences cancel between the collinear and the csoft anomalous dimension. The massless contributions at $\mathcal{O}(\alpha_s)$ and $\mathcal{O}(\alpha_s^2 C_F T_F)$ to γ_B and γ_S are given in App. B. In general when we use the term "beam function" we will refer to the subtracted beam function $B_i = \mathscr{B}_i \otimes \mathscr{S}_c^{-1}$, not to be confused with the unsubtracted matrix element $\mathscr{B}_i$.

For beam thrust the number of possible scale hierarchies with a massive quark is larger due to the fact that the (massless) collinear and soft modes have different invariant mass scales. The discussion for the hierarchies with $\sqrt{Q\mathcal{T}} \ll m$ where the massive quark cannot be produced via real emissions, is completely identical to $q_T \ll m$, since the quark mass effects in these cases are independent of the low-energy measurement. For $m \sim Q$, all mass effects are encoded by using the mass-dependent hard function from Sec. 2.1.2 in Eq. (2.75) together with setting $n_f = n_l$ in the rest of the factorization theorem. Similarly, the case $\sqrt{Q\mathcal{T}} \ll m \ll Q$ is described by using Eq. (2.75) with $n_f = n_l$, and replacing the hard function by the product of massless $(n_l + 1)$-flavor hard function and the soft and collinear mass-mode functions H_s and H_c, as for the case $q_T \ll m \ll Q$ in Sec. 2.1.3, i.e.

$$\frac{\mathrm{d}\sigma}{\mathrm{d}Q^2\, \mathrm{d}Y\, \mathrm{d}\mathcal{T}} = \sum_{i,j \in \{q,\bar{q}\}} H_{ij}^{(n_l+1)}(Q, \mu) H_c\left(m, \mu, \frac{\nu}{\omega_a}\right) H_c\left(m, \mu, \frac{\nu}{\omega_b}\right) H_s(m, \mu, \nu)$$
$$\times \int \mathrm{d}t_a\, \mathrm{d}t_b\, B_i^{(n_l)}(t_a, x_a, \mu)\, B_j^{(n_l)}(t_b, x_b, \mu) S^{(n_l)}\left(\mathcal{T} - \frac{t_a}{\omega_a} - \frac{t_b}{\omega_b}, \mu\right) \left[1 + \mathcal{O}\left(\frac{\mathcal{T}}{Q}, \frac{m^2}{Q^2}, \frac{Q\mathcal{T}}{m^2}\right)\right]. \tag{2.88}$$

We therefore proceed directly to the hierarchies $m \lesssim \sqrt{Q\mathcal{T}}$, where the massive quark can be produced in collinear and/or soft real radiation. The four possible hierarchies and the relevant EFT modes in the $p^+ p^-$-plane are illustrated in Fig. 2.12, and are discussed in the following subsections.

36

(a) $\mathcal{T} \ll m \sim \sqrt{Q\mathcal{T}}$

(b) $\mathcal{T} \ll m \ll \sqrt{Q\mathcal{T}}$

(c) $\mathcal{T} \sim m \ll \sqrt{Q\mathcal{T}}$

(d) $m \ll \mathcal{T} \ll \sqrt{Q\mathcal{T}}$
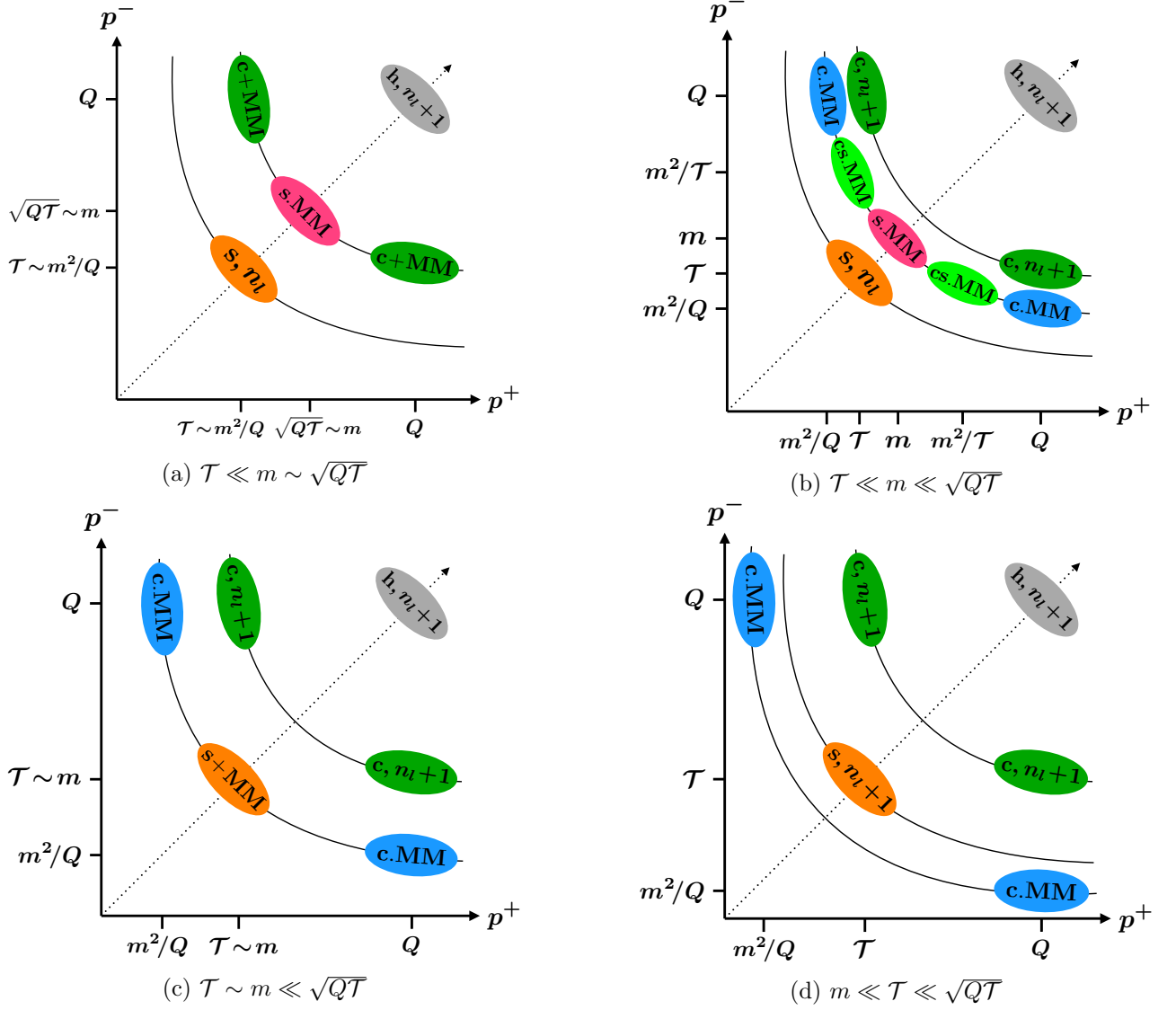
Figure 2.12: Effective theory modes for the beam thrust spectrum with massive quarks for $m^2/Q \lesssim \mathcal{T} \ll Q$ and $m \gg \Lambda_{\mathrm{QCD}}$.

2.2.2 Quark mass effects for $\sqrt{Q\mathcal{T}} \sim m \ll Q$

For $\sqrt{Q\mathcal{T}} \sim m \ll Q$ massive quarks can be produced via collinear initial-state radiation, but not via soft real radiation. After the hard matching, carried out with $n_l + 1$ massless quark flavors as discussed in Sec. 2.1.3, the degrees of freedom in the EFT are collinear and soft modes with the scaling

$$
\begin{aligned}
n_a\text{-collinear + MM:}\quad & p_{n_a}^{\mu} \sim (\mathcal{T}, Q, \sqrt{Q\mathcal{T}}) \sim \left(\frac{m^2}{Q}, Q, m\right), \\
n_b\text{-collinear + MM:}\quad & p_{n_b}^{\mu} \sim (Q, \mathcal{T}, \sqrt{Q\mathcal{T}}) \sim \left(Q, \frac{m^2}{Q}, m\right), \\
\text{soft MM:}\quad & p_s^{\mu} \sim (m, m, m), \\
\text{usoft:}\quad & p_{us}^{\mu} \sim (\mathcal{T}, \mathcal{T}, \mathcal{T}),
\end{aligned}
\tag{2.89}
$$

as illustrated in Fig. 2.12a. While the usual usoft modes live at a lower virtuality scale than the collinear modes, the soft mass-modes are separated from the collinear modes only in rapidity, leading to a mix of SCET$_\mathrm{I}$ and SCET$_\mathrm{II}$ features. In particular, there will be mass-related rapidity divergences.

At the scale $\mu \sim \sqrt{Q\mathcal{T}} \sim m$ this theory with $n_l + 1$ dynamical quark flavors is matched onto a theory with n_l flavors, integrating out at the same time the massive flavor and also fluctuations related to initial-state collinear radiation of massless particles, which corresponds to standard matching of the (massless) beam functions onto the PDFs. The matching in the collinear sectors leads to mass-dependent beam function coefficients $\mathcal{I}_{ik}$,

$$\mathscr{B}_i^{(n_l+1)}\Big(t, m, x, \mu, \frac{\nu}{\omega}\Big) = \sum_{k \in \{q, \bar{q}, g\}} \int \mathrm{d}\ell\, \mathcal{I}_{ik}\Big(t - \omega\ell, m, x, \mu, \frac{\nu}{\omega}\Big) \otimes_x f_k^{(n_l)}(x, \mu)$$
$$\times \mathscr{S}_c^{(n_l)}(\ell, \mu)\Big[1 + \mathcal{O}\Big(\frac{\Lambda_{\mathrm{QCD}}^2}{m^2}, \frac{\Lambda_{\mathrm{QCD}}^2}{t}\Big)\Big], \qquad (2.90)$$

Note that both the PDF and the csoft matrix elements are evaluated with only n_l massless quarks. This leads to only scaleless integrals in the csoft matrix elements, which corresponds to subtracting the zero-bins for the massless quarks.

The beam function that then appears in the factorization theorem is given by

$$B_i^{(n_l+1)}\Big(t, m, x, \mu, \frac{\nu}{\omega}\Big) = \int \mathrm{d}\ell\, \mathscr{B}_i^{(n_l+1)}\Big(t - \omega\ell, m, x, \mu, \frac{\nu}{\omega}\Big)\Big(\mathscr{S}_c^{(n_l)}(\ell, \mu)\Big)^{-1}$$
$$= \sum_{k \in \{q, \bar{q}, g\}} \mathcal{I}_{ik}\Big(t, m, x, \mu, \frac{\nu}{\omega}\Big) \otimes_x f_k^{(n_l)}(x, \mu)\Big[1 + \mathcal{O}\Big(\frac{\Lambda_{\mathrm{QCD}}^2}{m^2}, \frac{\Lambda_{\mathrm{QCD}}^2}{t}\Big)\Big], \quad (2.91)$$

where $\mathcal{I}_{ik}(t, m, x, \mu, \frac{\nu}{\omega})$ is defined by the matching relation in Eq. (2.90). Note that here the subtraction of collinear-soft modes (as well as that of the PDFs) is performed with only n_l massless flavors, while the full collinear matrix element $\mathscr{B}$ is calculated with $n_l + 1$ flavors. This still leads to an IR finite matching coefficient because the contributions of a massive quark to $\mathscr{B}$ do not introduce additional IR divergences because for $m \sim \sqrt{Q\mathcal{T}}$ the mass is kept finite. We have for the first time calculated the previously unkown contributions from massive quarks to the virtuality dependent beam functions, some details on the calculations can be found in appendix D. The results at $\mathcal{O}(\alpha_s)$ and $\mathcal{O}(\alpha_s^2 C_F T_F)$ for the mass dependent $\mathcal{I}_{ik}$ are given in Sec. C.2.2. Since the massive flavor is integrated out at this scale it is absent in the lower energy effective theory and does therefore not contribute to the subtractions. In principle it would also be possible to not fully integrate out the heavy flavor and include it also in the subtractions, which corresponds to the definition of the beam function in the UF scheme. This approach and its relation to the MMF scheme presented in this chapter, where the heavy flavor is always completely integrated out at its respective mass scale, will be discussed in chapter 4.

The dependence on the rapidity scale ν here arises due to virtual secondary massive quark corrections and is the same as for the collinear mass-mode matching function H_c already given in Eq. (2.22), i.e.,

$$\nu \frac{\mathrm{d}}{\mathrm{d}\nu} B_i^{(n_l+1)}\Big(t, m, x, \mu, \frac{\nu}{\omega}\Big) = \gamma_{\nu, H_c}(m, \mu)\, B_i^{(n_l+1)}\Big(t, m, x, \mu, \frac{\nu}{\omega}\Big). \qquad (2.92)$$

In the soft sector the soft mass modes are integrated out, leaving only the usoft modes. This gives exactly the soft mass-mode matching function H_s already given in Eq. (2.22), which encodes the effects of virtual secondary massive quark radiation. As usual, also the strong coupling constant has to be matched from $n_l + 1$ to n_l flavors. The remaining contributions at the lower scales, the soft function and the PDFs, are given in terms of n_l massless flavors and in the (n_l)-scheme for α_s. The

resulting factorized cross section reads

$$
\frac{\mathrm{d}\sigma}{\mathrm{d}Q^2\,\mathrm{d}Y\,\mathrm{d}\mathcal{T}} = \sum_{i,j\in\{q,\bar{q},Q,\bar{Q}\}} H_{ij}^{(n_l+1)}(Q,\mu)\,H_s(m,\mu,\nu) \int \mathrm{d}t_a\,\mathrm{d}t_b
$$
$$
\times \left[\sum_{k\in\{q,\bar{q},g\}} \mathcal{I}_{ik}\Big(t_a,m,x_a,\mu,\frac{\nu}{\omega_a}\Big) \otimes_x f_k^{(n_l)}(x_a,\mu) \right]
$$
$$
\times \left[\sum_{k\in\{q,\bar{q},g\}} \mathcal{I}_{jk}\Big(t_b,m,x_b,\mu,\frac{\nu}{\omega_a}\Big) \otimes_x f_k^{(n_l)}(x_b,\mu) \right]
$$
$$
\times S^{(n_l)}\Big(\mathcal{T}-\frac{t_a}{\omega_a}-\frac{t_b}{\omega_b},\mu\Big) \left[1+\mathcal{O}\Big(\frac{\mathcal{T}}{Q},\frac{m^2}{Q^2},\frac{\mathcal{T}^2}{m^2},\frac{\Lambda_{\mathrm{QCD}}^2}{Q\mathcal{T}}\Big)\right]. \tag{2.93}
$$

The resummation of logarithms in Eq. (2.93) is obtained by evolving all functions from their natural scales, as illustrated in Fig. 2.13a. The mass-dependent ν evolution, which resums the rapidity logarithms $\ln(Q/m)$, is identical to the one for the hard functions H_c and H_s in Sec. 2.1.3. The μ evolution can be conveniently carried out by evolving the hard, beam, and soft functions with $n_l + 1$ active flavors above the mass scale and with n_l active flavors below the mass scale, which automatically takes into account the μ dependence of H_s. To see this, the consistency of RG running for Eq. (2.93) together with the consistency relation for $n_l + 1$ massless quarks in Eq. (2.86) implies

$$
\omega_a \gamma_{B,m}^{(n_l+1)}\Big(\omega_a\ell,m,\mu,\frac{\nu}{\omega_a}\Big) + \omega_b \gamma_{B,m}^{(n_l+1)}\Big(\omega_b\ell,m,\mu,\frac{\nu}{\omega_b}\Big) + \gamma_S^{(n_l)}(\ell,\mu) + \gamma_{H_s,\mu}(m,\mu,\nu)\,\delta(\ell)
$$
$$
= \omega_a \gamma_B^{(n_l+1)}(\omega_a\ell,\mu) + \omega_b \gamma_B^{(n_l+1)}(\omega_b\ell,\mu) + \gamma_S^{(n_l+1)}(\ell,\mu), \tag{2.94}
$$

where $\gamma_S^{(n_l)}$, $\gamma_S^{(n_l+1)}$, $\gamma_B^{(n_l+1)}$ are the anomalous dimensions for the soft and beam functions with n_l and $n_l + 1$ massless flavors as defined in Eq. (2.85), and $\gamma_{B,m}^{(n_l+1)}(t,m,\mu,\nu/\omega)$ is the anomalous dimension of the mass-dependent beam function,

$$
\mu\frac{\mathrm{d}}{\mathrm{d}\mu} B_i^{(n_l+1)}\Big(t,m,x,\mu,\frac{\nu}{\omega}\Big) = \int \mathrm{d}t'\,\gamma_{B,m}^{(n_l+1)}\Big(t-t',m,\mu,\frac{\nu}{\omega}\Big) B_i^{(n_l+1)}\Big(t',m,x,\mu,\frac{\nu}{\omega}\Big). \tag{2.95}
$$

The consistency relation in Eq. (2.94) can be confirmed explicitly at two loops with the expressions in eqs. (B.11), (B.18), (C.9), and (C.23). Note that this relation does *not* imply that $\gamma_{B,m}^{(n_l+1)}(t,m,\mu,\nu/\omega)$ and $\gamma_B^{(n_l+1)}(t,\mu)$ are the same, which is indeed not the case for the massive quark corrections as is shown explicitly in Sec. C.2. The reason is that the presence of the quark mass leads to a SCET$_{\mathrm{II}}$-type theory, in which the required rapidity regularization redistributes the μ anomalous dimension between soft and collinear corrections with individually regularization scheme dependent pieces. Only their sum, as given on the left-hand side of Eq. (2.94), is independent of the regularization scheme and yields the combined running for beam and soft functions with $n_l + 1$ massless flavors above $\mu_m \sim m$, as given on the right-hand side of Eq. (2.94).

2.2.3 Quark mass effects for $\mathcal{T} \ll m \ll \sqrt{Q\mathcal{T}}$

When the beam scale becomes larger than the mass scale, but the soft scale is still smaller than the mass, which happens for $m^2/Q \ll \mathcal{T} \ll m$, the beam function matching coefficients $\mathcal{I}_{ik}$ encode only fluctuations related to initial-state collinear radiation with $n_l + 1$ massless quarks, i.e. the heavy flavor is treated as an additional massless quark in that matching. The EFT below $\sqrt{Q\mathcal{T}}$ contains the usual collinear and soft mass modes scaling as $p_{m,n_a}^\mu \sim (m^2/Q,Q,m)$, $p_{m,n_b}^\mu \sim (Q,m^2/Q,m)$ and $p_{m,s}^\mu \sim (m,m,m)$ that can not contribute to the beam thrust measurement in this hierarchy. Integrating out these modes leads to the PDF matching coefficients $\mathcal{M}_{ij}$ and the soft mass mode matching function H_s, respectively.

(a) $\mathcal{T} \ll m \sim \sqrt{Q\mathcal{T}}$ (b) $\mathcal{T} \ll m \ll \sqrt{Q\mathcal{T}}$ (c) $\mathcal{T} \sim m \ll \sqrt{Q\mathcal{T}}$
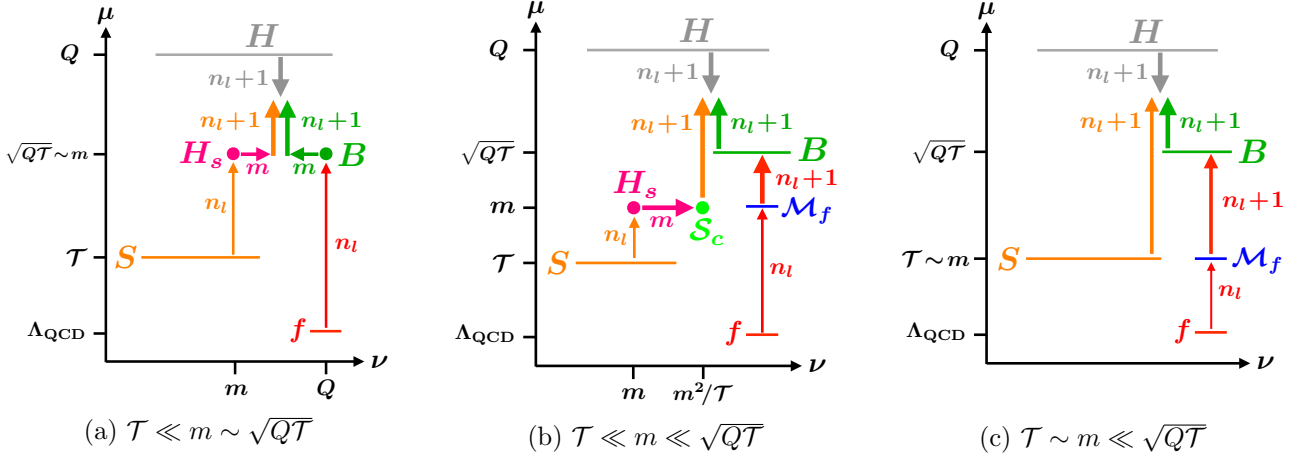
Figure 2.13: Illustration of the renormalization group evolution for beam thrust of the hard, beam, soft, and parton distribution function in virtuality μ (vertical) and rapidity ν (horizontal). The anomalous dimensions for each evolution step involve the displayed number of active quark flavors. The label m indicates that the corresponding evolution is mass dependent.

However, besides these there are also the collinear-soft modes as described in Eq. (2.80). They were defined as collinear modes at an invariant mass scale k^2 smaller than the beam scale and the scaling of their momentum components determined by the condition that they can have a dynamic impact on the $\mathcal{T}$ spectrum, as illustrated also in Fig. 2.12b. For massive modes their invariant mass is set by the on-shell constraint $k^2 \sim m^2$, yielding the scaling for the collinear-soft mass modes

$$n_a\text{-csoft MM:} \quad p^{\mu}_{cs,n_a} \sim \left(\mathcal{T}, \frac{m^2}{\mathcal{T}}, m\right),$$
$$n_b\text{-csoft MM:} \quad p^{\mu}_{cs,n_b} \sim \left(\frac{m^2}{\mathcal{T}}, \mathcal{T}, m\right). \tag{2.96}$$

The matching in the collinear sector can be performed in two steps as in Eqs. (2.29) and (2.30). After integrating out all of the mass modes, the PDF and the soft function are still given in a (n_l)-flavor theory. Thus the factorization formula reads

$$\frac{\mathrm{d}\sigma}{\mathrm{d}Q^2\,\mathrm{d}Y\,\mathrm{d}\mathcal{T}} = \sum_{i,j\in\{q,\bar{q},Q,\bar{Q}\}} H^{(n_l+1)}_{ij}(Q,\mu)\,H_s(m,\mu,\nu)\int\mathrm{d}k_a\,\mathrm{d}k_b\,\mathcal{S}_c(k_a,m,\mu,\nu)\,\mathcal{S}_c(k_b,m,\mu,\nu)$$
$$\times \int\mathrm{d}t_a\left[\sum_{k\in\{q,\bar{q},Q,\bar{Q},g\}}\sum_{l\in\{q,\bar{q},g\}}\mathcal{I}^{(n_l+1)}_{ik}(t_a,x_a,\mu)\otimes_x\mathcal{M}_{kl}(x_a,m,\mu)\otimes_x f^{(n_l)}_l(x_a,\mu)\right]$$
$$\times \int\mathrm{d}t_b\left[\sum_{k\in\{q,\bar{q},Q,\bar{Q},g\}}\sum_{l\in\{q,\bar{q},g\}}\mathcal{I}^{(n_l+1)}_{jk}(t_b,x_b,\mu)\otimes_x\mathcal{M}_{kl}(x_b,m,\mu)\otimes_x f^{(n_l)}_l(x_b,\mu)\right]$$
$$\times S^{(n_l)}\left(\mathcal{T}-\frac{t_a}{\omega_a}-\frac{t_b}{\omega_b}-k_a-k_b,\mu\right)\left[1+\mathcal{O}\left(\frac{\mathcal{T}}{Q},\frac{m^2}{Q\mathcal{T}},\frac{\mathcal{T}^2}{m^2},\frac{\Lambda^2_{\mathrm{QCD}}}{m^2}\right)\right]. \tag{2.97}$$

The beam function matching coefficient $\mathcal{I}^{(n_l+1)}(t,x,\mu)$ arises from integrating out hard-collinear modes in the (n_l+1)-flavor theory at the scale $\mu\sim\sqrt{Q\mathcal{T}}\gg m$. Since the matching scale is

much larger than the mass scale, all quarks can be considered massless

$$B_i^{(n_l+1)}(t, x, \mu) = \int \mathrm{d}\ell \, \mathscr{B}_i^{(n_l+1)}(t - \omega\ell, x, \mu) \left(\mathscr{S}_c^{(n_l+1)}(\ell, \mu) \right)^{-1}$$

$$= \sum_{k \in \{q, \bar{q}, Q, \bar{Q}, g\}} \mathcal{I}_{ik}^{(n_l+1)}(t, x, \mu) \otimes_x f_k^{(n_l+1)}(x, \mu) \left[1 + \mathcal{O}\left(\frac{\Lambda_{\text{QCD}}^2}{t} \right) \right]. \qquad (2.98)$$

Since all quarks are treated as massless, all contributions in $\mathscr{S}_c^{(n_l+1)}$ are in fact again scaleless and only render the matching coefficient IR finite by converting IR to UV divergences through the scaleless integrals.

The functions $\mathcal{S}_c$ in Eq. (2.97) are the csoft matching functions encoding the interactions of the collinear-soft radiation at the invariant mass scale $\mu \sim m$ and the rapidity scale $\nu \sim m^2/\mathcal{T}$. They arise from integrating out collinear-soft fluctuations of the heavy flavor at the mass scale and are defined as the matching coefficient of the collinear-soft matrix elements between the theories with and without the heavy flavor

$$\mathscr{S}_c^{(n_l+1)}(\ell, m, \mu, \nu) = \int \mathrm{d}\ell' \, \mathcal{S}_c(\ell - \ell', m, \mu, \nu) \, \mathscr{S}_c^{(n_l)}(\ell', \mu). \qquad (2.99)$$

At the matching scale $\mu \sim m$ the full mass dependence is kept in the $(n_l + 1)$-flavor theory, such that the collinear-soft matrix elements including the heavy flavor $\mathscr{S}_c^{(n_l+1)}$ now give non-vanishing contributions, in contrast to Eq. (2.98) where all quarks were treated as massless. The previously unknown csoft function $\mathcal{S}_c$ at $\mathcal{O}(\alpha_s^2)$ is calculated in Sec. D.5, the results are summarized in Sec. C.4.2.

The $\mathcal{M}_{ij}$ correspond to the well-known PDF matching correction incorporating the effect of the collinear mass modes, as in Eq. (2.31), with the results at $\mathcal{O}(\alpha_s)$ and $\mathcal{O}(\alpha_s^2 C_F T_F)$ given in Sec. C.2.3. The virtual soft massive quark corrections are still described by the function H_s at the rapidity scale $\nu \sim m$ as in the factorization theorem for $m \sim \sqrt{Q\mathcal{T}}$ in Eq. (2.93).

The RG evolution for Eq. (2.97) is illustrated in Fig. 2.13b. The csoft function satisfies the same rapidity RGE as the collinear mass-mode functions H_c appearing in the factorization theorem for $\sqrt{Q\mathcal{T}} \ll m \ll Q$ in Eq. (2.88) and the massive beam functions for $m \sim \sqrt{Q\mathcal{T}}$ in Eq. (2.92), i.e.,

$$\nu \frac{\mathrm{d}}{\mathrm{d}\nu} \mathcal{S}_c(k, m, \mu, \nu) = \gamma_{\nu, H_c}(m, \mu) \, \mathcal{S}_c(k, m, \mu, \nu). \qquad (2.100)$$

The only difference with respect to the rapidity evolution in the factorization theorem for $m \sim \sqrt{Q\mathcal{T}}$ in Eq. (2.93) is that it now happens between H_s with $\nu \sim m$ and $\mathcal{S}_c$ with $\nu_{\mathcal{S}_c} \sim m^2/\mathcal{T}$ rather than between H_s and the beam functions with $\nu_B \sim Q$, such that now the rapidity logarithms $\ln(m/\mathcal{T})$ are resummed. The μ evolution can be performed with $n_l + 1$ flavors for the hard function H_{ij}, the beam and soft function above the mass scale and with n_l flavors below. This automatically accounts for the μ dependence of $\mathcal{S}_c$ and H_s above $\mu_m \sim m$, which precisely gives the difference between the evolution of the soft function with $n_l + 1$ and n_l flavors, as implied by the consistency of RG running for Eq. (2.97) and the relation in Eq. (2.86) with $n_l + 1$ massless quarks,

$$\gamma_S^{(n_l)}(\ell, \mu) + 2\gamma_{\mathcal{S}_c}(\ell, m, \mu, \nu) + \delta(\ell) \, \gamma_{H_s}(m, \mu, \nu) = \gamma_S^{(n_l+1)}(\ell, \mu), \qquad (2.101)$$

where

$$\mu \frac{\mathrm{d}}{\mathrm{d}\mu} \mathcal{S}_c(k, m, \mu, \nu) = \int \mathrm{d}k' \, \gamma_{\mathcal{S}_c}(k - k', m, \mu, \nu) \, \mathcal{S}_c(k, m, \mu, \nu). \qquad (2.102)$$

At two loops, the consistency relation Eq. (2.101) can be confirmed with the explicit expressions given in Eqs. (B.18), (C.33), and (C.9).

2.2.4 Quark mass effects for $\mathcal{T} \sim m$ and $m \ll \mathcal{T}$

For $\mathcal{T} \sim m$ the csoft and soft mass modes in the previous section merge with the usual usoft modes,

$$\text{usoft:} \quad p_s^\mu \sim (\mathcal{T}, \mathcal{T}, \mathcal{T}) \sim \left(\mathcal{T}, \frac{m^2}{\mathcal{T}}, m\right) \sim (m, m, m). \tag{2.103}$$

In this hierarchy massive quarks can be also produced in soft real radiation leading to a soft function at the scale $\mu \sim \mathcal{T}$ that depends on the quark mass. In addition, there are the massless collinear modes as well as the collinear mass modes, as illustrated in Fig. 2.12c. Since we still have $m \ll \sqrt{Q\mathcal{T}}$, the matching in the collinear sectors is the same as for the case $\mathcal{T} \ll m \ll \sqrt{Q\mathcal{T}}$ discussed in the previous subsection. The factorization formula reads

$$
\begin{aligned}
\frac{\mathrm{d}\sigma}{\mathrm{d}Q^2\,\mathrm{d}Y\,\mathrm{d}\mathcal{T}} &= \sum_{i,j\in\{q,\bar{q},Q,\bar{Q}\}} H_{ij}^{(n_l+1)}(Q,\mu) \int \mathrm{d}t_a\,\mathrm{d}t_b \\
&\times \left[\sum_{k\in\{q,\bar{q},Q,\bar{Q},g\}} \sum_{l\in\{q,\bar{q},g\}} \mathcal{I}_{ik}^{(n_l+1)}(t_a, x_a, \mu) \otimes_x \mathcal{M}_{kl}(x_a, m, \mu) \otimes_x f_l^{(n_l)}(x_a, \mu) \right] \\
&\times \left[\sum_{k\in\{q,\bar{q},Q,\bar{Q},g\}} \sum_{l\in\{q,\bar{q},g\}} \mathcal{I}_{jk}^{(n_l+1)}(t_b, x_b, \mu) \otimes_x \mathcal{M}_{kl}(x_b, m, \mu) \otimes_x f_l^{(n_l)}(x_b, \mu) \right] \\
&\times S^{(n_l+1)}\left(\mathcal{T} - \frac{t_a}{\omega_a} - \frac{t_b}{\omega_b}, m, \mu\right) \left[1 + \mathcal{O}\left(\frac{\mathcal{T}}{Q}, \frac{m^2}{Q\mathcal{T}}, \frac{\Lambda_{\mathrm{QCD}}^2}{m^2}\right)\right].
\end{aligned}
\tag{2.104}
$$

Now all rapidity divergences cancel within the soft function and do not leave behind any potentially large rapidity logarithms. The RG evolution for this case is illustrated in Fig. 2.13c. The massive quark corrections at $\mathcal{O}(\alpha_s^2 C_F T_F)$ to the soft function $S(\mathcal{T}, m, \mu)$ are given in Sec. C.4.3.

Finally for $m \ll \mathcal{T}$, if expressed in terms of the $n_l + 1$-flavor scheme for α_s, the massless limit can be taken in the soft funciton $S^{(n_l+1)}(\mathcal{T}, m, \mu)$ without encountering any IR singularities. Otherwise, Eq. (2.104) remains unchanged, such that now the only dependence on the mass scale arises in the PDF matching corrections $\mathcal{M}_{ij}$. The hard, beam, and soft functions can now be always evolved with $n_l + 1$ massless flavors and only the evolution of the PDF changes, when crossing the flavor threshold.

2.2.5 Relations between hierarchies

We now discuss how the functions appearing in the different factorization formulae are related to each other. The relations between the modes and their contributions are illustrated in Fig. 2.14 for the different possible hierarchies. As in Sec. 2.1.6, these relations show how one can combine the resummation of logarithms relevant in one regime with the power-suppressed fixed-order content that becomes important in the neighboring regimes, enabling a systematic inclusion of mass corrections across the entire $\mathcal{T}$ spectrum. For a specific way of implementing these power corrections, discussed for the example of DIS in the endpoint region, we refer to Sec. 4.2.1. Here and in the following we will use the notation of Eqs. (2.33) and (2.36) when giving explicit results at one and two-loops.

Similar to Eq. (2.38) for the TMD beam functions, the mass-dependent beam function coefficients appearing for $\sqrt{Q\mathcal{T}} \sim m$ (incorporating massive quark fluctuation as discussed in Sec. 2.2.2) are related to those for $\sqrt{Q\mathcal{T}} \ll m$ with n_l massless quarks and the collinear mass-mode function H_c by

$$\mathcal{I}_{ik}\left(t, m, x, \mu, \frac{\nu}{\omega}\right) \overset{t \ll m^2}{=} H_c\left(m, \mu, \frac{\nu}{\omega}\right) \mathcal{I}_{ik}^{(n_l)}(t, x, \mu) \left[1 + \mathcal{O}\left(\frac{t}{m^2}\right)\right]. \tag{2.105}$$

At the same time, the mass-dependent beam function also encodes information about the fixed-order content for $\mathcal{T} \ll m \ll \sqrt{Q\mathcal{T}}$. Comparing Eqs. (2.93) and (2.97), they are related to those with $n_l + 1$

$\sqrt{Q\mathcal{T}} \ll m \sim Q$ | $\sqrt{Q\mathcal{T}} \ll m \ll Q$ | $\sqrt{Q\mathcal{T}} \sim m \ll Q$ | $\mathcal{T} \ll m \ll \sqrt{Q\mathcal{T}}$ | $\mathcal{T} \sim m \ll \sqrt{Q\mathcal{T}}$ | $m \ll \mathcal{T} \ll \sqrt{Q\mathcal{T}}$

hard+m → **hard, n_l+1** — $\mu \sim Q$

coll. MM
soft MM

coll., n_l ← **coll.+MM** → **coll., n_l+1** — $\mu \sim \sqrt{Q\mathcal{T}}$
soft MM

coll. MM
csoft MM
soft MM

soft, n_l ← **soft+MM** → **soft, n_l+1** — $\mu \sim \mathcal{T}$
coll. MM

coll. MM

coll., n_l — $\mu \sim \Lambda_{\mathrm{QCD}}$
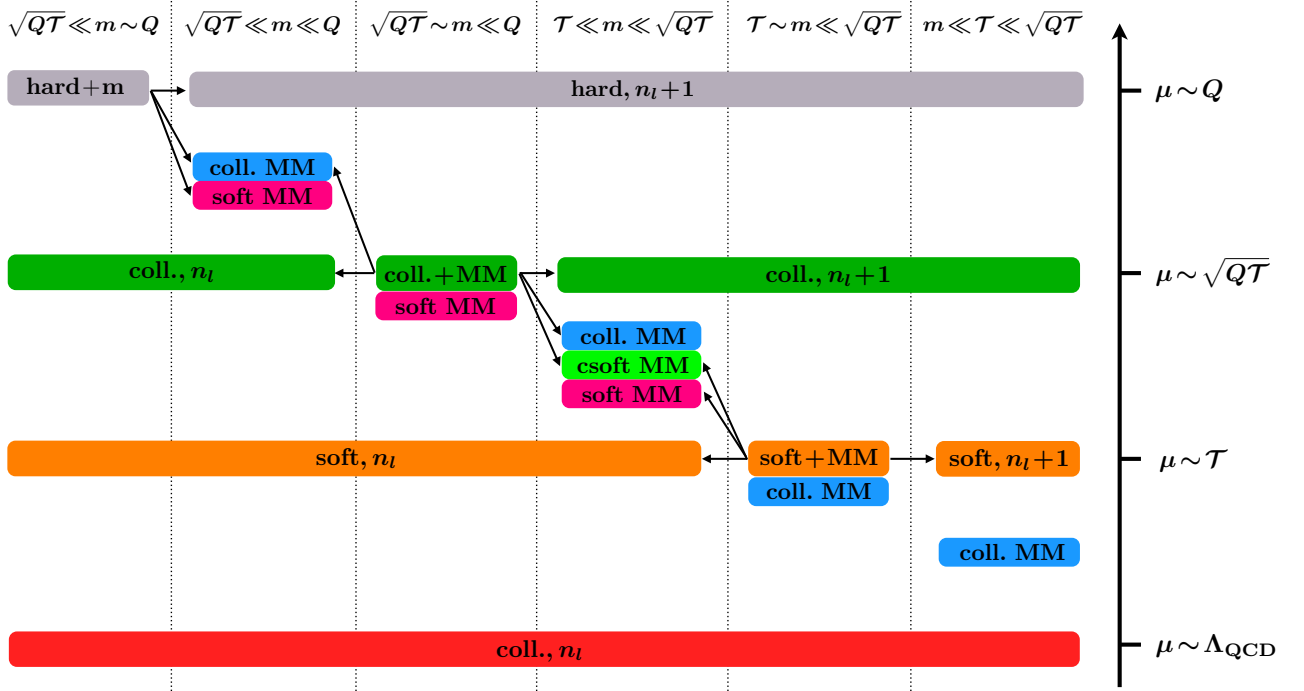
Figure 2.14: Relevant modes for the beam thrust spectrum with $\mathcal{T} \ll Q$ for different hierarchies between the quark mass m and the scales $\mathcal{T}$, $\sqrt{Q\mathcal{T}}$ and Q. The directions of the arrows indicate how a particular mode contribution is separated when the expansion of another hierarchy is used.

massless flavors, the PDF matching functions, and the csoft function $\mathcal{S}_c$ by

$$\mathcal{I}_{ik}\Big(t, m, x, \mu, \frac{\nu}{\omega}\Big) \overset{m^2 \ll t}{=} \sum_{j=\{q,\bar{q},Q,\bar{Q},g\}} \int \mathrm{d}\ell\, \mathcal{I}_{ij}^{(n_l+1)}(t - Q\ell, x, \mu) \otimes_x \mathcal{M}_{jk}(x, m, \mu)\, \mathcal{S}_c(\ell, m, \mu, \nu)$$
$$\times \Big[1 + \mathcal{O}\Big(\frac{m^2}{t}\Big)\Big]. \tag{2.106}$$

The mass-dependent soft function for $\mathcal{T} \sim m$ in Eq. (2.104) contains massive quark fluctuations that for $\mathcal{T} \ll m$ get split into the massless soft function with n_l flavors, the soft mass mode function H_s, and the csoft function $\mathcal{S}_c$ in Eq. (2.97) as

$$S^{(n_l+1)}(\ell, m, \mu) \overset{\ell \ll m}{=} H_s(m, \mu, \nu) \int \mathrm{d}\ell'\, S^{(n_l)}(\ell - \ell', \mu)\, \mathcal{S}_c(\ell', m, \mu, \nu)\Big[1 + \mathcal{O}\Big(\frac{\ell^2}{m^2}\Big)\Big]. \tag{2.107}$$

Finally, as already mentioned below Eq. (2.104), the soft function approaches its massless limit for $m \ll \mathcal{T}$,

$$S^{(n_l+1)}(\ell, m, \mu) \overset{m \ll \ell}{=} S^{(n_l+1)}(\ell, \mu)\Big[1 + \mathcal{O}\Big(\frac{m^2}{\ell^2}\Big)\Big]. \tag{2.108}$$

In the following we will verify the relations betweent the different hiearchies discussed above for the beam and soft functions up to $\mathcal{O}(\alpha_s^2)$. We also scrutinize the numerical impact of the power corrections for these functions. We focus in particular on the $\mathcal{O}(m^2/Q\mathcal{T})$ corrections the $\mathcal{T}$ spectrum for b quarks, which are contained in the factorization theorem Eq. (2.93) for $\sqrt{Q\mathcal{T}} \sim m$ but not in the small mass limit for $m \ll \sqrt{Q\mathcal{T}}$ in Eqs. (2.97) and (2.104).

For the numerical results we use the MMHT2014 NNLO PDFs [72] and evaluate the contributions for $\mu = m_b = 4.8$ GeV, $\omega = m_Z$, and $E_{\mathrm{cm}} = 13$ TeV. The main qualitative features of the results do not depend on these specific input parameters.

The virtuality-dependent massive quark beam function coefficient at one loop is given in Eq. (C.19). In the limit $t \ll m^2$ the primary massive quarks correctly decouple,

$$\mathcal{I}_{Qg}^{(1)}(t, m, z) \stackrel{t \ll m^2}{=} \mathcal{O}\left(\frac{t}{m^2}\right). \tag{2.109}$$

In the opposite limit $m^2 \ll t$ we get

$$\mathcal{I}_{Qg}^{(1)}(t, m, z) \stackrel{m^2 \ll t}{=} T_F \, \theta(1-z)\theta(z) \left\{ 2P_{qg}(z) \frac{1}{\mu^2} \mathcal{L}_0\left(\frac{t}{\mu^2}\right) + \delta(t) \left[2P_{qg}(z)\left(-L_m + \ln\frac{1-z}{z}\right) \right. \right.$$
$$\left. \left. + 4z(1-z) \right] \right\} + \mathcal{O}\left(\frac{m^2}{t}\right)$$
$$= \mathcal{I}_{qg}^{(1)}(t, z, \mu) + \delta(t) \, \mathcal{M}_{Qg}^{(1)}(m, z, \mu) + \mathcal{O}\left(\frac{m^2}{t}\right), \tag{2.110}$$

as required by the relation (2.106). The massless one-loop matching coefficient $\mathcal{I}_{qg}^{(1)}$ and the PDF matching coefficient $\mathcal{M}_{Qg}^{(1)}$ are given in Eqs. (B.9) and (C.24), respectively.

The secondary massive quark corrections to the virtuality-dependent quark beam function $\mathcal{I}_{qq}^{(2,h)}(t, m, z)$ are given in Eq. (C.20). In the decoupling limit $t \ll m^2$ all its nondistributional terms become $\mathcal{O}(t/m^2)$ power suppressed. Combining the remaining distributional terms in t with the contributions arising from changing the scheme of the strong coupling from $n_l + 1$ to n_l flavors according to Eq. (2.34), yields[9]

$$T_F \mathcal{I}_{qq}^{(2,h)}\left(t, m, z, \mu, \frac{\nu}{\omega}\right) - \frac{4}{3} T_F L_m \mathcal{I}_{qq}^{(1)}(t, z, \mu) \stackrel{t \ll m^2}{=} \delta(t)\delta(1-z) \, H_c^{(2)}\left(m, \mu, \frac{\nu}{\omega}\right) + \mathcal{O}\left(\frac{t}{m^2}\right), \tag{2.111}$$

in agreement with Eq. (2.105). The massless result for $\mathcal{I}_{qq}^{(1)}$ and the collinear mass-mode function $H_c^{(2)}$ are given in Eqs. (B.9) and (C.10), respectively. In the limit $m^2 \ll t$ we get

$$T_F \mathcal{I}_{qq}^{(2,h)}\left(t, m, z, \mu, \frac{\nu}{\omega}\right)$$
$$\stackrel{m^2 \ll t}{=} T_F \mathcal{I}_{qq}^{(2,l)}(t, z, \mu) + \delta(t) \, \mathcal{M}_{qq}^{(2)}(m, z, \mu) + \delta(1-z) \frac{1}{\omega} \mathcal{S}_c^{(2)}\left(\frac{t}{\omega}, m, \mu, \nu\right) + \mathcal{O}\left(\frac{m^2}{t}\right). \tag{2.112}$$

All infrared mass dependence is contained in the PDF matching coefficient and the csoft function, as required by Eq. (2.106). The functions on the right-hand side are given in eqs. (B.10), (C.25), and (C.32), respectively.

There are also secondary massive quark corrections at $\mathcal{O}(\alpha_s^2 T_F^2)$ to the Compton-type gluon initiated process shown in Fig. 2.7, encoded in the coefficient $\mathcal{I}_{qg}^{(2,h)}(t, m, z)$. Since they arise only from virtual corrections to an external gluon line, the limiting behavior for this coefficient is trivial, since it vanishes identically in the (n_l)-flavor scheme for α_s, and in the $(n_l + 1)$-flavor scheme for α_s it is exactly

$$T_F \, \mathcal{I}_{qg}^{(2,h)}(t, m, z, \mu) = \mathcal{I}_{qg}^{(1)}(t, z, \mu) \otimes_z \mathcal{M}_{gg}^{(1)}(m, z, \mu). \tag{2.113}$$

The mass-dependent $\mathcal{O}(\alpha_s^2)$ corrections to the (beam) thrust soft function are given in Eq. (C.34). In the limit $\ell \ll m$ all its nondistributional ℓ-dependent terms become $\mathcal{O}(\ell^2/m^2)$ power suppressed. Combining the remaining distributional terms with the contributions arising from changing the scheme of the strong coupling from $n_l + 1$ to n_l flavors yields

$$T_F S^{(2,h)}(\ell, m, \mu) - \frac{4}{3} T_F L_m S^{(1)}(\ell, \mu) \stackrel{\ell \ll m}{=} \delta(\ell) \, H_s^{(2)}(m, \mu, \nu) + \mathcal{S}_c^{(2)}(\ell, m, \mu, \nu) + \mathcal{O}\left(\frac{\ell^2}{m^2}\right), \tag{2.114}$$

---

[9]We remind the reader that this scheme change of α_s to the n_l flavor scheme is necessary to recover the decoupling limit, while for the massless limit we need α_s in the $n_l + 1$ flavor scheme.
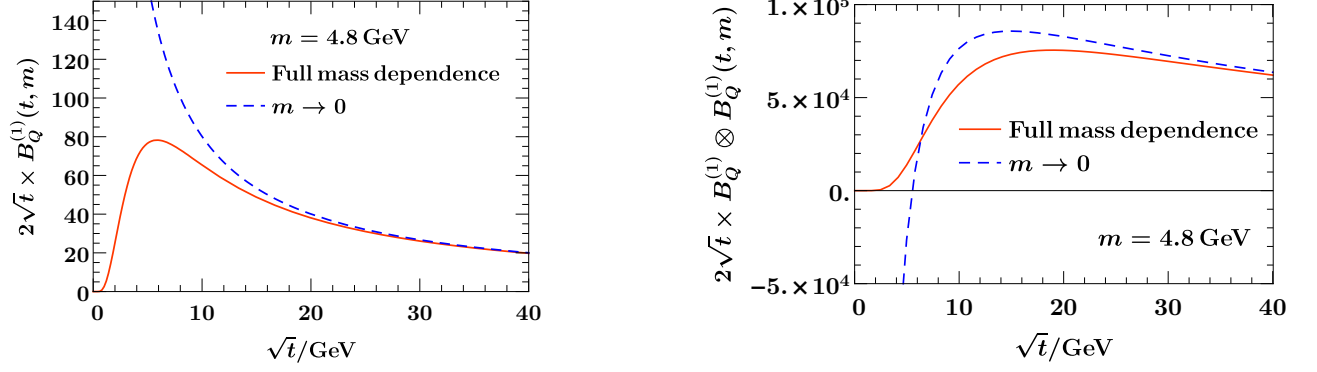
Figure 2.15: Massive b-quark beam function (left panel) and the convolution between two of these (right panel) together with the $m \to 0$ limit as a function of $\sqrt{t} \sim \sqrt{Q\mathcal{T}}$.
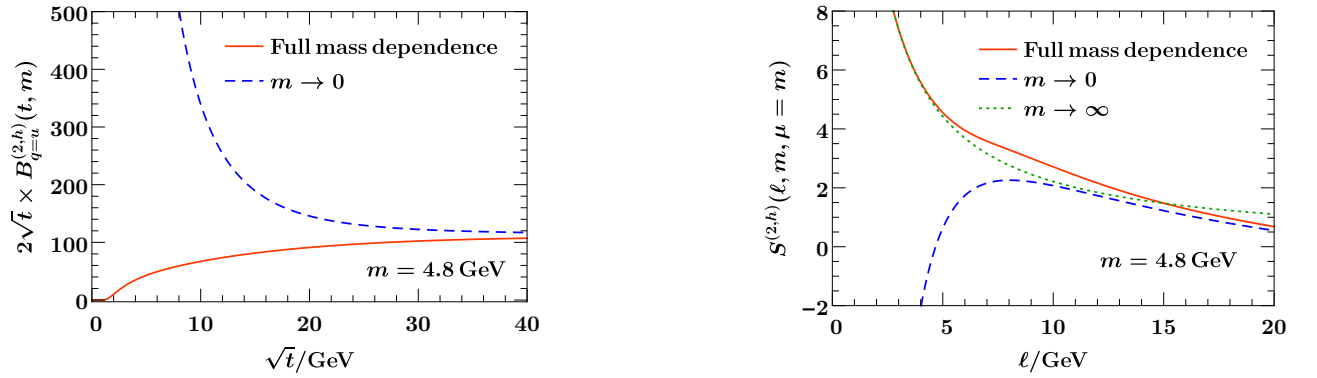
Figure 2.16: Secondary massive b-quark corrections to the u-quark beam function for $Y = 0$ (left panel) and the soft function (right panel) at $\mathcal{O}(\alpha_s^2 C_F T_F)$ for $\mu = m_b$ as functions of $\sqrt{t} \sim \sqrt{Q\mathcal{T}}$ and $\ell \sim \mathcal{T}$, respectively.

(a) $\omega_a \sim \omega_b \sim Q$　　　　　　　　　　　(b) $\omega_b \ll Q \ll \omega_a$
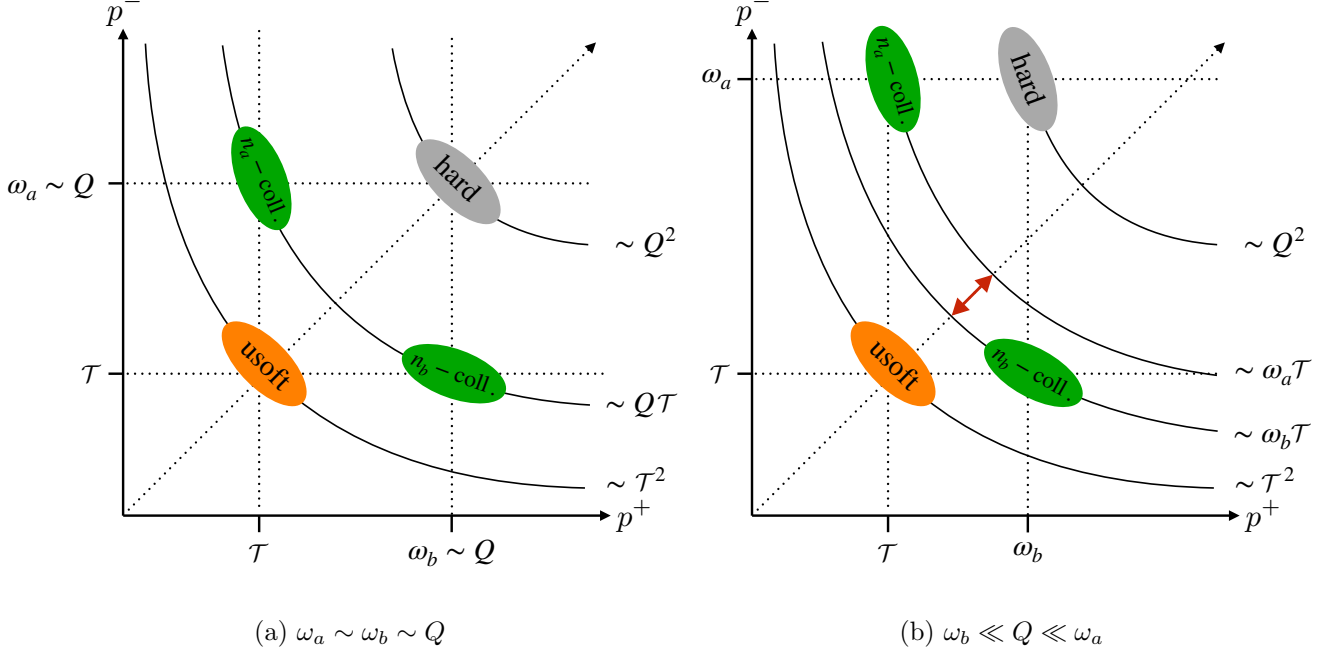
Figure 2.17: EFT modes for the massless factorization theorem for hadronic beam thrust for $\omega_a \sim \omega_b \sim Q$ (left) and $\omega_b \ll Q \ll \omega_a$ (right).

in agreement with Eq. (2.107). The massless one-loop thrust soft function $S^{(1)}$, the soft mass-mode function $H_s^{(2)}$, and the csoft function $\mathcal{S}_c^{(2)}$ can be found in eqs. (B.16), (C.8), and (C.32), respectively. For $m \ll \ell$ the correct massless result is recovered,

$$S^{(2,h)}(\ell, m, \mu) \overset{m \ll \ell}{=} S^{(2,l)}(\ell, \mu) + \mathcal{O}\!\left(\frac{m^2}{\ell^2}\right), \qquad (2.115)$$

which was already checked in Ref. [95].

In Fig. 2.15, we show the numerical results for the one-loop massive beam function and the convolution between two of these (which is the leading order correction from primary massive quarks for the Z-boson production) as a function of $\sqrt{t} \sim \sqrt{Q\mathcal{T}}$. The mass effects become relevant for $\sqrt{t} \sim m_b \sim 5$ GeV (corresponding to $\mathcal{T} \lesssim 1$ GeV for $Q = m_Z$). In Fig. 2.16, we show the result for the secondary $\mathcal{O}(\alpha_s^2 C_F T_F)$ corrections to the beam and soft function. The corrections to the massless limit for the beam function remain sizable even for $\sqrt{t} \gtrsim 2m_b$. For the soft function, the mass effects are important for $\mathcal{T} \sim \ell \sim m_b$ and become small for $\ell > 10\,\text{GeV} \sim 2m_b$.

2.2.6　Factorization theorems for large rapidities and partonic beam thrust

In the previous subsections we always assumed the scaling $\omega_a \sim \omega_b \sim Q$, such that one needs to consider only one beam scale $\mu_B = \mu_{B_a} = \mu_{B_b} \sim \sqrt{Q\mathcal{T}}$. The form of the massive factorization theorems for beam thrust in the previous sections are therefore only valid for the case of not too large rapidities of the color-singlet state, i.e. $e^Y \sim 1$. But the massless factorization theorem in Eq. (2.75) is in principle valid also for $e^{|Y|} \gg 1$, as long as the condition $\mathcal{T}e^{|Y|} \ll Q$ is fulfilled. In the following we will extend the massive factorization theorems to the more general case of rapidities in the range $1 \ll e^{|Y|} \ll Q/\mathcal{T}^{10}$. We will also explain that the issue of large rapidities does not show up when using a different definition of beam thrust. These issues when dealing with larger rapidities in the massive case were not discussed in Ref. [1] where $e^Y \sim 1$ was always assumed implicitly. The content of the

---

[10]As before we will always assume that $e^{|Y|} \ll E_{\text{cm}}/Q$ in order to avoid large threshold logarithms.

following section of this thesis is new and provides a framework capable of dealing with situations where Y is not small.

The scaling of the light-cone components of the momenta of the relevant collinear and ultra-soft modes of SCET and the hard fluctuations that are integrated out is determined by the momentum entering the hard interaction, which sets the larger light-cone components of the collinear modes to ω_a and ω_b, and the beam thrust measurement that fixes the small light-cone components to $\mathcal{T}$. Combining these conditions with the typical collinear and ultra-soft scaling of the SCET modes gives

$$
\begin{aligned}
\text{hard:} \quad & p_h^\mu \sim (\omega_b, \omega_a, \sqrt{\omega_a \omega_b})\,, \\
n_a\text{-collinear:} \quad & p_{n_a}^\mu \sim (\mathcal{T}, \omega_a, \sqrt{\omega_a \mathcal{T}})\,, \\
n_b\text{-collinear:} \quad & p_{n_b}^\mu \sim (\omega_b, \mathcal{T}, \sqrt{\omega_b \mathcal{T}})\,, \\
\text{usoft:} \quad & p_{us}^\mu \sim (\mathcal{T}, \mathcal{T}, \mathcal{T})\,,
\end{aligned}
\tag{2.116}
$$

as shown in Fig. 2.17. This implies that in principle one effectively introduces two separate beam scales in the factorization theorems

$$
\mu_{B_a} \sim \sqrt{\omega_a \mathcal{T}} \sim \mu_B \, \mathrm{e}^{Y/2}\,, \qquad\qquad \mu_{B_b} \sim \sqrt{\omega_b \mathcal{T}} \sim \mu_B \, \mathrm{e}^{-Y/2}\,.
\tag{2.117}
$$

For the rest of this section we will always assume that $Y > 0$, such that $\mu_{B_b} < \mu_{B_a}$. In the case of a rapidity $Y < 0$ one can just swap the two beam directions $a \leftrightarrow b$. Only in the case of not too large rapidities the two beam scales are of the same order and can be replaced by one global beam scale μ_B. If Y is becoming larger, a large hierarchy is introduced between the two beam scales, $\mu_{B_b} \ll \mu_{B_a}$, see Fig. 2.17b. While this does not affect the structure of the massless factorization theorem, as long as both of them are still clearly separated from the hard scale Q, this can be different in the massive case, where the scaling of the mass of the heavy flavor with respect to the other kinematic scales is of importance.

In the cases of $m \ll \sqrt{Q\mathcal{T}}\mathrm{e}^{-Y/2}$ or $m \gg \sqrt{Q\mathcal{T}}\mathrm{e}^{Y/2}$, i.e. the mass being much smaller than the smaller beam scale or much greater than the larger beam scale, the structure of the factorization theorems is unaffected. For $m \ll \sqrt{Q\mathcal{T}}\mathrm{e}^{-Y/2}$ the mass effects are encoded in the csoft or the soft function, and both beam functions (as well as the hard function) are the ones for $n_l + 1$ massless flavors. For $m \gg \sqrt{Q\mathcal{T}}\mathrm{e}^{Y/2}$ the mass effects are contained in the hard or the current mass mode matching functions, and both beam functions (as well as the soft function) are the ones for n_l massless flavors.

But if the mass is in the range $\sqrt{Q\mathcal{T}}\mathrm{e}^{-Y/2} \lesssim m \lesssim \sqrt{Q\mathcal{T}}\mathrm{e}^{Y/2}$, it has a different scaling with respect to one beam scale than with respect to the other one, leading to asymmetric factorization theorems, for which we need to consider three different possible hierarchies. Since the mass in these three hierarchies is always much smaller than the hard scale and much greater than the soft scale, we can always write the hard function with $n_l + 1$ massless flavors and the soft function with n_l massless flavors. Additionally there is the soft current mass mode matching function H_s from integrating out the heavy flavor in the soft sector. But in the collinear sector the structure of the factorization theorems varies for the three different possible hierarchies.

Factorization theorem for $\sqrt{Q\mathcal{T}}\mathrm{e}^{-Y/2} \ll m \sim \sqrt{Q\mathcal{T}}\mathrm{e}^{Y/2}$

In this hierarchy the mass is of order of the large beam scale and therefore - because here we are always assuming $\mu_{B_b} \ll \mu_{B_a}$ - much larger than the second beam scale, $\mu_{B_b} \ll \mu_{B_a} \sim m$. This means that when integrating out the heavy flavor at the mass scale, it happens at the same scale where hard collinear radiation is integrated out when matching the beam function for beam a on the PDF, which results in a mass dependent matching coefficient $\mathcal{I}_{ik}$. On the other hand, in beam b the mass scale is still much greater than the beam scale, which means that the heavy flavor is integrated out in the full SCET current, leading to a collinear current mass mode matching function H_c. The beam function

for beam b is then the same as in the massless case with n_l massless flavors. The full factorization theorem for this hierarchy reads

$$
\frac{\mathrm{d}\sigma}{\mathrm{d}Q^2\,\mathrm{d}Y\,\mathrm{d}\mathcal{T}} = \sum_{\substack{i\in\{q,\bar{q},Q,\bar{Q}\} \\ j\in\{q,\bar{q}\}}} H_{ij}^{(n_l+1)}(Q,\mu)\,H_s(m,\mu,\nu)H_c\Big(m,\mu,\frac{\nu}{\omega_b}\Big)\int \mathrm{d}t_a\,\mathrm{d}t_b
$$
$$
\times\left[\sum_{k\in\{q,\bar{q},g\}}\mathcal{I}_{ik}\Big(t_a,m,x_a,\mu,\frac{\nu}{\omega_a}\Big)\otimes_x f_k^{(n_l)}(x_a,\mu)\right]
$$
$$
\times\left[\sum_{k\in\{q,\bar{q},g\}}\mathcal{I}_{jk}^{(n_l)}(t_b,x_b,\mu)\otimes_x f_k^{(n_l)}(x_b,\mu)\right]
$$
$$
\times\,S^{(n_l)}\Big(\mathcal{T}-\frac{t_a}{\omega_a}-\frac{t_b}{\omega_b},\mu\Big)\left[1+\mathcal{O}\Big(\frac{\mathcal{T}\mathrm{e}^{|Y|}}{Q},\frac{m^2}{Q^2},\frac{Q\mathcal{T}\mathrm{e}^{-|Y|}}{m^2},\frac{\Lambda_{\mathrm{QCD}}^2\mathrm{e}^{|Y|}}{Q\mathcal{T}}\Big)\right]. \qquad (2.118)
$$

The logarithms of ratios of the involved scales can be resummed in RG evolution of the different functions starting from their respective natural scale to a common renormalization scale. Again it can be most conveniently carried out by only evolving the hard, beam and soft functions with n_l massless flavors below and with n_l+1 massless flavors above the mass scale. The rapidity logarithms can be resummed in rapidity evolution of the current matching functions H_c and H_s and the mass-dependent beam function matching coefficient.

In neutral current Drell-Yan, mass effects of the heavy flavor are relevant in the factorization theorem only for secondary radiation, as in Fig. 1.1b. In the beam function with $\mu_{B_a}\sim\sqrt{Q\mathcal{T}}\mathrm{e}^{Y/2}\sim m$, primary massive quark effects can in principle be relevant, leading to heavy quark matching coefficients of the form $\mathcal{I}_{Qg}^{(1)}$ at $\mathcal{O}(\alpha_s)$. But in the second beam function, at the scale $\mu_{B_b}\sim\sqrt{Q\mathcal{T}}\mathrm{e}^{-Y/2}\ll m$, effects of heavy flavor production are suppressed as $\mu_{B_b}^2/m^2$ and the heavy flavor is therefore already integrated out as an active degree of freedom above the beam scale μ_{B_b}. In this beam the mass effects of the heavy flavor are contributing at leading order in the power counting only via virtual effects in the current matching function H_c. Therefore there is no corresponding real heavy (anti-)quark as an active degree of freedom in that beam to enter the hard interaction, such that there are no primary massive quark effects as in Fig. 1.1a in the case of neutral current Drell-Yan in this hierarchy. In charged current Drell-Yan, however, primary m_c-effects start to contribute already at order $\mathcal{O}(\alpha_s)$, because the light strange quark can be generated non-perturbatively in the proton, which allows for primary massive quark effects also in this hierarchy, with the heavy flavor (in this case a charm quark) produced only in one of the beams. We emphasize again that in the case of charged current Drell-Yan our results currently only allow for NNLL resummation, as compared to NNLL$'$ resummation in the case of neutral current Drell-Yan, because of unknown $\mathcal{O}(\alpha_s^2)$ primary massive contributions.

Factorization theorem for $\sqrt{Q\mathcal{T}}\mathrm{e}^{-Y/2}\ll m\ll\sqrt{Q\mathcal{T}}\mathrm{e}^{Y/2}$

In this hierarchy the mass lies between the two beam scales, such that it is parametrically separated from both, $\mu_{B_b}\ll m\ll\mu_{B_a}$. In beam b, the beam scale is much smaller than the mass scale. Here, when the heavy flavor is integrated out at the mass scale, this still happens in the SCET current, leading to a collinear current matching function H_c. Since the heavy flavor is then already integrated out at the beam scale, the beam function is just the same as in the massless case with n_l massless flavors. In beam a the mass is much smaller than the beam scale. This means that when matching the beam function on the PDF in this beam, the heavy flavor can still be treated as massless, leading to a massless beam function matching coefficient with n_l+1 flavors. The heavy flavor is then integrated out at a lower scale, leading to a PDF matching coefficient $\mathcal{M}$ and csoft function $\mathcal{S}_c$. The factorization

theorem for this hierarchy reads

$$\frac{\mathrm{d}\sigma}{\mathrm{d}Q^2\,\mathrm{d}Y\,\mathrm{d}\mathcal{T}} = \sum_{\substack{i\in\{q,\bar{q},Q,\bar{Q}\}\\ j\in\{q,\bar{q}\}}} H_{ij}^{(n_l+1)}(Q,\mu)\,H_s(m,\mu,\nu)H_c\Big(m,\mu,\frac{\nu}{\omega_b}\Big)\int \mathrm{d}k_a\,\mathcal{S}_c(k_a,m,\mu,\nu)$$

$$\times \int \mathrm{d}t_a\left[\sum_{k\in\{q,\bar{q},Q,\bar{Q},g\}}\sum_{l\in\{q,\bar{q},g\}}\mathcal{I}_{ik}^{(n_l+1)}(t_a,x_a,\mu,)\otimes_x \mathcal{M}_{kl}(x_a,m,\mu)\otimes f_l^{(n_l)}(x_a,\mu)\right]$$

$$\times \int \mathrm{d}t_b\left[\sum_{k\in\{q,\bar{q},g\}}\mathcal{I}_{jk}^{(n_l)}(t_b,x_b,\mu)\otimes_x f_k^{(n_l)}(x_b,\mu)\right]$$

$$\times S^{(n_l)}\Big(\mathcal{T}-\frac{t_a}{\omega_a}-\frac{t_b}{\omega_b},\mu\Big)\left[1+\mathcal{O}\Big(\frac{\mathcal{T}\mathrm{e}^{|Y|}}{Q},\frac{m^2\mathrm{e}^{-|Y|}}{Q\mathcal{T}},\frac{Q\mathcal{T}\mathrm{e}^{-|Y|}}{m^2},\frac{\Lambda_{\mathrm{QCD}}^2\mathrm{e}^{|Y|}}{Q\mathcal{T}}\Big)\right].\quad (2.119)$$

The logarithms of ratios of the involved scales can be resummed in RG evolution of the different functions starting from their respective natural scale to a common renormalization scale. Again it can be most conveniently carried out by only evolving the hard, beam and soft functions with n_l massless flavors below and with n_l+1 massless flavors above the mass scale. The rapidity logarithms can be resummed in rapidity evolution of the current matching functions H_c and H_s and the csoft function $\mathcal{S}_c$.

Also in this hierarchy primary massive quark effects are included only for charged current Drell-Yan, because the heavy flavor is already integrated out as an active degree of freedom in one of the beam functions.

Factorization theorem for $m\sim\sqrt{Q\mathcal{T}}\mathrm{e}^{-Y/2}\ll\sqrt{Q\mathcal{T}}\mathrm{e}^{Y/2}$

In this hierarchy the mass is of order of the smaller beam scale (beam b) and therefore much smaller than the scale of beam a, i.e. $m\sim\mu_{B_b}\ll\mu_{B_a}$. In beam b, where the beam scale is of order of the mass scale, the heavy flavor is integrated out at the same scale where the beam function is matched on the PDF, giving a mass dependent beam function matching coefficient $\mathcal{I}_{jk}$. In beam a, the heavy flavor can still be treated massless when performing the matching on the PDF, giving a beam function matching coefficient with n_l+1 massless flavors. Integrating out the heavy flavor at a lower scale leads to a PDF matching coefficient $\mathcal{M}$ and a csoft function $\mathcal{S}_c$. The factorization theorem for this hierarchy reads

$$\frac{\mathrm{d}\sigma}{\mathrm{d}Q^2\,\mathrm{d}Y\,\mathrm{d}\mathcal{T}} = \sum_{i,j\in\{q,\bar{q},Q,\bar{Q}\}} H_{ij}^{(n_l+1)}(Q,\mu)\,H_s(m,\mu,\nu)\int \mathrm{d}k_a\,\mathcal{S}_c(k_a,m,\mu,\nu)$$

$$\times \int \mathrm{d}t_a\left[\sum_{k\in\{q,\bar{q},Q,\bar{Q},g\}}\sum_{l\in\{q,\bar{q},g\}}\mathcal{I}_{ik}^{(n_l+1)}(t_a,x_a,\mu)\otimes_x \mathcal{M}_{kl}(x_a,m,\mu)\otimes_x f_l^{(n_l)}(x_a,\mu)\right]$$

$$\times \int \mathrm{d}t_b\left[\sum_{k\in\{q,\bar{q},g\}}\mathcal{I}_{jk}\Big(t_b,m,x_b,\mu,\frac{\nu}{\omega_b}\Big)\otimes_x f_k^{(n_l)}(x_b,\mu)\right]$$

$$\times S^{(n_l)}\Big(\mathcal{T}-\frac{t_a}{\omega_a}-\frac{t_b}{\omega_b}-k_a-k_b,\mu\Big)\left[1+\mathcal{O}\Big(\frac{\mathcal{T}\mathrm{e}^{|Y|}}{Q},\frac{m^2\mathrm{e}^{-|Y|}}{Q\mathcal{T}},\frac{\mathcal{T}^2}{m^2},\frac{\Lambda_{\mathrm{QCD}}^2\mathrm{e}^{|Y|}}{Q\mathcal{T}},\frac{\Lambda_{\mathrm{QCD}}^2}{m^2}\Big)\right].$$
$$(2.120)$$

The logarithms of ratios of the involved scales can be resummed in RG evolution of the different functions starting from their respective natural scale to a common renormalization scale. Again it can be most conveniently carried out by only evolving the hard, beam and soft functions with n_l massless flavors below and with n_l+1 massless flavors above the mass scale. The rapidity logarithms

can be resummed in rapidity evolution of the current matching functions H_s, the mass-dependent beam function matching coefficient and the csoft function $\mathcal{S}_c$.

In this hierarchy primary heavy quarks can be produced at leading order in the power counting in both beams, so there are primary massive contributions also to neutral current Drell-Yan.

Factorization theorems for partonic beam thrust

So far we have always considered the definition of beam thrust in the hadronic center of mass frame as given in Eq. (2.72). It is the sum of the projections of the momenta of all hadronic final-state particles on one of the two light-like vectors n_a and n_b, depending on which hemisphere the particle is in. The hemispheres are defined as perpendicular to the beam axis in the lab frame (the hadronic center of mass frame), such that particles with rapidity $y > 0$ are assigned to hemisphere a and particles with rapidity $y < 0$ to hemisphere b. The above definition uses the momenta of the final-state particles and the hemispheres perpendicular to the beam axis in the hadronic center of mass frame. Therefore this observable is referred to as hadronic beam thrust $\mathcal{T}$.

A similar definition of beam thrust, that is in fact the original definition in Ref. [13], is in the partonic center of mass frame. Here partonic center of mass frame refers to the frame that is related to the hadronic center of mass frame by a boost along the beam axis such that the rapidity of the color singlet state becomes zero, i.e. it is not the exact partonic center of mass frame because the color singlet state could still have transverse momentum. Then all momenta of the hadronic final-state particles in the partonic center of mass frame are projected on the two light-like vectors n_a and n_b, with the two hemispheres being perpendicular to the beam axis in the partonic center of mass frame. That observable is called partonic beam thrust $\hat{\mathcal{T}}$

$$\hat{\mathcal{T}} = \sum_i \min\{n_a \cdot \hat{p}_i, n_b \cdot \hat{p}_i\} = \sum_i \mathrm{e}^{-|\hat{y}_i|}\sqrt{|\vec{p}_{\perp,i}|^2 + m_i^2}\,, \qquad (2.121)$$

where $\hat{p}_i$ and $\hat{y}_i$ are now the momenta of the hadronic final-state particles and their rapidities in the partonic center of mass frame. Boosting back to the hadronic center of mass frame, the definition of partonic beam thrust becomes

$$\hat{\mathcal{T}} = \sum_i \min\{\mathrm{e}^Y n_a \cdot p_i, \mathrm{e}^{-Y} n_b \cdot p_i\} = \sum_i \mathrm{e}^{-|y_i - Y|}\sqrt{|\vec{p}_{\perp,i}|^2 + m_i^2}\,, \qquad (2.122)$$

where Y is again the rapidity of the color-singlet state, that defines the boost between the partonic and the hadronic center of mass frames. This means that the momenta of particles in hemisphere a/b are weighted by an additional factor of $\mathrm{e}^{\pm Y}$, but also that the definition of the hemispheres in the lab frame is changed. Particles are now assigned to the hemispheres according to the condition $y > Y$ for hemisphere a and $y < Y$ or hemisphere b. This means that for $Y \neq 0$ the hemispheres are no longer symmetric with respect to the beam axis. Using the definition of partonic beam thrust provides an observable that is invariant under boost along the beam axis, and always ensures a symmetry between the two beam scales in the factorization theorem as we will see below.

To derive the massless factorization theorem for partonic beam thrust in the lab frame, we first start with its counter part for hadronic beam thrust in Eq. (2.75). It can be written in the form

$$\frac{\mathrm{d}\sigma}{\mathrm{d}Q^2\,\mathrm{d}Y\,\mathrm{d}\mathcal{T}} = \sum_{i,j\in\{q,\bar{q}\}} H_{ij}^{(n_f)}(Q,\mu) \int \mathrm{d}t_a\,\mathrm{d}t_b\,\mathrm{d}k_a^+\,\mathrm{d}k_b^-\, B_i^{(n_f)}(t_a,x_a,\mu)\,B_j^{(n_f)}(t_b,x_b,\mu)$$

$$\times\, S_{\mathrm{hemi}}^{(n_f)}(k_a^+,k_b^-,\mu\,|0)\,\delta\Big(\mathcal{T} - k_a^+ - k_b^- - \frac{t_a}{\omega_a} - \frac{t_b}{\omega_b}\Big)\Big[1 + \mathcal{O}\Big(\frac{\mathcal{T}}{Q\mathrm{e}^{-|Y|}}\Big)\Big]. \qquad (2.123)$$

Here $S_{\mathrm{hemi}}(k_a^+,k_b^-,\mu\,|\mathcal{Y})$ is the hemisphere soft function. It measures the light-cone components $k_a^+ = n_a \cdot k_a$ and $k_b^- = n_b \cdot k_b$ of momenta of the soft radiation in the hemispheres a and b, defined

such that particles with rapidity $y > \mathcal{Y}$ belong to hemisphere a and particles with rapidity $y < \mathcal{Y}$ to hemisphere b. The hemisphere soft function S_{hemi} is related to the thrust soft function S used before by

$$S(k,\mu) = \int \mathrm{d}k_a^+ \, \mathrm{d}k_b^- \, S_{\text{hemi}}(k_a^+, k_b^-, \mu \,|0) \, \delta(k - k_a^+ - k_b^-) \,. \tag{2.124}$$

To change the observable from $\mathcal{T}$ to $\hat{\mathcal{T}}$, one can now start from the factorization theorem in Eq. (2.123) and, according to the differences between partonic and hadronic beam thrust, change the definition of the hemispheres in the hemisphere soft function (the beam functions are independent of the hemisphere definition), and weight all momenta in hemisphere a by a factor e^Y and all momenta in hemisphere b by e^{-Y} in the measurement δ-function that relates the measured momenta to the beam thrust observable

$$
\begin{aligned}
\frac{\mathrm{d}\sigma}{\mathrm{d}Q^2\,\mathrm{d}Y\,\mathrm{d}\hat{\mathcal{T}}} &= \sum_{i,j\in\{q,\bar{q}\}} H_{ij}^{(n_f)}(Q,\mu) \int \mathrm{d}t_a\,\mathrm{d}t_b\,\mathrm{d}k_a^+\,\mathrm{d}k_b^-\, B_i^{(n_f)}(t_a,x_a,\mu)\, B_j^{(n_f)}(t_b,x_b,\mu) \\
&\quad \times S_{\text{hemi}}^{(n_f)}(k_a^+,k_b^-,\mu\,|Y)\,\delta\!\left(\hat{\mathcal{T}} - \mathrm{e}^Y k_a^+ - \mathrm{e}^{-Y} k_b^- - \frac{\mathrm{e}^Y t_a}{\omega_a} - \frac{\mathrm{e}^{-Y} t_b}{\omega_b}\right)\left[1 + \mathcal{O}\!\left(\frac{\hat{\mathcal{T}}}{Q}\right)\right] \\
&= \sum_{i,j\in\{q,\bar{q}\}} H_{ij}^{(n_f)}(Q,\mu) \int \mathrm{d}t_a\,\mathrm{d}t_b\,\mathrm{d}k_a^+\,\mathrm{d}k_b^-\, B_i^{(n_f)}(t_a,x_a,\mu)\, B_j^{(n_f)}(t_b,x_b,\mu) \\
&\quad \times S_{\text{hemi}}^{(n_f)}(\mathrm{e}^{-Y} k_a^+,\mathrm{e}^Y k_b^-,\mu\,|Y)\,\delta\!\left(\hat{\mathcal{T}} - k_a^+ - k_b^- - \frac{t_a}{Q} - \frac{t_b}{Q}\right)\left[1 + \mathcal{O}\!\left(\frac{\hat{\mathcal{T}}}{Q}\right)\right],
\end{aligned}
\tag{2.125}
$$

Using the property of the transformation of the hemisphere soft function under a boost along the beam axis

$$S_{\text{hemi}}(\mathrm{e}^{-Y} k_a^+, \mathrm{e}^Y k_b^-, \mu\,|Y) = S_{\text{hemi}}(k_a^+, k_b^-, \mu\,|0) \,, \tag{2.126}$$

and Eq. (2.124) to express everything again in terms of the thrust soft function, we arrive at

$$
\begin{aligned}
\frac{\mathrm{d}\sigma}{\mathrm{d}Q^2\,\mathrm{d}Y\,\mathrm{d}\hat{\mathcal{T}}} &= \sum_{i,j\in\{q,\bar{q}\}} H_{ij}^{(n_f)}(Q,\mu) \int \mathrm{d}t_a\,\mathrm{d}t_b\, B_i^{(n_f)}(t_a,x_a,\mu)\, B_j^{(n_f)}(t_b,x_b,\mu) \\
&\quad \times S^{(n_f)}\!\left(\hat{\mathcal{T}} - \frac{t_a}{Q} - \frac{t_b}{Q},\mu\right)\left[1 + \mathcal{O}\!\left(\frac{\hat{\mathcal{T}}}{Q}\right)\right].
\end{aligned}
\tag{2.127}
$$

This is the massless factorization theorem for partonic beam thrust also derived in Ref. [13]. It is very similar to the one for hadronic beam thrust, but with the difference that it is symmetric in the two beam directions, giving only one global beam scale $\mu_B = \sqrt{Q\hat{\mathcal{T}}}$, independent of the rapidity Y.

Exactly the same steps to derive the factorization theorems of partonic beam thrust from those of hadronic beam thrust also apply in the massive case, with the only complication arising in the hierarchy $\mathcal{T} \ll m \ll \sqrt{Q\mathcal{T}}$ in Eq. (2.97), which is the hierarchy where the csoft functions $\mathcal{S}_c$ appear as an additional structure in the factorization theorem. Like the beam functions also the csoft functions are independent of the definition of the hemispheres, but they are not invariant under a boost along the beam axis, but have the rescaling property

$$\mathrm{e}^{\mp Y}\,\mathcal{S}_c\!\left(\mathrm{e}^{\mp Y} k_{a,b}^\pm, m, \mu, \nu\right) = \mathcal{S}_c\!\left(k_{a,b}^\pm, m, \mu, \nu\mathrm{e}^{\mp Y}\right)\,. \tag{2.128}$$

Here the rescaling of the rapidity scale as $\nu \to \nu\mathrm{e}^{\mp Y}$ for the csoft function in the a/b direction only holds in case of using the symmetric Wilson line regulator η as rapidity regulator. For other choices of regulators this can in general be different. This rescaling of the rapidity scale ν by a factor $\mathrm{e}^{\pm Y}$ in

fact cancels between the two csoft functions for the two different hemispheres. This can be checked by solving the rapidity RGE of the csoft function in Eq. (2.100), to get the evolution equation

$$\mathcal{S}_c(k, m, \mu, \nu_1) = \exp\left[\gamma_{\nu, \mathcal{S}_c}(m, \mu) \ln\left(\frac{\nu_1}{\nu_0}\right)\right] \mathcal{S}_c(k, m, \mu, \nu_0). \tag{2.129}$$

In the special case of $\nu_0 = \nu$ and $\nu_1 = \nu e^{\pm Y}$ the evolution equation simply becomes

$$\mathcal{S}_c(k, m, \mu, \nu e^{\pm Y}) = \exp\left[\pm Y \gamma_{\nu, \mathcal{S}_c}(m, \mu)\right] \mathcal{S}_c(k, m, \mu, \nu), \tag{2.130}$$

and it is easy to see from Eq. (2.130) that this implies a cancellation of the Y-dependent terms in the case of two csoft functions in different hemispheres

$$\mathcal{S}_c(k_a, m, \mu, \nu e^{-Y}) \mathcal{S}_c(k_b, m, \mu, \nu e^{Y}) = \mathcal{S}_c(k_a, m, \mu, \nu) \mathcal{S}_c(k_b, m, \mu, \nu). \tag{2.131}$$

The same also holds for the virtuality-dependent beam functions with secondary massive quark corrections and the mass mode matching functions H_c, since they all follow the same rapidity evolution equation as the csoft function in Eq. (2.129), such that

$$B_i\left(t_a, m, x_a, \mu, \frac{\nu}{\omega_a}\right) B_j\left(t_b, m, x_b, \mu, \frac{\nu}{\omega_b}\right) = B_i\left(t_a, m, x_a, \mu, \frac{\nu}{Q}\right) B_j\left(t_b, m, x_b, \mu, \frac{\nu}{Q}\right), \tag{2.132}$$

$$H_c\left(m, \mu, \frac{\nu}{\omega_a}\right) H_c\left(m, \mu, \frac{\nu}{\omega_b}\right) = H_c\left(m, \mu, \frac{\nu}{Q}\right) H_c\left(m, \mu, \frac{\nu}{Q}\right). \tag{2.133}$$

With this we can give a simple "recipe" for translating all the factorization theorems for hadronic beam thrust $\mathcal{T}$ in Secs. 2.2.1 – 2.2.4 to partonic beam thrust $\hat{\mathcal{T}}$, by simply replacing $\omega_{a,b} \to Q$ everywhere in the factorization theorem. Note that this only applies for the factorization theorems for $\mathcal{T}$ assuming $\omega_a \sim \omega_b \sim Q$ as in Secs. 2.2.1 – 2.2.4, but not for the asymmetric factorization theorems presented in the beginning of this section in Eqs. (2.118) – (2.120), since the factorization theorems in $\hat{\mathcal{T}}$ are by construction always symmetric in the two beam scales. There are no corresponding factorization theorems in $\hat{\mathcal{T}}$ to the ones in Eqs. (2.118) – (2.120), because the situation of a different scaling of the mass with respect to the two beam scales is not possible for partonic beam thrust. With this recipe one can construct variable flavor number schemes for partonic beam thrust in Drell-Yan for any scaling of the mass of the heavy flavor with respect to the other scales, where the structure of the factorization theorems is unaffected by large rapidities of the lepton pair.

Chapter 3

Variable Flavor Number Scheme for DIS in the Endpoint Region

Deep inelastic scattering (DIS), the high energetic scattering of a lepton on a hadron, is a benchmark process for the extraction of PDFs. For this reason a precise understanding of quark mass effects is of importance in order to provide a theoretical framework suitable for PDF fits with better control over theoretical uncertainties.

In this chapter we will investigate effects of secondary massive quarks on the factorization and resummation properties in DIS in the kinematic endpoint $(1-x) \ll 1$. In this region the hadronic final state is collimated in one high energetic jet with additional soft radiation. This leads to a large separation of the kinematic scales, namely the partonic center of mass energy, that sets the hard scattering scale of the process, and the invariant mass of the final state jet, which makes the resummation of logarithms of ratios of these scales necessary. We will again use the framework of soft-collinear effective theory to factorize and resum the cross section in this region, which has been done for the process of DIS in the endpoint region in the massless case already several times [96–101].

The QCD current relevant for DIS is related to DY by crossing symmetry, by going from time-like to space-like momentum transfer of the virtual gauge boson and changing an incoming for an outgoing quark. Therefore many features of the factorization theorems are similar, especially those related to the hard function (that is just the square of the Wilson coefficient of the current matching from QCD to SCET) and the inclusion of mass effects in the evolution of the current. But since one incoming jet is now replaced by an outgoing jet, new features arise like the appearance of a jet function describing the dynamics of the final state jet instead of a beam function that covered the physics of the initial state radiation. Additionally the restriction of the phase space to the region $(1-x) \ll 1$ also has effects on the evolution of the PDFs and also leads to large rapidity logarithms $\sim \ln(1-x)$ in the PDF threshold matching coefficients when including heavy flavors that need to be resummed.

Including mass effects of heavy quarks introduces a new scale, that leads to additional logarithms of the ratio of the quark mass and the other scales of the process. To resum also these quark mass related logarithms, including also the additional rapidity logarithms that arise due to secondary massive quark effects, a VFNS scheme can be constructed that correctly includes the relevant number of active flavors in the RG evolution of the different structures in the factorization theorem. Different schemes have been developed to achieve this in the OPE region $(1-x) \sim \mathcal{O}(1)$, see e.g. Ref. [102] for an overview.

In this chapter we will set up a VFNS valid in the endpoint region $(1-x) \ll 1$ that is capable of resumming all secondary quark mass related logarithms and is valid for any hierarchy of the quark mass with respect to the kinematic scales, using the MMF approach discussed in the previous chapter for DY. The MMF approach for factorization and resummation of massive quark effects in DIS in the

endpoint was not discussed Ref. [1] and is done here for the first time in this thesis. In Refs. [2, 20] a VFNS for secondary massive quarks for DIS in the endpoint based on the UF approach introduced in Refs. [11, 12] was constructed. This framework allows for resummation logarithms including all massive power corrections, by using different renormalization schemes for the functions appearing in the factorization theorem below and above the mass scale, introducing so-called threshold corrections when switching between the renormalization schemes. Because of the universality of the threshold corrections and consistency relations between them, this allowed for the extraction of the $\mathcal{O}(\alpha_s^3)$ coefficient of a single rapidity logarithm for all threshold corrections in the factorization theorem from known results. But since a VFNS for secondary massive quarks for DIS in the endpoint based on the MMF approach, analogous to the massive factorization setup for Drell-Yan presented in chapter 2, has never been discussed in literature, we consider it worthwhile to first set up the VFNS based on the MMF approach for the various hierarchies of the mass with respect to the other scales in this chapter, and postpone the discussion of the universal factorization approach to chapter 4, where we will also analyze the relation of the two factorization approaches for massive quarks for the example of DIS in the endpoint region.

We will only deal with secondary massive quark effects for DIS in this chapter, because effects of primary massive quarks are suppressed for $x \to 1$ because all flavor mixing terms in the DGLAP evolution of the PDFs are suppressed in this limit. Many of the mass mode matching coefficients arising from integrating out the heavy flavor will be identical to those encountered in DY, demonstrating the universality of these functions. With the results presented in this thesis one can achieve a resummation of logarithms related to quark mass effects up NNLL$'$ in the logarithmic counting, i.e. NNLL resummation with NNLO order boundary conditions.

3.1 Factorization for massless quarks

Before discussing quark mass effects we briefly describe the kinematic setup and the factorization theorem for DIS in the endpoint region $1 - x \ll 1$ for massless quarks. Here we display the mode setup, highlight the relevant steps for its derivation specifically for the hierarchy $1 - x \gg \Lambda_{\text{QCD}}/Q$ and show that it can be readily combined with the commonly considered scaling $1 - x \sim \Lambda_{\text{QCD}}/Q$. This section of the thesis is partly taken from Sec. II of Ref. [2].

In the following we consider the scattering of an electron off a proton via photon exchange. We denote the proton momentum by P^μ, the momentum of the incoming (outgoing) electron by k^μ (k'^μ), the incoming momentum of the virtual photon by $q^\mu = k^\mu - k'^\mu$ with spacelike invariant mass $q^2 = -Q^2 < 0$ and the momentum of the outgoing hadronic final state X by P_X^μ. The Lorentz invariant Bjorken scaling variable x is defined by

$$x = -\frac{q^2}{2P \cdot q} = \frac{Q^2}{2P \cdot q} \tag{3.1}$$

with the kinematic constraint $0 \leq x \leq 1$. We will work in the Breit frame, where q^μ does not have an energy component and the initial state proton is $\bar{n}$-collinear. Neglecting the proton mass the relevant momenta in the Breit frame in terms of lightcone coordinates read

$$q^\mu = \frac{Q}{2} n^\mu - \frac{Q}{2} \bar{n}^\mu, \quad P^\mu = \frac{Q}{2x} \bar{n}^\mu,$$
$$P_X^\mu = \frac{Q}{2} n^\mu + \frac{Q(1-x)}{2x} \bar{n}^\mu. \tag{3.2}$$

In the endpoint region the hadronic final state is an n-collinear jet with an invariant mass $P_X^2 \approx Q^2(1-x) \ll Q^2$.

The differential cross section for DIS can be decomposed in terms of a leptonic and a hadronic tensor. The latter is defined by

$$W^{\mu\nu}(P,q) = \frac{1}{2\pi} \text{Im} \left[i \int \mathrm{d}^4 z \, e^{iqz} \langle P | T[J^{\mu\dagger}(z)J^\nu(0)] | P \rangle \right], \tag{3.3}$$

with $|P\rangle$ denoting the initial proton state and the current $J^\mu(z) = \sum_{q_i} e_{q_i}^2 \, \bar{q}_i \gamma^\mu q_i(z)$ summed over all quark flavors q_i with corresponding electric charges e_{q_i}. We will just deal with unpolarized DIS, so that a spin average is always implied. Using current conservation, which implies $q^\mu W_{\mu\nu} = 0$, one can decompose the hadronic tensor for the parity conserving vector current into the two structure functions $F_1(x,Q^2)$ and $F_2(x,Q^2)$,

$$\begin{aligned} W^{\mu\nu}(P,q) &= -\left(g_{\mu\nu} - \frac{q^\mu q^\nu}{q^2} \right) F_1(x,Q) + \frac{1}{P \cdot q} \left(P^\mu + \frac{q^\mu}{2x} \right) \left(P^\nu + \frac{q^\nu}{2x} \right) F_2(x,Q) \\ &= -g_\perp^{\mu\nu} F_1(x,Q) + \frac{1}{2x} \left(\frac{n^\mu}{2} + \frac{\bar{n}^\mu}{2} \right) \left(\frac{n^\nu}{2} + \frac{\bar{n}^\nu}{2} \right) F_L(x,Q). \end{aligned} \tag{3.4}$$

with $g_\perp^{\mu\nu} = g^{\mu\nu} - 1/2(n^\mu \bar{n}^\nu + \bar{n}^\mu n^\nu)$. Here the longitudinal structure function $F_L(x,Q)$ reads

$$F_L(x,Q) = F_2(x,Q) - 2xF_1(x,Q), \tag{3.5}$$

in terms of $F_1(x,Q)$ and $F_2(x,Q)$. These structure functions contain physics at different invariant mass scales and thus require to be factorized to resum the corresponding large logarithms.

In this section we briefly discuss the factorization theorem for inclusive DIS for massless quarks in the endpoint region $1 - x \ll 1$ in the framework of SCET. The factorization can be performed in a multi-step matching procedure and has been carried out already a number of times [96–101]. The only relevant scales in the process are the scale of the hard interaction Q, the invariant mass of the final state jet $Q\sqrt{1-x}$ and the non-perturbative scale Λ_{QCD}. In the massive case the mass m of the heavy flavor will give an additional scale in the process. Note that there is no physics related to the scale $Q(1-x)$, which means that the scaling of $Q(1-x)$ with respect to Λ_{QCD} or the mass of a heavy flavor has no relevance. This already implies that the factorization theorems are the same for all the possible hierarchies that these scales can have with respect to $Q(1-x)$, especially that they adopt the same form in the two cases $\Lambda_{\text{QCD}} \sim Q(1-x)$ and $\Lambda_{\text{QCD}} \ll Q(1-x)$, a statement that has already been made e.g. in Refs. [97, 103]. However, Ref. [97] uses a different mode setup including non-perturbative modes at a scale $\Lambda_{\text{QCD}}\sqrt{1-x} \ll \Lambda_{\text{QCD}}$, while Ref. [103] never explicitly displays the scaling of the modes, such that we think it is worthwhile to sketch the derivation of the factorization theorem using our mode setup with collinear-soft modes of virtuality Λ_{QCD} in the case where $\Lambda_{\text{QCD}} \ll Q(1-x)$.

The relevant modes are

$$\begin{aligned} n\text{-collinear:} \quad & p_n^\mu \sim \left(Q(1-x), Q, Q\sqrt{1-x} \right), \\ \bar{n}\text{-collinear:} \quad & p_{\bar{n}}^\mu \sim \left(Q, \Lambda_{\text{QCD}}^2/Q, \Lambda_{\text{QCD}} \right), \\ \bar{n}\text{-collinear-soft:} \quad & p_{\bar{c}s}^\mu \sim \left(Q(1-x), \Lambda_{\text{QCD}}^2/(Q(1-x)), \Lambda_{\text{QCD}} \right), \end{aligned} \tag{3.6}$$

where we have used the decomposition

$$p^\mu \sim (n \cdot p, \bar{n} \cdot p, p_\perp). \tag{3.7}$$

These modes are also displayed in Fig. 3.1. The non-perturbative $\bar{n}$-collinear modes describing the initial state proton in the Breit frame have always the same scaling $p_{\bar{n}}^\mu = (n \cdot p_{\bar{n}}, \bar{n} \cdot p_{\bar{n}}, p_{\bar{n}}^\perp) \sim (Q, \Lambda_{\text{QCD}}^2/Q, \Lambda_{\text{QCD}})$. The final state is strongly collimated for $x \to 1$ with a large momentum Q and an
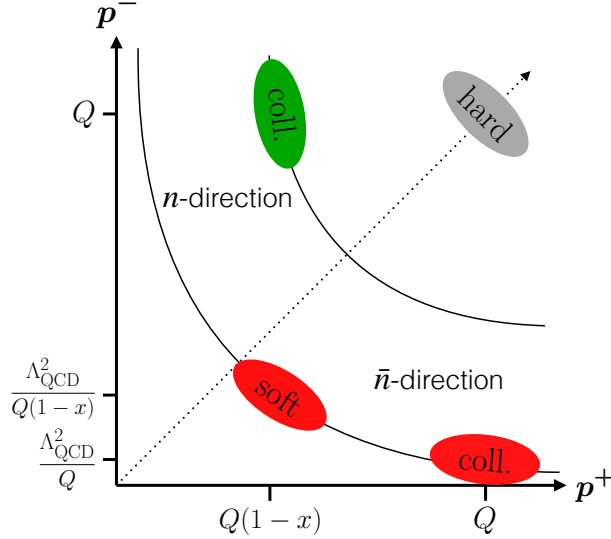
Figure 3.1: Relevant modes for inclusive DIS in the endpoint region $x \to 1$ with $1 - x \gg \Lambda_{\mathrm{QCD}}/Q$ in the $p^+ p^-$-plane, with $p^+ = n \cdot p$ and $p^- = \bar{n} \cdot p$.

invariant mass $Q\sqrt{1-x}$ and is thus described by n-collinear modes scaling as $p_n^\mu \sim Q(1-x, 1, \sqrt{1-x})$. The kinematics in the Breit frame prohibits the appearance of a final $\bar{n}$-collinear state, as can be seen from Eq. (3.2). This has the important consequence that the $\bar{n}$-collinear sector just enters the factorization theorem via a component which is local both in label space as well as in the residual coordinate, as has been also pointed out in Ref. [101]. The remaining relevant low-energy modes contribute to the measurement of x or equivalently to the squared invariant mass $\sim Q^2(1-x)$ via a component $n \cdot p \sim Q(1-x)$ (i.e. they have to lie on the vertical line below the n-coll. modes in Fig. 3.1). In fact all such modes give vanishing contributions in perturbation theory in the massless case, since no physical scale is associated with the other momentum components which results in scaleless integrals. This holds in particular also for ultrasoft modes scaling as $Q(1-x, 1-x, 1-x)$ as stated e.g. in Refs. [96, 97, 103]. Thus any additional relevant modes can only be nonperturbative and scale like $p_{cs}^\mu \sim (Q(1-x), \Lambda_{\mathrm{QCD}}^2/Q(1-x), \Lambda_{\mathrm{QCD}})$. These modes are also boosted in the Breit frame if $\Lambda_{\mathrm{QCD}} \ll Q(1-x)$, and therefore referred to as collinear-soft modes. The momenta of theses modes have a collinear scaling but with a softer virtuality than the n-coll. modes. Compared to the non-perturbative $\bar{n}$-coll. modes they have the same virtuality but are less boosted by a factor $(1-x)$. In the special case where $Q(1-x) \sim \Lambda_{\mathrm{QCD}}$ the csoft modes become soft modes with the momentum scaling $\Lambda_{\mathrm{QCD}}(1, 1, 1)$.

To derive the factorization theorem we employ a multistep matching procedure. First the QCD current is matched to the SCET current in the standard way at the scale Q^2. The Wilson coefficient of this matching is related to the one in DY encountered in the previous chapter because of crossing symmetry by analytic continuation $Q^2 \to -Q^2 - i0$. The square of the Wilson coefficient gives the hard function $\hat{H}$, describing the physics of the hard scattering process at the scale $\mu_H \sim Q$. The virtuality of the collinear and soft modes in SCET can then be lowered without any non-trivial matching to the scale $\mu_J \sim Q\sqrt{1-x}$. This is the scale at which the final state jet, with invariant mass $Q\sqrt{1-x}$, is started to be resolved and the corresponding n-collinear modes need to be integrated out. The vacuum correlator of the collinear SCET fields is

$$\mathcal{J}(Q r_n^+, \mu) \equiv \frac{-1}{2\pi N_c Q} \operatorname{Im} \left[i \int d^4 z \, e^{i r_n \cdot z} \langle 0| \mathrm{T} \left\{ \bar{\chi}_{n,Q}(0) \frac{\slashed{\bar{n}}}{2} \chi_n(z) \right\} |0\rangle \right], \tag{3.8}$$

with momenta of the collinear SCET fields χ_n exhibiting the scaling

$$n\text{-coll.:}\qquad p_n^\mu \sim Q\Big(1-x, 1, \sqrt{1-x}\Big). \tag{3.9}$$

All color and spin indices are traced implicitly. This is matched onto a theory where the collinear modes with virtuality $Q(1-x)$ in the n-direction are integrated out and only n-collinear-soft modes are remaining

$$\mathcal{J}^{(n_f)}(s,\mu) = \int \mathrm{d}\ell\, J^{(n_f)}(s-Q\ell,\mu)\mathscr{S}_c^{(n_f)}(\ell,\mu). \tag{3.10}$$

The superscript n_f indicates the number of flavors. Here J is the matching coefficient, the jet function as it will appear in the factorization theorem, and $\mathscr{S}_c$ are the matrix elements of collinear-soft (csoft) Wilson lines

$$\mathscr{S}_c(\ell,\mu) = \frac{1}{N_c}\,\mathrm{tr}\,\Big\langle 0\Big|\overline{\mathrm{T}}\big[X_n^\dagger(0)V_n(0)\big]\delta(\ell - n\cdot\hat{p})\mathrm{T}\big[V_n^\dagger(0)X_n(0)\big]\Big|0\Big\rangle, \tag{3.11}$$

where the collinear-soft Wilson lines are

$$X_n = \sum_{\text{perms}} \exp\left[-\frac{g}{n\cdot\mathcal{P}}\frac{\nu^{\eta/2}}{(\bar{n}\cdot\mathcal{P})^{\eta/2}}\,n\cdot A_{cs}\right], \quad V_n = \sum_{\text{perms}} \exp\left[-\frac{g}{\bar{n}\cdot\mathcal{P}}\frac{\nu^{\eta/2}}{(\bar{n}\cdot\mathcal{P})^{\eta/2}}\,\bar{n}\cdot A_{cs}\right], \tag{3.12}$$

and $\mathcal{P}$ is the momentum operator. Here the η-regulator [40, 41] has been expanded using the n-collinear-soft scaling $\bar{n}\cdot\mathcal{P} \gg n\cdot\mathcal{P}$. These are the same collinear-soft matrix elements and Wilson lines already discussed for the case of beam thrust in DY[1] in Sec. 2.2, written down here another time for the convenience of the reader.

The matching coefficient $J(s,\mu)$ is the jet function that appears in the final factorization theorem. It is infrared finite since all IR divergences cancel between the hard collinear and the collinear-soft matrix elements on both sides of the matching equation, and it describes the dynamics of the outgoing jet with invariant mass $\mu_J \sim Q\sqrt{1-x}$. The collinear-soft matrix elements only give scaleless contributions in the massless case, i.e. their only effect is to cancel the corresponding IR divergences in the collinear matrix element, but give rise to non-trivial contributions once effects of secondary massive quarks are included. This definition of the jet function as a matching coefficient gives equivalent results as defining the jet function only as the hard collinear vacuum correlator in Eq. (3.8), but defined with the necessary zero-bin subtraction to avoid double counting with the soft region, see also the discussion after Eq. (2.76).

The modes of lower virtuality than the jet scale, that remain after integrating out the n-collinear modes, encode fluctuations that contribute to the measurement of the invariant mass of the final state $\sim Q\sqrt{1-x}$ but arise from lower virtualities than the collinear scale. Thus the scaling of their momenta is

$$n\text{-csoft:}\qquad p_{\mathrm{cs}}^\mu \sim \Big(Q(1-x), \frac{k^2}{Q(1-x)}, \sqrt{k^2}\Big), \tag{3.13}$$

where k^2 is some virtuality below the jet scale, i.e. $k^2 \ll Q^2(1-x)$. In the discussion about the n-collinear-soft matrix element above we implicitly assumed $k^2 \gg \big(Q(1-x)\big)^2$, which led to these modes being boosted in the n-direction, such that they were still separated from the soft modes. But this restriction has no physical relevance, since the scale $\mu \sim Q(1-x)$ is not a physical scale of the process. Because there is no other perturbative scale associated with the process below the jet scale $\mu \sim Q\sqrt{1-x}$, the virtuality of the n-collinear-soft, soft and $\bar{n}$-collinear modes that are left

---

[1]Changing one incoming to an outgoing Wilson line when going from Drell-Yan to DIS does not change the csoft matrix elements at two-loops, which is the order we are working here. See also Ref. [82] where this was discussed for hemisphere soft functions.

after integrating out the n-collinear modes as in Eq. (3.10) at the scale $\mu \sim Q\sqrt{1-x}$, can be lowered further without non-trivial matching. At the scale $\mu \sim Q(1-x)$ the collinear-soft and the soft modes are not separated any more by rapidity and become identical. This results in the n-csoft Wilson lines X_n, V_n of csoft gluon fields A_{cs} in Eq. (3.12) being replaced by Wilson lines $S_n, S_{\bar{n}}$ of soft gluon fields A_s

$$S_n = \sum_{\text{perms}} \exp\left[-\frac{g}{n \cdot \mathcal{P}} \frac{\nu^{\eta/2}}{|2\mathcal{P}_3|^{\eta/2}} \, n \cdot A_s \right], \tag{3.14}$$

where and $\mathcal{P}_3$ is the third component of the momentum operator. Because the soft modes have the scaling $n \cdot \mathcal{P} \sim \bar{n} \cdot \mathcal{P}$, this cannot be expanded as in the case of the n-collinear modes, where we used that $\bar{n} \cdot \mathcal{P} \gg n \cdot \mathcal{P}$. If $Q(1-x) \sim \Lambda_{\text{QCD}}$ this already corresponds to the lowest scale in the process. In that case the non-perturbative matrix element of the soft and $\bar{n}$-coll. fields with the proton initial state is the PDF in endpoint region $x \to 1$

$$\phi_q(\ell, \mu) = \langle P | \bar{\chi}_{\bar{n}} S_{\bar{n}}^\dagger S_n \frac{\slashed{n}}{2} \delta(\ell - n \cdot \mathcal{P}) S_n^\dagger S_{\bar{n}} \chi_{\bar{n},Q} | P \rangle \,. \tag{3.15}$$

The PDF in the endpoint can also be factorized as

$$\phi_q(1-z, \mu) = Q \int \mathrm{d}\ell \, g_q(Q(1-z) - \ell, \mu) \, \mathscr{S}(\ell, \mu) \,, \tag{3.16}$$

where $g_q(\ell, \mu)$ denotes a local collinear matrix element

$$g_q(\ell, \mu) = \langle P | \bar{\chi}_{\bar{n}}(0) \frac{\slashed{n}}{2} \chi_{\bar{n},Q}(0) | P \rangle \, \delta(\ell) \,, \tag{3.17}$$

and $\mathscr{S}$ is a matrix element of soft Wilson lines

$$\mathscr{S}(\ell, \mu) = \frac{1}{N_c} \operatorname{tr} \left\langle 0 \left| \overline{\mathrm{T}} \big[S_n^\dagger(0) S_{\bar{n}}(0) \big] \delta(\ell - n \cdot \hat{p}) \mathrm{T} \big[S_{\bar{n}}^\dagger(0) S_n(0) \big] \right| 0 \right\rangle \,. \tag{3.18}$$

In the case where $\Lambda_{\text{QCD}} \ll Q(1-x)$ the virtuality of the soft and $\bar{n}$-coll. modes can be lowered further below the scale $Q(1-x)$. As doing so, the soft modes become boosted in the $\bar{n}$-direction, because their $n \cdot p$ light-cone component is fixed to $\sim Q(1-x)$ in order to give leading contributions to the measurement[2]. In this way they become the $\bar{n}$-collinear-soft modes described in the beginning of this section. This means that the soft Wilson lines get replaced by Wilson lines $\bar{X}_n, \bar{V}_n$ of $\bar{n}$-csoft gluon fields $A_{\bar{c}s}$

$$\bar{X}_n = \sum_{\text{perms}} \exp\left[-\frac{g}{n \cdot \mathcal{P}} \frac{\nu^{\eta/2}}{(n \cdot \mathcal{P})^{\eta/2}} \, n \cdot A_{\bar{c}s} \right], \quad \bar{V}_n = \sum_{\text{perms}} \exp\left[-\frac{g}{\bar{n} \cdot \mathcal{P}} \frac{\nu^{\eta/2}}{(n \cdot \mathcal{P})^{\eta/2}} \, \bar{n} \cdot A_{\bar{c}s} \right]. \tag{3.19}$$

Here the η-regulator has been expanded using the $\bar{n}$-collinear-soft scaling $n \cdot \mathcal{P} \gg \bar{n} \cdot \mathcal{P}$. The only other scale in the process that sets the virtuality of the $\bar{n}$-collinear-soft and the $\bar{n}$-coll. modes is the non-perturbative scale Λ_{QCD}. In this way we arrive at the mode setup shown in Fig. 3.1. The only change compared to the case where $Q(1-x) \sim \Lambda_{\text{QCD}}$ is that the soft matrix element $\mathscr{S}$ in Eq. (3.16) gets replaced by the matrix element $\mathscr{S}_{\bar{c}}$ of Wilson lines of $\bar{n}$-csoft gluon fields

$$\mathscr{S}_{\bar{c}}(\ell, \mu) = \frac{1}{N_c} \operatorname{tr} \left\langle 0 \left| \overline{\mathrm{T}} \big[\bar{X}_n^\dagger(0) \bar{V}_n(0) \big] \delta(\ell - n \cdot \hat{p}) \mathrm{T} \big[\bar{V}_n^\dagger(0) \bar{X}_n(0) \big] \right| 0 \right\rangle \,, \tag{3.20}$$

with the Wilson lines as in Eq. (3.19). Note that also in the case of measuring beam thrust in DY in Sec. 2.2 we had two collinear-soft matrix elements, one for collinear-soft modes boosted in the n_a

---

[2]We do not consider ultrasoft modes modes of virtuality $< \Lambda_{\text{QCD}}$ since they do not contribute to the measurement as stated before.

and one for collinear-soft modes boosted in the n_b direction. But in each of them the measurement function $\delta(\ell - n_{a,b} \cdot \hat{p})$ was measuring the smaller light-cone component, such that they gave identical results when using the symmetric η-regulator, which is the reason why we denoted both as $\mathscr{S}_c$, not distinguishing from which collinear-soft sector they were arising. In other words the two collinear-soft matrix elements were simply related by renaming $n_a \leftrightarrow n_b$, which does not change any result. The n-collinear-soft modes contributing to the matrix element in Eq. (3.11) are boosted in the n-direction and the measurement function $\delta(\ell - n \cdot \hat{p})$ measures their smaller light-cone component $n \cdot p$, which means these matrix elements $\mathscr{S}_c$ are indeed the same as in the case of beam thrust in DY. But the $\bar{n}$-collinear-soft modes in Eq. (3.20) are boosted in the $\bar{n}$-direction (the direction of the incoming proton), while still the, now larger, light-component $n \cdot \hat{p}$ is measured. This matrix element of collinear-soft fields is therefore in principle different from the one encountered above, and therefore denoted as $\mathscr{S}_{\bar{c}}$. So while we had two collinear-soft matrix elements from modes being boosted in different directions in the case of beam thrust in DY that gave identical results and therefore both denoted as $\mathscr{S}_c$, we distinguish the n-collinear-soft and $\bar{n}$-collinear-soft matrix elements for DIS, denoting them as $\mathscr{S}_c$ and $\mathscr{S}_{\bar{c}}$, respectively, depending on whether the smaller or larger light-cone component is measured. But in fact the difference between them arises only by the special choice of the rapidity regulator η, as discussed below.

The different soft, n-collinear-soft and $\bar{n}$-collinear-soft Wilson lines in Eqs. (3.14), (3.12) and (3.19) have the same structure apart of the different expansion of the rapidity regulator. In the massless case, where all the soft, n-csoft and $\bar{n}$-csoft matrix elements give in fact only scaleless contributions in pure dimensional regularization, the rapidity regulator does not matter and can as well be set to zero. Without this additional rapidity regulator that breaks the boost invariance, all these matrix elements, that are related only by a simple boost of the gluon fields $A_{cs} \to A_s \to A_{\bar{c}s}$, are in fact equivalent. This is the reason why the factorization theorem takes the same form in the two cases $\Lambda_{\mathrm{QCD}} \sim Q(1-x)$ and $\Lambda_{\mathrm{QCD}} \ll Q(1-x)$, because the simple replacement of the soft gluon fields by $\bar{n}$-collinear-soft gluons fields does not change the structure of the massless (c)soft matrix elements.

The full massless factorization theorem reads (to all orders in α_s and at leading order in $1-x$)

$$F_1(x, Q) = \frac{1}{2x} F_2(x, Q) = \frac{1}{2} \sum_{i=q,\bar{q}} \hat{H}_i^{(n_f)}(Q, \mu) \int \mathrm{d}s \, J^{(n_f)}(s, \mu) \, \phi_i^{(n_f)}\left(1 - x - \frac{s}{Q^2}, \mu\right), \qquad (3.21)$$

where the superscript (n_f) indicates the number of active quark flavors relevant for the RG evolution of all renormalized structures including in particular also the strong coupling constant. Note that the hadronic tensor becomes transverse in the limit $x \to 1$, such that $F_L(x, Q) = 0$ and the Callan-Gross relation $F_2(x, Q) = 2xF_1(x, Q)$ is satisfied to all orders in α_s. The massless fixed-order hard and jet functions, $\hat{H}^{(n_f)}(Q, \mu_H)$ and $J^{(n_f)}(s, \mu_J)$, are known up to $\mathcal{O}(\alpha_s^2)$ and $\mathcal{O}(\alpha_s^3)$, respectively, the anomalous dimensions up to $\mathcal{O}(\alpha_s^3)$. Results can be found e.g. in Ref. [97], the contributions at $\mathcal{O}(\alpha_s)$ and $\mathcal{O}(\alpha_s^2 C_F T_F)$ are given in Eqs (B.2) and (B.19).

The factorization theorem of Eq. (3.21) is written with all its components at the common renormalization scale μ, which can be chosen independently from the respective characteristic scales $\mu_H \sim Q$ for the hard function, $\mu_J \sim Q\sqrt{1-x}$ for the jet function and $\mu_\phi \sim \Lambda_{\mathrm{QCD}}$ for the PDF. Since the choice of μ necessarily differs widely from at least two of the characteristic scales, it is mandatory to sum large logarithmic terms. The corresponding RG equations are

$$\mu \frac{\mathrm{d}}{\mathrm{d}\mu} \hat{H}_i^{(n_f)}(Q, \mu) = \gamma_H^{(n_f)}(Q, \mu) \, \hat{H}_i^{(n_f)}(Q, \mu),$$

$$\mu \frac{\mathrm{d}}{\mathrm{d}\mu} J^{(n_f)}(s, \mu) = \int \mathrm{d}s' \, \gamma_J^{(n_f)}(s - s', \mu) \, J^{(n_f)}(s', \mu),$$

$$\mu \frac{\mathrm{d}}{\mathrm{d}\mu} \phi_i^{(n_f)}(1 - z, \mu) = \int \mathrm{d}z' \, \gamma_\phi^{(n_f)}(1 - z - z', \mu) \, \phi_i^{(n_f)}(z', \mu). \qquad (3.22)$$

The anomalous dimensions γ at $\mathcal{O}(\alpha_s)$ and $\mathcal{O}(\alpha_s^2 C_F T_F)$ are given in Eqs. (B.3), (B.20) and (B.12).

Note that the convolutional structure of the RG equation for the PDF in the limit $x \to 1$ (denoted as $\phi_i(1 - x, \mu)$) in the third line of Eq. (3.22) is different from the DGLAP equation for the full PDF (denoted as $f_i(x, \mu)$) in Eq. (2.17). To see how the standard DGLAP evolution for the PDF $f_i(x, \mu)$ in Eq. (2.17), involving a Mellin-type convolution as in the first line of Eq. (3.23) below, can be expanded in the endpoint region $x \to 1$ to become the evolution equation shown in the third line of Eq. (3.22), valid for the PDF in the endpoint, we first write out the RG evolution equation for the full PDF

$$
\begin{aligned}
\mu \frac{\mathrm{d} f_i(x, \mu)}{\mathrm{d}\mu} &= \sum_j \int_x^1 \frac{\mathrm{d}z}{z} \, \gamma_{f,ij}\Big(\frac{x}{z}, \mu\Big) f_j(z, \mu) \\
&= \sum_j \int_0^{1-x} \frac{\mathrm{d}z}{1-z} \, \gamma_{f,ij}\Big(\frac{1 - (1-x)}{1-z}, \mu\Big) f_j(1 - z, \mu) \\
&= \sum_j \int_0^{1-x} \mathrm{d}z \, \gamma_{f,ij}(x + z, \mu) f_j(1 - z, \mu) \times \Big[1 + \mathcal{O}(1 - x)\Big],
\end{aligned}
\tag{3.23}
$$

where in the last line we expanded simultaneously in $(1 - x) \sim z \ll 1$. Defining the PDF and its anomalous dimension in the endpoint as an expansion in $x \to 1$ of the full PDF and anomalous dimension, keeping only the leading order terms

$$
\begin{aligned}
\phi_i(1 - x, \mu) &= f_i(x, \mu) \times \Big[1 + \mathcal{O}(1 - x)\Big], \\
\gamma_{\phi,ij}(1 - x, \mu) &= \gamma_{f,ij}(x, \mu) \times \Big[1 + \mathcal{O}(1 - x)\Big],
\end{aligned}
\tag{3.24}
$$

this can be written as

$$
\mu \frac{\mathrm{d}\phi_i(1 - x, \mu)}{\mathrm{d}\mu} = \sum_j \int_0^{1-x} \mathrm{d}z \, \gamma_{\phi,ij}(1 - x - z, \mu) \phi_j(z, \mu).
\tag{3.25}
$$

We can further use the fact that all off-diagonal anomalous dimensions, i.e. $\gamma_{\phi,qg}$ and $\gamma_{\phi,gq}$, are suppressed by $\mathcal{O}(1 - x)$ with respect to the diagonal terms $\gamma_{\phi,qq}$ and $\gamma_{\phi,gg}$, such that to leading order in $1 - x$ no flavor mixing takes place in the evolution of the PDFs. Due to Furry's theorem gluon initiated processes do not contribute to the hard function for the electromagnetic vector current, and are therefore not included. This means we only need the quark PDFs in the endpoint, and by replacing $\gamma_{\phi,ij} = \delta_{ij}\gamma_\phi$, where γ_ϕ is an abbreviation for the quark-quark anomalous dimension $\gamma_{\phi,qq}$, this reduces to the evolution equation for the quark PDFs in the endpoint without flavor mixing shown in Eq. (3.22).

3.2   Variable flavor number scheme for secondary massive quarks

In the following sections we will set up a variable flavor number scheme for secondary massive quark effects in DIS in the endpoint region, using the mass mode factorization approach. Since the massless factorization theorem has a SCET_I type structure where the soft and the collinear scale are different, this will involve similar structures as in the case of beam thrust in DY. The only new structure compared to DY is the jet function, that replaces the beam functions in the collinear sector. We will always assume $m \gg \Lambda_{\text{QCD}}$ such that the mass can always be treated as a perturbative scale. This discussion of secondary massive quark effects for DIS in the endpoint region following the MMF approach as presented in this section of the thesis is new and has not been published before, because Ref. [1] was only studying the DY process and Ref. [2] was using the UF approach for DIS.
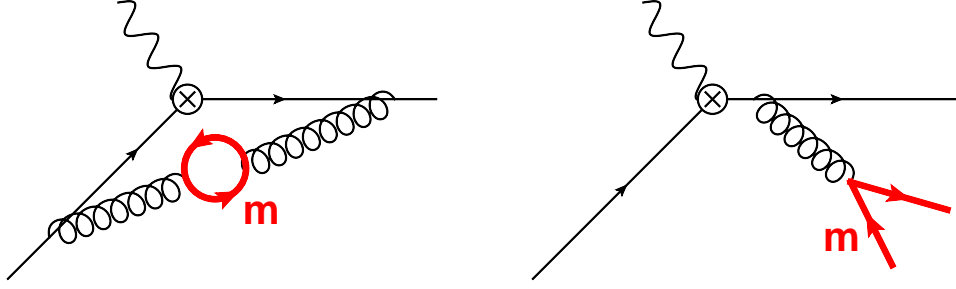
Figure 3.2: Exemplary diagrams for secondary massive quark contributions in DIS at $\mathcal{O}(\alpha_s^2 C_F T_F)$.

An important feature of the factorization theorem in Eq. (3.21) is that there are no flavor mixing terms between quarks and gluons in any of the EFT contributions in the hard current matching, the jet function, the PDF and their evolution factors, due to the power suppression of off-diagonal terms in the PDF evolution in the limit $(1-x) \ll 1$. This means that at leading order in $(1-x)$ the parton extracted out of the PDF at the low scale $\sim \Lambda_{\text{QCD}}$ is also the one interacting with the hard photon and entering the final state jet. Since we assume $m \gg \Lambda_{\text{QCD}}$, so that the heavy quarks are not produced nonperturbatively out of the proton, this has the consequence that massive quarks enter the EFT components of the factorization theorem only via secondary corrections, i.e. via contributions which are initiated by massless quarks and where massive quarks are produced through the radiation of virtual gluons that split into a massive quark-antiquark pair, see Fig. 3.2. In the case were $Q\sqrt{1-x} \ll m$, i.e. when the heavy quark cannot be produced via real emission, the changes in the factorization theorem are identical to the case of Drell-Yan in that hierarchy.

For $m \sim Q$ the mass effects are completely encoded in the massive hard function $\hat{H}$ as in Sec. 2.1.2, and the massless jet function and PDFs with n_l flavors are used

$$F_1(x,m,Q) = \frac{1}{2} \sum_{i=q,\bar{q}} \hat{H}_i(Q,m,\mu) \int \mathrm{d}s\, J^{(n_l)}(s,\mu)\, \phi_i^{(n_l)}\left(1-x-\frac{s}{Q^2},\mu\right) \left[1 + \mathcal{O}\left(1-x, \frac{Q^2(1-x)}{m^2}\right)\right].$$

(3.26)

Note that the mass corrections to the hard function $\hat{H}$ for DIS differ from the ones to the hard function H for DY because of the analytic continuation $Q^2 \to -Q^2 - i0$ in the current. The results for DIS are given in Eq. (C.6).

The case $Q\sqrt{1-x} \ll m \ll Q$ is described by using the massless $n_l + 1$ flavor hard function, the massless n_l flavor jet function and PDFs and additionally the mass mode current matching functions H_c and H_s as in Sec. 2.1.3.

$$F_1(x,m,Q) = \frac{1}{2} \sum_{i=q,\bar{q}} \hat{H}_i^{(n_l+1)}(Q,\mu)\, H_c\left(m,\mu,\frac{\nu}{Q}\right) H_c\left(m,\mu,\frac{\nu}{Q}\right) H_s(m,\mu,\nu)$$

$$\times \int \mathrm{d}s\, J^{(n_l)}(s,\mu)\, \phi_i^{(n_l)}\left(1-x-\frac{s}{Q^2},\mu\right) \left[1 + \mathcal{O}\left(1-x, \frac{m^2}{Q^2}, \frac{Q^2(1-x)}{m^2}\right)\right].$$

(3.27)

As already mentioned when discussing massive quark effects in DY in chapter 2, the two collinear mass mode matching functions H_c in the n and $\bar{n}$ sector are identical only when using a symmetric Wilson-line rapidity regulator as we always do here, but can in general be different from each other when using other rapidity regulators. The results for our choice of the symmetric η-regulator at $\mathcal{O}(\alpha_s^2)$ are given in Sec. C.1.3.

(a) $m \sim Q\sqrt{1-x}$

(b) $Q(1-x) \ll m \ll Q\sqrt{1-x}$

(c) $m \sim Q(1-x)$
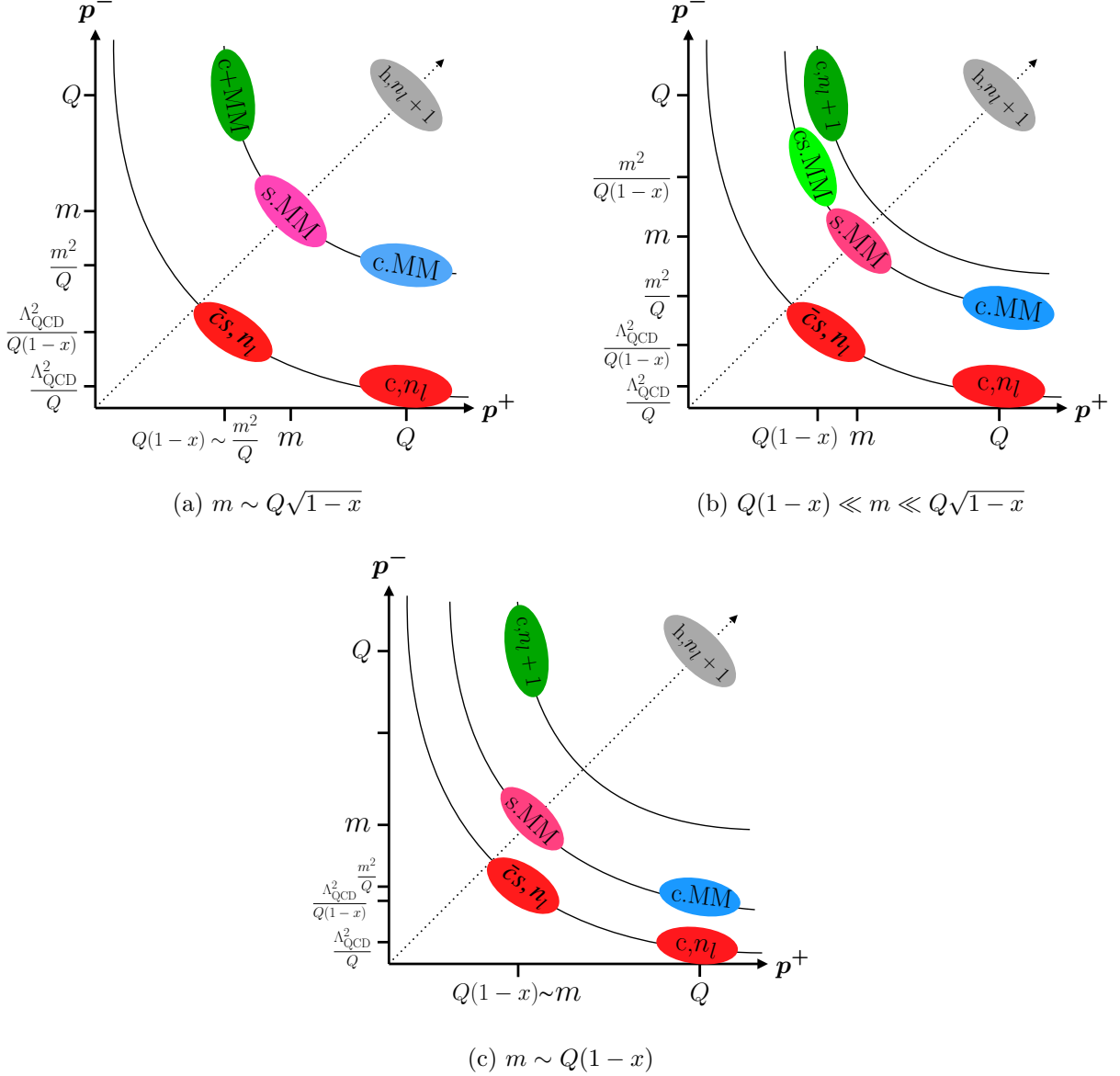
Figure 3.3: Effective theory modes with massive quarks for $\Lambda_{\text{QCD}} \ll m \lesssim Q\sqrt{1-x} \ll Q$.

3.2.1 Quark mass effects for $Q\sqrt{1-x} \sim m \ll Q$

If the quark mass is of the order of the jet scale, i.e. $Q\sqrt{1-x} \sim m$, the heavy flavor becomes a dynamical degree of freedom in the theory. Since the mass modes as well as the other modes in SCET have a scaling parametrically much smaller than the hard scale $\mu \sim Q$, the matching from QCD to SCET at the hard scale happens for all the modes simultaneously and leads to the massless hard function $n_l + 1$ flavors. In the soft and $\bar{n}$-collinear (i.e. collinear to the incoming proton) sector the mass modes are widely separated from the other (non-perturbative) modes in these sectors because we always assume $\Lambda_{\text{QCD}} \ll Q\sqrt{1-x}$. This means that integrating out the soft and $\bar{n}$-collinear mass modes at the mass scale leads to the same matching coefficients H_s and H_c as in the hierarchy $Q\sqrt{1-x} \ll m$, given in Eqs. (C.8) and (C.10), respectively.

The n-collinear mass modes now have the same virtuality as the other n-collinear modes in SCET, as illustrated in Fig 3.3a. Integrating out all these collinear fluctuations leads to a matching of a theory

with $n_l + 1$ hard collinear modes onto a theory with n_l collinear-soft modes only.

$$\mathcal{J}^{(n_l+1)}\Big(s,m,\mu,\frac{\nu}{Q}\Big) = \int d\ell\, J\Big(s - Q\ell, m, \mu, \frac{\nu}{Q}\Big)\mathscr{S}_c^{(n_l)}(\ell, \mu)\,. \tag{3.28}$$

Here $\mathcal{J}^{(n_l+1)}$ are the collinear matrix elements of light quark fields as in Eq. (3.8), with corrections from the heavy flavor via real and virtual secondary massive quark effects, and $\mathscr{S}_c^{(n_l)}$ the collinear-soft matrix elements as in Eq. (3.11) with n_l massless flavors. The matching coefficient J is the now explicitly mass-dependent jet function (called mass mode jet function, to distinguish from the mass dependent jet function as it will appear in the UF approach in chapter 4). The contributions from secondary massive quarks at $\mathcal{O}(\alpha_s^2 C_F T_F)$ are given in Eq. (C.27). We remind the reader that due to the suppression of flavor mixing in the DGLAP evolution of the PDFs in the endpoint region $x \to 1$ we do not need to consider primary massive quarks (for the primary massive quark jet function see Ref. [19]). Note that in Eq. (3.28) the subtraction of collinear-soft modes is performed with only n_l massless flavors, while the full collinear matrix element $\mathcal{J}$ is calculated with $n_l + 1$ flavors. This still leads to an IR finite matching coefficient because the contributions of a massive quark to $\mathcal{J}$ do not introduce additional IR divergences as long as the mass is kept finite. Since the massive flavor is integrated out at this scale it is absent in the lower energy effective theory and does therefore not contribute to the subtractions. In principle it would also be possible not to fully integrate out the heavy flavor and include it also in the subtractions, which corresponds to the definition of the jet function in the universal factorization scheme [71]. This approach and its relation to the mass mode factorization scheme presented in this chapter, where the heavy flavor is always completely integrated out at its respective mass scale, will be discussed in chapter 4.

The mass mode jet function's anomalous dimension for evolution in the energy scale μ is the same as for the virtuality-dependent beam function in Sec. 2.2.2

$$\mu \frac{d}{d\mu} J\Big(s,m,\mu,\frac{\nu}{Q}\Big) = \int ds'\, \gamma_{J,m}\Big(s - s', m, \mu, \frac{\nu}{Q}\Big) J\Big(s', m, \mu, \frac{\nu}{Q}\Big)\,, \tag{3.29}$$

with the contributions of the massive flavor at $\mathcal{O}(\alpha_s^2 C_F T_F)$ given in Eq. (C.29). We emphasize once again that these contributions are not the same as for an additional massless flavor.

The dependence of the mass mode jet function on the rapidity scale ν is the same as for the collinear mass-mode matching function H_c and the virtuality-dependent beam function

$$\nu \frac{d}{d\nu} J\Big(s,m,\mu,\frac{\nu}{Q}\Big) = \gamma_{\nu,H_c}(m,\mu) J\Big(s,m,\mu,\frac{\nu}{Q}\Big)\,, \tag{3.30}$$

with the rapidity anomalous dimension given in Eq. (C.11).

In the soft and the $\bar{n}$-collinear sector no measurement takes place at this scale, such that the soft and $\bar{n}$-collinear mass modes are integrated out in the current which leads to the same mass mode matching functions H_s and H_c as before. The full factorization theorem for this hierarchy reads

$$F_1(x,m,Q) = \frac{1}{2} \sum_{i \in \{q,\bar{q}\}} \hat{H}_i^{(n_l+1)}(Q,\mu) H_c\Big(m,\mu,\frac{\nu}{Q}\Big) H_s(m,\mu,\nu) \int ds\, J\Big(s,m,\mu,\frac{\nu}{Q}\Big)$$

$$\times \phi_i^{(n_l)}\Big(1 - x - \frac{s}{Q^2}, \mu\Big)\Big[1 + \mathcal{O}\Big(1 - x, \frac{m^2}{Q^2}, \frac{\Lambda_{\text{QCD}}^2}{m^2}\Big)\Big]\,. \tag{3.31}$$

The μ evolution can be carried out by evolving the hard and jet functions and the PDF with their massless anomalous dimensions with n_l active flavors below the mass scale and $n_l + 1$ active flavors above the mass scale, as indicated by the vertical arrows in Fig. 3.4a, which automatically takes into account the μ dependence of the mass mode matching functions H_s and H_c, because of the relation

$$Q^2 \gamma_{J,m}\Big(Q^2(1 - z), m, \mu, \frac{\nu}{Q}\Big) + \gamma_\phi^{(n_l)}(1 - z, \mu) + \delta(1 - z)\gamma_{H_s}(m, \mu, \nu) + \delta(1 - z)\gamma_{H_c}\Big(m, \mu, \frac{\nu}{Q}\Big)$$

$$= Q^2 \gamma_J^{(n_l+1)}(Q^2(1 - z), \mu) + \gamma_\phi^{(n_l+1)}(1 - z, \mu)\,. \tag{3.32}$$

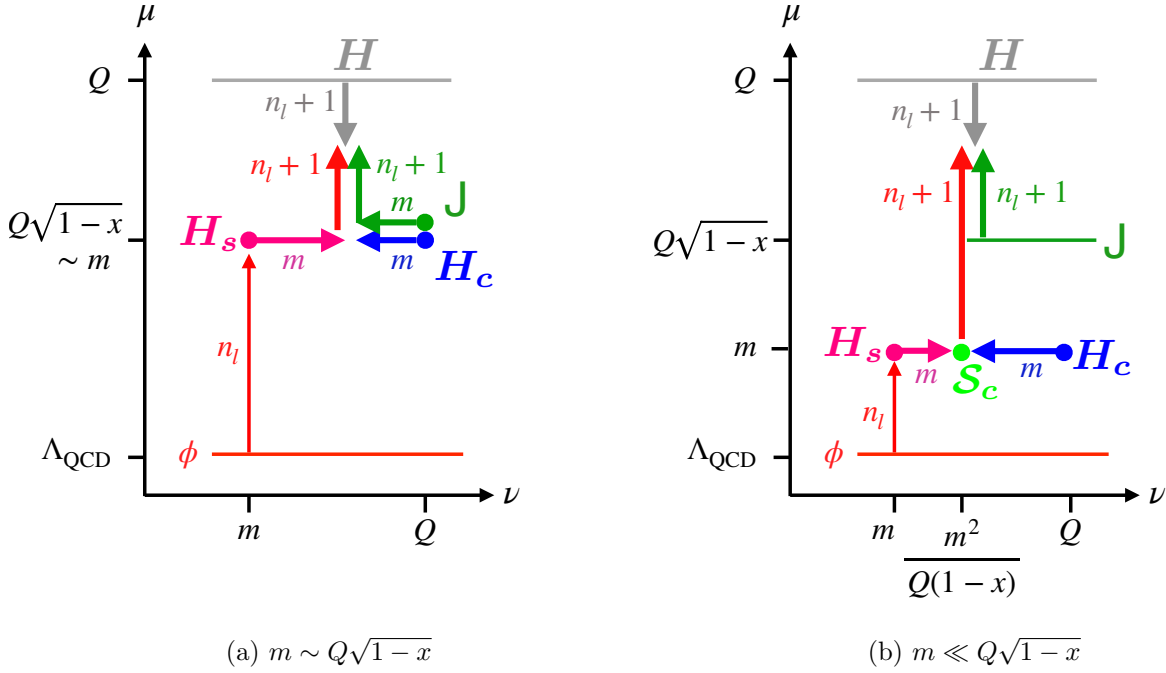(a) $m \sim Q\sqrt{1-x}$ (b) $m \ll Q\sqrt{1-x}$

Figure 3.4: Illustration of the renormalization group evolution of the hard and jet functions and the parton distribution function in the limit $x \to 1$ in virtuality μ (vertical) and rapidity ν (horizontal). The anomalous dimensions for each evolution step involve the displayed number of active quark flavors. The label m indicates that the corresponding evolution is mass dependent.

This can be checked explicitly at two-loops with the results given in Eqs (B.20), (B.12), (C.9), (C.11) and (C.29). The rapidity evolution is carried out between the massive jet function and the current matching function H_c at the rapidity scale $\nu \sim Q$ and the soft current matching function H_s at the rapidity scale $\nu \sim m$, as indicated by the horizontal arrows in Fig. 3.4a. It is identical to the one involving only the hard functions H_s and H_c in Sec.2.1.3

3.2.2 Quark mass effects for $m \ll Q\sqrt{1-x}$

If the jet scale becomes much larger than the mass scale, i.e $m \ll Q\sqrt{1-x}$, the heavy flavor can be considered massless up to power corrections of order $\sim m^2/(Q^2(1-x))$ when integrating out the n-collinear modes at the jet scale, leading to the standard $n_l + 1$ flavor massless jet function. The analogous statement also holds for the hard function. Integrating out the mass modes at the mass scale, that is now much smaller than the jet scale (but still much larger than the non-perturbative scale Λ_{QCD}), leads to a larger number of matching functions compared to Eq. (3.31) above.

After integrating out the n-collinear modes as in Eq. (3.10) with $n_f = n_l + 1$, where all flavors are treated as massless, such that it gives the massless $n_l + 1$ flavor jet function as a matching coefficient, we are left with a theory with $n_l + 1$ n-collinear-soft, soft and $\bar{n}$-collinear modes. The virtuality of these modes can be lowered down to the mass scale, where the heavy flavor is integrated out. The matching at the mass scale can involve different mass modes (n-collinear-soft, soft, $\bar{n}$-collinear-soft), depending on how the mass m scales with respect to $Q(1-x)$, because this is the scale where the collinear-soft modes become soft (compare Fig. 3.3b and 3.3c). This matching procedure, however, always leads to identical results for the combination of all relevant matching coefficients. This is clear from the fact that the only physical scales in the process besides the mass are the hard scale Q, the jet scale $Q\sqrt{1-x}$ and the non-perturbative scale Λ_{QCD}, so that it is obvious that only the

relative scaling of the mass with respect to these scales can have an effect, but not the scaling with respect to the non-dynamical scale $Q(1-x)$. So whether one does the matching of the $n_l + 1$ to the n_l flavor theory when integrating out the heavy flavor in the scenario where $m \ll Q\sqrt{1-x}$ with (a) n-collinear-soft mass modes (corresponding to the case where $m \gg Q(1-x)$), or (b) soft mass modes (corresponding to the case $m \sim Q(1-x)$), or (c) $\bar{n}$-collinear-soft mass modes (corresponding to the case $m \ll Q(1-x)$), is just a technicality changing some details of the calculations and the mode-setup, depending on the choice of the rapidity regulator, but is not changing any of the final analytical results when combing all matching coefficients that arise, as will be discussed below.

If $m \gg Q(1-x)$, the mass modes have the momentum scaling

$$
\begin{aligned}
&\bar{n}\text{-coll. MM:} \quad p_{\bar{c}}^{\mu} \sim \left(Q, \frac{m^2}{Q}, m \right), \\
&\text{soft MM:} \quad p_s^{\mu} \sim (m, m, m), \\
&n\text{-csoft MM:} \quad p_{cs}^{\mu} \sim \left(Q(1-x), \frac{m^2}{Q(1-x)}, m \right),
\end{aligned}
\tag{3.33}
$$

as also indicated in Fig. 3.3b. When integrating out the heavy flavor, this leads to separate matching coefficients in each of the three sectors. In the $\bar{n}$-coll. and the soft sector, the mass modes can not contribute to the measurement and are therefore integrated out in the SCET current, leading to the mass mode matching functions H_s and H_c as before, with the result at two-loops given in Eqs. (C.8) and (C.10).

The momentum scaling of the n-collinear-soft mass modes in Eq. (3.33) is determined by the on-shell condition and that the component $n \cdot p$ coincides with the respective dynamical momentum component of the collinear modes, i.e. $n \cdot p \sim Q(1-x)$. In this way the collinear-soft mass modes can contribute the measurement of the invariant mass of the final state $P_X^2 \sim Q^2(1-x)$. Integrating out the heavy flavor in the n-collinear-soft sector therefore leads to the matching relation between non-local collinear-soft matrix elements in the $n_l + 1$ and n_l flavor theories

$$
\mathscr{S}_c^{(n_l+1)}(\ell, m, \mu, \nu) = \int \mathrm{d}\ell' \, \mathcal{S}_c(\ell - \ell', m, \mu, \nu) \, \mathscr{S}_c^{(n_l)}(\ell', \mu, \nu) \,,
\tag{3.34}
$$

with the collinear-soft matrix elements $\mathscr{S}_c$ defined in Eq. (3.11). This gives the matching coefficient $\mathcal{S}_c$, the csoft function, with the contributions up to $\mathcal{O}(\alpha_s^2)$ given in Eq. (C.32). The csoft function is the same that also appeared in the factorization theorem for beam thrust in Drell-Yan in Sec. 2.2.3. The virtuality of the remaining n_l massless modes can then be lowered without any further matching down to the non-perturbative scale, where they contribute to the PDF as in the massless case in Eq. (3.15).

The factorization theorem, consisting of the $n_l + 1$ flavor massless hard and jet functions, the n_l flavor PDF and the mass mode matching functions H_s, H_c and $\mathcal{S}_c$, reads

$$
F_1(x, m, Q) = \frac{1}{2} \sum_{i \in \{q, \bar{q}\}} \hat{H}_i^{(n_l+1)}(Q, \mu) H_c\left(m, \mu, \frac{\nu}{Q}\right) H_s(m, \mu, \nu) \int \mathrm{d}s \, \mathrm{d}\ell \, J^{(n_l+1)}(s, \mu) \mathcal{S}_c(\ell, m, \mu, \nu)
$$

$$
\times \phi_i^{(n_l)}\left(1 - x - \frac{s}{Q^2} - \frac{\ell}{Q}, \mu\right) \left[1 + \mathcal{O}\left(1 - x, \frac{m^2}{Q^2(1-x)}, \frac{\Lambda_{\mathrm{QCD}}^2}{m^2}\right)\right].
\tag{3.35}
$$

The μ evolution can be carried out by evolving the hard and jet functions and the PDF with their massless anomalous dimensions with n_l active flavors below the mass scale and $n_l + 1$ active flavors above the mass scale, as indicated in Fig. 3.4b, which automatically takes into account the μ dependence of the mass mode matching functions H_s, H_c and $\mathcal{S}_c$, because of the relation

$$
Q\gamma_{\mathcal{S}_c}\big(Q(1-z), m, \mu, \nu\big) + \delta(1-z)\gamma_{H_s}(m, \mu, \nu) + \delta(1-z)\gamma_{H_c}\left(m, \mu, \frac{\nu}{Q}\right) + \gamma_\phi^{(n_l)}(1-z, \mu)
$$

$$
= \gamma_\phi^{(n_l+1)}(1-z, \mu).
\tag{3.36}
$$

65

This can be checked explicitly at two-loops with the results given in Eqs (B.12), (C.9), (C.11) and (C.33).

The rapidity evolution is carried out between the collinear-soft function at the rapidity scale $\nu \sim m^2/(Q(1-x))$ and the collinear current matching function H_c at the rapidity scale $\nu \sim Q$ and the soft current matching function H_s at the rapidity scale $\nu \sim m$, as indicated in Fig. 3.4b. The anomalous dimensions and the structure of the solutions of the rapidity RGE are the same as for the case involving only the hard functions H_s and H_c in Sec.2.1.3

The factorization theorem in Eq. (3.35) was derived assuming the scaling $Q(1-x) \ll m \ll Q\sqrt{1-x}$, such that the n-collinear-soft and soft mass modes in Eq. (3.33) are clearly separated. This led to the two matching coefficients $\mathcal{S}_c$ and H_s in the csoft and the soft sector, respectively. If the mass is of order $m \sim Q(1-x)$, the momentum scaling of the n-collinear-soft mass modes in Eq. (3.33) coincides with that of the soft mass modes. In that situation, when integrating out the mass modes at the mass scale, there is only a $\bar{n}$-collinear and a soft sector, see Fig. 3.3c. In the $\bar{n}$-collinear sector nothing has changed compared to the situation where $Q(1-x) \ll m$, i.e. the heavy flavor is integrated out in the collinear SCET current, giving the same mass mode matching coefficient H_c as before. But now the soft mass modes can contribute to the measurement via their momentum component $n \cdot p \sim m \sim Q(1-x)$. While in the situation where $Q(1-x) \ll m$ they could contribute only via virtual effects and integrating out the heavy flavor in the soft SCET current only gave a local matching coefficient H_s, in the situation where $m \sim Q(1-x)$ the matching takes place between soft matrix elements with a non-local measurement function

$$\mathscr{S}^{(n_l+1)}(\ell, m, \mu, \nu) = \int d\ell' \, \mathcal{S}(\ell - \ell', m, \mu, \nu) \, \mathscr{S}^{(n_l)}(\ell', \mu, \nu) \,, \qquad (3.37)$$

where the soft matrix elements $\mathscr{S}$ are defined in Eq. (3.18). This matching relation has the same form as the one in the csoft case in Eq. (3.34), but with the csoft matrix elements replaced by soft matrix elements, and the matching coefficient is therefore the new soft function $\mathcal{S}$. In this way when going from the scenario $Q\sqrt{1-x} \gg m \gg Q(1-x)$ to $m \sim Q(1-x)$, the matching coefficients arising from integrating out the heavy flavor in the factorization theorem in Eq. (3.35), are changed from $H_c \times H_s \times \mathcal{S}_c$ to $H_c \times \mathcal{S}$. As we will discuss below the two expressions are in fact identical.

In the case where $m \ll Q(1-x)$ (but still as always assumed here much larger than Λ_{QCD}), the virtuality of the soft modes gets lowered even further, such that they become $\bar{n}$-collinear-soft when they reach the mass scale where the heavy flavor is integrated out. Their momentum scaling is

$$p_{\bar{c}s}^\mu \sim \left(Q(1-x), \frac{m^2}{Q^2(1-x)}, m \right) \,, \qquad (3.38)$$

which implies that they are boosted in the $\bar{n}$-direction because $m \ll Q(1-x)$, in contrast to the n-collinear-soft modes in Eq. (3.33) for $m \gg Q(1-x)$. This implies that the soft matrix elements in Eq. (3.37) get replaced by $\bar{n}$-collinear-soft matrix elements, leading to a matching relation for integrating out the heavy flavor of the form

$$\mathscr{S}_{\bar{c}}^{(n_l+1)}(\ell, m, \mu, \nu) = \int d\ell' \, \mathcal{S}_{\bar{c}}(\ell - \ell', m, \mu, \nu) \, \mathscr{S}_{\bar{c}}^{(n_l)}(\ell', \mu, \nu) \,, \qquad (3.39)$$

with the $\bar{n}$-collinear-soft matrix elements $\mathscr{S}_{\bar{c}}$ defined in Eq. (3.20). Nothing is changed in the $\bar{n}$-collinear sector compared to the case $m \sim Q(1-x)$, i.e. integrating out the heavy flavor in the collinear SCET current leads to same the mass mode matching function H_c, such that the only change in the factorization theorem when the mass becomes much smaller than $Q(1-x)$ is the replacement of the soft function $\mathcal{S}$ by the $\bar{n}$-collinear-soft function $\mathcal{S}_{\bar{c}}$, that is defined by the matching relation in Eq. (3.39).

Since we know that the only physical scales in the process besides the mass m of the heavy flavor are the hard scale Q, the invariant mass of the hadronic final state $Q\sqrt{1-x}$ and the hadronic scale

Λ_{QCD}, the factorization theorem cannot depend on the scaling of the mass with respect to the non-dynamical scale $Q(1-x)$. This implies that all results for the matching coefficients for the three cases $m \gg Q(1-x)$, $m \sim Q(1-x)$ and $m \ll Q(1-x)$ have to agree, leading to the relation

$$H_s(m,\mu,\nu)\mathcal{S}_c(\ell,m,\mu,\nu) = \mathcal{S}(\ell,m,\mu,\nu) = \mathcal{S}_{\bar{c}}(\ell,m,\mu,\nu)\,, \qquad (3.40)$$

between the various mass mode matching coefficients in the n-collinear-soft, soft and $\bar{n}$-collinear-soft sectors. These relations are independent of the choice of the rapidity regulator, though the results for the individual functions depend on which rapidity regulator is employed. In this thesis all contributions are always calculated with the symmetric η Wilson-line regulator [40], the results for H_s and $\mathcal{S}_c$ at $\mathcal{O}(\alpha_s^2)$ are given in Eqs. (C.8) and (C.32). The soft and $\bar{n}$-collinear-soft matching functions $\mathcal{S}$ and $\mathcal{S}_{\bar{c}}$ with the η-regulator have been calculated in Sec. V of Ref. [2]. With these results Eq. (3.40) can be checked to two-loop order. We remark that the distinction between $\mathcal{S}_c$, $\mathcal{S}$ and $\mathcal{S}_{\bar{c}}$ is only introduced by the choice of a rapidity regulator (here the η-regulator with its action on n-collinear-soft, soft and $\bar{n}$-collinear-soft Wilson lines given in Eqs. (3.12), (3.14) and (3.19)) that distinguishes between different boosts of the gluon momenta, and is for example absent when using instead the regulator $\frac{1}{k^-} \rightarrow \frac{1}{k^-}\left(\frac{\nu}{k^-}\right)^{\alpha}$ for the gluon loop momentum suggested in Ref. [104]. This regulator does not distinguish between different boosts of the gluon momentum, such that the matrix elements $\mathscr{S}_c$, $\mathscr{S}$ and $\mathscr{S}_{\bar{c}}$ are identical already at the integrand level[3]. All corrections beyond tree level to the local soft current mass mode matching function H_s are scaleless when using this regulator and therefore vanish, such that Eq. (3.40) trivially holds. We emphasize again that when using this regulator the results for the collinear current mass mode matching functions H_c are not anymore identical for the n- and the $\bar{n}$-direction.

In the following we will adopt the form of the factorization theorem in Eq. (3.35) with the current matching function H_s and the n-collinear-soft function $\mathcal{S}_c$ as for $Q(1-x) \ll m$, regardless of the relation of m and $Q(1-x)$. This may seem an unnecessary complication compared to writing it with only $\mathcal{S}$ or $\mathcal{S}_{\bar{c}}$ because instead of having just one mass mode matching function it is split into two separate functions, but it will turn out to be more convenient when comparing with the other factorization theorems for beam thrust in Drell-Yan discussed in Sec. 2.2 and thrust in $e^+e^- \rightarrow$ jets discussed in appendix A, and also when incorporating the mass related power corrections in Sec. 4.2.1. In this way the matching functions are completely universal, such that in the factorization theorems for all three processes discussed here - beam thrust in DY, DIS in the endpoint and thrust in $e^+e^- \rightarrow$ jets - the mass mode matching functions are always the same H_s, H_c and $\mathcal{S}_c$. This also implies that the rapidity evolution related to secondary massive quark effects is universal for all three observables, an important result that was not directly clear from Refs. [1,2,12], where the resummation of secondary massive quark effects in DY, DIS and $e^+e^- \rightarrow$ jets were discussed separately.

3.2.3   Relations between hierarchies

We will now discuss how the ingredients in the different factorization theorems for the different hierarchies presented in the previous sections are related with each other, in analogy to the presentation in Secs. 2.1.6 and 2.2.5 for the case of DY. Here we only give a collection of the various relations existing between the mass dependent hard and jet functions and their massless counterparts in the n_l and $n_l + 1$ flavor schemes and provide the equations to check them with our results up to $\mathcal{O}(\alpha_s^2)$, without discussing them further. But in Sec. 4.2.1 theses relations between the various functions in the massless and the decoupling limit form the basis of the UF approach which is a variable flavor number scheme where the mass dependent power corrections that are omitted in the MMF approach are included for any scale hierarchy, so that it is applicable for an arbitrary scaling of the mass relative

---

[3]When using the η-regulator the soft function $\mathcal{S}$ and the $\bar{n}$-collinear-soft function $\mathcal{S}_{\bar{c}}$ are still identical, but the individual virtual and real radiation diagrams are not. Only the sum of all diagrams is identical, see Sec. V of Ref. [2] for details of the calculation.

to the other scales. The relations between the modes for DIS in the endpoint in the different regimes are summarized in Fig. 3.5.

The massless results at $\mathcal{O}(\alpha_s)$ and $\mathcal{O}(\alpha_s^2 C_F T_F)$ are collected in appendix B, the contributions from secondary massive quarks at $\mathcal{O}(\alpha_s^2)$ in appendix C. The relations between the hard and the jet functions in the different hierarchies given here can be checked explicitly up to $\mathcal{O}(\alpha_s^2)$ with the results there.

The hard functions of DIS in the hierarchies $m \sim Q$ and $m \ll Q$ have the same relation as the hard functions for Drell-Yan shown in Eq. (2.37)

$$\hat{H}(Q,m,\mu) \overset{m \ll Q}{=} \hat{H}^{(n_l+1)}(Q,\mu) H_c\Big(m,\mu,\frac{\nu}{Q}\Big) H_c\Big(m,\mu,\frac{\nu}{Q}\Big) H_s(m,\mu,\nu) + \mathcal{O}\Big(\frac{m^2}{Q^2}\Big). \qquad (3.41)$$

The mass dependent hard function used for $m \sim Q$ also shows the correct decoupling behavior in the limit $Q \ll m$, i.e.

$$\hat{H}(Q,m,\mu) \overset{Q \ll m}{=} \hat{H}^{(n_l)}(Q,\mu) + \mathcal{O}\Big(\frac{Q^2}{m^2}\Big). \qquad (3.42)$$

The mass mode jet function in the hierarchy $m \sim Q\sqrt{1-x}$ is related to the massless jet function with n_l flavors and the collinear mass mode matching function H_c by

$$J\Big(s,m,\mu,\frac{\nu}{Q}\Big) \overset{s \ll m^2}{=} H_c\Big(m,\mu,\frac{\nu}{Q}\Big) J^{(n_l)}(s,\mu) \times \Big(1 + \mathcal{O}\Big(\frac{s}{m^2}\Big)\Big), \qquad (3.43)$$

which is the same relation that also holds in the same limit for the mass dependent beam function matching coefficients, both the q_T and the virtuality dependent ones, expressed in Eqs. (2.38) and (2.105), respectively. In the small mass limit the mass mode jet function is related to the massless jet function with $n_l + 1$ flavors and the csoft function by

$$J\Big(s,m,\mu,\frac{\nu}{Q}\Big) \overset{m^2 \ll s}{=} \int \mathrm{d}\ell\, J^{(n_l+1)}(s - Q\ell,\mu) \mathcal{S}_c(\ell,m,\mu,\nu) \times \Big(1 + \mathcal{O}\Big(\frac{m^2}{s}\Big)\Big). \qquad (3.44)$$

With our results we can check these relations at $\mathcal{O}(\alpha_s^2)$. We will use the notation of Eqs. (2.33) and (2.36) and remind the reader once again that to get the correct limiting behavior the appropriate flavor scheme for the strong coupling has to be used, i.e. the $n_l + 1$ flavor scheme for the small mass limit and the n_l flavor scheme for the heavy mass limit. The small mass limit of the mass dependent hard function expressed in Eq. (3.41) can be checked with the results in Eqs. (C.6), (B.2), (C.8) and (C.10)

$$T_F \hat{H}^{(2,h)}(Q,m,\mu) \overset{m \ll Q}{=} T_F \hat{H}^{(2,l)}(Q,\mu) + H_c^{(2)}\Big(m,\mu,\frac{\nu}{Q}\Big) + H_{\bar{c}}^{(2)}\Big(m,\mu,\frac{\nu}{Q}\Big) + H_s^{(2)}(m,\mu,\nu) + \mathcal{O}\Big(\frac{m^2}{Q^2}\Big). \qquad (3.45)$$

The decoupling limit at $\mathcal{O}(\alpha_s^2)$ in Eq. (3.42) can be seen from Eq. (C.6)

$$\hat{H}^{(2,h)}(Q,m,\mu) - \frac{4}{3} L_m \hat{H}^{(1)}(Q,\mu) \overset{Q \ll m}{=} \mathcal{O}\Big(\frac{Q^2}{m^2}\Big). \qquad (3.46)$$

The heavy mass limit of the mass mode jet function in Eq. (3.43) at $\mathcal{O}(\alpha_s^2)$ can be checked with the result in Eqs. (C.27), (B.19) and (C.10)

$$T_F J^{(2,h)}\Big(s,m,\mu,\frac{\nu}{Q}\Big) - \frac{4}{3} T_F L_m J^{(1)}(s,\mu) \overset{s \ll m^2}{=} H_c^{(2)}\Big(m,\mu,\frac{\nu}{Q}\Big) \delta(s) + \mathcal{O}\Big(\frac{s}{m^2}\Big), \qquad (3.47)$$

and the small mass limit of the mass mode jet function in Eq. (3.44) with Eqs. (C.27), (B.19) and (C.32)

$$T_F J^{(2,h)}\Big(s,m,\mu,\frac{\nu}{Q}\Big) \overset{m^2 \ll s}{=} T_F J^{(2,l)}(s,\mu) + \frac{1}{Q} \mathcal{S}_c^{(2)}\Big(\frac{s}{Q},m,\mu,\nu\Big) + \mathcal{O}\Big(\frac{m^2}{s}\Big). \qquad (3.48)$$
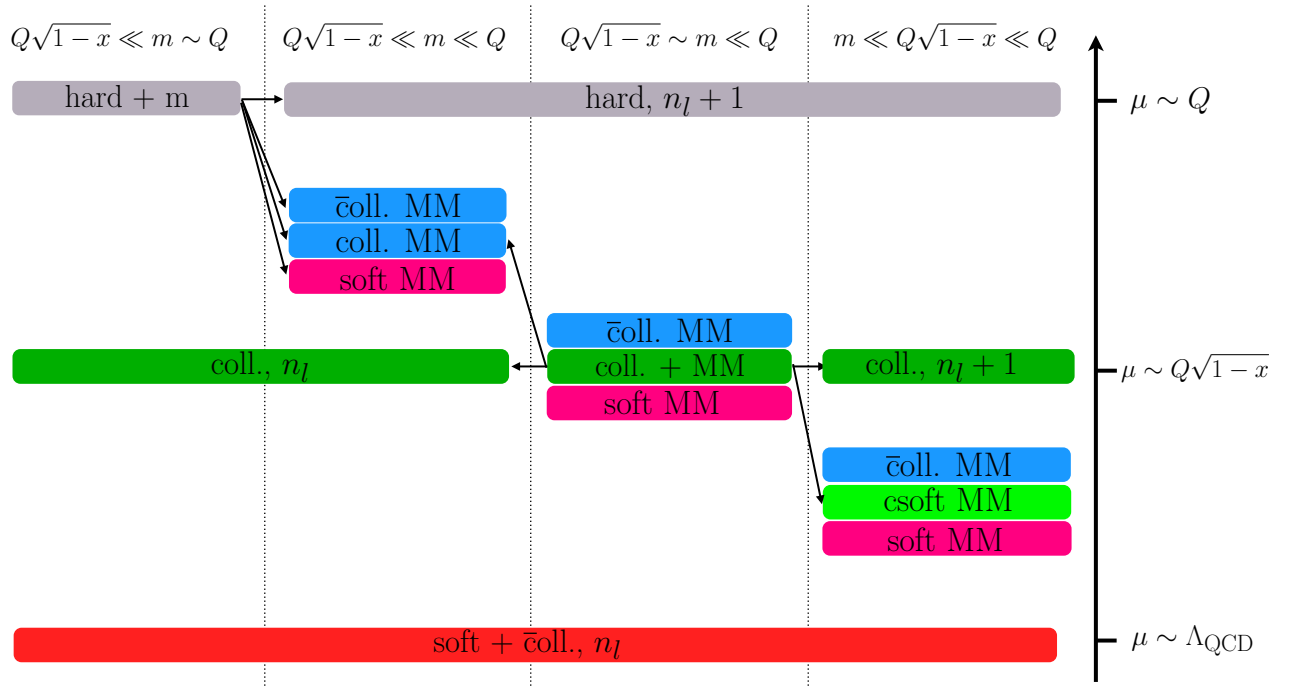
Figure 3.5: Relevant modes DIS in the endpoint $(1 - x) \ll 1$ for different hierarchies between the quark mass m and the scales $Q\sqrt{1-x}$ and Q. The directions of the arrows indicate how a particular mode contribution is separated when the expansion of another hierarchy is used.

Chapter 4

An Alternative Way of Constructing the Variable Flavor Number Schemes

In this section we will present an alternative approach on how to construct a VFNS called universal factorization (UF) approach, and compare it to the MMF approach that was used in the previous sections. The resulting factorization theorems have an equivalent content to the ones in the MMF approach for all possible hierarchies (see Sec. 4.2). The UF approach provides a different setup on how to include the mass effects, leading to factorization theorems for the different hierarchies that correctly resum all logarithms but in addition also show a smooth transition from one to the other when the scaling of the mass relative to the other scales is changed, i.e. no strict separation of the scales needs to be assumed and all mass related power correction are automatically included.

The idea of the UF approach is to have the same structures that appear in the massless factorization theorems, e.g. the jet function, the soft function etc., as the universal building blocks. The goal is to have a definition of these functions containing all contributions from massive quarks that allows for

a) a smooth transition between all different hierarchies that the mass can have with respect to the other kinematic scales, i.e. a description that does not specifically rely on a large separation of the mass scale from other scales and does not contain any expansions in the mass,

b) resummation of all rapidity logarithms within those functions themselves, such that each function can be defined as an already resummed building block that can then be inserted in any factorization theorem for a practical implementation.

In this way this approach differs from the MMF approach, where always a fixed scaling of the mass with respect to other scales was assumed and all subleading contributions were always strictly expanded away, leading to a framework where the resulting structures in the factorization theorems are in general valid only in one strict hierarchy, and rapidity logarithms are always resummed in an evolution in rapidity between the different functions in the factorization theorems.

The UF framework was first developed in Refs. [11,12] for thrust in the peak region in e^+e^--collisions (see also appendix A for the corresponding setup in the mass mode factorization approach), and then applied to DIS in the endpoint region in Ref. [2]. It is also discussed in great detail in Ref. [20], and we will therefore only give a short summary on how the UF scheme is implemented for the various functions in the factorization schemes in Sec. 4.1. In Sec. 4.2 we will compare the UF and the MMF approach for secondary massive quarks, show how they are equivalent and discuss where they differ. A similar comparison for the primary massive quark jet functions in the MMF and the UF approach was given in Ref. [71].

4.1   The universal factorization scheme

The basic idea to get functions in the factorization theorems that keep the full mass dependence and are therefore applicable over the full range of possible hierarchies, is to not integrate out the heavy flavor at its mass scale, but use different renormalization schemes for the massive contributions, depending on whether the mass is above or below the natural kinematic scale of the function. This idea follows and extends the treatment of mass corrections in inclusive heavy flavor production (e.g. in the calculation of quark mass effects in the hadronic R-ratio), where an appropriate choice of the renormalization scheme of the coupling, either in a scheme with n_l active flavors in the RG evolution (when contributions from the heavy flavor are renormalized with a low-momentum subtraction) when the scale is below the quark threshold or in a scheme with $n_l + 1$ active flavors (when contributions from the heavy flavor are renormalized in the $\overline{\text{MS}}$ scheme) when the scale is above the quark threshold, leads to the correct massless and decoupling limits for the heavy flavor [105–107].

This concept can be extended to factorized differential cross sections, involving different gauge invariant functions that describe the physics at the various energy scales involved in the process [11, 12]. To achieve a setup that allows for resummation of logarithms that contain the quark mass as a scale, while keeping the full mass dependence in all functions in the factorization theorem with the correct massless and decoupling limit, the strategy of changing between the mass independent $\overline{\text{MS}}$ renormalization scheme and a low-momentum subtraction scheme has to be applied not only to the renormalization of the coupling, but to the renormalization of each of the UV divergent structures in the factorization theorem. Since all of the SCET matrix elements involved in the matching relations defining the hard, jet, beam and (c)soft functions in the previous chapters are UV divergent, they require an additional renormalization (beyond that associated to the strong coupling) where the UV divergences are absorbed into a counterterm. As always there is the freedom of which finite terms are additionally absorbed into the counterterm, leading to different renormalization schemes. One scheme that will be used in the construction of the different functions in the factorization theorems in the UF approach is the standard $\overline{\text{MS}}$ scheme, where only the $\frac{1}{\epsilon}$-divergences are absorbed into the counterterm. The other renormalization scheme that will be used corresponds to a low-momentum subtraction scheme, where all contributions from the heavy flavor that do not automatically decouple in the limit $m \to \infty$ are absorbed into the counterterm. Those are typically the mass-dependent distributional terms appearing in the functions, while contributions related to real production of the heavy quarks will have the correct decoupling limit due to kinematic thresholds and are therefore not absorbed into the counterterm. Motivated by the on-shell renormalization scheme we will refer to this low-momentum subtractions with respect to the massive quark also as "on-shell" (OS) subtractions.

We will discuss the UF scheme for a generic function $F(y, \mu)$, where F can stand for any hard, beam, jet or soft function or PDF as they appear in the factorization schemes discussed in the previous chapters. The variable y stands for the kinematic variable that this function depends on, like e.g. the center of mass energy Q in the case of the hard function or the virtuality t in case of the virtuality dependent beam function. We denote the natural kinematic scale, i.e. the scale that minimizes the logarithms in $F(y, \mu)$ in the massless case, as μ_F (e.g. for the hard function $\mu_F \sim Q$), and the mass scale as $\mu_m \sim m$.

Then the rule to get the mass-dependent function $F(y, m, \mu)$ as it is implemented in the universal factorization scheme is as follows: If $\mu_F < \mu_m$, the massive quark corrections to F are renormalized in the OS scheme that was described above. Also the contributions from the massive flavor to the strong coupling are renormalized with the OS subtraction, such that a scheme of n_l active flavors for the strong coupling is implemented. In this way the heavy flavor does not contribute to the RG evolution of F and automatically decouples in the heavy quark limit $m \to \infty$. If $\mu_m < \mu_F$ the massive quark corrections in F are renormalized the $\overline{\text{MS}}$ scheme, and the same is also done for massive quark contributions to the running of α_s, i.e. a $n_l + 1$ flavor scheme is used for the strong coupling. In this way the massive quark constitutes an additional active flavor in the RG evolution.

72

In this renormalization scheme the function F reduces to the correct massless function with one extra massless flavor in the limit $m \to 0$. Contributions from massless quarks are always renormalized in the $\overline{\text{MS}}$ scheme. The distinction between $\overline{\text{MS}}$ and OS subtractions is thus only to be made for effects of the massive flavor, including its contributions to the running of the coupling. We will denote the function F renormalized with the $\overline{\text{MS}}$ and OS subtractions by $F^{\overline{\text{MS}}}$ and F^{OS}, respectively, and emphasize again that this does not only refer to the renormalization with respect to the massive quark of F itself, but also to the renormalization scheme used with respect to the massive quark in the strong coupling.[1]

Written out explicitly this means that when the contributions from the massive flavor are renormalized with the $\overline{\text{MS}}$ subtraction, they contribute to the running of the $\overline{\text{MS}}$ renormalized F as an active flavor the same way as the massless quarks do

$$\mu \frac{\mathrm{d}}{\mathrm{d}\mu} F^{\overline{\text{MS}}}(y, m, \mu) = \gamma_F^{(n_l+1)}(y, \mu) \otimes F^{\overline{\text{MS}}}(y, m, \mu) \,, \tag{4.1}$$

where $\gamma_F^{(n_l+1)}$ is the anomalous dimension of F for $n_l + 1$ massless flavors. Here the symbol $\otimes$ should be understood as either a simple product or as a convolution in y, depending on whether the evolution of the function F is local or not. When the contributions from the massive flavor are renormalized in the OS scheme, they do not contribute to the running of the OS renormalized F

$$\mu \frac{\mathrm{d}}{\mathrm{d}\mu} F^{\text{OS}}(y, m, \mu) = \gamma_F^{(n_l)}(y, \mu) \otimes F^{\text{OS}}(y, m, \mu) \,, \tag{4.2}$$

where $\gamma_F^{(n_l)}$ is the anomalous dimension of F for n_l massless flavors.

With the $\overline{\text{MS}}$ subtraction the massive contributions reduce to those of an extra massless flavor in the limit $m \to 0$

$$F^{\overline{\text{MS}}}(y, m, \mu) = F^{(n_l+1)}(y, \mu) \times \left(1 + \mathcal{O}\Big(\frac{m^2}{y}\Big)\right). \tag{4.3}$$

But the $\overline{\text{MS}}$ scheme does not exhibit a decoupling behavior in the heavy quark limit.

With the OS subtraction all effects of massive quarks that do not decouple in the heavy quark limit are absorbed into the counter term for F, which means that F^{OS} automatically has the correct decoupling limit

$$F^{\text{OS}}(y, m, \mu) = F^{(n_l)}(y, \mu) \times \left(1 + \mathcal{O}\Big(\frac{y}{m^2}\Big)\right). \tag{4.4}$$

On the other hand those terms that are absorbed in the counter term are now missing to cancel other terms that are divergent in the limit $m \to 0$, such that the massless limit is not feasible with the OS subtraction. Therefore it is import to always keep the contributions of the massive flavor renormalized in the OS scheme when the mass scale is above the natural scale of F and in the $\overline{\text{MS}}$ scheme when the mass is below the natural scale, such that both limits can be reached smoothly and correctly.

It is important to note again that in the definition of F no expansion in the mass with respect to any other scale is made, which means that F contains the full mass dependence and does not only exhibit the correct limiting behavior in the small and large mass limit as indicated in Eqs. (4.3) and (4.4), but is also correct when $m^2 \sim y$. This is one of the differences of how the various functions in the factorization theorems are defined in the UF approach compared to the MMF approach. In the latter these functions are always valid only in a certain scaling of the mass with respect to the kinematic

---

[1]This notation with the superscripts $\overline{\text{MS}}$ and OS differs from the notation used in Refs. [2, 12], where instead the superscripts $(n_l + 1)$ and (n_l) where used to indicate when a function is renormalized with $\overline{\text{MS}}$ subtractions (i.e. with $n_l + 1$ active flavors in the RG running) or with OS subtractions (i.e. with n_l active flavors in the RG running).

scale that is assumed in defining them, and the missing power corrections of $\mathcal{O}(y/m^2)$ and $\mathcal{O}(m^2/y)$ have to be implemented by a dedicated additional procedure, as discussed in Sec. 4.2.1.

Since we want to have F to be renormalized with the OS subtraction when its dynamical scale is below and with the $\overline{\text{MS}}$ subtraction when it is above the mass scale, the renormalization scheme needs to be changed when the mass scale is crossed in the evolution of F. This is done by the insertion of so called threshold corrections, that are analogous to the matching conditions that arise when relating the strong coupling in the $n_l + 1$ and the n_l flavor scheme. The threshold corrections $\mathcal{M}_F^{\pm}$ are just the ratio of F with the OS and the $\overline{\text{MS}}$ subtractions

$$\mathcal{M}_F^+(y, m, \mu_m) = F^{\overline{\text{MS}}}(y, m, \mu_m) \otimes \left(F^{\text{OS}}(y, m, \mu_m) \right)^{-1},$$

$$\mathcal{M}_F^-(y, m, \mu_m) = F^{\text{OS}}(y, m, \mu_m) \otimes \left(F^{\overline{\text{MS}}}(y, m, \mu_m) \right)^{-1}, \tag{4.5}$$

and therefore take F from one scheme to the other. $\mathcal{M}_F^+$ is used when the mass scale is crossed from below in the evolution (which means that the heavy flavor is added as an active flavor in the RG evolution), and $\mathcal{M}_F^-$ when the mass scale is crossed from above (when the heavy flavor is removed from the RG evolution as an active flavor). To avoid large logarithms in the threshold corrections the matching has to be done at the mass scale $\mu_m \sim m$. In this way the μ-dependence of the threshold correction is by construction exactly the difference of the running of F in the $(n_l + 1)$ and the (n_l) flavor scheme

$$\mu \frac{\mathrm{d}}{\mathrm{d}\mu} \mathcal{M}_F^{\pm}(y, m, \mu) = \pm \left[\gamma_F^{(n_l+1)}(y, \mu) - \gamma_F^{(n_l)}(y, \mu) \right] \otimes \mathcal{M}_F^{\pm}(y, m, \mu), \tag{4.6}$$

such that the renormalized F is effectively always evolved with n_l flavors below the mass scale (where F^{OS} must be used) and with $n_l + 1$ flavors above the mass scale (where $F^{\overline{\text{MS}}}$ must be used).

To resum logarithms in F in the massless case, the function is first evaluated at its natural scale μ_F where all logarithms are small, and then evolved in a RG evolution to the common renormalization scale μ of the factorizaton theorem. This is done in a convolution with an evolution kernel U_F, such that

$$F(y, \mu, \mu_F) = U_F^{(n_f)}(y, \mu, \mu_F) \otimes F(y, \mu_F). \tag{4.7}$$

The superscript (n_f) indicates that the evolution is carried out for n_f massless flavors. It is these resummed functions $F(y, \mu, \mu_F)$ that then finally appear in the factorization theorems, when they are not evaluated at fixed order but are used to resum large logarithms.

In the massive case there are in total four different possibilities how the function F is implemented in the factorization theorem, depending on how the global renormalization scale μ, the mass scale μ_m and the natural scale of the function μ_F lie with respect to each other.

$\mu_F < \mu_m < \mu$:

$$F(y, m, \mu, \mu_m, \mu_F) = U_F^{(n_l+1)}(y, \mu, \mu_m) \otimes \mathcal{M}_F^+(y, m, \mu_m) \otimes U_F^{(n_l)}(y, \mu_m, \mu_F) \otimes F^{\text{OS}}(y, m, \mu_F). \tag{4.8}$$

Here F is evaluated with the OS subtraction for the massive quark contributions at its natural scale μ_F, then evolved with n_l active flavors to the mass scale μ_m, where the scheme switch from the OS to the $\overline{\text{MS}}$ subtractions is done. From there it is evolved with $n_l + 1$ active flavors to the global renormalization scale μ.

$\mu < \mu_m < \mu_F$:

$$F(y, m, \mu, \mu_m, \mu_F) = U_F^{(n_l)}(y, \mu, \mu_m) \otimes \mathcal{M}_F^-(y, m, \mu_m) \otimes U_F^{(n_l+1)}(y, \mu_m, \mu_F) \otimes F^{\overline{\text{MS}}}(y, m, \mu_F). \tag{4.9}$$

Here F is evaluated with the $\overline{\text{MS}}$ subtraction for the massive quark contributions at its natural scale μ_F, then evolved with $n_l + 1$ active flavors to the mass scale μ_m, where the scheme switch from the

$\overline{\text{MS}}$ to the OS subtractions is done. From there it is evolved with n_l active flavors to the global renormalization scale μ.

$$\mu_m < \mu, \mu_F : \qquad F(y, m, \mu, \mu_m, \mu_F) = U_F^{(n_l+1)}(y, \mu, \mu_F) \otimes F^{\overline{\text{MS}}}(y, m, \mu_F). \qquad (4.10)$$

Here F is evaluated with the $\overline{\text{MS}}$ subtraction for the massive quark contributions and then evolved to the global renormalization scale μ with $n_l + 1$ active flavors. The mass scale is never crossed.

$$\mu, \mu_F < \mu_m : \qquad F(y, m, \mu, \mu_m, \mu_F) = U_F^{(n_l)}(y, \mu, \mu_F) \otimes F^{\text{OS}}(y, m, \mu_F). \qquad (4.11)$$

Here F is evaluated with with the OS subtraction for the massive quark contributions and then evolved to the global renormalization scale μ with n_l active flavors. The mass scale is never crossed.

The factorization theorems for the various processes including the full mass dependence in the resummation then take the same form as in the massless case, but each hard, jet, beam and soft function that had the form $F(y, \mu, \mu_F)$ as in Eq. (4.7) in the massless case, being replaced by its massive form $F(y, m, \mu, \mu_m, \mu_F)$ as in Eqs. (4.8)-(4.11).

In general all rapidity logarithms that can become large if the scales μ_F and μ_m are widely separated and therefore need to be resummed are contained the threshold corrections $\mathcal{M}_F$. In Refs. [11, 12] it was shown that these logarithms can be resummed by factorizing the threshold corrections into contributions arising from different modes or from radiation into different hemispheres, as we will discuss below.

In the following sections we will briefly sketch how the UF scheme is implemented for treatment of massive quark effects in the jet, beam, soft and hard functions and the PDF in the endpoint. Except for the beam functions this is discussed in more detail in Refs. [2, 11, 12, 20]. We will not write down the explicit results for the various functions in the different renormalization schemes and the threshold corrections here, but show how they can be constructed from the ingredients of the MMF approach in Sec. 4.2.2.

4.1.1 Jet function

We will first discuss how the UF scheme is implemented for the hemisphere jet function. We will again consider only secondary massive quark effects here, a similar discussion also for the primary massive quark jet function in the UF and the MMF approach can be found in Ref. [71]. As explained above, the massive flavor is never integrated out, such that the massive jet function is always a matching coefficient between a theory with $n_l + 1$ hard-collinear modes and a theory with $n_l + 1$ collinear-soft modes that remain after the hard-collinear modes have been integrated out from the theory. This differs from its definition in the previous sections in the MMF scheme, where we either had only massless flavors in the matching or, in the case where the mass was of order of the jet scale, the matching was between $n_l + 1$ hard-collinear and only n_l collinear-soft modes, since the heavy quark got integrated out completely at that scale. In the UF approach the relative scaling of the mass scale to the jet scale only changes the renormalization scheme, such that we have two different definitions of the renormalized jet function, either with OS or $\overline{\text{MS}}$ subtractions for the massiv quark

$$\mathcal{J}^{\text{OS}}(s, m, \mu) = \int d\ell \, J^{\text{OS}}(s - Q\ell, m, \mu) \mathscr{S}_c^{\text{OS}}(\ell, m, \mu),$$

$$\mathcal{J}^{\overline{\text{MS}}}\left(s, m, \mu, \frac{\nu}{Q}\right) = \int d\ell \, J^{\overline{\text{MS}}}(s - Q\ell, m, \mu) \mathscr{S}_c^{\overline{\text{MS}}}(\ell, m, \mu, \nu). \qquad (4.12)$$

Here $\mathcal{J}$ and $\mathscr{S}_c$ are the collinear and collinear-soft matrix elements defined in Eqs. (3.8) and (3.11), respectively, with n_l massless and one massive flavor, and the matching coefficient J is the jet function that appears in the factorization theorem. Again the superscripts OS and $\overline{\text{MS}}$ only indicate which

subtraction scheme is used for the contributions from the massive quark, and contributions from massless quarks are always renormalized with $\overline{\text{MS}}$ subtractions. Since the massive contributions to the collinear-soft matrix element $\mathscr{S}_c$ are purely distributional and do not exhibit any kinematic threshold and therefore do not decouple in the heavy quark limit, they are completely absorbed into the on-shell counterterm, such that the OS renormalized csoft matrix element is equal to the csoft matrix element with only n_l massless flavors, i.e. $\mathscr{S}_c^{\text{OS}}(\ell, m, \mu) = \mathscr{S}_c^{(n_l)}(\ell, \mu)$. In this way the UF jet function in the $\overline{\text{MS}}$ scheme has the correct massless limit, while the UF jet function in the OS scheme exhibits the correct decoupling limit. Note that even though the matrix elements in the $\overline{\text{MS}}$ scheme have a dependence on the rapidity scale ν, the resulting jet function is independent of ν since the ν dependence completely cancels between the collinear and the collinear-soft matrix elements. The jet function defined in this way does also not contain any large rapidity logarithms.

The threshold correction $\mathcal{M}_J$ for the jet function, defined as in Eq. (4.5), contains rapidity logarithms of the form $\ln(s/m^2)$, that can be resummed by factorizing the threshold correction into contributions coming from the collinear matrix element $\mathcal{J}$ and the csoft matrix element $\mathscr{S}_c$

$$\mathcal{M}_{\mathcal{J}}^+\Big(s, m, \mu_m, \frac{\nu}{Q}\Big) = \int \mathrm{d}s' \, \mathcal{J}^{\overline{\text{MS}}}\Big(s - s', m, \mu_m, \frac{\nu}{Q}\Big)\Big(\mathcal{J}^{\text{OS}}(s', m, \mu_m)\Big)^{-1}, \qquad (4.13)$$

$$\mathcal{M}_{\mathscr{S}_c}^+(\ell, m, \mu_m, \nu) = \int \mathrm{d}\ell' \, \mathscr{S}_c^{\overline{\text{MS}}}(\ell - \ell', m, \mu_m, \nu)\Big(\mathscr{S}_c^{\text{OS}}(\ell', m, \mu_m)\Big)^{-1} \qquad (4.14)$$

such that

$$\mathcal{M}_J^\pm(s, m, \mu_m) = \int \mathrm{d}\ell \, \mathcal{M}_{\mathcal{J}}^\pm\Big(s - Q\ell, m, \mu_m, \frac{\nu}{Q}\Big)\Big(\mathcal{M}_{\mathscr{S}_c}^\pm(\ell, m, \mu_m, \nu)\Big)^{-1}. \qquad (4.15)$$

The result for $\mathcal{M}_J$ in terms of the mass mode matching functions of the MMF approach is given in Eq. (4.52).

Each of the separate threshold corrections $\mathcal{M}_{\mathcal{J}}$ and $\mathcal{M}_{\mathscr{S}_c}$ now has a dependence on the rapidity renormalization scale ν, which can be used to resum the logarithms by evaluating them both at their respective natural rapidity scale that minimizes the logarithms and then run them to a common rapidity renormalization scale in a rapidity RG evolution. How this is related to the resummation of rapidity logarithms in the MMF scheme is discussed in Sec. 4.2.2. To further avoid large logarithms in virtuality the threshold correction should be evaluated at a scale $\mu_m \sim m$.

In Refs. [2, 11, 12] the jet function was not defined as a matching coefficient onto a theory containing collinear-soft modes only, but only as the collinear matrix element with the relevant subtractions from lower virtualities made as a zero-bin subtraction, see also the discussion after Eq. (3.10) and Eq. (2.76). We will now briefly discuss how the jet function in the UF approach can be defined also in that way. To avoid double counting and make sure that the massive jet function has the correct massless limit in the $\overline{\text{MS}}$ scheme, any non-vanishing regions in the integrals contributing to the jet function from virtualities lower than the jet scale must be subtracted. In the MMF scheme the massive quark was integrated out at the jet scale when its mass was of the order of the jet scale, such that it did not contribute to the soft function that then contained only purely massless quarks. Therefore also the zero-bin subtractions in the jet function, that should remove any double counting with the soft function, had to be done only for the n_l massless quarks in the jet function. But in the UF scheme also the massive flavor contributes to the soft function because it is never integrated out, such that in this case the subtractions in the jet function must also account for the contributions from the massive quark.

The collinear matrix element is evaluated with the normal collinear scaling

$$k^+ \sim s/Q, \qquad k^- \sim Q, \qquad k_\perp^2 \sim k^+ k^- \sim s, \qquad (4.16)$$

and the only region with lower virtuality that does not lead to scaleless or power suppressed integrals is[2]

$$k^+ \sim s/Q \,, \qquad k^- \ll Q \,, \qquad k_\perp^2 \sim k^+ k^- \ll s \,. \qquad (4.17)$$

Because we want to keep the full mass dependence, regardless of the scaling of the mass with respect to the other scales, we never do an expansion in the mass m in the integrands, i.e. in the calculation we always treat the mass as if it had the scaling $m^2 \sim k^2$, even if we are in a scenario where $m^2 \gg s$ or $m^2 \ll s$, such that no expansion in m is done. While expanding the integrands in the loop momenta using the scaling in Eq. (4.17) leads only to scaleless integrals in the massless case, which corresponds to the standard zero-bin subtractions, in the massive case this is no longer true and and we get non-trivial contributions that need to be subtracted to get a jet function that correctly includes the full mass dependence. When doing this with the massive quark contributions renormalized either in the $\overline{\text{MS}}$ or OS scheme, this leads to the same jet functions as the definition in Eq. (4.12), because the subtraction terms arising when expanding for the scaling in Eq. (4.17) in the massive case are identical to the collinear-soft matrix element.

In order to resum rapidity logarithms in the threshold correction $\mathcal{M}_J$, it needs to be factorized into two separate parts that get contributions from different regions in rapidity. In the definition of the jet function as in Eq. (4.12) those were coming from the collinear and collinear-soft matrix elements in Eqs. (3.8) and (3.11), leading to the factorized form of $\mathcal{M}_J$ as in Eq. (4.15). These are each by themselves matrix elements of gauge invariant operators, that get renormalized separately and can then be evolved in a RG running. In the case where the jet function is defined as the collinear matrix element with the subtractions from lower momentum regions as a zero-bin subtraction as discussed above, the threshold corrections can be factorized into contributions coming from the naive collinear matrix element and contributions coming from the subtractions. In order to do so both contributions must be renormalized separately, with the rapidity divergences, that cancel only in combination of contributions from the massive flavor, absorbed into two separate counterterms. One counterterm for the contributions coming from the pure collinear matrix element in Eq. (3.8) without subtractions, and one counterterm for the contributions coming from the subtraction when using the scaling in Eq. (4.17). In this way one does not renormalize two separate gauge-invariant operators, but rather assigns an individual counterterm to the contributions coming from a specific region in an integral. In this way one can define rapidity anomalous dimensions for the unsubtracted matrix element and the zero-bin subtractions and the rapidity logarithms can be resummed in a rapidity RG evolution, analogous to the definition with the collinear-soft matrix elements in Eq. (4.15). Because the results of the zero-bin subtractions for massive quarks are the same as for the csoft matrix elements for massive quarks, this results in the same form of the resummed threshold correction $\mathcal{M}_J$.

4.1.2 Virtuality-dependent beam function

The discussion of the virtuality-dependent beam function is similar to that of the jet function in the previous section. The difference in the definition of the beam function matching coefficient $\mathcal{I}$ with massive quarks compared to the MMF case in Eq. (2.90) is again that the massive flavor is never

---

[2]In Ref. [11] the subtraction was made using the scaling

$$k^+ \sim m \,, \qquad k^- \sim m \,, \qquad k_\perp^2 \sim k^+ k^- \sim m^2 \,,$$

what was called a soft mass mode bin subtraction, with the additional change in the scaling of the invariant mass of the jet to $s \sim mQ$. This leads to exactly the same integrals after doing the expansion and therefore also the same result for the jet function, but conceptually is not the correct region to subtract. This should instead be the collinear-soft region at a lower virtuality as in Eq. (4.17). Indeed, without the somewhat artificial change of the scaling of the jet invariant mass s, the soft mass mode bin subtraction does not give non-vanishing contributions and is therefore considered not relevant in the light of our discussion here.

integrated out, i.e. also the csoft matrix elements and the PDFs contain the full $n_l + 1$ flavors, and only the renormalization scheme for the heavy flavor is changed

$$\mathscr{B}_i^{\mathrm{OS}}(t, m, x, \mu) = \sum_{k \in \{q, \bar{q}, g\}} \int \mathrm{d}\ell \, \mathcal{I}_{ik}^{\mathrm{OS}}(t - \omega\ell, m, x, \mu) \otimes_x f_k^{\mathrm{OS}}(x, m, \mu)$$
$$\times \, \mathscr{S}_c^{\mathrm{OS}}(\ell, m, \mu) \,,$$
$$\mathscr{B}_i^{\overline{\mathrm{MS}}}\left(t, m, x, \mu, \frac{\nu}{\omega}\right) = \sum_{k \in \{q, \bar{q}, g\}} \int \mathrm{d}\ell \, \mathcal{I}_{ik}^{\overline{\mathrm{MS}}}(t - \omega\ell, m, x, \mu) \otimes_x f_k^{\overline{\mathrm{MS}}}(x, m, \mu)$$
$$\times \, \mathscr{S}_c^{\overline{\mathrm{MS}}}(\ell, m, \mu, \nu) \,. \tag{4.18}$$

The dependence on the rapidity renormalization scale ν cancels between the collinear and the collinear-soft matrix elements such that $\mathcal{I}$ is independent of ν for both the OS and the $\overline{\mathrm{MS}}$ subtraction schemes for the massive quark. The matching coefficients $\mathcal{I}$ defined in this way have the correct massless limit when using the $\overline{\mathrm{MS}}$ subtractions and the correct decoupling limit when using the OS subtractions for the massive flavor. In both cases they are free of rapidity logarithms.

Remember that the csoft modes eventually only manifest themselves as part of the soft function, such that the RG running in the collinear sector is caused only by the matching coefficients $\mathcal{I}$ and the PDFs f. The relevant threshold correction, that encodes the change of the renormalization scheme in the functions that contribute to the running in the collinear sector, that one needs to calculate is therefore that of the beam function with subtraction from csoft contributions already made, i.e. $B = \mathscr{B} \otimes \mathscr{S}_c^{-1} = \mathcal{I} \otimes_x f$, which is also the function that appears in the factorization theorem. The threshold correction to the light quark beam function $\mathcal{M}_B$ contains rapidity logarithms from secondary massive quarks of the form $\ln(t/m^2)$ that can be resummed in a similar manner as for the jet function threshold correction by splitting it into contributions coming from only the purely collinear matrix element and from the csoft matrix element

$$\mathcal{M}_{\mathscr{B}}^+\left(t, m, x, \mu_m, \frac{\nu}{\omega}\right) = \int \mathrm{d}t' \, \mathscr{B}^{\overline{\mathrm{MS}}}\left(t - t', m, x, \mu_m, \frac{\nu}{\omega}\right)\left(\mathscr{B}^{\mathrm{OS}}(t', m, x, \mu_m)\right)^{-1} \,, \tag{4.19}$$

such that

$$\mathcal{M}_B^{\pm}(t, m, x, \mu_m) = \int \mathrm{d}\ell \, \mathcal{M}_{\mathscr{B}}^{\pm}\left(t - \omega\ell, m, x, \mu_m, \frac{\nu}{\omega}\right)\left(\mathcal{M}_{\mathscr{S}_c}^{\pm}(\ell, m, \mu_m, \nu)\right)^{-1} \,, \tag{4.20}$$

with $\mathcal{M}_{\mathscr{S}_c}$ as in Eq. (4.14). The result for $\mathcal{M}_B$ in terms of the mass mode matching functions of the MMF approach is given in Eq. (4.52). The logarithms are resummed in an rapidity RG evolution of the threshold corrections $\mathcal{M}_{\mathscr{B}}$ and $\mathcal{M}_{\mathscr{S}_c}$, each from its natural rapidity scale to a common renormalization scale.

Also for the beam function one can define the matching coefficient $\mathcal{I}_{ik}$ and the threshold corrections $\mathcal{M}_B^{\pm}$ with zero-bin subtractions in the spirit of the calculations in Refs. [2,11,12] instead of a matching on collinear-soft modes, see also the discussion after Eq. (2.76). The definition that leads to the identical matching coefficients $\mathcal{I}_{ik}$ then reads

$$B_i^{\mathrm{OS}}(t, m, x, \mu) = \sum_{k \in \{q, \bar{q}, g\}} \mathcal{I}_{ik}^{\mathrm{OS}}(t, m, x, \mu) \otimes_x f_k^{\mathrm{OS}}(x, m, \mu) \,,$$
$$B_i^{\overline{\mathrm{MS}}}(t, m, x, \mu) = \sum_{k \in \{q, \bar{q}, g\}} \mathcal{I}_{ik}^{\overline{\mathrm{MS}}}(t, m, x, \mu) \otimes_x f_k^{\overline{\mathrm{MS}}}(x, m, \mu) \,, \tag{4.21}$$

with B defined with subtractions to avoid double counting with the soft region.

The beam function without subtractions with partonic initial states is evaluated with the normal collinear scaling

$$k^+ \sim t/\omega \,, \qquad k^- \sim \omega \,, \qquad k_\perp^2 \sim k^+ k^- \sim t \,, \tag{4.22}$$

where we keep again the full mass dependence in the calculation, irregardless of the scaling of the mass with respect to the loop momentum, i.e. effectively always treating the mass as $m^2 \sim k^2$.

For primary massive quarks at one-loop, i.e. B_Q, the only other region that does not lead to vanishing or power suppressed contributions is

$$ k^+ \ll t/\omega \,, \qquad k^- \sim \omega \,, \qquad k_\perp^2 \sim k^+ k^- \ll t \,. \qquad (4.23) $$

This corresponds to the collinear region of lower virtuality that is already covered by the PDF and must therefore *not* be subtracted again, because it is already subtracted from the matching coefficient when matching the full beam function onto the PDF, such that no double counting takes place.

For secondary massive quarks at two-loops, i.e. corrections from the heavy flavor to the light quark beam function B_q, one can identify different regions of lower virtuality that lead to non-vanishing and non-suppressed contributions

$$
\begin{aligned}
k^+ &\ll t/\omega \,, & k^- &\sim \omega \,, & k_\perp^2 &\sim k^+ k^- \ll t \,, \\
k^+ &\sim t/\omega \,, & k^- &\ll \omega \,, & k_\perp^2 &\sim k^+ k^- \ll t \,.
\end{aligned} \qquad (4.24)
$$

The first corresponds again to collinear fluctuations covered already by the PDF and does not need to be subtracted again. The second corresponds to regions that have an overlap with the soft region and must be subtracted to avoid double counting between the beam and the soft function. Subtracting this region from the beam function leads to identical beam function matching coefficients $\mathcal{I}_{ik}$ in Eqs. (4.18) and (4.21) and also to the same threshold corrections $\mathcal{M}_B^\pm$. In the massless case these contributions are scaleless and correspond to the standard zero-bin subtractions.

The resummation of rapidity logarithms in the threshold correction to the light quark beam function $\mathcal{M}_B$ defined with these subtraction can again be achieved by renormalizing and evolving the subtractions from the soft regions in the integrals separately, as it was the case also for the jet function in the previous section.

4.1.3 Hard function

The hard function in the UF scheme is always the matching coefficient for a matching between the QCD and the SCET currents with all $n_l + 1$ flavors, in contrast to the MMF scheme where the numbers of flavors on the two sides of the matching relation depended on the relative scaling of the quark mass and the hard scale $\mu_H \sim Q$. In the UF scheme only the renormalization scheme for the massive quark is changed between the OS and $\overline{\text{MS}}$ subtractions, depending on whether $m > \mu_H$ or $m < \mu_H$

$$
\begin{aligned}
J_{\text{QCD}}(Q, m, \mu) &= C^{\text{OS}}(Q, m, \mu) \times J_{\text{SCET}}^{\text{OS}}(Q, m, \mu) \,, \\
J_{\text{QCD}}(Q, m, \mu) &= C^{\overline{\text{MS}}}(Q, m, \mu) \times J_{\text{SCET}}^{\overline{\text{MS}}}(Q, m, \mu) \,,
\end{aligned} \qquad (4.25)
$$

with $H(Q, m, \mu) = |C(Q, m, \mu)|^2$. The full QCD vector current form factor J_{QCD} is UV finite and does not require an additional counterterm.

Since the SCET current gets correction only from purely virtual contributions that do not vanish in the heavy quark limit, all contributions from the massive flavor are absorbed into the counterterm when using the OS subtraction scheme, i.e. $J_{\text{SCET}}^{\text{OS}}(Q, m, \mu) = J_{\text{SCET}}^{(n_l)}(Q, \mu)$. We recall that the contributions from massless flavors are always renormalized in the $\overline{\text{MS}}$ scheme. The two resulting hard functions $H^{\text{OS}}(Q, m, \mu)$ and $H^{\overline{\text{MS}}}(Q, m, \mu)$ are then independent of any rapidity renormalization scale and free of rapidity logarithms and have the correct decoupling and massless limit respectively. They are related by the threshold correction $\mathcal{M}_H$, defined as the ratio of the hard function in the two different renormalization schemes. In fact the QCD current cancels in that ratio, such that the

threshold correction for the hard function is just the ratio of the SCET current in the OS and the $\overline{\text{MS}}$ scheme

$$\mathcal{M}_H^+(Q, m, \mu_m) = \left| \frac{J_{\text{SCET}}^{\text{OS}}(Q, m, \mu_m)}{J_{\text{SCET}}^{\overline{\text{MS}}}(Q, m, \mu_m)} \right|^2 , \tag{4.26}$$

and as always $\mathcal{M}_H^- = (\mathcal{M}_H^+)^{-1}$. The result for $\mathcal{M}_H$ in terms of the mass mode matching functions of the MMF approach is given in Eq. (4.52). It contains rapidity logarithms of the form $\ln(m^2/Q^2)$ that become large and need to be resummed to all orders when $m \ll Q$. They can be resummed by factorizing the threshold correction into three factors by splitting the full SCET current into contributions coming from the different collinear and soft sectors $J_{\text{SCET}} = J_{\text{SCET,n}} \times J_{\text{SCET,\bar{n}}} \times J_{\text{SCET,s}}$, such that the threshold correction $\mathcal{M}_H^\pm$ can be written as

$$\mathcal{M}_H^\pm(Q, m, \mu_m) = \mathcal{M}_{H_c}^\pm\left(Q, m, \mu_m, \frac{\nu}{Q}\right) \times \mathcal{M}_{H_c}^\pm\left(Q, m, \mu_m, \frac{\nu}{Q}\right) \times \mathcal{M}_{H_s}^\pm(Q, m, \mu_m, \nu) , \tag{4.27}$$

where each $\mathcal{M}_{H_i}$ is a current threshold correction as in Eq. (4.26), but only with contributions from one single collinear or soft sector.[3] Each of these threshold corrections in the different sectors now has an explicit dependence on the rapidity renormalization scale ν that cancels only in the sum of all three of them, such that the full threshold correction for the hard function is independent of ν. The rapidity logarithms can then be resummed in an rapidity RG evolution of these three separate threshold corrections.

4.1.4 PDF in the endpoint

The PDF is a non-perturbative object that cannot be calculated in perturbation theory, but since its dependence on the renormalization scale can be determined perturbatively, also its threshold correction in the endpoint region $\mathcal{M}_\phi$, that encodes the scheme change from renormalizing the heavy flavor in the PDF in the limit $x \to 1$ with OS and $\overline{\text{MS}}$ subtractions, can be calculated perturbatively by evaluating the PDF operator in Eq. (3.15) with partonic initial states. The resulting threshold correction contains rapidity logarithms of the form $\ln(1 - x)$ that need to be resummed to all orders because we are assuming the limit $(1 - x) \ll 1$.

The resummation of these logarithms has been achieved in Ref. [2]. The full threshold correction can be split into two parts that get contributions from different rapidity scales by separating the PDF into a collinear and a soft matrix element (or likewise a $\bar{n}$-csoft matrix element, see the discussion after Eq. (3.40)) as in Eq. (3.16). The individual threshold corrections for these two functions are then defined as

$$\mathcal{M}_g^+\left(\ell, m, \mu_m, \frac{\nu}{Q}\right) = \int \mathrm{d}\ell' \, g_{q/q}^{\overline{\text{MS}}}\left(\ell - \ell', m, \mu_m, \frac{\nu}{Q}\right) \left(g_{q/q}^{\text{OS}}(\ell', m, \mu_m)\right)^{-1} ,$$

$$\mathcal{M}_{\mathscr{S}}^+(\ell, m, \mu_m, \nu) = \int \mathrm{d}\ell' \, \mathscr{S}^{\overline{\text{MS}}}(\ell - \ell', m, \mu_m, \nu) \left(\mathscr{S}^{\text{OS}}(\ell', m, \mu_m)\right)^{-1} , \tag{4.28}$$

with the collinear and the soft matrix elements defined in Eqs. (3.17) and (3.18), respectively, such that

$$\mathcal{M}_\phi^\pm(1 - z, m, \mu_m) = Q \int \mathrm{d}\ell \, \mathcal{M}_g^\pm\left(Q(1 - z) - \ell, m, \mu_m, \frac{\nu}{Q}\right) \mathcal{M}_{\mathscr{S}}^\pm(\ell, m, \mu_m, \nu) . \tag{4.29}$$

The result for $\mathcal{M}_\phi$ in terms of the mass mode matching functions of the MMF approach is given in Eq. (4.52). The collinear and the soft threshold corrections $\mathcal{M}_g$ and $\mathcal{M}_{\mathscr{S}}$ can then both be first evaluated at their natural rapidity scale that minimizes the logarithms and then evolved to a common rapidity renormalization scale.

---

[3]We remind the reader the fact that the threshold corrections for n- and the $\bar{n}$-collinear sector take the form only holds for the case of a symmetric rapidity regulator.

4.1.5 Thrust soft function

The (beam) thrust soft function with the massive quark corrections renormalized in either the OS or $\overline{\text{MS}}$ scheme automatically encodes all mass corrections. It has the correct decoupling limit in the OS scheme and the correct massless limit in the $\overline{\text{MS}}$ scheme, without any further matching because the soft function is already free of IR divergences. The threshold correction $\mathcal{M}_S$, defined as in Eq. (4.5), contains rapidity logarithms of the form $\ln(\ell/m)$, that become large and need to be resummed when the mass scale is much larger then the soft scale. In Ref. [11, 12] this resummation was achieved by splitting the full soft function into different contributions coming from virtual radiation and real radiation in the two different hemispheres[4]. Then the threshold corrections of these, defined in the usual way as the ratio of the OS and $\overline{\text{MS}}$ contributions, can be calculated separately such the threshold correction for the full soft function can be written as

$$\mathcal{M}_S(\ell, m, \mu_m) = \int d\ell_a d\ell_b \, \mathcal{M}_{S_{r_a}}(\ell_a, m, \mu_m, \nu) \mathcal{M}_{S_{r_b}}(\ell_b, m, \mu_m, \nu) \mathcal{M}_{S_v}(\ell - \ell_a - \ell_b, m, \mu_m, \nu) \,. \quad (4.30)$$

The result for $\mathcal{M}_S$ in terms of the mass mode matching functions of the MMF approach is given in Eq. (4.52).

The threshold corrections from the real radiation in the two hemispheres $\mathcal{M}_{S_{r_a}}$ (from real radiation contributions where both heavy quarks are radiated into hemisphere a) and $\mathcal{M}_{S_{r_b}}$ (from real radiation contributions where both heavy quarks are radiated into hemisphere b) and the threshold correction coming from the purely virtual contributions $\mathcal{M}_{S_v}$ have different natural rapidity scales ν, such that an incomplete cancellation of these logarithms when evaluated at fixed order leads to a rapidity logarithms of the form $\ln(\ell/m)$ in the full soft function threshold correction $\mathcal{M}_S$. When each threshold correction is first evaluated at its natural rapidity scale that minimizes the logarithms and then evolved to a common rapidity renormalization scale, these logarithms are resummed in the rapidity RG running.

This means that in the UF approach different real and virtual corrections to the soft function need to be renormalized separately and then evolved with their own anomalous dimension in rapidity. That is in contrast to the MMF approach where all the mass mode matching functions that are evolved in rapidity are defined as matching coefficients between matrix elements of well-defined gauge invariant operators.

4.1.6 TMD beam and soft functions

We will now discuss how the transverse momentum dependent functions, the beam and the soft function, are implemented in an UF setup. Also for these SCET_{II} type functions the UF scheme can provide a convenient way for getting the full mass dependence without any additional massive power corrections by switching between the OS and $\overline{\text{MS}}$ subtractions. Since the TMD functions are rapidity divergent already in the massless case, the dependence on the rapidity renormalization scale ν is intrinsic to them and not only a feature of the secondary massive quark corrections. Also the threshold corrections $\mathcal{M}_i$ for the TMD functions show this explicit ν-dependence. It is, however, possible to construct an object as a combination of both the TMD soft and beam function that is free of rapidity divergences and for which also the threshold correction is independent of the rapidity scale, see below. In this way the resummation of rapidity logarithms related only to the secondary massive quark effects can be performed in the threshold correction, in a similar way as for the SCET_{I} type functions discussed before.

---

[4]There are also virtual-real contributions, but they are purely massless at two-loops and therefore cancel in the threshold correction, because contributions from massless quark are always renormalized in the $\overline{\text{MS}}$ scheme. There are further contributions from secondary massive quarks where the two quarks go into different hemispheres, but also these cancel in the threshold correction because these real radiation effects of massive particles automatically decouple in the heavy quark limit, which means they are equivalent, both when using the OS and $\overline{\text{MS}}$ subtractions.

For the TMD beam function the definitions of the matching coefficient $\mathcal{I}$ with the different subtraction schemes for contributions form massive quarks are

$$B_i^{\mathrm{OS}}\left(\vec{p}_T, m, x, \mu, \frac{\nu}{Q}\right) = \sum_{k \in \{q, \bar{q}, g\}} \mathcal{I}_{ik}^{\mathrm{OS}}\left(\vec{p}_T, m, x, \mu, \frac{\nu}{Q}\right) \otimes_x f_k^{\mathrm{OS}}(x, m, \mu),$$

$$B_i^{\overline{\mathrm{MS}}}\left(\vec{p}_T, m, x, \mu, \frac{\nu}{Q}\right) = \sum_{k \in \{q, \bar{q}, g\}} \mathcal{I}_{ik}^{\overline{\mathrm{MS}}}\left(\vec{p}_T, m, x, \mu, \frac{\nu}{Q}\right) \otimes_x f_k^{\overline{\mathrm{MS}}}(x, m, \mu). \tag{4.31}$$

The matching coefficients $\mathcal{I}$ then have the correct massless limit when using the $\overline{\mathrm{MS}}$ subtractions and the correct decoupling limit when using the OS subtractions.

Since this is a $\mathrm{SCET_{II}}$ setup there is no soft scale of lower virtuality that could inflict some double counting with the beam function as we found it for the virtuality-dependent beam function. Therefore no subtractions from these regions need to be made. This is also visible by expanding the integrals that contribute to the massive beam function. The only momentum region other than the normal collinear one that gives non-scaleless and non-suppressed integrals is

$$k^+ \ll p_T/\omega, \qquad k^- \sim \omega, \qquad k_\perp^2 \sim k^+ k^- \ll p_T^2, \tag{4.32}$$

in both the primary and the secondary massive beam function. This corresponds to the collinear region of lower virtuality that is already covered by the PDF, such that no additional subtraction needs to be made since no double counting is made in $\mathcal{I}$.

The threshold correction for the beam function $\mathcal{M}_B$, defined as in Eq. (4.5), contains an explicit dependence on the rapidity renormalization scale ν coming from secondary massive quark contributions, because in contrast to the virtuality-dependent beam function (after subtraction of the collinear-soft contributions) the TMD beam function has an explicit ν-dependence that does not exactly cancel between the OS and the $\overline{\mathrm{MS}}$ scheme. This leaves a threshold correction of the form $\mathcal{M}_B\left(\vec{p}_T, m, x, \mu_m, \frac{\nu}{\omega}\right)$, where the ν-dependence cancels only against the threshold correction of the soft function $\mathcal{M}_S(\vec{p}_T, m, \mu_m, \nu)$. The results for $\mathcal{M}_B$ and $\mathcal{M}_S$ in terms of the mass mode matching functions of the MMF approach are given in Eq. (4.52).

The threshold corrections of the TMD beam and soft functions $\mathcal{M}_B$ and $\mathcal{M}_S$ have different natural rapidity scales, which means that the ν dependence in the logarithms cancels when the two are combined but the cancellation of the rapidity logarithms is not complete and leaves logarithms of the form $\ln(m^2/Q^2)$, that need to be resummed when $m^2 \ll Q^2$. These can be resummed by first evaluating each threshold correction at its natural rapidity scale and then evolving both to a common rapidity renormalization scale. In this way one gets a resummed threshold correction when combining them, that is by consistency of RG running just the same as the one for the hard function $\mathcal{M}_H$. But because of the explicit ν-dependence it is not possible to have a resummed threshold correction for the individual beam or soft functions, what has been a feature of the UF scheme for the $\mathrm{SCET_I}$ type functions so far.

But it is possible to construct what is called the TMDPDF[5]

$$f_i^{\mathrm{TMD}}(\vec{p}_T, m, x, \omega, \mu) = \int \mathrm{d}^2 p_T' \, B_i\left(\vec{p}_T - \vec{p}_T', m, x, \mu, \frac{\nu}{\omega}\right) \sqrt{S(\vec{p}_T', m, \mu, \nu)}, \tag{4.33}$$

where the root is defined in the sense that

$$\int \mathrm{d}^2 p_T' \sqrt{S(\vec{p}_T - \vec{p}_T', m, \mu, \nu)} \sqrt{S(\vec{p}_T', m, \mu, \nu)} = S(\vec{p}_T, m, \mu, \nu), \tag{4.34}$$

---

[5]In literature sometimes also the collinear matrix element B_i is referred to as the TMDPDF and the distinction between B_i and f_i^{TMD} is not always clearly made. We use the language following e.g. Ref. [57] and strictly call B_i the TMD beam function and only f_i^{TMD} defined as in Eq. (4.33) the TMDPDF.

which leads to a single function that is free of rapidity divergences and independent of the rapidity scale ν. The threshold correction of this TMDPDF is then also independent of ν, and the rapidity logarithms it contains can be resummed between the different contributions from the beam and the soft function. In this way one can achieve to have one universal function that is resummed in rapidity in the UF scheme, analogous to the SCET$_\mathrm{I}$ cases.

4.2 Relation between the two approaches

We will now compare the MMF approach in Sec. 3.2 and the UF approach for DIS in the endpoint region and discuss where they differ and in which sense they are equivalent. Here we will only discuss the relation between the two approaches for DIS in the endpoint region as an example, but the situation is similar for exclusive Drell-Yan (see chapter 2) and thrust in $e^+e^- \to 2$ jets in the peak region (see appendix A).

4.2.1 Power corrections in the mass mode factorization scheme

So far, in the MMF approach for Drell-Yan in chapter 2 and for DIS in Sec. 3.2, we only kept the full mass dependence in the various functions in the factorization theorems in the case that $m \sim \mu_i$, where μ_i is the natural scale of that function, i.e. the scale that minimizes all logarithms. Otherwise we always neglected power corrections of the form m^2/μ_i^2 whenever we assumed the hierarchy $m \ll \mu_i$ and corrections of the form μ_i^2/m^2 for $\mu_i \ll m$, by always using the massless hard, beam, jet or soft function in either the $n_l + 1$ or n_l flavor scheme. This approach does not provide a smooth transition from one hierarchy to another, because each of those factorization theorems is only valid in the strict hierarchy of the scales it was derived for. This is one of the differences of the MMF approach as presented above compared to the UF, where we were able to always keep the full mass dependence.

In this section we discuss how to include these massive power corrections in the MMF approach and thereby keep the full mass dependence and achieve a smooth transition between all hierarchies for the example of DIS in the endpoint region as discussed in Sec. 3.2. It is straightforward to do the same for the factorization theorems for Drell-Yan discussed in Secs. 2.1 and 2.2, and the results will be presented at the end of this section.

For convenience of the reader we write down again the factorization theorems including the secondary mass effects (remember that we do not deal with primary mass effects for DIS) for the different

hierarchies for DIS in the endpoint region

$\underline{Q \ll m\ :}$
$$F_1(x,m,Q) = \frac{1}{2} \sum_{i \in \{q,\bar{q}\}} \hat{H}_i^{(n_l)}(Q,\mu) \int ds\, J^{(n_l)}(s,\mu)\, \phi_i^{(n_l)}\Big(1-x-\frac{s}{Q^2},\mu\Big), \qquad (4.35)$$

$\underline{m \sim Q\ :}$
$$F_1(x,m,Q) = \frac{1}{2} \sum_{i \in \{q,\bar{q}\}} \hat{H}_i(Q,m,\mu) \int ds\, J^{(n_l)}(s,\mu)\, \phi_i^{(n_l)}\Big(1-x-\frac{s}{Q^2},\mu\Big), \qquad (4.36)$$

$\underline{Q\sqrt{1-x} \ll m \ll Q\ :}$
$$F_1(x,m,Q) = \frac{1}{2} \sum_{i \in \{q,\bar{q}\}} \hat{H}_i^{(n_l+1)}(Q,\mu) H_c\Big(m,\mu,\frac{\nu}{Q}\Big) H_c\Big(m,\mu,\frac{\nu}{Q}\Big) H_s(m,\mu,\nu)$$
$$\times \int ds\, J^{(n_l)}(s,\mu)\, \phi_i^{(n_l)}\Big(1-x-\frac{s}{Q^2},\mu\Big), \qquad (4.37)$$

$\underline{m \sim Q\sqrt{1-x}\ :}$
$$F_1(x,m,Q) = \frac{1}{2} \sum_{i \in \{q,\bar{q}\}} \hat{H}_i^{(n_l+1)}(Q,\mu) H_c\Big(m,\mu,\frac{\nu}{Q}\Big) H_s(m,\mu,\nu)$$
$$\times \int ds\, J\Big(s,m,\mu,\frac{\nu}{Q}\Big) \phi_i^{(n_l)}\Big(1-x-\frac{s}{Q^2},\mu\Big), \qquad (4.38)$$

$\underline{m \ll Q\sqrt{1-x}\ :}$
$$F_1(x,m,Q) = \frac{1}{2} \sum_{i \in \{q,\bar{q}\}} \hat{H}_i^{(n_l+1)}(Q,\mu) H_c\Big(m,\mu,\frac{\nu}{Q}\Big) H_s(m,\mu,\nu)$$
$$\times \int ds\, d\ell\, J^{(n_l+1)}(s,\mu)\, \mathcal{S}_c(\ell,m,\mu,\nu)\, \phi_i^{(n_l)}\Big(1-x-\frac{s}{Q^2}-\frac{\ell}{Q},\mu\Big). \qquad (4.39)$$

The factorization theorems in Eqs. (4.35), (4.37) and (4.39), valid whenever the mass scale is clearly separated from all the other scales, resum all logarithms between the mass and the other scales that need to be considered large in these hierarchies with widely separated scales. But they only use the massless hard and jet functions, either in the n_l or the n_l+1 scheme depending on whether the mass is above or below the hard or jet scale, and therefore do not include power corrections of the form $\mathcal{O}\big(\frac{Q^2}{m^2}, \frac{Q^2\sqrt{1-x}}{m^2}\big)$ when the mass becomes larger than the hard or the jet scale, and terms of the form $\mathcal{O}\big(\frac{m^2}{Q^2}, \frac{m^2}{Q^2\sqrt{1-x}}\big)$ when the mass becomes small. Therefore these factorization theorems can only be used in the strict hierarchies for which they were derived.

On the other hand as was shown in Sec. 3.2, the factorization theorems in Eqs. (4.36) and (4.38) do include all these terms correctly for the hard function when $m \sim Q$ and the jet function when $m \sim Q\sqrt{1-x}$, respectively. But they can not resum logarithms of the form $\log\big(Q^2/m^2\big)$ in the case of Eq. (4.36) and logarithms of the form $\log\big(Q^2(1-x)/m^2\big)$ in the case of Eq. (4.38), that become large if the mass scale is widely separated from the hard or the jet scale. Consequently also those factorization theorems can only be applied in the strict hierarchy for which they were derived.

One can construct factorization theorems that smoothly connect those different hierarchies and are valid regardless of whether the mass is close to one of the other scales μ_i – which makes it suitable to keep the full mass dependence not neglecting terms of the form $\mathcal{O}\big(\mu_i^2/m^2\big)$ or $\mathcal{O}\big(m^2/\mu_i^2\big)$ – or whether

there is a large hierarchy between the mass and the other scale – which makes it necessary to resum logarithms of the form $\log\left(\mu_i^2/m^2\right)$ – that are therefore more in the spirit of the UF approach discussed in Sec. 4.1, but still keeping the advantage of the MMF approach, i.e. that all the threshold matching functions in the factorization theorem are matching coefficients between matrix elements containing quantum fluctuations at a single scale and (rapidity) logarithms are only resummed between several of these matching coefficients. To achieve this one simply has to add back the full mass dependence that is encoded in hard and jet functions appearing in the factorization theorems in Eq. (4.36) and (4.38) to the factorization theorems in Eqs. (4.35), (4.37) and (4.39).

To identify the missing power corrections one can look at the small and large mass limits of the massive hard and mass mode jet functions (for primary massless quarks), that were already discussed in Sec. 3.2.3. For example from Eq. (3.44) it can be seen that the mass mode jet function can be written in the form

$$J\left(s,m,\mu,\frac{\nu}{Q}\right) = \int \mathrm{d}s'\,\mathrm{d}\ell\, J^{(n_l+1)}(s-s'-Q\ell,\mu)\,\mathcal{S}_c(\ell,m,\mu,\nu)\,P_{J_{m<Q\sqrt{1-x}}}(s',m,\mu)\,, \qquad (4.40)$$

where $P_{J_{m<Q\sqrt{1-x}}}$ stands for the power corrections that vanish in the limit $m\to 0$. In order to write down a factorization theorem that resums all the logarithms and includes all the mass related power corrections, one can add the appropriate power corrections to the massless functions. We define the new hard and jet functions including the power corrections from secondary massive quarks as

$$\hat{H}_{m>Q}(Q,m,\mu) = \hat{H}^{(n_l)}(Q,\mu)\times P_{H_{m>Q}}(Q,m,\mu)\,,$$
$$\hat{H}_{m<Q}(Q,m,\mu) = \hat{H}^{(n_l+1)}(Q,\mu)\times P_{H_{m<Q}}(Q,m,\mu)\,,$$
$$J_{m>Q\sqrt{1-x}}(s,m,\mu) = \int \mathrm{d}s'\, J^{(n_l)}(s-s',\mu)P_{J_{m>Q\sqrt{1-x}}}(s',m,\mu)$$
$$J_{m<Q\sqrt{1-x}}(s,m,\mu) = \int \mathrm{d}s'\, J^{(n_l+1)}(s-s',\mu)P_{J_{m<Q\sqrt{1-x}}}(s',m,\mu)\,, \qquad (4.41)$$

where the P-functions are defined to contain only the power corrections in the respective limits

$$P_{H_{m>Q}}(Q,m,\mu) = 1 + \mathcal{O}\left(\frac{Q^2}{m^2}\right)\,,$$
$$P_{H_{m<Q}}(Q,m,\mu) = 1 + \mathcal{O}\left(\frac{m^2}{Q^2}\right)\,,$$
$$P_{J_{m>Q\sqrt{1-x}}}(s,m,\mu) = \delta(s)\left[1 + \mathcal{O}\left(\frac{s}{m^2}\right)\right]\,,$$
$$P_{J_{m<Q\sqrt{1-x}}}(s,m,\mu) = \delta(s)\left[1 + \mathcal{O}\left(\frac{m^2}{s}\right)\right]\,. \qquad (4.42)$$

Using Eqs. (3.42), (3.41), (3.43) and (3.44), where the large and small mass limits are discussed for the hard and jet functions, one finds the following solutions

$$\hat{H}_{m>Q}(Q,m,\mu) = \hat{H}(Q,m,\mu)\,,$$
$$\hat{H}_{m<Q}(Q,m,\mu) = \hat{H}(Q,m,\mu)H_c^{-1}\left(m,\mu,\frac{\nu}{Q}\right)H_c^{-1}\left(m,\mu,\frac{\nu}{Q}\right)H_s^{-1}(m,\mu,\nu)\,,$$
$$J_{m>Q\sqrt{1-x}}(s,m,\mu) = J\left(s,m,\mu,\frac{\nu}{Q}\right)H_c^{-1}\left(m,\mu,\frac{\nu}{Q}\right)\,,$$
$$J_{m<Q\sqrt{1-x}}(s,m,\mu) = \int \mathrm{d}\ell\, J\left(s-Q\ell,m,\mu,\frac{\nu}{Q}\right)\mathcal{S}_c^{-1}(\ell,m,\mu,\nu)\,, \qquad (4.43)$$

where the contributions from secondary massive quarks at order $\mathcal{O}(\alpha_s^2)$ to the hard and jet functions $\hat{H}$ and J that appear on the right-hand sides are given in Eqs. (C.6) and (C.27) and H_s, H_c and $\mathcal{S}_c$ in Eqs. (C.8), (C.10) and (C.32). The ν dependence of the functions on the right side of the equations

cancels. The massive hard and jet functions defined in this way have the same anomalous dimensions as their massless counterparts, with either n_l or $n_l + 1$ flavors, depending on whether the function below or above the mass scale is used

$$\mu \frac{\mathrm{d}}{\mathrm{d}\mu} \hat{H}_{m>Q}(Q, m, \mu) = \gamma_H^{(n_l)}(Q, \mu) \, \hat{H}_{m>Q}(Q, m, \mu) \,,$$

$$\mu \frac{\mathrm{d}}{\mathrm{d}\mu} \hat{H}_{m<Q}(Q, m, \mu) = \gamma_H^{(n_l+1)}(Q, \mu) \, \hat{H}_{m<Q}(Q, m, \mu) \,,$$

$$\mu \frac{\mathrm{d}}{\mathrm{d}\mu} J_{m>Q\sqrt{1-x}}(s, m, \mu) = \int \mathrm{d}s' \, \gamma_J^{(n_l)}(s - s', \mu) \, J_{m>Q\sqrt{1-x}}(s', m, \mu) \,,$$

$$\mu \frac{\mathrm{d}}{\mathrm{d}\mu} J_{m<Q\sqrt{1-x}}(s, m, \mu) = \int \mathrm{d}s' \, \gamma_J^{(n_l+1)}(s - s', \mu) \, J_{m<Q\sqrt{1-x}}(s', m, \mu) \,. \qquad (4.44)$$

Here γ_H and γ_J are the anomalous dimensions of the massless hard and the jet functions, with the contributions at order $\mathcal{O}(\alpha_s)$ and $\mathcal{O}(\alpha_s^2 C_F T_F)$ given in Eqs (B.3) and (B.20). All these functions have the correct limiting behavior in the small and large mass limit

$$\hat{H}_{m>Q}(Q, m, \mu) = \hat{H}^{(n_l)}(Q, \mu) + \mathcal{O}\Big(\frac{Q^2}{m^2}\Big) \,,$$

$$\hat{H}_{m<Q}(Q, m, \mu) = \hat{H}^{(n_l+1)}(Q, \mu) + \mathcal{O}\Big(\frac{m^2}{Q^2}\Big) \,,$$

$$J_{m>Q\sqrt{1-x}}(s, m, \mu) = J^{(n_l)}(s, \mu) \times \Big(1 + \mathcal{O}\Big(\frac{s}{m^2}\Big)\Big) \,,$$

$$J_{m<Q\sqrt{1-x}}(s, m, \mu) = J^{(n_l+1)}(s, \mu) \times \Big(1 + \mathcal{O}\Big(\frac{m^2}{s}\Big)\Big) \,, \qquad (4.45)$$

and do not contain any large logarithms when evaluated at their respective natural scale

$$\mu_H \sim Q \,, \qquad \mu_J \sim Q\sqrt{1-x} \,. \qquad (4.46)$$

In this way we do not need to treat the situations where the mass scale is widely separated from one of the kinematic scales, like $m \ll \mu_i$, separately from the case where the mass becomes of the same order of that scale $m \lesssim \mu_i$, but only need to distinguish three scenarios:

Scenario I: $Q < m$:

$$F_1(x, Q) = \frac{1}{2} \sum_{i \in \{q, \bar{q}\}} \hat{H}_{i, m>Q}(Q, m, \mu) \times \int \mathrm{d}s \, J_{m>Q\sqrt{1-x}}(s, m, \mu) \, \phi_i^{(n_l)}\Big(1 - x - \frac{s}{Q^2}, \mu\Big) \qquad (4.47)$$

The functions $\hat{H}_{m>Q}$ and $J_{m>Q\sqrt{1-x}}$ have the same anomalous dimensions as the massless hard and jet functions for n_l dynamical flavors. The same holds for the PDF.

Scenario II: $Q\sqrt{1-x} < m < Q$:

$$F_1(x, Q) = \frac{1}{2} \sum_{i \in \{q, \bar{q}\}} \hat{H}_{i, m<Q}(Q, m, \mu) H_c\Big(m, \mu, \frac{\nu}{Q}\Big) H_c\Big(m, \mu, \frac{\nu}{Q}\Big) H_s(m, \mu, \nu)$$

$$\times \int \mathrm{d}s \, J_{m>Q\sqrt{1-x}}(s, m, \mu) \, \phi_i^{(n_l)}\Big(1 - x - \frac{s}{Q^2}, \mu\Big) \qquad (4.48)$$

The functions $\hat{H}_{m<Q}$ and $J_{m>Q\sqrt{1-x}}$ have the same anomalous dimensions as the massless hard and jet functions with $n_l + 1$ and n_l dynamical flavors, respectively. Again the effects of the μ-running of the mass mode matching functions H_s and H_c are most conveniently taken into account by running only the hard and jet functions and the PDF, but with $n_l + 1$ active flavors above and with n_l active

flavors below the mass scale (see Eq. (2.23)). The rapidity logarithms are resummed in the rapidity RG running of the matching functions H_s and H_c.

Scenario III: $m < Q\sqrt{1-x}$:

$$F_1(x,Q) = \frac{1}{2}\sum_{i\in\{q,\bar{q}\}} \hat{H}_{i,m<Q}(Q,m,\mu) H_s(m,\mu,\nu) H_c\left(m,\mu,\frac{\nu}{Q}\right)$$

$$\times \int ds\, d\ell\, J_{m<Q\sqrt{1-x}}(s,m,\mu)\, \mathcal{S}_c(\ell,m,\mu,\nu)\, \phi_i^{(n_l)}\left(1-x-\frac{s}{Q^2}-\frac{\ell}{Q},\mu\right) \quad (4.49)$$

The functions $\hat{H}_{m<Q}$ and $J_{m<Q\sqrt{1-x}}$ have the same anomalous dimensions as the massless hard and jet functions with n_l flavors. Again the effects of the μ-running of the mass mode matching functions H_s, H_c and $\mathcal{S}_c$ are most conveniently taken into account by running only the hard and jet functions and the PDF, but with $n_l + 1$ active flavors above and with n_l active flavors below the mass scale (see Eq. (3.36)). The rapidity logarithms are resummed in the rapidity RG running of the matching functions H_s, H_c and $\mathcal{S}_c$.

Using Eq. (4.45) it is easy to see that the factorization theorems in Eqs. (4.47)-(4.49) reduce to the ones in Eqs. (4.35) - (4.39) in the hierarchies $m \sim Q$, $Q\sqrt{1-x} \ll m \ll Q$, $m \sim Q\sqrt{1-x}$ and $m \ll Q\sqrt{1-x}$, for which the original factorization theorems where derived, plus power corrections that are formally small in these strict hierarchies (but can be non-negligible). In the factorization theorems in Eqs. (4.47)-(4.49) the same logarithmic terms are resummed since all functions have the same anomalous dimensions as before, but the massive hard and jet functions $H_{m\lessgtr Q}$ and $J_{m\lessgtr Q\sqrt{1-x}}$ have a smooth transition between the small and large mass limit and can therefore be used for an arbitrary scaling of the mass with respect to the other scales. In this way one can formulate the factorization theorem for the three different scenarios $Q < m$, $Q\sqrt{1-x} < m < Q$ and $m < Q\sqrt{1-x}$ with all mass related power corrections in the hard and jet functions included, such that no large hierarchies between the mass and the kinematic scales needs to be assumed.

In close analogy one can also define the soft and beam functions including the full mass dependence using the relation between the various function in the different hierarchies given in Sec. 2.1.6 and 2.2.5

$$S_{m>\mathcal{T}}(\ell,m,\mu) = H_s^{-1}(m,\mu,\nu)\int d\ell'd\ell''\, S(\ell-\ell'-\ell'',m,\mu)\mathcal{S}_c^{-1}(\ell',m,\mu,\nu)\mathcal{S}_c^{-1}(\ell'',m,\mu,\nu)\,,$$

$$S_{m<\mathcal{T}}(\ell,m,\mu) = S(\ell,m,\mu)\,,$$

$$S_{m>p_T}(\vec{p}_T,m,\mu,\nu) = S(\vec{p}_T,m,\mu,\nu)H_s^{-1}(m,\mu,\nu)\,,$$

$$S_{m<p_T}(\vec{p}_T,m,\mu,\nu) = S(\vec{p}_T,m,\mu,\nu)\,,$$

$$\mathcal{I}_{ik,m>\sqrt{Q\mathcal{T}}}(t,m,x,\mu) = \mathcal{I}_{ik}\left(t,m,x,\mu,\frac{\nu}{Q}\right)H_c^{-1}\left(m,\mu,\frac{\nu}{Q}\right)\,,$$

$$\mathcal{I}_{ik,m<\sqrt{Q\mathcal{T}}}(t,m,x,\mu) = \int d\ell\, \mathcal{I}_{ij}\left(t-Q\ell,m,x,\mu,\frac{\nu}{Q}\right)\mathcal{S}_c^{-1}(\ell,m,\mu,\nu)\otimes_x \mathcal{M}_{jk}^{-1}(x,m,\mu)\,,$$

$$\mathcal{I}_{ik,m>p_T}\left(\vec{p}_T,m,x,\mu,\frac{\nu}{Q}\right) = \mathcal{I}_{ik}\left(\vec{p}_T,m,x,\mu,\frac{\nu}{Q}\right)H_c^{-1}\left(m,\mu,\frac{\nu}{Q}\right)\,,$$

$$\mathcal{I}_{ik,m<p_T}\left(\vec{p}_T,m,x,\mu,\frac{\nu}{Q}\right) = \mathcal{I}_{ij}\left(\vec{p}_T,m,x,\mu,\frac{\nu}{Q}\right)\otimes_x \mathcal{M}_{jk}^{-1}(x,m,\mu)\,. \quad (4.50)$$

4.2.2 Consistency between universal factorization and mass mode factorization

In the previous section we have derived factorization theorems for the various scenarios for DIS in the endpoint region that used generalizations of the ingredients of the MMF scheme that allow for a smooth transition between all scenarios, which was one of the key points of the UF approach. We shall now compare these two schemes directly, as it will turn out that they are in fact equivalent.

Comparing the results from the previous section with the results in Refs. [2,12] we directly see that the hard and jet functions with the OS and the $\overline{\text{MS}}$ subtractions for secondary massive quarks in the UF approach and the hard and jet functions of the mass mode factorization for secondary massive quarks including the mass related power corrections derived in Sec. 4.2.1, are in fact equivalent, i.e.

$$\hat{H}_{m>Q}(Q,m,\mu) = \hat{H}^{\text{OS}}(Q,m,\mu)\,,$$
$$\hat{H}_{m<Q}(Q,m,\mu) = \hat{H}^{\overline{\text{MS}}}(Q,m,\mu)\,,$$
$$J_{m>Q\sqrt{1-x}}(s,m,\mu) = J^{\text{OS}}(s,m,\mu)\,,$$
$$J_{m<Q\sqrt{1-x}}(s,m,\mu) = J^{\overline{\text{MS}}}(s,m,\mu)\,. \tag{4.51}$$

The analogous relations hold also for the beam and soft functions. The remaining functions in the factorization theorems are the matching functions, the threshold corrections $\mathcal{M}_i$ in the case of the universal factorization approach, and H_c, H_s and $\mathcal{S}_c$ for the mass mode factorization approach. Comparing Eqs. (C.8), (C.10) and (C.32) with the results from Refs. [2,12] we see that the threshold matching coefficients $\mathcal{M}_i^\pm$ that appear in the universal factorization approach can be written in terms of the matching functions from the mass mode factorization as[6]

$$\mathcal{M}_H^-(Q,m,\mu) = H_c\Big(m,\mu,\frac{\nu}{Q}\Big)H_c\Big(m,\mu,\frac{\nu}{Q}\Big)H_s(m,\mu,\nu)\,,$$
$$\mathcal{M}_J^-(s,m,\mu) = \frac{1}{Q}H_c^{-1}\Big(m,\mu,\frac{\nu}{Q}\Big)\mathcal{S}_c\Big(\frac{s}{Q},m,\mu,\nu\Big)\,,$$
$$\mathcal{M}_\phi^+(1-z,m,\mu) = QH_c\Big(m,\mu,\frac{\nu}{Q}\Big)H_s(m,\mu,\nu)\mathcal{S}_c\big(Q(1-z),m,\mu,\nu\big)\,,$$
$$\mathcal{M}_S^+(\ell,m,\mu) = H_s(m,\mu,\nu)\int d\ell'\,\mathcal{S}_c(\ell-\ell',m,\mu,\nu)\mathcal{S}_c(\ell',m,\mu,\nu)\,,$$
$$\mathcal{M}_B^-(t,x,m,\mu) = \delta(1-x)\frac{1}{\omega}H_c^{-1}\Big(m,\mu,\frac{\nu}{\omega}\Big)\mathcal{S}_c\Big(\frac{t}{\omega},m,\mu,\nu\Big)\,,$$
$$\mathcal{M}_B^+\Big(\vec{p}_T,m,x,\mu,\frac{\nu}{\omega}\Big) = \delta(1-x)\delta^{(2)}(\vec{p}_T)H_c\Big(m,\mu,\frac{\nu}{\omega}\Big)\,,$$
$$\mathcal{M}_S^+(\vec{p}_T,m,\mu,\nu) = \delta^{(2)}(\vec{p}_T)H_s(m,\mu,\nu)\,, \tag{4.52}$$

which tells us that all the factorization theorems for all the different scenarios derived in the UF approach and those in the MMF approach are equivalent, once the latter are supplemented by power corrections as described in Sec. 4.2.1.

After simply stating the fact of equivalence of the two approaches once the power corrections are included by comparing to the results from literature, we will now take a closer look on how the definitions of the different mass dependent structures in the factorization theorems in the two approaches differ and what their relation is. We will do this for the example of the hemisphere jet function and will again focus only on the secondary massive quark corrections to the primary massless jet function, i.e. the case where the quark entering the hard interaction and initiating the jet is massless and the heavy flavor only contributes via virtual effects or a gluon splitting into a heavy $Q\bar{Q}$ pair. The discussion is analogous for all other functions appearing in the factorization theorems. A similar comparison between the definitions of the jet function in the MMF and the UF approach, also including primary massive quark effects, was done in Ref. [71]. One of the results found there was that the relation between the jet function defined in the UF and the MFF approach is not affected by primary massive quark effects, which is due to the fact that the csoft matrix elements are independent of the primary quark's mass.

---

[6]The threshold correction for the virtuality-dependent beam function is the same as for the jet function by consistency with the hard function and the thrust soft function that are the same in the factorization theorems for thrust in the peak region in $e^+e^- \to$ jets and beam thrust in DY. The threshold corrections for the TMD beam and soft functions can be inferred from consistency with the hard function.

In the following we will use the subscripts "uf" and "mm" to distinguish the jet functions defined in the UF scheme and in the MMF scheme, respectively. In the universal factorization approach in Sec. 4.1 we defined the jet function J_{uf} for $m \lesssim Q\sqrt{1-x} \sim \mu_J$ as the collinear matrix element $\mathcal{J}$ in Eq. (3.8) renormalized with $\overline{\mathrm{MS}}$ subtractions for all flavors, thereby always including the massive quark as an active flavor, with a subtraction of the collinear-soft region for all $n_l + 1$ quarks (either as a zero-bin or a csoft matrix elements defined in Eq (3.11))

$$J_{\mathrm{uf}}^{\overline{\mathrm{MS}}} = \mathcal{J}^{(n_l+1),\overline{\mathrm{MS}}} \otimes \left(\mathscr{S}_c^{(n_l+1),\overline{\mathrm{MS}}} \right)^{-1} . \tag{4.53}$$

The subtraction of modes of lower virtuality for all $n_l + 1$ flavors ensures that the jet function $J_{\mathrm{uf}}^{\overline{\mathrm{MS}}}$ is IR finite, because all IR divergences cancel between the collinear and the collinear-soft contributions. This is true both in the case of only massless quarks and in the case of massive quarks, such that the jet function defined in that way has the correct, IR finite, massless limit. This is the reason why the jet function in the UF scheme can be used for any $m \lesssim \mu_J$, because the full mass dependence, relevant for $m \sim \mu_J$ is kept, while at the same time the correct massless limit, relevant for $m \ll \mu_J$, can be reached, which is one of the main ideas behind the UF approach.

In the MMF approach the renormalized jet function for $m \sim \mu_J$ is defined as (in the MMF scheme contributions from all flavors, massless and massive, always get renormalized in the $\overline{\mathrm{MS}}$ scheme)

$$J_{\mathrm{mm}} = \mathcal{J}^{(n_l+1),\overline{\mathrm{MS}}} \otimes \left(\mathscr{S}_c^{(n_l),\overline{\mathrm{MS}}} \right)^{-1} . \tag{4.54}$$

Here the csoft matrix elements contain only n_l flavors, because in contrast to the UF scheme the heavy flavor is completely integrated out from the theory at its mass scale. This is the reason why the MM jet function does not recover the correct massless limit, because the IR subtractions from the csoft matrix elements are missing for that flavor to cancel those of the collinear matrix element, such that J_{mm} is not free of IR singularities in the massless limit. The MM jet function also does not show the correct decoupling limit, because all contributions are renormalized in the $\overline{\mathrm{MS}}$ scheme, which is a mass-independent renormalization scheme and does not allow for a decoupling behavior of heavy quarks.

Comparing Eqs. (4.53) and (4.54) one can establish the relation

$$J_{\mathrm{uf}}^{\overline{\mathrm{MS}}} = J_{\mathrm{mm}} \otimes \mathscr{S}_c^{(n_l),\overline{\mathrm{MS}}} \otimes \left(\mathscr{S}_c^{(n_l+1),\overline{\mathrm{MS}}} \right)^{-1} = J_{\mathrm{mm}} \otimes \mathcal{S}_c^{-1} , \tag{4.55}$$

where we have used the definition of the csoft function $\mathcal{S}_c$ in Eq. (3.34).

In the case $m \gtrsim Q\sqrt{1-x} \sim \mu_J$ the jet function in the UF scheme was defined with all contributions from the heavy quark renormalized with OS subtractions

$$J_{\mathrm{uf}}^{\mathrm{OS}} = \mathcal{J}^{(n_l+1),\mathrm{OS}} \otimes \left(\mathscr{S}_c^{(n_l+1),\mathrm{OS}} \right)^{-1} . \tag{4.56}$$

Renormalizing with OS subtractions for the massive quark means that all terms that do not vanish as $m \to \infty$ are absorbed into the counter terms. This is the reason why the UF jet function with OS subtractions for the massive flavor can be used for any $m \gtrsim \mu_J$ and gives the correct decoupling limit. In the collinear matrix element this leaves only contributions from real production of a heavy quark pair. In the csoft matrix element, that is purely distributional, all contributions from the heavy flavor are absorbed into the counter term, such that Eq. (4.56) can be written as

$$J_{\mathrm{uf}}^{\mathrm{OS}} = \mathcal{J}_{\mathrm{virt}}^{(n_l),\overline{\mathrm{MS}}} \otimes \mathcal{J}_{\mathrm{real}}^{(n_l+1)} \otimes \left(\mathscr{S}_c^{(n_l),\overline{\mathrm{MS}}} \right)^{-1} . \tag{4.57}$$

Comparing with Eq. (4.54) one finds the relation

$$J_{\mathrm{uf}}^{\mathrm{OS}} = J_{\mathrm{mm}} \otimes \mathcal{J}_{\mathrm{virt}}^{(n_l),\overline{\mathrm{MS}}} \otimes \left(\mathcal{J}_{\mathrm{virt}}^{(n_l+1),\overline{\mathrm{MS}}} \right)^{-1} = J_{\mathrm{mm}} \times H_c^{-1} . \tag{4.58}$$

89

Here we have used the fact that the purely virtual contributions $J_{\rm virt}$ in the collinear matrix element are just the same as for the collinear SCET current, since they are not sensitive to any measurement.

Eqs. (4.55) and (4.58) just express the equivalence of the UF jet function and the MMF jet function after the inclusion of the power corrections as in Eq. (4.43). The UF scheme provides a method of directly including the full mass dependence over the whole range of possible hierarchies, while the MMF scheme first strictly separates all hierarchies and then achieves a smooth transition only when supplementing it with of the massive power corrections. It can be seen as a pure matter of taste which way is preferred, since both approaches agree exactly with each other.

The two approaches differ in how the resummation of rapidity logarithms is organized. In the MMF scheme (with the power corrections included) the only basic structures that need to be evolved to achieve rapidity resummation related to secondary massive quarks are the three matching functions H_s, H_c and $\mathcal{S}_c$. They appear in different combinations, depending on the process and on the specific scale hierarchy, but are completely universal in the sense that all corrections resulting from integrating out the massive quark as an active flavor and therefore also all resummation of rapidity logarithms related to secondary massive quark effects can be expressed with only these three functions for all the processes and all the hierarchies discussed here. This also makes the universality of the structure of the rapidity logarithms from secondary massive quark effects manifest.

In the UF scheme each function (beam, jet, soft, ...) in the factorization theorem requires its own threshold correction $\mathcal{M}_i$, of which each then has to be resummed in rapidity. This procedure gives the same results and resums the same logarithms, but it makes it not explicit that the rapidity evolution related to secondary massive quarks has in fact always the same structure in all the factorization theorems for the different processes discussed here and in all the scale hierarchies, always related to the three mass mode matching functions H_s, H_c and $\mathcal{S}_c$ (see Eq. (4.52) for the relation of the threshold corrections $\mathcal{M}_i$ to the matching function of the MMF scheme).

We will consider the example of DIS in the endpoint to discuss how the rapidity resummation in the UF scheme can be carried out with the help of the mass mode matching functions defined in the MMF scheme. When the mass is between the jet and the hard scale, in the UF scheme the three threshold corrections $\mathcal{M}_H^-$ (for an evolution below the mass scale) and $\mathcal{M}_J^+$ and $\mathcal{M}_\phi^+$ (for an evolution above the mass scale) are needed. By consistency of RG running they fulfill the relation

$$\delta(1-z)\mathcal{M}_H^-(Q,m,\mu_m) = \int \mathrm{d}s\, \mathcal{M}_J^+(s,m,\mu_m)\mathcal{M}_\phi^+\left(1-z-\frac{s}{Q^2},m,\mu_m\right). \qquad (4.59)$$

Using the relations given in Eq. (4.52) this can be rewritten as

$$\delta(1-z)\,\underbrace{H_c\left(m,\mu_m,\frac{\nu}{Q}\right)\times H_c\left(m,\mu_m,\frac{\nu}{Q}\right)\times H_s(m,\mu_m,\nu)}_{\mathcal{M}_H^-(Q,m,\mu_m)}$$

$$= \int \mathrm{d}s\,\underbrace{\frac{1}{Q}H_c\times\left(m,\mu_m,\frac{\nu}{Q}\right)\left(\mathcal{S}_c\left(\frac{s}{Q},m,\mu_m,\nu\right)\right)^{-1}}_{\mathcal{M}_J^+(s,m,\mu_m)}$$

$$\times\underbrace{Q\mathcal{S}_c\left(Q(1-z)-\frac{s}{Q},m,\mu_m,\nu\right)\times H_s(m,\mu_m,\nu)\times H_c\left(m,\mu_m,\frac{\nu}{Q}\right)}_{\mathcal{M}_\phi^+\left(1-z-\frac{s}{Q^2},m,\mu_m\right)}. \qquad (4.60)$$

On the RHS of Eq. (4.60) we have inserted a csoft function $\mathcal{S}_c$ and its inverse $\mathcal{S}_c^{-1}$ such that

$$\int \mathrm{d}s\,\left(\mathcal{S}_c\left(\frac{s}{Q},m,\mu_m,\nu\right)\right)^{-1}\mathcal{S}_c\left(Q(1-z)-\frac{s}{Q},m,\mu_m,\nu\right) = \delta(1-z) \qquad (4.61)$$

The rapidity evolution factors $V_i(m, \mu, \nu, \nu_0)$, that evolve one function from one rapidity scale ν_0 to another scale ν, fulfill the consistency relation

$$V_{H_c}^{-\frac{1}{2}} = V_{\mathcal{S}_c}^{-\frac{1}{2}} = V_{H_s} = V \, , \tag{4.62}$$

with V given in Eq. (2.53). The resummed threshold corrections then read

$$\mathcal{M}_H^-(Q, m, \mu_m, \nu_Q, \nu_m) = H_c\big(m, \mu_m, \frac{\nu_Q}{Q}\big) \times H_c\big(m, \mu_m, \frac{\nu_Q}{Q}\big)$$
$$\times \left[V(m, \mu_m, \nu_Q, \nu_m) \times H_s(m, \mu_m, \nu_m) \right] , \tag{4.63}$$

$$\mathcal{M}_J^+(s, m, \mu_m, \nu_Q, \nu_{\mathcal{S}_c}) = \frac{1}{Q} H_c\big(m, \mu_m, \frac{\nu_Q}{Q}\big) \times \left[V^{\frac{1}{2}}(m, \mu_m, \nu_Q, \nu_{\mathcal{S}_c}) \times \mathcal{S}_c^{-1}\big(\frac{s}{Q}, m, \mu_m, \nu_{\mathcal{S}_c}\big) \right] , \tag{4.64}$$

$$\mathcal{M}_\phi^+(1-z, m, \mu_m, \nu_Q, \nu_{\mathcal{S}_c}, \nu_m) = Q H_c\big(m, \mu_m, \frac{\nu_Q}{Q}\big) \times \left[V(m, \mu_m, \nu_Q, \nu_m) \times H_s(m, \mu_m, \nu_m) \right]$$
$$\times \left[V^{-\frac{1}{2}}(m, \mu_m, \nu_Q, \nu_{\mathcal{S}_c}) \times \mathcal{S}_c(Q(1-z), m, \mu_m, \nu_{\mathcal{S}_c}) \right] , \tag{4.65}$$

where we have chosen the rapidity scale ν_Q of the collinear mass mode current matching function as the common global rapidity renormalization scale. To make sure that all remaining rapidity logarithms are small the scaling

$$\nu_Q \sim Q \, , \qquad\qquad \nu_m \sim \mu_m \, , \qquad\qquad \nu_{\mathcal{S}_c} \sim \frac{\mu_m^2}{Q(1-x)} \, , \tag{4.66}$$

is implied. To further minimize also the virtuality logarithms the scaling $\mu_m \sim m$ is used.

If the global renormalization scale is chosen below the mass scale, $\mu < m$, only the threshold corrections for the hard function $\mathcal{M}_H^-$ in Eq. (4.63), taking the hard function from the $(n_l + 1)$ to the (n_l) flavor scheme, appears in the factorization theorem. In this case the rapidity resummation is carried out in the same ways as it would have been done in the pure MMF scheme, between the hard matching functions H_c and H_s, and therefore between the rapidity scales $\nu_Q \sim Q$ and $\nu_m \sim m$. If the global renormalization scale is instead chosen to be above the mass scale, $\mu > m$, then according to the UF the threshold corrections $\mathcal{M}_J^+$ and $\mathcal{M}_\phi^+$ in Eqs. (4.64) and (4.65) have to be implemented, taking the jet function and the PDF from the n_l to the $n_l + 1$ flavor scheme. Here the rapidity evolution takes place between the scales $\nu_{\mathcal{S}_c} > Q$ and $\nu_m \sim m$, i.e. over a wider range. But the evolution between the scales ν_Q and $\nu_{\mathcal{S}_c}$, that appears in both $\mathcal{M}_J^+$ and $\mathcal{M}_\phi^+$, exactly cancels between the two threshold corrections. This is due to including one time the csoft function and one time its inverse in Eq. (4.60). In the scenario $m < Q\sqrt{1-x}$ there is a similar cancellation of a factor H_c between $\mathcal{M}_H^-$ and $\mathcal{M}_J^-$ when the global renormalization scale is chosen to be below the mass. In this sense the MMF scheme is more efficient, such that the rapidity evolution when resumming all rapidity logarithms related to secondary massive quarks is carried out with the minimal set of mass mode matching functions, without any cancellations between them taking place.

The UF and the MMF approach discussed in the previous chapters were derived in different ways and led to different definitions of the various structures and combinations of those. The MMF approach led to an efficient and clear way of performing the rapidity resummation related to secondary massive quark effects, reducing everything to three universal matching functions and one evolution kernel. In the UF approach it might be seen as less obvious how to arrange the rapidity resummation, but it has the advantage that each function in the factorization theorem like the jet function, the soft function etc. can be defined as one single universal object for which a closed resummed form can be written down, that then only needs to be inserted in the factorization theorem as a universal building block. Using the MMF scheme to write down the universal rapidity evolution and using the UF scheme as a guideline on how to combine the different building blocks in a convenient way as in Eqs. (4.63)-(4.65) may be the most practical combination of the advantages of both approaches.

Chapter 5

Conclusion

In this part of the thesis we have discussed how to set up VFNS, based on the SCET factorization framework, to systematically incorporate massive quark correction into exclusive differential cross sections for hadronic collisions. We focused on the Drell-Yan process, where we studied the q_T and the beam thrust spectrum in the limit of two (beam-)jets as prototypical examples for SCET_{II} and SCET_{I} factorization theorems, and DIS and the endpoint region $x \to 1$. We have established two different approaches, the MMF and the UF approach, for how to achieve the resummation of all logarithms related to the mass of a heavy flavor in the process for any possible (perturbative) hierarchy of the quark mass with respect to the other kinematic scales, and showed that the two approaches lead to equivalent results. We showed how the quark mass affects the resummation of rapidity logarithms in the q_T spectrum for DY. We furthermore established the universality of rapidity logarithms associated with secondary massive quarks for beam thrust in the exclusive region in DY, DIS in the endpoint and thrust in $e^+e^- \to 2$ jets, where the resummation of these rapidity logarithms can always be carried out in a rapidity RG evolution of three universal matching functions (here called H_c, H_s and $\mathcal{S}_c$).

We also calculated all the missing ingredients for NNLL$'$ resummation of massive quark effects in neutral current DY for small $q_T/\mathcal{T}$, namely the mass-dependent TMD and virtuality beam function matching coefficients for primary massive quarks at $\mathcal{O}(\alpha_s)$ and for secondary massive quarks at $\mathcal{O}(\alpha_s^2)$, as well as the TMD soft function and the csoft function with secondary massive quarks at $\mathcal{O}(\alpha_s^2)$. Several of our results are also immediately relevant for other processes at the LHC besides Drell-Yan. The primary massive quark beam functions are relevant for any heavy-quark initiated process, for example exclusive $b\bar{b}H$-production. The mass-dependent TMD soft function and rapidity anomalous dimension at $\mathcal{O}(\alpha_s^2)$ satisfy Casimir scaling and can be therefore also utilized for the description of gluon-fusion processes, e.g. the Higgs q_T-spectrum. Our results for the beam thrust spectrum also allow for a systematic inclusion of massive quark effects into the Geneva Monte-Carlo program [76,77] at NNLL$'$+NNLO in its underlying jet resolution variable.

This work focused on the conceptual part of how to consistently set up the VNFS for all the different hierarchies and resum the mass-dependent logarithms in rapidity and virtuality, and on calculating the mass-dependent one- and two-loop functions relevant for NNLL$'$ resummation, while full phenomenological analyses with our results are still missing and postponed to future work. An important application of our framework will be the precise theoretical description of the Drell-Yan q_T spectrum. Especially in the ratio of the W- and Z-boson spectra, which is important for the precision measurement of the W-boson mass at the LHC, bottom and charm mass effects are expected to be relevant because they enter at different order in perturbation theory in W- and Z-boson production. Our results are, however, not limited to this particular application and can be relevant for many measurements at hadron colliders, where bottom and charm mass effects are often neglected in the resummation when calculating differential cross sections to high order in the logarithmic counting, but can be expected to become relevant with increasing precision.

Part II

On the Cutoff Dependence of the Quark Mass Parameter in Angular Ordered Parton Showers

Chapter 6

Introduction

Large sections of this part of the thesis and corresponding appendices were taken from Ref. [3]. Some theoretical discussions of the cutoff dependence of NLO matched showers, that were not directly part of the work of the author of this thesis, are omitted here. They can be found in Sec. 7.7 of Ref. [3]. Some additional calculations for the unreleased contributions to the soft and jet functions with an angular cut, not contained in Ref. [3], are provided in appendix H.

6.1 Prelude and review

A precise determination of the top quark mass m_t represents one of the most important measurements in the context of studies of the Standard Model (SM) as well as of new physics, in particular in the context of electroweak symmetry breaking. The most precise top mass measurements are obtained from template and matrix element fits which are based on the idea of accessing m_t by directly reconstructing the kinematic properties of a top quark "particle". These types of measurements naturally yield a very high sensitivity to the top quark mass because they involve endpoints, thresholds or resonant structures in kinematic distributions which substantially reduces the impact of uncertainties that affect poperties such as their normalization. The most recent reconstruction measurements are $m_t^{\mathrm{MC}} = 172.44(49)$ GeV (CMS) [108], $m_t^{\mathrm{MC}} = 172.69(48)$ GeV (ATLAS) [109] and $m_t^{\mathrm{MC}} = 174.34(64)$ GeV (Tevatron) [110].

The characteristic property of these measurements, however, is that the observables employed for the reconstruction analyses are too complicated to be calculated in a systematically improvable way and, in addition, involve sizeable perturbative and non-perturbative corrections due to soft gluon emission which, in the vicinity of kinematic endpoints or thresholds, are not power-suppressed. The theoretical computations used for these measurements are therefore based on multi-purpose Monte Carlo (MC) event generators since they can produce predictions for essentially any conceivable observable. As a consequence, in these direct mass measurements the top mass parameter m_t^{MC} of the MC generator employed in the analyses is determined. The experimental collaborations provide estimates of the theoretical uncertainty in the extracted value of m_t^{MC} concerning the quality of the modelling of non-perturbative effects, e.g. by using different tunes or MC generators, or concerning theoretical uncertainties, e.g. by variations of theory parameters. The improvement of the theoretical basis of MC event generators and of methods to estimate their uncertainties is an ongoing effort [111–113].

However, the intrinsic, i.e. quantum field theoretic meaning of m_t^{MC} has up to now not been rigorously specified. Since this matter goes beyond the task of properly estimating or reducing MC modelling uncertainties and is also tied to the constructive elements incorporated to the MC's perturbative and non-perturbative components, it is much harder to quantify. Issues one has to consider do not only involve the truncations of perturbative QCD expansions, but also MC specific implementations such

as the cut on the parton shower (PS) evolution or even modifications that are formally subleading but play numerically important roles in reaching better agreement with data or are part of the implementation of the hadronization model. It should also be remembered that the level of theoretical rigor of MC event generators depends on the observable. Since the theoretical description of thresholds and endpoints in general involves the resummation of QCD radiation to all orders, the perturbative aspect of how to interpret m_t^{MC} thus significantly depends on the implementation of the parton showers that are used in the MC generators and to the extent that NLO fixed-order QCD corrections have been systematically implemented for the observables that are relevant for the reconstruction analyses. Apart from that, the interface between the perturbative components and the hadronization models, which involves the structure of the infrared cut of the shower evolution, $Q_0 \sim 1$ GeV, or the treatment of the top quarks finite width, $\Gamma_t \sim 1.4$ GeV, and other finite lifetime effects can play essential roles. Finally, it should also be mentioned that m_t^{MC} may also be affected by non-perturbative MC modelling effects as a consequence of the tuning process partly compensating for approximations and model-like features implemented into the MC perturbative components.

So, although m_t^{MC} is by construction closely related to the concept of a kinematic top quark mass, the identification to a particular kinematic mass scheme is far from obvious - also because there are several options for kinematic masses including schemes such the pole mass m_t^{pole} or short-distance threshold masses as they are employed for the top pair threshold cross section at a future Linear Collider [114–116] or in the context of massive quark initiated jets [117,118]. As shown in Ref. [119], these kinematic mass schemes can differ by more than 1 GeV. Given that the reconstruction analyses have reached uncertainties at the level of 0.5 GeV it appears evident that systematic and quantitative examinations on the field theoretic meaning of the MC top mass m_t^{MC} are compulsory. This scrutiny may involve examinations of different MC generators, as well as the respective interplay of their perturbative and non-perturbative components.

So far, only a limited number of theoretical considerations dedicated to this issue exist in the literature. In Ref. [120], based on the analogy of the MC components to the QCD factorization for boosted top quark initiated jet masses in the peak region derived in the factorization framework of Soft-Collinear-Effective Theory (SCET) and boosted Heavy-Quark-Effective-Theory (bHQET) [18, 19], it was conjectured that the relation between m_t^{MC} and the pole mass is given by $m_t^{\mathrm{pole}} - m_t^{\mathrm{MC}} = R_{\mathrm{sc}}(\alpha_s/\pi)$, where the scale R_{sc} should be closely related to the shower cut Q_0. The conjecture was based on general considerations how an infrared cut affects perturbative calculations but did not provide a precise quantitative relation. It was, however, argued that the uncertainty in the relation is unlikely to exceed the level of 1 GeV. A similar conclusion was drawn in Ref. [121] where it was argued that m_t^{MC}, due to the effects of the hadronization models, may have properties analogous to the mass of a top (heavy-light) meson. Based on the concepts of heavy quark symmetry [122,123] the relation $m_t^{\mathrm{MC}} = m_t^{\mathrm{MSR}}(R) + \Delta_{t,\mathrm{MC}}(R)$ was conjectured, where m_t^{MSR} is the MSR mass [124,125], the term $\Delta_{t,\mathrm{MC}}$ contains perturbative as well as non-perturbative corrections and $R = 1$ GeV represents a factorization scale separating perturbative and non-perturbative effects. From a comparison of B meson and bottom quark masses, and using heavy quark symmetry, it was concluded that $\Delta_{t,\mathrm{MC}}$ could in principle be at the level of 1 GeV. We also refer to Ref. [126] for a related discussion.

In Ref. [118] the concrete numerical relation $m_t^{\mathrm{MC}} = m_t^{\mathrm{MSR}}(1\,\mathrm{GeV}) + (0.18 \pm 0.22)$ GeV was obtained from fitting NNLL (next-to-next-to-leading logarithmic) and $\mathcal{O}(\alpha_s)$ matched factorized hadron level predictions for the 2-jettiness distribution in the peak region for boosted top production in e^+e^- annihilation [18,19] to corresponding pseudo-data samples obtained by PYTHIA 8.2 [127] with the default Monash tune [128] correctly accounting for the dominant top quark width effects in the factorized calculation. Here the quoted error is the theoretical uncertainty of the factorized NNLL+$\mathcal{O}(\alpha_s)$ prediction and also includes an estimate for the intrinsic uncertainty of the PYTHIA 8.2 calculation. Using the pole mass scheme in the factorized NNLL+$\mathcal{O}(\alpha_s)$ prediction, the corresponding analysis yielded $m_t^{\mathrm{MC}} = m_t^{\mathrm{pole}} + (0.57 \pm 0.28)$ GeV. While this analysis provided a concrete numerical result, it can only be generalized to LHC measurements if one makes the additional assumption that the

MC top mass has a universal meaning covering in particular also the LHC environment and the substantially more complicated observables included in the direct mass measurements, for which currently no first principle calculations exist. In addition, systematic uncertainties in the modelling of non-perturbative effects at hadron colliders, such as multi parton interactions, or the description of the pile-up effects are much harder to control. An analogous analysis for the LHC environment was subsequently carried out in Ref. [129] using factorized NLL soft-drop groomed [130,131] hadron level jet mass distributions showing results that are compatible with, but less precise than those of [118]. We also refer to Ref. [132] for a related analysis.

Aside from the previously mentioned examinations, recently, a number of complementary studies were conducted focusing on various sources of uncertainties in the perturbative description of top production and decay and the non-perturbative modelling of final states involved in top mass measurements. While these studies mainly aimed at examining the potential size of uncertainties in top mass determinations from reconstruction as well as from alternative methods (see Refs. [133–135] and references therein), some of their findings may also be relevant for addressing the question how m_t^{MC} obtained from reconstruction should be interpreted field theoretically.

In Ref. [136] the sensitivity of m_t^{MC} determinations from exclusive hadronic variables such as the B-meson energy E_B [137], the B-lepton invariant mass $m_{B\ell}$ [138] or the transverse mass variables m_{T_2} [139–142] to variations of the parameters of the MC hadronization models in PYTHIA 8 and HERWIG 6 was studied. They found that for top mass determinations based on these distributions to be competitive with direct reconstruction methods these hadronization parameters would have to be constrained significantly more precisely than what is possible from usual multi-purpose tuning. In addition, they made the observation that the top mass dependent endpoints of these distributions are, compared to the overall shape of the distributions, largely insensitive to variations of the hadronization parameters, indicating that these kinematic endpoints only depend on global and inclusive properties of the final state dynamics.

In Ref. [143] top mass determinations from distributions such as the b-jet and lepton invariant mass $m_{b_j\ell}$ and the variable m_{T_2} [139] were analyzed within fixed-order perturbation theory comparing the full NLO QCD result for $W^+W^-b\bar{b}$ production with different approximations in the narrow width approximation (NWA) concerning NLO QCD corrections in the production and the decay of the top quarks as well as using the parton shower from SHERPA [144] after top production. Using pseudo-data fits they found that the extracted top mass can depend significantly (at the level of 1 GeV or even more) on the approximation used, indicating that incomplete descriptions of finite-lifetime effects can lead to systematic deviations in the value of the extracted top mass of order Γ_t.

In Ref. [145] the NLO-PS matched POWHEG [146,147] top production generators hvq [148], $t\bar{t}dec$ [149] and $b\bar{b}4\ell$ [150] interfaced to PYTHIA 8.2 [127] and HERWIG 7.1 [151,152] were studied comparatively examining the peak position of the particle level b-jet and W invariant mass m_{b_jW}, the peak of the b-jet energy E_{b_j} [137] and moments of various lepton observables [153] in view of an extraction of the top quark mass. They found that the m_{b_jW} peak is largely insensitive to variations of the generators and the shower MC as well as to input quantities such as the strong coupling and the PDFs or the b-jet definition, and concluded that changes in the top mass due to these variations do not exceed 200 MeV in the absence of experimental resolution effects. They also indicated that the good agreement between the three POWHEG generators may imply that m_{b_jW} is not sensitive to additional finite lifetime effects. Once the smearing due to experimental resolution effects is accounted for, however, they found an increased sensitivity to the differences in the parton showers of PYTHIA 8.2 and HERWIG 7.1 that correspond to variations in the extracted top mass at the level of 1 GeV or more. For E_{b_j} the dependence of the extracted top mass on the shower type and on the b-jet definition is in general at the level of 1 GeV. For the leptonic observables variations of this size arise from PDF uncertainties and from changing the shower type.

6.2 About this work

The aim of this work is to initiate dedicated individual examinations of the different components of MC event generators with the aim to gain insights concerning the field theoretic meaning and potential limitations of the MC top mass parameter m_t^{MC} *from first principles*. We start with an examination of the parton shower evolution with respect to the dependence on the infrared shower cut Q_0.

Apart from the perturbative hard interaction matrix elements that encode the basic hard process that can be described by MC generators, the parton shower describes the parton branching for energies below the hard interaction scale and represents the perturbative component of MC generators responsible for the low energy dynamics in MC predictions. While common analytic calculations in perturbative QCD are carried out in the limit of a vanishing infrared regulator, event generators based on parton showers rely on the existence of an infrared cut in order to prevent infinite parton multiplicities and to ensure that the parton shower description does not leave the realm of perturbation theory.

From the field theoretic point of view, Q_0 represents a factorization scale that separates the perturbative components of MC event generators and their hadronization models. While it is generally accepted that a finite value for Q_0 restricts the amount of real radiation and multiplicity generated by the shower evolution, it is not per se obvious to which extend it may also affect the meaning of QCD parameters such as the MC quark mass parameters. Due to the unitarization property of the shower evolution which is responsible for the coherent summation of real as well as infrared virtual radiative corrections for scales above Q_0, it is also plausible that the MC top mass parameter m_t^{MC} should acquire a dependence on the value of Q_0 unless one makes the additional assumption the Q_0 effects are negligible. In this work we examine this dependence and find that is is not negligible. We emphasize that in the discussions of this work we ignore all issues related to (the shower cut dependence of) hadronization because the primary aim is to concentrate on the perturbative aspects of the relation between m_t^{MC} and field theoretic mass schemes. We are aware that the properties of the hadronization modelling in MC event generators may have a significant impact on the interpretation of m_t^{MC}, but we believe that examining perturbative and non-perturbative MC components separately in this respect is essential to gain full conceptual insight.

Because the top quark has color charge its mass is - following the principles of heavy quark symmetry - linearly affected by the momenta of *ultra-collinear* gluons [18, 19], which are the gluons that are soft in the top quark rest frame. The role of these ultra-collinear gluons turns out to be essential for our conceptual considerations concerning the shower cut dependence of the top quark mass. Compared to the radiation pattern of massless quarks the additional effects coming from the ultra-collinear gluons is for example responsible for the dead cone effect [154, 155] which is generally considered as coming from the top mass regulating the emergence of collinear singularities in the quasi-collinear limit. The radiation in the dead-cone region, however, is still non-zero and to the extent that it is unresolved becomes part of the energy (i.e. mass) of the measured top quark state. It is this quantum mechanical feature that goes beyond the classic picture of an unambiguous top quark "particle" whose total energy could be determined in the direct mass measurements. Since the parton showers in all state-of-the-art MC generators account for the dead cone effect [156], it appears obvious that the meaning of m_t^{MC} should naturally have a linear dependence on the shower cut Q_0 restricting the ultra-collinear radiation – unless there is a mechanism that leads to a power suppressed effect of order Q_0^2 or higher which we may then safely neglect for the case of the top quark. Therefore, to examine the intrinsic field theoretical meaning of the MC top quark mass parameter m_t^{MC} it is essential to start with a careful examination of the production of the top quarks and the ultra-collinear gluons. From this point of view, studies of the top decay and the treatment of the observable final states are important to quantify to which extent the ultra-collinear gluons are unresolved and how they enter a particular observable.

In this work we aim to focus primarily on the production aspect, and we are therefore studying an observable that is maximally insensitive on details of the final state dynamics and its theoretical modeling. This observable is the peak (i.e. resonance) position of hemisphere jet masses in e^+e^- annihilation, explained in more detail in Sec. 7.1. The basic outcome of our considerations concerning the field theoretic meaning of m_t^{MC}, however, should be general and shall be systematically extended to other types of observables and to the LHC environment in subsequent work. As a further simplification we consider the narrow width approximation (NWA), i.e. the case of quasi-stable top quarks which allows to rigorously factorize top production and decay, the case of boosted (i.e. large-p_T) top quarks and the coherent branching formalism which is related to angular ordered showers, see Refs. [157–159] for massless and Refs. [160] for massive quarks, and also Refs. [161, 162]. Since the limit of stable and quasi-collinear heavy quarks is the theoretical basis of all parton shower formulations for top (and other heavy) quarks, it is natural to investigate the physics in this limit first to avoid that the conclusions are affected by the additional approximations that need to be made in the attempt to account for the effects of slow and unstable top quarks. Our current focus on angular ordered showers is, on the other hand, of purely practical nature: Our considerations here require explicit analytic solutions of the shower evolution, and angular ordered showers based on the coherent branching formalism can be more easily tackled by well known analytic methods [163] applicable to global event shapes. So our current results are directly relevant for the HERWIG MC generator which employs an angular ordered PS. Generalizations to other MC generators shall be treated elsewhere.

In this context our work is structured around the following three questions:

(A) Can state-of-the-art partons showers in principle describe the single top resonance mass and related thresholds with NLO precision?

(B) What is the impact of the shower cut Q_0 on the resonance value of the jet masses?

(C) Does the shower cut imply that the MC top quark mass parameter m_t^{MC} is a low-scale threshold short-distance mass, and how can this be proven from first principles at the field theoretic level?

Question A is relevant because, only if parton showers can describe the threshold or resonance mass with NLO precision, the question of which mass scheme is employed can be addressed systematically in a meaningful way. In the course of our examination we show that this is indeed the case as long as NLL order logarithmic terms are resummed, and we also show that the additional NLO corrections implemented by NLO matched parton showers do not further increase the precision. Question B concerns the dependence of the resonance value of the jet mass on Q_0. We show that the jet mass at the resonance peak depends linearly on Q_0 which means that for the field theoretic meaning of m_t^{MC} the finite shower cut is essential and cannot be neglected. Finally, question C addresses to which extent the linear dependence on Q_0 must be interpreted as a Q_0-dependence of the MC top quark mass. As we will show, only a part of the linear Q_0-dependence of the peak jet mass is related to ultra-collinear radiation and thus to the top quark mass. Overall, the shower cut also restricts the radiation of large angle soft gluons unrelated to the top quark and the ultra-collinear radiation. Only the latter is related to the top quark mass, and its dominant linear Q_0-dependence caused by the shower cut can be shown to automatically imply a mass redefinition which differs from the pole mass by a term proportional to $\alpha_s(Q_0)\,Q_0$. This result implies that m_t^{MC} is equivalent to the top quark pole mass, in the limit $Q_0 = 0$ which is however practically inaccessible for parton showers. In the formal limit $m_t \to 0$ the effects of the ultra-collinear radiation and its Q_0-dependence vanish and only the cutoff dependence on the soft radiation remains. This cutoff dependence represents the factorization interface between perturbative soft radiation and hadronization effects governed by the MC hadronization models. Since in this context the understanding of the shower cut dependence of the soft radiation is a prerequisite to the examination of the ultra-collinear radiation, we also analyze carefully the case of massless quark production in parallel to our discussions on the top quark.

6.3   Outline

The outline of this part is as follows: In Sec. 7.1 we set up our theoretical framework by explaining the hemisphere mass observable τ and reviewing the corresponding NLL and hadron level factorized QCD predictions in the resonance region for massless as well as massive quark production. We also provide details on the hadronization model shape function which is important for the numerical analyses carried out in the subsequent sections. In this section we also prove, using the factorized predictions, that NLL resummation of logarithms is sufficient to achieve NLO precision for the position of the peak in the τ distribution.

In Sec. 7.2 we review the coherent branching formalism, provide the analytic evolution equation for the jet mass distribution for massless and massive quark production at NLL order and give some details on the practical implementation of the angular order parton shower based on the coherent branching formalism in the HERWIG 7 event generator.

In Sec. 7.3 we show – in the absence of any infrared cutoff and in the context of strict perturbative computations – that the NLL predictions for the hemisphere mass τ distribution in the resonance region obtained from the coherent branching formalism are fully equivalent to the NLL factorized QCD predictions for massless quark production as well as for massive quark production in the pole mass scheme. This result proves, that in the context of strict perturbative computations for massive quarks in the limit $Q_0 = 0$ the MC generator mass is equivalent to the pole mass. This conclusion, however, does not apply for MC event generators because their parton shower algorithm strictly requires a finite shower cut Q_0 in order to terminate and to avoid infinite multiplicities.

The impact of the shower cut Q_0 is then analyzed in detail in Sec. 8.1, which represents the core of this work. Here we analyze the power counting of the relevant modes entering the hemisphere mass in the resonance region in the massless and massive quark case and we focus on a coherent view of the factorized QCD and the coherent branching approach. We calculate analytically the NLO corrections caused by the shower cut Q_0 in comparison with the results without any cut in the coherent branching formalism and the factorized QCD approach focusing on the dominant effects linear in Q_0. We show that the results obtained for the linear Q_0 contributions in coherent branching and factorized QCD are compatible, and we use the direct connection of the factorized QCD computation to field theory to unambiguously distinguish shower cut effects related to soft hadronization corrections and the quark mass parameter. By coherently examining massless and massive quark production we prove that using a finite shower cut Q_0 in the coherent branching formalism – and thus also in angular ordered parton showers – automatically implies that one employs a short-distance mass scheme different from the pole mass, called the *coherent branching (CB) mass, $m^{\mathrm{CB}}(Q_0)$*. We explicitly calculate the relation of the coherent branching mass to the pole mass at NLO, i.e. $\mathcal{O}(\alpha_s)$.

In Sec. 8.2 the conceptual results obtained in the previous sections are summarized coherently to set up the numerical examinations we carry out in Sec. 9. In Sec. 9 we compare the results obtained in Sec. 8.1 with analytic methods and conceptual considerations with numerical results running simulations for the hemisphere mass variable τ in HERWIG 7 using different values of the shower cut Q_0. Focusing mostly on the peak position of τ we show that the simulations are in full agreement with our conceptual results. We also show explicitly that NLO corrections added in the context of NLO matched parton showers have extremely small effects in the resonance location and do not modify any of the previous results, confirming that NLL accurate parton showers are already NLO accurate as far as the resonance region is concerned. Furthermore, we also demonstrate that the results we have obtained in the context the hemisphere mass variable τ are also compatible with numerical simulations for the more exclusive kinematic variables $m_{b_j\ell}$ and m_{b_jW} supporting the view that our results are universal.

Finally, Sec. 10 contains our conclusions and an outlook for some of the remaining questions that should be addressed in the future. There we also provide a brief numerical analysis how $m^{\mathrm{CB}}(Q_0)$ is related to other mass renormalization schemes. We also provide appendices containing some sup-

plemental material relevant for our work. In App. G we provide details on the computations of the effects of the shower cut Q_0 in the context of the factorized QCD predictions. In App. H we present anaologous calculations with an additional angular cut and in App. I we collect results for loop integrals in the presence of the shower cut Q_0. Finally, in App. K we give information on the HERWIG 7 settings we have employed for our simulation studies.

Chapter 7

Resummation and the Coherent Branching Formalism

7.1 The observable: squared hemisphere mass sum

The observable we consider in this work is the sum of the squared hemisphere masses defined with respect to the thrust axis in e^+e^--collisions normalized to the square of the c.m. energy Q,

$$\tau \equiv \frac{M_1^2 + M_2^2}{Q^2}. \tag{7.1}$$

In the lower endpoint region the τ distribution has a resonance peak which is dominated by back-to-back 2-jet configurations which arise from LO quark-antiquark production, and it is the location of the resonance, τ_{peak}, which we focus on mostly in our study. For massless quarks this resonance region is located close to $\tau = 0$ and represents the threshold region for dijet production. Non-perturbative effects shift the observable peak towards positive τ values by an mount of $\mathcal{O}(\Lambda/Q)$, where Λ is a scale of around 1 GeV. For massive quark production the resonance region and the peak are located close to $\tau = 2m_Q^2/Q^2$, and for the case of the top quark for $Q \gg m_t$ is dominated by boosted back-to-back top quark initiated jets. As for the case of massless quark production non-perturbative effects shift the observable peak towards positive τ values by an mount of $\mathcal{O}(\Lambda/Q)$. The scale of $\Lambda \approx 1$ GeV is generated from non-perturbative effects, but its value is numerically larger than Λ_{QCD} because it accounts for the cumulative hadronization effect from both hemispheres [164]. In the peak region, τ is closely related to the classic thrust variable [165] in the case of massless quark production [163], and to 2-Jettiness [166] for massive quarks [18]. To be concrete, concerning the structure of large logarithms and of terms singular in the $\tau \to \tau_{\mathrm{min}}$ limit, which dominate the shape and position of the peak, the hemisphere mass variable τ, thrust and 2-jettiness are equivalent for large Q. We therefore frequently refer to τ simply as "thrust" in this work.

For our examinations for top quarks we also consider the rescaled thrust variable

$$M_\tau \equiv \frac{Q^2 \tau}{2m_Q}. \tag{7.2}$$

The variable M_τ is peaked close to $M_\tau = m_Q$ and allows for a more transparent interpretation of the shower cut Q_0-dependence from the point of view of the top quark mass than τ. Note that the scheme dependence of the quark mass parameter m_Q appearing in the definition (7.2) represents an effect that is $\mathcal{O}(\alpha_s^2)$-suppressed in the context of our examinations and therefore irrelevant at the order we are working.

An essential aspect of the examinations in this work is that for boosted top quarks events related to top decay products being radiated outside the parent top quark's hemisphere are $(m_t/Q)^2$ power

suppressed [18]. So, because thrust depends on the sum of momenta in each hemisphere, effects of the top quark decay in the thrust distribution are power suppressed as well, and the situation of a finite top quark width is smoothly connected to the NWA and the stable top quark limit. This is compatible with the factorized treatment of top production and decay used in contemporary parton showers and also allows us to carry out analytic QCD calculations for stable top quarks which are essential for the chain of arguments we use. In this way thrust is an ideal observable for the examinations made in this work since it allows to study the mass of the top quark accounting in particular for the contribution of the unresolved ultra-collinear gluon cloud around it.

However, in thrust the effects of large angle soft radiation are maximized, and the impact of the shower cut Q_0 on the meaning of the top quark mass parameter interferes with that Q_0 has on large angle soft radiation. Since the latter is not related to the top quark mass, but represents the interface to hadronization effects [163, 167], it is important that both effects are disentangled unambiguously. As we will show, for thrust in the peak region this can be carried out in a straightforward way owing to soft-collinear factorization [168, 169]. Since the structure of large angle soft radiation is equivalent for the production of massless quarks and boosted massive quarks [18, 19], we discuss the case of massless quark production before we examine boosted top quarks.

Since our discussion requires the analytic comparison of the thrust distribution determined from the parton shower evolution based on the coherent branching formalism at NLL order (where we follow the approach of [163, 170]) and of corresponding resummed QCD calculations based on soft-collinear factorization, we briefly review the latter in the following two subsections for massless and massive quark production.

7.1.1 Factorized QCD cross section: massless quarks

Resummed calculations for the thrust distribution in the peak region require the summation of terms that are logarithmically enhanced and singular in the limit $\tau \to \tau^{\min} = 0$, where the partonic threshold is located. In the context of conventional perturbative QCD, factorized calculations for massless quarks have been carried out in Ref. [169] at NLL order. In the context of SCET the corresponding results have been obtained at NLL+$\mathcal{O}(\alpha_s)$ in Ref. [171] and were extended to N^{3}LL+$\mathcal{O}(\alpha_s^3)$ in Ref. [164, 172]. Using the notations from Ref. [164] the observable hadron level thrust distribution in the peak region can be written in the form

$$\frac{\mathrm{d}\sigma}{\mathrm{d}\tau}(\tau, Q) = \int\limits_0^{Q\tau} \mathrm{d}\ell \, \frac{\mathrm{d}\hat{\sigma}_s}{\mathrm{d}\tau}\Big(\tau - \frac{\ell}{Q}, Q\Big) \, S_{\mathrm{mod}}(\ell) \tag{7.3}$$

where $\mathrm{d}\hat{\sigma}_s/\mathrm{d}\tau$ contains the factorized resummed singular partonic QCD corrections (containing δ-function terms of the form $\alpha_s^n \delta(\tau)$ and plus-distributions of the form $\alpha_s^n [\ln^k(\tau)/\tau]_+$) and $S_{\mathrm{mod}}(\ell)$ is the soft model shape function that describes the non-perturbative effects. It has support for positive values of ℓ, exhibits a peaked behavior for ℓ values around 1 GeV and is strongly falling for larger values. We further assume that it vanishs at zero momentum, $S_{\mathrm{mod}}(0) = 0$.[1] Due to the smearing caused by the non-perturbative function the visible peak of the thrust distribution is shifted to positive values by an amount of order $(1 \text{ GeV})/Q$. The dominant perturbative corrections to the factorized cross section in Eq. (7.3) are coming from so-called non-singular contributions containing terms of the form $\alpha_s^n \ln^k(\tau)$. For our considerations in the resonance region these corrections are power-suppressed by a *additional factor* of order $(1 \text{ GeV})/Q$, i.e. they cause a shift in the peak position by an amount $(1 \text{ GeV})^2/Q^2$ which we can safely neglect.

---

[1]The typical scale of the non-perturbative function S^{mod} is about twice the typical hadronization scale $\Lambda_{\mathrm{QCD}} \lesssim 0.5$ GeV as it accounts for non-perturbative from both hemispheres [164]. The property $S_{\mathrm{mod}}(0) = 0$ is assumed for all shape functions treated in the literature and physically motivated from the hadronization gap.

The resummed factorized singular partonic QCD cross section has the form

$$\frac{1}{\sigma_0}\frac{\mathrm{d}\hat{\sigma}_s}{\mathrm{d}\tau}(\tau, Q) = Q\, H_Q(Q,\mu_H) \int\limits_0^{Q^2\tau} \mathrm{d}s \int\limits_0^s \mathrm{d}s'\, U_J(s',\mu_H,\mu_J)\, J^{(\tau)}(s-s',\mu_J) \tag{7.4}$$

$$\times \int\limits_0^{Q\tau-s/Q} \mathrm{d}k\ U_S(k,\mu_H,\mu_S)\, S^{(\tau)}\!\left(Q\tau - \frac{s}{Q} - k, \mu_S\right)$$

where σ_0 is the total partonic e^+e^- tree-level cross section. The term H_Q is the hard function describing effects at the production scale Q, $J^{(\tau)}$ is the jet function describing the distribution of the squared invariant mass s due to collinear radiation coming from *both*[2] jets and $S^{(\tau)}$ is the soft function containing the effects of large angle soft radiation. They depend on the renormalizations scales $\mu_H \sim Q$, $\mu_J \sim Q\sqrt{\tau}$ and $\mu_S \sim Q\tau$, which are chosen such that no large logs appear in hard, jet and soft functions respectively. Large logarithmic contributions are resummed in the different U factors which are evolved from the corresponding renormalization scale μ_H, μ_J or μ_S to a common renormalization scale. Since it most closely resembles the analytic form of the resummation formulae obtained in the coherent branching formalism, we have set in Eq. (7.4) the common renormalization scale equal to the hard scale μ_H, so that there is no evolution factor U_H for the hard function. So, U_J sums logarithms between the jet scale μ_J and the hard scale μ_H, and U_S sum logarithms between the soft scale μ_S and the hard scale. For our discussions we need the expressions for the U factors at NLL and the hard, soft and jet function at $\mathcal{O}(\alpha_s)$.

The $\mathcal{O}(\alpha_s)$ the hard, jet and soft functions appearing in the dominant singular partonic contributions of the 2-jettiness factorization theorem obtained in SCET for massless quarks have the form [171] (see also Refs. [164, 172])

$$H_Q(Q,\mu) = 1 + \frac{\alpha_s(\mu)C_F}{4\pi}\left(-2\ln^2\frac{Q^2}{\mu^2} + 6\ln\frac{Q^2}{\mu^2} - 16 + \frac{7\pi^2}{3}\right) + \mathcal{O}(\alpha_s^2), \tag{7.5}$$

$$J^{(\tau)}(s,\mu) = \delta(s) + \frac{\alpha_s(\mu)C_F}{4\pi}\left(\frac{8}{\mu^2}\left[\frac{\mu^2\ln\frac{s}{\mu^2}}{s}\right]_+ - \frac{6}{\mu^2}\left[\frac{\mu^2}{s}\right]_+ + (14-2\pi^2)\delta(s)\right) + \mathcal{O}(\alpha_s^2), \tag{7.6}$$

$$S^{(\tau)}(k,\mu) = \delta(k) + \frac{\alpha_s(\mu)C_F}{4\pi}\left(-\frac{16}{\mu}\left[\frac{\mu\ln\frac{k}{\mu}}{k}\right]_+ + \frac{\pi^2}{3}\delta(k)\right) + \mathcal{O}(\alpha_s^2), \tag{7.7}$$

with the plus distributions defined in App. J.

Their respective anomalous dimensions can (to all orders) be written in the form

$$\mu\frac{d}{d\mu}U_H(Q,\mu_H,\mu) = \left(\Gamma_H[\alpha_s(\mu)]\ln\left(\frac{\mu^2}{Q^2}\right) + \gamma_H[\alpha_s(\mu)]\right)U_H(Q,\mu_H,\mu), \tag{7.8}$$

$$\mu\frac{d}{d\mu}U_J(s,\mu,\mu_J) = \int ds'\left(-\frac{\Gamma_{J^{(\tau)}}[\alpha_s(\mu)]}{\mu^2}\left[\frac{\mu^2\theta(s-s')}{s-s'}\right]_+ + \gamma_{J^{(\tau)}}[\alpha_s(\mu)]\delta(s-s')\right)$$
$$\times U_J(s-s',\mu,\mu_J), \tag{7.9}$$

$$\mu\frac{d}{d\mu}U_S(k,\mu,\mu_J) = \int dk'\left(-\frac{2\Gamma_S[\alpha_s(\mu)]}{\mu}\left[\frac{\mu\theta(k-k')}{k-k'}\right]_+ + \gamma_S[\alpha_s(\mu)]_+\delta(k-k')\right)$$
$$\times U_S(k-k',\mu,\mu_S), \tag{7.10}$$

where the coeffients at NLL precision needed for discussions are given in Eqs. (7.17), (7.18) and (7.34). These results have been obtained using dimensional regularization to regulate ultraviolet as well as

---

[2] Note that here the thrust jet function $J^{(\tau)}$ is accounting for the collinear radiation in both jets (the same is true for the bHQET jet function J_B), whereas in the first part of the thesis we defined the single hemisphere jet function J describing only one jet, i.e. $J^{(\tau)} = J \otimes J$ (see also Eq. (B.21)).

infrared divergences and do not account for any other infrared cutoff. Ultraviolet renormalization has been carried out in the $\overline{\text{MS}}$ scheme.

Expanded to first order in the strong coupling and setting $\mu_H = \mu_J = \mu_S = \mu$ in Eq. (7.4) we obtain the well-known $\mathcal{O}(\alpha_s)$ singular fixed-order thrust distribution

$$\frac{1}{\sigma_0}\frac{\mathrm{d}\hat{\sigma}_s}{\mathrm{d}\tau}(\tau, Q) = \delta(\tau) + \frac{\alpha_s C_F}{4\pi}\left\{ -8\left[\frac{\theta(\tau)\ln\tau}{\tau}\right]_+ - 6\left[\frac{\theta(\tau)}{\tau}\right]_+ + \left(\frac{2\pi^2}{3} - 2\right)\delta(\tau)\right\} + \mathcal{O}(\alpha_s^2). \quad (7.11)$$

Transforming the partonic massless quark thrust distribution of Eq. (7.4) to Laplace space with the convention

$$\tilde{\sigma}(\nu, Q) = \int\limits_0^\infty \mathrm{d}\tau\, e^{-\nu\tau}\, \frac{1}{\sigma_0}\frac{\mathrm{d}\hat{\sigma}_s}{\mathrm{d}\tau}(\tau, Q) \quad (7.12)$$

the NLL thrust distribution can be written in the condensed form

$$\tilde{\sigma}(\nu, Q) = \exp\left[K(\Gamma_{J(\tau)}, \mu_{H,\nu}, \mu_{J,\nu}) + K(\Gamma_S, \mu_{H,\nu}, \mu_{S,\nu}) \right.$$
$$\left. + \frac{1}{2}\Big(\omega(\gamma_{J(\tau)}, \mu_{H,\nu}, \mu_{J,\nu}) + \omega(\gamma_S, \mu_{H,\nu}, \mu_{S,\nu}) \Big) \right], \quad (7.13)$$

where evolution functions K and ω have the form

$$K(\Gamma, \mu, \mu_0) = 2\int_{\alpha_s(\mu_0)}^{\alpha_s(\mu)} \frac{\mathrm{d}\alpha_s}{\beta[\alpha_s]}\, \Gamma[\alpha_s]\int_{\alpha_s(\mu_0)}^{\alpha_s}\frac{\mathrm{d}\alpha_s'}{\beta[\alpha_s']}, \quad (7.14)$$

$$\omega(\Gamma, \mu, \mu_0) = 2\int_{\alpha_s(\mu_0)}^{\alpha_s(\mu)} \frac{\mathrm{d}\alpha_s}{\beta[\alpha_s]}\, \Gamma[\alpha_s]. \quad (7.15)$$

The QCD beta function is defined as

$$\mu\frac{\mathrm{d}\alpha_s(\mu)}{\mathrm{d}\mu} = \beta[\alpha_s(\mu)] = -2\alpha_s(\mu)\sum_{n=0}\beta_n\left(\frac{\alpha_s(\mu)}{4\pi}\right)^{n+1} \quad (7.16)$$

with $\beta_0 = 11 - \frac{2}{3}n_f$ and $\beta_1 = 102 - \frac{38}{3}n_f$, and the cusp and non-cusp anomalous dimensions read

$$\Gamma_{J(\tau)}[\alpha_s] = -2\Gamma_S[\alpha_s] = 4\,\Gamma^{\text{cusp}}[\alpha_s],$$
$$\gamma_{J(\tau)}[\alpha_s] = 12 C_F\left(\frac{\alpha_s}{4\pi}\right),$$
$$\gamma_S[\alpha_s] = 0 \quad (7.17)$$

with

$$\Gamma^{\text{cusp}}[\alpha_s] = \Gamma_0^{\text{cusp}}\left(\frac{\alpha_s}{4\pi}\right) + \Gamma_1^{\text{cusp}}\left(\frac{\alpha_s}{4\pi}\right)^2,$$
$$\Gamma_0^{\text{cusp}} = 4 C_F,$$
$$\Gamma_1^{\text{cusp}} = C_F\left[C_A\left(\frac{268}{9} - \frac{4\pi^2}{3}\right) - \frac{80}{9}T_F n_f \right], \quad (7.18)$$

The scales $\mu_{H,\nu}$, $\mu_{J,\nu}$ and $\mu_{S,\nu}$ are given by

$$\mu_{H,\nu} = Q\,, \qquad \mu_{J,\nu} = Q(\nu\,e^{\gamma_E})^{-1/2}\,, \qquad \mu_{S,\nu} = Q(\nu\,e^{\gamma_E})^{-1}\,. \quad (7.19)$$

These scales are fixed to the expressions shown and arise from the combination of the renormalization scale dependent NLL U evolution factors *and* the Laplace transformed $\mathcal{O}(\alpha_s)$ corrections in the hard,

jet and soft functions shown in Eqs. (7.5), (7.6) and (7.7) that are logarithmic or plus-distributions. Dropping a π^2 term arising in the Laplace transform of the $(\ln \tau/\tau)_+$ distributions, in this combination the dependence on the renormalization scales μ_H, μ_J and μ_S cancels and the result shown in Eq. (7.13) with the physical scales given in Eqs. (7.19) emerges. Since the structure of these $\mathcal{O}(\alpha_s)$ corrections is already unambiguously known from the NLL renormalization properties, *we consider them part of the NLL logarithmic contributions.* (We refer to Ref. [173] for an extensive discussion on this issue.) Using in Eq. (7.13) the renormalization scales μ_i instead of the scales $\mu_{i,\nu}$ ($i = H, J, S$) one recovers the renormalization scale dependent results coming from the U evolution factors alone.

As we show in Sec. 7.3.1 all terms displayed in Eq. (7.13) are also precisely obtained by the coherent branching formalism at NLL order.

7.1.2   Factorized QCD cross section: massive quarks

In the case of boosted massive quark production the thrust distribution has been determined at NNLL+$\mathcal{O}(\alpha_s)$ in Refs. [18, 19, 118]. Adopting the *pole mass scheme*, the τ distribution as defined in Eq. (7.1) has its partonic threshold at

$$\tau_{\min}^{\text{pole}} = \frac{2(m^{\text{pole}})^2}{Q^2}. \tag{7.20}$$

The observable thrust distribution in the resonance region for $\tau \gtrsim \tau_{\min}^{\text{pole}}$, can be written in a form analogous to the case of massless quarks and has the form

$$\frac{\mathrm{d}\sigma}{\mathrm{d}\tau}(\tau, Q, m^{\text{pole}}) = \int_0^{Q\tau} \mathrm{d}\ell \, \frac{\mathrm{d}\hat{\sigma}_s}{\mathrm{d}\tau}\left(\tau - \frac{\ell}{Q}, Q, m^{\text{pole}}\right) S_{\text{mod}}(\ell), \tag{7.21}$$

where $\mathrm{d}\hat{\sigma}_s/\mathrm{d}\tau$ is the resummed singular massive quark partonic QCD cross section, which contains terms of the form $\alpha_s^n \delta(\tau - \tau_{\min}^{\text{pole}})$ and $\alpha_s^n [\ln^k(\tau - \tau_{\min}^{\text{pole}})/(\tau - \tau_{\min}^{\text{pole}})]_+)$. The non-singular corrections to the factorized cross section in Eq. (7.21) are coming from terms of the form $\alpha_s^n \ln^k(\tau - \tau_{\min}^{\text{pole}})$. In the resonance region these corrections are power-suppressed by a *additional factor* of order $(1 \text{ GeV})/Q$ or $(1 \text{ GeV})/m$ and can, in analogy to the case of massless quark production, be safely neglected for top quark production. In an arbitrary mass scheme m with $\delta m = m^{\text{pole}} - m$ we can write the observable thrust distribution in the form

$$\frac{\mathrm{d}\sigma}{\mathrm{d}\tau}(\tau, Q, m, \delta m) = \int_0^{Q\tau} \mathrm{d}\ell \, \frac{\mathrm{d}\hat{\sigma}_s}{\mathrm{d}\tau}\left(\tau - \frac{\ell}{Q}, Q, m, \delta m\right) S_{\text{mod}}(\ell), \tag{7.22}$$

where the additional argument δm indicates the dependence on the mass scheme changing contributions in the perturbation series for the partonic cross section.

For the rescaled thrust variable defined in Eq. (7.2) the relation analogous to Eq. (7.21) reads

$$\frac{\mathrm{d}\sigma}{\mathrm{d}M_\tau}(M_\tau, Q, m^{\text{pole}}) = \int_0^{2m^{\text{pole}}M_\tau/Q} \mathrm{d}\ell \, \frac{\mathrm{d}\hat{\sigma}_s}{\mathrm{d}M_\tau}\left(M_\tau - \frac{Q\ell}{2m^{\text{pole}}}, Q, m^{\text{pole}}\right) S_{\text{mod}}(\ell), \tag{7.23}$$

where

$$\frac{\mathrm{d}\hat{\sigma}_s}{\mathrm{d}M_\tau}(M_\tau, Q, m^{\text{pole}}) \equiv \frac{2m^{\text{pole}}}{Q^2} \frac{\mathrm{d}\hat{\sigma}_s}{\mathrm{d}\tau}\left(\frac{2m^{\text{pole}}M_\tau}{Q^2}, Q, m^{\text{pole}}\right). \tag{7.24}$$

The generalization of Eqs. (7.23) and (7.24) to an arbitrary mass scheme is straightforward.

The singular partonic cross section in the resonance region can be written in the factorized form

$$\frac{\mathrm{d}\hat{\sigma}_s}{\mathrm{d}\tau}(\tau, Q, m^{\text{pole}}) = \sigma_0 \, Q \, H_Q(Q, \mu_H) U_H(Q, \mu_H, \mu_m) H_m(Q, m^{\text{pole}}, \mu_m) U_m\left(\frac{Q}{m^{\text{pole}}}, \mu_m, \mu_H\right)$$

$$\times \int_0^{Q^2(\tau-\tau_{\text{pole}}^{\text{min}})} \mathrm{d}s \int_0^{s/m} \mathrm{d}\hat{s}' \; U_{J_B}(\hat{s}', \mu_H, \mu_{J_B}) \, J_B\left(\frac{s}{m^{\text{pole}}} - \hat{s}', m^{\text{pole}}, \delta m = 0, \mu_{J_B}\right)$$

$$\times \int_0^{Q(\tau-\tau_{\text{pole}}^{\text{min}})-s/Q} \mathrm{d}k \; U_S(k, \mu_H, \mu_S) \, S^{(\tau)}\left(Q(\tau - \tau_{\text{min}}^{\text{pole}}) - \frac{s}{Q} - k, \mu_S\right), \tag{7.25}$$

where σ_0 is again the total partonic e^+e^- tree-level cross section. The hard function H_Q, the soft function $S^{(\tau)}$ and the soft evolution factor U_S, as well as the soft model function S_{mod} in Eq. (7.25) are identical to the case of massless quarks [18, 19]. Their effects are universal for massless and boosted massive quarks, because large angle soft radiation cannot distinguish between the color flow associated to massless and boosted massive quarks. The relation of the soft function renormalization scale to τ is, however, modified to the form $\mu_S \sim Q(\tau - \tau_{\text{min}})$ because the quark mass shifts the τ threshold from zero to τ_{min}. For the other components of the factorization formula the quark mass represents an additional intermediate scale which leads to modifications. The term $J_B^{(\tau)}(\hat{s})$ is the bHQET jet function [18, 19] which describes the linearized distribution of the invariant mass of *both* jets *with respect to the partonic threshold*,

$$\hat{s} = \frac{s - (2m^{\text{pole}})^2}{m^{\text{pole}}}, \tag{7.26}$$

due to ultra-collinear gluon radiation in the region where $\hat{s}$ is much smaller than the mass, $\hat{s} \ll m$. It depends on the renormalization scale $\mu_{J_B} \sim Q\mu_S/m \sim Q^2(\tau - \tau_{\text{min}})/m$, and its expression at $\mathcal{O}(\alpha_s)$ in an arbitrary mass scheme m, $J_B^{(\tau)}(\hat{s}, m, \delta m, \mu_{J_B})$, with $\delta m = m^{\text{pole}} - m \neq 0$ is shown in Eq. (7.28). At NLL+$\mathcal{O}(\alpha_s)$ the bHQET jet function completely controls the quark mass scheme dependence of the singular partonic cross section. So at this order the singular partonic cross section in an arbitrary mass scheme, $\frac{\mathrm{d}\hat{\sigma}_s}{\mathrm{d}\tau}(\tau, Q, m, \delta m)$, is obtained from Eq. (7.25), by employing the bHQET jet function $J_B^{(\tau)}(\hat{s}, m, \delta m, \mu_{J_B})$ and setting $m^{\text{pole}} \to m$ everywhere else. This is because $J_B^{(\tau)}$ has mass sensitivity already at tree level through the dependence on τ_{min}, see Eq. (7.20). Physically the ultra-collinear radiation is, owing to heavy quark symmetry, related to the soft radiation governing the mass of heavy-light mesons. The mass mode factor H_m contains fluctuations at the scale of the quark mass $\mu_m \sim m$ coming from the massive quark field fluctuations that are off-shell in the resonance region and integrated out. Its expression at $\mathcal{O}(\alpha_s)$ is shown in Eq. (7.27) and a detailed discussion on its definition and properties can be found in Ref. [19]. The factor U_{J_B} sums logarithms between the ultra-collinear jet scale μ_{J_B} and the hard scale μ_H, U_S sums logarithms between the soft scale μ_S and the hard scale, and U_m sum logarithms between the quark mass scale μ_m and the hard scale.

The $\mathcal{O}(\alpha_s)$ results for the mass mode and the bHQET jet functions read [19]

$$H_m(m, \mu) = 1 + \frac{\alpha_s(\mu)C_F}{4\pi}\left(2\ln^2\frac{m^2}{\mu^2} - 2\ln\frac{m^2}{\mu^2} + 8 + \frac{\pi^2}{3}\right) + \mathcal{O}(\alpha_s^2), \tag{7.27}$$

$$m J_B(\hat{s}, m, \delta m, \mu) = \delta(\hat{s}) - 4\,\delta m\,\delta'(\hat{s}) + \frac{\alpha_s(\mu)C_F}{4\pi}\left(\frac{16}{\mu}\left[\frac{\mu\ln\frac{\hat{s}}{\mu}}{\hat{s}}\right]_+ - \frac{8}{\mu}\left[\frac{\mu}{\hat{s}}\right]_+\right.$$

$$\left. + (8 - \pi^2)\delta(\hat{s})\right) + \mathcal{O}(\alpha_s^2), \tag{7.28}$$

where the result for the bHQET jet function has been displayed for a general quark mass renormalization scheme m which is related to the pole mass scheme by the relation $\delta m = m_{\text{pole}} - m$. So

in Eq. (7.28) we have $\hat{s} = (s - m^2)/m$. Also here the bHQET jets function already accounts for the ultra-collinear radiation in both hemispheres. Their respective anomalous dimensions can (to all orders) be written in the form

$$\mu \frac{d}{d\mu} U_m \left(\frac{Q}{m}, \mu_m, \mu \right) = \left(\Gamma_m[\alpha_s(\mu)] \ln \left(\frac{m^2}{Q^2} \right) + \gamma_m[\alpha_s(\mu)] \right) U_m \left(\frac{Q}{m}, \mu_m, \mu \right) \qquad (7.29)$$

$$\mu \frac{d}{d\mu} U_{J_B}(\hat{s}, \mu, \mu_{J_B}) = \int d\hat{s}' \left(-\frac{\Gamma_{J_B}[\alpha_s(\mu)]}{\mu} \left[\frac{\mu \theta(\hat{s} - \hat{s}')}{\hat{s} - \hat{s}'} \right]_+ + \gamma_{J_B}[\alpha_s(\mu)] \delta(\hat{s} - \hat{s}') \right) \qquad (7.30)$$
$$\times U_{J_B}(\hat{s} - \hat{s}', \mu, \mu_{J_B}),$$

where the coeffients at NLL precision are given in Eqs. (7.34), see also Eqs. (7.17) and (7.18). These results have been obtained using dimensional regularization to regulate ultraviolet as well as infrared divergences and do not account for any other infrared cutoff. Ultraviolet renormalization has been carried out in the $\overline{\text{MS}}$ scheme.

From a physical point of view it appears more appropriate to evolve the factors U_{J_B}, U_S and U_m to the quark mass scale μ_m (at which point the factor U_m could be dropped) rather than the hard scale. This is because the logarithms resummed in U_{J_B} and U_m physically arise from scales below the quark mass. The form we have adopted here is equivalent due to renormalization group consistency conditions [19] and matches better to the form of the log resummations obtained from the coherent branching formalism as discussed in Sec. 7.3.2. For our examinations we need the expressions for the U factors at NLL and the hard, mass matching, soft and the bHQET jet functions at $\mathcal{O}(\alpha_s)$. Expanding to first order in the strong coupling and setting $\mu_H = \mu_{J_B} = \mu_S = \mu$ we obtain the $\mathcal{O}(\alpha_s)$ singular fixed-order massive quark thrust distribution in the pole mass scheme ($L_m = \ln \frac{(m^{\text{pole}})^2}{Q^2}$):

$$\frac{1}{\sigma_0} \frac{d\hat{\sigma}_s}{d\tau}(\tau, Q, m^{\text{pole}}) = \delta(\tau - \tau_{\min}^{\text{pole}}) + \frac{\alpha_s C_F}{4\pi} \left\{ -8(1 + L_m) \left[\frac{\theta(\tau - \tau_{\min}^{\text{pole}})}{\tau - \tau_{\min}^{\text{pole}}} \right]_+ \right.$$
$$\left. + (4L_m^2 + 2L_m + 2\pi^2) \delta(\tau - \tau_{\min}^{\text{pole}}) \right\} + \mathcal{O}(\alpha_s^2). \qquad (7.31)$$

In Eq. (7.31), changing to another mass scheme m leads to the additional term $\delta'(\tau - \tau_{\min}^{\text{pole}}) \, 4m \, \delta m / Q^2$ on the RHS, and this term has to be counted as a NLL contributions as well.

We note that in Eq. (7.31) the dead cone effect [154, 155] is manifest as a $\tau \to \tau_{\min}$ behavior that is less singular than the $\tau \to 0$ limit for massless quark production displayed in Eq. (7.11). However, one can see from the form of the bHQET jet function in Eq. (7.28), that ultra-collinear radiation still involves soft-collinear double-logarithmic singularities which arise from the coherent effect of ultra-collinear gluons physically originating from the associated top quark and its opposite hemisphere [18, 19]. So, in the context of QCD factorization based on SCET and bHQET the deadcone effect arises from a cancellation of double logarithmic singularities between the ultra-collinear and the large-angle soft radiation (radiated in the collinear direction and called collinear-soft radiation in the following). This can be seen from the expression for the partonic soft function $S^{(\tau)}$ given in Eq. (7.7) which exhibits the same double-logarithmic singularity as the bHQET jet function, but with the opposite sign. So the origin of the deadcone effect from the perspective of QCD factorization, which is manifestly gauge invariant, is due to a cancellation of ultra-collinear and collinear-soft radiation. This is somewhat different (but not contradictory) to the conventional and gauge-dependent view that the deadcone originates from the suppression of collinear radiation off the boosted top quarks due to the finite top quark mass. The relation between these two views is subtle because in the canonical SCET/bHQET approach (ultra-)collinear jet functions are defined with a zero-bin subtraction [88] to avoid a double counting between (ultra-)collinear and collinear-soft radiation.

Transforming the partonic massive quark thrust distribution to Laplace space with the convention

$$\tilde{\sigma}(\nu, Q, m^{\mathrm{pole}}) = \int_{\tau_{\min}^{\mathrm{pole}}}^{\infty} \mathrm{d}\tau \, e^{-\nu\tau} \frac{1}{\sigma_0} \frac{\mathrm{d}\hat{\sigma}_s}{\mathrm{d}\tau}(\tau, Q, m^{\mathrm{pole}}) \tag{7.32}$$

the NLL thrust distribution can be written in the condensed form

$$\tilde{\sigma}(\nu, Q, m^{\mathrm{pole}}) = \exp\left[-K(\Gamma_{H_m}, \mu_{H,\nu}, \mu_{m,\nu}) + K(\Gamma_{J_B}, \mu_{H,\nu}, \mu_{J_B,\nu}) + K(\Gamma_S, \mu_{H,\nu}, \mu_{S,\nu})\right]$$

$$\times \exp\left[\frac{1}{2}\Big(\omega(\gamma_{H_m} - \gamma_{H_Q}, \mu_{H,\nu}, \mu_{m,\nu}) + \omega(\gamma_{J_B}, \mu_{H,\nu}, \mu_{J_B,\nu}) + \omega(\gamma_S, \mu_{H,\nu}, \mu_{S,\nu})\Big)\right] \tag{7.33}$$

where the evolution functions K and ω have been given in Eqs. (7.14) and the cusp and non-cusp anomalous dimensions not already displayed in Eqs. (7.17) and (7.18) read

$$\Gamma_{J_B}[\alpha_s] = -\Gamma_{H_m}[\alpha_s] = -\Gamma_{H_Q}[\alpha_s] = 2\Gamma^{\mathrm{cusp}}[\alpha_s]\,,$$
$$\gamma_H[\alpha_s] = -12C_F\left(\frac{\alpha_s}{4\pi}\right),$$
$$\gamma_{H_m}[\alpha_s] = -8C_F\left(\frac{\alpha_s}{4\pi}\right),$$
$$\gamma_{J_B}[\alpha_s] = 8C_F\left(\frac{\alpha_s}{4\pi}\right) \tag{7.34}$$

and the scales μ_H, μ_m, $\mu_{J_B,\nu}$ and $\mu_{S,\nu}$ are given by

$$\mu_{H,\nu} = Q\,, \qquad \mu_{m,\nu} = m^{\mathrm{pole}}\,, \qquad \mu_{J_B,\nu} = \frac{Q^2}{m^{\mathrm{pole}}}(\nu\, e^{\gamma_E})^{-1}\,, \qquad \mu_{S,\nu} = Q(\nu\, e^{\gamma_E})^{-1}\,. \tag{7.35}$$

As for the case of massless quark production these scales are fixed to the expressions shown and arise from the combination of the renormalization scale dependent NLL U evolution factors *and* the Laplace transformed $\mathcal{O}(\alpha_s)$ corrections in the hard, mass mode, bHQET jet and soft functions, shown in Eqs. (7.5), (7.27), (7.28) and (7.7) respectively, which are logarithmic and plus-distributions. In this combination the dependence on the renormalization scales μ_H, μ_m, μ_{J_B} and μ_S cancels and the result shown in Eq. (7.33) with the physical scales given in Eqs. (7.35) emerges. Like in the case of massless quarks, since the structure of these $\mathcal{O}(\alpha_s)$ corrections is already unambiguously known from the NLL renormalization properties, we consider them part of the NLL logarithmic contributions. Using in Eq. (7.33) the renormalization scales μ_i instead of the scales $\mu_{i,\nu}$ ($i = H, m, J_B, S$) one recovers the renormalization scale dependent results coming from the U evolution factors alone. The mass dependence of the scales in Eq. (7.35) and in the rescaled thrust variable M_τ defined in Eq. (7.2) is subleading and does not generate NLL contributions when the quark mass scheme is changed.

As we show in Sec. 7.3.2 all terms shown in Eq. (7.33) are also precisely obtained by the coherent branching formalism at NLL order.

We finally note that all functions and U factors that appear in Eqs. (7.4) and (7.25) have been determined using dimensional regularization to regularize infrared and ultraviolet divergences and the $\overline{\mathrm{MS}}$ renormalization scheme. At this point the partonic soft function $S^{(\tau)}(k)$ does *not* contain any gap subtraction [174] to remove its $\mathcal{O}(\Lambda_{\mathrm{QCD}})$ renormalon ambiguity related to the partonic threshold at $k = 0$.

7.1.3 Importance of the shape function

The soft model shape function S_{mod} appearing in Eqs. (7.3) and (7.21) represents an essential part of the thrust factorization theorems since it accounts for the hadronization effects that affect the observable thrust distribution. The shape function leads to a smearing of the parton level contributions

and an additional shift of the peak position since the hadronization effects increase the hemisphere masses by non-perturbative contributions. It is also essential as far as the shape of the distribution in the resonance region is concerned where the thrust distribution is peaked.

Since in this work we are mainly interested in the Q_0-dependence of the partonic contributions, one may conclude that one should better drop the effects of the shape function S_{mod} in our analysis such that it does not interfere with the perturbative effects. However, this is not possible since analyzing the singular partonic corrections of the thrust distribution (and their Q_0 dependence) alone without any smearing does not allow for a correct interpretation of their contributions to the observable distribution. This can be easily seen for example from the $\mathcal{O}(\alpha_s)$ fixed-order parton level results for the massless and massive quark thrust distributions shown in Eqs. (7.11) and (7.31). Here the partonic contributions to the observable distribution contained in the δ-functions and in the regularized singularity structures of the plus distributions at the partonic thresholds at $\tau = 0$ and $\tau = \tau_{\mathrm{min}}$, respectively, remain invisible if one simply studies the partonic contributions at a function of τ. One may in particular conclude wrongly, that the observable peak position is independent of Q_0 simply because the partonic threshold always remains at $\tau = 0$ and $\tau = \tau_{\mathrm{min}}$ for massless and massive quarks, respectively. The essential point is that the complete set of singular structures in the (infinitesimal) vicinity of the threshold contributes in the resonance region and non-trivially affect the observable peak location. Thus, the partonic thresholds alone do not govern the observable peak position and some smearing is crucial to fully resolve the effects of all parton level contributions.

As a consequence, in our analysis of the partonic effects coming from the shower cut Q_0, it is still important that we account for the hadronic smearing of the shape function S_{mod}. For the analysis of the partonic effects coming from the shower cut Q_0 we therefore include a shape function that is Q_0-independent. It has the simple form

$$S_{\mathrm{mod}}(\ell) \;=\; \frac{128\,\ell^3}{3\,\Lambda_{\mathrm{m}}^4}\,\exp\!\Big(-\frac{4\ell}{\Lambda_{\mathrm{m}}}\Big)\,, \tag{7.36}$$

and the important properties

$$\int_0^\infty \mathrm{d}\ell\,S_{\mathrm{mod}}(\ell) \;=\; 1 \quad \text{and} \quad \int_0^\infty \mathrm{d}\ell\,\ell\,S_{\mathrm{mod}}(\ell) \;=\; \Lambda_{\mathrm{m}}\,, \tag{7.37}$$

where we consider Λ_{m} values between 1 and 5 GeV for our conceptual discussions. (See also our comment after Eq. (7.3).) We use this shape function for our analytic calculations as well as for the parton level numerical results we obtain from the HERWIG event generator. This way we can ensure that the smearing is precisely equivalent for both types of results. We note that the exact form of S_{mod} and the size of the smearing scale Λ_{m} affect the form and the absolute value of peak location of the distribution in the resonance region. However, for our analysis only the relative dependence of the peak position on the cut value Q_0 is essential, for which the exact form of the shape function turns out to be irrelevant. We further note that for our numerical studies for top quark production we use the smearing due to S_{mod} to also mimic effects of the top quark width even though the form of S_{mod} does not provide a fully consistent description.

As we show in Sec. 8.1, for making physical predictions the soft model function has to compensate for the dependence of the parton level large angle soft radiation on the Q_0 cut. This is because for large angle soft radiation the shower cut represents a factorization scale that separates the parton level and non-perturbative regions. The point of our examination, however, is not to make physical predictions, but to conceptually quantify the dependence on Q_0 with the aim to disentangle it unambiguously from the effect Q_0 has on the mass parameter. Along the same lines, we also do not account for the possible effects of a finite experimental resolution. The latter results in an additional smearing of the resonance distribution that, particularly in the context of hadron colliders, may by far exceed the smearing caused by the hadronization effects. While the overall norm still remains irrelevant for the peak position, properties of the theoretical distribution far away from the resonance region could

then affect the experimentally observed peak position in a non-negligible way. In such a case the non-singular corrections may have to be included for a reliable description. This is straightforward, but beyond the scope of this work.

7.1.4 NLO precision for the resonance location

Within quantum field theory a consistent discussion of a quark mass (renormalization) scheme is only meaningful if the theoretical description of the observable of interest has all or at least the dominant $\mathcal{O}(\alpha_s)$ corrections implemented. In the factorization theorems of Eqs. (7.3) and (7.21) we can neglect the nonsingular corrections since they are power-suppressed in the resonance region. To be concrete, they lead to negligible shifts in the peak position of order $(1\,\text{GeV})^2/Q^2$ and $(1\,\text{GeV})^2/m^2$, respectively, upon including the smearing effects coming from the soft model shape function S_{mod}. It is now obvious to ask the question if, apart from the summation of logarithms at NLL order, also the full set of $\mathcal{O}(\alpha_s)$ non-logarithmic fixed-order corrections contained in the hard, mass mode, jet and soft functions are needed to achieve $\mathcal{O}(\alpha_s)$ precision in the resonance region. These corrections are either constant (originating from the functions H_Q and H_m, see Eqs. (7.5) and (7.27), respectively) or proportional to the delta-function (coming from the functions $J^{(\tau)}$, $J_B^{(\tau)}$ and $S^{(\tau)}$, see Eqs. (7.6),(7.28) and (7.7), respectively), and their sum is displayed in Eqs. (7.11) and (7.31). If one considers all aspects of the thrust distribution in the resonance region, obviously both, NLL resummation and the full set of $\mathcal{O}(\alpha_s)$ fixed-order corrections are needed. For example, the one-loop corrections in the hard function lead to $\mathcal{O}(\alpha_s)$ corrections in the norm of the thrust distributions. This in general favors the so-called "primed" counting scheme [164] where NLL$'$ order refers to the resummation of logarithms at NLL order combined with all additional fixed-order corrections at $\mathcal{O}(\alpha_s)$.

However, the mass sensitivity of the thrust distribution in the peak region mainly comes from the location of the resonance peak, τ_{peak}, and properties such as the overall norm of the distribution are less important. For most practical considerations of such kinematic distributions, the norm is even eliminated on purpose by considering distributions that are normalized to a restricted interval in the kinematic variable. Therefore, in our analysis we mainly focus on the resonance peak position of the thrust distribution and do not consider the overall norm. Interestingly, as we show in the following, when discussing the peak position with NLO (i.e. $\mathcal{O}(\alpha_s)$) precision, we only have to account for the NLL resummed cross section, and we can neglect the $\mathcal{O}(\alpha_s)$ non-logarithmic corrections. The reason why these non-logarithmic $\mathcal{O}(\alpha_s)$ corrections do not contribute to the peak position τ_{peak} at NLO is that they are represent corrections proportional to the LL cross section.

To see this more explicitly let us rewrite the NLL+$\mathcal{O}(\alpha_s)$ thrust distributions of Eqs. (7.3) and (7.21) in the generic form

$$f_{\text{NLL}+\alpha_s}(\tau) \;=\; \int_0^\tau \text{d}\bar{\tau}\, \hat{f}_{\text{NLL}+\alpha_s}(\bar{\tau})\, \bar{S}_{\text{mod}}(\tau - \bar{\tau})\,, \qquad (7.38)$$

where f and $\hat{f}$ stand for the hadron and parton level thrust distributions, respectively, and $\bar{S}_{\text{mod}}$ for the hadronization shape function after variable rescaling. The NLL+$\mathcal{O}(\alpha_s)$ partonic thrust distribution can then be written in the form

$$\hat{f}_{\text{NLL}+\alpha_s}(\tau) \;=\; \hat{f}_{\text{LL}}(\tau) \;+\; \alpha_s\left(\Delta\hat{f}_{\text{NLL}}(\tau) + c\hat{f}_{\text{LL}}(\tau)\right) \qquad (7.39)$$

where $\hat{f}_{\text{LL}}$ represents the LL cross section (which provides the complete leading order approximation), the term $\alpha_s\Delta f_{\text{NLL}}$ contains all NLL corrections in the NLL resummed cross section, and $\alpha_s c$ stands for the non-logarithmic $\mathcal{O}(\alpha_s)$ corrections mentioned above. The latter corrections are related to the LL tower of logarithms associated to the term $(2\pi^2/3-2)\delta(\tau)$ in Eq. (7.11) and the term $2\pi^2\delta(\tau - \tau_{\text{min}}^{\text{pole}})$ in Eq. (7.31). Note that corrections arising from a change in the quark mass scheme are proportional to derivatives of $\delta(\tau - \tau_{\text{min}}^{\text{pole}})$ and therefore *always* contained in the term $\alpha_s\Delta f_{\text{NLL}}$.

The LL peak position τ_{peak}^0 is determined from the equality

$$0 \overset{!}{=} f'_{\text{LL}}(\tau_{\text{peak}}^0) = \int_0^{\tau_{\text{peak}}^0} \mathrm{d}\bar{\tau}\, \hat{f}_{\text{LL}}(\bar{\tau})\, \bar{S}'_{\text{mod}}(\tau_{\text{peak}}^0 - \bar{\tau}). \tag{7.40}$$

At the NLL level, writing the $\mathcal{O}(\alpha_s)$ correction to the peak position as $\delta\tau_{\text{peak}}$, the corresponding equality reads

$$0 \overset{!}{=} f'_{\text{NLL}+\alpha_s}(\tau_{\text{peak}}^0 + \delta\tau_{\text{peak}}) \tag{7.41}$$

$$= \int_0^{\tau_{\text{peak}}^0 + \delta\tau_{\text{peak}}} \mathrm{d}\bar{\tau}\, \left[\hat{f}_{\text{LL}}(\bar{\tau}) + \alpha_s \left(\Delta\hat{f}_{\text{NLL}}(\bar{\tau}) + c\hat{f}_{\text{LL}}(\bar{\tau}) \right) \right] \bar{S}'_{\text{mod}}(\tau_{\text{peak}}^0 + \delta\tau_{\text{peak}} - \bar{\tau})$$

$$= \delta\tau_{\text{peak}} \int_0^{\tau_{\text{peak}}^0} \mathrm{d}\bar{\tau}\, \hat{f}_{\text{LL}}(\bar{\tau})\, \bar{S}''_{\text{mod}}(\tau_{\text{peak}}^0 - \bar{\tau})$$

$$+ \alpha_s \int_0^{\tau_{\text{peak}}^0} \mathrm{d}\bar{\tau}\, \left[\Delta\hat{f}_{\text{NLL}}(\bar{\tau}) + c\hat{f}_{\text{LL}}(\bar{\tau}) \right] \bar{S}'_{\text{mod}}(\tau_{\text{peak}}^0 - \bar{\tau}) + \mathcal{O}(\alpha_s^2)$$

$$= \delta\tau_{\text{peak}} \int_0^{\tau_{\text{peak}}^0} \mathrm{d}\bar{\tau}\, \hat{f}_{\text{LL}}(\bar{\tau})\, \bar{S}''_{\text{mod}}(\tau_{\text{peak}}^0 - \bar{\tau})$$

$$+ \alpha_s \int_0^{\tau_{\text{peak}}^0} \mathrm{d}\bar{\tau}\, \Delta\hat{f}_{\text{NLL}}(\bar{\tau})\, \bar{S}'_{\text{mod}}(\tau_{\text{peak}}^0 - \bar{\tau}) + \mathcal{O}(\alpha_s^2),$$

where in the third line we have dropped terms of $\mathcal{O}(\alpha_s^2)$ and in the fourth we used the LL constraint of Eq. (7.40) for the non-logarithmic $\mathcal{O}(\alpha_s)$ fixed-order corrections with are proportional to the LL cross section.

The outcome is that the non-logarithmic $\mathcal{O}(\alpha_s)$ fixed-order corrections contained in the hard, jet and soft function are not relevant for discussing the peak position τ_{peak} as far as $\mathcal{O}(\alpha_s)$ precision is concerned and would only enter when $\mathcal{O}(\alpha_s^2)$ corrections are considered. Since the peak position represents the dominant characteristics of the thrust distribution entering the mass determination, we can therefore conclude that the resummation of logarithmic correction at the NLL level is sufficient to achieve $\mathcal{O}(\alpha_s)$ precision for a mass determination based on the resonance peak position. Going along the line of arguments we use in the subsequent sections this important result also means that to the extent that parton showers systematically and *correctly sum all NLL logarithmic terms*, the peak position of the thrust distribution generated by their evolution is already $\mathcal{O}(\alpha_s)$ precise, even *without* including any additional NLO fixed-order corrections by an NLO matching prescription.

7.2 Coherent branching formalism

The coherent branching formalism has proven to be a very powerful tool for analytic resummation of a large number of observables. Besides the analytic use, it forms the core rationale behind coherent parton shower algorithms, notably the angular ordered algorithms of the Herwig family [151, 152, 175] of event generators. Following earlier work of Ref. [163, 167] we use this framework to calculate the parton level jet mass distributions $\mathcal{J}(s, Q^2)$ for massless quarks and $\mathcal{J}(s, Q^2, m^2)$ for massive quarks originating from successive gluon radiation off the progenitor quark and anti-quark pair generated by the hard interaction at c.m. energy Q. Here the variable $s = M_{\text{jet}}^2$ stands for the resulting squared jet invariant mass. This determines the partonic thrust distribution in the peak region as defined in Eq. (7.1) as

$$\frac{\mathrm{d}\hat{\sigma}^{\text{cb}}}{\mathrm{d}\tau}(\tau, Q) = \sigma_0 \int \mathrm{d}s_1\, \mathrm{d}s_2\, \delta\left(\tau - \frac{s_1 + s_2}{Q^2}\right) \mathcal{J}(s_1, Q^2)\mathcal{J}(s_2, Q^2),$$

$$\frac{\mathrm{d}\hat{\sigma}^{\text{cb}}}{\mathrm{d}\tau}(\tau, Q, m) = \sigma_0 \int \mathrm{d}s_1\, \mathrm{d}s_2\, \delta\left(\tau - \frac{s_1 + s_2}{Q^2}\right) \mathcal{J}(s_1, Q^2, m^2)\mathcal{J}(s_2, Q^2, m^2), \tag{7.42}$$

for massless and massive quark cases, respectively. The jet mass distributions obtained in the context of coherent branching incorporate coherently the dynamic effects of soft as well as (ultra-)collinear radiation and are UV-finite quantities. Thus they differ from the jet functions $J^{(\tau)}$ and $J_B^{(\tau)}$ in the QCD factorization approach which describe the factorized collinear and ultra-collinear gluon effects, respectively, and are determined from UV-divergent effective theory matrix elements that need to be renormalized. In order to obtain the observable hadron level thrust distribution, the contributions of the non-perturbative effects are accounted for in exactly the same way as for the QCD factorization approach by an additional convolution with a soft model shape function, as shown in Eqs. (7.3) and (7.21), see Refs. [163, 167, 176].

We note that in Eqs. (7.42) we have used the superscript 'cb' to indicate the cross sections obtained in the coherent branching formalism. We use this notation throughout this work, when suitable, to distinguish results based on the coherent branching formalism from those obtained in the factorization approach.

While an analytic treatment of the coherent branching formalism in the strict context of perturbation theory does not rely on the presence of any infrared cutoff,[3] it is, however, required within the realm of an event generator for several reasons. These include the Landau pole singularity of the strong coupling, which emerges because its renormalization scale is tied to shower evolution variables, and that the particle multiplicities diverge when the shower evolves to infrared scales. In addition, in the limit of small scales the perturbative treatment of the parton splitting breaks down anyway, and it is therefore mandatory to terminate the shower at a low scale where the perturbative description is still valid and hand over the partonic ensemble generated through the shower emissions to a phenomenological model of hadronization.

The variables we consider in the following of this section are used both to derive analytic results, but we also stress that they precisely correspond to the variables employed in the angular ordered parton shower of the HERWIG 7 event generator. The results obtained from the HERWIG 7 event generator only differ from the analytic framework by the implementation of exact momentum conservation with respect to the momenta of all final state particles that emerge when the shower has terminated at its infrared cutoff Q_0. This implementation of momentum conservation shall not change the jet mass distribution and is explained in more detail in Sec. 7.2.3. There we also briefly discuss some HERWIG 7 (version 7.1.2) specific implementations in its default setting that go beyond the coherent branching formalism and that we do not use in the context of the conceptual studies carried out in this work.

7.2.1 Massless case

Starting from an initial, color-connected $q\bar{q}$-pair with momenta p and $\bar{p}$, the momenta of the partons emerging from the shower evolution of the quark carrying the momentum p are parametrized based on

$$k_i^\mu = \alpha_i \, p^\mu + \beta_i \, \bar{n}^\mu + k_{i,\perp}^\mu \,, \tag{7.43}$$

where k_i is the quarks momentum after the i-th emission. In the massless case we use $\bar{n} = \bar{p}$ as the reference direction to specify the collinear limit, with $k_{i,\perp} \cdot p = k_{i,\perp} \cdot n = 0$, $k_{i,\perp}^2 < 0$ and β_i being determined by the virtualities $k_i \cdot k_i = k_i^\mu k_{i\mu} = k_i^2$ as

$$\beta_i = \frac{-k_{i,\perp}^2 + k_i^2}{2\alpha_i(p \cdot \bar{n})} \,. \tag{7.44}$$

---

[3]We refer to strict perturbation theory as expanding in α_s at a constant renormalization scale such that the evolution is described by higher powers of α_s and logarithms only, and that virtual loop and real radiation phase space integrals can be carried out down to zero momenta.
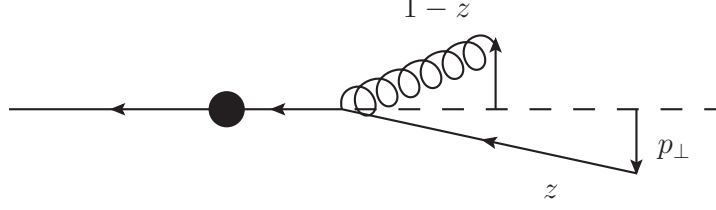
Figure 7.1: A gluon branching off a back-to-back quark/anti-quark system. The radiated gluon is assumed to carry a fraction $1 - z$ of the parent's momentum and is emitted at a transverse momentum which equals the one acquired by, in this case, the anti-quark after the emission.

The radiation off the anti-quark with momentum $\bar{p}$ is described similarly with a reference direction $n = p$. Expressing k_i^μ in terms of the momentum of the emitter before the i-th branching we find

$$k_i^\mu = z_i \, k_{i-1}^\mu + \frac{z_i^2 k_{i-1,\perp}^2 - k_{i,\perp}^2 + k_i^2 - z_i^2 k_{i-1}^2}{2 z_i (k_{i-1} \cdot \bar{n})} \bar{n}^\mu + q_{i,\perp}^\mu \tag{7.45}$$

where the physical splitting variables relative to the quark's momentum k_{i-1} before the i-th emission relate to the global light-cone decomposition Eq. (7.43) as

$$z_i = \frac{\alpha_i}{\alpha_{i-1}} , \tag{7.46}$$

$$q_{i,\perp}^\mu = k_{i,\perp}^\mu - z_i k_{i-1,\perp}^\mu , \tag{7.47}$$

where $\alpha_0 = 1$ as well as $q_{0,\perp}^\mu = 0$ are understood. This means that for the first emission the physical branching variables coincide with the global parametrization. We have depicted the variables of one branching in Fig. 7.1. Soft gluon coherence is encoded through ordering emissions in an angular variable [159],

$$\tilde{q}_i^2 = \frac{p_{i,\perp}^2}{z_i^2 (1 - z_i)^2} , \tag{7.48}$$

where $p_{i,\perp}^2 = -q_{i,\perp}^2$ is the magnitude of the transverse momentum, which is purely spacelike and perpendicular to the emitter axis in the centre-of-mass system of the momenta k_i and $\bar{n}$. The explicit restrictions of decreasing opening angle of subsequent emissions following a branching at scale $\tilde{q}_i$ from the evolving quark or anti-quark at scale $\tilde{q}_{i+1}^2$, and the radiated gluon at scale $\tilde{k}_i^2$ are imposed by the conditions

$$\tilde{q}_{i+1}^2 < z_i^2 \, \tilde{q}_i^2 \qquad \text{and} \qquad \tilde{k}_i^2 < (1 - z_i)^2 \, \tilde{q}_i^2 . \tag{7.49}$$

In the context of these variables, the Altarelli-Parisi splitting functions explicitly show the full Eikonal radiation pattern and the correct collinear limit, see *e.g.* Ref. [177] for an overview and comparison to dipole-type parton showers. The formalism is appropriate to resum higher order logarithmic corrections for observables that are inclusive concerning the collinear radiation in the same jet *and* in the sense that the information that large-angle soft gluon radiation originates from a particular collinear parton is unresolved and can hence be described to originate from the net collinear color charge of the whole jet. Momentum conservation in the branching $i - 1 \rightarrow i$ implies

$$k_{i-1}^2 = \frac{k_i^2}{z_i} + \frac{q_i^2}{1 - z_i} + z_i(1 - z_i)\tilde{q}_i^2 , \tag{7.50}$$

where q_i^2 is the virtuality of the emitted gluon, the momentum of which is parametrized in a decomposition similar to Eq. (7.43).
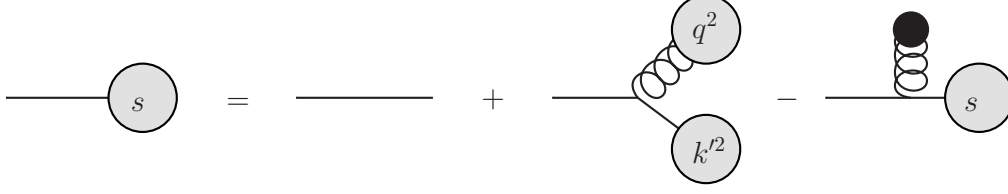
Figure 7.2: Graphical representation of the evolution equation Eq. 7.51: Grey blobs denote the quark and gluon jet function at a given jet mass, a single line implies a δ-function at mass zero, while the black dot represents a factor of one and implies an unconstrained integration over the gluon's emission scale and momentum fraction.

We follow Ref. [163] and start with an analytic approach for which the evolution equation for the jet mass distribution starting at a hard scale $\tilde{q}^2 = Q^2$ has the form

$$\mathcal{J}(s, Q^2) = \delta(s) + \int_0^{Q^2} \frac{\mathrm{d}\tilde{q}^2}{\tilde{q}^2} \int_0^1 \mathrm{d}z \, P_{qq}\Big[\alpha_s\big(z(1-z)\tilde{q}\big), z\Big] \tag{7.51}$$

$$\times \left[\int_0^\infty \mathrm{d}k'^2 \int_0^\infty \mathrm{d}q^2 \delta\Big(s - \frac{k'^2}{z} - \frac{q^2}{1-z} - z(1-z)\tilde{q}^2\Big) \mathcal{J}(k'^2, z^2\tilde{q}^2) \mathcal{J}_g(q^2, (1-z)^2\tilde{q}^2) \right.$$

$$\left. - \mathcal{J}(s, \tilde{q}^2) \right],$$

where $\mathcal{J}_g(s, Q^2)$ is the gluon jet mass distribution defined in analogy to the jet mass distribution $\mathcal{J}(s, Q^2)$ for the quarks. We have illustrated the evolution schematically in Fig. 7.2. The splitting function is given by

$$P_{qq}\Big[\alpha_s, z\Big] = \frac{\alpha_s C_F}{2\pi} \frac{1 + z^2}{1 - z} = \frac{\alpha_s C_F}{2\pi} \left[\frac{2}{1-z} - (1+z) \right] \tag{7.52}$$

where the second equality makes the cusp and non-cusp terms explicit, which stem from soft $(z \to 1)$ and hard collinear emissions, respectively.

We note that the evolution equation for the jet mass distribution shown in Eq. (7.51) can be rendered NLL precise by correctly implementing the analytic form of the two-loop cusp term in quark splitting function P_{qq}. By using the relative transverse momentum of the splitting,

$$p_\perp^2 = z^2(1-z)^2\tilde{q}^2, \tag{7.53}$$

as the renormalization scale for the strong coupling the leading $\ln(1-z)/(1-z)$ behavior of the cusp term in the two-loop splitting function is reproduced exactly. The remaining non-logarithmic term from the two-loop cusp anomalous dimension and can be incorporated by either scaling

$$\alpha_s \to \alpha_s \left(1 + K_g \frac{\alpha_s}{2\pi}\right), \tag{7.54}$$

or, equivalently, (up to terms of $\mathcal{O}(\alpha_s^3)$) by adopting a change in renormalization scheme through the rescaling

$$\Lambda_{\overline{\text{MS}}} \to \Lambda_{\text{MC}} = \Lambda_{\overline{\text{MS}}} \exp\left(\frac{K_g}{\beta_0}\right) \tag{7.55}$$

The constant K_g commonly used in this context relates to the two-loop cusp anomalous dimension as $\Gamma_1^{\text{cusp}} = 8C_F K_g$ shown in Eqs. (7.18). This approach to implement NLL precision in parton showers is called the CMW ("Catani-Marchesini-Webber") or Monte Carlo scheme [159]. We note that in

the HERWIG event generator, the transverse momentum argument (7.53) is used as the scale of the strong coupling, but that in the default settings the CMW scheme of Eqs. (7.54) and (7.55) is not used explicitly. Instead the precise value of α_s is obtained from tuning to LEP data along with the parameters of the hadronization model and the shower cut Q_0. The result, however, numerically resembles the CMW factor in the relation between $\Lambda_{\overline{\text{MS}}}$ and Λ_{MC}. Indeed, for example for a one-loop running the CMW correction implies that

$$\alpha_s^{\text{MC}}(M_Z) = \frac{\alpha_S^{\overline{\text{MS}}}(M_Z)}{1 - \alpha_S^{\overline{\text{MS}}}(M_Z)\frac{K_g}{2\pi}} = 0.126 \quad \text{at} \quad \alpha_S^{\overline{\text{MS}}}(M_Z) = 0.118 \ , \quad n_f = 5 \ , \quad (7.56)$$

and the larger value is exactly is the tuned value, with a similar converted value for $\alpha_s^{\overline{\text{MS}}}(M_Z)$ for the two loop running actually employed in the HERWIG shower. For our numerical analyses in Secs. 9.4 and 9.5, where we compare analytic calculations and HERWIG results concerning the shower cut Q_0 dependence of the thrust peak position, we therefore use the strong coupling as implemented in HERWIG.

The evolution equation for the jet mass distribution given in Eq. (7.51) is an explicit representation of the coherent branching algorithm. Consider the distribution of the first emitter's virtuality $k_0^2 \equiv k^2$ and one iteration of the branching algorithm, where one choses $\tilde{q}^2 \equiv \tilde{q}_1^2$, $z \equiv z_1$, as well as $k'^2 \equiv k_1^2$ and the gluon's virtuality is denoted by $q^2 \equiv q_1^2$ as displayed in Fig. 7.2. There is a contribution without any branching or virtual effects, encoded in the first δ-function term in Eq. (7.51). It describes a vanishing jet mass that corresponds to the tree-level contribution and also constitutes the initial condition for the shower evolution at $\tilde{q}^2 = Q^2$. In addition, we need to take into account a resolvable branching at a scale $\tilde{q}^2$ below the hard scale Q^2, which gives rise to a subsequent evolution of the quark and gluon jet mass distributions at the scales imposed by the angular ordering criterion of Eq. (7.49). This contribution is itself constrained by the momentum conservation criterion of Eq. (7.50). The last contribution originates from an unresolved emission, which gives rise to an evolution of the quark mass distribution starting at scale $\tilde{q}^2$ but being unconstrained otherwise. Notice that the momentum conservation constraint links the evolution scale to the specific kinematics that is considered. No further constraints to the integration over the momenta involved in the emission are present.

As already mentioned, in the context of an event generator the evolution has to be terminated by imposing infrared cutoff Q_0. This is typically done by a requiring a minimum transverse momentum for the emissions with respect to the momentum direction of the emitter. This restricts the integral over $\tilde{q}^2$ and z to a region where

$$p_\perp^2 = \tilde{q}^2 \, z^2 (1-z)^2 > Q_0^2 \ . \quad (7.57)$$

We note that also other choices are in principle possible and have been discussed in the context of radiation within the 'dead cone' for massive quarks [160]. In principle any prescription that simultaneously cuts off both the collinear $\tilde{q} \to 0$ and soft $z \to 1$ (as well as $z \to 0$ for a gluon branching) limits, and also avoids low transverse momenta appearing in the argument of the strong coupling, is appropriate.

We also note that an analogous evolution equation holds for the gluon jet mass distribution $\mathcal{J}_g(s, Q^2)$. The evolution of the gluon jet is governed by the gluon splitting function, and also describes gluon branching into a quark/anti-quark pair. However, as far as the jet mass distributions in the resonance region is are concerned, the contribution of the gluon jet mass to the quark jet mass is at least at NLL precision suppressed due to the angular ordering constraint, see e.g. Ref. [163]. Therefore, at NLL several simplifying approximations are in principle possible to solve the evolution equation for the quark jet mass distribution, which are particularly useful for analytic calculations of the jet mass distribution: (i) we can neglect the contribution to the jet mass due to the branching of emitted gluons by the replacement $\mathcal{J}_g((1-z)\tilde{q}^2) \to \delta(q^2)$ for the gluon jet mass distribution and (ii) we can can take the limit $z \to 1$ for some terms that do not acquire an enhancement in the soft limit. Interestingly, this also includes that, once prescription (i) is applied, we can remove the remaining, strict angular ordering

constraint in the quark jet mass distribution through modifying the starting scale of the subsequent emission contained in the quark jet mass distribution by the replacement $\mathcal{J}(k'^2, z^2\tilde{q}^2) \rightarrow \mathcal{J}(k'^2, \tilde{q}^2)$. In Sec. 9.3 we explicitly verify these simplifications from numerical simulations using the HERWIG 7 event generator.

7.2.2 Massive case

Moving on to radiation off massive quarks, we consider the generalizations of coherent branching developed in Ref. [160], based on splitting functions and factorization *in the quasi-collinear limit* for which the emitted parton's transverse momenta is restricted from above by the mass of the emitting quark and furthermore small compared to the scale of the previous emission, $p_{i,\perp}^2 \lesssim m_i^2 \ll 2(k_{i-1}\cdot\bar{n})$. In this case we consider a system of a massive quark and anti-quark, $p^2 = \bar{p}^2 = m^2$. However we still use light-like backward directions $\bar{n}$ and n in the momentum parametrization such as (7.43), with three-momenta pointing along the direction of the massive momenta, *i.e.* $\bar{n} = (|\vec{p}|, -\vec{p})$ and $n = (|\vec{p}|, \vec{p})$. This modifies the form of the β_i variables to take into account the mass effect,

$$\beta_i = \frac{-k_{i,\perp}^2 + k_i^2 - \alpha_i^2\, m^2}{2\alpha_i(p\cdot\bar{n})} \,, \tag{7.58}$$

while the parametrization of the momenta from the massless case given in Eq. (7.43) and the relation to the branching variables in Eqs. (7.46) and (7.47) remain unchanged. Following Ref. [160] the evolution variable is generalized to the expression

$$\tilde{q}_i^2 = \frac{p_{i,\perp}^2 + (1-z_i)^2 m^2}{z_i^2(1-z_i)^2} \,. \tag{7.59}$$

Consequently, the generalization of Eq. (7.50) also adopts a mass term and reads

$$k_{i-1}^2 = \frac{k_i^2 - (1-z_i)m^2}{z_i} + \frac{q_i^2}{1-z_i} + z_i(1-z_i)\tilde{q}_i^2 \,. \tag{7.60}$$

The arguments we discussed for the massless quark case concerning the mass of the gluon jet apply in the analogous way in the massive quark case. Therefore we do not have to consider the fully general formalism for our analytic calculations at NLL order and can restrict ourselves to the case of gluon emission from a massive quark. We note that gluon splitting into massive quarks is also a negligible effect for the jet mass distribution in the resonance region since the corresponding splitting function is suppressed with respect to the gluon emission case due to a lack of soft enhancement (even in the absence of angular ordering). The variables considered here are precisely those used in the HERWIG 7 angular ordered shower, which, in its current version is not relying on a finite Q_g parameter as quoted in [160], but is instead using a cutoff on the transverse momentum.

The evolution equation of the massive quark jet mass distribution then has the form

$$\mathcal{J}(s, Q^2, m^2) = \delta(s - m^2) + \int_{m^2}^{\bar{Q}^2} \frac{\mathrm{d}\tilde{q}^2}{\tilde{q}^2} \int_0^1 \mathrm{d}z\, P_{QQ}\left[\alpha_s(\mu_R^2(\tilde{q}^2, z)), z, \frac{m^2}{\tilde{q}^2}\right] \tag{7.61}$$

$$\times \left[\int_0^\infty \mathrm{d}k'^2 \int_0^\infty \mathrm{d}q^2 \delta\left(s - \frac{k'^2 - (1-z)m^2}{z} - \frac{q^2}{1-z} - z(1-z)\tilde{q}^2\right)\right.$$

$$\times\, \mathcal{J}(k'^2, z^2\tilde{q}^2, m^2)\mathcal{J}_g(q^2, (1-z)^2\tilde{q}^2)$$

$$\left. - \mathcal{J}(s, \tilde{q}^2, m^2)\right].$$

The initial hard scale of the evolution in $\tilde{q}^2$ is chosen as

$$\tilde{Q}^2 = \frac{1}{2}Q^2\left(1 + \sqrt{1 - \frac{4m^2}{Q^2}}\right) \tag{7.62}$$

which amounts to the 'symmetric' phase space choice for the $Q\bar{Q}$ system as suggested in Sec. 3.2 of Ref. [160], so that the shower evolution off the progenitors Q and $\bar{Q}$ only cover physically distinct phase space regions. For the situation of boosted quarks ($m^2/Q^2 \ll 1$) we consider in this work, however, we can safely replace $\tilde{Q}^2 \to Q^2$ for all analytic calculations. The shower cutoff condition in the massive quark case reads

$$p_\perp^2 = z^2(1-z)^2\tilde{q}^2 - (1-z)^2m^2 > Q_0^2\,, \tag{7.63}$$

and the splitting function in the quasi-collinear limit generalizes to

$$P_{QQ}\left[\alpha_s, z, \frac{m^2}{\tilde{q}^2}\right] = \frac{\alpha_s C_F}{2\pi}\left[\frac{1+z^2}{1-z} - \frac{2m^2}{z(1-z)\tilde{q}^2}\right]. \tag{7.64}$$

In contrast to the massless quark case where the coherent branching formalism has a solid conceptual basis related to the different kinematics of soft and collinear phase space regions, the corresponding formalism for massive quarks has in its present form higher order ambiguities, which makes e.g. the determination $\mathcal{O}(\alpha_s^2)$ corrections to the quasi-collinear splitting functions ambiguous. This is related to the more complicated structure of collinear, ultra-collinear, mass mode and soft dynamics and phase space regions that emerge in the presence of the quark mass and which (as we show explicitly in Sec. 7.3.2) depends in addition on the relation between the jet invariant mass $\sqrt{s}$ and the quark mass m. This is manifest in the fact that, in contrast to the massless quark case, there is no unique choice of the renormalization scale of α_s as a function of z, $\tilde{q}$ and the quark mass m. As such, different choices for $\mu_R^2(\tilde{q}^2, z)$ which reduce to Eq. (7.53) in the massless limit may be considered. The default choice is the generalized transverse momentum, $\mu_R^2(\tilde{q}^2, z) = \tilde{q}^2 z^2(1-z)^2$, which adds an additional mass-dependent contribution relative to the physical transverse momentum given in Eq. (7.63). We demonstrate in Sec. 7.3.2 that this choice is fully consistent with the QCD factorization approach for massive quarks at NLL order. (See also the power counting shown in Tab. 8.2: In the soft gluon region the m^2 term is suppressed and irrelevant, and in the ultra-collinear region the $\tilde{q}^2$ and the m^2 terms are of the same order.)

7.2.3   Coherent branching in the Herwig 7 event generator

The coherent branching formalism and its variables outlined in the previous two subsections form the core of the angular ordered parton shower in the HERWIG 7 event generator [151, 152, 175], covering the massless and the massive quark cases as discussed in Secs. 7.2.1 and 7.2.2, respectively. In the HERWIG 7 parton shower algorithm, a sequence of random values for the variables $\tilde{q}$ and z is generated, distributed according to the Sudakov form factor that depends on the splitting function. This provides a solution to the evolution of the jet mass distribution accounting for the branching and no-branching probabilities in terms of explicit events.

A major difference to a purely analytic computation of the jet mass distributions encoded in the evolution equations (7.51) and (7.61), however, is related to the virtualities, i.e. the off-shell invariant masses of the branching partons. While an analytic calculation of the jet mass distribution just focuses on the description of the overall invariant mass of the final state particles produced by the emissions from the progenitor parton originating from the hard process, event generators have to face an additional constraint: they have to evolve the progenitor parton to a final state consisting of partons *on their physical mass shell consistent with overall energy-momentum conservation* at the

point when the shower terminates. This procedure is called *'kinematic reconstruction'*. It is the kinematic reconstruction procedure that fixes the virtualities to the partons before showering (which are, however, approximated as on-shell in the splitting function). The kinematic reconstruction is based on the information of the entire evolution tree, the momentum decomposition based on Eq. (7.43), four-momentum conservation at each vertex, and the knowledge of the $\tilde{q}$ and z values of each branching to determine explicit particle momenta and to relate the kinematics of the subsequent emissions to the associated off-shell invariant masses.

In this context an additional important issue the kinematic reconstruction procedure has to deal with is that the sizes of the physical virtualities are kinematically limited by the available phase space. However, this phase space constraint is *not* imposed by the parton shower evolution itself, such that physically inaccessible (i.e. too large) invariant masses can be generated. Given the decomposition of the momenta based on Eq. (7.43), and a sequence of $\tilde{q}$ and z values, the kinematic reconstruction algorithms are designed such that one single solution for the final state momenta is obtained. However, physically, the final state momenta cannot be determined uniquely such that ambiguities arise in the way how overall energy-momentum conservation is restored in the event.

To illustrate the kinematic reconstruction procedure more concretely, consider the production of a quark/anti-quark progenitor pair produced in e^+e^- annihilation carrying on-shell momenta

$$p = \left(\sqrt{\mathbf{p}^2 + m^2}, \mathbf{p} \right) \qquad \text{and} \qquad \bar{p} = \left(\sqrt{\mathbf{p}^2 + m^2}, -\mathbf{p} \right) , \tag{7.65}$$

respectively, with the initial tree-level process constraint $Q = 2\sqrt{\mathbf{p}^2 + m^2}$ at the starting point of the parton shower evolution. At the end of the parton shower evolution their showered counterparts will have gained virtualities $M^2 \geq m^2$ and $\bar{M}^2 \geq m^2$ with momenta

$$P = \left(\sqrt{M^2 + \mathbf{P}^2}, \mathbf{P} \right) \qquad \bar{P} = \left(\sqrt{\bar{M}^2 + \bar{\mathbf{P}}^2}, \bar{\mathbf{P}} \right) \tag{7.66}$$

and an overall restoration of energy-momentum conservation is mandatory. The strategy in this case (and similarly its generalizations to more final and initial state partons) is to transform the reconstructed momenta of the children coming from the now off-mass-shell shower progenitors into their common centre-of-mass frame where three-momentum conservation is guaranteed. Their spatial momentum components will then be re-scaled by a common parameter such that the overall invariant mass is consistent with energy-momentum conservation, $(P + \bar{P})^2 = Q^2$. This procedure is equivalent to specific boosts along the $\mathbf{P}$ and the $\bar{\mathbf{P}}$ directions, respectively, for the progenitor quark and anti-quark sides. In cases that the shower evolution, which – as we have mentioned before has no notion of global energy-momentum conservation – has generated virtualities which are inconsistent with the available centre-of-mass energy Q, the procedure just outlined is not possible.

Different choices for re-interpreting the branching variables when setting up the full kinematics, with the aim of reducing the occurrence of unphysically large virtualities have been implemented in HERWIG 7. The default setting in the released version of HERWIG 7, `set ShowerHandler:ReconstructionOption OffShell5`, imposes an additional constraint in the intermediate evolution by explicitly altering the intermediate splitting variables $\tilde{q}$ and z (which are originally obtained in the approximation the partons after the splitting are on-shell). This scheme absorbs the invariant mass of the children of the branching parton [178] into a redefinition of the splitting variables to preserve the originally generated virtuality of the splitting parton. This approach, however, intrinsically changes the original form of the coherent branching algorithm as outlined in the previous two subsections, and we therefore do not consider this default option in the numerical analyses carried out in Sec. 9. Instead, the setting `set ShowerHandler:ReconstructionOption CutOff` is used. It directly uses the variables generated for the splittings, and does not redefine the variables used to set up the full kinematics. Events with unphysically large virtualities are discarded.

An additional difference of the HERWIG 7 parton shower to the analytic computation of the jet mass distributions encoded in Eqs. (7.51) and (7.61), is that its default (cluster-type) hadronization

model [179], imposes, in addition, constituent mass on-shell conditions for all partons that emerge when the shower is switched off. This includes in particular a constituent mass for the gluons of around 1 GeV. These parton constituent masses represent tunable parameters of the hadronization model and are thus part of the hadronization model even though they enter the HERWIG 7 parton level output. In particular, the constituent mass allows for a splitting into quark/anti-quark pairs such that the primary non-perturbative clusters can be formed. Within our parton level examination concerning the dependence on the shower cut Q_0, parton constituent masses would represent additional infrared cutoff scales that non-trivially interfere with Q_0 and in addition may cause gauge-invariance issues in higher order perturbative QCD calculations. Since we anyway do not use the HERWIG 7 hadronization model in our numerical analyses of Sec. 9, as already explained in Sec. 7.1.3, we do not account for these constituent masses in our analytic calculations and when generating parton level results from HERWIG 7. We set all quark constituent masses to $m_q^c = 0.01$ MeV, and the gluon mass parameter to $m_g^c = 2m_q^c$, which is the lower bound dictated by constraints from the cluster hadronization model. This effectively eliminates any effect coming from the constituent masses. We note that string hadronization models do not require to assign a mass to the gluons produced by the shower.

7.3 Hemisphere mass distribution from coherent branching without cut

In this section we show that – in the context of strict perturbative computations – the coherent branching formalism and the factorized QCD predictions provide identical results concerning the NLL resummation of logarithmic corrections for the thrust distribution in the absence of any infrared cut, i.e. for $Q_0 = 0$. In the context of our discussions in Sec. 7.1.4, this equivalence means that for the thrust distribution the coherent branching formalism with NLL log resummation is already $\mathcal{O}(\alpha_s)$ precise as far as the peak position is concerned. For the thrust distribution for massive quarks this allows us to identify at $\mathcal{O}(\alpha_s)$ the coherent branching (CB) mass parameter and the pole mass m^{pole} *as long as we consider the resonance peak location as the observable*. We phrase this restricted equivalence by the relation

$$m^{\text{CB}}(Q_0 = 0) \overset{\text{peak}}{=} m^{\text{pole}} + \mathcal{O}(\alpha_s^2). \qquad (7.67)$$

We stress that an exact solution for the jet mass distributions in Eqs. (7.51) and (7.61) (i.e. a solution that does not rely on any perturbative expansion or rearrangement of the expressions) is impossible without imposing any infrared cut because of the singularities in the soft and collinear regions of the $(z, \tilde{q})$ plane caused by the Landau pole of the strong coupling. So applying the coherent branching formalism without any infrared cut implies (and requires) that the running of the strong coupling is treated strictly perturbatively (see also footnote 2). The equivalence relation (7.67) must therefore be understood strictly in the perturbative sense. From the point of view of an exact solution of the coherent branching formalism the limit $Q_0 \to 0$ is impossible to reach. This illustrates the well-known problem of the pole mass being a purely perturbative concept that, however, cannot be associated directly to any physical process at the exact, non-perturbative level.

In the following two subsections we calculate the jet mass distribution in Eqs. (7.51) and (7.61) obtained from the coherent branching formalism analytically at NLL order for massless and massive quark, respectively, and show that the results agree identically with those obtained from the factorized QCD calculations for thrust reviewed in Secs. 7.1.1 and 7.1.2. For the case of massless quarks this equivalence is well known and has already been studied thoroughly in the literature, see e.g. Refs. [173, 180]. We nevertheless lay out the analysis for massless quarks in some detail because it sets the stage for the more complicated discussion for massive quarks in the resonance region, where – to the best of our knowledge – such a study has never been carried out before. Moreover, the manipulations are setting the stage for Sec. 8.1.2 where we examine the impact of the infrared shower cut Q_0 on the

resonance location τ_{peak}. The reader not interested in these computational details may safely skip these two subsection and continue reading with Sec. 8.1.

For simplicity we carry out the bulk of the calculations in Laplace space and define the Laplace transform of the jet mass distributions as

$$
\tilde{\mathcal{J}}(\bar{\nu}, Q) = \int_0^\infty \mathrm{d}s\, e^{-\bar{\nu}s}\, \mathcal{J}(s, Q) \,,
$$
$$
\tilde{\mathcal{J}}(\bar{\nu}, Q, m) = \int_{m^2}^\infty \mathrm{d}s\, e^{-\bar{\nu}(s-m^2)}\, \mathcal{J}(s, Q, m) \,, \tag{7.68}
$$

such that the Laplace space thrust distributions as defined in Eqs. (7.12) and (7.32) adopt the simple form

$$
\tilde{\sigma}^{\text{cb}}(\nu, Q) = \left[\tilde{\mathcal{J}}\left(\frac{\nu}{Q^2}, Q \right) \right]^2 ,
$$
$$
\tilde{\sigma}^{\text{cb}}(\nu, Q, m) = \left[\tilde{\mathcal{J}}\left(\frac{\nu}{Q^2}, Q, m \right) \right]^2 . \tag{7.69}
$$

To keep our notation simple we write the heavy quark mass paramter simply as m instead of $m^{\text{CB}}(Q_0 = 0)$ in the rest of Sec. 7.3.

7.3.1 NLL resummation for massless quarks

To analytically determine the NLL jet mass distribution for massless quarks in the peak region from Eq. (7.51) we follow Ref. [163] and replace z by 1 in all functions that are slowly varying in the limit $z \to 1$, *except* in the splitting function. As already discussed at the end of Sec. 7.2.1, this means that the angular ordering constraint can be dropped in the peak region, giving

$$
\tilde{\mathcal{J}}(\bar{\nu}, Q) = 1 + \int_0^{Q^2} \frac{\mathrm{d}\tilde{q}^2}{\tilde{q}^2} \int_0^1 \mathrm{d}z\, P_{qq}\Big[\alpha_s\big((1-z)\tilde{q}\big), z\Big] \Big(e^{-\bar{\nu}(1-z)\tilde{q}^2} - 1 \Big) \tilde{\mathcal{J}}(\nu, \tilde{q}) \,, \tag{7.70}
$$

for the Laplace space integral equation for the jet mass distribution. From this we find the differential equation

$$
\frac{\mathrm{d}\tilde{\mathcal{J}}(\bar{\nu}, Q)}{\tilde{\mathcal{J}}(\bar{\nu}, Q)} = \frac{\mathrm{d}Q^2}{Q^2} \int_0^1 \mathrm{d}z\, P_{qq}\Big[\alpha_s\big((1-z)Q\big), z\Big] \Big(e^{-\bar{\nu}(1-z)Q^2} - 1 \Big) \,, \tag{7.71}
$$

with the solution

$$
\ln \tilde{\mathcal{J}}(\bar{\nu}, Q) = \int_0^{Q^2} \frac{\mathrm{d}\tilde{q}^2}{\tilde{q}^2} \int_0^1 \mathrm{d}z\, P_{qq}\Big[\alpha_s\big((1-z)\tilde{q}\big), z\Big] \Big(e^{-\bar{\nu}(1-z)\tilde{q}^2} - 1 \Big) \,. \tag{7.72}
$$

With the substitutions

$$
\tilde{q}^2 = \frac{q^2}{1-z} \quad \text{and} \quad z = 1 - \frac{q'^2}{q^2} \tag{7.73}
$$

and using the explicit form of the NLL splitting function in terms of the cusp anomalous dimension of Eq. (7.18) and a subleading non-cusp term,

$$
P_{qq}[\alpha_s, z] = \frac{\Gamma^{\text{cusp}}[\alpha_s]}{1-z} - \left(\frac{C_F \alpha_s}{2\pi} \right)(1+z) \,, \tag{7.74}
$$

we arrive at

$$
\ln \tilde{\mathcal{J}}(\bar{\nu}, Q) = \int_0^{Q^2} \frac{\mathrm{d}q^2}{q^2} \left(e^{-\bar{\nu}q^2} - 1 \right) \int_{\frac{(q^2)^2}{Q^2}}^{q^2} \frac{\mathrm{d}q'^2}{q'^2} \left[\Gamma^{\text{cusp}}[\alpha_s(q')] - \left(\frac{C_F \alpha_s(q')}{2\pi} \right) \left(2 - \frac{q'^2}{q^2} \right) \frac{q'^2}{q^2} \right] . \tag{7.75}
$$

124

For the second non-cusp term we rewrite $\alpha_s(q')$ in terms of $\alpha_s(q)$ and powers of $\ln(q'^2/q^2)$ and notice that at NLL precision we only have to keep terms that are proportional to $\alpha_s^{n+1}(q)\ln^n(q^2/Q^2)$ after the q' integration. Here only a single term for $n=0$ has to be kept,

$$-\int_{\frac{(q^2)^2}{Q^2}}^{q^2} \frac{\mathrm{d}q'^2}{q'^2} \left(\frac{C_F\alpha_s(q')}{2\pi}\right)\left(2-\frac{q'^2}{q^2}\right)\frac{q'^2}{q^2} \stackrel{\text{NLL}}{=} -3\,C_F\left(\frac{\alpha_s(q)}{4\pi}\right) = -\frac{1}{4}\gamma_{J(\tau)}[\alpha_s(q)], \qquad (7.76)$$

which we have, anticipating the form of the final result, identified with the non-cusp anomalous dimension of the jet function in the factorized QCD cross section. Rewriting in the remaining integral $\alpha_s(q)$ in terms of $\alpha_s(Q)$ and powers of $\ln(q^2/Q^2)$, we can further simplify the integral by noticing, that for obtaining all NLL logarithmic terms correctly, we can use the replacement

$$\mathrm{e}^{-\bar{\nu}q^2} - 1 \stackrel{\text{NLL}}{=} -\theta(q^2 - w) \qquad \text{with} \qquad w = (\mathrm{e}^{\gamma_E}\bar{\nu})^{-1} = Q^2(\mathrm{e}^{\gamma_E}\nu)^{-1}\,. \qquad (7.77)$$

This replacement technically acts like an infrared cutoff for the q integration. It is, however, not a physical cutoff because it is derived in the context of a strict perturbative expansion (where no infrared Landau Pole singularity arises) and is furthermore not correct beyond NLL order. One should therefore better think of the replacement simply as an algebraic relation that simplifies the perturbative analytic NLL resummation calculation.

For the remaining double integral with the cusp-anomalous dimension we can now switch the order of integration,

$$-\int_{\frac{w^2}{Q^2}}^{w} \frac{\mathrm{d}q^2}{q^2}\, \Gamma^{\text{cusp}}[\alpha_s(q^2)]\int_w^{qQ} \frac{\mathrm{d}q'^2}{q'^2} - \int_w^{Q^2} \frac{\mathrm{d}q^2}{q^2}\, \Gamma^{\text{cusp}}[\alpha_s(q^2)]\int_{q^2}^{qQ} \frac{\mathrm{d}q'^2}{q'^2}\,, \qquad (7.78)$$

and reshuffle the q' integrations,

$$\int_w^{qQ} \frac{\mathrm{d}q'^2}{q'^2} = \frac{1}{2}\int_{\frac{w^2}{Q^2}}^{q^2} \frac{\mathrm{d}q'^2}{q'^2}\,,$$

$$\int_{q^2}^{qQ} \frac{\mathrm{d}q'^2}{q'^2} = -\int_w^{q^2} \frac{\mathrm{d}q'^2}{q'^2} + \frac{1}{2}\int_{\frac{w^2}{Q^2}}^{q^2} \frac{\mathrm{d}q'^2}{q'^2}\,, \qquad (7.79)$$

to obtain

$$-\frac{1}{2}\int_{\frac{w^2}{Q^2}}^{Q^2} \frac{\mathrm{d}q^2}{q^2}\, \Gamma^{\text{cusp}}[\alpha_s(q^2)]\int_{\frac{w^2}{Q^2}}^{q^2} \frac{\mathrm{d}q'^2}{q'^2} + \int_w^{Q^2} \frac{\mathrm{d}q^2}{q^2}\, \Gamma^{\text{cusp}}[\alpha_s(q^2)]\int_w^{q^2} \frac{\mathrm{d}q'^2}{q'^2}\,. \qquad (7.80)$$

Noticing the scale identifications

$$Q^2 = \mu_{H,\nu}^2\,, \quad w = \mu_{J,\nu}^2\,, \quad w^2/Q^2 = \mu_{S,\nu}^2 \qquad (7.81)$$

according to Eqs. (7.19) and (7.77), we see that at this point we have separated the collinear and soft evolution to the hard scale. The non-cusp term

$$\frac{1}{4}\int_w^{Q^2} \frac{\mathrm{d}q^2}{q^2}\, \gamma_{J(\tau)}[\alpha_s(q)]\,, \qquad (7.82)$$

on the other hand, describes only a collinear evolution to the hard scale consistent with our assignment in Eq. (7.76). Accounting for Eq. (7.16) for the QCD beta function and Eq. (7.69), we then arrive at the following form of the NLL Laplace space thrust distribution,

$$\ln\tilde{\sigma}^{\text{cb}}(\nu,Q) = 8\int_{\alpha_s(\mu_{J,\nu})}^{\alpha_s(Q)} \frac{\mathrm{d}\alpha_s}{\beta[\alpha_s]}\, \Gamma^{\text{cusp}}[\alpha_s]\int_{\alpha_s(\mu_{J,\nu})}^{\alpha_s} \frac{\mathrm{d}\alpha_s'}{\beta[\alpha_s']}$$

$$-4\int_{\alpha_s(\mu_{S,\nu})}^{\alpha_s(Q)} \frac{\mathrm{d}\alpha_s}{\beta[\alpha_s]}\, \Gamma^{\text{cusp}}[\alpha_s]\int_{\alpha_s(\mu_{S,\nu})}^{\alpha_s} \frac{\mathrm{d}\alpha_s'}{\beta[\alpha_s']}$$

$$+\int_{\alpha_s(\mu_{J,\nu})}^{\alpha_s(Q)} \frac{\mathrm{d}\alpha_s}{\beta[\alpha_s]}\, \gamma_{J(\tau)}[\alpha_s]\,. \qquad (7.83)$$

In terms of the K and ω evolution factors defined in Eq. (7.14) this can be rewritten as

$$
\begin{aligned}
\tilde{\sigma}^{\text{cb}}(\nu, Q) &= \exp\left[4\,K(\Gamma^{\text{cusp}}, \mu_{H,\nu}, \mu_{J,\nu}) - 2\,K(\Gamma^{\text{cusp}}, \mu_{H,\nu}, \mu_{S,\nu}) + \frac{1}{2}\omega(\gamma_{J(\tau)}, \mu_{H,\nu}, \mu_{J,\nu})\right] \\
&= \exp\left[K(\Gamma_{J(\tau)}, \mu_{H,\nu}, \mu_{J,\nu}) + K(\Gamma_S, \mu_{H,\nu}, \mu_{S,\nu}) + \frac{1}{2}\omega(\gamma_{J(\tau)}, \mu_{H,\nu}, \mu_{J,\nu})\right],
\end{aligned} \tag{7.84}
$$

where in the last line we have used the cusp and non-cusp identities of Eqs. (7.17). This agrees identically with the factorized QCD cross section for massless quarks of Eq. (7.13).

7.3.2 NLL resummation for massive quarks

To analytically determine the NLL jet mass distribution for massive quarks in the peak region from Eq. (7.61) we initially proceed in the same way as for the massless quark case. Taking the large z approximation of Ref. [163] and in addition the limit of large boost ($Q^2 \gg m^2$), the Laplace space integral equation for the jet mass distribution adopts the form

$$
\tilde{\mathcal{J}}(\bar{\nu}, Q, m) = 1 + \int_{m^2}^{Q^2} \frac{\mathrm{d}\tilde{q}^2}{\tilde{q}^2} \int_0^1 \mathrm{d}z \, P_{QQ}\left[\alpha_s\big((1-z)\tilde{q}\big), z, \frac{m^2}{\tilde{q}^2}\right]\left(e^{-\bar{\nu}(1-z)\tilde{q}^2} - 1\right)\tilde{\mathcal{J}}(\nu, \tilde{q}), \tag{7.85}
$$

with

$$
P_{QQ}\left[\alpha_s, z, \frac{m^2}{\tilde{q}^2}\right] = \frac{\Gamma^{\text{cusp}}[\alpha_s]}{1-z} - \left(\frac{C_F \alpha_s}{2\pi}\right)(1+z) - \left(\frac{C_F \alpha_s}{\pi}\right)\frac{m^2}{(1-z)\tilde{q}^2}, \tag{7.86}
$$

where we have dropped a factor $1/z$ from the mass correction term for a consistent expansion in the $z \to 1$ limit, see also Sec. 7.2. Its solution reads

$$
\ln \tilde{\mathcal{J}}(\bar{\nu}, Q, m) = \int_{m^2}^{Q^2} \frac{\mathrm{d}\tilde{q}^2}{\tilde{q}^2} \int_0^1 \mathrm{d}z \, P_{QQ}\left[\alpha_s\big((1-z)\tilde{q}\big), \tilde{q}, m, z\right]\left(e^{-\bar{\nu}(1-z)\tilde{q}^2} - 1\right), \tag{7.87}
$$

and with the substitutions of Eq. (7.73) we arrive at

$$
\begin{aligned}
\ln \tilde{\mathcal{J}}(\bar{\nu}, Q, m) = \int_w^{Q^2} \frac{\mathrm{d}q^2}{q^2} \int_{\frac{(q^2)^2}{Q^2}}^{q^2} \frac{\mathrm{d}q'^2}{q'^2} &\left[-\Gamma^{\text{cusp}}[\alpha_s(q')]\right. \\
&\left.+ \left(\frac{C_F \alpha_s(q')}{2\pi}\right)\left(2 - \frac{q'^2}{q^2}\right)\frac{q'^2}{q^2} + \left(\frac{C_F \alpha_s(q')}{\pi}\right)\frac{m^2 q'^2}{(q^2)^2}\right]\theta(q^2 - q'm)
\end{aligned} \tag{7.88}
$$

for the NLL resummed Lapace space thrust distribution. We have already implemented the NLL relation of Eq.(7.77) to simplify the q^2 integration, since it is also valid in the context of massive quarks.

It it easy to see that the massive quark constraint $q^2 > q'm$ is irrelevant for $w = \mu_{J,\nu}^2 > m^2$, which refers to the situation where the hemisphere jet masses are larger than the mass of the quark. In this kinematic situation the mass correction in the splitting function represents the only modification due to the quark mass, but the struture of the log resummation is otherwise in complete analogy to the massless quark case. In the context of the factorized QCD calculations, one can then employ usual SCET factorization where the collinear sector of the effective Lagrangian is extended trivially by just accounting for the finite quark mass [18, 19]. In this work, however, we are interested in the peak region where the hemisphere jet masses are close to the quark mass, i.e. where $w < m^2$. Here the ultra-collinear sector emerges and the QCD factorization requires that the off-shell fluctuations of the massive quark field are integrated out [18, 19]. So the quark mass effects are much more complicated

and lead to a substantial rearrangement the structure of the resummed logarithms. The physical meaning of w is also modified and the scale identifications read

$$Q^2 = \mu_{H,\nu}^2\,, \quad m^2 = \mu_{m,\nu}^2\,, \quad w^2/m^2 = \mu_{B,\nu}^2\,, \quad w^2/Q^2 = \mu_{S,\nu}^2 \tag{7.89}$$

Let us now have a closer look at the calculation for the cusp term. Reversing the order of integration we have to distinguish three integration regions and find

$$-\int_{\frac{w^2}{Q^2}}^{\frac{w^2}{m^2}} \frac{\mathrm{d}q^2}{q^2}\,\Gamma^{\mathrm{cusp}}[\alpha_s(q^2)] \int_{w}^{qQ} \frac{\mathrm{d}q'^2}{q'^2} - \int_{\frac{w^2}{m^2}}^{m^2} \frac{\mathrm{d}q^2}{q^2}\,\Gamma^{\mathrm{cusp}}[\alpha_s(q^2)] \int_{mq}^{Qq} \frac{\mathrm{d}q'^2}{q'^2}$$
$$-\int_{m^2}^{Q^2} \frac{\mathrm{d}q^2}{q^2}\,\Gamma^{\mathrm{cusp}}[\alpha_s(q^2)] \int_{q^2}^{Qq} \frac{\mathrm{d}q'^2}{q'^2}\,. \tag{7.90}$$

The q' integrations can be reshuffled using

$$\int_{w}^{qQ} \frac{\mathrm{d}q'^2}{q'^2} = \frac{1}{2} \int_{\frac{w^2}{Q^2}}^{q^2} \frac{\mathrm{d}q'^2}{q'^2}\,, \tag{7.91}$$

$$\int_{mq}^{Qq} \frac{\mathrm{d}q'^2}{q'^2} = -\frac{1}{2} \int_{\frac{w^2}{m^2}}^{q^2} \frac{\mathrm{d}q'^2}{q'^2} + \frac{1}{2} \int_{\frac{w^2}{Q^2}}^{q^2} \frac{\mathrm{d}q'^2}{q'^2}\,, \tag{7.92}$$

$$\int_{q^2}^{Qq} \frac{\mathrm{d}q'^2}{q'^2} = -\frac{1}{2} \int_{m^2}^{q^2} \frac{\mathrm{d}q'^2}{q'^2} - \frac{1}{2} \int_{\frac{w^2}{m^2}}^{q^2} \frac{\mathrm{d}q'^2}{q'^2} + \frac{1}{2} \int_{\frac{w^2}{Q^2}}^{q^2} \frac{\mathrm{d}q'^2}{q'^2}\,, \tag{7.93}$$

such that we get

$$\frac{1}{2}\int_{m^2}^{Q^2} \frac{\mathrm{d}q^2}{q^2}\,\Gamma^{\mathrm{cusp}}[\alpha_s(q^2)] \int_{m^2}^{q^2} \frac{\mathrm{d}q'^2}{q'^2} + \frac{1}{2}\int_{\frac{w^2}{m^2}}^{Q^2} \frac{\mathrm{d}q^2}{q^2}\,\Gamma^{\mathrm{cusp}}[\alpha_s(q^2)] \int_{\frac{w^2}{m^2}}^{q^2} \frac{\mathrm{d}q'^2}{q'^2}$$
$$-\frac{1}{2}\int_{\frac{w^2}{Q^2}}^{Q^2} \frac{\mathrm{d}q^2}{q^2}\,\Gamma^{\mathrm{cusp}}[\alpha_s(q^2)] \int_{\frac{w^2}{Q^2}}^{q^2} \frac{\mathrm{d}q'^2}{q'^2}$$
$$= K(\Gamma^{\mathrm{cusp}}, \mu_{H,\nu}, \mu_{m,\nu}) + K(\Gamma^{\mathrm{cusp}}, \mu_{H,\nu}, \mu_{J_B,\nu}) - K(\Gamma^{\mathrm{cusp}}, \mu_{H,\nu}, \mu_{S,\nu})\,. \tag{7.94}$$

At this point we have separated mass-dependent, ultra-collinear and soft evolution to the hard scale and have rewritten the result using the evolution function K of Eq. (7.14) and the scale identifications of Eq. (7.89).

For the non-cusp term, rewriting the constraint $q^2 > q'm$ in terms of integration limits,

$$\int_{w}^{Q^2} \frac{\mathrm{d}q^2}{q^2} \int_{\frac{(q^2)^2}{Q^2}}^{q^2} \frac{\mathrm{d}q'^2}{q'^2}\,\theta(q^2 - q'm) = \int_{w}^{m^2} \frac{\mathrm{d}q^2}{q^2} \int_{\frac{(q^2)^2}{Q^2}}^{\frac{(q^2)^2}{m^2}} \frac{\mathrm{d}q'^2}{q'^2} + \int_{m^2}^{Q^2} \frac{\mathrm{d}q^2}{q^2} \int_{\frac{(q^2)^2}{Q^2}}^{q^2} \frac{\mathrm{d}q'^2}{q'^2} \tag{7.95}$$

we can use the considerations already applied in the massless quark case and find that only the second integration contributes at NLL order. This gives

$$\int_{m^2}^{Q^2} \frac{\mathrm{d}q^2}{q^2}\left[3\,C_F\Big(\frac{\alpha_s(q)}{4\pi}\Big)\right] = \frac{1}{4}\int_{m^2}^{Q^2} \frac{\mathrm{d}q^2}{q^2}\left[-\gamma_H[\alpha_s(q)] + \gamma_{J_B}[\alpha_s(q)] + \gamma_{H_m}[\alpha_s(q)]\right], \tag{7.96}$$

where we have written the expression in terms of the the non-cusp anomalous dimensions of the hard, the mass mode and the bHQET jet functions, anticipating already the form of the final result.

For the mass correction term in the splitting function we reverse integration order in analogy to our manipulation for the cusp term in Eq. (7.90),

$$\int_{\frac{w^2}{Q^2}}^{\frac{w^2}{m^2}} \frac{dq^2}{q^2} \left(\frac{C_F \alpha_s(q')}{\pi}\right) \int_{w}^{qQ} \frac{dq'^2}{q'^2} \frac{m^2 q^2}{(q^{2\prime})^2} + \int_{\frac{w^2}{m^2}}^{m^2} \frac{dq^2}{q^2} \left(\frac{C_F \alpha_s(q')}{\pi}\right) \int_{mq}^{Qq} \frac{dq'^2}{q'^2} \frac{m^2 q^2}{(q^{2\prime})^2}$$

$$+ \int_{m^2}^{Q^2} \frac{dq^2}{q^2} \left(\frac{C_F \alpha_s(q')}{\pi}\right) \int_{q^2}^{Qq} \frac{dq'^2}{q'^2} \frac{m^2 q^2}{(q^{2\prime})^2} . \tag{7.97}$$

In the limit of a boosted massive quark $(Q^2 \gg m^2)$ only the second term can contribute NLL logarithms. Using

$$\int_{mq}^{Qq} \frac{dq'^2}{q'^2} \frac{m^2 q^2}{(q^{2\prime})^2} = \frac{1}{2} + \mathcal{O}\left(\frac{m^2}{Q^2}\right), \tag{7.98}$$

the contribution from the mass correction term at NLL accuracy then reads

$$\int_{\frac{w^2}{m^2}}^{m^2} \frac{dq^2}{q^2} \left[2C_F\left(\frac{\alpha_s(q)}{4\pi}\right)\right] = \frac{1}{4} \int_{\frac{w^2}{m^2}}^{Q^2} \frac{dq^2}{q^2} \gamma_{J_B}[\alpha_s(q)] - \frac{1}{4} \int_{m^2}^{Q^2} \frac{dq^2}{q^2} \gamma_{J_B}[\alpha_s(q)] \tag{7.99}$$

Taking the sum of the NLL contributions from the non-cusp term in Eq. (7.96) and the mass corrections term in Eq. (7.99) we obtain

$$\frac{1}{4} \int_{m^2}^{Q^2} \frac{dq^2}{q^2} \left[-\gamma_H[\alpha_s(q)] + \gamma_{H_m}[\alpha_s(q)]\right] + \frac{1}{4} \int_{\frac{w^2}{m^2}}^{Q^2} \frac{dq^2}{q^2} \gamma_{J_B}[\alpha_s(q)]$$

$$= \frac{1}{4}\Big(\omega(\gamma_{H_m} - \gamma_{H_Q}, \mu_{H,\nu}, \mu_{m,\nu}) + \omega(\gamma_B, \mu_{H,\nu}, \mu_{J_B,\nu}) + \omega(\gamma_S, \mu_{H,\nu}, \mu_{S,\nu})\Big) \tag{7.100}$$

where in the second line we have rewritten the result in using the evolution function ω of Eq. (7.14) using the scale identities of Eq. (7.89) and that $\gamma_S[\alpha_s] = 0$ at NLL. Combining Eqs. (7.94) and (7.100) and using (7.69) we arrive at the final form for the NLL Laplace space thrust distribution

$$\tilde{\sigma}^{\text{cb}}(\nu, Q, m^{\text{pole}}) = \exp\left[-K(\Gamma_{H_m}, \mu_{H,\nu}, \mu_{m,\nu}) + K(\Gamma_{J_B}, \mu_{H,\nu}, \mu_{J_B,\nu}) + K(\Gamma_S, \mu_{H,\nu}, \mu_{S,\nu})\right]$$

$$\times \exp\left[\frac{1}{2}\Big(\omega(\gamma_{H_m} - \gamma_{H_Q}, \mu_{H,\nu}, \mu_{m,\nu}) + \omega(\gamma_{J_B}, \mu_{H,\nu}, \mu_{J_B,\nu}) + \omega(\gamma_S, \mu_{H,\nu}, \mu_{S,\nu})\Big)\right], \tag{7.101}$$

which agrees identically with the factorized QCD cross section for massive quarks of Eq. (7.33).

Chapter 8

Cutoff Dependence of Jet Observables

8.1 Hemisphere mass distribution with shower cut Q_0

In this section we study analytically the impact of the shower evolution cut Q_0 on the thrust distribution in the resonance regions for massless and massive quark production. The main focus is on the effects that cause a dependence of the hemisphere masses that is linear on Q_0. The Q_0 cut is defined as the restriction $p_\perp^2 > Q_0^2$ on the transverse momentum of the emission with respect to the momentum of the emitter. In the context of the coherent branching formalism the dependence of the transverse momentum on the shower evolution variables $\tilde{q}$ and z for the massless and the massive quark cases are given in Eqs. (7.48) and (7.59), respectively, leading to the constraints in Eqs. (7.57) and (7.63).

Since *in the framework of strict perturbative calculations* the Q_0 cut represents an artificial restriction of the radiation generated by the shower, we call the emissions that are allowed by the Q_0 cut *released* and the emissions that is not allowed by the Q_0 cut *unreleased*. As we will show, the dominant (linear in Q_0) effect of removing the unreleased radiation from the calculation in the resonance region must be *reinterpreted as a redefinition of parameters in a perturbative calculation without Q_0 cut.*

To elucidate this we compare the effects of the unreleased radiation in the context of the coherent branching formalism for the jet mass distributions as described in Secs. 7.2.1 and 7.2.2, and in the context of QCD factorization using the SCET approach for the thrust distribution as described in Secs. 7.1.1 and 7.1.2. This comparison, together with the facts that in the absence of the Q_0 cut coherent branching and QCD factorization provide equivalent results at NLL order and both are $\mathcal{O}(\alpha_s)$ precise for the resonance peak mass, allows us to relate the quark mass parameter of the coherent branching formalism with Q_0 cut (and thus of angular ordered parton showers) to an explicit field theoretic mass renormalization scheme at $\mathcal{O}(\alpha_s)$.

In subsection 8.1.1 we outline the collinear and soft phase space regions and QCD modes relevant for the thrust distribution in the resonance region in the context of coherent branching and QCD factorization, respectively, and we show where a linear Q_0 dependence can possibly emerge. In subsections 8.1.3 to 8.1.2 we calculate the effects of the unreleased radiation each for massless and massive quarks for QCD factorization and coherent branching and analyze in detail the effects linear in Q_0.

8.1.1 Phase space regions with and without Q_0 cut

To initiate the analytic examinations it is illustrative to first discuss the structure of the phase space and the QCD modes relevant for the resonance region. To define our counting variable we
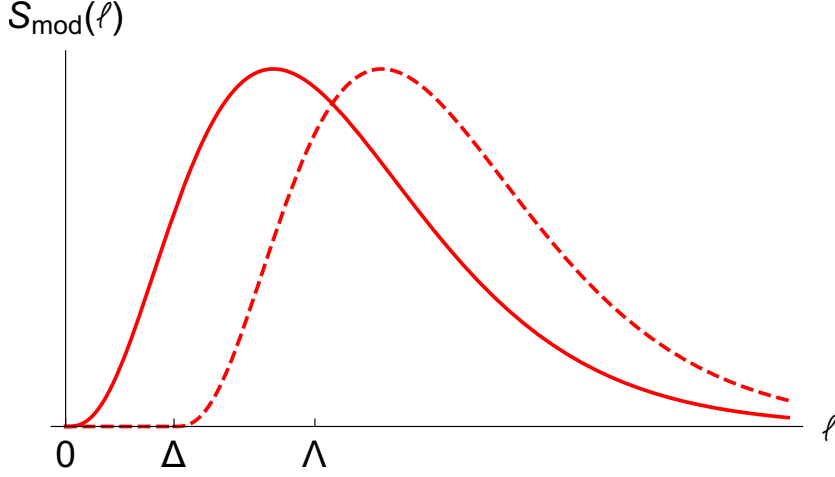
Figure 8.1: Generic form of the soft model shape function $S_{\mathrm{mod}}(\ell)$ in arbitray units for illustration. The original soft model shape function $S_{\mathrm{mod}}(\ell)$ is represented by the solid red line and the soft model shape function with a gap shift, $S_{\mathrm{mod}}(\ell - \Delta)$ for the case $0 < \Delta < \Lambda$, by the dashed red line.

start from the hadron level thrust distributions given in Eqs. (7.3) and (7.21), where the partonic thrust distribution is convoluted with the soft model shape function $S_{\mathrm{mod}}(\ell)$. The parameters of the shape function may be either determined from fits to experimental data or from non-perturbative methods. The shape function has support for positive ℓ values and exhibits a peak for $\ell \approx \Lambda$, where Λ parametrizes the overall energy the non-perturbative effects add to the parton level hemisphere masses. For larger ℓ values the shape function falls quickly and one usually assumes an exponential behavior. A typical generic form for S_{mod} is displayed in Fig. 8.1. The effect of the shape function on the hadron level prediction is twofold: it smears out the distributive and singular structures of the partonic cross section, and it leads to a shift of the observable resonance peak position in the thrust distribution towards larger values with respect to the partonic thresholds, $\tau_{\mathrm{min}} = 0$ for massless quarks and $\tau_{\mathrm{min}} = 2m^2/Q^2$ for massive quarks:

$$\tau_{\mathrm{peak}} - \tau_{\mathrm{min}} \sim \frac{\Lambda}{Q} \ll 1 . \tag{8.1}$$

It is therefore natural to adopt Λ/Q as the counting parameter in the resonance region.

In Fig. 8.2a we show the generic form of the $(z, \tilde{q})$ phase space populated by coherent branching for the jet mass distribution for massless quarks, see Eq. (7.51). The gray area represents the phase space without Q_0 cut and the hatched area the phase space with Q_0 cut. In the peak region the thrust distribution is dominated by soft and collinear gluon radiation, which are also indicated. In QCD factorization the soft and the collinear modes are separated at the operator level by imposing power-counting contraints on the momentum fluctuations these operators can generate. These constraints are most efficiently formulated in the light cone basis where

$$p^\mu = n \cdot p \frac{\bar{n}^\mu}{2} + \bar{n} \cdot p \frac{n^\mu}{2} + p_\perp^\mu \tag{8.2}$$

where n and $\bar{n}$ are back-to-back light-like vectors than can be directed along the momenta of the progenitor quark-antiquark pair produced by the primary hard scattering. The momentum components in this basis are then denoted by $p^\mu = (p^+, p^-, p_\perp) = (n \cdot p, \bar{n} \cdot p, p_\perp)$ where the momentum square reads $p^2 = p^+ p^- - p_\perp^2$, see also Secs. 7.2.1 and 7.2.2. The Λ counting of the collinear and soft regions formulated in the coherent branching and in the QCD factorization approaches can be connected by
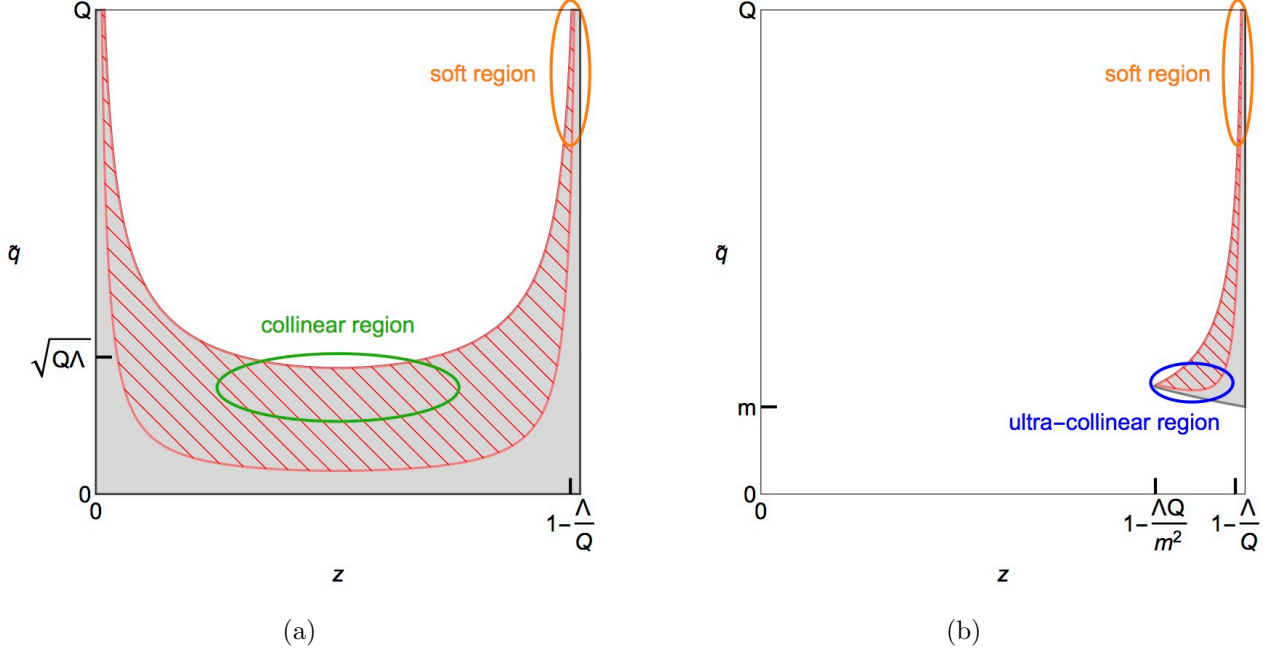
Figure 8.2: $(z, \tilde{q})$ phase space for coherent branching in the (a) massless and (b) massive case, with indication of the relevant soft, collinear and ultra-collinear regions. The hatched area corresponds to the phase space populated in the presence of a shower cut Q_0. The soft, collinear and ultra-collinear phase space regions are indicated.

the relation

$$(p^+, p^-, p_\perp) \;=\; Q(1-z)\left(\frac{\tilde{q}^2}{Q^2}, 1, \frac{\tilde{q}}{Q}\right) \tag{8.3}$$

for soft and n-collinear modes. For the $\bar{n}$ collinear modes, the plus and the minus components on the RHS have to be swapped. The momentum power counting for both approaches for massless quark production is summarized in Tab. 8.1.

phase space regions for $\tau_{\mathrm{peak}} \sim \dfrac{\Lambda}{Q} \ll 1$, $m = 0$		
	coherent branching	QCD factorization
n-collinear	$z \sim (1-z) \sim 1$ $\tilde{q} \sim (Q\Lambda)^{\frac{1}{2}}$ $q_\perp \sim (Q\Lambda)^{\frac{1}{2}}$	$q^\mu \sim (\Lambda, Q, (Q\Lambda)^{\frac{1}{2}})$
soft	$1 - z \sim \dfrac{\Lambda}{Q}$, $z \sim 1$ $\tilde{q} \sim Q$ $q_\perp \sim \Lambda$	$q^\mu \sim (\Lambda, \Lambda, \Lambda)$

Table 8.1: Power counting for coherent branching and QCD factorization for massless quarks.

Imposing the Q_0 cut, one has to note that it represents a cut on the transverse momentum of the emission with respect to the momentum of the emitter and not with respect to the momenta of the progenitor quarks. In the coherent branching approach this is automatically taken care of in the definition of the transverse momentum variable $q_{i,\perp}^\mu$ of Eq. (7.47) which parametrizes the i-th

branching. In QCD factorization, on the other hand, the constraint has a more complicated structure, because the momenta of all radiated partons are usually formulated in one common frame based on Eq. (8.2). Fortunately at NLL+$\mathcal{O}(\alpha_s)$ precision, the order we consider in this work, only the first emission has to be calculated in the QCD factorization approach to determine the effects linear in Q_0. At this level the transverse momentum variable in coherent branching defined in Eq. (7.47) and the transverse momentum in QCD factorization defined in Eq. (8.2) agree and can be identified. So at NLL+$\mathcal{O}(\alpha_s)$ precision we can implement the shower cut constraint in the factorized calculation by simply imposing a cut on the transverse momentum in Eq. (8.2) without further complications. For the rest of this work we therefore identify the transverse momenta in both apporaches to keep the presentation simple, and we frequently refer to the shower cut Q_0 also as the cut on the transverse momentum $p_\perp$ without further specification.

From a conceptual point of view the numerical value for Q_0 should be chosen such that it is unresolved, i.e. it should be smaller than the typical values $p_\perp$ can adopt for the observable of interest. From Tab. 8.1 we can see that soft radiation imposes the strongest constraint and requires that Q_0 should in principle be smaller than $\Lambda \sim 1$ GeV. This is the hierarchy we assume for some of the arguments presented below. For practical parton showers, however, this constraint cannot be satisfied in terms of a strong hierarchy (if at all) due to computational reasons and the proximity to the Landau pole of the strong coupling. As we show in our numerical analysis in Sec. 9 using the approximation $Q_0 \ll \Lambda$ in our analytic calculations does very well, even for cases where the both scales are similar in size. In any case, since Q_0 represents the smallest scale for the strong coupling, integrations over its Landau pole are prevented as long as Q_0 is chosen larger than Λ_{QCD}, and, moreover, for finite Q_0 there are no renormalon ambiguities in perturbative calculations.

In the context of QCD factorization we can see already at the level of the factorization theorem (7.4) that a linear dependence on the $p_\perp$ cut Q_0 can only arise in the partonic soft function S because it is linear in the light cone momentum ℓ. In the jet function J, however, we expect a quadratic behavior for simple dimensional reasons. This consideration can be confirmed explicitly applying the soft and collinear $(z, \tilde{q})$ counting shown Tab. 8.1 to the quark jet mass distribution defined in Eq. (7.51): In the collinear region $z \sim (1-z) \sim 1$ and the cut-dependence arises where $\tilde{q}^2 \sim Q_0^2$. This leads to changes proportional to Q_0^2 on the invariant mass s due to the δ function constraint. In the soft region we have $\tilde{q} \sim Q$ and $z \sim 1$, and the cut dependence arises where $(1-z) \sim Q_0/Q$. This then leads to changes in s proportional to QQ_0 due to the δ function constraint. This simple counting is confirmed by the explicit calculations carried out in Secs. 8.1.2 and 8.1.3.

In Fig. 8.2b we show the generic form of the $(z, \tilde{q})$ phase space populated by coherent branching for the jet mass distribution in the resonance region for a massive quark, see Eq. (7.61), where the coloring is the same as for the massless quark case. Again the gray region represents the allowed phase space without Q_0 cut and the hatched region when the Q_0 cut is imposed. We see that the allowed phase space is considerably different from the massless quark case and overall confined to the region of large z. This is particular to the resonance region, where $s - m^2 \ll m^2$. Here the massive quark thrust distribution is dominated by soft and ultra-collinear gluon radiation, which are also indicated. While the soft region is equivalent to the case of massless quarks, the ultra-collinear region differs substantially from the collinear region for massless quarks because it is related to gluon radiation that is soft in the massive quark rest frame and only becomes collinear due to the massive quark boost. As such the ultra-collinear radiation originating from a boosted massive quark with a given energy is substantially less energetic than the typical collinear radiation originating from a massless quark with the same energy. The resulting power counting is shown in Tab. 8.2, where we see e.g. that ultra-collinear gluons have a typical energy of order $Q^2\Lambda/m^2$, compared to collinear gluons which have a typical energy of order Q. Note that if we would consider the situation $s - m^2 \gg m^2$ the allowed phase space would look similar to the massless case and we would recover the collinear counting. It is a remarkable fact that, despite its limitations, the coherent branching formalism for massive quarks is capable of describing both limits correctly and provides a smooth connection between them. We also

note that, since $(p_\perp^2 + (1-z)^2 m^2)^{1/2}$ is the renormalization scale of the strong coupling, integrations over its Landau pole are strictly prevented as long as Q_0 is chosen larger than Λ_{QCD}. Therefore there are no renormalon ambiguities in perturbative calculations in the presence of the $p_\perp$ cut Q_0.

phase space regions for $\tau_{\mathrm{peak}} - \tau_{\mathrm{min}} \sim \dfrac{\Lambda}{Q} \ll 1,\ m \neq 0$		
	coherent branching	QCD factorization
n-ultra-collinear	$1 - z \sim \dfrac{Q\Lambda}{m^2},\ z \sim 1$ $\tilde{q} \sim m$ $q_\perp \sim \dfrac{Q}{m}\Lambda$	$q^\mu \sim (\Lambda, \dfrac{Q^2}{m^2}\Lambda, \dfrac{Q}{m}\Lambda)$
soft	$1 - z \sim \dfrac{\Lambda}{Q},\ z \sim 1$ $\tilde{q} \sim Q$ $q_\perp \sim \Lambda$	$q^\mu \sim (\Lambda, \Lambda, \Lambda)$

Table 8.2: Power counting for coherent branching and QCD factorization for massive quarks.

To conclude this section let us also discuss in which sectors we should expect a linear dependence on Q_0 for the case of massive quark production. In the context of QCD factorization, inspecting the factorization theorem (7.25), we see that a linear dependence on the $p_\perp$ cut Q_0 can arise not only in the partonic soft function S but also in the bHQET jet function J_B because it has, in contrast to the massless quark jet function, a linear kinematic dependence on the reduced invariant mass variable $\hat{s}$, see Eq (7.26). This simple dimensional argument can again be confirmed applying the ultra-collinear momentum counting shown in Tab. 8.2 to the quark jet mass distribution defined in Eq. (7.61): We have $z \sim 1$, $\tilde{q} \sim m$ and the cut-dependence arises where $(1 - z) \sim Q_0/m$. This leads to changes in the squared invariant mass relative to the threshold of order $s - m^2 \sim mQ_0$. This simple counting is confirmed by the explicit calculations carried out in Secs. 8.1.2 and 8.1.4.

8.1.2 Unreleased radiation: coherent branching

To calculate the effects of the $p_\perp$ cut Q_0 on the thrust distribution in the peak region in the context of the coherent branching formalism we can start from the corresponding Laplace space expressions given in Eq. (7.72) for massless quarks and Eq. (7.87) for massive quarks. In contrast to the calculations we carried out for our examinations concerning the summation of logarithms in Secs. 7.3.1 and 7.3.2, where the finite quark mass represented a non-trivial modification, we can treat the massless and the massive quark case within the same computation because $Q_0 < m$. We can therefore begin from the Laplace space thrust distribution

$$
\begin{aligned}
\ln \tilde{\sigma}^{\mathrm{cb}}(\nu, Q, m, Q_0) = {}& 2 \int_{m^2}^{Q^2} \frac{\mathrm{d}\tilde{q}^2}{\tilde{q}^2} \int_0^1 \mathrm{d}z\, \theta\!\left(\tilde{q}^2 - m^2 - \frac{Q_0^2}{(1-z)^2}\right) \\
& \times P_{QQ}\!\left[\alpha_s\!\left(\tilde{q}^2(1-z)^2\right), z, \frac{m^2}{\tilde{q}^2}\right]\!\left(\mathrm{e}^{-\nu \tilde{q}^2(1-z)/Q^2} - 1\right) \\
= {}& \int_{Q_0^2}^{Q^2} \mathrm{d}q_\perp^2 \int_0^{1-\frac{q_\perp}{Q}} \mathrm{d}z\, \frac{1}{q_\perp^2 + m^2(1-z)^2} \\
& \times P_{QQ}\!\left[\alpha_s\!\left(q_\perp^2 + m^2(1-z)^2\right), z, \frac{m^2(1-z)^2}{q_\perp^2 + m^2(1-z)^2}\right] \\
& \times \left(\mathrm{e}^{-\nu(q_\perp^2 + m^2(1-z)^2)/Q^2(1-z)} - 1\right),
\end{aligned}
\tag{8.4}
$$

where we have implemented the $p_\perp$ cut Q_0 according to Eqs. (7.57) and (7.63). In the second line we changed the integration variable from $\tilde{q}$ to $q_\perp$ and used that $m^2/Q^2 \ll 1$. From the second line one can see that we can write the Laplace space thrust distribution with Q_0 cut as

$$\tilde{\sigma}^{\mathrm{cb}}(\nu, Q, m, Q_0) = \mathrm{e}^{-\mathcal{I}(\nu, Q, m, Q_0)} \times \tilde{\sigma}^{\mathrm{cb}}(\nu, Q, m) \,, \tag{8.5}$$

where $\tilde{\sigma}^{\mathrm{cb}}(\nu, Q, m)$ is the distribution without Q_0 cut and the function

$$
\begin{aligned}
\mathcal{I}(\nu, Q, m, Q_0) = {} & 2 \int_0^{Q_0^2} \mathrm{d}q_\perp^2 \int_0^{1 - \frac{q_\perp}{Q}} \mathrm{d}z \, \frac{1}{q_\perp^2 + m^2(1-z)^2} \\
& \times P_{QQ}\left[\alpha_s\big(q_\perp^2 + m^2(1-z)^2\big), z, \frac{m^2(1-z)^2}{q_\perp^2 + m^2(1-z)^2} \right] \\
& \times \left(\mathrm{e}^{-\nu(q_\perp^2 + m^2(1-z)^2)/Q^2(1-z)} - 1 \right)
\end{aligned}
\tag{8.6}
$$

describes the contributions of the unreleased radiation. Since we are interested in the dominant contribution linear in Q_0 we can expand to linear order in ν and change variables to $q^2 = p_\perp^2 + m^2(1 - z)^2$ to obtain

$$
\begin{aligned}
\mathcal{I}(\nu, Q, m, Q_0) = {} & -\frac{4 C_F \nu}{\pi Q^2} \Bigg\{ (Q - 2m) \int_0^{Q_0} \mathrm{d}q \, \alpha_s(q) \\
& + m \int_{Q_0}^{m} \mathrm{d}q \, \alpha_s(q) \, \frac{\big(q - \sqrt{q^2 - Q_0^2}\big)^2}{q\sqrt{q^2 - Q_0^2}} \Bigg\} + \mathcal{O}\!\left(\nu^2, Q_0^2, \frac{m^2 Q_0}{Q^3}\right).
\end{aligned}
\tag{8.7}
$$

where we have dropped terms which are down by additional powers of Q_0/m and m/Q. In addition, to linear order in Q_0 we can extend the upper limit of the second integral up to infinity. From this we obtain at $\mathcal{O}(\alpha_s)$ the final result

$$\mathcal{I}(\nu, Q, m, Q_0) = -\left[16 \frac{Q_0}{Q} - 8\pi \frac{Q_0 m}{Q^2} \right] \frac{C_F \alpha_s(Q_0)}{4\pi} \nu + \mathcal{O}\!\left(\nu^2, Q_0^2, \frac{m^2 Q_0}{Q^3}, \alpha_s^2\right), \tag{8.8}$$

for the unreleased radiation, where we can fix the scale of the strong coupling to Q_0 because it represents the only scale the integral depends. For the case of massless quark production the term proportional to m is zero. A similar calculation for the massless quark case (relevant for an analysis in the effective coupling model) was carried out in Ref. [170].

For the thrust distributions obtained from the coherent branching formalism the relations (8.5) and (8.8) in connection with Laplace space identities imply that up to terms quadratic in Q_0, the strong coupling and m/Q the effect of the $p_\perp$ cut is a simple shift in τ with respect to the thrust distribution without $p_\perp$ cut:

$$\frac{\mathrm{d}\sigma^{\mathrm{cb}}}{\mathrm{d}\tau}(\tau, Q, Q_0) = \frac{\mathrm{d}\sigma^{\mathrm{cb}}}{\mathrm{d}\tau}\left(\tau + 16\frac{Q_0}{Q}\frac{C_F \alpha_s(Q_0)}{4\pi}, Q, Q_0 = 0\right) \tag{8.9}$$

$$\frac{\mathrm{d}\sigma^{\mathrm{cb}}}{\mathrm{d}\tau}(\tau, Q, m, Q_0) = \frac{\mathrm{d}\sigma^{\mathrm{cb}}}{\mathrm{d}\tau}\left(\tau + \left[16\frac{Q_0}{Q} - 8\pi\frac{Q_0 m}{Q^2}\right]\frac{C_F \alpha_s(Q_0)}{4\pi}, Q, m, Q_0 = 0\right) \tag{8.10}$$

These shifts are valid for the parton level distributions and through the convolutions of Eqs. (7.3) and (7.21) also for the hadron level distributions. Numerically, these shifts are far from negligible for $Q_0 \sim 1$ GeV, which is the typical size of the shower cut values used in state-of-the-art Monte-Carlo event generators.

Within the coherent branching formalism it is, however, not possible to systematically address the question if these shifts should be interpreted as modifications of QCD parameters such as the mass. This is because the coherent branching formalism provides a convenient computational method to sum cross section contributions that are singular in the soft and collinear limits, but does not provide a field theoretic background where this issue can be discussed conceptually from first principles. We will therefore examine the effects of $p_\perp$ cut Q_0 again in the next two subsections in the framework of the factorization theorems (7.4) and (7.25) for massless and massive quarks, respectively.

<div style="text-align:center">

SCET Jet Function, $\mu = Q_0$ Soft Function, $\mu = Q_0$
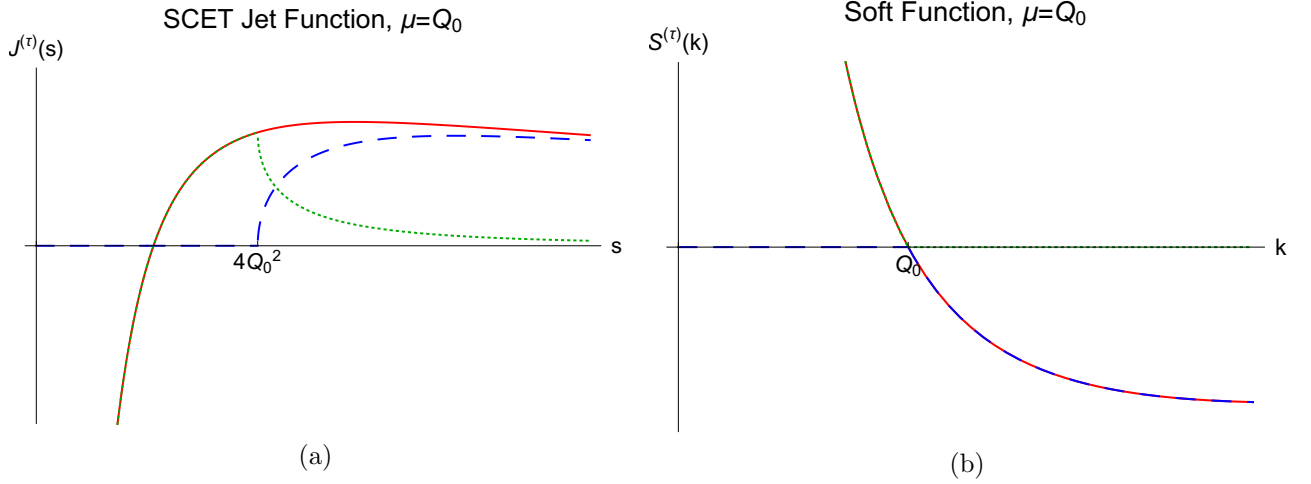
(a)   (b)

</div>

Figure 8.3: SCET jet function for massless quarks (a) and soft function (b) without cut (solid red), unreleased (dotted green) and with cut (dashed blue) for $\mu = Q_0$.

8.1.3 Unreleased radiation for massless quarks: QCD factorization

In the context of QCD factorization the hard, soft and collinear effects are separated at the operator level and the modifications caused the by the $p_\perp$ cut Q_0 can be determined in each sector individually. Possible cross terms and exponentiation effects are automatically taken care of by the multiplicative structure of the factorization theorem (7.4). It is then straightforward to see that there is no change in the U factors which sum the large logarithms, since the $p_\perp$ cut acts in the infrared and does not lead to any new types of UV-divergences. As far as the hard function H_Q is concerned, the $p_\perp$ cut contributes only through terms of order Q_0^2/Q^2, which are strongly power-suppressed and negligible at the order we are working. So we only have to analyze the jet function $J^{(\tau)}$ and the soft function $S^{(\tau)}$ as they describe radiation where the $p_\perp$ cut Q_0 can leave a non-trivial impact.

We write the jet function $J^{(\tau)}$ and the soft function $S^{(\tau)}$ in the presence of the $p_\perp$ cut Q_0 in the form

$$J^{(\tau)}(s, \mu_J, Q_0) = J^{(\tau)}(s, \mu_J) - J^{(\tau)}_{\mathrm{ur}}(s, Q_0), \tag{8.11}$$

$$S^{(\tau)}(k, \mu_S, Q_0) = S^{(\tau)}(k, \mu_S) - S^{(\tau)}_{\mathrm{ur}}(k, Q_0) \tag{8.12}$$

where $J^{(\tau)}(s, \mu_J)$ and $S^{(\tau)}(k, \mu_S, Q_0)$ are the renormalization scale dependent jet and soft functions from Eq. (7.4) determined using dimensional regularization for the momentum integrations and defined in the $\overline{\mathrm{MS}}$ renormalization scheme. Their expressions at $\mathcal{O}(\alpha_s)$ are displayed in Eqs. (7.6) and (7.7), respectively. The functions $J^{(\tau)}_{\mathrm{ur}}(s, Q_0)$ and $S^{(\tau)}_{\mathrm{ur}}(k, Q_0)$ represent the unreleased radiation coming from regions *below* the $p_\perp$ cut Q_0, i.e. they describes the perturbative radiation that is prevented if Q_0 is finite. Since the $p_\perp$ cut does not lead to any genuine UV divergences, $J^{(\tau)}_{\mathrm{ur}}$ and $S^{(\tau)}_{\mathrm{ur}}$ are renormalization group invariant, which we have indicated by dropping the renormalization scale dependence from their arguments. The calculations for $S^{(\tau)}_{\mathrm{ur}}$ and $J^{(\tau)}_{\mathrm{ur}}$ at $\mathcal{O}(\alpha_s)$ are straightforward and described in detail in App. G.1 and App. G.4, respectively.

The result for the unreleased jet function has the form $[s' = s/Q_0^2, \ w(z) = (1 - 4/z)^{1/2}]$

$$
\begin{aligned}
J^{(\tau)}_{\mathrm{ur}}(s, Q_0) = \frac{\alpha_s(Q_0) C_F}{4\pi} \Bigg\{ & \left(12 - \frac{4\pi^2}{3} \right) \delta(s) \\
& + \theta(4Q_0^2 - s) \left(-\frac{6}{Q_0^2} \left[\frac{\theta(s')}{s'} \right]_+ + \frac{8}{Q_0^2} \left[\frac{\theta(s') \ln s'}{s'} \right]_+ \right) \\
& + \theta(s - 4Q_0^2) \frac{1}{s} \left[6(w(s') - 1) - 8 \left(\ln\left(\frac{1 + w(s')}{1 - w(s')} \right) - \ln s' \right) \right] \Bigg\} + \mathcal{O}(\alpha_s^2).
\end{aligned}
\tag{8.13}
$$

<div style="text-align:center">

135

</div>

In Fig. 8.3a the $\mathcal{O}(\alpha_s)$ corrections for jet function without $p_\perp$ cut, $J^{(\tau)}(s, \mu_J)$ (solid red line), the unreleased jet function $J_{\mathrm{ur}}^{(\tau)}(s, Q_0)$ (dotted green), and the full jet function with $p_\perp$ cut, $J^{(\tau)}(s, \mu_J, Q_0)$ (dashed blue line) are shown for $\mu_J = Q_0$ using arbitrary units. For this scale choice the $p_\perp$ cut completely eliminates the plus distributions for $s < 4Q_0^2$ in $J^{(\tau)}(s, \mu_J, Q_0)$ and slightly reduces the collinear jet mass distribution for s larger than $4Q_0^2$. As already argued in Sec. 8.1.1, the unreleased radiation in the collinear sector depends quadratially on Q_0 except for the δ-function term, which is however, not affecting the peak location τ_{peak} at $\mathcal{O}(\alpha_s)$, see the discussion of Sec. 7.1.4. The contributions from $s < 4Q_0^2$ as well as from $s > 4Q_0^2$ lead to effects of order Q_0^2 in the observable thrust distribution upon integration over the soft model shape function, which corresponds to a smearing in s over an interval of order $Q\Lambda$ which is much larger than Q_0^2, see Eq. (7.3). Since we are interested in effects that are linear in Q_0, the unreleased radiation in the collinear sector can thus be ignored in our discussion.

The result for the unreleased soft function reads [$k' = k/Q_0$]

$$S_{\mathrm{ur}}^{(\tau)}(k, Q_0) = \frac{\alpha_s(Q_0)C_F}{4\pi} \, 16 \, \theta(Q_0 - k) \left\{ -\frac{1}{Q_0}\left[\frac{\theta(\tilde{k})\ln\tilde{k}}{\tilde{k}}\right]_+ \right\} + \mathcal{O}(\alpha_s^2) \,. \tag{8.14}$$

In Fig. 8.3b the $\mathcal{O}(\alpha_s)$ corrections to the soft function without $p_\perp$ cut, $S^{(\tau)}(k, \mu_S)$ (solid red line), the unreleased jet function $S_{\mathrm{ur}}^{(\tau)}(k, Q_0)$ (dotted green), and the full jet function with $p_\perp$ cut, $S^{(\tau)}(s, \mu_S, Q_0)$ (dashed blue line) are shown for $\mu_S = Q_0$ for arbitrary units. Similar to the case of the jet function, for this scale choice, the $p_\perp$ cut just eliminates the plus distributions for $k < Q_0$ in $S^{(\tau)}(k, \mu_S, Q_0)$, and but has no effects for $k > Q_0$. As already anticipated on general grounds in Sec. 8.1.1, the $p_\perp$ cut indeed leads to a linear dependence on Q_0.

As can be seen from the factorization formula (7.3), the soft model shape function causes a smearing in k over an interval of order Λ which we assume to be larger than Q_0. Since the unreleased soft function has support only for light cone momenta $k < Q_0$, we can therefore quantify its effect more transparently in terms of a multipole expansion,

$$S_{\mathrm{ur}}^{(\tau)}(k, Q_0) \, = \, -\Delta_{\mathrm{soft}}(Q_0) \, \delta'(k) \, + \, \mathcal{O}(Q_0^2) \,, \tag{8.15}$$

where the term $\Delta_{\mathrm{soft}}(Q_0)$ is the first moment of the unreleased soft function,

$$\Delta_{\mathrm{soft}}(Q_0) \, = \, \int \mathrm{d}k' \, k' \, S_{\mathrm{ur}}^{(\tau)}(k', Q_0) \, = \, 16 \, Q_0 \, \frac{\alpha_s(Q_0)C_F}{4\pi} \,. \tag{8.16}$$

Mathematically, this multipole term appears to cause a shift of the partonic soft function threshold by $-\Delta_{\mathrm{soft}}(Q_0)$ since it can absorbed into the tree level soft function, $\delta(k) + \Delta_{\mathrm{soft}}(Q_0) \, \delta'(k) \approx \delta(k + \Delta_{\mathrm{soft}}(Q_0)) + \mathcal{O}(\alpha_s^2)$. In the context of the thrust factorization theorem (7.3) we thus see that this shift agrees identically with the result which we determined from the coherent branching formalism given in Eq. (8.9). However, as we have already mentioned before, in the coherent branching formalism there was no rigorous field theoretical background that strictly enforced this view *in the context of perturbation theory* because a perturbative modification of the threshold of a kinematic variable can only be implemented by a renormalization scheme change of a dimensionful parameter. Such a parameter does also not exists for the soft function because is arises from the dynamics of massless gluons and only depends on a light-cone momentum. In the context of the factorization formula (7.3) the correct view is that the linear effect caused by the $p_\perp$ cut Q_0 can be reinterpreted as a *shift of the soft model shape function S_{mod} [163, 167, 176], called "gap" in Ref. [174]*. Following the presentation of Ref. [174] we can write the convolution of the partonic soft function and the non-perturbative shape

function as

$$\int d\ell\, S^{(\tau)}(k - \ell, \mu_S, Q_0)\, S_{\text{mod}}(\ell) = \int d\ell \left[S^{(\tau)}(k - \ell, \mu_S) - S_{\text{ur}}^{(\tau)}(k - \ell, Q_0) \right] S_{\text{mod}}(\ell),$$

$$= \int d\ell\, S^{(\tau)}\!\left(k - \ell + \Delta_{\text{soft}}(Q_0), \mu_S \right) S_{\text{mod}}(\ell) + \mathcal{O}(\alpha_s^2, \alpha_s Q_0^2)$$

$$= \int d\ell\, S^{(\tau)}(k - \ell, \mu_S)\, S_{\text{mod}}\!\left(\ell + \Delta_{\text{soft}}(Q_0) \right) + \mathcal{O}(\alpha_s^2, \alpha_s Q_0^2). \tag{8.17}$$

This relation shows that the dominant effect of the $p_\perp$ cut Q_0 is to modify the interface between perturbation theory and non-perturbative physics and – from the point of view of a partonic computation carried out without Q_0 cut – acts as a modification of the hadronization contribution from $S_{\text{mod}}(\ell)$ to $S_{\text{mod}}\!\left(\ell + \Delta_{\text{soft}}(Q_0) \right)$ as shown in the last line of Eq. (8.17). As long as the scale Q_0 is in the perturbative regime, this scheme change can be described perturbatively. This shows that the correct way to deal with a change in Q_0 when making physical predictions – from the point of view of a partonic computation with a Q_0 cut – is to modify the non-perturbative effects by a corresponding change of the shape function gap in order to leave the physical prediction unchanged.

One of the motivations of discussing "gapped" soft functions in Ref. [174] was to devise a way consistent with QCD factorization and field theory to eliminate the $\mathcal{O}(\Lambda_{\text{QCD}})$ renormalon from the partonic soft function. This $\mathcal{O}(\Lambda_{\text{QCD}})$ renormalon arises from large factorially growing coefficients in its perturbation series and renders, from the non-perturbative, i.e. beyond perturbation theory point of view, the partonic threshold ambiguous to an amount of order of Λ_{QCD}. While for a massive particle threshold this can be achieved by a modification of the mass scheme, there is no such parameter for gluonic thresholds. Our argumentation that the effects linear in the $p_\perp$ cut Q_0 should be interpreted as a soft function gap are therefore further supported, if the $p_\perp$ cut eliminates the $\mathcal{O}(\Lambda_{\text{QCD}})$ renormalon behavior of the partonic soft function. To examine this we restrict our discussion to the effects of dressing the gluon propagator with massless fermion bubble chains using the replacement [181]

$$\frac{1}{q^2 + i\epsilon} \longrightarrow \frac{4\pi}{\alpha_s(\mu)\beta_0} \left(\frac{e^{5/3}}{\mu^2} \right)^{-u} \frac{-1}{(-q^2 - i\epsilon)^{1+u}}, \tag{8.18}$$

to compute the Borel transform, using the convention $\beta[\alpha_s] = -2\beta_0(\alpha_s^2/4\pi) + \ldots$ for defining the coefficients of the β-function (see also Eq. (7.16)), and focusing on poles in the Borel variable u located a $u = 1/2$. The term $e^{5/3}$ is related to using the usual $\overline{\text{MS}}$ renormalization scheme for the strong coupling. In passing we note that using the bubble chain method does not represent a strict all order proof that the $p_\perp$ cut eliminates the $\mathcal{O}(\Lambda_{\text{QCD}})$ renormalon. However, it is sufficient for our discussion that focuses on angular ordered showers which have NLL order precision.

As was shown in Ref. [174], the Laurent expansion of the Borel transform of the partonic soft function $S^{(\tau)}(k, \mu_S)$ around $u = 1/2$ reads

$$B\!\left[S^{(\tau)}(k, \mu) \right]\!\left(u \approx \frac{1}{2} \right) = \frac{16 C_F e^{-5/6}}{\pi \beta_0} \frac{\mu}{u - \frac{1}{2}} \delta'(k). \tag{8.19}$$

The $\mathcal{O}(\Lambda_{\text{QCD}})$ renormalon is canceled by the $p_\perp$ cut, if the unreleased soft function $S_{\text{ur}}^{(\tau)}$ exhibits also a Borel pole at $u = 1/2$ and if the residue agrees with the one shown in Eq. (8.19). Some details on the calculation of the Borel transform of the unreleased soft function can be found in App. G.1. The result reads

$$B\!\left[S_{\text{ur}}^{(\tau)}(k, Q_0) \right]\!\left(u \approx \frac{1}{2} \right) = \frac{16 C_F e^{-5/6}}{\pi \beta_0} \frac{\mu}{u - \frac{1}{2}} \delta'(k), \tag{8.20}$$

and is identical to Eq. (8.19) when, consistently, the same scale choice is adopted for the strong coupling. The agreement shows that in the presence of the $p_\perp$ cut Q_0 the $\mathcal{O}(\Lambda_{\text{QCD}})$ renormalon

is indeed removed from the partonic soft function due to Eq. (8.12). Thus the $p_\perp$ cut eliminates the $\mathcal{O}(\Lambda_{\rm QCD})$ renormalon and leads to a more convergent large-order behavior of the partonic soft function. This analysis also reconfirms the view that soft gluon radiation in (at least angular ordered) parton showers used in MC event generators does not suffer from $\mathcal{O}(\Lambda_{\rm QCD})$ renormalon ambiguities, in contrast to perturbative calculations without finite infrared cuts.

8.1.4   Unreleased radiation for massive quarks: QCD factorization

For the massive quark thrust distribution factorization theorem (7.4) we proceed in a way analogous to the massless quark case. The $p_\perp$ cut does not lead to any modifications for the U factors that sum large logarithms since it does not lead to any new types of UV-divergences. The hard function H_Q is the same as for massless quarks, and the $p_\perp$ cut contributes terms of order Q_0^2/Q^2. The mass mode factor H_m, which arises from off-shell massive quark fluctuations, obtains modifications of order Q_0^2/m^2. Both effects are strongly power-suppressed and negligible at the order we are working. Since the massive and massless quark factorization theorems contain the same partonic soft function $S^{(\tau)}$ and the same non-perturbative model shape function $S_{\rm mod}$, the effects of the $p_\perp$ cut we have discussed for them in the massless quark case also apply for massive quarks: the $p_\perp$ cut leads to a linear sensitivity to Q_0 can can be associated to a gapped soft function, as shown in Eqs. (8.16) and (8.17). This takes care of the m-independent shift contribution shown in Eq. (8.10).

What remains to be examined is the bHQET jet function $J_B^{(\tau)}$ which contains the dynamics of the ultra-collinear radiation and which, as we have argued in Sec. 8.1.1, can also have a linear sensitivity to the $p_\perp$ cut Q_0. The aim is to show from the field theory perspective that we can associate the m-dependent term in Eq. (8.10) to a modification of the quark mass scheme different from the pole mass. This examination of the bHQET jet function represents the central part of our discussion because at NLL+$\mathcal{O}(\alpha_s)$ order the bHQET jet function completely controls the quark mass scheme. We note that the bHQET jet function dominates the mass dependence also at higher orders, while the mass dependence coming from other parts of the factorization formula is subleading.

We write the bHQET jet function $J_B^{(\tau)}$ in the presence of the $p_\perp$ cut Q_0 in the form

$$J_B^{(\tau)}(\hat{s}, m^{\rm pole}, \mu_B, Q_0) = J_B^{(\tau)}(\hat{s}, m^{\rm pole}, \delta m = 0, \mu_B) - J_{B,{\rm ur}}^{(\tau)}(\hat{s}, Q_0), \qquad (8.21)$$

where $J_B^{(\tau)}(\hat{s}, m^{\rm pole}, \delta m = 0, \mu_B)$ is the renormalization scale dependent bHQET jet from Eq. (7.25) *in the pole mass scheme* determined using dimensional regularization for the momentum integrations and defined in the $\overline{\rm MS}$ renormalization scheme. Its expression at $\mathcal{O}(\alpha_s)$ is displayed in Eqs. (7.28). The function $J_{B,{\rm ur}}^{(\tau)}(\hat{s}, Q_0)$ describes the unreleased radiation coming from regions *below* the $p_\perp$ cut Q_0. The $p_\perp$ cut does not lead to any genuine UV divergences, so $J_{B,{\rm ur}}^{(\tau)}$ is renormalization group invariant, which we have indicated by dropping the renormalization scale dependence from its arguments. The calculation of $J_{B,{\rm ur}}^{(\tau)}$ is described in detail in App. G.3.

The result for the unreleased bHQET jet function reads [$\tilde{s} = \hat{s}/Q_0$, $w(z) = (1 - 4/z)^{1/2}$]

$$\begin{aligned}
m^{\rm pole} J_{B,{\rm ur}}^{(\tau)}(\hat{s}, Q_0) = \frac{\alpha_s(Q_0) C_F}{4\pi} \Bigg\{ & -8\pi Q_0 \delta'(\hat{s}) + 2\Big(4 - \frac{\pi^2}{3}\Big)\delta(\hat{s}) \\
& + \theta(2Q_0 - \hat{s})\Big(-\frac{8}{Q_0}\Big[\frac{\theta(\tilde{s})}{\tilde{s}}\Big]_+ + \frac{16}{Q_0}\Big[\frac{\theta(\tilde{s})\ln\tilde{s}}{\tilde{s}}\Big]_+ \Big) \\
& + \theta(\hat{s} - 2Q_0)\frac{8}{\hat{s}}\Big[(w(\tilde{s}^2) - 1) - \Big(\ln\Big(\frac{1 + w(\tilde{s}^2)}{1 - w(\tilde{s}^2)}\Big) - 2\ln\tilde{s}\Big)\Big] \Bigg\} + \mathcal{O}(\alpha_s^2)
\end{aligned} \qquad (8.22)$$

In Fig. 8.4 the $\mathcal{O}(\alpha_s)$ corrections to the bHQET jet function without $p_\perp$ cut, $J_B^{(\tau)}(\hat{s}, \mu_B)$ (solid red line), the unreleased jet function $J_{B,{\rm ur}}^{(\tau)}(\hat{s}, Q_0)$ (dotted green), and the full jet function with the $p_\perp$
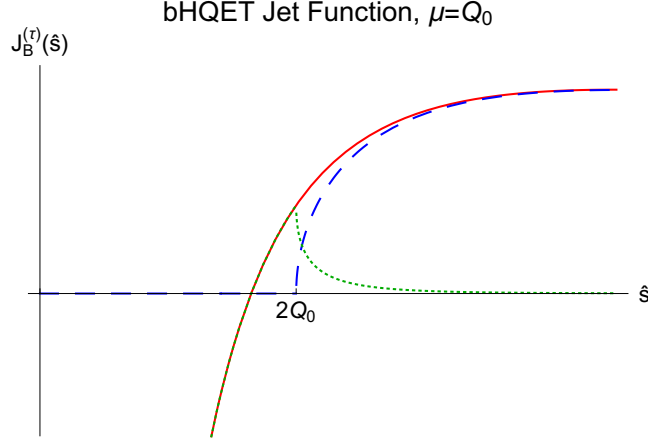
Figure 8.4: bHQET jet function without cut (solid red), unreleased (dotted green) and with cut (dashed blue) for $\mu = Q_0$.

cut, $J_B^{(\tau)}(\hat{s}, \mu_B, Q_0)$ (dashed blue line) are shown for $\mu_B = Q_0$ for arbitrary units. We see that the effect of the $p_\perp$ cut has features common to the massless quark jet function: the $p_\perp$ cut eliminates the plus distributions for $\hat{s} < 2Q_0$ and slightly reduces the ultra-collinear jet mass distributions for $\hat{s}$ larger than $2Q_0$, compare to Fig. 8.3a. However, the difference is that the overall dependence on Q_0 is linear, as anticipated in Sec. 8.1.1, and the singular structure at $\hat{s} = 0$ is more complicated due to the appearance of the term proportional to the derivative of the delta function, $\delta'(\hat{s})$. This term arises from the on-shell cuts of the self-energy diagram of the heavy quark with the $p_\perp$ cut Q_0, see App. G.3 for details.

To understand the result for the unreleased bHQET jet function in Eq. (8.22), it is important to recall that for the soft function the interpretation of the effects of the $p_\perp$ cut is related to the interface between partonic cross section and the non-perturbative shape function that describes hadronization effects and that there is no partonic parameter involved in the argumentation. This differs from the bHQET jet function which contains the quark mass as a partonic parameter that depends on an explicit decision about its renormalization condition. In the expression for the $\mathcal{O}(\alpha_s)$ corrections to the bHQET jet function in Eq. (7.28) this dependence is manifest in the term $-\frac{4\delta m}{m^{\text{pole}}}\delta'(\hat{s})$, where $\delta m = m_{\text{pole}} - m$ is the difference of the employed mass renormalization scheme to the pole mass. From the structure of the convolutions in the factorization formulae (7.21) and (7.25), due to the combination $\hat{s}\, m/Q - k$ appearing in the partonic soft function $S^{(\tau)}$, it is also evident that the effects linear in Q_0 contained in Eq. (8.22) cannot be associated to a universal (i.e. m/Q-independent) change of the soft function model gap. It is therefore mandatory to interpret these contributions from the point of a perturbative mass change alone.

In the absence of the $p_\perp$ cut, i.e. when only dimensional regularization is used to regularize infrared and ultraviolet divergences, the bHQET on-shell heavy quark self energy is a scaleless integral and vanishes to all orders. So in bHQET the quark mass renormalization scheme is automatically the pole mass when we set $\delta m = 0$. A change to another scheme is realized by explicitly adopting a finite expressions for δm (which is a series that starts at $\mathcal{O}(\alpha_s)$). In the presence of the $p_\perp$ cut Q_0, however, the on-shell self-energy depends on the scale Q_0 and does not vanish any more, see App. G.3 for details of this calculation. This is the origin of the $\delta'(\hat{s})$ term in Eq. (8.22), and it means that *in the presence of the $p_\perp$ cut Q_0 the pole mass m^{pole}, as defined in perturbation theory without any infrared cut, does not any more represent the pole position of the heavy quark propagator.*[1] Rather,

---

[1] At this point one may object that in the calculation of the unreleased bHQET jet function one can decide whether one applies the $p_\perp$ cut Q_0 in the on-shell self-energy diagram or not. However, this corresponds to using different infrared regulators for virtual and real radiation corrections which is inconsistent. In fact, dropping the $p_\perp$ cut Q_0 in

the pole is located at the Q_0-dependent mass

$$m^{\mathrm{CB}}(Q_0) = m^{\mathrm{pole}} - \delta m^{\mathrm{CB}}(Q_0) \,, \tag{8.23}$$

with

$$\begin{aligned}
\delta m^{\mathrm{CB}}(Q_0) &= \frac{\alpha_s(Q_0)C_F}{4\pi}\, 2\pi\, Q_0 + \mathcal{O}(\alpha_s^2) \\
&= \frac{2}{3}\alpha_s(Q_0)\, Q_0 + \mathcal{O}(\alpha_s^2)\,.
\end{aligned} \tag{8.24}$$

We stress that this means that the pole of the heavy quark propagator is not physical and implicitly depends on the infrared regularization scheme employed. The pole of the heavy quark propagatpr is unique only in the limit of vanishing infrared regulators. We call $m^{\mathrm{CB}}(Q_0)$ the scale-dependent *coherent branching (CB) mass*. It is possible to absorb the $\delta'(\hat{s})$ correction term into the mass scheme (of the tree-level bHQET jet function) which changes it from m^{pole} to the coherent branching mass $m^{\mathrm{CB}}(Q_0)$. The essential point is that this scheme change is *implicitly carried out within the coherent branching formalism (and in angular ordered parton showers) because there the $\delta'(\hat{s})$ term never arises.* This means that the mass parameter in the coherent branching formalism in the presence of the $p_\perp$ cut Q_0 *agrees with the pole of the heavy quark propagator which is the CB mass $m^{\mathrm{CB}}(Q_0)$.* As we show in the following, only within this context we find that the result of Eq. (8.22) is compatible with the mass-dependent shift in Eq. (8.10) obtained from the coherent branching formalism in the presence of the $p_\perp$ cut, recalling the definitions of the thrust variable τ and the linearized invariant mass variable $\hat{s}$ given in Eqs. (7.1) and (7.26), respectively.

The subtle issue to fully understand (and appreciate) our conclusion is that all the terms shown in Eq. (8.22) are required to allow the interpretation that the effects of the $p_\perp$ cut that are linear in Q_0 represent a modification of the mass scheme. The crucial consistency requirement for this interpretation is that the sum of all modifications due to the contributions linear in the cutoff scale Q_0 given in Eq. (8.22) vanish. This is because a change of the quark mass scheme (and of the renormalization scheme of any QCD parameter) leaves the theoretical prediction invariant and essentially represents a mutual exchange of perturbative corrections between the mass parameter and the dynamical matrix elements. It is therefore mandatory that the contributions linear in Q_0 of the remaining corrections (other than the $\delta'(\hat{s})$ term) in the unreleased bHQET jet function given in Eq. (8.22) have the same magnitude but the opposite sign as the contribution coming from the $\delta'(\hat{s})$ term. Since the soft model in the factorization theorem (7.21) causes a smearing in $\hat{s}$ of order $Q\Lambda/m \gg Q_0$, we can - in analogy to our discussion on the unreleased soft function in Sec. 8.1.3 - use again the multipole expansion to proceed. In contrast to our discussion on the soft function, we do not have to argue about the validity of the multipole expansion because for boosted top quarks we have $Q/m \gg 1$ so that the multipole expansion is well applicable even if Q_0 and Λ are similar in size. The outcome is that we need to show that *the total integral (i.e. the zeroth moment) as well as the first moment of the unreleased bHQET jet function vanish identically.* If these conditions are satisfied, we can interpret all effects of the $p_\perp$ cut that are linear in Q_0 as a change in the quark mass renormalization scheme.

It is straightforward to check from the result in Eq. (8.22) that these properties are indeed satisfied:

$$\int \mathrm{d}\hat{s}\, J_{B,\mathrm{ur}}^{(\tau)}(\hat{s}, Q_0) = 0 \,, \tag{8.25}$$

$$\begin{aligned}
\int \mathrm{d}\hat{s}\, \hat{s}\, J_{B,\mathrm{ur}}^{(\tau)}(\hat{s}, Q_0) &= \left[\frac{\alpha_s(Q_0)C_F}{4\pi}\, 8\pi\, Q_0\right]_{\delta'} - \left[\frac{\alpha_s(Q_0)C_F}{4\pi}\, 8\pi\, Q_0\right]_{\mathrm{non}-\delta'} \\
&= \left[4\delta m^{\mathrm{CB}}(Q_0)\right]_{\delta'} - \left[4\delta m^{\mathrm{CB}}(Q_0)\right]_{\mathrm{non}-\delta'} = 0 \,,
\end{aligned} \tag{8.26}$$

---

the on-shell self-energy diagram only and keeping it in the rest of the calculation is just equivalent to switching from the pole mass scheme to $m^{\mathrm{CB}}(Q_0)$.

where for the first moment we have indicated by subscripts the contributions from the $\delta'(\hat{s})$ term and the rest. Given the complicated structure of the result for the unreleased bHQET jet function in Eq. (8.22), the results appear highly non-trivial. From the physical point of view, however, the vanishing zeroth moment is related to the fact that the total (e^+e^- hadronic) cross section is not linearly sensitive to infrared momenta, which is well known. The vanishing of the first moment expresses that, physically, the mass-dependent kinematics threshold generated by the ultra-collinear radiation is not linearly sensitive to infrared momenta either. Linear sensitivity to infrared moments is only introduced by hand when one imposes the pole scheme for the heavy quark mass (defined in the common way by the one-particle irreducible on-shell self energy diagrams in the absence of any infrared regulator)[2]. This feature is well known since a long time see e.g. Ref. [182]. We can therefore expect that the zeroth and the first moments of the unreleased bHQET jet function vanish to all orders in perturbation theory.

At this point our prove is complete and we have field theoretically shown that – if one always employs a mass scheme that agrees with the pole of the perturbative heavy quark propagator – all effects of the $p_\perp$ cut that are linear in Q_0 not only can, but rather must be interpreted as a change of the quark mass scheme from the pole mass to the coherent branching mass:

$$J_B^{(\tau)}(\hat{s}, m^{\text{pole}}, \mu_B, Q_0) = J_B^{(\tau)}(\hat{s}, m^{\text{pole}}, \delta m = 0, \mu_B) - J_{B,\text{ur}}^{(\tau)}(\hat{s}, Q_0)$$

$$= J_B^{(\tau)}\Big(\hat{s}, m^{\text{CB}}(Q_0), \delta m^{\text{CB}}(Q_0), \mu_B\Big) + \mathcal{O}(Q_0^2)\,, \qquad (8.27)$$

where at $\mathcal{O}(\alpha_s)$, keeping in mind Eq. (8.21) and the form of Eq. (7.28), the term $\delta m^{\text{CB}}(Q_0)$ in the 2nd line of Eq. (8.27) is generated by the non-δ' terms in the unreleased bHQET jet function of Eq. (8.22). Recalling the definitions of the thrust variable τ and the linearized invariant mass variable $\hat{s}$ given in Eqs. (7.1), (7.2) and (7.26), we see that the mass dependent τ shift in Eq. (8.10) agrees with the τ shift generated by $\delta m^{\text{CB}}(Q_0)$ in the 2nd line of Eq. (8.27). This implies that the mass parameter in the coherent branching formalism (as well as in angular ordered parton showers) in the presence of the $p_\perp$ cut Q_0 *is* the CB mass $m^{\text{CB}}(Q_0)$. The result of Eq. (8.27) gives us full control over the quark mass scheme in the presence of the $p_\perp$ cut Q_0 since, with the help of relation (8.23), we can relate the coherent branching mass $m^{\text{CB}}(Q_0)$ to any other scheme at $\mathcal{O}(\alpha_s)$.

It is now natural to ask if the change from the pole mass to the scale-dependent CB mass cures the $\mathcal{O}(\Lambda_{\text{QCD}})$ renormalon problem of the thrust distribution in the pole mass scheme. We address this question using again the dressed gluon propagator approach of Eq. (8.18) to determine the Borel transform in the region around $u = 1/2$. As was shown in Refs. [183, 184], the Laurent expansion of the Borel transform of the perturbative series in $\alpha_s(\mu)$ for the pole mass in terms of the $\overline{\text{MS}}$ mass around $u = 1/2$ reads

$$B\Big[m^{\text{pole}} - \overline{m}(\mu)\Big]\Big(u \approx \frac{1}{2}\Big) = -\frac{2C_F e^{-5/6}}{\beta_0}\frac{\mu}{u - \frac{1}{2}}\,. \qquad (8.28)$$

The corresponding result for the perturbative series in $\alpha_s(\mu)$ for the pole mass in terms of the CB mass is calculated in App. G.3 and reads

$$B\Big[m^{\text{pole}} - m^{\text{CB}}(Q_0)\Big]\Big(u \approx \frac{1}{2}\Big) = -\frac{2C_F e^{-5/6}}{\beta_0}\frac{\mu}{u - \frac{1}{2}}\,. \qquad (8.29)$$

We see that the result is identical to Eq. (8.28). This shows that the scale-dependent CB mass $m^{\text{CB}}(Q_0)$ is a low-scale short-distance mass. This is not unexpected, of course, because the CB mass is defined from the bHQET on-shell massive quark self-energy with a transverse momentum infrared

_____

[2]In this work we define the pole mass scheme m^{pole} strictly in the generally accepted canonical way, namely in the context of perturbation theory in the limit of vanishing infrared regularization.

cut which prevents the low-virtuality contributions from the evolution of the strong coupling that are responsible for the emergence of infrared renormalons. It is also straightforward to check that the Borel ambiguities coming from the $\delta'(\hat{s})$ self-energy term and the other contributions in the unreleased jet function (calculated from the perturbative series in $\alpha_s(\mu)$) cancel exactly:

$$
\begin{aligned}
B\left[J_{B,\mathrm{ur}}^{(\tau)}(\hat{s}, Q_0)\right]\left(u \approx \frac{1}{2}\right) &= \left[\frac{8C_F e^{-5/6}}{\beta_0} \frac{\mu}{u - \frac{1}{2}} \delta'(\hat{s})\right]_{\delta'} - \left[\frac{8C_F e^{-5/6}}{\beta_0} \frac{\mu}{u - \frac{1}{2}} \delta'(\hat{s})\right]_{\mathrm{non}-\delta'} \\
&= 0 \,.
\end{aligned}
\tag{8.30}
$$

This reconfirms the relation (8.27) also beyond the NLO precision level (at least in the large-β_0 approximation). As a consequence, imposing the $p_\perp$ cut Q_0 in the massive quark thrust distributions implies that one uses the CB mass scheme of Eq. (8.23) and that all $\mathcal{O}(\Lambda_{\mathrm{QCD}})$ infrared renormalon issues are removed.

8.2   Summary of all theoretical considerations

In this section we summarize all theoretical and conceptual results we have obtained in the previous sections in the context of the massless and massive quark thrust distributions (see Eq. (7.1) and (7.2) in Sec. 7.1) obtained in the coherent branching formalism and the QCD factorization approach. These findings provide the basis of the field theoretic reinterpretation of the effects of the $p_\perp$ cut Q_0 *that are linear in Q_0* as a modification of hadronization contributions and a redefinition of the heavy quark mass scheme, valid for boosted massive quarks in the narrow width approximation. We also discuss the meaning of these results in the context of angular ordered parton showers, which are based on the coherent branching formalism and for which a $p_\perp$ cut on the parton shower evolution is mandatory. These considerations set the stage for the numerical studies we carry out in Sec. 9 using the HERWIG 7 event generator [151, 152, 175].

Since the QCD factorization approach provides the closest relation to field theory and allows to systematically address issues concerning the interpretation of partonic and non-perturbative parameters, the examinations in the previous sections were built around establishing a one-to-one correspondence between the factorized cross sections for thrust and the corresponding results obtained from the coherent branching formalism. For massive quarks the latter is known to be valid for quasi-collinear and the former for boosted massive quarks, which here correspond to equivalent kinematic situations. Because the peak resonance region of the thrust distribution, and in particular the peak position, provide the strongest and cleanest top mass sensitivity we have focused our considerations on the thrust resonance peak position.

In Sec. 7.1.4 we have shown that, for the factorized predictions, resummed results at full NLL order (where the dynamical logarithmic terms in the fixed-order matrix elements of the factorized predictions are understood to be part of full NLL) are sufficient to describe the peak position with NLO precision, i.e. up to higher order terms that enter only at $\mathcal{O}(\alpha_s^2)$ and beyond. In Secs. 7.3.1 and 7.3.2 we then established for massless and massive quarks, respectively, that in the absence of any infrared cut the NLL resummed results provided by the coherent branching formalism and by the usual factorized approach are equivalent. Since the massive quark results in the factorized approach we were using for the comparison were determined in the strict pole mass scheme m^{pole}, we could prove that *in the coherent branching formalism with NLL resummation of logarithms and in the absence of an infrared cut (i.e. for $Q_0 = 0$) the quark mass parameter is equivalent to the pole mass m^{pole} at $\mathcal{O}(\alpha_s)$:*

$$
m^{\mathrm{CB}}(Q_0 = 0) \overset{\mathrm{peak}}{=} m^{\mathrm{pole}} + \mathcal{O}(\alpha_s^2) \,,
\tag{8.31}
$$

where m^{CB} is the quark mass parameter in the coherent branching formalism and called the coherent branching (CB) mass.

This relation, however, is only valid in the context of strict QCD perturbation theory, i.e. in calculations based on expanding in α_s at a constant renormalization scale such that evolution effects are encoded entirely in powers of logarithms and virtual loop and real radiation phase space integrals can be carried out down to zero momenta. Such a strict perturbative approach, however, *cannot be applied for angular ordered parton shower algorithms implemented in state-of-the-art MC event generators*, so that it is not possible to use them without an infrared cut on the parton shower evolution. There are two main reasons for that. The first is related to the fact that for the parton showers implemented in multi-purpose MC event generators the renormalization scale of the strong coupling is a function of kinematic variables that decrease in the course of the shower evolution. In this way parton showers can account for important subleading NLL information. Without an infrared cut the strong coupling would therefore run into its Landau pole once the evolution reached virtualities and momenta close to $\Lambda_{\rm QCD}$. The second reason is that in the absence of the infrared cut the particle multiplicities generated by the shower became infinite and made event generation impossible for pure computational reasons. *Thus, relation (8.31) does not apply for parton showers that are used in MC event generators.*

In Sec. 8.1 we then analyzed the impact of the transverse momentum $p_\perp$ cut Q_0 that is imposed on angular ordered parton showers. In the evolution described by the coherent branching formalism this cut is paraphrased in the conditions (7.57) and (7.63) for the massless and massive quark case, respectively. In the factorization approach it represents, at NLL+$\mathcal{O}(\alpha_s)$, a simple cut on the transverse momentum of (virtual or real) gluons with respect to the thrust axis in the hard, soft and jet functions. In the presence of the cut Q_0 the descriptions provided by angular ordered parton showers, based on the coherent branching formalism and the one provided by the factorized approach are all equivalent, and we were thus able to unambiguously track the field theoretic meaning and interpretation of the dominant contributions *linear* in the $p_\perp$ cut Q_0 through the results obtained in the factorized approach. At this point we emphasize that our conclusions related to the meaning and reinterpretation of QCD parameters in the context of computations with the finite $p_\perp$ cut are made *from the perspective of computations without any infrared cut*, since the canonical way how perturbative calculations and the renormalization procedure are carried out in collider physics applications is in the limit of zero infrared cutoff. Based on our examinations in Secs. 8.1.2, 8.1.3 and 8.1.4 we proved the following two statements *valid in the peak region of the thrust distribution*:

(1) For massless quark production the dominant linear effects of the shower cut Q_0 represent a factorization scale[3] at the interface of perturbative and non-perturbative large angle soft radiation, and changes in Q_0 can be reinterpreted as a modification of the non-perturbative contributions in the resonance peak region. In the coherent branching formalism and in the QCD factorization approach this modification is related to a shift in the non-perturbative model shape function, called "gap" in Ref. [174][4], that can be computed perturbatively. For the thrust distribution in the peak region obtained in QCD factorization this is expressed quantitatively by the relation

$$\frac{\mathrm{d}\sigma}{\mathrm{d}\tau}(\tau, Q, Q_0) = \int\limits_0^{Q\tau} \mathrm{d}\ell \, \frac{\mathrm{d}\hat{\sigma}_s}{\mathrm{d}\tau}\left(\tau - \frac{\ell}{Q}, Q, Q_0\right) S_{\rm mod}(\ell) \tag{8.32}$$

$$= \int\limits_0^{Q\tau} \mathrm{d}\ell \, \frac{\mathrm{d}\hat{\sigma}_s}{\mathrm{d}\tau}\left(\tau - \frac{\ell}{Q}, Q, Q_0 = 0\right) S_{\rm mod}(\ell + \Delta_{\rm soft}(Q_0)) + \mathcal{O}(\alpha_s^2, Q_0^2)$$

where $\mathrm{d}\hat{\sigma}/\mathrm{d}\tau$ stands for the partonic and $\mathrm{d}\sigma/\mathrm{d}\tau$ for the hadron level distribution, $S_{\rm mod}$ is the soft model shape function incorporating the hadronization effects (see Sec. 7.1.3), and having Q_0

---

[3]We adopt the canonical approach of factorization where the factorization scale that separates perturbative and non-perturbative effects is chosen small, but also sufficiently large such that the interface can be described within perturbative QCD.

[4]The name "gap" is motivated by the hadronization gap of the hadron mass spectrum.

in the argument of a function refers to a calculation with the Q_0 cut imposed. Here, $\Delta_{\mathrm{soft}}(Q_0)$ is the Q_0-dependent gap that has the form

$$\Delta_{\mathrm{soft}}(Q_0) = 16\,Q_0\,\frac{\alpha_s(Q_0)C_F}{4\pi} + \mathcal{O}(\alpha_s^2 Q_0)\,. \tag{8.33}$$

The gap function $\Delta_{\mathrm{soft}}(Q_0)$ satisfies the renormalization group equation

$$R\,\frac{\mathrm{d}}{\mathrm{d}R}\,\Delta_{\mathrm{soft}}(R) = 16\,R\,\frac{\alpha_s(R)C_F}{4\pi} + \mathcal{O}(\alpha_s^2 R)\,, \tag{8.34}$$

which, due to the appearance of the scale R on the RHS, describes evolution that is *linear in the renormalization scale* and is called R-evolution [124,125,185,186]. R-evolution differs from usual renormalization group equations such as for the strong coupling, which describe logarithmic evolution. In the context of multi-purpose MC event generators, where an angular ordered parton shower is combined with a hadronization model, the relation means that a change of the shower cut Q_0 needs to be compensated by a retuning of the hadronization model parameters in order to keep physical predictions effectively unchanged. At the level of the hadron level thrust factorization theorem valid in the peak region, which involves the convolution of the partonic distribution $\frac{\mathrm{d}\hat{\sigma}}{\mathrm{d}\tau}$ with the soft model shape function, this feature is quantitatively encoded in the relation

$$\frac{\mathrm{d}\sigma}{\mathrm{d}\tau}(\tau, Q, Q_0) = \int_0^{Q\tau}\mathrm{d}\ell\,\frac{\mathrm{d}\hat{\sigma}}{\mathrm{d}\tau}\Big(\tau - \frac{\ell}{Q}, Q, Q_0'\Big)\,S_{\mathrm{mod}}(\ell + \Delta_{\mathrm{soft}}(Q_0) - \Delta_{\mathrm{soft}}(Q_0'))\,, \tag{8.35}$$

where the difference of the gap functions at the scales Q_0 and Q_0' is

$$\Delta_{\mathrm{soft}}(Q_0) - \Delta_{\mathrm{soft}}(Q_0') = 16\int_{Q_0'}^{Q_0}\mathrm{d}R\,\Big[\frac{\alpha_s(R)C_F}{4\pi} + \mathcal{O}(\alpha_s^2)\Big]\,, \tag{8.36}$$

which is manifestly infrared insensitive. Relation (8.35) states that the dominant linear effects of a change of the shower cut form Q_0' to Q_0 can be compensated, to keep the prediction unchanged, by a modification of the soft model shape function of the form

$$S_{\mathrm{mod}}(\ell) \to \bar{S}_{\mathrm{mod}}(\ell) = S_{\mathrm{mod}}\Big(\ell - \Delta_{\mathrm{soft}}(Q_0) + \Delta_{\mathrm{soft}}(Q_0')\Big)\,. \tag{8.37}$$

We note that relations (8.32) and (8.35) also have the important implication that the size of hadronization corrections for event-shape distributions that are encoded in MC event generators (i.e. the difference between parton and hadron level output) depends the value of the shower cut. A discussion of the feature is, however, beyond the scope of this work. We also remark that in practice a change in the shower cut Q_0 may not be entirely compensated by a modification of the gap function alone because of additional non-linear dependence on the shower cut.

(2) For massive quark production, the dominant linear effects of the shower cut Q_0 on the thrust distribution at the resonance peak can be interpreted, from the perspective of a computation in QCD factorization without infrared cutoff in the pole mass scheme m^{pole}, as a modification of the non-perturbative contribution from large angle soft radiation and a change of the quark mass scheme from m^{pole} to the scale-dependent coherent branching (CB) mass scheme $m^{\mathrm{CB}}(Q_0)$. The modification concerning the non-perturbative effects from large angle soft radiation is universal and the same as for massless quark production. The modification concerning the quark mass scheme originates from the restriction the shower cut Q_0 imposes on the *ultra-collinear radiation*, which corresponds to soft radiation in the massive quark rest frame and which has to be partly considered as an unresolved contribution to the observable top quark state. *The shower cut Q_0*

144

changes the position of the pole of the massive quark propagator to $m^{\mathrm{CB}}(Q_0)$ and also provides the associated scheme change corrections. Starting from a QCD factorization computation of the thrust distribution in the pole mass scheme, this is expressed quantitatively by the relation

$$\frac{\mathrm{d}\sigma}{\mathrm{d}\tau}(\tau, Q, m^{\mathrm{pole}}, Q_0) = \int\limits_0^{Q\tau} \mathrm{d}\ell \, \frac{\mathrm{d}\hat{\sigma}_s}{\mathrm{d}\tau}\left(\tau - \frac{\ell}{Q}, Q, m^{\mathrm{pole}}, Q_0\right) S_{\mathrm{mod}}(\ell) \tag{8.38}$$

$$= \int\limits_0^{Q\tau} \mathrm{d}\ell \, \frac{\mathrm{d}\hat{\sigma}_s}{\mathrm{d}\tau}\left(\tau - \frac{\ell}{Q}, Q, m^{\mathrm{CB}}(Q_0), \delta m^{\mathrm{CB}}(Q_0), Q_0 = 0\right) S_{\mathrm{mod}}(\ell + \Delta_{\mathrm{soft}}(Q_0))$$

$$+ \, \mathcal{O}(\alpha_s^2, Q_0^2)$$

where $\mathrm{d}\hat{\sigma}_s/\mathrm{d}\tau$ stands for the parton level and $\mathrm{d}\sigma/\mathrm{d}\tau$ for the hadron level distribution, S_{mod} is the soft model shape function incorporating the hadronization effects, having Q_0 in the argument of a function refers to a calculation with the Q_0 cut imposed coherently in virtual and real radiation calculations, and the argument $\delta m^{\mathrm{CB}}(Q_0)$ in $\mathrm{d}\hat{\sigma}_s/\mathrm{d}\tau$ indicates the modification of the perturbative series due to the scheme change from m^{pole} to $m^{\mathrm{CB}}(Q_0)$. The soft function gap $\Delta_{\mathrm{soft}}(Q_0)$ is given in Eq. (8.33) and the scale-dependent CB (coherent branching) mass scheme is defined by

$$m^{\mathrm{CB}}(Q_0) = m^{\mathrm{pole}} - \delta m^{\mathrm{CB}}(Q_0) \,, \tag{8.39}$$

with

$$\delta m^{\mathrm{CB}}(Q_0) = \frac{2}{3}\alpha_s(Q_0)\,Q_0 + \mathcal{O}(\alpha_s^2 Q_0) \,. \tag{8.40}$$

The scale-dependent CB mass $m^{\mathrm{CB}}(Q_0)$ is a short-distance mass and thus does not suffer from the $\mathcal{O}(\Lambda_{\mathrm{QCD}})$ renormalon ambiguity inherent to the pole mass m^{pole}. It satisfies the R-evolution equation [124, 125, 186]

$$R\frac{\mathrm{d}}{\mathrm{d}R}m^{\mathrm{CB}}(R) = -\frac{2}{3}R\,\alpha_s(R) + \mathcal{O}(\alpha_s^2 R) \,, \tag{8.41}$$

and evolves linearly in R in the same way as the soft function gap $\Delta_{\mathrm{soft}}(R)$. The difference of the CB masses for the cutoff scales Q_0' and Q_0 can then be expressed by solving the R-evolution equation

$$m^{\mathrm{CB}}(Q_0) - m^{\mathrm{CB}}(Q_0') = -\frac{2}{3}\int\limits_{Q_0'}^{Q_0} \mathrm{d}R\left[\alpha_s(R) + \mathcal{O}(\alpha_s^2)\right] \,, \tag{8.42}$$

which is manifestly infrared insensitive. In the context of angular ordered partons showers with a transverse momentum cut Q_0 the result implies – because the parton shower quark mass parameter is implicitly identified with the pole of the quark propagator – that the parton shower quark mass parameter is the scale-dependent CB mass $m^{\mathrm{CB}}(Q_0)$. In the context of multi-purpose Monte-Carlo event generators, where an angular ordered parton shower is combined with a hadronization model this means that a change of the shower cut from Q_0' to Q_0 needs to be compensated by a retuning of the hadronization model parameters compatible with Eq. (8.37) *and* a change of the value of the CB mass from $m^{\mathrm{CB}}(Q_0')$ to $m^{\mathrm{CB}}(Q_0)$ according to Eq. (8.42) in order to keep physical predictions unchanged. This puts a stringent field theoretic constraint on properties of the hadronization models, since it is forbidden that they modify by themselves the mass scheme through the retuning procedure.

Statements (1) and (2) can be cross checked numerically from the side of MC event generators by the analysis of the thrust peak position τ_{peak} as a function of the shower cut Q_0 *when leaving the hadronization model as well as the numerical value of the generator mass unchanged.* In that case the sizable linear effects in the $p_\perp$ cut Q_0 remain uncompensated and are directly visible in a characteristic dependence of the thrust peak position, $\tau_{\text{peak}}(Q_0)$, on Q_0. The resulting Q_0-dependence of $\tau_{\text{peak}}(Q_0)$ can be directly read off Eqs. (8.32), (8.33), (8.38) and (8.40) giving the relation

$$\tau_{\text{peak}}(Q_0) \;=\; \tau_{\text{peak}}(Q_0') - \frac{1}{Q}\Big[16 - 8\pi\frac{m}{Q}\Big] \int\limits_{Q_0'}^{Q_0} \mathrm{d}R\, \frac{C_F\,\alpha_s(R)}{4\pi}\,, \tag{8.43}$$

where m is the generator mass and Q_0' is some reference cutoff scale. Here it is understood that only cutoff values $Q_0 \ll m$ are employed, and we also remind the reader that the results have been derived in the limit of boosted massive quarks where $m \ll Q$. For the rescaled thrust variable M_τ, see Eq. (7.2), which is suitable for an analysis for top quarks, the analogous relation reads

$$M_{\tau,\,\text{peak}}(Q_0) \;=\; M_{\tau,\,\text{peak}}(Q_0') - \Big[8\frac{Q}{m} - 4\pi\Big] \int\limits_{Q_0'}^{Q_0} \mathrm{d}R\, \frac{C_F\,\alpha_s(R)}{4\pi}\,. \tag{8.44}$$

We note that in relations (8.43) and (8.44) the cutoff dependence coming from the large angle soft and the ultra-collinear radiation have an opposite sign. This is a characteristic property of these two different types of effects, which may be used to differentiate between them in the context of quark mass sensitive observables which are more exclusive concerning the soft radiation. In the next section we confront these relations numerically with parton-level simulations carried out with the HERWIG 7 event generator [151, 152, 175].

Chapter 9

Event generation with Herwig 7

In this section we confront the conceptual and theoretical considerations summarized in Sec. 8.2 and in particular our predictions for the shower cutoff dependence of the peak position of the thrust distributions given in Eqs. (8.43) and (8.44) and our main conclusion that the presence of a shower cutoff Q_0 implies that the top quark mass parameter used in an angular ordered parton shower is the scale-dependent CB mass given in Eq.(8.39) with numerical simulations for e^+e^- collisions using the Herwig 7 event generator [151, 152, 175] in version 7.1.2. The angular ordered parton shower algorithm of Herwig 7 implements the coherent branching algorithm outlined in Secs. 7.2.1 and 7.2.2, for massless and massive quarks, respectively. Since the treatment of the top quark decay goes beyond the coherent branching formalism outlined in these sections, we provide some more details of event generation in Herwig 7 for top quarks in Sec. 9.1. In Sec. 9.2 we explain a number of special setting we use for our Herwig 7 simulations such that they are precisely in accordance to the coherent branching formalism. In Sec. 9.3, using simulations results obtained with Herwig 7, we reconfirm some approximations used in our analytic calculations in Secs. 7.3.1, 7.3.2 and 8.1.2 within the coherent branching formalism, and the insensitivity of thrust to the cut governing the parton shower evolution of the top decay products. Our predictions for the shower cutoff dependence of the thrust peak position for the massless quark and top quark case are then confronted with Herwig 7 in Secs. 9.4 and 9.5, respectively. Here we demonstrate that our conceptual predictions for the shower cut dependence of the peak position of the thrust distributions given in Eqs. (8.43) and (8.44) are indeed reproduced by the Herwig 7 simulations. In Sec. 9.6 we address the universality of our findings for thrust by discussing the reconstructed (b-jet and W boson) top quark invariant mass $m_{b_j W}$ and the endpoint region of the b-jet and lepton invariant mass $m_{b_j \ell}$. Finally, in Sec. 9.7 we comment on the (ir)relevance of NLO-matched simulations with respect to the cutoff dependence of the thrust distribution in the resonance region and the kinematic mass sensitivity of the reconstructed observables $m_{b_j W}$ and $m_{b_j \ell}$.

9.1 Event generation for top quark production

Within Herwig 7 events with top quarks account for the top quark decay in a factorized narrow width approach: The top quarks are considered stable at the stage of their production, with momenta p^μ which satisfy the on-shell condition $p^2 = m_t^2$, where m_t is the Herwig top mass parameter. In the default setting for the `LEP-Matchbox.in` simulation setup, no smearing with any Breit-Wigner-type distribution is applied, so that off-shell effects coming from the finite top quark width are absent. This default setting is mainly rooted in considerations related to NLO matched predictions, where the smearing disrupts the cancellation of virtual and real infrared cancellations. The angular ordered parton shower then attaches radiation to the production process terminated by the $p_\perp$ cutoff Q_0, including radiation off the top quarks (and possibly other colored partons involved in the hard

scattering). After the kinematic reconstruction following the production stage parton shower, the final state top quarks have definite momenta p'^μ which satisfy the on-shell condition $p'^2 = m_t^2$, and the progenitor top quarks, which initiated the showering, have acquired a virtual mass, see the discussion in Sec. 7.2.3. At this point the top quarks decay, where we for simplicity only consider leptonic decays of the W bosons coming from the top decays assuming perfect neutrino identification. This is not a restriction for the thrust distributions we examine, but simplifies their numerical analyses. The partons originating from the top decays, $t \to b\, W^+$ and $\bar{t} \to \bar{b}\, W^-$, then radiate according to the decay parton shower algorithm from Refs. [160] and [187] which is terminated by the $p_\perp$ cutoff $Q_{0,b}$. The radiation from the decay stage parton shower exactly preserves the 4-momenta of the decaying top and antitop quarks, respectively, and hence their mass shell condition, in a separate kinematic reconstruction procedure. Within this procedure the b-quark shower progenitor that initiates the b-jet is allowed to acquire a virtuality according to the decay stage parton shower.

In the conceptual considerations of the preceding sections we were discussing the effects of the production stage parton shower cutoff Q_0. The thrust variable is by construction independent of details of the top decay and therefore also insensitive to the value of the decay state parton shower cutoff $Q_{0,b}$. In HERWIG 7 the values of Q_0 and $Q_{0,b}$ can be chosen independently, which allows us to explicitly check the insensitivity of thrust to variations of $Q_{0,b}$. This check is carried out in Sec. 9.3.

9.2 Settings for MC simulations

To compare the predictions obtained from analytic examinations of the preceding sections with the HERWIG predictions, which are based on the previously described algorithms and methods, we use a number of special settings. These settings are used to eliminate default features in HERWIG 7 which go beyond the coherent branching formalism as described in Sec. 7.2 or interfere with the Q_0 dependence of the *parton level predictions* we aim to analyze. We emphasize that the purpose of these settings is to allow for a direct comparison of HERWIG simulations with our analytic results *at the parton level* in a conceptually clean and controlled setup. So these special settings may serve as the starting point of further examinations, also accounting for the effects and properties of hadronization models, where the impact of default settings used in HERWIG (or other MC event generators) can be studied in more detail, or for upcoming releases. We emphasize, however, that these special HERWIG 7 settings should be taken with some care since they are not appropriate to carry out full hadron level simulations.

As already explained in Sec. 7.2.3 we set the (constituent) masses of all quarks and the mass of the gluons that have emerged after the parton showers have terminated to very small values to effectively remove their effects in the parton level results.[1] Zero constituent quark and gluon masses are required to allow a comparison with our analytic QCD calculations; they are, however, not compatible with the default HERWIG 7 cluster hadronization model. Furthermore, in our HERWIG simulations we do not include any QED radiation or any matrix element corrections, except in our discussion of NLO matching carried out in Sec. 9.7. As already discussed in Sec. 7.2.3 we also choose the `CutOff` option for the kinematic reconstruction as this does not alter the correspondence to the underlying coherent branching algorithm as described in in Secs. 7.2.1 and 7.2.2. Finally we note that most analyses we have developed are based on Rivet [188], except those focusing on particle multiplicities for which an entirely in-house analysis code is used. In App. K we give the complete set of input file changes required to reproduce the parton level results within our special settings, both for the massless and massive case.

---

[1]We note that in HERWIG all light quarks (i.e. up, down and strange quarks) and gluons are treated as exactly massless during the shower evolution and that constituent quark mass and gluon mass conditions are only imposed kinematically for the partons that emerge after shower terminations. The constituent quark and gluon masses have to be considered as part of the hadronization model.
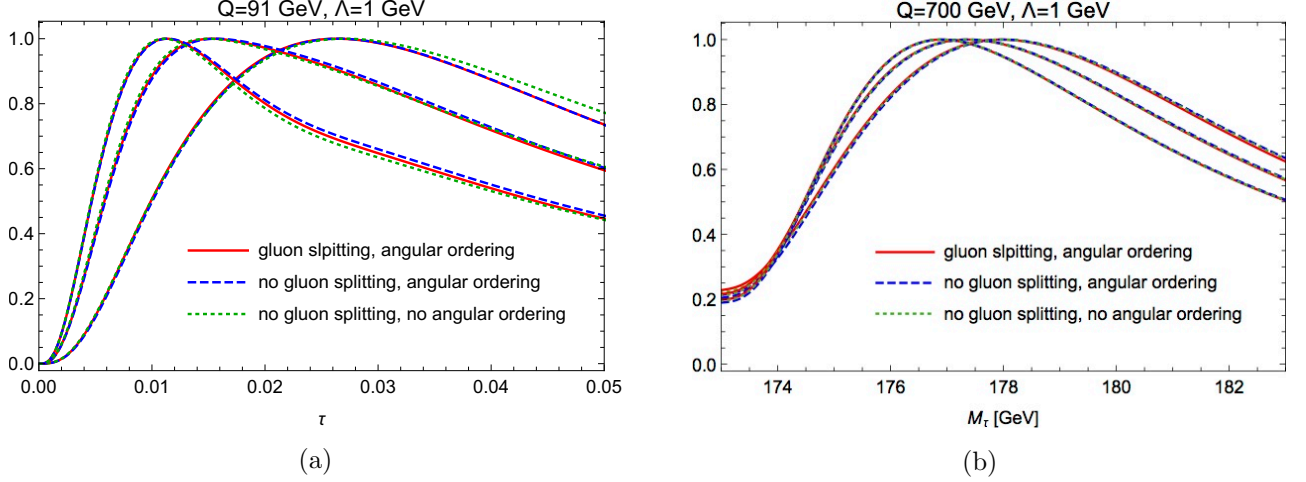
Figure 9.1:   Thrust at the parton level in the peak region generated by HERWIG 7 for (a) massless quarks at c.m. energy $Q = 91$ GeV and (b) top quarks with mass $m_t = 173$ GeV at $Q = 700$ GeV. The HERWIG 7 parton level results are smeared with a soft model shape function with smearing parameter $\Lambda = 1$ GeV, see Sec. 7.1.3. Displayed are simulation results for shower cuts $Q_0 = 1$ GeV (right set of curves), $Q_0 = 1.5$ GeV (middle set of curves) and $Q_0 = 2$ GeV (left set of curves) and with gluon splitting and angular ordering both turned on (solid red curves), with gluon splitting turned off, but angular ordering turned on (dashed blue curves) and with gluon splitting and angular ordering both turned off (dotted green curves).

9.3   Monte Carlo tests of approximations for analytic thrust calculations

In our analytic calculations of the parton level massless and massive quark jet mass distributions at NLL order in Secs. 7.3.1, 7.3.2 and 8.1.2 within the coherent branching formalism we used two approximations which were crucial to allow for an analytic all order exponentiation of the computation, see e.g. Eqs. (7.70) to (7.72). In the integral equations for the jet mass distributions shown in Eqs. (7.51) and (7.61) these approximations involve (i) neglecting the parton branching of the gluon (i.e. switching off the $g \to gg$ and $g \to q\bar{q}$ branchings) and (ii) using the $z \to 1$ limit in the parts which are slowly varying in the soft limit. These approximations were already discussed (and used for analytic calculations) in the seminal coherent branching papers for massless quarks, see e.g. Ref. [163, 167]. The former approximation is – *for the thrust distribution in the peak region* – related to the fact that due to angular ordering the showered gluons originating from the progenitor quarks can themselves not radiate to pick up any significant virtuality. The latter approximation implies – *again for the thrust distribution in the peak region* – that once gluon splitting is turned off, also strict angular ordering can be dropped from the calculations. For simplicity reasons we therefore refer to the latter approximation as "angular ordering switched off" in the following discussion.

Adopting the settings discussed in Sec. 9.2, these two approximations can be explicitly verified numerically using HERWIG 7 to generate the parton level thrust distribution for massless and massive quark production. In Fig. 9.1a the parton level thrust distribution, defined in Eq. (7.1), obtained from HERWIG 7 for massless quarks at c.m. energy $Q = 91$ GeV is displayed for shower cuts $Q_0 = 1$ GeV (right set of curves), $Q_0 = 1.5$ GeV (middle set of curves) and $Q_0 = 2$ GeV (left set of curves) with gluon splitting and angular ordering both turned on (solid red curves), with gluon splitting turned off, but angular ordering turned on (dashed blue curves) and with gluon splitting and angular ordering both turned off (dotted green curves). All curves are normalized such that at their respective maximum they evaluate to unity, which is particularly suitable to discuss the peak region. We also remind the reader that all curves are produced by convolution of the HERWIG 7 parton level results with
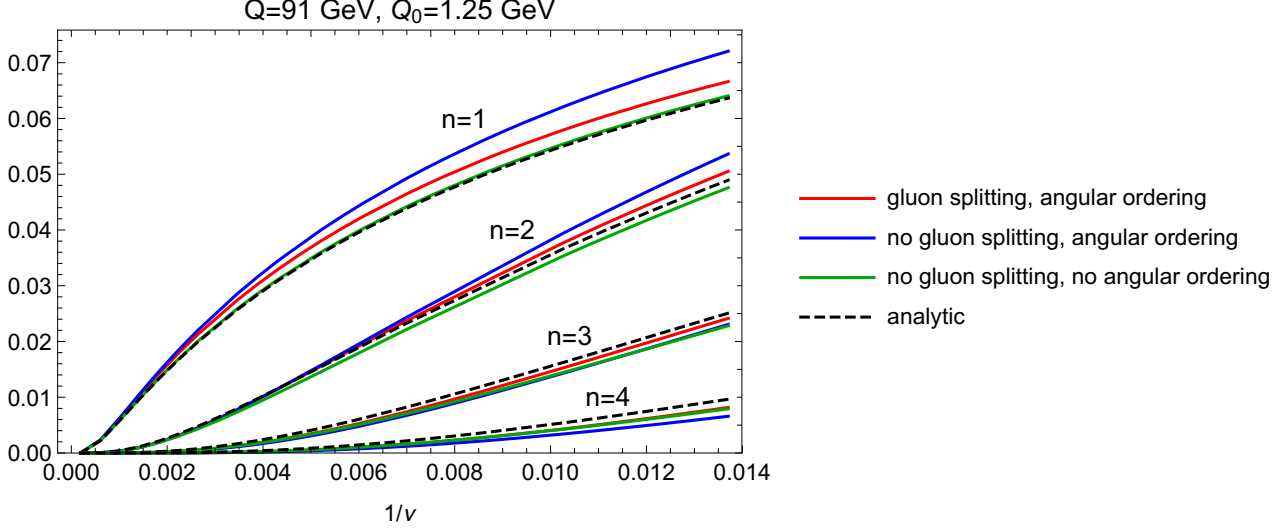
Figure 9.2: Laplace space parton level thrust distribution over $1/\nu$ in the peak region for $Q = 91$ GeV and $Q_0 = 1.25$ GeV shown for the final state parton multiplicities $n = 1, 2, 3, 4$. Displayed are the analytic results (dashed black curves) and simulation results with gluon splitting and angular ordering both turned on (red curves), with gluon splitting turned off, but angular ordering turned on (blue curves) and with gluon splitting and angular ordering both turned off (green curves).

the soft model shape function of Eq. (7.36) for $\Lambda_{\mathrm{m}} = \Lambda$ with $\Lambda = 1$ GeV according to Eq. (7.3). As discussed in Sec. 7.1.3, this is essential to obtain a smooth distribution in the peak region that can be interpreted properly. In Fig. 9.1b the parton level rescaled thrust distribution, as defined in Eq. (7.2), obtained from HERWIG 7 for top quarks at c.m. energy $Q = 700$ GeV and with the generator mass set to $m_t = 173$ GeV is displayed in the same way and for the same choices for the shower cut Q_0 and concerning gluon splitting and angular ordering. For the top quark case we employed a convolution over the same shape function according to Eq. (7.23) with $\Lambda_{\mathrm{m}} = \Lambda + 4 m_t \Gamma_t / Q$ and $\Gamma_t = 1.5$ GeV. For the top quark case the smearing parameter is larger than for the massless quarks in order to simulate the additional smearing effects of the top quark width. Note, however, that this does not represent a systematic treatment of width effects for the top quark.

From the results in Figs. 9.1a and 9.1b we clearly see that the impact of the gluon splitting is very small in the peak region and, furthermore, that once gluon splitting is turned off the numerical effects of angular ordering are very small as well. For the rescaled thrust distribution in the case of top production these three settings lead to variations in the peak position of less than $\Delta\tau_{\mathrm{peak}} \sim 10^{-3}$ in the massless case and less than $\Delta M_{\tau,\mathrm{peak}} \sim 100$ MeV in the massive case for Q_0 between 1 and 2 GeV. In any case, these variation are considerably smaller than the variations caused by changes in the shower cut Q_0 which we focus on in our subsequent examinations. While the validity of the two approximations concerning gluon splitting and angular ordering for thrust for massless quarks has already been known since Ref. [163], our analysis shows that they are also applicable for the massive quark case, which is new. We note that in our analysis of the dependence of the thrust peak position on the shower cut Q_0 in Secs. 9.4 and 9.5, we consider HERWIG 7 simulations using all three options: (i) full simulation, (i) simulations with gluon branchings switched off and (iii) simulations with gluon branchings and angular ordering both switched off. The differences of the HERWIG 7 results obtained from these three options should be viewed as an illustration of possible subleading effects even though they should not be overinterpreted as a systematic error estimate.

In the context of these results an obvious question to ask is whether the suppression of effects coming from the gluon branching in the thrust peak region is only a cumulative effect visible in the distribution upon accounting for the sum of all emissions, or whether the suppression takes place literally at the
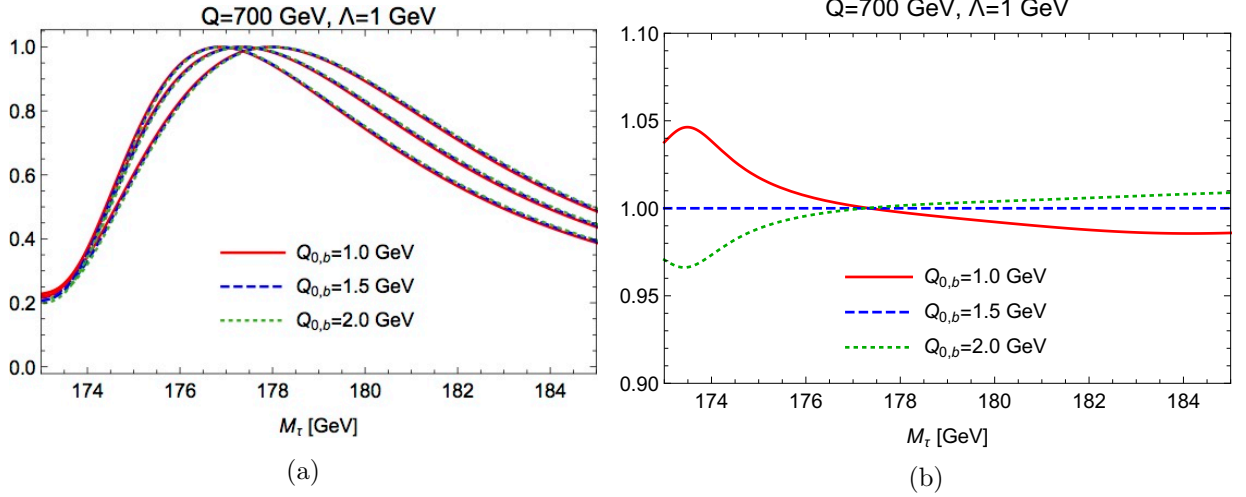
Figure 9.3: Parton level rescaled thrust for top quarks with $m_t = 173$ GeV and $Q = 700$ GeV in the peak region generated by HERWIG 7 and smeared with a soft model shape function with smearing parameter $\Lambda = 1$ GeV, see Sec. 7.1.3. Displayed are simulation results for production stage shower cuts $Q_0 = 1$ GeV (right set of curves), $Q_0 = 1.5$ GeV (middle set of curves) and $Q_0 = 2$ GeV (left set of curves) and decay stage shower cuts $Q_{0,b} = 1$ GeV (solid red curves), $Q_{0,b} = 1.5$ GeV (dashed blue curves) and $Q_{0,b} = 2$ GeV (dotted green curves).

level of the individual parton multiplicities. To answer this question we can analyze the parton level massless quark thrust distribution for a fixed number of final state parton multiplicity, where we define the multiplicity n as the total number of partons emitted from the progenitor quark-antiquark pair. Interestingly, for the Laplace space parton level distribution (7.12) for massless quarks the contribution for a given multiplicity n can be determined analytically, in the approximation that gluon splitting and angular ordering are switched off, simply from Eq. (7.84) by taking the n-th term in the Taylor expansion of the exponential function. In Fig. 9.2 the Laplace space parton level thrust distribution for massless quarks at $Q = 91$ GeV with shower cut $Q_0 = 1.25$ GeV is shown as a function of $1/\nu$ in the peak region $1/\nu \sim \tau_{\text{peak}} \ll 1$ for multiplicities $n = 1, 2, 3, 4$. Shown are the HERWIG 7 full simulation results with gluon splitting and angular ordering both turned on (solid red curves), with gluon splitting turned off, but angular ordering turned on (solid blue curves) and with gluon splitting and angular ordering both turned off (solid green curves) and the analytic result from Eq. (7.84), which is calculated in the approximation with gluon splitting and angular ordering both turned off (dashed black curves). The curves do not include any smearing effects from the shape function because the Laplace integral of Eq. (7.12) already provides a sufficient amount of smearing. We see that HERWIG 7 and the analytic results in the various approximations agree very well. The outcome shows that that the approximations we used in our analytic calculations are also appropriate at the level of fixed parton multiplicities and may therefore have a more general validity.

At this point we emphasize that the examination of the effects of gluon splitting and angular ordering we have just carried out solely serves as a cross check for the approximations we used in our analytic calculation for thrust using the coherent branching formalism in Sec. 7.3 and 8.1.2 and that these approximation are *not* a viable option for general phenomenological studies. These approximations do also not *in any way* constitute conceptual guidelines for predictions based on QCD factorization (or SCET). In addition, the consistent use of these approximations for thrust involves that the effects angular ordering are only small once the gluon branchings are *already* switched off. Indeed, the converse, a simulation with gluon branchings but strict angular ordering switched off leads to a dramatic increase of parton radiation and multiplicities and to physically meaningless outcomes.

As already elaborated in Sec. 9.1, for event generation involving top quarks HERWIG 7 uses a factorized

treatment of production and decay stage parton shower evolution. As we argued in Sec. 7.1 the thrust variable is by construction independent of details of the top decay and should therefore be insensitive to the value of the decay state parton shower cutoff $Q_{0,b}$. In Fig. 9.3a the parton level distribution of the rescaled thrust M_τ in the peak region obtained from HERWIG 7 is shown for the c.m. energy $Q = 700$ GeV and generator mass $m_t = 173$ GeV with production stage shower cuts $Q_0 = 1$ GeV (right set of curves), $Q_0 = 1.5$ GeV (middle set of curves) and $Q_0 = 2$ GeV (left set of curves), and decay state shower cuts of $Q_{0,b} = 1$ GeV (solid red curves), $Q_{0,b} = 1.5$ GeV (dashed blue curves) and $Q_{0,b} = 2$ GeV (dotted green curves). In Fig 9.3b a ratio plot for the curves for the three choices of $Q_{0,b}$ is shown for $Q_0 = 1$ GeV. For all curves a shape function smearing with $\Lambda = 1$ GeV has been included following the prescription given above. The results confirm that the dependence of the thrust distribution on the decay stage shower cut $Q_{0,b}$ is extremely weak and in particular significantly smaller than the corresponding dependence on the production stage shower cut Q_0. In the resonance region variations due to changes of $Q_{0,b}$ are at the percent level and negligible as far as the peak position is concerned. The results confirm that the thrust variable is ideal to study the production stage shower cutoff dependence and essentially insensitive to differential details of the top quark decay. For our studies of the shower cutoff dependence of the thrust peak position in Secs. 9.4 and 9.5 we set $Q_{0,b} = Q_0$, which is the default HERWIG 7 setting.

9.4   Thrust peak position for massless quarks

In this section we confront our analytic parton level prediction for the Q_0 dependence of the thrust peak position for massless quarks,

$$\tau_{\text{peak}}(Q_0) \,=\, \tau_{\text{peak}}(Q_0') - \frac{16}{Q} \int\limits_{Q_0'}^{Q_0} \mathrm{d}R \, \frac{C_F \, \alpha_s(R)}{4\pi} \,, \tag{9.1}$$

with parton level simulations in HERWIG 7 using the specific settings discussed in Sec. 9.2. To determine the distribution for a given c.m. energy Q and shower cut Q_0 we generated 10^9 events. The resulting binned distribution (with bin size $\Delta\tau = 2 \times 10^{-4}$) was numerically convoluted using a discretized version of Eq. (7.3) with the soft model shape function S_{mod} given in Eq. (7.36) for a given smearing parameter Λ_{m}. The peak position was then determined from fitting a quadratic function to the bin values in the peak region with heights that differ from the maximum by at most 1 per mille. This leads to statistical uncertainties in the peak position well below 10^{-3} which is an order of magnitude smaller than the size of the Q_0 variations we obtain in our analysis. The results can thus be considered exact for all practical purposes and we refrain from quoting any statistical uncertainties in the results we obtain in the simulations.

In Fig. 9.4 the peak position τ_{peak} obtained from HERWIG 7 is shown as a function of the shower cut Q_0 for $Q = 91$ GeV (upper panels) and $Q = 300$ GeV (lower panels) for the smearing parameter $\Lambda_{\text{m}} = 1$ GeV (left panels) and $\Lambda_{\text{m}} = 3$ GeV (right panels). The (center of the) colored squares show the corresponding results from the full simulation, i.e. with gluon splitting and angular ordering both turned on (red squares), with gluon splitting turned off, but angular ordering turned on (blue squares) and with gluon splitting and angular ordering both turned off (green squares). The solid blue line represents the analytic prediction of Eq. (9.1) with $Q_0' = 1.25$ GeV as the reference peak position taken form the HERWIG 7 simulation and using the strong coupling employed by the HERWIG 7 parton shower to calculate τ_{peak} for Q_0 different from Q_0'. We have shown the results for shower cut values in the range between $(0.5 \text{ GeV}) < Q_0 < (2.0 \text{ GeV})$ even though the perturbative treatment is expected to break down for scales below 1 GeV. Nevertheless, HERWIG 7 can carry out simulations for values of Q_0 even below 0.5 GeV since for scales below 1 GeV the strong coupling used in its parton shower is frozen to the value at 1 GeV. The choice of Q_0 in the simulations is in practice limited from below
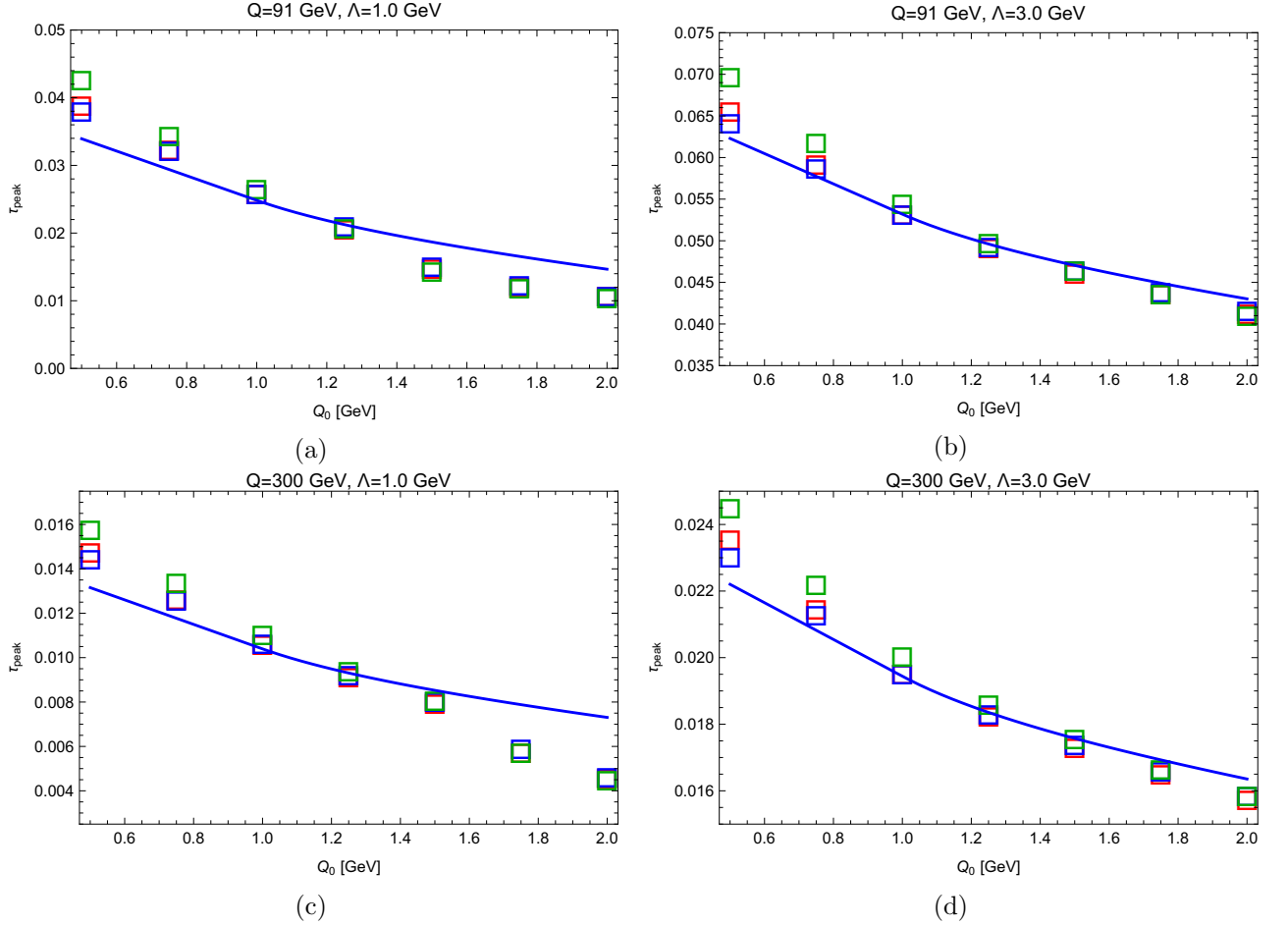
Figure 9.4: Peak position τ_{peak} at the parton level obtained from Herwig 7 as a function of of the shower cut Q_0 and including a smearing with $\Lambda = 1$ GeV (left panels) and $\Lambda = 3$ GeV (right panels) for massless quarks and $Q = 91$ GeV (upper panels) and $Q = 300$ GeV (lower panels). Displayed are the results from the full simulation (red squares), with gluon splitting turned off, but angular ordering turned on (blue squares) and with gluon splitting and angular ordering both turned off (green squares). The blue solid line is the analytic prediction of Eq. (9.1) taking the Herwig 7 result for $Q_0' = 1.25$ GeV as the reference.
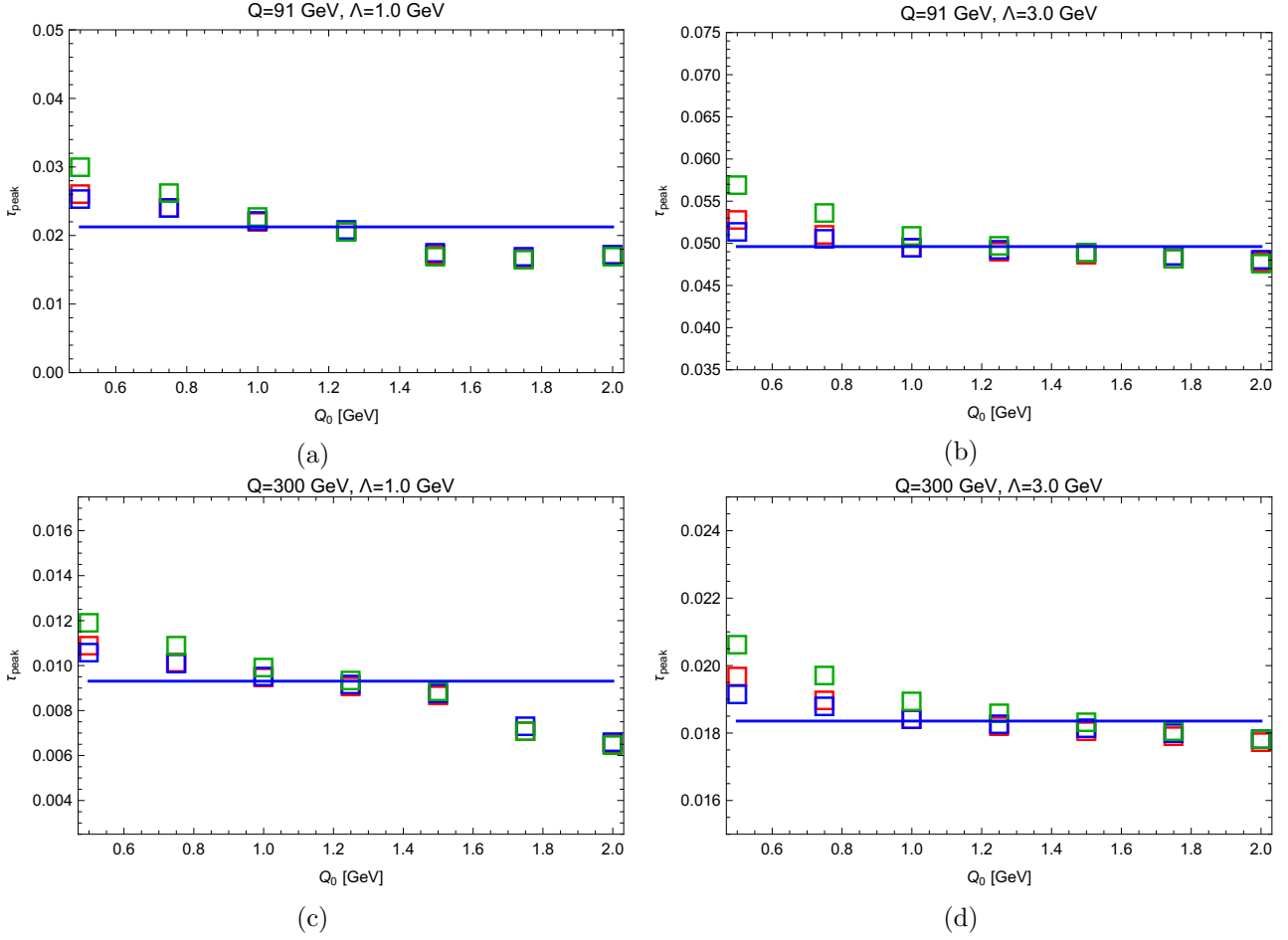
Figure 9.5: Peak position τ_{peak} at the parton level obtained from HERWIG 7 for the parameters used in Fig. 9.4, but including the soft function gap calculated analytically to achieve results that eliminate the linear dependence on the shower cut Q_0 taking $Q_0' = 1.25$ GeV as the reference. The blue solid line represents the corresponding analytic prediction.

only by computation time since the parton mulplicities strongly increase for decreasing shower cut. For theoretical considerations, however, only shower cut values of 1 GeV and larger can be considered seriously, because Q_0 conceptually represents a factorization scale and should be located well within the regime of perturbation theory. In fact, indications of a breakdown of the perturbative description for $Q_0 < 1$ GeV are visible in Figs. 9.4 (and also in Figs. 9.5 and the corresponding results for top quarks in the following subsection) as the increased spread in the HERWIG 7 results arising from the different choices concerning gluon branching and angular ordering.

Overall we see quite good agreement between the HERWIG 7 simulations and the analytic prediction for τ_{peak} for $\Lambda_{\text{m}} = 1$ GeV and excellent agreement for $\Lambda_{\text{m}} = 3$ GeV. While $\Lambda_{\text{m}} = 1$ GeV corresponds to the actual size of hadronization effects compatible with experimental data, the choice $\Lambda_{\text{m}} = 3$ GeV is motivated by the possible size of additional experimental resolution effects. That we find a much better agreement for larger smearing scale is related to the fact that the evolution equation (9.1) only accounts for the dominant linear dependence on Q_0 which was in our analytic calculations in Secs. 8.1.2, 8.1.3 and 8.1.4 derived by employing the multipole expansion for the contributions of the unreleased radiation, i.e. the radiation originating from below the shower cut. This expansion is formally an expansion in Q_0/Λ_{m}, and we see from the agreement between simulation and analytic prediction in Fig. 9.4 that this expansion works already well for $Q_0 \sim \Lambda_{\text{m}}$ and even better for $\Lambda_{\text{m}} > Q_0$. Since in realistic simulations and actual experimental measurements there are additional resolution effects that always lead to a smearing scale that is effectively larger than 1 GeV, we can conclude that

the linear dependence on the shower cut Q_0 expressed by Eq. (9.1) represents the dominant effects in all cases and that effects quadratic in Q_0 or of even higher power are small in practice.

At this point it is also illustrative to explicitly show the quality of relation (8.35) which states that the observed peak position can be rendered shower cut independent, if the gap of the soft model function used in the convolution is modified as described in Eq. (8.37). In Fig. 9.5 the thrust peak positions obtained from the HERWIG 7 simulations already shown in Fig. 9.4 are displayed once again as a function of Q_0, however, with the corresponding modification of the soft function gap for the reference shower cut value $Q_0' = 1.25$ GeV. As expected, we see that the shower cut dependence is substantially reduced for the smearing scale $\Lambda_\mathrm{m} = 1$ GeV and almost vanishes for the smearing scale $\Lambda_\mathrm{m} = 3$ GeV in the region $Q_0 \geq 1$ GeV, i.e. where perturbation theory can be employed.

9.5   Thrust peak position for top quarks

In this section we finally confront our analytic prediction for the Q_0 dependence of the rescaled thrust peak position for top quarks

$$M_{\tau,\,\mathrm{peak}}(Q_0) \;=\; M_{\tau,\,\mathrm{peak}}(Q_0') - \Big[8\frac{Q}{m_t} - 4\pi\Big] \int\limits_{Q_0'}^{Q_0} \mathrm{d}R \, \frac{C_F \, \alpha_s(R)}{4\pi}\,. \qquad (9.2)$$

with simulations in HERWIG 7. We again used the specific settings discussed in Sec. 9.2 and generated 10^9 events for a given c.m. energy Q and shower cut Q_0. For the convolution with the soft model shape function S_mod given in Eq. (7.36) we employed the discretized version of Eq. (7.23) with $\Lambda_\mathrm{m} = \Lambda + 4m_t\Gamma_t/Q$ with $\Gamma_t = 1.5$ GeV for the soft function smearing parameter. It effectively accounts for the additional smearing caused by the top quark width. Since the resonance region in τ is substantially more narrow compared to the massless case we used a bin size that corresponds to $\Delta\tau = 8 \times 10^{-6}$ and used the same method to determine the peak position as for the massless quark case.

In Fig. 9.6 the peak position $M_{\tau,\,\mathrm{peak}}$ obtained from HERWIG 7 with the top quark generator mass $m_t = 173$ GeV is shown as a function of the shower cut Q_0 for $Q = 700$ GeV (upper panel) and $Q = 1$ TeV (lower panel) for the smearing parameter $\Lambda = 1$ GeV (left column) and $\Lambda = 3$ GeV (right column). The (center of the) colored squares show the corresponding results from the full simulation, i.e. with gluon splitting and angular ordering both turned on (red squares), with gluon splitting turned off, but angular ordering turned on (blue squares) and with gluon splitting and angular ordering both turned off (green squares). The solid blue line represents the analytic prediction of Eq. (9.2) with $Q_0' = 1.25$ GeV as the reference peak position taken form the HERWIG 7 simulation and using the strong coupling employed by HERWIG 7 parton shower to calculate $M_{\tau,\,\mathrm{peak}}$ for Q_0 different from Q_0'. The dashed blue line represents the analytic prediction of Eq. (9.2), but only accounting for the large angle soft radiation contributions which are multiplied with the Q/m_t factor, in order to visualize the size of the Q_0 dependence coming from the ultra-collinear radiation that affects the interpretation of the mass scheme alone. As in the massless quark case we have shown the results for shower cut values in the range between $(0.5 \text{ GeV}) < Q_0 < (2.0 \text{ GeV})$ and remind the reader that the results for Q_0 below 1 GeV are only shown for illustration, as already explained in Sec. 9.4.

We observe that the agreement between the HERWIG 7 simulations and the analytic prediction for $M_{\tau,\,\mathrm{peak}}$ is very good for $\Lambda_\mathrm{m} = 1$ GeV as well as for $\Lambda_\mathrm{m} = 3$ GeV. This shows that for the top quark case, where the width provides an additional irreducible smearing effect, the linear dependence on the shower cut Q_0, which we have determined in our analytic calculations, fully captures the complete Q_0 dependence and that contributions proportional to higher powers of Q_0 are negligible for all practical purposes.
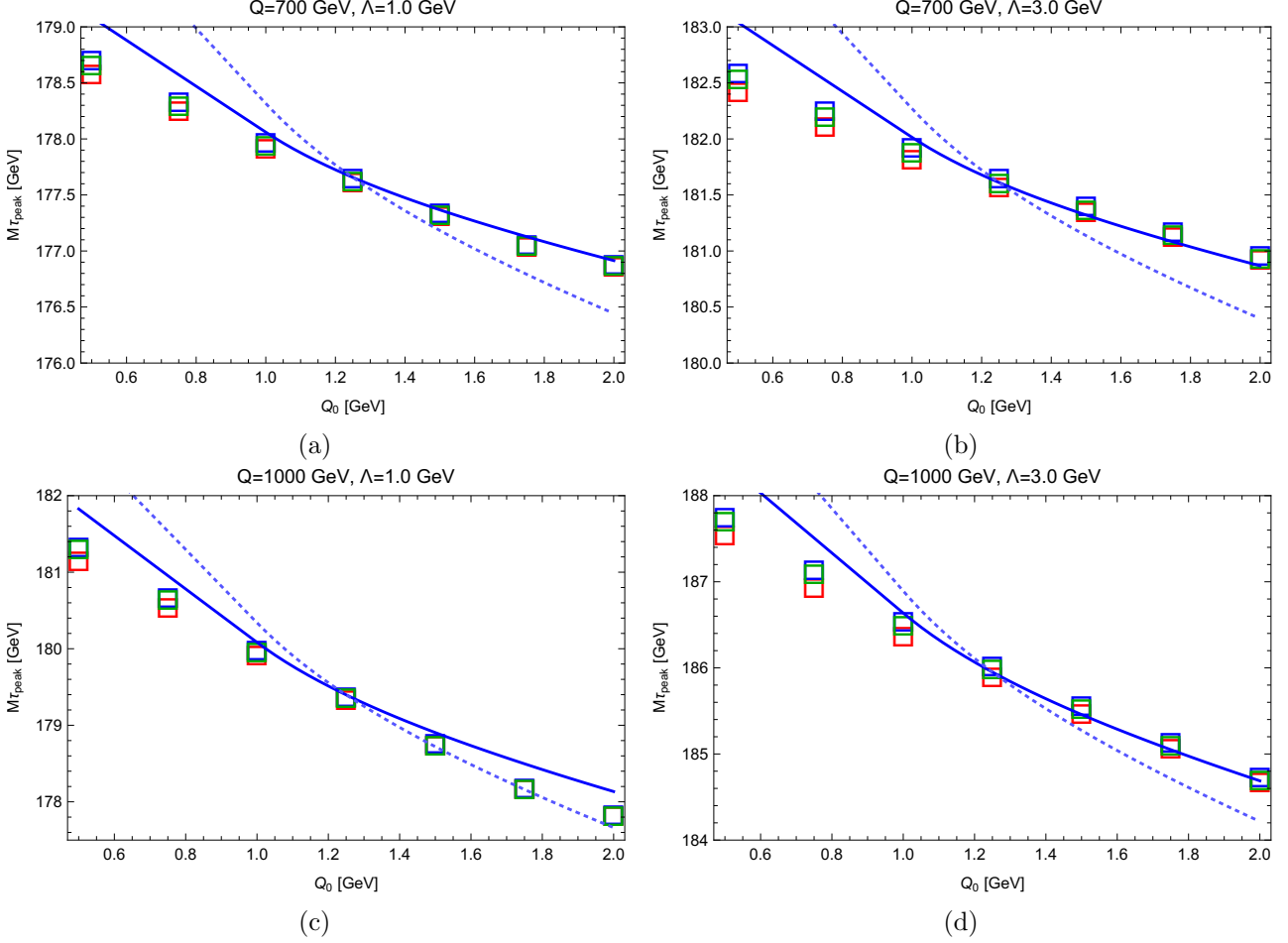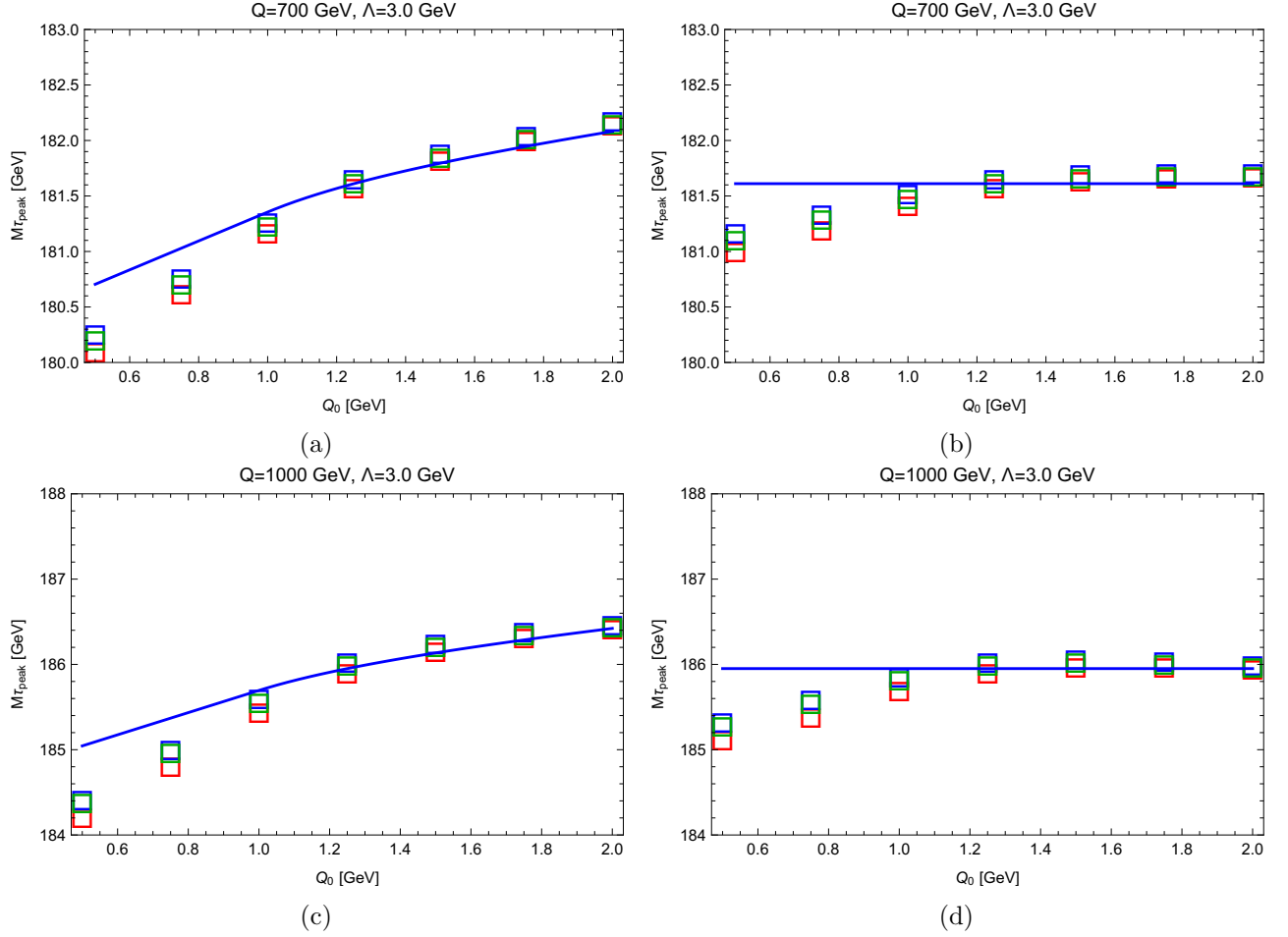
Figure 9.6: Peak position $M_{\tau,\text{peak}}$ at the parton level obtained from HERWIG 7 for the top quark generator mass $m_t = 173$ GeV as a function of the shower cut Q_0 for $Q = 700$ GeV (upper panels) and $Q = 1$ TeV (lower panels) for smearing $\Lambda = 1$ GeV (left panels) and $\Lambda = 3$ GeV (right panels). Displayed are the results from the full simulation (red squares), with gluon splitting turned off, but angular ordering turned on (blue squares) and with gluon splitting and angular ordering both turned off (green squares). The blue solid line is the analytic prediction of Eq. (9.2) taking the HERWIG 7 result for $Q_0' = 1.25$ GeV as the reference. The dashed blue line is the analytic prediction of Eq. (9.2), but only accounting for the large angle soft radiation contributions which are multiplied with the Q/m_t factor.

Figure 9.7: Peak position $M_{\tau,\text{peak}}$ at the parton level obtained from HERWIG 7 for the top quark generator mass $m_t = 173$ GeV as a function of the shower cut Q_0 for $Q = 700$ GeV (upper panels) and $Q = 1$ TeV (lower panels) for smearing with $\Lambda = 3$ GeV. Left panels: In addition to the results shown in Fig. 9.6 we have included the soft function gap calculated analytically to remove the shower cut dependence due to the large angle soft radiation. Right panels: In addition to the results of the left panels we have set the generator mass to $m^{\text{CB}}(Q_0)$ such that the peak position becomes independent of the shower cut Q_0. The blue solid line represents the corresponding analytic prediction for the remaining cutoff scale dependence. For all results we used $Q'_0 = 1.25$ GeV as the reference scale.

It is now illustrative to explicitly demonstrate that the observed peak position can be rendered shower cut independent, if - taking $Q'_0 = 1.25$ GeV as the reference - the gap of the soft model function used in the convolution is modified according to Eqs. (8.36) and (8.37) and if the generator mass m_t is modified by

$$m_t \to m_t + m_t^{\text{CB}}(Q_0) - m_t^{\text{CB}}(Q'_0) \tag{9.3}$$

according to Eq. (8.42). In Fig. 9.7 the rescaled thrust peak positions obtained from the HERWIG 7 simulations for $Q = 700$ GeV (upper panel) and $Q = 1$ TeV (lower panel) are displayed once again as a function of Q_0 for $\Lambda = 3$ GeV. In the left panels we have in addition to the corresponding curves shown in Fig. 9.6 included the corresponding modification of the soft function gap for the reference shower cut value $Q'_0 = 1.25$ GeV. This removes the shower cut dependence coming from the large angle soft radiation such that the remaining Q_0 dependence explicitly illustrates the shower cut dependence of the generator mass alone.[2] Compared to the results shown in Fig. 9.6 we see that the slope in Q_0

---

[2]The rescaled thrust variable M_τ defined in Eq. (7.2) is normalized such that the Q_0 slope shown in the left panels of Fig. 9.7 is minus twice the one of the generator mass.

has an opposite sign which means that the Q_0 dependent CB mass scheme that has to be employed to keep the physical prediction unchanged is decreasing with Q_0 as expressed by the renormalization group equation (8.41). In the right panels we have then also modified, in addition to the figures in the left column, the generator mass according to Eq. (9.3) and taking $m^{\mathrm{CB}}(Q_0' = 1.25\,\mathrm{GeV}) = 173\,\mathrm{GeV}$ as the reference top quark mass. We see that once both modifications are implemented, the shower cut dependence has essentially disappeared.

In Ref. [189] our numerical checks on the cutoff dependence of the thrust peak position were repeated for a Nagy-Soper dipole shower with $p_\perp$ as evolution variable [190,191] (similar to Herwig's dipole shower [177,192] that is also implemented in the event generator as a second option besides its default angular orderd shower) and compared to our analytic results in Eqs. (9.1) and (9.2). They found a very good agreement with our results for the peak shift as a function of the cutoff also for that type of parton shower, which indicates that our results may be more universal and not restricted only to angular ordered parton showers. However, a clear theoretical understanding of how to correctly interpret that cutoff dependence in terms of consistently implementing a short-distance mass scheme, as summarized in Sec. 8.2 for the coherent branching formalism, is missing for the dipole shower, because it is hardly accessible analytically and the connection to the QCD factorization theorem at NLL, as established in our work here for coherent branching, has not been made.

It is interesting to also analyze to which extent the shower cut dependent modifications of the soft function gap and the generator mass we have just discussed for the thrust peak position also holds for the whole distribution function in the resonance region. This is shown in Figs. 9.8 were the rescaled thrust distributions in the peak region are shown for $Q = 700\,\mathrm{GeV}$ for $Q_0 = 1\,\mathrm{GeV}$ (dotted green curves), $Q_0 = 1.5\,\mathrm{GeV}$ (solid red curves) and $Q_0 = 2\,\mathrm{GeV}$ (dashed blue curves) obtained from the full simulation. The left panels show the distributions in the peak region for fixed generators mass $m_t = 173\,\mathrm{GeV}$ with smearing parameter $\Lambda = 1\,\mathrm{GeV}$ (upper left panel) and $\Lambda = 3\,\mathrm{GeV}$ (lower left panel). The corresponding right panels show, using $Q_0' = 1.5\,\mathrm{GeV}$ as the reference scale, the distributions including the Q_0 dependent soft function gap according to Eq (8.37) and the Q_0 dependent generator mass according to Eq. (9.3) to keep the peak position cutoff independent. We see that the resonance distribution tends to be narrower for increasing cutoff Q_0, but that this effect is weaker for a larger smearing. This behavior can be explained from the fact that for increasing cutoff Q_0 the no-branching probability (which describes production stage multiplicity $n = 0$ events and contributes to the coefficient of the tree-level δ-function located at the partonic threshold) is becoming bigger and, correspondingly, the weight of events with branching (which correspond to production stage multiplicities $n > 0$ and lead to jet masses above the partonic threshold) is becoming smaller. For a larger smearing this width effects is washed out and therefore less pronounced for $\Lambda = 3\,\mathrm{GeV}$. Thus depending on the size of the experimental resolution the effects that a variation of the shower cut Q_0 has on the whole peak distribution may be more complicated than a simple modification of the soft function gap and the generator mass. Since the contributions from ultra-collinear radiation in this context are m_t/Q-suppressed, see Eq. (9.2), these width effects mostly originate from large angle soft radiation. One can therefore conclude that these effects may be properly taken into account during the retuning procedure which has to be carried out upon a change of the shower cut Q_0 in MC event generators used for experimental analyses, and which is substantially more involved than an a simple modification of the soft function gap.

9.6 Reconstructed observables and universality

After our analysis of the Q_0 shower cut dependence of the MC generator top mass for angular ordered parton showers using the thrust distribution in the resonance region there is one obvious question to be asked: Is our main conclusion concerning the equivalence the MC generator top quark mass and the shower cut dependent CB mass defined in Eq. (8.39) only valid for thrust (or very similar event shape
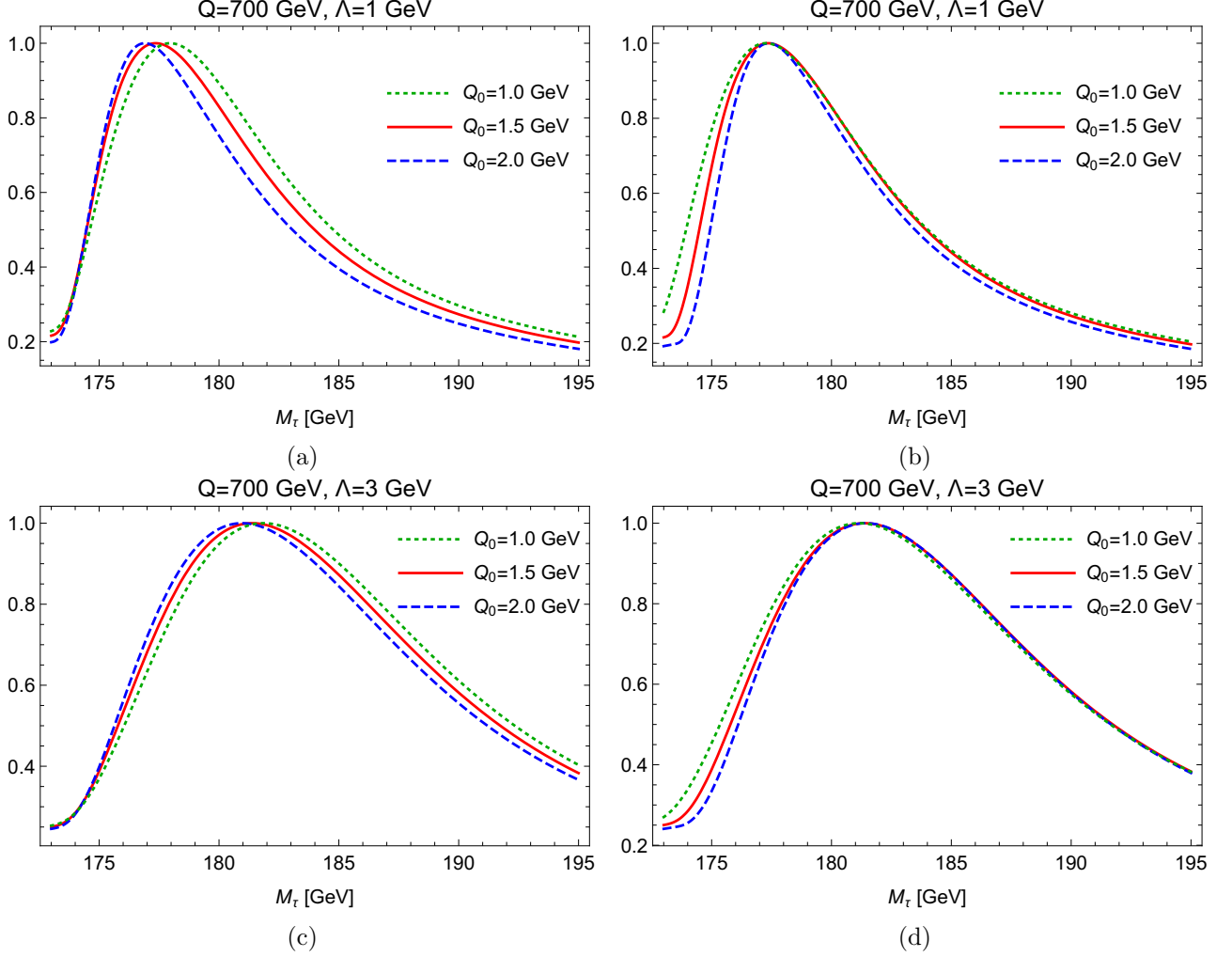
Figure 9.8: Parton level rescaled thrust distribution in the peak region obtained from HERWIG 7 full simulations for $Q = 700$ GeV and smearing with $\Lambda = 1$ GeV (upper panels) and $\Lambda = 3$ GeV (lower panels) for shower cut values $Q_0 = 1$ GeV (dotted green curves), $Q_0 = 1.5$ GeV (solid red curves) and $Q_0 = 2$ GeV (dashed blue curves). Left panels: Simulations with generator input mass $m_t = 173$ GeV and using the same soft model shape function for all shower cut values. Right panels: Same distributions, but using a Q_0-dependent soft function gap to eliminate the shower cut dependence due to large angle soft radiation and using $m^{\text{CB}}(Q_0 = 1.0) = 173.22$ GeV (green), $m^{\text{CB}}(Q_0 = 1.5) = 173$ GeV (red) and $m^{\text{CB}}(Q_0 = 2) = 172.86$ GeV (blue) as the generator masses, according to Eq. (8.42), to render the peak location independent of the shower cut Q_0.

type observables), or is it universal? Clearly, examinations at the same level of depth as we carried out for thrust, where we employed analytic calculations within the coherent branching formalism and the QCD factorization approach together with numerical MC simulations, will be difficult for most other observables with strong kinematic quark mass dependence – most notably because hadron level first principles and factorized predictions (which would allow directly for conclusions at the field theoretic level) are not available for them. The question of universality is also made difficult by the fact that the shower cut dependence not only affects the meaning of the generator mass for heavy quarks (or potentially other QCD parameters), but also modifies the description of non-perturbative effects through its effects on large angle soft radiation (or other types of long-range gluon effects), so that the issue may not be resolved completely restricting the considerations only to partonic cross sections.

At this point one may also have to define general criteria to prove universality systematically. Although we hope to address this issue in forthcoming work, at this time such a systematic and universal approach is lacking. However – *if universality applies* – the dependence of MC parton level predictions on the shower cut Q_0, which was one of the main instrument of our thrust examinations, should be visible in a predictable, simple and universal way also for other observables and furthermore allow for non-trivial consistency checks. While consistency concerning the Q_0 dependence among thrust and other kinematic observables represents *only a necessary condition* for claiming universality, it still provides some evidence that universality indeed applies. Furthermore, computing the shower cut Q_0 dependence analytically for general observables and carrying out the corresponding MC simulations as a cross check is a relatively straightforward and easy task and may even be testable in consistency checks confronting MC generators with experimental data or in the context of pseudo-data analyses. In this section we therefore examine exemplarily two completely different observables with very strong kinematic top mass dependence and which are based on a jet clustering procedure acting on the full set of partons after production and decay stage parton showers have terminated. In this work we restrict our examinations to a numerical analysis of the shower cut dependence of these observables, and we demonstrate that it can be easily predicted and interpreted. Interestingly, we find that the results are compatible with our examinations for the thrust distribution. A more coherent test of consistency in the context of pseudo-data analyses which specifically addresses the shower cut dependence of the generator mass shall be addressed elsewhere.

The first observable is the b-jet and lepton invariant mass $m_{b_j\ell}$ and the second the reconstructed b-jet and W invariant mass m_{b_jW}. Both types of observables have been studied intensely in the context of top quark mass measurements at the LHC. The kinematic sensitivity of $m_{b_j\ell}$ to the top quark mass m_t arises from the upper endpoint of its distribution, which is, for stable W bosons and at tree-level, located at $(m_t^2 - m_W^2)^{1/2}$ neglecting the mass effects of the b-jet. But also the bulk of the $m_{b_j\ell}$ distribution has kinematic top mass sensitivity because the region where $m_{b_j\ell}$ is maximal depends on the boost of the W boson in the top rest frame which depends kinematically on the top quark mass. The direct kinematic sensitivity of m_{b_jW} to the top mass arises simply from the kinematic location of the resonance which is tied to m_t in a way very similar to thrust, see Eqs. (7.1). In the following we refer to the top mass sentivities of the endpoint location for $m_{b_j\ell}$ and the peak location for m_{b_jW} simply as 'the kinematic top mass dependence' of these two variables. Typical results for the $m_{b_j\ell}$ and m_{b_jW} distributions using the b-jet clustering described below and generated with HERWIG 7 are displayed in Fig. 9.9 for $Q = 700$ GeV and top quark masses 172, 173 and 174 GeV. Overall, we see that m_{b_jW} has a somewhat stronger top mass dependence than $m_{b_j\ell}$.

We consider the production of boosted top quarks at $Q = 700$ GeV in e^+e^- annihilation and use HERWIG 7.1.2 with the same settings as for the thrust analyses discussed in the previous sections (see Sec. 9.2). For simplicity we again generate only leptonically decaying W bosons and assume perfect neutrino identification. Furthermore we neglect any combinatorial background, i.e. we assume perfect b-jet lepton pairing and perfectly reconstructed top or antitop quarks. While these simplications are not fully realistic, they are, however, fully adequate for our examination of the shower cut Q_0
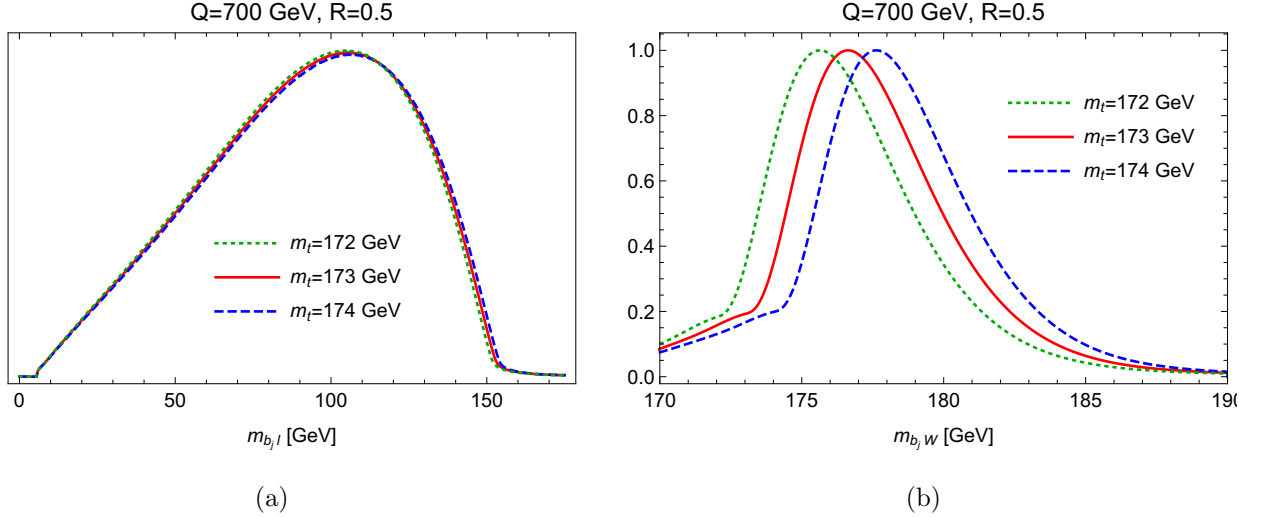
Figure 9.9: The $m_{b_j\ell}$ (left panel) and m_{b_jW} distributions (right panel) generated by HERWIG 7 for top masses between $m_t = 172$ (dotted green), 173 (solid red) $m_t = 174$ GeV (dashed blue) for $Q = 700$ GeV, jet radius $R = 0.5$ and Cambridge-Aachen-type b-jet clustering.

dependence. For the b-jet clustering we use the FastJet package [193] and employ the generalized k_t algorithm for e^+e^- collisions in the inclusive mode with the inter-particle and inclusive jet distance measures

$$d_{ij} = \min(E_i^{2p}, E_j^{2p}) \frac{1 - \cos\theta_{ij}}{1 - \cos R},$$

(9.4)

$$d_{iB} = E_i^{2p},$$

where E_i refers to energy, R is the jet radius[3], and θ_{ij} is the relative angle between two momenta. The exponent $p = 1$ corresponds to the k_t-type generalized clustering algorithm, $p = 0$ to the Cambridge-Aachen, and $p = -1$ to the anti-k_t-type variant, and we consider all three types of algorithms in our analysis. In Fig. 9.9a and 9.9b we show the $m_{b_j\ell}$ distribution and the m_{b_jW} distribution in the peak region, respectively, generated by HERWIG 7 *at the parton level* with jet radius $R = 0.5$ and Cambridge-Aachen-type jet clustering for generator masses $m_t = 172$ GeV (green dashed curves), $m_t = 173$ GeV (solid red curves) and $m_t = 174$ GeV (dashed blue curves). For m_{b_jW} we have smeared the distribution according to Eq. (7.23) using smearing parameter $\Lambda = 1$ GeV as described in Sec. 9.5. Since the $m_{b_j\ell}$ distribution is already smooth by itself at the parton level we did not account for any additional smearing. For both distributions we see that the top mass dependence is essentially linear and particularly strong in the endpoint region for $m_{b_j\ell}$ and in the peak region for m_{b_jW}.

The interesting conceptual aspect of the reconstructed observables $m_{b_j\ell}$ and m_{b_jW} is that, due to the b-jet clustering, they are more exclusive than the hemisphere masses entering the thrust variable of Eq. (7.1). In particular, $m_{b_j\ell}$ and m_{b_jW} depend on the b-jet radius R. For large $R \sim \pi/2$ we can expect their shower cut dependence to be very similar to the one for thrust since the ultra-collinear as well as major portions of large angle soft radiation are clustered into the b-jet. On the other hand, due to the boosted top kinematics which confines the top decay products as well as the ultra-collinear radiation inside a cone with angle $\sim m_t/Q$ with respect to the top momentum direction, the clustering should always retain most of the ultra-collinear radiation that is soft in the top rest frame and thus inherently tied to the physical top quark state. Thus for small $R \sim m_t/Q$ we can expect

---

[3]We note that we use the variable R also for the R-evolution equations (8.34) and (8.41) and the corresponding relations in Eqs. (8.36), (8.42)-(8.44), (9.1), (9.2), (9.5) and (9.6). Since jet radius and R-evolution are different concepts, the meaning of R should be clear from the context.
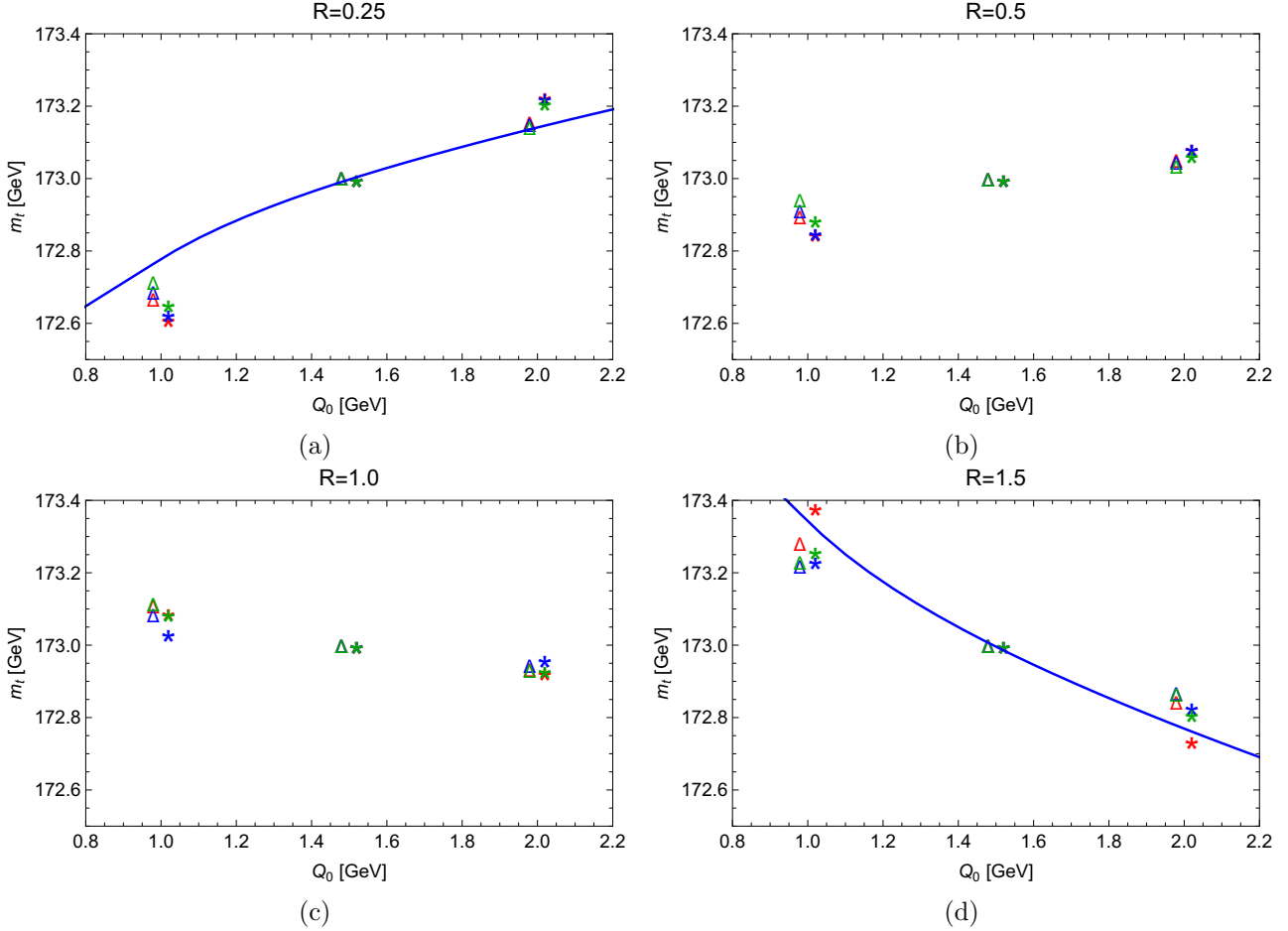
Figure 9.10: Fitted top quark mass as a function of the shower cut $Q_0 = Q_{0,b}$ for $Q = 700$ GeV obtained from the $m_{b_j\ell}$ endpoint (stars) and the $m_{b_j W}$ resonance region (triangles) using the k_t-type-type algorithm (green), the Cambridge-Aachen-type algorithm (blue) and the anti-k_t-type algorithm (red) for b-jet clustering. Displayed are the results for b-jet radii $R = 0.25$, 0.5, 1.0 and 1.5. The solid blue line in the lower right panel corresponds to Eq. (9.5) and the one in the upper left panel corresponds to Eq. (9.6) using $Q_0' = 1.5$ as the reference scale.

that the majority of the ultra-collinear radiation is still clustered into the b-jet while the majority of the large-angle soft radiation is removed. As a consequence we can expect that the shower cut dependence coming from the large-angle soft radiation is reduced when R is lowered, while the one from ultra-collinear radiation is kept.

To quantify the dependence of $m_{b_j\ell}$ and $m_{b_j W}$ generated from HERWIG 7 on the shower cut we use the following procedure: For a given jet radius R and clustering algorithm (as well as matching scheme for the analysis in Sec. 9.7) we take the results for $Q_0 = Q_{0,b} = 1.5$ GeV as the default and generate $m_{b_j\ell}$ and $m_{b_j W}$ distributions for different generator masses m_t in the range between 172 and 174 GeV, which we subsequently use to fit the top quark mass from the distributions generated for $m_t = 173$ GeV but with different choices of Q_0 or $Q_{0,b}$. The shower cut dependence of the parts of the $m_{b_j\ell}$ and $m_{b_j W}$ distributions used for the fits are then directly transferred into deviations of the fitted top masses with respect to the default mass $m_t = 173$ GeV (for $Q_0 = Q_{0,b} = 1.5$ GeV), which can then be compared with our theoretical expectations. Due to the high number of events we use, statistical uncertainties are negligible and therefore not specified in the following. We emphasize that the shower cut dependence of the fitted top mass we obtain in this analysis is a representation of the shower cut dependence of $m_{b_j\ell}$ and $m_{b_j W}$ themselves and not equivalent to the shower cut dependence of the generator mass.

In Figs. 9.10 the dependence of the fitted top mass on the shower cut is shown, where production stage and decay stage shower cuts are identified, using for $Q_{0,b} = Q_0$ the values 1.0, 1.5 and 2.0 GeV for jet radii $R = 0.25$ (upper left panel), $R = 0.5$ (upper right panel), $R = 1.0$ (lower left panel) and $R = 1.5$ (lower right panel). The top masses obtained from the $m_{b_j \ell}$ endpoint region are shown as colored stars and have been obtained from fits in the $m_{b_j \ell}$ interval $[150, 155]$ GeV. The top masses obtained from the $m_{b_j W}$ resonance region are shown as colored triangles and have been obtained from fits using the highest 20% of the distribution around to the peak. To allow for an easier visual identification we have slightly displaced the stars and the triangles horizontally. We have carried out the analyses for all three jet clustering algorithm where we use green color for the k_t-type algorithm ($p = 1$), blue color for the Cambridge-Aachen-type algorithm ($p = 0$) and red color for the anti-k_t-type algorithm ($p = -1$). We see that for large hemisphere-type b-jet cones the fitted top mass decreases with the shower cut. This means that the mass of the reconstructed top quark state, to which $m_{b_j \ell}$ and $m_{b_j W}$ are kinematically sensitive (and which for hemisphere-type b-jets includes the effects of large angle soft radiation), decreases when Q_0 is increased. So the behavior indeed follows the one of thrust we have observed in Sec. 9.5. Analytically, the expected Q_0 dependence for ideal hemisphere-type b-jets has the form

$$m_{t,\,\text{fit}}^{R=\pi/2}(Q_0) \;=\; m_{t,\,\text{fit}}^{R=\pi/2}(Q_0') - \left[4\frac{Q}{m_t} - 2\pi \right] \int\limits_{Q_0'}^{Q_0} \mathrm{d}R \, \frac{C_F \, \alpha_s(R)}{4\pi} \tag{9.5}$$

and is ploted in the lower right panel of Fig. 9.10 as the blue solid line using $Q_0' = 1.5$ GeV as the reference scale. The RHS of Eq. (9.5) is a factor two smaller than the one for the rescaled thrust $M_{\tau,\,\text{peak}}$ in Eq. (8.44) since the reconstructed top mass is linear in the top mass while the rescaled thrust variable $M_{\tau,\,\text{peak}}$ is quadratic in the top mass, see Eqs. (7.1) and (7.2). We see that the expected behavior agrees very well with the results obtained from the fit. The actual fit results for all clustering algorithms except for anti-k_t tend to have a slightly smaller slope than Eq. (9.5), which is mainly due to the fact that even for $R = \pi/2$ the b-jets are typically not full hemisphere jets because they are in general not exactly back-to-back and compete with each other in the clustering process. For decreasing jet radius R, on the other hand, we see that the slope in Q_0 of the fitted top mass increases continuously and becomes positive for $R \lesssim 0.5$. This confirms the expectation that the shower cut dependence originating from large-angle soft radiation (which is the contribution proportional to Q/m in Eq. (9.5)) becomes suppressed when R is reduced, while the shower cut-dependence associated to the ultra-collinear radiation is kept. For visualization we have plotted in upper left panel Fig. 9.10 the relation

$$m_{t,\,\text{fit}}^{R\sim m_t/Q}(Q_0) \;=\; m_{t,\,\text{fit}}^{R\sim m_t/Q}(Q_0') + 2\pi \int\limits_{Q_0'}^{Q_0} \mathrm{d}R \, \frac{C_F \, \alpha_s(R)}{4\pi} \tag{9.6}$$

with $Q_0' = 1.5$ GeV as the reference scale as the blue solid line. This is just Eq. (9.5) but with the Q/m_t term dropped, that originates from large angle soft radiation. Again we see good agreement between the expected shower cut dependence and the actual fit results. It is also conspicuous that the shower cut dependence of the fitted top quark masses we obtain from $m_{b_j \ell}$ and $m_{b_j W}$ for the different jet radii and jet algorithms are essentially equivalent and do not exhibit any systematic difference. This analysis thus supports universality concerning the equivalence of the MC generator top quark mass and the shower cut dependent CB mass defined in Eq. (8.39).

However, in the absence of a systematic factorized analytic approach to the kinematic top mass dependence of the $m_{b_j \ell}$ and $m_{b_j W}$ this universality cannot be strictly proven because, in contrast to thrust, $m_{b_j \ell}$ and $m_{b_j W}$ are affected substantially by the MC modelling and the dynamics of the final state and, in particular, by the choice of the decay stage shower cut $Q_{0,b}$. This makes the conceptual background to be examined more involved. In particular, for our *parton-level studies* a strict proof
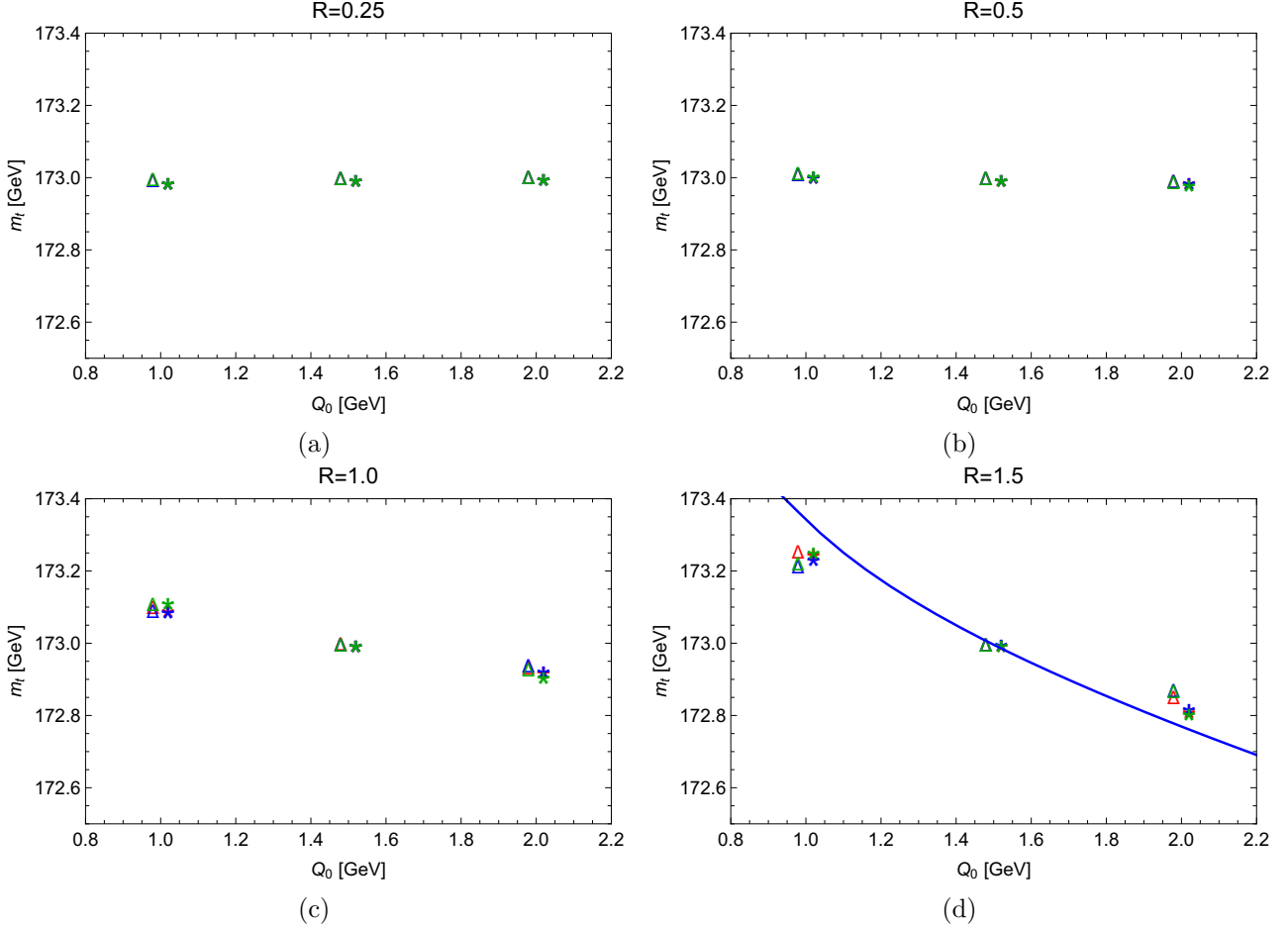
Figure 9.11: Fitted top quark mass as a function of the production stage shower cut Q_0 with decay stage shower cut fixed to $Q_{0,b} = 1.5$ GeV for $Q = 700$ GeV obtained from the $m_{b_j\ell}$ endpoint (stars) and the m_{b_jW} resonance region (triangles) using the k_t-type algorithm (green), the Cambridge-Aachen algorithm (blue) and the anti-k_t-type algorithm (red) for b-jet clustering. Displayed are the results for b-jet radii $R = 0.25$, 0.5, 1.0 and 1.5. The solid blue line in the lower right panel corresponds to Eq. (9.5) using $Q'_0 = 1.5$ as the reference scale.

would require that we could analytically track the role played by the decay stage shower cut $Q_{0,b}$ for the interpretation of the generator top quark mass in a systematic manner.

To visualize the relevance of the decay stage shower cut $Q_{0,b}$ for small b-jet radii we show in Figs. 9.11 again the dependence of the fitted top mass on the production stage shower cut Q_0 for the same cases displayed in Figs. 9.10, but using a fixed decay stage shower cut $Q_{0,b} = 1.5$ GeV. We see that for a large hemisphere-type b-jet radius $R = 1.5$ the results are equivalent to the corresponding ones for $Q_{0,b} = Q_0$ shown in lower right panel of Figs. 9.10. For decreasing jet radii we see that the dependence of the fitted top mass on Q_0 decreases continuously remains essentially flat for $R < 0.5$ in contrast to Figs. 9.10 where a positive slope in Q_0 was emerging. This shows that for small jet radii the shower cut dependence of the kinematic top mass sensitivity of $m_{b_j\ell}$ and m_{b_jW} arises from the decay stage shower cut $Q_{0,b}$. Even though it appears hard to believe that the good agreement we observed for small b-jet radii and $Q_{0,b} = Q_0$ between the fit results and the naive expectations is purely accidental, the case of small jet radii is strictly speaking not covered by the conceptual considerations we have carried out for thrust. A first approach to calculate the dependence on the production stage shower cut Q_0 as a function of the jet radius R is given in appendix H, where we find a cancellation to leading order in R for small jet radii between the effects of ultra-collinear and the remaining soft radiation that was not accounted for in Eq. (9.6), which could explain why the dependence on the production stage shower cut esentially vanishes for small $R \sim m_t/Q$.

To conclude the question of universality, at the present stage, we can say that the shower cut dependence we observe for the kinematic top mass dependence of $m_{b_j\ell}$ and m_{b_jW} is compatible with the one we have proven for thrust and thus supports universality. This is quite encouraging and motivates further systematic and more general consistency studies that may be carried out with MC simulations and relatively simple analytical computations alone. However, a strict conceptual proof would also involve a precise quantification of the role of the decay stage shower cut $Q_{0,b}$ (and maybe other issues relevant for exclusive observables with strong kinematic top sensitivity), preferably in the context of a factorized approach where the types of radiation relevant for the interpretation of the top quark mass can be ambiguously separated from other types of radiation and discussed at the field theoretic level. This strongly motivates the development of factorized predictions for reconstructed and exclusive observables such as $m_{b_j\ell}$ and m_{b_jW}.

At this point we would also like to remind the reader that all our examinations above have been carried out for boosted top quarks. The direct reconstruction top mass measurements at the LHC are, on the other hand, based on top quarks with p_T values in the range of 50 to 100 GeV, which corresponds predominantly to unboosted top quarks. We stress that for unboosted top quarks a classification of the radiation modes relevant for a systematic discussion of the meaning of the generator mass is currently lacking and that, in particular, the concepts of large angle soft and ultra-collinear radiation do not apply. Therefore, none of the above considerations or argumentations are applicable for the reconstructed observables $m_{b_j\ell}$ and m_{b_jW} for unboosted top quarks.

9.7   Impact of NLO matching

A crucial precondition of our examinations on the shower cut dependence was that NLL precise angular ordered parton showers, based on the coherent branching formalism described in Secs. 7.2.1 and 7.2.2, are already NLO precise *as far as the dominant linear shower cut dependence of the thrust peak position is concerned*, see Sec. 7.1.4. This means in turn that the $\mathcal{O}(\alpha_s)$ QCD corrections added to simulations in NLO matched MC setups (see [146, 192, 194–196] for initial development concerning multi-purpose event generators as well as a general review), should show very small or even negligible effects in the numerical studies that we have carried out in Secs. 9.3, 9.4 and 9.5. It is the purpose of this section to demonstrate this explicitly by comparing HERWIG 7 simulations with and without NLO matching.
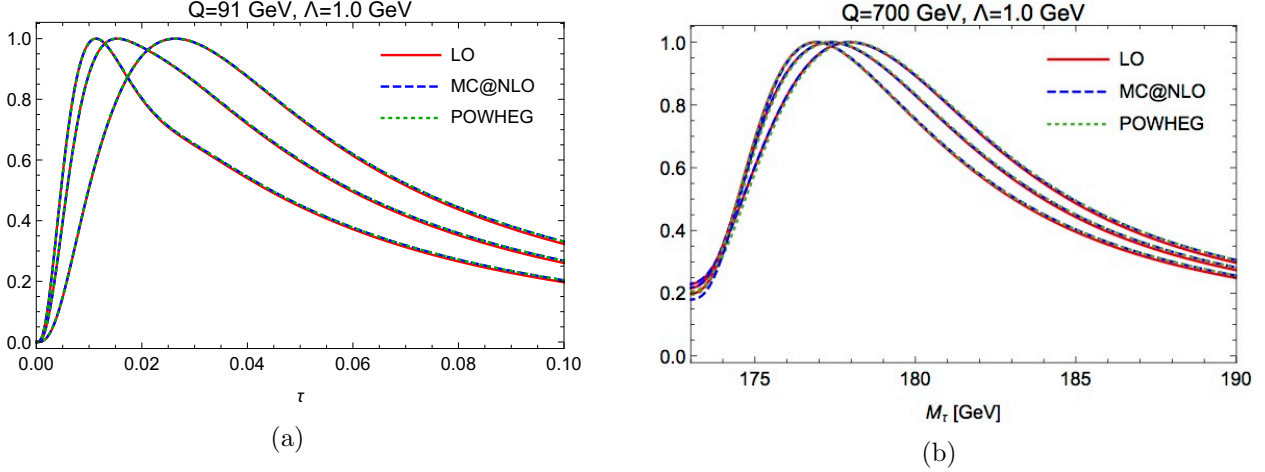
Figure 9.12: Thrust at the parton level in the peak region generated with HERWIG 7 full simulations for (a) massless quarks at c.m. energy $Q = 91$ GeV and (b) top quarks with mass $m_t = 173$ GeV at $Q = 700$ GeV. The parton level results are smeared with a soft model shape function with smearing parameter $\Lambda = 1$ GeV, see Sec. 7.1.3. Displayed are simulation results for shower cuts $Q_0 = 1.0$ GeV (right set of curves), $Q_0 = 1.5$ GeV (middle set of curves) and $Q_0 = 2$ GeV (left set of curves) at LO (i.e. without any NLO matching, solid red curves), with MC@NLO-type matching (dashed blue curves) and POWHEG-type matching (dotted green curves).

For a theoretical discussion of the effect of NLO matching on the cutoff dependence we refer to Sec. 7.7 of Ref. [3]. The bottom line is that in NLO matched partons showers the contributions leading to a linear cutoff dependence are still present and do not modify the principle precision with respect to the unmatched NLL parton showers in the resonance region.

Let us now compare numerical results obtained with HERWIG 7 without NLO matching – referred to as 'LO' ('leading-order') for the rest of this section – (which is the setup we have used for our simulation studies in Secs. 9.3, 9.4, 9.5 and 9.6) and with NLO matching using the MC@NLO-type [194] and the POWHEG-type [146] matching within the HERWIG 7 event generator's MATCHBOX module [192]. In Figs. 9.12 we show the thrust distribution for massless quark production at $Q = 91$ GeV (left panel) and the rescaled thrust distribution for top quark production with $m_t = 173$ GeV at $Q = 700$ GeV (right panel) for $Q_0 = Q_{0,b} = 1.0$ GeV (right set of curves), 1.5 GeV (middle set of curves) and 2.0 GeV (left set of curves) at LO (solid red), with MC@NLO-type matching (dashed blue curves) and with POWHEG-type matching (dotted green curves). All curves are normalized to unity at the peak position. We hardly see any difference between the LO and NLO matched simulations in the resonance regions. Visible effects arise only in the tails away from the resonances, which can be understood from the fact that the hardest gluon emission, which is improved to full NLO precision by the matching procedure, only obtains sizable NLO corrections away from the singular resonance region. In the resonance region, however, the NLL splitting function approach already provides a fully adequate description and the genuine non-singular NLO corrections are very small. For the cases shown in Figs. 9.12 the peak shifts due to NLO effects are typically less than $\Delta\tau_{\text{peak}} \sim 10^{-4}$ in the massless case and less than $\Delta M_{\tau,\text{peak}} \sim 100$ MeV in the massive case which is considerably smaller than the effects of the shower cut dependence we consider. We have checked that this property is generic and valid for all energies and shower cut values we have examined in our earlier studies. The results confirm that NLO matched parton shower simulations do not add more precision in the thrust resonance region and, in particular, do not modify the shower cut dependence of the simulations without NLO matching.

At this point it is also instructive to examine the impact of NLO matching to the reconstructed observables $m_{b_j\ell}$ and m_{b_jW}, which we have already examined at LO in Sec. 9.6. Within HERWIG 7,
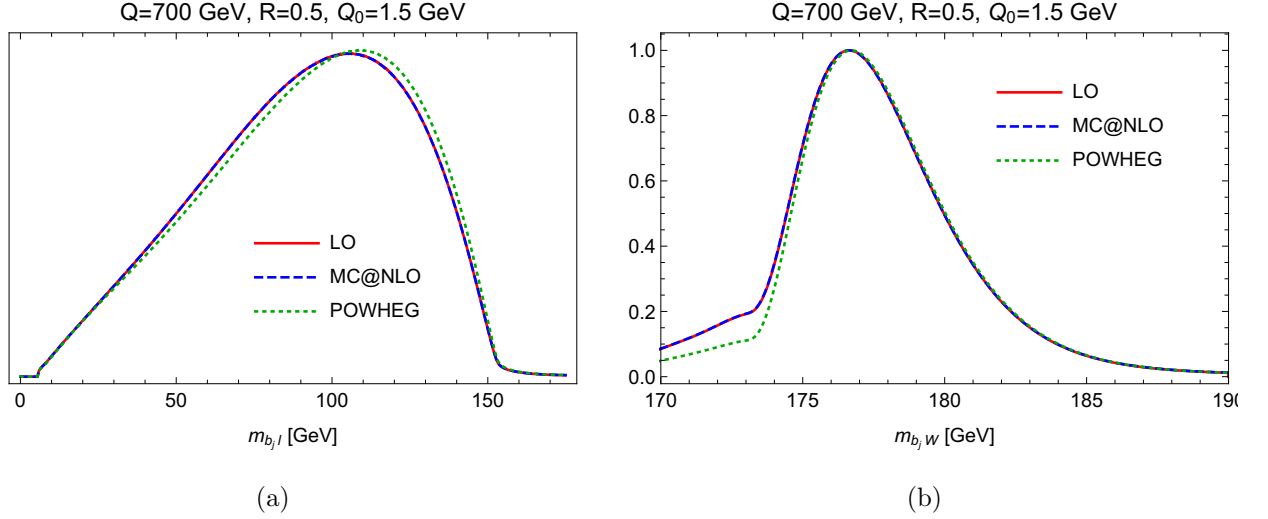
166

Figure 9.13: The $m_{b_j\ell}$ (left panel) and m_{b_jW} distributions (right panel) generated with HERWIG 7 full simulations for $m_t = 173$ GeV for $Q = 700$ GeV, jet radius $R = 0.5$ and Cambridge-Aachen-type b-jet clustering. Show are results at LO (solid red curves), with MC@NLO-type matching (dashed blue curves) and POWHEG-type matching (dotted green curves).

concerning the description of top quarks, the MC@NLO-type matching provides only NLO improved simulations concerning the production of the top quarks while the POWHEG-type matching provides NLO improved simulations concerning the production and the decay of the top quarks, where we refer to Ref. [187] for more details. In our LO examination in Sec. 9.6 we have already seen that $m_{b_j\ell}$ and m_{b_jW} are quite sensitive to the modeling of the decay for b-jet clustering for small jet radii as they are used in experimental reconstruction analyses. At the same time, for small jet radii $m_{b_j\ell}$ and m_{b_jW} are by construction insensitive to details of the top quark production. We can therefore expect that the LO and MC@NLO-type simulation results are very similar, while the POWHEG-type results may receive notable NLO corrections. This is shown in Figs. 9.13 where the $m_{b_j\ell}$ (left panel) and the m_{b_jW} distributions are displayed for $Q = 700$ GeV, $m_t = 173$ GeV, $R = 0.5$ and $Q_0 = Q_{0,b} = 1.5$ GeV at LO (solid red curve), with MC@NLO-type matching (dashed blue curve) and POWHEG-type matching (dotted green curve). As expected, we see that the MC@NLO-type matching for top production has essentially no impact, while we find visible effects in the distribution for POWHEG-type matching. However, in the top mass sensitive regions these are substantially smaller for m_{b_jW} than for $m_{b_j\ell}$, which is particularly conspicuous when comparing the curves in Figs. 9.13 to the corresponding ones shown in Figs. 9.9, where the dependence on the top quark mass was illustrated.

Focusing on the shower cut dependence of the kinematic top mass sensitivity of $m_{b_j\ell}$ and m_{b_jW} we again use the approach of Sec. 9.6 by fits of the top quark mass with respect to the default shower cut setting $Q_0 = Q_{0,b} = 1.5$ GeV (see the paragraph prior to Eq. (9.5) in Sec. 9.6 for the description of the fitting approach). In Figs. 9.14 and Figs. 9.15 the dependence of the fitted top mass obtained from the $m_{b_j\ell}$ endpoint region (stars) and from the m_{b_jW} resonance region (triangles), respectively, is displayed at LO and with NLO matching using the same settings as in Figs. 9.10 where we only displayed the LO results. We again show the results for shower cuts $Q_{0,b} = Q_0 = 1.0$, 1.5 and 2.0 GeV for jet radii $R = 0.25$ (upper left panels), $R = 0.5$ (upper right panels), $R = 1.0$ (lower left panels) and $R = 1.5$ (lower right panels), and we have carried out the analyses for b-jet clustering using the k_t-type algorithm (green symbols), the Cambridge-Aachen-type algorithm (blue symbols) and the anti-k_t-type algorithm (red symbols). To allow for an easier visual identification of the results we have slightly displaced the symbols horizontally, where for each Q_0 value the respective left set of symbols come from the LO simulations (already displayed in Figs. 9.10), the respective middle set of symbols come from simulations with MC@NLO-type matching and the respective right set of symbols
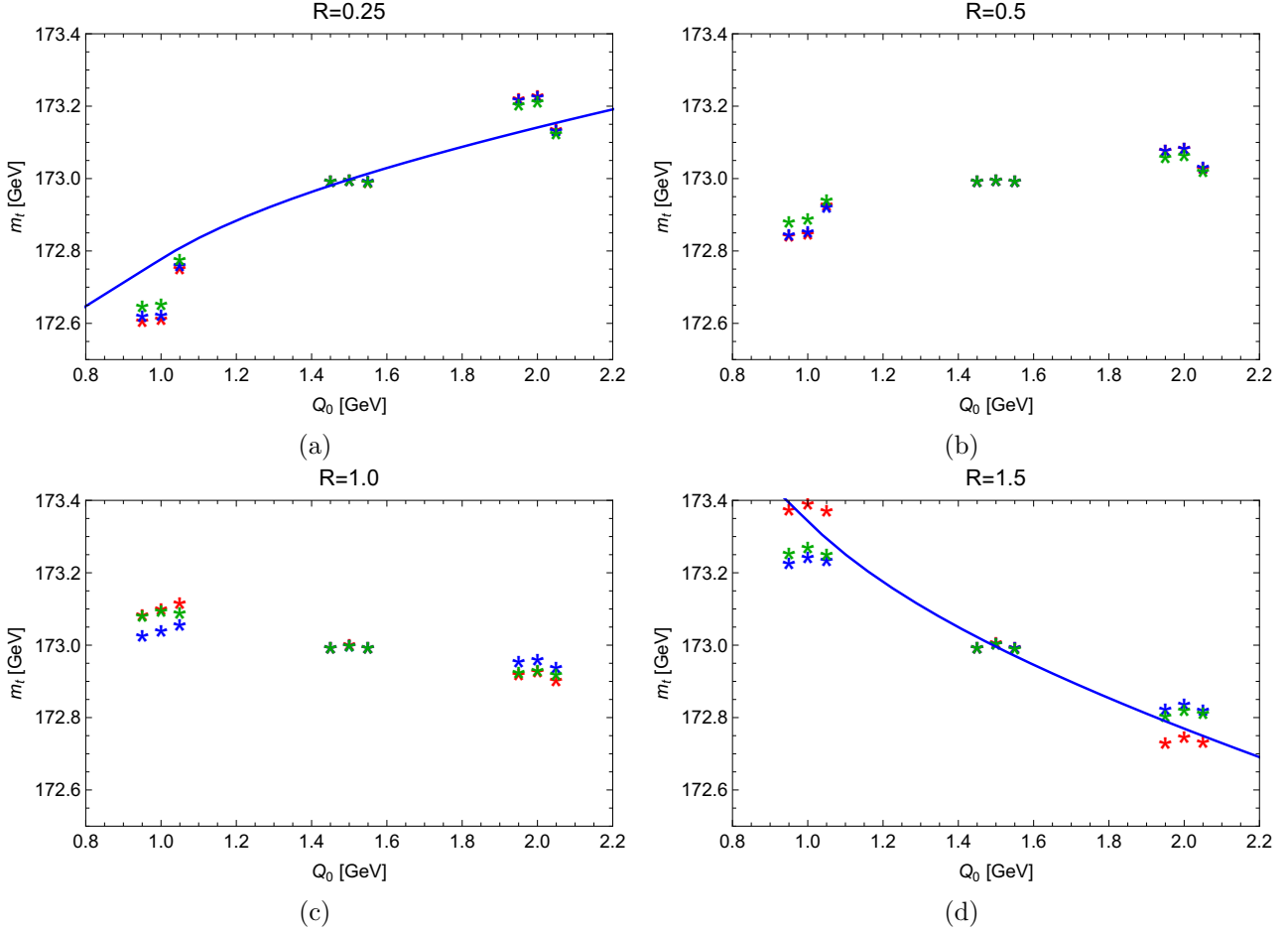
167

Figure 9.14: Fitted top quark mass obtained from the $m_{b_j\ell}$ endpoint region for shower cut values $Q_0 = Q_{0,b} = 1.0$, 1.5 and 2.0 GeV for $Q = 700$ GeV using the k_t-type algorithm (green), the Cambridge-Aachen algorithm (blue) and the anti-k_t-type algorithm (red) for b-jet clustering. For each Q_0 value the respective left set of symbols come from the LO simulations, the respective middle set of symbols come from simulations with MC@NLO-type matching and the respective right set of symbols from simulations with POWHEG-type matching. Displayed are the results for b-jet radii $R = 0.25$, 0.5, 1.0 and 1.5. The solid blue line in the lower right panel corresponds to Eq. (9.5) and the one in the upper left panel corresponds to Eq. (9.6) using $Q_0' = 1.5$ as the reference scale.

from simulations with POWHEG-type matching.

We see that the NLO matching has essentially no impact on the fitted top mass for large jet radii and the cutoff dependence agrees again very well with Eq. (9.5), which is displayed in the lower right panel ($R = 1.5$) as the solid blue line with $Q_0' = 1.5$ GeV as the reference scale. This is expected since $m_{b_j\ell}$ and $m_{b_j W}$ with large b-jet clustering radius are by construction neither sensitive to the top production mechanism and nor to details of the top quark decay. It is conspicuous, however, that there is also very good agreement between the LO and NLO fitted top masses for small jet radii. For comparison we have displayed again Eq. (9.6) with $Q_0' = 1.5$ GeV as the reference scale in the upper left panel ($R = 0.25$). We recall that Eq. (9.6) describes the expected shower cut dependence for $R \sim m_t/Q$ with the contributions coming from large angle soft radiation being removed while those from the ultra-collinear radiation being kept. So we see that, even though the POWHEG-type matching has sizable nominal effects on the distributions for the reconstructed observables, particularly for $m_{b_j\ell}$, the relative shower cut dependence itself it essentially unchanged.

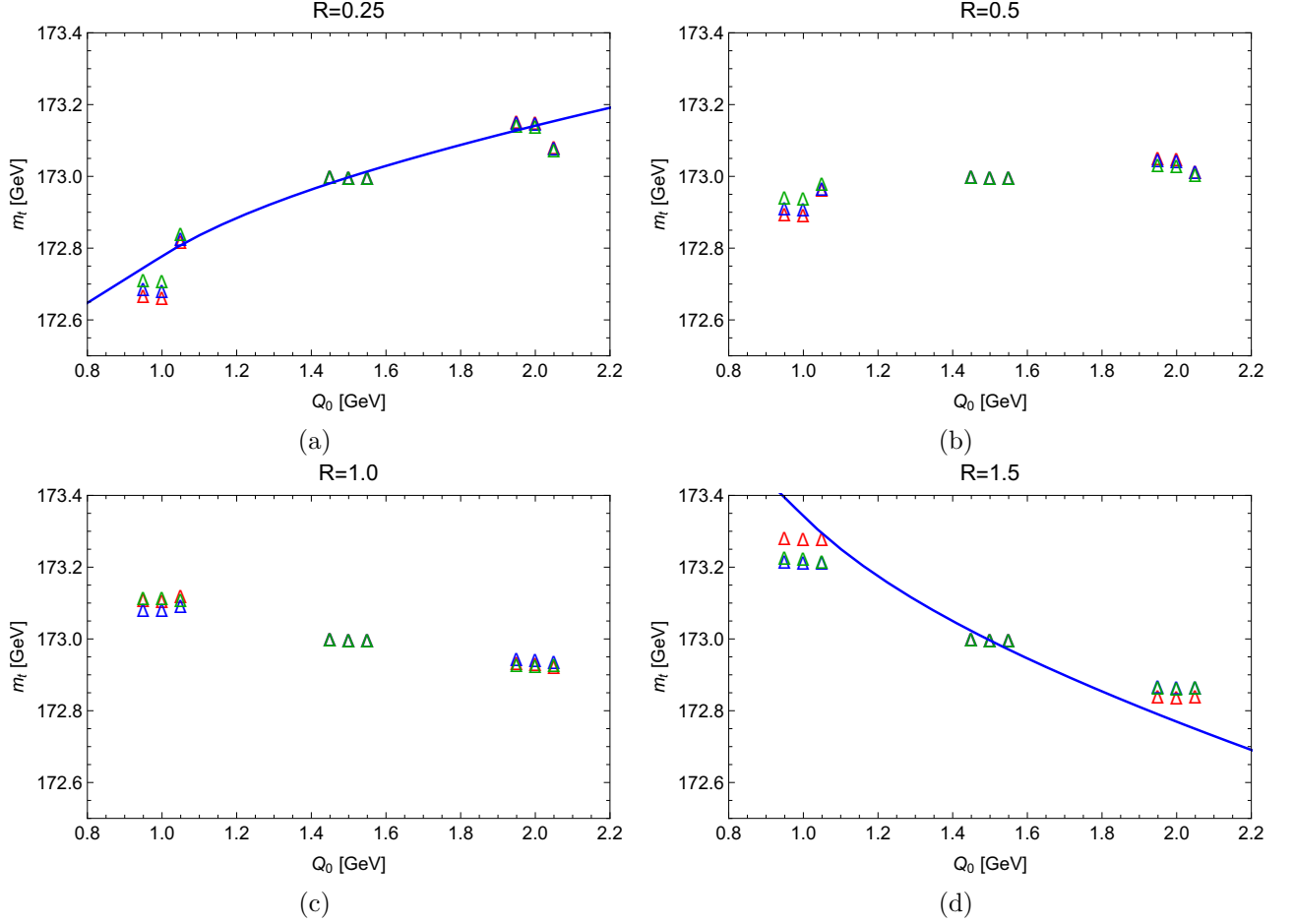This outcome again fully supports the idea of universality of the shower cut dependence and its

Figure 9.15: Fitted top quark mass obtained from the m_{b_jW} resonance region for shower cut values $Q_0 = Q_{0,b} = 1.0$, 1.5 and 2.0 GeV for $Q = 700$ GeV using the k_t-type algorithm (green), the Cambridge-Aachen algorithm (blue) and the anti-k_t-type algorithm (red) for b-jet clustering. For each Q_0 value the respective left set of symbols come from the LO simulations, the respective middle set of symbols come from simulations with MC@NLO-type matching and the respective right set of symbols from simulations with POWHEG-type matching. Displayed are the results for b-jet radii $R = 0.25$, 0.5, 1.0 and 1.5. The solid blue line in the lower right panel corresponds to Eq. (9.5) and the one in the upper left panel corresponds to Eq. (9.6) using $Q'_0 = 1.5$ as the reference scale.

independence concerning NLO matched predictions, and it is precisely what is to be expected if the equivalence of the MC generator top mass and the shower cut dependent CB mass of Eq. (8.39) is universal. However, as already noted in Sec. 9.6, a strict proof would require a a thorough quantitative (and preferably analytic) understanding of the b-jet clustering for exclusive observables such as $m_{b_j \ell}$ and $m_{b_j W}$ to unambiguously track the shower cut dependence. We emphasize again, that such quantitative understanding should at best be achieved in the context of a QCD factorization approach as it allows for a direct, clean and unambiguous field theoretical association of the different types of radiation concerning dynamical physical effects and contributions affecting the interpretation of QCD parameters such as the top quark mass.

Chapter 10

Conclusion

The emergence of infrared divergences and their proper treatment to achieve meaningful physics predictions represents one of the major conceptual and technical issues in modern applications of perturbative QCD in the context of collider physics. These divergences emerge in partonic computations in the (unphysical) limit of infinitesimally small resolution concerning infrared energies and momenta and are resolved by treating partonic configurations below the resolution scale as contributions to the same observable configuration. Within this approach, infrared cuts used to regulate the infrared divergences at the intermediate steps of the perturbative calculations, can then be sent to zero, where the limit of this procedure typically defines what is commonly perceived as the perturbative component of cross section predictions. In the context of multi-purpose MC event generators, where the parton showers are responsible for the description of the parton dynamics below the hard interaction scale, the same principles are applied. However, the infrared shower cut Q_0 which terminates the parton shower evolution is finite, typically in the range of 1 GeV, and leads to a power-like dependence of the parton-level predictions on Q_0 depending on the mass dimension and the infrared sensitivity of the observable. As we have discussed in this work for observables with kinematic top mass sensitivity this dependence on the shower cut Q_0 turns out to be linear and non-negligible given that the current experimental precision in top quark mass determinations based on direct reconstruction methods already reached the level of 0.5 GeV.

In this work we analyzed in detail the role of the shower cut Q_0 in angular ordered parton showers based on the coherent branching formalism *for quasi-collinear, i.e. boosted, massive quarks* at NLL. We have demonstrated, using an eventshape-type observable based on hemisphere masses and closely related to thrust (see Eqs. (7.1) and (7.2)) in the resonance region where the highest kinematic top mass sensitivity is located, that the finite shower cut automatically implies that the generator top quark mass is the Q_0-dependent *coherent branching* (CB) mass, $m_t^{\mathrm{MC}} = m_t^{\mathrm{CB}}(Q_0)$, even though the underlying analytic expressions that go into the formulation of the parton shower are derived in the pole mass scheme. The CB mass is a low-scale short-distance mass and free of an $\mathcal{O}(\Lambda_{\mathrm{QCD}})$ renormalon ambiguity. At $\mathcal{O}(\alpha_s)$ its relation to the pole mass m_t^{pole} reads

$$m_t^{\mathrm{CB}}(Q_0) - m_t^{\mathrm{pole}} = -\frac{2}{3}\,\alpha_s(Q_0)\,Q_0 \,+\, \mathcal{O}(\alpha_s^2 Q_0)\,. \tag{10.1}$$

The inclusion of NLO corrections in the context of NLO-matched parton showers does not add more precision to this relation as the additional NLO information improves the perturbative description of configurations that are located outside the resonance region, i.e. outside the region where the main kinematic top mass sensitivity arises. In Sec. 8.2 we have provided a detailed summary of all our theoretical findings and in Sec. 9 we have confronted them with parton-level simulations carried out using the HERWIG 7 event generator. The simulation results fully confirm our conceptual conclusions concerning the equivalence of the generator top mass and the shower-cut-dependent CB mass, and we also gathered evidence that the equivalence is universal and also applies for other

more exclusive observables such as the b-jet and lepton invariant mass $m_{b_j\ell}$ and the reconstructed top invariant mass m_{b_jW} in the limit of boosted top quarks. In the course of our examinations we also analyzed in detail the shower cut dependence coming from large-angle soft radiation which is universal for the production of massless quarks and boosted top quarks and which represents an interface to the hadronization model used in the MC event generator. These results have implications for the hadronization corrections in event-shape distribution and the extraction of α_s which we have, however, not addressed in this work and will be discussed elsewhere.

To conclude this part of thesis we address two important questions which have not been addressed in the main body of this work. The first is about the remaining conceptual issues that have to be resolved to universally explore the meaning of the MC generator top quark mass in the context of state-of-the-art MC event generators that are used in the experimental analyses. The second is about how to best convert $m_t^{\rm CB}(Q_0)$ to other top quark mass schemes. This issue gains particular importance if one assumes that the MC top quark mass $m_t^{\rm MC}$ determined in direct reconstruction methods at hadron colliders is indeed equal to the coherent branching mass $m_t^{\rm CB}(Q_0)$.

Before we address these issues we would like to emphasize that the proper field theoretic specification of the generator top quark mass $m_t^{\rm MC}$ as a particular mass renormalization scheme does not touch in any way the important questions how MC modeling uncertainties such as for the description of multi parton interactions or relevant for the event selection and the description of hadronization effects in the final states such as color reconnection affect the top mass measurements. These uncertainties are and shall continue to be under scrutiny, and their study may lead to improved MC generators in the future. The focus of the present work, on the other hand, is that the principle field theoretic meaning of the cutoff-dependence of the generator top quark mass can be studied and resolved independently of these issues and thus deserves particular attention by itself. Associated dedicated studies cover subtle effects that are, however, already relevant in view of the current experimental uncertainties in top quark mass determinations and may in a complementary way contribute to improved MC generators.

Let us now address the first issue. The basic simplifications for the examinations carried out in this work were that we used (i) parton level studies, (ii) the narrow width approximation, (iii) boosted (quasi-collinear) top quark kinematics and (iv) hemiphere masses in e^+e^- collisions closely related to the thrust/2-jettiness event-shape. In the context of hemisphere mass studies, the extension to MC hadron level studies is straightforward and shall be carried out in forthcoming works. Here the main question to be addressed is how well the MC hadronization models are compatible with the parton-hadron level factorization of Eqs. (7.3) and (7.21), which is an intrinsic property of QCD. The main point then to be clarified is, whether MC hadronization models have the capability to retune the top quark mass – a property that would make the MC top quark generator mass a hadronization parameter und mean that there are additional MC dependent non-perturbative contributions that have to be accounted for in the relation between the MC generator top mass $m_t^{\rm MC}$ and the coherent branching mass $m_t^{\rm CB}(Q_0)$. Concerning the narrow width approximation, we note that state-of-the-art parton showers for massive quarks do not have the capability to describe unstable particle effects from first principles. These unstable particle effects include the top quark intrinsic Breit-Wigner smearing of its invariant mass as well as interference effects connecting top and non-top processes through equivalent top decay final states. Accounting for unstable particle effects may be possible in the context of MC generators matched to calculations including the full top production and decay process or in the context of new MC generators which incorporate unstable particle effects in terms of systematic expansions that are more general than the narrow width approximation. Such studies are in reach and may be addressed in the near future. Concerning the approximation of boosted top quark kinematics, imagining systematic studies for slow top quarks comparable to the examinations carried out in this work, the prospects are far less clear. This is because the existing parton shower formalisms for massive quarks are by construction designed to be valid in the quasi-collinear limit - even though the bulk of the top quarks entering current experimental analyses have relatively low transverse momenta

between 50 and 100 GeV and cannot be considered to be quasi-collinear. So progressing into this direction involves general studies of the MC modeling for top quarks that in principle go beyond the problem of the MC top quark generator mass. Finally, concerning the extension of examinations at the level of those carried out in this work to other types of observables covering also hadronic collisions at the LHC, such studies require the development of new types of factorization theorems. For groomed fat jet masses for boosted top quark production at the LHC a factorization approach was recently developed [129], but factorization theorems for more exclusive variables such as $m_{b_j \ell}$ or $m_{b_j W}$, which are currently absent, are desirable as well. Furthermore, pushing the existing factorization approach for thrust and the description of the shower cut dependence to one higher order would be useful as well since it would allow for an explicit check of the $\mathcal{O}(\alpha_s^2)$ corrections to relation (10.1).

Let us now address the second issue. Assuming that the currently most precise top quark mass measurements of m_t^{MC} can be identified with a measurement of the CB mass $m_t^{\mathrm{CB}}(Q_0)$ defined in relation (10.1), how well can it be converted to other mass schemes? Given that most theoretical predictions for top quark physics at the LHC are carried out in the pole mass scheme, one may simply convert the CB mass to the pole mass using Eq. (10.1). The HERWIG 7 event generator uses $Q_0 = 1.25$ GeV as the default value for the shower cut, and using the $\overline{\mathrm{MS}}$ scheme for the strong coupling with $\alpha_s^{\overline{\mathrm{MS}},(n_f=5)}(M_Z) = 0.118$ we obtain $m_t^{\mathrm{pole}} - m_t^{\mathrm{CB}}(Q_0 = 1.25 \text{ GeV}) = 330$ MeV, where we have evaluated the strong coupling in the 3-flavor scheme using $\alpha_s^{(n_f=5)}(M_Z) = 0.118$ as the input. On the other hand, using the Monte Carlo (MC) scheme for α_s, which accounts for the two-loop cusp anomalous dimension contained in the NLL quark splitting function and which is effectively used in HERWIG 7 (see Eq. (7.56) in Sec. 7.2.1 on the MC scheme for the strong coupling), we obtain $m_t^{\mathrm{pole}} - m_t^{\mathrm{CB}}(Q_0 = 1.25 \text{ GeV}) = 520$ MeV. The difference of about 200 MeV between both conversions can be viewed as an illustration of the currently unknown $\mathcal{O}(\alpha_s^2)$ corrections and indicates that the convergence is not particularly good. This is, however, expected since the pole mass has an $\mathcal{O}(\Lambda_{\mathrm{QCD}})$ renormalon ambiguity. From the analysis of Ref. [186], where a determination of the pole mass from a short-distance mass at the scale 1.3 GeV was studied in detail, we can expect that $\mathcal{O}(\alpha_s^2)$ and $\mathcal{O}(\alpha_s^3)$ corrections are also needed to determine the pole mass value and that at $\mathcal{O}(\alpha_s^3)$ there is a remaining irreducible uncertainty of around 250 MeV due to the $\mathcal{O}(\Lambda_{\mathrm{QCD}})$ renormalon ambiguity of the pole mass (see also [197] for an alternative view on the size of the renormalon ambiguity of the pole mass). Thus the determination of the currently unknown $\mathcal{O}(\alpha_s^2)$ and $\mathcal{O}(\alpha_s^3)$ corrections to Eq. (10.1) is important to reliably determine the pole mass. To determine the $\mathcal{O}(\alpha_s^2)$ corrections in the factorization approach the effects of the shower cut need to be implemented into the bHQET jet function at $\mathcal{O}(\alpha_s^2)$. To determine the $\mathcal{O}(\alpha_s^2)$ corrections in the context of coherent branching formalism (or angular ordered parton showers) the effects of the shower cut have to be analyzed in the context of a fully consistent next-to-next-to-leading order evolution. The overall conclusion is that the difference between the pole mass and the CB mass, $m_t^{\mathrm{pole}} - m_t^{\mathrm{CB}}(Q_0 = 1.25 \text{ GeV})$, is likely at least as large as the current uncertainties in top quark mass measurements from direct reconstruction of around 500 MeV (see Sec. 6.1) and requires the determination of two and three-loop corrections. Even when these corrections become available, there will be is an irreducible uncertainty of 250 MeV. So, for a reliable determination of the pole mass the unknown higher order corrections to Eq. (10.1) are very important, and the ultimate uncertainty in the pole mass is at the same level as the precision of 200 MeV that may be achieved for measurements of m_t^{MC} in the future high-luminosity run of the LHC [198, 199].

Alternatively, since physical observables are not tied conceptually to the pole mass scheme in any way and its $\mathcal{O}(\Lambda_{\mathrm{QCD}})$ ambiguity is a pure artefact of the pole mass definition, one can as well parametrize calculations using suitable short-distance top quark mass schemes. In this approach the sizeable corrections and the renormalon ambiguity associated to the pole mass scheme – as well as any controversial discussion on the actual size of this ambiguity – can be avoided entirely. To illustrate this approach let us consider a determination of the MSR mass $m_t^{\mathrm{MSR}}(Q_0)$ from a given value of the CB mass $m_t^{\mathrm{CB}}(Q_0)$. At $\mathcal{O}(\alpha_s)$ the relation between the scale-dependent MSR mass [124, 125] and the pole

mass reads $m_t^{\mathrm{MSR}}(Q_0) - m_t^{\mathrm{pole}} = -4\,\alpha_s(Q_0)Q_0/(3\pi)$. For the strong coupling in the $\overline{\mathrm{MS}}$ scheme this gives $m_t^{\mathrm{MSR}}(Q_0) - m_t^{\mathrm{CB}}(Q_0 = 1.25\,\mathrm{GeV}) = 120\,\mathrm{MeV}$ compared to 190 MeV in the Monte Carlo scheme. As expected from the fact that the difference of MSR and CB masses does not contain any $\mathcal{O}(\Lambda_{\mathrm{QCD}})$ renormalon ambiguity, the scheme corrections to obtain the MSR mass are small, and one can also expect that they exhibit good convergence because MSR and CB masses are both short-distance mass schemes. The difference of 70 MeV can be viewed as an illustration of the currently unknown $\mathcal{O}(\alpha_s^2)$ corrections and indicates that the knowledge of the two-loop corrections in Eq. (10.1) may be sufficient to convert the CB mass to the MSR with a precision of better than 50 MeV. Compared to the current uncertainties in top quark mass measurements from direct reconstruction of around 500 MeV these corrections are small and the knowledge of these two-loop corrections is not required. Furthermore, as was shown in Ref. [125], one can convert the MSR mass to all other commonly used short-distance mass schemes, such as the 1S [200–202], the PS [203] or the $\overline{\mathrm{MS}}$ schemes, with a precision of 10 MeV (see also the REvolver library [204] for automated running and matching). The overall conclusion is that, when using only short-distance mass schemes, the achievable precision in converting the MC/CB mass to other mass schemes is already at this stage substantially higher than the current experimental uncertainties and also than extrapolations concerning the future high-luminosity run of the LHC which indicate that a precision of 200 MeV [198, 199] for a determination of the top quark mass can be reached.

Appendix

Appendix A

Variable Flavor Number Scheme for Thrust in the Peak Region in e^+e^- Collisions

For completeness we also write down a VFNS for secondary massive quarks following the mass mode factorization approach for thrust [165]

$$\tau = 1 - \max_{\vec{n}} \sum_i \frac{|\vec{n} \cdot \vec{p}_i|}{Q} \,, \tag{A.1}$$

in the process e^+e^- to jets in the peak region $\tau \ll 1$, which is the third process that is related to Drell-Yan and DIS by crossing symmetry. A VFNS for secondary massive quarks for thrust in the peak region following the universal factorization approach was discussed in Refs. [11, 12]. Here we will discuss the same in the MMF approach.

The massless SCET factorization theorem [171] in the dijet region $\tau \ll 1$ reads

$$\frac{\mathrm{d}\sigma}{\mathrm{d}\tau} = \sigma_0 \, H(Q,\mu) \int \mathrm{d}s_a \mathrm{d}s_b \, J(s_a,\mu) J(s_b,\mu) S\Big(Q\tau - \frac{s_a}{Q} - \frac{s_b}{Q}, \mu\Big) \,, \tag{A.2}$$

with the hard function H and the soft function S the same as for beam thrust in Drell-Yan in Sec. 2.2, and the hemisphere jet function J the same in Sec. 3. The natural scales of the functions that minimize the logarithms are

$$\mu_H \sim Q \,, \qquad\qquad \mu_J \sim Q\sqrt{\tau} \,, \qquad\qquad \mu_S \sim Q\tau \,, \tag{A.3}$$

which gives a typical SCET I scenario with $\mu_S \ll \mu_J$. It is therefore similar to the factorization theorem for beam thrust discussed in Sec. 2.2, with the beam function replaced by the hemisphere jet function.

We will briefly discuss the massive factorization theorems for the different hierarchies for secondary massive quarks, i.e. virtual and real radiation contributions that arise form a gluon splitting into a massive quark pair. These factorization theorems will have a structure very similar to the ones for beam thrust in Sec. 2.2. We will ignore any effects of primary massive quarks here. They would lead to new structures in the factorization theorems because one encounters also a region where boosted Heavy Quark Effective Theory is needed to correctly resum all massive logarithms, see Refs. [18, 19]. This is beyond the scope of this work and we will only discuss the effects of secondary massive quarks that can be treated in analogy to the previous sections.

We give the form of the factorization theorems already including the massive power corrections in the notation of Sec. 4.2.1. All the mass mode matching functions that appear in the following

factorization theorems have already been introduced in the previous sections, which demonstrates again the universality of this method that is providing single building blocks that, once calculated, can be reused in various different factorization theorems including massive quarks. Since also the massive hard, jet and soft functions have been discussed before, no additional calculation is needed at all to provide all relevant functions for the factorization theorem for thrust with secondary massive quarks at NNLL$'$.

Again all of the hard, jet and soft functions are evolved with $n_l + 1$ active flavor above and with n_l active flavors below the mass scale with the standard massless anomalous dimensions, the mass mode matching functions H_s, H_c and $\mathcal{S}_c$ are then only evolved in rapidity.

Scenario I: $Q < m$:

$$H_{m>Q}(Q, m, \mu) \times \int \mathrm{d}s_a \mathrm{d}s_b \, J_{m>Q\sqrt{\tau}}(s_a, m, \mu) J_{m>Q\sqrt{\tau}}(s_b, m, \mu) S_{m>Q\tau}\Big(Q\tau - \frac{s_a}{Q} - \frac{s_b}{Q}, m, \mu\Big) \quad \text{(A.4)}$$

The massive flavor is integrated out at the hard scale and is therefore no dynamic degree of freedom in SCET. There are no large rapidity logarithms to be resummed. In the limit $m \gg Q$ this reduces to the massless factorization theorem in Eq. (A.2) with n_l massless flavors.

Scenario II: $Q\sqrt{\tau} < m < Q$:

$$H_{m<Q}(Q, m, \mu) H_c\Big(m, \mu, \frac{\nu}{\omega_a}\Big) H_c\Big(m, \mu, \frac{\nu}{\omega_b}\Big) H_s(m, \mu, \nu)$$
$$\times \int \mathrm{d}s_a \mathrm{d}s_b \, J_{m>Q\sqrt{\tau}}(s_a, m, \mu) J_{m>Q\sqrt{\tau}}(s_b, m, \mu) S_{m>Q\tau}\Big(Q\tau - \frac{s_a}{Q} - \frac{s_b}{Q}, m, \mu\Big) \quad \text{(A.5)}$$

The massive flavor is integrated out between the hard and the jet scale. The rapidity logarithms are resummed in the rapidity RG evolution of the matching functions H_c and H_s.

Scenario III: $Q\tau < m < Q\sqrt{\tau}$:

$$H_{m<Q}(Q, m, \mu) H_s(m, \mu, \nu)$$
$$\times \int \mathrm{d}s_a \mathrm{d}s_b \mathrm{d}\ell_a \mathrm{d}\ell_b \, J_{m<Q\sqrt{\tau}}(s_a, m, \mu) J_{m<Q\sqrt{\tau}}(s_b, m, \mu)$$
$$\times \mathcal{S}_c(\ell_a, m, \mu, \nu) \mathcal{S}_c(\ell_b, m, \mu, \nu) S_{m>Q\tau}\Big(Q\tau - \frac{s_a}{Q} - \frac{s_b}{Q} - \ell_a - \ell_b, \mu\Big) \quad \text{(A.6)}$$

The massive flavor is integrated out between the jet and the soft scale. The rapidity logarithms are resummed in the rapidity RG evolution of the matching functions H_s and $\mathcal{S}_c$.

Scenario IV: $m < Q\tau$:

$$H_{m<Q}(Q, m, \mu) \int \mathrm{d}s_a \mathrm{d}s_b \, J_{m<Q\sqrt{\tau}}(s_a, m, \mu) J_{m<Q\sqrt{\tau}}(s_b, m, \mu) S_{m<Q\tau}\Big(Q\tau - \frac{s_a}{Q} - \frac{s_b}{Q}, m, \mu\Big) \quad \text{(A.7)}$$

The mass is below the soft scale and therefore the massive flavor is a dynamic degree of freedom in all the components of the SCET factorization theorem. There are no large rapidity logarithms to be resummed. In the limit $m \ll Q\tau$ this reduces to the massless factorization theorem in Eq. (A.2) with $n_l + 1$ massless flavors.

All the hard, jet and soft functions have the correct limiting behavior in the small and large mass limit and give a smooth transition between the different scenarios. Theses results are equivalent to the universal factorization approach for thrust in the peak region presented in Refs. [11, 12].

Appendix B

Results for massless quarks

Here we summarize the relevant results with massless quarks for the hard, beam, jet and soft functions used in part I. We will use the notation of Eqs. (2.33) and (2.36) to give the explicit results at $\mathcal{O}(\alpha_s)$ and $\mathcal{O}(\alpha_s^2 C_F T_F)$ (the terms that are relevant for massive quark effects at NNLL′).

The notation of Eqs. (2.33) and (2.36) is used. The plus-distributions $\mathcal{L}_n(\vec{p}_T, \mu)$ and $\mathcal{L}_n(x)$ are defined in appendix J.

B.1   Hard function

The massless quark hard function is directly related to the QCD form factor and has been computed at $\mathcal{O}(\alpha_s^2)$ in Ref. [205]. The loop-corrections entering the two hard functions for DIS and DY are related by analytic continuation $Q^2 \rightarrow -Q^2 - i0$ in the SCET current Wilson coefficient C, where $H = |C|^2$. The $\mathcal{O}(\alpha_s)$ and $\mathcal{O}(\alpha_s^2 C_F T_F)$ corrections to the hard function in Drell-Yan and $e^+ e^- \rightarrow$ jets read (with $L_Q = \ln(Q^2/\mu^2)$)

$$H_{ij}^{(1)}(Q, \mu) = H_{ij}^{(0)}(Q)\, C_F \left(-2L_Q^2 + 6L_Q - 16 + \frac{7\pi^2}{3} \right), \tag{B.1}$$

$$H_{ij}^{(2,l)}(Q, \mu) = H_{ij}^{(0)}(Q)\, C_F \left[-\frac{8}{9}L_Q^3 + \frac{76}{9}L_Q^2 - \left(\frac{836}{27} - \frac{16\pi^2}{9} \right)L_Q + \frac{4085}{81} - \frac{182\pi^2}{27} + \frac{8\zeta_3}{9} \right],$$

where $H_{ij}^{(0)}$ is the tree-level contribution. Note that for a single quark flavor there is in addition a nonvanishing correction to the axial current contribution relevant for Z-boson production, which cancels within an isospin doublet for massless quarks.

The hard function for neutral current DIS reads (with $L_Q = \ln(Q^2/\mu^2)$)

$$\hat{H}_i^{(1)}(Q, \mu) = \hat{H}_i^{(0)}(Q)\, C_F \left(-2L_Q^2 + 6L_Q - 16 + \frac{\pi^2}{3} \right), \tag{B.2}$$

$$\hat{H}_i^{(2,l)}(Q, \mu) = \hat{H}_i^{(0)}(Q)\, C_F \left[-\frac{8}{9}L_Q^3 + \frac{76}{9}L_Q^2 - \left(\frac{836}{27} + \frac{8\pi^2}{9} \right)L_Q + \frac{4085}{81} + \frac{46\pi^2}{27} + \frac{8\zeta_3}{9} \right].$$

The corresponding anomalous dimensions are the same for the DY and DIS hard functions and read

$$\gamma_H^{(1)}(Q, \mu) = C_F \left(8L_Q - 12 \right),$$

$$\gamma_H^{(2,l)}(Q, \mu) = C_F \left(-\frac{160}{9}L_Q + \frac{520}{27} + \frac{8\pi^2}{3} \right). \tag{B.3}$$

B.2 Beam functions and PDF

B.2.1 TMD beam function

The matching coefficients entering the TMD beam function have been computed at $\mathcal{O}(\alpha_s^2)$ in various schemes [54–56,206] and are obtained for the symmetric η-regulator in Ref. [57]. The results at $\mathcal{O}(\alpha_s)$ are

$$\mathcal{I}_{qg}^{(1)}(\vec{p}_T, z, \mu) = \theta(z)\theta(1-z)\,T_F\left[2P_{qg}(z)\mathcal{L}_0(\vec{p}_T, \mu) + 4z(1-z)\delta^{(2)}(\vec{p}_T)\right], \tag{B.4}$$

$$\mathcal{I}_{qq}^{(1)}\left(\vec{p}_T, z, \mu, \frac{\nu}{\omega}\right) = \theta(z)\,C_F\left\{\mathcal{L}_0(\vec{p}_T, \mu)\left[-\left(4\ln\frac{\nu}{\omega} + 3\right)\delta(1-z) + 2P_{qq}(z)\right]\right.$$
$$\left. + 2\delta^{(2)}(\vec{p}_T)\,\theta(1-z)(1-z)\right\}, \tag{B.5}$$

The splitting functions are

$$P_{qg}(z) = z^2 + (1-z)^2\,, \qquad P_{qq}(z) = 2\mathcal{L}_0(1-z) + \frac{3}{2}\delta(1-z) - \theta(1-z)(1+z)\,. \tag{B.6}$$

At $\mathcal{O}(\alpha_s^2 C_F T_F)$ the massless matching coefficient is given by

$$\mathcal{I}_{qq}^{(2,l)}\left(\vec{p}_T, z, \mu, \frac{\nu}{\omega}\right) = \theta(z)\,C_F\left\{\mathcal{L}_1(\vec{p}_T, \mu)\left[\frac{16}{3}\mathcal{L}_0(1-z) - \frac{16}{3}\ln\frac{\nu}{\omega}\delta(1-z) - \frac{8}{3}\theta(1-z)(1+z)\right]\right.$$
$$+ \mathcal{L}_0(\vec{p}_T, \mu)\left[-\frac{80}{9}\mathcal{L}_0(1-z) + \frac{80}{9}\ln\frac{\nu}{\omega}\delta(1-z)\right.$$
$$\left. + \theta(1-z)\left(-\frac{8}{3}\frac{1+z^2}{1-z}\ln z + \frac{16}{9} + \frac{64z}{9}\right)\right]$$
$$+ \delta^{(2)}(\vec{p}_T)\left[\frac{224}{27}\mathcal{L}_0(1-z) - \frac{224}{27}\ln\frac{\nu}{\omega}\delta(1-z)\right.$$
$$\left.\left. + \theta(1-z)\left(\frac{2}{3}\frac{1+z^2}{1-z}\ln^2 z + \frac{20}{9}\frac{1+z^2}{1-z}\ln z - \frac{148}{27} - \frac{76z}{27}\right)\right]\right\}. \tag{B.7}$$

The anomalous dimensions of the massless quark TMD beam function, as defined in Eq. (2.17), are given at $\mathcal{O}(\alpha_s)$ and $\mathcal{O}(\alpha_s^2 C_F T_F)$ by

$$\gamma_B^{(1)}\left(\frac{\nu}{\omega}\right) = C_F\left(8\ln\frac{\nu}{\omega} + 6\right),$$

$$\gamma_B^{(2,l)}\left(\frac{\nu}{\omega}\right) = C_F\left(-\frac{160}{9}\ln\frac{\nu}{\omega} - \frac{4}{3} - \frac{16\pi^2}{9}\right),$$

$$\gamma_{\nu,B}^{(1)}(\vec{p}_T, \mu) = -C_F\,4\mathcal{L}_0(\vec{p}_T, \mu),$$

$$\gamma_{\nu,B}^{(2,l)}(\vec{p}_T, \mu) = C_F\left[-\frac{16}{3}\mathcal{L}_1(\vec{p}_T, \mu) + \frac{80}{9}\mathcal{L}_0(\vec{p}_T, \mu) - \frac{224}{27}\delta^{(2)}(\vec{p}_T)\right]. \tag{B.8}$$

B.2.2 Virtuality-dependent beam function

The virtuality-dependent beam functions for massless quarks are known to two loop order [86, 87]. The matching coefficients at $\mathcal{O}(\alpha_s)$ read

$$\mathcal{I}_{qg}^{(1)}(t, z, \mu) = \theta(z)\theta(1-z)\, T_F \left\{ 2P_{qg}(z)\frac{1}{\mu^2}\mathcal{L}_0\left(\frac{t}{\mu^2}\right) + \delta(t)\left[2P_{qg}(z)\ln\frac{1-z}{z} + 4z(1-z)\right] \right\},$$

$$\begin{aligned} \mathcal{I}_{qq}^{(1)}(t, z, \mu) = \theta(z)\, C_F &\left\{ \frac{4}{\mu^2}\mathcal{L}_1\left(\frac{t}{\mu^2}\right)\delta(1-z) + \frac{1}{\mu^2}\mathcal{L}_0\left(\frac{t}{\mu^2}\right)\left[2P_{qq}(z) - 3\delta(1-z)\right] \right. \\ &+ \delta(t)\left[4\mathcal{L}_1(1-z) - \frac{\pi^2}{3}\delta(1-z) \right. \\ &\left.\left. + \theta(1-z)\left[2(1-z-2(1+z)\ln(1-z) - 2\frac{1+z^2}{1-z}\ln z\right]\right] \right\}. \end{aligned} \tag{B.9}$$

The massless matching coefficient at order $\mathcal{O}(\alpha_s^2 C_F T_F)$ for one quark flavor reads

$$\mathcal{I}_{qq}^{(2,l)}(t, z, \mu) \tag{B.10}$$

$$\begin{aligned} = \theta(z)\, C_F &\left\{ \frac{8}{3}\frac{1}{\mu^2}\mathcal{L}_2\left(\frac{t}{\mu^2}\right)\delta(1-z) \right. \\ &+ \frac{1}{\mu^2}\mathcal{L}_1\left(\frac{t}{\mu^2}\right)\left[\frac{16}{3}\mathcal{L}_0(1-z) - \frac{80}{9}\delta(1-z) - \frac{8}{3}\theta(1-z)(1+z)\right] \\ &+ \frac{1}{\mu^2}\mathcal{L}_0\left(\frac{t}{\mu^2}\right)\left[\frac{16}{3}\mathcal{L}_1(1-z) - \frac{80}{9}\mathcal{L}_0(1-z) + \delta(1-z)\left(\frac{224}{27} - \frac{8\pi^2}{9}\right)\right. \\ &\left. + \theta(1-z)\left(-\frac{8}{3}(1+z)\ln(1-z) - \frac{16(1+z^2)}{3(1-z)}\ln z + \frac{16}{9} + \frac{64z}{9}\right)\right] \\ &+ \delta(t)\left[\frac{8}{3}\mathcal{L}_2(1-z) - \frac{80}{9}\mathcal{L}_1(1-z) + \mathcal{L}_0(1-z)\left(\frac{224}{27} - \frac{8\pi^2}{9}\right)\right. \\ &+ \delta(1-z)\left(-\frac{656}{81} + \frac{10\pi^2}{9} + \frac{40\zeta_3}{9}\right) + \theta(1-z)\left(-\frac{8(1+z^2)}{3(1-z)}\mathrm{Li}_2(1-z)\right. \\ &- \frac{4}{3}(1+z)\ln^2(1-z) - \frac{16(1+z^2)}{3(1-z)}\ln(1-z)\ln z + \frac{10\left(1+z^2\right)}{3(1-z)}\ln^2 z \\ &\left.\left.+ \left(\frac{16}{9} + \frac{64z}{9}\right)\ln(1-z) + \frac{4(5 - 2z + 7z^2)}{3(1-z)}\ln z - \frac{148}{27} - \frac{76z}{27} + \frac{4\pi^2}{9}(1+z)\right)\right] \right\}. \end{aligned}$$

The anomalous dimension of the massless quark beam function at order $\mathcal{O}(\alpha_s)$ and $\mathcal{O}(\alpha_s^2 C_F T_F)$ are given by

$$\gamma_B^{(1)}(t, \mu) = C_F\left[-\frac{8}{\mu^2}\mathcal{L}_0\left(\frac{t}{\mu^2}\right) + 6\delta(t)\right],$$

$$\gamma_B^{(2,l)}(t, \mu) = C_F\left[\frac{160}{9}\frac{1}{\mu^2}\mathcal{L}_0\left(\frac{t}{\mu^2}\right) + \delta(t)\left(-\frac{484}{27} - \frac{8\pi^2}{9}\right)\right]. \tag{B.11}$$

B.2.3 PDF

The anomalous dimensions of the PDFs are known to three-loops [207, 208], and partially known to four-loops [209]. The anomalous dimension of the quark PDF in the limit $z \to 1$ at order $\mathcal{O}(\alpha_s)$ and

$\mathcal{O}(\alpha_s^2 C_F T_F)$ needed here is

$$\gamma_\phi^{(1)}(1-z,\mu) = C_F\left[8\mathcal{L}_0(1-z) + 6\delta(1-z)\right],$$

$$\gamma_\phi^{(2,l)}(1-z,\mu) = C_F\left[-\frac{160}{9}\mathcal{L}_0(1-z) - \left(\frac{4}{3} + \frac{16\pi^2}{9}\right)\delta(1-z)\right]. \tag{B.12}$$

B.3 Soft functions

B.3.1 TMD soft function

The TMD soft function for massless quarks with the symmetric η-regulator has been computed at two loops in Ref. [57]. At $\mathcal{O}(\alpha_s)$ and $\mathcal{O}(\alpha_s^2 C_F T_F)$ it is given by

$$S^{(1)}(\vec{p}_T,\mu,\nu) = C_F\left[-4\mathcal{L}_1(\vec{p}_T,\mu) + 8\ln\frac{\nu}{\mu}\mathcal{L}_0(\vec{p}_T,\mu) - \frac{\pi^2}{3}\delta^{(2)}(\vec{p}_T)\right], \tag{B.13}$$

$$S^{(2,l)}(\vec{p}_T,\mu,\nu) = C_F\left[-\frac{16}{3}\mathcal{L}_2(\vec{p}_T,\mu) + \mathcal{L}_1(\vec{p}_T,\mu)\left(\frac{32}{3}\ln\frac{\nu}{\mu} + \frac{80}{9}\right) - \mathcal{L}_0(\vec{p}_T,\mu)\left(\frac{160}{9}\ln\frac{\nu}{\mu} + \frac{8\pi^2}{9}\right)\right.$$
$$\left. + \delta^{(2)}(\vec{p}_T)\left(\frac{448}{27}\ln\frac{\nu}{\mu} - \frac{656}{81} + \frac{10\pi^2}{9} - \frac{8\zeta_3}{9}\right)\right]. \tag{B.14}$$

The corresponding anomalous dimensions are

$$\gamma_S^{(1)}(\mu,\nu) = -C_F\,16\ln\frac{\nu}{\mu},$$

$$\gamma_S^{(2,l)}(\mu,\nu) = C_F\left(\frac{320}{9}\ln\frac{\nu}{\mu} - \frac{448}{27} + \frac{8\pi^2}{9}\right),$$

$$\gamma_{\nu,S}^{(1)}(\vec{p}_T,\mu) = C_F\,8\mathcal{L}_0(\vec{p}_T,\mu),$$

$$\gamma_{\nu,S}^{(2,l)}(\vec{p}_T,\mu) = C_F\left[\frac{32}{3}\mathcal{L}_1(\vec{p}_T,\mu) - \frac{160}{9}\mathcal{L}_0(\vec{p}_T,\mu) + \frac{448}{27}\delta^{(2)}(\vec{p}_T)\right]. \tag{B.15}$$

B.3.2 Thrust soft function

The thrust soft function is known to two loops [83, 84]. At $\mathcal{O}(\alpha_s)$ and $\mathcal{O}(\alpha_s^2 C_F T_F)$ it is given by

$$S^{(1)}(\ell,\mu) = C_F\left[-16\frac{1}{\mu}\mathcal{L}_1\left(\frac{\ell}{\mu}\right) + \frac{\pi^2}{3}\delta(\ell)\right], \tag{B.16}$$

$$S^{(2,l)}(\ell,\mu) = C_F\left[-\frac{64}{3}\frac{1}{\mu}\mathcal{L}_2\left(\frac{\ell}{\mu}\right) + \frac{320}{9}\frac{1}{\mu}\mathcal{L}_1\left(\frac{\ell}{\mu}\right) + \frac{1}{\mu}\mathcal{L}_0\left(\frac{\ell}{\mu}\right)\left(-\frac{448}{27} + \frac{16\pi^2}{9}\right)\right.$$
$$\left. + \delta(\ell)\left(\frac{80}{81} + \frac{74\pi^2}{27} - \frac{232}{9}\zeta_3\right)\right]. \tag{B.17}$$

The corresponding μ anomalous dimension is given by

$$\gamma_S^{(1)}(\ell,\mu) = 16C_F\frac{1}{\mu}\mathcal{L}_0\left(\frac{\ell}{\mu}\right),$$

$$\gamma_S^{(2,l)}(\ell,\mu) = C_F\left[-\frac{320}{9}\frac{1}{\mu}\mathcal{L}_0\left(\frac{\ell}{\mu}\right) + \delta(\ell)\left(\frac{448}{27} - \frac{8\pi^2}{9}\right)\right]. \tag{B.18}$$

B.4 Jet function

The massless quark jet function is known to three loop order [210, 211]. The terms relevant here at $\mathcal{O}(\alpha_s)$ and $\mathcal{O}(\alpha_s^2 C_F T_F)$ are

$$J^{(1)}(s,\mu) = C_F \left[4 \frac{1}{\mu^2} \mathcal{L}_1\left(\frac{s}{\mu^2}\right) - 3 \frac{1}{\mu^2} \mathcal{L}_0\left(\frac{s}{\mu^2}\right) + \delta(s)\left(7 - \pi^2\right) \right], \tag{B.19}$$

$$J^{(2,l)}(s,\mu) = C_F \left[\frac{8}{3} \frac{1}{\mu^2} \mathcal{L}_2\left(\frac{s}{\mu^2}\right) - \frac{116}{9} \frac{1}{\mu^2} \mathcal{L}_1\left(\frac{s}{\mu^2}\right) + \frac{1}{\mu^2} \mathcal{L}_0\left(\frac{s}{\mu^2}\right)\left(\frac{494}{27} - \frac{8\pi^2}{9}\right) \right.$$
$$\left. + \delta(s)\left(-\frac{4057}{162} + \frac{68\pi^2}{27} + \frac{16}{9}\zeta_3\right) \right].$$

The corresponding μ anomalous dimension is the same as for the virtuality-dependent beam function in Eq. (B.11).

$$\gamma_J^{(1)}(s,\mu) = C_F \left[-\frac{8}{\mu^2} \mathcal{L}_0\left(\frac{s}{\mu^2}\right) + 6\delta(s) \right],$$

$$\gamma_J^{(2,l)}(s,\mu) = C_F \left[\frac{160}{9} \frac{1}{\mu^2} \mathcal{L}_0\left(\frac{s}{\mu^2}\right) + \delta(s)\left(-\frac{484}{27} - \frac{8\pi^2}{9}\right) \right]. \tag{B.20}$$

Note that in the second part of the thesis a different notation is used where we defined the thrust jet function $J^{(\tau)}$ as

$$J^{(\tau)}(s,\mu) = \int \mathrm{d}s' \, J(s - s', \mu) J(s', \mu), \tag{B.21}$$

accounting already for both hemispheres, whereas in the first part of the thesis the function $J(s,\mu)$ always stands for the single hemisphere jet function.

Appendix C

Results for massive quarks

In this section we present our results for the contributions from primary massive quarks at $\mathcal{O}(\alpha_s)$ and from secondary massive quarks at $\mathcal{O}(\alpha_s^2)$ to all components of the various factorization theorems discussed in part I. The results in this section are only given for a single massive quark flavor and with the rapidity divergences regularized by the symmetric Wilson line regulator introduced in Refs. [40,41]. The actual computations of the primary and secondary massive quark corrections to the beam, jet and soft functions are carried out in some detail in App. D.

We will use the notation of Eqs. (2.33) and (2.36) (which use the convention the expansion is always done in terms of the strong coupling in the $n_l + 1$ flavor scheme $\alpha_s^{(n_l+1)}$) to give the explicit results at $\mathcal{O}(\alpha_s)$ and $\mathcal{O}(\alpha_s^2 C_F T_F)$. The plus-distributions $\mathcal{L}_n(\vec{p}_T, \mu)$ and $\mathcal{L}_n(x)$ are defined in appendix J.

C.1   Hard matching functions

All the hard matching functions are insensitive to the measurement performed at a lower scale. The hard functions for q_T and $\mathcal{T}$ measurements are therefore the same, by crossing symmetry also the hard function for thrust in $e^+e^- \to 2$ jets in Refs. [12,70]. The DIS hard function is related to the others by crossing symmetry via the analytic continuation $Q^2 \to -Q^2 - i0$ in the current matching coefficient. The hard mass mode matching functions H_s and H_c are also insensitive to the measurement and additionally not sensitive to the scale Q^2, and are therefore identical for all processes discussed here.

C.1.1   Massive quark corrections to the DY hard function

The secondary massive quark corrections to the hard function in Eq. (2.20) read

$$H^{(2,h)}(Q, m, \mu) = H^{(0)}(Q) C_F h_{\text{virt}}\left(\frac{m^2}{Q^2}\right) + \frac{4}{3} L_m \, H^{(1)}(Q, \mu) \,, \tag{C.1}$$

where $H^{(0)}$ denotes the tree-level normalization and $H^{(1)}$ the massless one-loop contribution given in Eq. (B.1). The function h_{virt} contains the $\mathcal{O}(\alpha_s^2 C_F T_F)$ virtual massive quark bubble correction in full QCD shown in Fig. 1.1. It has been calculated in Refs. [212, 213] and is given by

$$
\begin{aligned}
h_{\text{virt}}(x) = {}& \left(16x^2 - \frac{8}{3}\right)\left[-4\text{Li}_3\left(\frac{r-1}{r+1}\right) - \frac{1}{3}\ln^3\frac{r-1}{r+1} + \frac{2\pi^2}{3}\ln\frac{r-1}{r+1} + 4\zeta_3\right] \\
& + r\left(\frac{184}{9}x + \frac{76}{9}\right)\left[4\text{Li}_2\left(\frac{r-1}{r+1}\right) + \ln^2\frac{r-1}{r+1} - \frac{2\pi^2}{3}\right] + \left(\frac{880}{9}x + \frac{1060}{27}\right)\ln x \\
& + \frac{1904}{9}x + \frac{6710}{81} \,,
\end{aligned}
\tag{C.2}
$$

with $r = \sqrt{1 + 4x}$. For $m \to \infty$ the decoupling of the massive quark is encoded in the fact that $h_{\text{virt}}(x) \to 0$ for $x \to \infty$.

For Z-boson production there is an additional primary massive quark contribution to the axial vector current, namely the massive quark triangle correction in Fig. 1.1, which we denote by Δh_{axial}. Using the narrow width approximation comes with the same prefactor $H^{(0)}(Q)$ as for h_{virt}. It has been computed in Refs. [67–69] and is given by

$$\Delta h_{\text{axial}}(Q, m, \mu) = \frac{8 a_q a_Q}{v_q^2 + a_q^2} \left[3 \ln \frac{Q^2}{\mu^2} - 9 + \frac{\pi^2}{3} + \theta(Q^2 - 4m^2) \, G_1\left(\frac{m^2}{Q^2}\right) \right.$$
$$\left. + \theta(4m^2 - Q^2) \, G_2\left(\frac{m^2}{Q^2}\right) \right], \tag{C.3}$$

where the vector and axial vector couplings for up- and down-type quarks are proportional to $v_u = 1 - 8/3 \sin^2 \theta_W$, $v_d = -1 + 4/3 \sin^2 \theta_W$, $a_u = 1$, $a_d = -1$. The functions G_1 and G_2 are given in Eqs. (2.8) and (2.9) of Ref. [68]. In the small mass limit $m \ll Q$ the function $G_1(m^2/Q^2)$ vanishes, such that Δh_{axial} gives the same result as for a massless flavor in the loop,

$$\Delta h_{\text{axial}}(Q, m, \mu) = \frac{8 a_q a_Q}{v_q^2 + a_q^2} \left[3 \ln \frac{Q^2}{\mu^2} - 9 + \frac{\pi^2}{3} + \mathcal{O}\left(\frac{m^2}{Q^2}\right) \right]. \tag{C.4}$$

For a massless isospin partner this correction is thus canceled within the $SU(2)_L$ doublet, while for different masses (as for $m_b \ll m_t$) there is a (μ-independent) remainder. Note that for $Q \ll m$ the function Δh_{axial} gives a nonvanishing contribution

$$\Delta h_{\text{axial}}(Q, m, \mu) = \frac{8 a_q a_Q}{v_q^2 + a_q^2} \left[3 \ln \frac{m^2}{\mu^2} + \frac{3}{2} + \mathcal{O}\left(\frac{Q^2}{m^2}\right) \right]. \tag{C.5}$$

In this case one would integrate out the heavy quark at the scale $\mu_m \sim m$ and evolve the axial current to $\mu_H \sim Q$ to resum logarithms $\ln(m^2/Q^2)$.

C.1.2   Massive quark corrections to the DIS hard function

The two-loop contributions of a massive flavor to the DIS hard function are

$$\hat{H}^{(2,h)}(Q, m, \mu) = \hat{H}^{(0)}(Q) C_F \hat{h}_{\text{virt}}\left(\frac{m^2}{Q^2}\right) + \frac{4}{3} L_m \, \hat{H}^{(1)}(Q, \mu), \tag{C.6}$$

where $\hat{H}^{(0)}$ denotes the tree-level normalization and $\hat{H}^{(1)}$ the massless one-loop contribution given in Eq. (B.2). Also the function $\hat{h}_{\text{virt}}$ can be inferred from the results in Refs. [67–69] and reads

$$\hat{h}_{\text{virt}}(x) = \left(16x^2 - \frac{8}{3}\right) \left[-2\text{Li}_3\left(\frac{\hat{r} - 1}{\hat{r} + 1}\right) - 2\text{Li}_3\left(\frac{\hat{r} + 1}{\hat{r} - 1}\right) + 4\zeta_3 \right]$$
$$+ \hat{r}\left(\frac{184}{9}x - \frac{76}{9}\right) \left[-2\text{Li}_2\left(\frac{\hat{r} - 1}{\hat{r} + 1}\right) + 2\text{Li}_2\left(\frac{\hat{r} + 1}{\hat{r} - 1}\right) \right] - \left(\frac{880}{9}x - \frac{1060}{27}\right) \ln x$$
$$- \frac{1904}{9}x + \frac{6710}{81}, \tag{C.7}$$

with $\hat{r} = \sqrt{1 - 4x}$. For $m \to \infty$ the decoupling of the massive quark is encoded in the fact that $h_{\text{virt}}(x) \to 0$ for $x \to \infty$.

C.1.3 Soft and collinear mass-mode matching functions

The contributions to the mass-mode matching functions originate only from secondary radiation. The soft mass-mode function H_s appearing in Eqs. (2.22), (2.93), and (2.97) has been computed at two loops with the symmetric η-regulator in Ref. [70]. It is given by

$$H_s(m,\mu,\nu) = 1 + \frac{\alpha_s^2 C_F T_F}{16\pi^2} \left[-\left(\frac{16}{3}L_m^2 + \frac{160}{9}L_m + \frac{448}{27} \right) \ln\frac{\nu}{\mu} + \frac{8}{9}L_m^3 + \frac{40}{9}L_m^2 \right.$$
$$\left. + \left(\frac{448}{27} - \frac{4\pi^2}{9} \right)L_m + \frac{656}{27} - \frac{10\pi^2}{27} - \frac{56\zeta_3}{9} \right] + \mathcal{O}(\alpha_s^3). \tag{C.8}$$

Since there are no $\mathcal{O}(\alpha_s)$ corrections, the flavor scheme for α_s does not affect the results at $\mathcal{O}(\alpha_s^2)$. Its anomalous dimensions are

$$\gamma_{H_s}(m,\mu,\nu) = \frac{\alpha_s^2 C_F T_F}{16\pi^2} \left[\left(\frac{64}{3}L_m + \frac{320}{9} \right) \ln\frac{\nu}{\mu} - \frac{448}{27} + \frac{8\pi^2}{9} \right] + \mathcal{O}(\alpha_s^3),$$
$$\gamma_{\nu,H_s}(m,\mu) = \frac{\alpha_s^2 C_F T_F}{16\pi^2} \left[-\frac{16}{3}L_m^2 - \frac{160}{9}L_m - \frac{448}{27} \right] + \mathcal{O}(\alpha_s^3). \tag{C.9}$$

The rapidity anomalous dimension is even known at $\mathcal{O}(\alpha_s^3)$, see Ref. [2].

The result for the collinear mass-mode function H_c in Eq. (2.22) can be inferred at $\mathcal{O}(\alpha_s^2)$ from the computations in Refs. [12, 70] and reads

$$H_c\left(m,\mu,\frac{\nu}{\omega}\right) = 1 + \frac{\alpha_s^2 C_F T_F}{16\pi^2} \left[\left(\frac{8}{3}L_m^2 + \frac{80}{9}L_m + \frac{224}{27} \right) \ln\frac{\nu}{\omega} \right.$$
$$\left. + 2L_m^2 + \left(\frac{2}{3} + \frac{8\pi^2}{9} \right)L_m + \frac{73}{18} + \frac{20\pi^2}{27} - \frac{8\zeta_3}{3} \right] + \mathcal{O}(\alpha_s^3). \tag{C.10}$$

Its anomalous dimensions are

$$\gamma_{H_c}\left(m,\mu,\frac{\nu}{\omega}\right) = \frac{\alpha_s^2 C_F T_F}{16\pi^2} \left[-\left(\frac{32}{3}L_m + \frac{160}{9} \right) \ln\frac{\nu}{\omega} - 8L_m - \frac{4}{3} - \frac{16\pi^2}{9} \right] + \mathcal{O}(\alpha_s^3),$$
$$\gamma_{\nu,H_c}(m,\mu) = \frac{\alpha_s^2 C_F T_F}{16\pi^2} \left(\frac{8}{3}L_m^2 + \frac{80}{9}L_m + \frac{224}{27} \right) + \mathcal{O}(\alpha_s^3). \tag{C.11}$$

One can easily verify that the relation in Eq. (2.37) between the massive hard function in Eq. (C.1), the hard function contribution for a massless flavor in Eq. (B.1), and the two mass mode matching functions H_s and H_c in Eqs. (C.8) and (C.10), respectively, is satisfied,

$$H^{(2,h)}(Q,m,\mu) = H^{(2,l)}(Q,\mu) + H_c^{(2)}\left(m,\mu,\frac{\nu}{\omega_a}\right) + H_c^{(2)}\left(m,\mu,\frac{\nu}{\omega_b}\right) + H_s^{(2)}(m,\mu,\nu) + \mathcal{O}\left(\frac{m^2}{Q^2}\right). \tag{C.12}$$

The same relation also holds for the DIS hard function $\hat{H}$ with the massive and massless results given in Eqs. (C.6) and (B.2).

C.2 Beam functions

Here we give our results for the massive quark beam function coefficient $\mathcal{I}_{Qg}$ at $\mathcal{O}(\alpha_s)$ and the secondary massive quark corrections to the light-quark coefficients $\mathcal{I}_{qq}$ at $\mathcal{O}(\alpha_s^2)$, which appear in Eqs. (2.26) and (2.93) for the q_T and beam thrust measurement. We also give the massive quark contributions to the beam function anomalous dimensions. We also give the well-known results for the corresponding PDF matching coefficients $\mathcal{M}_{Qg}$ at $\mathcal{O}(\alpha_s)$ and $\mathcal{M}_{qq}$ at $\mathcal{O}(\alpha_s^2)$ appearing in Eqs. (2.31), (2.97) and (2.104).
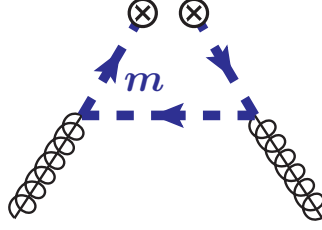
Figure C.1: Feynman diagram for the massive quark beam function at one loop.
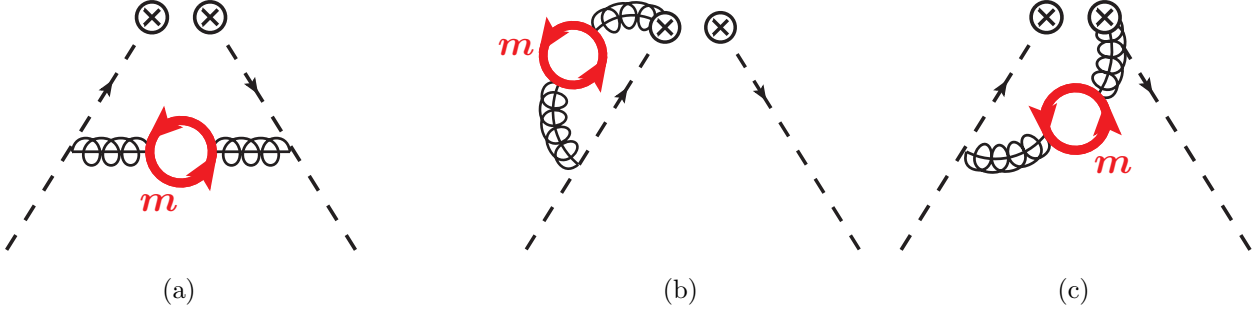

Figure C.2: Secondary massive quark corrections for the light-quark beam function at $\mathcal{O}(\alpha_s^2)$. In addition, also the wave-function renormalization correction and the mirror diagrams for (b) and (c) have to be included.

C.2.1   TMD beam function coefficients

The matching coefficient $\mathcal{I}_{Qg}$ generating a massive beam function from a gluon splitting is calculated at $\mathcal{O}(\alpha_s)$ in Sec. D.1 and corresponds to the diagram shown in Fig. C.1. The result reads $(p_T^2 = |\vec{p}_T|^2)$

$$\mathcal{I}_{Qg}(\vec{p}_T, m, z) = \mathcal{I}_{\bar{Q}g}(\vec{p}_T, m, z) = \frac{\alpha_s T_F}{4\pi^2}\, \theta(z)\, \theta(1-z)\, \frac{2}{p_T^2 + m^2} \left[P_{qg}(z) + \frac{2m^2 z(1-z)}{p_T^2 + m^2} \right] + \mathcal{O}(\alpha_s^2)\,, \tag{C.13}$$

with the splitting function

$$P_{qg}(z) = z^2 + (1-z)^2\,. \tag{C.14}$$

This result is equivalent to the Fourier transform of the mass-dependent matching functions $\mathcal{C}_{h/G}$ in Ref. [45]. After performing an appropriate crossing it also agrees with the massive final-state splitting functions [214, 215] or fragmenting jet function [216].

The contributions from secondary massive quarks to the matching coefficient $\mathcal{I}_{qq}$ are computed in

Sec. D.3 at $\mathcal{O}(\alpha_s^2)$. The corresponding diagrams are shown in Fig. C.2. The result is given by

$$
\begin{aligned}
\mathcal{I}_{qq}^{(2,h)}&\left(\vec{p}_T, m, z, \mu, \frac{\nu}{\omega}\right)\\
&= \theta(z)C_F\Bigg\{\delta^{(2)}(\vec{p}_T)\,\delta(1-z)\left[\left(\frac{8}{3}L_m^2 + \frac{80}{9}L_m + \frac{224}{27}\right)\ln\frac{\nu}{\omega} + 2L_m^2 + \left(\frac{2}{3} + \frac{8\pi^2}{9}\right)L_m\right.\\
&\qquad\left. + \frac{73}{18} + \frac{20\pi^2}{27} - \frac{8\zeta_3}{3}\right]\\
&\quad + \frac{16}{9\pi p_T^2}\left[\mathcal{L}_0(1-z) - \delta(1-z)\ln\frac{\nu}{\omega}\right]\left[-5 + 12\hat{m}^2 + 3c(1-2\hat{m}^2)\ln\frac{c+1}{c-1}\right]\\
&\quad + \frac{16}{9\pi p_T^2}\theta(1-z)\left[\frac{3}{2d(1-z)}\left[(1+z^2)(1+2\hat{m}^2 z) + 4\hat{m}^4 z^2(-5 + 6z - 5z^2)\right]\ln\frac{d+1}{d-1}\right.\\
&\qquad\left.\left. - \frac{3c(1-2\hat{m}^2)}{1-z}\ln\frac{c+1}{c-1} + 1 + 4z + 3\hat{m}^2(-4 + z - 5z^2)\right]\right\}\\
&\quad + \frac{4}{3}L_m\,\mathcal{I}_{qq}^{(1)}\left(\vec{p}_T, z, \mu, \frac{\nu}{\omega}\right),
\end{aligned}
\tag{C.15}
$$

where

$$
\hat{m} \equiv \frac{m}{p_T}, \qquad c = \sqrt{1 + 4\hat{m}^2}, \qquad d = \sqrt{1 + 4\hat{m}^2 z}, \tag{C.16}
$$

and the one-loop term $\mathcal{I}_{qq}^{(1)}$ is given in Eq. (B.5).

In the $(n_l + 1)$-flavor scheme for α_s there is also a correction from a virtual massive quark loop to the flavor-nondiagonal matching coefficient $\mathcal{I}_{qg}^{(2)}$. This contribution is trivial, since it factorizes into a vacuum polarization correction corresponding to the matching of α_s between the (n_l) and $(n_l + 1)$-flavor schemes, and the one-loop contribution, such that

$$
\mathcal{I}_{qg}^{(2,h)}(\vec{p}_T, m, z, \mu) = \frac{4}{3}L_m\,\mathcal{I}_{qg}^{(1)}(\vec{p}_T, z, \mu), \tag{C.17}
$$

with $\mathcal{I}_{qg}^{(1)}$ given in Eq. (B.4). In the (n_l)-flavor scheme for α_s the $\mathcal{I}_{qg}^{(2,h)}$ contribution vanishes.

The contributions from a massive flavor to the beam function anomalous dimensions are

$$
\begin{aligned}
\gamma_B^{(2,h)}\left(\frac{\nu}{\omega}\right) &= C_F\left(-\frac{160}{9}\ln\frac{\nu}{\omega} - \frac{4}{3} - \frac{16\pi^2}{9}\right),\\
\gamma_{\nu,B}^{(2,h)}(\vec{p}_T, m, \mu) &= C_F\left\{-\frac{16}{3}L_m\mathcal{L}_0(\vec{p}_T, \mu) + \delta^{(2)}(\vec{p}_T)\left(\frac{8}{3}L_m^2 + \frac{80}{9}L_m + \frac{224}{27}\right)\right.\\
&\qquad\left. + \frac{16}{9\pi p_T^2}\left[5 - 12\hat{m}^2 - 3c(1-2\hat{m}^2)\ln\frac{c+1}{c-1}\right]\right\}.
\end{aligned}
\tag{C.18}
$$

The $\mathcal{L}_0(\vec{p}_T, \mu)$ distribution is defined in appendix J. The μ anomalous dimension here is the same as for a massless quark flavor, $\gamma_B^{(2,h)} = \gamma_B^{(2,l)}$ [see Eq. (B.8)]. The rapidity anomalous dimension is explicitly mass dependent and only reproduces the result for a massless flavor in the limit $m \ll p_T$.

C.2.2 Virtuality-dependent beam function coefficients

The massive quark-gluon virtuality beam function matching coefficient at $\mathcal{O}(\alpha_s)$ shown in Fig. C.1 is given by

$$
\mathcal{I}_{Qg}(t, m, z) = \frac{\alpha_s T_F}{4\pi}\,\theta(t)\,\theta(z)\,\theta\left[\frac{t(1-z)}{z} - m^2\right]\frac{2}{t}\left[P_{qg}(z) + \frac{2m^2 z^2}{t}\right] + \mathcal{O}(\alpha_s^2). \tag{C.19}
$$

The contributions from secondary massive quarks to the light-quark coefficient at $\mathcal{O}(\alpha_s^2)$ as shown in Fig. C.2 are given by

$$
\begin{aligned}
\mathcal{I}_{qq}^{(2,h)}&\left(t, m, z, \mu, \frac{\nu}{\omega}\right)\\
&= \theta(z) C_F \Bigg\{ \delta(t)\,\delta(1-z) \left[\left(\frac{8}{3} L_m^2 + \frac{80}{9} L_m + \frac{224}{27} \right) \ln \frac{\nu}{\omega} + 2L_m^2 + \left(\frac{2}{3} + \frac{8\pi^2}{9} \right) L_m \right.\\
&\quad \left. + \frac{73}{18} + \frac{20\pi^2}{27} - \frac{8\zeta_3}{3} \right]\\
&\quad + \theta\!\left(t - \frac{4m^2 z}{1-z} \right) \frac{8}{9t(1-z)} \left[-\frac{3}{u} \left[(1+z^2)(1-2\hat{m}_t^2 z) - 4\hat{m}_t^4 z^2 (2 - 3z + 5z^2) \right] \ln \frac{u-v}{u+v} \right.\\
&\quad \left. - 2v \left[4 - 3z + 4z^2 + \frac{z(11 - 21z + 29z^2 - 15z^3)}{1-z} \hat{m}_t^2 \right] \right] \Bigg\} + \frac{4}{3} L_m \, \mathcal{I}_{qq}^{(1)}(t, z, \mu) \,, \qquad \text{(C.20)}
\end{aligned}
$$

with

$$
\hat{m}_t = \frac{m}{\sqrt{t}} \qquad u = \sqrt{1 - 4\hat{m}_t^2 z}\,, \qquad v = \sqrt{1 - \frac{4\hat{m}_t^2 z}{1-z}}\,, \qquad \text{(C.21)}
$$

and the one-loop term $\mathcal{I}_{qq}^{(1)}$ is given in Eq. (B.9).

In the $(n_l + 1)$-flavor scheme for α_s there is also the analogous contribution to Eq. (C.17) to the flavor-nondiagonal coefficient

$$
\mathcal{I}_{qg}^{(2,h)}(t, m, z, \mu) = \frac{4}{3} L_m \, \mathcal{I}_{qg}^{(1)}(t, z, \mu) \,, \qquad \text{(C.22)}
$$

with $\mathcal{I}_{qg}^{(1)}$ given in Eq. (B.9). In the (n_l)-flavor scheme for α_s the $\mathcal{I}_{qg}^{(2,h)}$ contribution vanishes.

The contribution from the massive flavor to the μ anomalous dimension at $\mathcal{O}(\alpha_s^2)$ is given by

$$
\gamma_{B,m}^{(2,h)}\left(t, \frac{\nu}{\omega}\right) = C_F \,\delta(t) \left(-\frac{160}{9} \ln \frac{\nu}{\omega} - \frac{4}{3} - \frac{16\pi^2}{9} \right) \,. \qquad \text{(C.23)}
$$

We emphasize that the massive quark contribution to the μ anomalous dimension is not the same as for a massless flavor, but is in fact the same as for the TMD beam function in Eq. (C.18). This is required by consistency with the large mass limit $\sqrt{Q\mathcal{T}}, q_T \ll m$, where the massive flavor can only contribute to the (local) running of the common current operators, which are independent of the measurement. Only in combination with the soft mass-mode function H_s and the soft function, the combined μ evolution above the mass scale is the same as for $n_l + 1$ massless flavors as discussed in Eq. (2.94).

The secondary massive quarks introduce rapidity divergences and associated logarithms also in the virtuality-dependent beam function. The ν anomalous dimension induced by the secondary massive effects is the same as for the collinear mass-mode function, see Eq. (2.92), given in Eq. (C.11).

C.2.3 PDF matching coefficients

The matching coefficients relating the PDFs in the $(n_l + 1)$ and the (n_l)-flavor scheme are all known at two loops [217] and partially beyond (see e.g. Refs. [218–220] and references therein). The matching coefficient for a primary massive quark originating from an initial-state gluon at $\mathcal{O}(\alpha_s)$ is

$$
\mathcal{M}_{Qg}(m, z, \mu) = -\frac{\alpha_s T_F}{4\pi} \theta(1-z)\theta(z)\, 2P_{qg}(z) L_m + \mathcal{O}(\alpha_s^2) \,. \qquad \text{(C.24)}
$$

The matching coefficient coming from secondary massive quark corrections to the light-quark PDFs reads up to $\mathcal{O}(\alpha_s^2)$

$$
\begin{aligned}
\mathcal{M}_{qq}(m,z,\mu) = 1 + \frac{\alpha_s^2 C_F T_F}{16\pi^2}\,\theta(z)\Bigg\{ & \mathcal{L}_0(1-z)\left(\frac{8}{3}L_m^2 + \frac{80}{9}L_m + \frac{224}{27}\right) \\
& + \delta(1-z)\left[2L_m^2 + \left(\frac{2}{3}+\frac{8\pi^2}{9}\right)L_m + \frac{73}{18} + \frac{20\pi^2}{27} - \frac{8\zeta_3}{3}\right] \\
& + \theta(1-z)\left[-\frac{4}{3}L_m^2(1+z) + L_m\left(\frac{8}{9}-\frac{88}{9}z + \frac{8}{3}\frac{1+z^2}{1-z}\ln z\right) + \frac{2}{3}\frac{1+z^2}{1-z}\ln^2 z\right. \\
& \left. + \frac{\ln z}{1-z}\left(\frac{44}{9}-\frac{16}{3}z+\frac{44}{9}z^2\right) + \frac{44}{27} - \frac{268}{27}z\right]\Bigg\} + \mathcal{O}(\alpha_s^3)\,. \tag{C.25}
\end{aligned}
$$

Because there are no corrections at $\mathcal{O}(\alpha_s)$, the specification of the flavor scheme of α_s is not relevant at order $\mathcal{O}(\alpha_s^2)$.

The matching coefficient between the gluon PDF in the (n_l) and $(n_l + 1)$-flavor schemes at $\mathcal{O}(\alpha_s)$, which is also required for Drell-Yan at $\mathcal{O}(\alpha_s^2)$, is equivalent to the matching relation for α_s

$$
\mathcal{M}_{gg}(m,z,\mu) = \delta(1-z) + \frac{\alpha_s T_F}{4\pi}\,\delta(1-z)\,\frac{4}{3}L_m + \mathcal{O}(\alpha_s^2)\,. \tag{C.26}
$$

Note that taking into account the nondiagonal evolution of the PDFs the known $\mathcal{O}(\alpha_s^2)$ corrections for all matching factors $\mathcal{M}_{ij}$ become relevant at NNLL$'$.

C.3   Hemisphere jet function

The secondary massive quark corrections to the primary massless quark hemisphere jet function in the mass mode scheme (i.e. without subtractions concerning the massive flavor) was calculated at two-loops in Ref. [71] and are

$$
\begin{aligned}
J^{(2,h)}&\left(s,m,\mu,\frac{\nu}{\omega}\right) \\
&= C_F\Bigg\{\delta(s)\left[\left(\frac{8}{3}L_m^2 + \frac{80}{9}L_m + \frac{224}{27}\right)\ln\frac{\nu}{\omega} + 2L_m^2 + \left(\frac{2}{3}+\frac{8\pi^2}{9}\right)L_m + \frac{73}{18}\right. \\
&\quad \left. + \frac{20\pi^2}{27} - \frac{8\zeta_3}{3}\right] + \frac{\theta(s-4m^2)}{s}\left[-\frac{32}{3}\text{Li}_2\left(\frac{b-1}{1+b}\right) + \frac{16}{3}\ln\left(\frac{1-b^2}{4}\right)\ln\left(\frac{1-b}{1+b}\right)\right. \\
&\quad \left.\left. - \frac{8}{3}\ln^2\left(\frac{1-b}{1+b}\right) + \left(\frac{1}{2}b^4 - b^2 + \frac{241}{18}\right)\ln\left(\frac{1-b}{1+b}\right) - \frac{5}{27}b^3 + \frac{241}{9}b - \frac{8\pi^2}{9}\right]\right\} \\
&\quad + \frac{4}{3}L_m J^{(1)}(s,\mu)\,, \tag{C.27}
\end{aligned}
$$

with

$$
b = \sqrt{1-\frac{4m^2}{s}}\,, \tag{C.28}
$$

and the massless one-loop contribution $J^{(1)}$ given in Eq. (B.19). The contribution from the massive flavor to the μ anomalous dimension at $\mathcal{O}(\alpha_s^2)$ is the same as for the virtuality-dependent beam function in the mass mode scheme in Eq. (C.23).

$$
\gamma_{J,m}^{(2,h)}\left(s,\frac{\nu}{Q}\right) = C_F\,\delta(s)\left(-\frac{160}{9}\ln\frac{\nu}{Q} - \frac{4}{3} - \frac{16\pi^2}{9}\right)\,. \tag{C.29}
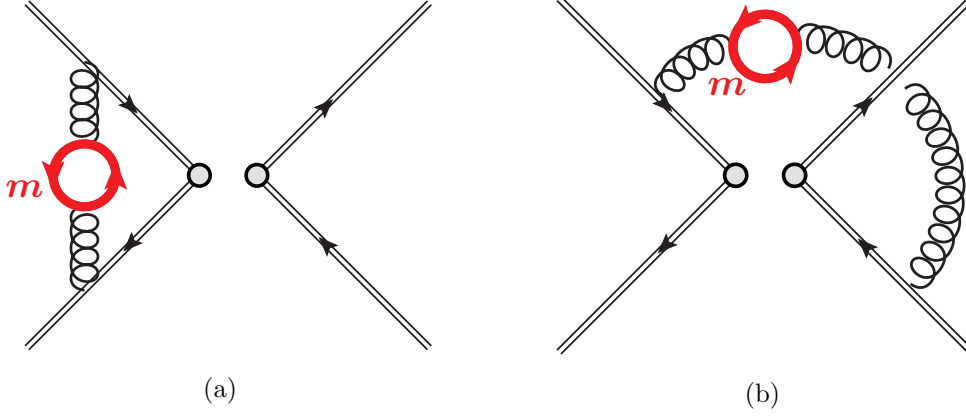$$

Figure C.3: Corrections from secondary massive quarks to the (c)soft function. Also the mirror diagrams need to be included.

We emphasize that it is not the same as for a massless flavor.

The secondary massive quarks introduce rapidity divergences and associated logarithms also in the jet function. The ν anomalous dimension induced by the secondary massive effects is the same as for the collinear mass-mode current matching function H_c given in Eq. (C.11).

C.4 Soft and collinear-soft functions

Here we give all massive quark corrections at $\mathcal{O}(\alpha_s^2)$ to the soft and csoft functions. They arise exclusively from secondary radiation. Note that the soft functions satisfy Casimir scaling at this order and can be thus applied also to color-singlet production in gluon-fusion by replacing an overall $C_F \to C_A$.

C.4.1 TMD soft function

The contributions from secondary massive quarks to the TMD soft function, which appears in Eq. (2.26) for $q_T \sim m$, are calculated in App. D.4 at $\mathcal{O}(\alpha_s^2)$ and correspond to the diagrams shown in Fig. C.3. The result reads

$$
\begin{aligned}
S^{(2,h)}(\vec{p}_T, m, \mu, \nu) = C_F &\bigg\{ \delta^{(2)}(\vec{p}_T) \bigg[\bigg(-\frac{16}{3}L_m^2 - \frac{160}{9}L_m - \frac{448}{27} \bigg) \ln\frac{\nu}{\mu} + \frac{8}{9}L_m^3 + \frac{40}{9}L_m^2 \\
&+ \bigg(\frac{448}{27} - \frac{4\pi^2}{9} \bigg)L_m + \frac{656}{27} - \frac{10\pi^2}{27} - \frac{56\zeta_3}{9} \bigg] \\
&+ \frac{16}{9\pi p_T^2} \bigg[2\Big[-5 + 12\hat{m}^2 + 3c(1 - 2\hat{m}^2)\ln\frac{c+1}{c-1} \Big] \ln\frac{\nu}{m} \\
&+ 3c(1 - 2\hat{m}^2)\bigg[\mathrm{Li}_2\bigg(\frac{(c-1)^2}{(c+1)^2} \bigg) + 2\ln\frac{c+1}{c-1}\ln\frac{\hat{m}(c+1)}{2c} - \frac{\pi^2}{6} \bigg] \\
&+ c(5 - 16\hat{m}^2)\ln\frac{c+1}{c-1} + 8\hat{m}^2 \bigg] \bigg\} + \frac{4}{3}L_m\, S^{(1)}(\vec{p}_T, \mu, \nu), \qquad (C.30)
\end{aligned}
$$

where $\hat{m} = m/p_T$ and $c = \sqrt{1 + 4\hat{m}^2}$ as in Eq. (C.16) and the one-loop soft function $S^{(1)}$ given in Eq. (B.13).

The massive quark contributions to the anomalous dimensions of the soft function are

$$\gamma_S^{(2,h)}(\vec{p}_T, \mu, \nu) = C_F \left(\frac{320}{9} \ln \frac{\nu}{\mu} - \frac{448}{27} + \frac{8\pi^2}{9} \right),$$

$$\gamma_{\nu,S}^{(2,h)}(\vec{p}_T, m, \mu) = C_F \left\{ \frac{32}{3} L_m \mathcal{L}_0(\vec{p}_T, \mu) + \delta^{(2)}(\vec{p}_T) \left(-\frac{16}{3} L_m^2 - \frac{160}{9} L_m - \frac{448}{27} \right) \right.$$

$$\left. + \frac{32}{9\pi p_T^2} \left[-5 + 12\hat{m}^2 + 3c(1 - 2\hat{m}^2) \ln \frac{c+1}{c-1} \right] \right\}. \tag{C.31}$$

The μ anomalous dimension here is the same as for an additional massless flavor, $\gamma_S^{(2,h)} = \gamma_S^{(2,l)}$ [see Eq. (B.15)]. The rapidity anomalous dimension is explicitly mass dependent and only reduces to the result for a massless flavor in the limit $m \ll p_T$.

C.4.2 Csoft function

The csoft function is a matching coefficient between an eikonal matrix element defined in Eq. (2.82) in the $n_l + 1$ and n_l flavor theories as in Eq. (D.50). The relevant diagrams at $\mathcal{O}(\alpha_s^2)$ are shown in Fig. C.3 and are calculated in Sec. D.5. The result is given by

$$\mathcal{S}_c(\ell, m, \mu, \nu) = \delta(\ell) + \frac{\alpha_s^2 C_F T_F}{16\pi^2} \left\{ \frac{\nu}{\mu^2} \mathcal{L}_0 \left(\frac{\ell \nu}{\mu^2} \right) \left(\frac{8}{3} L_m^2 + \frac{80}{9} L_m + \frac{224}{27} \right) \right. \tag{C.32}$$

$$\left. + \delta(\ell) \left[-\frac{8}{9} L_m^3 - \frac{40}{9} L_m^2 + \left(-\frac{448}{27} + \frac{4\pi^2}{9} \right) L_m - \frac{656}{27} + \frac{10\pi^2}{27} + \frac{56\zeta_3}{9} \right] \right\} + \mathcal{O}(\alpha_s^3).$$

Because there are no corrections at $\mathcal{O}(\alpha_s)$, the specification of the flavor scheme of α_s is not relevant at order $\mathcal{O}(\alpha_s^2)$. We can see that with the scale choices $\mu \sim m$ and $\nu \sim \mu^2/\ell \sim m^2/\mathcal{T}$ all large logarithms (including the implicit one inside the plus distribution) are minimized. The μ anomalous dimensions of the csoft matching function is given by

$$\gamma_{\mathcal{S}_c}(\ell, m, \mu, \nu) = \frac{\alpha_s^2 C_F T_F}{16\pi^2} \left[-\frac{\nu}{\mu^2} \mathcal{L}_0 \left(\frac{\ell \nu}{\mu^2} \right) \left(\frac{32}{3} L_m + \frac{160}{9} \right) + \delta(\ell) \left(\frac{448}{27} - \frac{8\pi^2}{9} \right) \right] + \mathcal{O}(\alpha_s^3). \tag{C.33}$$

The ν anomalous dimension is the same as for the collinear mass mode function in Eq. (C.11), $\gamma_{\nu,\mathcal{S}_c} = \gamma_{\nu,H_c}$.

C.4.3 (Beam) thrust soft function

The secondary massive quark corrections to the (beam) thrust soft function at $\mathcal{O}(\alpha_s^2)$ were calculated in Ref. [95] and are given by

$$S^{(2,h)}(\ell, m, \mu) = C_F \left\{ \frac{1}{\mu} \mathcal{L}_0 \left(\frac{\ell}{\mu} \right) \left(\frac{16}{3} L_m^2 + \frac{160}{9} L_m + \frac{448}{27} \right) \right.$$

$$+ \delta(\ell) \left[-\frac{8}{9} L_m^3 - \frac{40}{9} L_m^2 + \left(-\frac{448}{27} + \frac{4\pi^2}{9} \right) L_m - \frac{656}{27} + \frac{10\pi^2}{27} + \frac{56}{9} \zeta_3 \right]$$

$$+ \theta(\ell - 2m) \frac{1}{\ell} \left[\frac{64}{3} \text{Li}_2 \left(\frac{w-1}{w+1} \right) + \frac{16}{3} \ln^2 \frac{1-w}{1+w} - \frac{64}{3} \ln \frac{1-w}{1+w} \ln \hat{m}_\ell \right.$$

$$\left. - \frac{160}{9} \ln \frac{1-w}{1+w} - w \left(\frac{896}{27} + \frac{256}{27} \hat{m}_\ell^2 \right) + \frac{16\pi^2}{9} \right] \right\}$$

$$+ \Delta S_\tau(\ell, m) + \frac{4}{3} L_m S^{(1)}(\ell, \mu), \tag{C.34}$$

where

$$\hat{m}_\ell \equiv \frac{m}{\ell}\,, \qquad w = \sqrt{1 - 4\hat{m}_\ell^2}\,, \tag{C.35}$$

and the one-loop soft function $S^{(1)}$ is given in Eq. (B.16). The term $\Delta S_\tau(\ell, m)$ contains the correction from two real final-state emissions entering two opposite hemispheres, which vanishes both for $\ell \ll m$ and $m \ll \ell$ and is currently only known numerically. The integral expression for this numerically small contribution is given in Eq. (61) of Ref. [95], and a precise parametrization can be found in Ref. [12].

The massive quark contribution to the anomalous dimension is the same as for a massless flavor, $\gamma_S^{(2,h)}(\ell, \mu) = \gamma_S^{(2,l)}(\ell, \mu)$, given in Eq. (B.18).

Appendix D

Calculations of massive quark corrections

We calculate the quark mass dependent beam and soft functions for primary and secondary contributions at one and two loops, respectively. The final renormalized results are given and discussed in Sec. C. For the computation of the massive quark corrections we use the Feynman rules determined from the massive quark SCET Lagrangian [18, 221, 222]. First, we calculate the massive quark beam function in Sec. D.1, before discussing the computation of the secondary massive quark corrections for the massless quark beam and soft functions in secs. D.2 – D.5. All computations are carried out in Feynman gauge.

D.1 Massive quark beam function at $\mathcal{O}(\alpha_s)$

The massive quark beam function operator for a measurement function $\mathcal{M}$ is defined as (see e.g. Refs. [13, 41, 85, 223])

$$\mathcal{O}_Q(\{\mathcal{M}\}, \omega, m) = \overline{\chi}_{n,m}(0)\mathcal{M}(\mathcal{P}^\mu, \hat{p}^+)\frac{\slashed{\bar{n}}}{2}\left[\delta(\omega - \overline{\mathcal{P}}_n)\chi_{n,m}(0)\right], \tag{D.1}$$

where $\chi_{n,m}$ indicates a massive collinear quark field, $\mathcal{P}^\mu$ is the label momentum operator, and $\hat{p}^+$ extracts the residual momentum component $n \cdot k$. For the transverse momentum dependent (TMD), virtuality dependent, and fully differential case the measurement functions are

$$\mathcal{M}_\perp = \delta^{(2)}(\vec{p}_T - \vec{\mathcal{P}}_\perp), \quad \mathcal{M}_{p^+} = \delta(t - \omega\hat{p}^+), \quad \mathcal{M}_{\perp,p^+} = \delta^{(2)}(\vec{p}_T - \vec{\mathcal{P}}_\perp)\,\delta(t - \omega\hat{p}^+). \tag{D.2}$$

For convenience we discuss also the fully differential case here, from which the other two cases can be obtained by an integration over the respective other variable. The beam functions are proton matrix elements of the operators $\mathcal{O}_Q$. To compute the (perturbative) matching coefficients onto the PDFs, we take matrix elements with partonic states, denoting e.g.

$$B_{Qg}\left(\{\mathcal{M}\}, m, z = \frac{\omega}{p^-}\right) \equiv \langle g_n(p)|\mathcal{O}_Q(\{\mathcal{M}\}, \omega, m)|g_n(p)\rangle, \tag{D.3}$$

for an initial collinear gluon state with momentum $p^\mu = p^- n^\mu/2$.

At $\mathcal{O}(\alpha_s)$ the only contribution to the massive quark beam function originates from an initial collinear gluon splitting into a heavy quark-antiquark pair. The corresponding diagram is given in Fig. D.1. The kinematics of the on-shell final state is fully constrained at one loop, so that the diagram can be
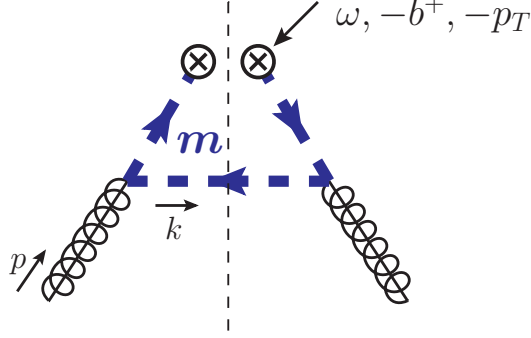
Figure D.1: One-loop diagram contributing to the massive quark beam function.

evaluated without performing any integration. For the fully differential case we obtain

$$
\begin{aligned}
B_{Qg}(t, \vec{p}_T, m, z)\big|_{\mathcal{O}(\alpha_s)} &= 8\pi\alpha_s T_F\, \theta(\omega)\, \theta(t) \int \frac{\mathrm{d}^4 k}{(2\pi)^4} \frac{|\vec{k}_\perp|^2 \left[(p^-)^2 - 2(p^- - k^-)k^-\right] + m^2(p^-)^2}{(p^-)^2(k^+)^2 k^-} \\
&\quad \times \delta(\omega - p^- + k^-)\, \delta(b^+ - k^+)\, \delta^{(2)}(\vec{p}_T - \vec{k}_\perp)\, 2\pi\delta(k^2 - m^2) \\
&= \frac{\alpha_s T_F}{4\pi^2}\, \theta(z)\, \theta(t)\, \delta\!\left(p_T^2 - \frac{t(1-z)}{z} + m^2\right) \frac{2}{t}\left(P_{qg}(z) + \frac{2m^2 z^2}{t}\right) \\
&= \frac{\alpha_s}{4\pi}\, \mathcal{I}_{Qg}^{(1)}(t, \vec{p}_T, m, z)\,,
\end{aligned}
\tag{D.4}
$$

where $P_{qg}(z) = z^2 + (1-z)^2$ is the leading-order gluon-quark splitting function. The correction B_{Qg} at $\mathcal{O}(\alpha_s)$ is UV and IR finite. It corresponds directly to the matching coefficient $\mathcal{I}_{Qg}^{(1)}$, given as the one-loop coefficient in an expansion in terms of α_s as in Eq. (2.33). The matching coefficients for the TMD and virtuality-dependent beam functions can be obtained here by a trivial integration of this result,

$$
\mathcal{I}_{Qg}^{(1)}(\vec{p}_T, m, z) = \int \mathrm{d}t\, \mathcal{I}_{Qg}^{(1)}(t, \vec{p}_T, m, z)\,, \qquad \mathcal{I}_{Qg}^{(1)}(t, m, z) = \int \mathrm{d}^2 p_T\, \mathcal{I}_{Qg}^{(1)}(t, \vec{p}_T, m, z)\,,
\tag{D.5}
$$

which yields the results in Eqs. (C.13) and (C.19). Note that in general, this integration has to be performed for the *bare* result with the full dependence on the UV and rapidity regulator. However, in this case all matrix elements are finite and do not require any renormalization at this order.

D.2 Dispersive technique for secondary massive quark corrections

For observables where only the sum over the final-state hadronic momenta enters the measurement, one can use dispersion relations to obtain the results for secondary massive quark radiation at $\mathcal{O}(\alpha_s^2)$ from the corresponding results for "massive gluon" radiation at $\mathcal{O}(\alpha_s)$. This has been discussed in detail in Ref. [12]. The key relation is that the insertion of a vacuum polarization function for massive quarks $\Pi_{\mu\nu}(m^2, p^2)$ between two gluon propagators can be written as

$$
\begin{aligned}
\frac{-i\, g^{\mu\rho}}{p^2 + i\epsilon}\, \Pi_{\rho\sigma}(m^2, p^2)\, \frac{-i\, g^{\sigma\nu}}{p^2 + i\epsilon} &= \frac{1}{\pi} \int \frac{\mathrm{d}M^2}{M^2}\, \frac{-i\left(g^{\mu\nu} - \frac{p^\mu p^\nu}{p^2}\right)}{p^2 - M^2 + i\epsilon}\, \mathrm{Im}\big[\Pi(m^2, M^2)\big] \\
&\quad - \frac{-i\left(g^{\mu\nu} - \frac{p^\mu p^\nu}{p^2}\right)}{p^2 + i\epsilon}\, \Pi(m^2, 0)\,.
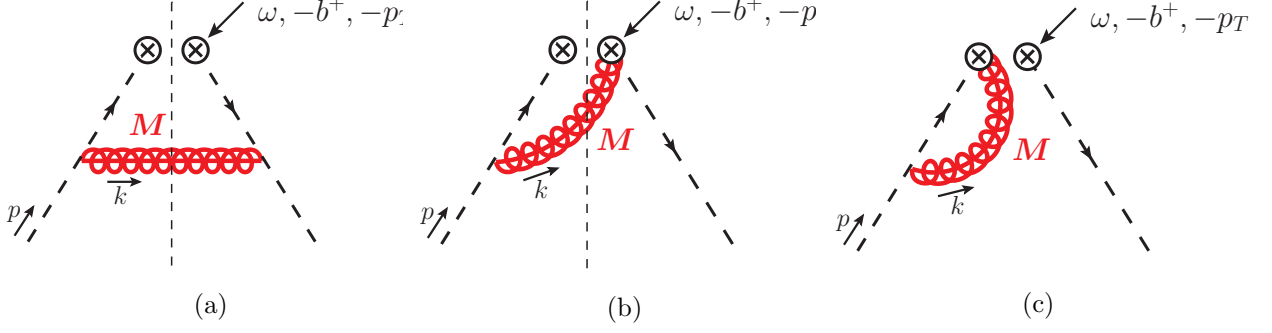\end{aligned}
\tag{D.6}
$$

Figure D.2: Light-quark beam function diagrams for massive gluon radiation at one loop. In addition, also the wave function renormalization correction and the mirror diagrams for (b) and (c) have to be included in the calculation.

The first term contains a gluon propagator with effective mass M and the absorptive part of the vacuum polarization function, which reads in $d = 4 - 2\epsilon$ dimensions

$$\mathrm{Im}\big[\Pi(m^2, p^2)\big] = \theta(p^2 - 4m^2)\, \frac{\alpha_s T_F}{4\pi}\, \frac{(4\mu^2 e^{\gamma_E})^\epsilon \pi^{3/2}}{\Gamma(\frac{5}{2} - \epsilon)}\Big(1 - \epsilon + \frac{2m^2}{p^2}\Big)(p^2)^{-\epsilon}\Big(1 - \frac{4m^2}{p^2}\Big)^{1/2 - \epsilon}. \quad \text{(D.7)}$$

To obtain the first term on the right-hand side in Eq. (D.6) the vacuum polarization function (and thus the strong coupling) was renormalized in the on-shell scheme with respect to the massive quark, i.e., with n_l active quark flavors. The second term in Eq. (D.6) translates back to an unrenormalized strong coupling and consists of a massless gluon propagator and the $\mathcal{O}(\alpha_s)$ vacuum polarization function at zero momentum transfer, which is given by

$$\Pi(m^2, 0) = \frac{\alpha_s T_F}{4\pi}\, \frac{4}{3}\, \Gamma(\epsilon)\Big(\frac{\mu^2 e^{\gamma_E}}{m^2}\Big)^\epsilon \equiv \frac{\alpha_s T_F}{4\pi}\, \Pi^{(1)}(m^2, 0)\,. \quad \text{(D.8)}$$

In the following we will first carry out the computation of the beam and soft functions at $\mathcal{O}(\alpha_s)$ for the radiation of a "massive gluon" and in a second step use the relation in Eq. (D.6) to obtain the associated results for massive quarks at $\mathcal{O}(\alpha_s^2 C_F T_F)$. In our calculations we drop the contributions from the terms proportional to $p^\mu p^\nu$, which vanish in total due to gauge invariance.

D.3 Secondary mass effects in light-quark beam functions

We compute the massive quark corrections to the TMD and virtuality-dependent light-quark beam function at $\mathcal{O}(\alpha_s^2 C_F T_F)$ starting with the massive gluon case at $\mathcal{O}(\alpha_s)$. Only the contributions to the matching coefficient $\mathcal{I}_{qq}$ are nontrivial, so we consider only diagrams with a quark in the initial state.

D.3.1 Quark beam function with a massive gluon at $\mathcal{O}(\alpha_s)$

Contributions to the fully-differential beam function   As in Sec. D.1 we start also here with the computation of the corrections for the fully-differential beam function. The contributing one-loop diagrams to the matrix element B_{qq} with massless quarks in the initial state, defined in analogy to Eq. (D.3), are displayed in Fig. D.2. They consist of a purely virtual and a real-radiation part,

$$B_{qq}^{(1,\text{bare})}(t, \vec{p}_T, M, \omega, z) = \delta(1 - z)\, \delta(t)\, \delta^{(2)}(\vec{p}_T)\, B_{qq,\text{virt}}^{(1,\text{bare})}(M, \omega) + B_{qq,\text{real}}^{(1,\text{bare})}(t, \vec{p}_T, M, \omega, z)\,. \quad \text{(D.9)}$$

The virtual massive gluon contributions in Fig. D.2c are the same as for other collinear quark operators like the current or the PDF and have been computed e.g. in Ref. [41]. Including the wave function renormalization diagrams the d-dimensional result reads [2]

$$B_{qq,\text{virt}}^{(1,\text{bare})}(M,\omega) = C_F \left(\frac{\mu^2 e^{\gamma_E}}{M^2} \right)^\epsilon \Gamma(\epsilon) \left\{ \frac{4}{\eta} + 4\ln\frac{\nu}{\omega} + 4H_{1-\epsilon} - \frac{2(1-\epsilon)}{2-\epsilon} + \mathcal{O}(\eta) \right\}, \qquad (\text{D}.10)$$

where $H_\alpha = \psi(1+\alpha) + \gamma_E$ is the Harmonic number. Here the rapidity divergences have been regulated using the symmetric η regulator acting on the Wilson lines [40,41], while UV divergences are regulated with dimensional regularization as usual. Furthermore, the gluon mass provides an IR cutoff.

The real radiation contributions in Figs. D.2a and D.2b can be easily evaluated, since all momentum components are fully determined by the measurement. For the first diagram we get

$$\begin{aligned}
B^{(a)} &= 8\pi\alpha_s C_F p^- \theta(\omega)\,\theta(t) \int \frac{\mathrm{d}^4 k}{(2\pi)^4} \frac{|\vec{k}_\perp|^2}{[(p-k)^2 + i\epsilon]^2} \delta(\omega - p^- + k^-)\,\delta(t - \omega k^+) \\
&\qquad \times \delta^{(2)}(\vec{p}_T - \vec{k}_\perp)\,2\pi\delta(k^2 - M^2) \\
&= \frac{\alpha_s C_F}{4\pi^2}\,\theta(z)\,\theta(t)\,\delta\!\left(p_T^2 - \frac{t(1-z)}{z} + M^2 \right) \frac{2\big(t(1-z) - zM^2\big)}{(t - zM^2)^2}\,. \qquad (\text{D}.11)
\end{aligned}$$

Since UV divergences do not appear for the real radiation corrections and the gluon mass regulates all IR divergences we do not need to employ dimensional regularization here. The second diagram in Fig. D.2b yields

$$\begin{aligned}
B^{(b)} &= -8\pi\alpha_s C_F p^- \theta(\omega)\,\theta(t) \int \frac{\mathrm{d}^4 k}{(2\pi)^4} \frac{(p^- - k^-)}{(p-k)^2 + i\epsilon} \frac{\nu^\eta}{(k^-)^{1+\eta}} \delta(\omega - p^- + k^-)\,\delta(t - \omega k^+) \\
&\qquad \times \delta^{(2)}(\vec{p}_T - \vec{k}_\perp)\,2\pi\delta(k^2 - M^2) \\
&= \frac{\alpha_s C_F}{4\pi^2}\,\theta(z)\,\theta(t)\,\delta\!\left(p_T^2 - \frac{t(1-z)}{z} + M^2 \right) \left(\frac{\nu}{\omega} \right)^\eta \frac{2z^{1-\eta}}{(t - zM^2)(1-z)^\eta}\,. \qquad (\text{D}.12)
\end{aligned}$$

While the fully-differential quark beam function itself does not contain any rapidity divergences, we have included here the η regulator, since we will use this result to obtain the TMD beam function by integrating over the virtuality, which results in rapidity divergences for this real radiation correction. The full real radiation contributions at one loop yield

$$\begin{aligned}
\frac{\alpha_s}{4\pi} B_{qq,\text{real}}^{(1,\text{bare})}(t,\vec{p}_T,M,\omega,z) &= B^{(a)} + 2B^{(b)} \\
&= \frac{\alpha_s C_F}{4\pi} \frac{1}{\pi}\,\theta(z)\,\theta(t)\,\delta\!\left(p_T^2 - \frac{t(1-z)}{z} + M^2 \right) \\
&\quad \times \frac{2}{t - zM^2} \left[\left(\frac{\nu}{\omega} \right)^\eta \frac{2z^{1-\eta}}{(1-z)^\eta} + \frac{t(1-z) - zM^2}{t - zM^2} \right]. \qquad (\text{D}.13)
\end{aligned}$$

For both virtual and real radiation corrections all soft-bin subtractions are parametrically power suppressed or scaleless and therefore do not contribute.

Contributions to the TMD beam function   The corrections for the TMD beam function with a massive gluon can be obtained by integrating the fully-differential beam function in Eq. (D.9) over the virtuality t. We write them again as

$$B_{qq}^{(1,\text{bare})}(\vec{p}_T,M,z) = \delta(1-z)\,\delta^{(2)}(\vec{p}_T)\,B_{qq,\text{virt}}^{(1,\text{bare})}(M,\omega) + B_{qq,\text{real}}^{(1,\text{bare})}(\vec{p}_T,M,\omega,z)\,, \qquad (\text{D}.14)$$

where $B_{qq,\mathrm{virt}}^{(1,\mathrm{bare})}$ is given in Eq. (D.10) and

$$
\begin{aligned}
B_{qq,\mathrm{real}}^{(1,\mathrm{bare})}(\vec{p}_T, M, \omega, z) &= \int \mathrm{d}t \, B_{qq,\mathrm{real}}^{(1,\mathrm{bare})}(t, \vec{p}_T, M, z) \\
&= C_F \, \theta(z) \, \theta(1-z) \, \frac{1}{\pi} \frac{2}{p_T^2 + zM^2} \left[\frac{p_T^2(1-z)}{p_T^2 + zM^2} + \frac{2z^{1-\eta}}{(1-z)^{1+\eta}} \left(\frac{\nu}{\omega} \right)^{\eta} \right] .
\end{aligned}
\tag{D.15}
$$

Here it is necessary to keep a nonvanishing value for η in the second term to regularize the rapidity divergence for $z \to 1$. Expanding for $\eta \to 0$ we get

$$
\begin{aligned}
B_{qq,\mathrm{real}}^{(1,\mathrm{bare})}(\vec{p}_T, M, \omega, z) &= C_F \, \theta(z) \, \frac{1}{\pi} \left\{ \frac{4}{p_T^2 + M^2} \left[-\delta(1-z) \left(\frac{1}{\eta} + \ln \frac{\nu}{\omega} \right) + \mathcal{L}_0(1-z) \right] \right. \\
&\left. + \theta(1-z) \frac{2p_T^2}{p_T^2 + zM^2} \left[\frac{1-z}{p_T^2 + zM^2} - \frac{2}{p_T^2 + M^2} \right] \right\} + \mathcal{O}(\eta) .
\end{aligned}
\tag{D.16}
$$

Contributions to the virtuality-dependent beam function The virtuality-dependent beam function with a massive gluon can be obtained by integrating the results for the fully-differential beam function over $\vec{p}_T$. We decompose the corrections again into a virtual and real radiation part,

$$
B_{qq}^{(1,\mathrm{bare})}(t, M, z) = \delta(1-z) \, \delta(t) \, B_{qq,\mathrm{virt}}^{(1,\mathrm{bare})}(M, \omega) + B_{qq,\mathrm{real}}^{(1,\mathrm{bare})}(t, M, z) ,
\tag{D.17}
$$

where $B_{qq,\mathrm{virt}}^{(1,\mathrm{bare})}$ is given in Eq. (D.10) and

$$
\begin{aligned}
B_{qq,\mathrm{real}}^{(1)}(t, M, z) &= \int \mathrm{d}^2 \vec{p}_T \, B_{qq,\mathrm{real}}^{(1,\mathrm{bare})}(t, \vec{p}_T, M, \omega, z) \\
&= C_F \, \theta(z) \, \theta(t) \, \theta\left(\frac{t(1-z)}{z} - M^2 \right) \frac{2}{t - zM^2} \left(\frac{2z}{1-z} + \frac{t(1-z) - zM^2}{t - zM^2} \right) ,
\end{aligned}
\tag{D.18}
$$

with the fully-differential real radiation contributions in Eq. (D.13). Here the η regulator has already been dropped, since for the virtuality-dependent beam function no rapidity divergences arise from the real radiation contributions.

D.3.2 Secondary massive quark effects in the TMD beam function

To obtain the secondary massive quark corrections from the one-loop results with a massive gluon, we first convolve the one-loop results with the imaginary part of the vacuum polarization function according to Eq. (D.6) and define

$$
\frac{\alpha_s T_F}{4\pi} B_{qq,\mathrm{virt}}^{(2,h,\mathrm{bare})}(m, \omega) = \frac{1}{\pi} \int \frac{\mathrm{d}M^2}{M^2} \, \mathrm{Im}\big[\Pi(m^2, M^2)\big] \times B_{qq,\mathrm{virt}}^{(1,\mathrm{bare})}(M, \omega) ,
$$

$$
\frac{\alpha_s T_F}{4\pi} B_{qq,\mathrm{real}}^{(2,h,\mathrm{bare})}(\vec{p}_T, m, \omega, z) = \frac{1}{\pi} \int \frac{\mathrm{d}M^2}{M^2} \, \mathrm{Im}\big[\Pi(m^2, M^2)\big] \times B_{qq,\mathrm{real}}^{(1,\mathrm{bare})}(\vec{p}_T, M, \omega, z) .
\tag{D.19}
$$

The results from these dispersion integrations are

$$
\begin{aligned}
B_{qq,\mathrm{virt}}^{(2,h,\mathrm{bare})}(m,\omega) = C_F &\left\{ \left(\frac{1}{\eta} + \ln\frac{\nu}{\omega}\right)\left[\frac{8}{3\epsilon^2} - \frac{1}{\epsilon}\left(\frac{16}{3}L_m + \frac{40}{9}\right) + \frac{16}{3}L_m^2 + \frac{80}{9}L_m + \frac{224}{27}\right. \right. \\
&\left. + \frac{4\pi^2}{9} + \mathcal{O}(\epsilon)\right] + \frac{2}{\epsilon^2} - \frac{1}{\epsilon}\left(4L_m + \frac{1}{3} + \frac{4\pi^2}{9}\right) + 4L_m^2 + \left(\frac{2}{3} + \frac{8\pi^2}{9}\right)L_m \\
&\left. + \frac{73}{18} + \frac{29\pi^2}{27} - \frac{8\zeta_3}{3}\right\},
\end{aligned}
\tag{D.20}
$$

$$
\begin{aligned}
B_{qq,\mathrm{real}}^{(2,h,\mathrm{bare})}(\vec{p}_T, m, \omega, z) = C_F \frac{1}{\pi p_T^2} &\left\{ \frac{16}{9\eta}\,\delta(1-z)\left[5 - 12\hat{m}^2 - 3c(1-2\hat{m}^2)\ln\left(\frac{c+1}{c-1}\right)\right] \right. \\
&\left. + b_{\mathrm{real}}^{q_T}\left(\frac{m^2}{p_T^2}, z, \frac{\nu}{\omega}\right)\right\},
\end{aligned}
\tag{D.21}
$$

with

$$
\begin{aligned}
b_{\mathrm{real}}^{q_T}\left(\hat{m}^2, z, \frac{\nu}{\omega}\right) = &\,\theta(z)\frac{16}{9}\left\{\left[5 - 12\hat{m}^2 - 3c(1-2\hat{m}^2)\ln\left(\frac{c+1}{c-1}\right)\right] \right. \\
&\times \left(\delta(1-z)\ln\frac{\nu}{\omega} - \mathcal{L}_0(1-z)\right) \\
&+ \theta(1-z)\left[\frac{3}{2d(1-z)}\left[1 + z^2 + 2\hat{m}^2 z(1+z^2) + 4\hat{m}^4 z^2(-5 + 6z - 5z^2)\right]\ln\left(\frac{d+1}{d-1}\right)\right. \\
&\left.\left. - \frac{3c(1-2\hat{m}^2)}{1-z}\ln\left(\frac{c+1}{c-1}\right) + 1 + 4z + 3\hat{m}^2(-4 + z - 5z^2)\right]\right\},
\end{aligned}
\tag{D.22}
$$

and $\hat{m}$, c, d defined in Eq. (C.16). Using Eq. (D.19) entails that the massive quark corrections to the strong coupling are renormalized in the on-shell scheme, i.e., the expansion is in terms of $\alpha_s = \alpha_s^{(n_l)}$. Since the beam function matrix element has to be renormalized entirely in the $n_l + 1$ flavor theory, we need to account for the second term in Eq. (D.6) (which switches back to an unrenormalized α_s) and renormalize the massive quark corrections to the strong coupling in the $\overline{\mathrm{MS}}$ scheme, such that the expansion is in terms of $\alpha_s = \alpha_s^{(n_l+1)}$. The beam function operator is renormalized according to

$$
\mathcal{O}_q^{(\mathrm{bare})}(\vec{p}_T, m, \omega) = \int \mathrm{d}^2 p_T'\, Z_B\left(\vec{p}_T - \vec{p}_T', m, \mu, \frac{\nu}{\omega}\right)\mathcal{O}_q(\vec{p}_T', m, \omega, \mu, \nu),
\tag{D.23}
$$

where the counterterm encodes also the rapidity divergences. This yields for the renormalized matrix element with initial state quarks at $\mathcal{O}(\alpha_s^2 C_F T_F)$ in terms of $\alpha_s = \alpha_s^{(n_l+1)}$

$$
\begin{aligned}
B_{qq}^{(2,h)}\left(\vec{p}_T, m, z, \mu, \frac{\nu}{\omega}\right) = &\,\delta^{(2)}(\vec{p}_T)\,\delta(1-z)\,B_{qq,\mathrm{virt}}^{(2,h,\mathrm{bare})}(m,\omega) + B_{qq,\mathrm{real}}^{(2,h,\mathrm{bare})}(\vec{p}_T, m, \omega, z) \\
&- \left(\Pi^{(1)}(m^2, 0) - \frac{4}{3\epsilon}\right)\underbrace{B_{qq}^{(1,\mathrm{bare})}(\vec{p}_T, \omega, z)}_{= B_{qq}^{(1)}(\vec{p}_T, z, \mu, \frac{\nu}{\omega}) + Z_B^{(1)}(\vec{p}_T, \mu, \frac{\nu}{\omega})\,\delta(1-z)} - \delta(1-z)Z_B^{(2,h)}\left(\vec{p}_T, m, \mu, \frac{\nu}{\omega}\right).
\end{aligned}
\tag{D.24}
$$

where the (bare) vacuum polarization function $\Pi^{(1)}(m^2, 0)$ is given in Eq. (D.8). The one-loop counterterm reads

$$
Z_B^{(1)}\left(\vec{p}_T, \mu, \frac{\nu}{\omega}\right) = C_F\left\{\delta^{(2)}(\vec{p}_T)\left[\frac{1}{\eta}\left(\frac{4}{\epsilon} + \mathcal{O}(\epsilon)\right) + \frac{1}{\epsilon}\left(3 + 4\ln\frac{\nu}{\omega}\right)\right] - \frac{1}{\eta}\left(4 + \mathcal{O}(\epsilon)\right)\mathcal{L}_0(\vec{p}_T, \mu)\right\}.
\tag{D.25}
$$

The two-loop counterterm $Z_B^{(2)}$ absorbs all remaining UV and rapidity divergences in Eq. (D.24) and is given by

$$
Z_B^{(2,h)}\left(\vec{p}_T, m, \mu, \frac{\nu}{\omega}\right) = C_F \left\{ \delta^{(2)}(\vec{p}_T) \left[\frac{1}{\eta}\left(\frac{8}{3\epsilon^2} - \frac{40}{9\epsilon} + \frac{8}{3}L_m^2 + \frac{80}{9}L_m + \frac{224}{27} + \mathcal{O}(\epsilon) \right) \right. \right.
$$
$$
\left. + \frac{1}{\epsilon^2}\left(2 + \frac{8}{3}\ln\frac{\nu}{\omega}\right) - \frac{1}{\epsilon}\left(\frac{1}{3} + \frac{4\pi^2}{9} + \frac{40}{9}\ln\frac{\nu}{\omega}\right) \right] - \frac{1}{\eta}\left(\frac{16}{3}L_m + \mathcal{O}(\epsilon)\right)\mathcal{L}_0(\vec{p}_T, \mu)
$$
$$
\left. + \frac{1}{\eta}\frac{16}{9\pi p_T^2}\left[5 - 12\hat{m}^2 - 3c(1 - 2\hat{m}^2)\ln\frac{c+1}{c-1}\right] \right\}. \tag{D.26}
$$

This yields the anomalous dimensions in Eq. (C.18). The renormalized one-loop partonic beam function $B_{qq}^{(1)}$ still contains IR divergences, so its exact form depends on the choice of the IR regulator.

The beam function matching coefficient $\mathcal{I}_{qq}$ as defined in (2.25) can be now easily obtained. Note that the PDFs are renormalized in an n_l-flavor theory with $\alpha_s = \alpha_s^{(n_l)}$ in contrast to the beam function. Thus, there is a contribution coming from the scheme change of α_s to $n_l + 1$ flavors for the (renormalized) one-loop PDF correction, i.e.

$$
\mathcal{I}_{qq}^{(2,h)}\left(\vec{p}_T, m, z, \mu, \frac{\nu}{\omega}\right) = B_{qq}^{(2,h)}\left(\vec{p}_T, m, z, \mu, \frac{\nu}{\omega}\right) - \delta^{(2)}(\vec{p}_T)\frac{4}{3}L_m f_{qq}^{(1)}(z, \mu)
$$
$$
= \delta^{(2)}(\vec{p}_T)\,\delta(1-z)B_{qq,\text{virt}}^{(2,h,\text{bare})}(m, \omega) + B_{qq,\text{real}}^{(2,h,\text{bare})}(\vec{p}_T, m, \omega, z)
$$
$$
- \delta(1-z)\left[\left(\Pi^{(1)}(m^2, 0) - \frac{4}{3\epsilon}\right)Z_B^{(1)}\left(\vec{p}_T, \mu, \frac{\nu}{\omega}\right) + Z_B^{(2,h)}\left(\vec{p}_T, m, \mu, \frac{\nu}{\omega}\right)\right]
$$
$$
+ \underbrace{\frac{4}{3}L_m\left(B_{qq}^{(1)}\left(\vec{p}_T, z, \mu, \frac{\nu}{\omega}\right) - \delta^{(2)}(\vec{p}_T)f_{qq}^{(1)}(z, \mu)\right)}_{=\mathcal{I}_{qq}^{(1)}(\vec{p}_T, z, \mu, \frac{\nu}{\omega})}. \tag{D.27}
$$

Here the IR divergences cancel between the one-loop beam function and the PDF to give the finite one-loop matching coefficient $\mathcal{I}_{qq}^{(1)}$, which is given in Eq. (B.5). Using Eqs. (D.20), (D.21), (D.25) and (D.26) we obtain the full result for the secondary massive quark corrections to the beam function matching coefficient given in Eq. (C.15).

D.3.3 Secondary massive quark effects in the virtuality-dependent beam function

We proceed with the virtuality-dependent beam function. While the virtual contributions are the same as for the TMD beam function given in Eq. (D.20), the dispersion integration for the real radiation terms yields

$$
\frac{\alpha_s T_F}{4\pi}B_{qq,\text{real}}^{(2,h)}(t, m, z) = \frac{1}{\pi}\int\frac{\mathrm{d}M^2}{M^2}\,\text{Im}\left[\Pi(m^2, M^2)\right] \times B_{qq,\text{real}}^{(1)}(t, M, z)
$$
$$
= \frac{\alpha_s T_F}{4\pi}\frac{C_F}{t}\,b_{\text{real}}^{\mathcal{T}}\left(\frac{m^2}{t}, z\right), \tag{D.28}
$$

with

$$
b_{\text{real}}^{\mathcal{T}}(\hat{m}^2, z) = \theta(z)\,\theta(v)\frac{8}{9(1-z)}\left\{ -\frac{3}{u}\ln\frac{u-v}{u+v}\left[1 + z^2 - 2\hat{m}_t^2 z(1+z^2) - 4\hat{m}_t^4 z^2(2-3z+5z^2)\right]\right.
$$
$$
\left. - 2v\left[4 - 3z + 4z^2 + \frac{z(11 - 21z + 29z^2 - 15z^3)}{1-z}\,\hat{m}_t^2\right]\right\}, \tag{D.29}
$$

and $\hat{m}_t$, u, v as in Eq. (C.21).

To obtain the quark mass dependent matching coefficient $\mathcal{I}_{qq}^{(2,h)}$ we carry out our calculation using a gluon mass $\Lambda \ll \sqrt{QT} \sim m$ as IR regulator. While the theory with $n_l + 1$ flavors (i.e. above the mass scale) contains collinear modes, the theory with n_l flavors (i.e. below the mass scale) contains collinear and csoft modes like in the mode setup of Sec. 2.2.3. The matching relation reads

$$\mathscr{B}_{qq}^{(n_l+1)}\left(t, m, z, \mu, \frac{\nu}{\omega}\right) = \int d\ell\, \mathcal{I}_{qq}\left(t - \omega\ell, m, z, \mu, \frac{\nu}{\omega}\right) \otimes_z f_{qq}^{(n_l)}(z, \mu)\, \mathscr{S}_c^{(n_l)}(\ell, \mu, \nu)\,, \tag{D.30}$$

where $\mathscr{B}_{qq}^{(n_l+1)}$ corresponds to the pure collinear matrix element and $\mathscr{S}_c^{(n_l)}$ represents the csoft matrix element.

In close analogy to Eq. (D.24) the renormalized collinear matrix element $\mathscr{B}_{qq}^{(n_l+1)}$ is given at $\mathcal{O}(\alpha_s^2 C_F T_F)$ by

$$\mathscr{B}_{qq}^{(2,h)}\left(t, m, z, \mu, \frac{\nu}{\omega}\right) = \delta(t)\,\delta(1-z)\, B_{qq,\text{virt}}^{(2,h,\text{bare})}(m, \omega) + B_{qq,\text{real}}^{(2,h)}(t, m, z) \tag{D.31}$$

$$- \left(\Pi^{(1)}(m^2, 0) - \frac{4}{3\epsilon}\right) \underbrace{B_{qq}^{(1,\text{bare})}(t, z)}_{= \mathscr{B}_{qq}^{(1)}(t, z, \mu, \frac{\nu}{\omega}) + Z_{\mathscr{B}}^{(1)}(t, \mu, \frac{\nu}{\omega})\,\delta(1-z)} - \delta(1-z) Z_{\mathscr{B}}^{(2,h)}\left(t, m, \mu, \frac{\nu}{\omega}\right)\,.$$

To separate UV, rapidity, and IR divergences properly from each other, we also employ an IR regulator (here a gluon mass Λ) for the one-loop expressions, and at this stage the renormalized matrix elements and the counterterms still depend on this IR regulator. The matching coefficient $\mathcal{I}_{qq}$ can now be calculated as (in an expansion in terms of $\alpha_s^{(n_l+1)}$)

$$\mathcal{I}_{qq}^{(2,h)}\left(t, m, z, \mu, \frac{\nu}{\omega}\right) = \mathscr{B}_{qq}^{(2,h)}\left(t, m, z, \mu, \frac{\nu}{\omega}\right) - \frac{4}{3} L_m \left[\delta(t) f_{qq}^{(1)}(z, \mu) + \delta(1-z)\frac{1}{\omega}\mathscr{S}_c^{(1)}\left(\frac{t}{\omega}, \mu, \nu\right)\right]$$

$$= \delta(t)\delta(1-z) B_{qq,\text{virt}}^{(2,h,\text{bare})}(m, \omega) + B_{qq,\text{real}}^{(2,h)}(t, m, z) - Z_{\mathscr{B}}^{(2,h)}\left(t, m, \mu, \frac{\nu}{\omega}\right)\delta(1-z)$$

$$- \left(\Pi^{(1)}(m^2, 0) - \frac{4}{3\epsilon}\right) Z_{\mathscr{B}}^{(1)}\left(t, \mu, \frac{\nu}{\omega}\right)\delta(1-z)$$

$$+ \frac{4}{3} L_m \underbrace{\left[\mathscr{B}_{qq}^{(1)}(t, z, \mu) - \delta(t) f_{qq}^{(1)}(z, \mu) - \delta(1-z)\frac{1}{\omega}\mathscr{S}_c^{(1)}\left(\frac{t}{\omega}, \mu, \nu\right)\right]}_{= \mathcal{I}_{qq}^{(1)}(t, z, \mu)}\,. \tag{D.32}$$

Here the IR divergences cancel between the one-loop beam function, the PDF, and the csoft matrix element and yield the finite one-loop matching coefficient $\mathcal{I}_{qq}^{(1)}$ given in Eq. (B.9). The counterterm $Z_{\mathscr{B}}$ is defined via

$$\mathscr{B}_{qq}^{(\text{bare})}(t, m, z) = \int dt'\, Z_{\mathscr{B}}^{(n_l+1)}\left(t - t', m, \mu, \frac{\nu}{\omega}\right) \mathscr{B}_{qq}^{(n_l+1)}\left(t', m, z, \mu, \frac{\nu}{\omega}\right)\,. \tag{D.33}$$

Using the results in Eqs. (D.17) and (D.10) for a massive gluon gives the associated expression for $Z_{\mathscr{B}}^{(1)}$ (expanded in η and ϵ)

$$Z_{\mathscr{B}}^{(1)}\left(t, \mu, \frac{\nu}{\omega}\right) = C_F\, \delta(t) \left\{\frac{4}{\eta}\left[\frac{1}{\epsilon} - \ln\frac{\Lambda^2}{\mu^2} + \mathcal{O}(\epsilon)\right] + \frac{1}{\epsilon}\left[4\ln\frac{\nu}{\omega} + 3\right]\right\}\,. \tag{D.34}$$

The two-loop counterterm $Z_{\mathscr{B}}^{(2,h)}$ cancels all divergences in Eq. (D.32) and reads[1]

$$Z_{\mathscr{B}}^{(2,h)}\left(t, m, \mu, \frac{\nu}{\omega}\right) = C_F\, \delta(t) \left\{\frac{1}{\eta}\left(\frac{8}{3\epsilon^2} - \frac{40}{9\epsilon} - \frac{16}{3}L_m \ln\frac{\Lambda^2}{\mu^2} + \frac{8}{3}L_m^2 + \frac{80}{9}L_m + \frac{224}{27} + \mathcal{O}(\epsilon)\right)\right.$$

$$\left. + \frac{1}{\epsilon^2}\left(\frac{8}{3}\ln\frac{\nu}{\omega} + 2\right) - \frac{1}{\epsilon}\left(\frac{40}{9}\ln\frac{\nu}{\omega} + \frac{1}{3} + \frac{4\pi^2}{9}\right)\right\}\,. \tag{D.35}$$

---

[1] While the $1/\eta$-divergences in the counterterm of the beam function matrix element still contain IR sensitivity, this also happens for the counterterm of the csoft matrix element in Eq. (D.30), such that the resulting rapidity anomalous dimension for the running at the boundary between the $n_l + 1$ and n_l theory is IR finite.
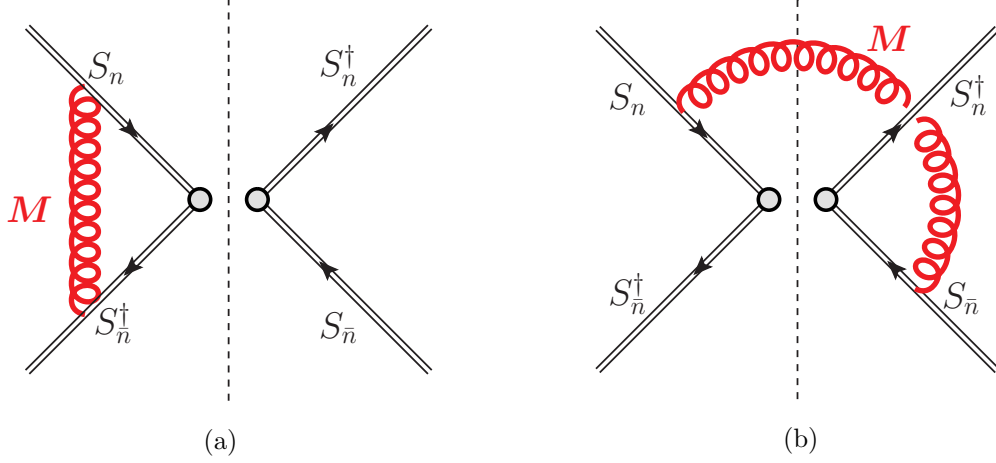
Figure D.3: Soft function corrections for a massive gluon at one-loop. The associated mirror diagrams need to be included in addition.

Using Eqs. (D.10), (D.28), (D.34), (D.35) and (B.9) in Eq. (D.32) we obtain the full two-loop result for the matching coefficient in Eq. (C.20).

D.4 Secondary mass effects in the TMD soft function

The TMD soft function is defined as

$$S(\vec{p}_T) = \frac{1}{N_c} \operatorname{tr} \left\langle 0 \left| \overline{\mathrm{T}} \left[S_n^\dagger(0) S_{\bar{n}}(0) \right] \delta^{(2)}(\vec{p}_T - \vec{\mathcal{P}}_\perp) \mathrm{T} \left[S_{\bar{n}}^\dagger(0) S_n(0) \right] \right| 0 \right\rangle ,$$ (D.36)

with the soft Wilson line S_n given by [41]

$$S_n = \sum_{\text{perms}} \exp \left[-\frac{g}{n \cdot \mathcal{P}} \frac{\nu^{\eta/2}}{|2\mathcal{P}_3|^{\eta/2}} \, n \cdot A_s \right] ,$$ (D.37)

and in analogy for the others. Again we will first calculate the one-loop corrections to the soft function with a massive gluon, which is used in a second step to obtain the corrections from secondary massive quarks at $\mathcal{O}(\alpha_s^2 C_F T_F)$.

D.4.1 TMD soft function with a massive gluon at $\mathcal{O}(\alpha_s)$

We decompose the soft function with a massive gluon at one loop in terms of virtual and real radiation corrections,

$$S^{(1)}(\vec{p}_T, M, \mu, \nu) = \delta^{(2)}(\vec{p}_T) \, S^{(1)}_{\text{virt}}(M, \mu, \nu) + S^{(1)}_{\text{real}}(\vec{p}_T, M, \nu) .$$ (D.38)

The virtual contributions from the diagram in Fig. D.3a (and its mirror diagram) are the same as for the Sudakov form factor computed in Ref. [41] and yield

$$S^{(1,\text{bare})}_{\text{virt}}(M) = C_F \left(\frac{\mu^2 e^{\gamma_E}}{M^2} \right)^\epsilon \Gamma(\epsilon) \left[-\frac{8}{\eta} - 8 \ln \frac{\nu}{M} - 4 H_{\epsilon-1} \right] + \mathcal{O}(\eta) .$$ (D.39)

203

The UV-finite and IR-finite real radiation diagram in Fig. D.3b gives

$$S^{(b)} = 8\pi\alpha_s C_F \int \frac{\mathrm{d}^4 k}{(2\pi)^4} \frac{1}{k^+ k^-} \frac{\nu^\eta}{|k^+ - k^-|^\eta} \delta^{(2)}(\vec{p}_T - \vec{k}_\perp) 2\pi\delta(k^2 - M^2)$$

$$= \frac{\alpha_s C_F}{4\pi} \frac{2\,\Gamma(\frac{\eta}{2})\Gamma(\frac{1-\eta}{2})}{\pi^{\frac{3}{2}}(p_T^2 + M^2)} \left(\frac{\nu}{2\sqrt{p_T^2 + M^2}}\right)^\eta . \tag{D.40}$$

After expanding in η and adding the mirror diagram, the real radiation contribution to the TMD soft function at one loop then reads

$$\frac{\alpha_s}{4\pi} S_{\text{real}}^{(1,\text{bare})}(\vec{p}_T, M) = 2S^{(b)} = \frac{\alpha_s C_F}{4\pi} \frac{4}{\pi(p_T^2 + M^2)} \left[\frac{2}{\eta} + \ln\left(\frac{\nu^2}{p_T^2 + M^2}\right)\right] + \mathcal{O}(\eta) . \tag{D.41}$$

D.4.2 Secondary corrections at $\mathcal{O}(\alpha_s^2 C_F T_F)$

To obtain the secondary massive quark corrections from the one-loop results with a massive gluon, we first convolve the one-loop results with the imaginary part of the vacuum polarization function,

$$\frac{\alpha_s T_F}{4\pi} S_{\text{virt}}^{(2,h,\text{bare})}(m) = \frac{1}{\pi} \int \frac{\mathrm{d}M^2}{M^2} \,\text{Im}\big[\Pi(m^2, M^2)\big] \times S_{\text{virt}}^{(1,\text{bare})}(M) ,$$

$$\frac{\alpha_s T_F}{4\pi} S_{\text{real}}^{(2,h,\text{bare})}(\vec{p}_T, m) = \frac{1}{\pi} \int \frac{\mathrm{d}M^2}{M^2} \,\text{Im}\big[\Pi(m^2, M^2)\big] \times S_{\text{real}}^{(1,\text{bare})}(\vec{p}_T, M) . \tag{D.42}$$

The results from these dispersion integrations are

$$S_{\text{virt}}^{(2,h,\text{bare})}(m) = C_F \left\{ \left[-\frac{16}{3\epsilon^2} + \frac{1}{\epsilon}\left(\frac{32}{3}L_m + \frac{80}{9}\right) - \frac{32}{3}L_m^2 - \frac{160}{9}L_m - \frac{448}{27} - \frac{8\pi^2}{9} + \mathcal{O}(\epsilon) \right] \right.$$

$$\times \left(\frac{1}{\eta} + \ln\frac{\nu}{\mu}\right) + \frac{4}{\epsilon^3} - \frac{1}{\epsilon^2}\left(\frac{16}{3}L_m + \frac{20}{9}\right) + \frac{1}{\epsilon}\left(\frac{8}{3}L_m^2 - \frac{112}{27} + \frac{2\pi^2}{3}\right) + \frac{40}{9}L_m^2$$

$$\left. + \left(\frac{448}{27} - \frac{8\pi^2}{9}\right)L_m + \frac{656}{27} - \frac{10\pi^2}{27} - 8\zeta_3 \right\} , \tag{D.43}$$

$$S_{\text{real}}^{(2,h,\text{bare})}(\vec{p}_T, m) = \frac{C_F}{\pi p_T^2} \left\{ \frac{32}{9\eta}\left[-5 + 12\hat{m}^2 + 3c(1 - 2\hat{m}^2)\ln\frac{c+1}{c-1} \right] + s_{\text{real}}^{q_T}\left(\frac{m^2}{p_T^2}, \frac{\nu}{m}\right) \right\} , \tag{D.44}$$

with

$$s_{\text{real}}^{q_T}\left(\hat{m}^2, \frac{\nu}{m}\right) = \frac{16}{9}\left\{ 2\left[-5 + 12\hat{m}^2 + 3c(1 - 2\hat{m}^2)\ln\frac{c+1}{c-1} \right]\ln\frac{\nu}{m} \right.$$

$$+ 3c(1 - 2\hat{m}^2)\left[\text{Li}_2\left(\frac{(c-1)^2}{(c+1)^2}\right) + 2\ln\frac{c+1}{c-1}\left(\ln\frac{c+1}{2c} + \ln\hat{m}\right) - \frac{\pi^2}{6} \right]$$

$$\left. + 8\hat{m}^2 + c(5 - 16\hat{m}^2)\ln\frac{c+1}{c-1} \right\} , \tag{D.45}$$

and $\hat{m}$ and c as in Eq. (C.16). Using Eq. (D.42) entails that the massive quark corrections to the strong coupling are renormalized in the on-shell scheme, i.e., the expansion is in terms of $\alpha_s = \alpha_s^{(n_l)}$. Since the soft function matrix element has to be renormalized entirely in the $n_l + 1$ flavor theory, we need to account for the second term in Eq. (D.6) (which switches back to an unrenormalized α_s) and renormalize the massive quark corrections to the strong coupling in the $\overline{\text{MS}}$ scheme, such that the expansion is in terms of $\alpha_s = \alpha_s^{(n_l+1)}$. The soft function is renormalized according to

$$S^{(\text{bare})}(\vec{p}_T, m) = \int \mathrm{d}^2 p_T' \, Z_S\left(\vec{p}_T - \vec{p}_T', m, \mu, \nu\right) S(\vec{p}_T', m, \mu, \nu) . \tag{D.46}$$

This yields for the renormalized matrix element with initial state quarks at $\mathcal{O}(\alpha_s^2 C_F T_F)$ in terms of $\alpha_s = \alpha_s^{(n_l+1)}$

$$S^{(2,h)}(\vec{p}_T, m, \mu, \nu) = \delta^{(2)}(\vec{p}_T) \, S_{\text{virt}}^{(2,h,\text{bare})}(m) + S_{\text{real}}^{(2,h,\text{bare})}(\vec{p}_T, m) \tag{D.47}$$
$$- \left(\Pi^{(1)}(m^2, 0) - \frac{4}{3\epsilon}\right) \underbrace{S^{(1,\text{bare})}(\vec{p}_T, \mu, \nu)}_{= S^{(1)}(\vec{p}_T, \mu, \nu) + Z_S^{(1)}(\vec{p}_T, \mu, \nu)} - \delta(1-z) \, Z_S^{(2,h)}(\vec{p}_T, m, \mu, \nu) \,,$$

where the (bare) vacuum polarization function $\Pi^{(1)}(m^2, 0)$ is given in Eq. (D.8) and the renormalized one-loop soft function $S^{(1)}$ is given in Eq. (B.13). The one-loop counterterm reads

$$Z_S^{(1)}(\vec{p}_T, \mu, \nu) = C_F \left\{ \delta^{(2)}(\vec{p}_T) \left[\frac{1}{\eta}\left(-\frac{8}{\epsilon} + \mathcal{O}(\epsilon)\right) + \frac{4}{\epsilon^2} - \frac{8}{\epsilon}\ln\frac{\nu}{\mu} \right] + \frac{1}{\eta}\left(8 + \mathcal{O}(\epsilon)\right) \mathcal{L}_0(\vec{p}_T, \mu) \right\} \,, \tag{D.48}$$

The two-loop counterterm $Z_S^{(2)}$ absorbs all remaining UV and IR divergences in Eq. (D.47) and is given by

$$Z_S^{(2,h)}(\vec{p}_T, m, \mu, \nu) = C_F \left\{ \delta^{(2)}(\vec{p}_T) \left[\frac{1}{\eta}\left(-\frac{16}{3\epsilon^2} + \frac{80}{9\epsilon} - \frac{16}{3}L_m^2 - \frac{160}{9}L_m - \frac{448}{27} + \mathcal{O}(\epsilon)\right) \right. \right.$$
$$\left. + \frac{4}{\epsilon^3} - \frac{1}{\epsilon^2}\left(\frac{20}{9} + \frac{16}{3}\ln\frac{\nu}{\mu}\right) + \frac{1}{\epsilon}\left(-\frac{112}{27} + \frac{2\pi^2}{9} + \frac{80}{9}\ln\frac{\nu}{\mu}\right) \right] + \frac{1}{\eta}\left(\frac{32}{3}L_m + \mathcal{O}(\epsilon)\right) \mathcal{L}_0(\vec{p}_T, \mu)$$
$$\left. + \frac{1}{\eta} \frac{32}{9\pi p_T^2}\left(-5 + 12\hat{m}^2 + 3c(1 - 2\hat{m}^2)\ln\frac{c+1}{c-1}\right) \right\} \,. \tag{D.49}$$

This yields the anomalous dimensions in Eq. (C.31). Using Eqs. (D.43), (D.44), (D.48), and (D.49) we obtain the full result for the secondary massive quark corrections to the TMD soft function in Eq. (C.30).

D.5 Csoft function at two loops

We compute the csoft function $\mathcal{S}_c$ for beam thrust appearing in the hierarchy $\mathcal{T} \ll m \ll \sqrt{Q\mathcal{T}}$ for DY and $m \ll Q\sqrt{1-x}$ for DIS. As in the computation for the beam function matching coefficient in App. D.3.3 we carry out the calculation using a gluon mass $\Lambda \ll m$ as an IR regulator. In this context the csoft function is the matching coefficient between the csoft matrix elements in the $n_l + 1$ and n_l flavor theories,

$$\mathcal{S}_c^{(n_l+1)}(\ell, m, \mu, \nu) = \int d\ell' \, \mathcal{S}_c(\ell - \ell', m, \mu, \nu) \, \mathcal{S}_c^{(n_l)}(\ell', \mu, \nu) \,. \tag{D.50}$$

The csoft matrix elements are defined for any direction n as

$$\mathcal{S}_c(\ell, \mu) = \frac{1}{N_c} \text{tr} \left\langle 0 \left| \overline{\text{T}}\left[X_n^\dagger(0) V_n(0)\right] \delta(\ell - n \cdot \hat{p}) \text{T}\left[V_n^\dagger(0) X_n(0)\right] \right| 0 \right\rangle \,, \tag{D.51}$$

with the csoft Wilson lines given by (see e.g. Refs. [89, 90])

$$X_n = \sum_{\text{perms}} \exp\left[-\frac{g}{n \cdot \mathcal{P}} \frac{\nu^{\eta/2}}{(\bar{n} \cdot \mathcal{P})^{\eta/2}} \, n \cdot A_{cs}\right], \quad V_n = \sum_{\text{perms}} \exp\left[-\frac{g}{\bar{n} \cdot \mathcal{P}} \frac{\nu^{\eta/2}}{(\bar{n} \cdot \mathcal{P})^{\eta/2}} \, \bar{n} \cdot A_{cs}\right], \tag{D.52}$$

Here we have also expanded out he η regulator according to the n-collinear soft scaling $\bar{n} \cdot \mathcal{P} \gg n \cdot \mathcal{P}$.

Changing one or two Wilson lines from incoming to outgoing when describing the differnet processes DY, DIS and $e^+e^- \to$ leads to identical results at two-loops (see also Ref. [82]), which is the order at which we are working here.

D.5.1 Csoft function with a massive gluon at $\mathcal{O}(\alpha_s)$

We will first calculate the one-loop corrections to the csoft matrix elements $\mathscr{S}_c$ with a massive gluon, that can then be used to obtain the two-loop corrections with secondary massive quarks using the dispersion technique described in Sec. D.2. The one-loop results for the csoft matrix elements can be written as

$$\mathscr{S}_c^{(1,\text{bare})}(\ell, M) = \delta(\ell)\,\mathscr{S}_{c,\text{virt}}^{(1,\text{bare})}(M) + \mathscr{S}_{c,\text{real}}^{(1,\text{bare})}(\ell, M)\,. \tag{D.53}$$

The relevant contributions at one loop are displayed in the diagrams in Fig. D.3, with the soft Wilson lines S_n and $S_{\bar{n}}$ replaced by the csoft Wilson lines X_n and V_n. With the choice of regularization in Eq. (2.83) the virtual diagram leads to a scaleless integral, such that $\mathscr{S}_{c,\text{virt}}^{(1,\text{bare})} = 0$. The real radiation diagram corresponding to Fig. D.3b yields

$$
\begin{aligned}
\mathscr{S}_c^{(b)} &= 8\pi\alpha_s C_F\tilde{\mu}^{2\epsilon}\int\frac{\mathrm{d}^d k}{(2\pi)^d}\frac{1}{k^- k^+}\left(\frac{\nu}{k^-}\right)^\eta \delta(\ell - k^+)\,2\pi\delta(k^2 - M^2)\\
&= \frac{\alpha_s C_F}{4\pi}\frac{2\,\Gamma(\epsilon+\eta)}{\Gamma(1+\eta)}\left(\frac{\mu^2 \mathrm{e}^{\gamma_E}}{M^2}\right)^\epsilon\left(\frac{\nu}{M^2}\right)^\eta\frac{\theta(\ell)}{\ell^{1-\eta}}\,.
\end{aligned}
\tag{D.54}
$$

Including also the mirror diagram and expanding in η the total real radiation contribution to the csoft matrix element with a massive gluon is

$$
\begin{aligned}
\frac{\alpha_s}{4\pi}\mathscr{S}_{c,\text{real}}^{(1,\text{bare})}(\ell, M) &= 2\mathscr{S}_c^{(b)}\\
&= \frac{\alpha_s C_F}{4\pi}\left(\frac{\mu^2 \mathrm{e}^{\gamma_E}}{M^2}\right)^\epsilon\Gamma(\epsilon)\left[\delta(\ell)\left(\frac{1}{\eta} - \ln\frac{M^2}{\mu^2} + H_{\epsilon-1}\right) + \frac{\nu}{\mu^2}\mathcal{L}_0\left(\frac{\ell\,\nu}{\mu^2}\right) + \mathcal{O}(\eta)\right].
\end{aligned}
\tag{D.55}
$$

D.5.2 Csoft function at $\mathcal{O}(\alpha_s^2)$

We convolve the one-loop results with the imaginary part of the vacuum polarization function, which yields for the nonvanishing contributions

$$\frac{\alpha_s T_F}{4\pi}\mathscr{S}_{c,\text{real}}^{(2,h,\text{bare})}(\ell, m) = \frac{1}{\pi}\int\frac{\mathrm{d}M^2}{M^2}\,\text{Im}\big[\Pi(m^2, M^2)\big]\times\mathscr{S}_{c,\text{real}}^{(1,\text{bare})}(\ell, M)\,. \tag{D.56}$$

The result of this dispersion integral is

$$
\begin{aligned}
\mathscr{S}_{c,\text{real}}^{(2,h,\text{bare})}(\ell, m) = C_F\Bigg\{&\left[\frac{8}{3\epsilon^2} - \frac{1}{\epsilon}\left(\frac{16}{3}L_m + \frac{40}{9}\right) + \frac{16}{3}L_m^2 + \frac{80}{9}L_m + \frac{224}{27} + \frac{4\pi^2}{9} + \mathcal{O}(\epsilon)\right]\\
&\times\left[\frac{1}{\eta}\delta(\ell) + \frac{\nu}{\mu^2}\mathcal{L}_0\left(\frac{\ell\,\nu}{\mu^2}\right)\right] + \delta(\ell)\left[-\frac{4}{\epsilon^3} + \frac{1}{\epsilon^2}\left(\frac{16}{3}L_m + \frac{20}{9}\right)\right.\\
&+ \frac{1}{\epsilon}\left(-\frac{8}{3}L_m^2 + \frac{112}{27} - \frac{2\pi^2}{3}\right) - \frac{40}{9}L_m^2 + \left(-\frac{448}{27} + \frac{8\pi^2}{9}\right)L_m\\
&\left.- \frac{656}{27} + \frac{10\pi^2}{27} + 8\zeta_3\right]\Bigg\}.
\end{aligned}
\tag{D.57}
$$

Using Eq. (D.56) entails that the massive quark corrections to the strong coupling are renormalized in the on-shell scheme, i.e., the expansion is in terms of $\alpha_s = \alpha_s^{(n_l)}$. To obtain the csoft function $\mathcal{S}_c$ we need to switch to $\alpha_s^{(n_l+1)}$ and furthermore subtract the correction $\mathscr{S}_c^{(2,n_l)}$ (with a strong coupling in the n_l flavor scheme) according to Eq. (D.50). All purely massless contributions cancel each other

and we obtain for the $\mathcal{O}(\alpha_s^2)$ corrections in an expansion in terms of $\alpha_s^{(n_l+1)}$

$$
\begin{aligned}
\mathcal{S}_c^{(2)}(\ell, m, \mu, \nu) &= \mathscr{S}_c^{(2,h)}(\ell, m, \mu, \nu) - \frac{4}{3} L_m \mathscr{S}_c^{(1)}(\ell, \mu, \nu) \\
&= \mathscr{S}_{c,\text{real}}^{(2,h,\text{bare})}(\ell, m) - \left(\Pi^{(1)}(m^2, 0) - \frac{4}{3\epsilon} \right) \mathscr{S}_c^{(1,\text{bare})}(\ell) \\
&\quad - Z_{\mathscr{S}_c}^{(2,h)}(\ell, m, \mu, \nu) - \frac{4}{3} L_m \mathscr{S}_c^{(1)}(\ell, \mu, \nu) \\
&= \mathscr{S}_{c,\text{real}}^{(2,h,\text{bare})}(\ell, m) - \left(\Pi^{(1)}(m^2, 0) - \frac{4}{3\epsilon} \right) Z_{\mathscr{S}_c}^{(1)}(\ell, \mu, \nu) - Z_{\mathscr{S}_c}^{(2,h)}(\ell, m, \mu, \nu) \,.
\end{aligned}
$$

(D.58)

Here the counterterm is defined via

$$
\mathscr{S}_c^{(\text{bare})}(\ell, m) = \int d\ell' \, Z_{\mathscr{S}_c}^{(n_l+1)}(\ell - \ell', m, \mu, \nu) \, \mathscr{S}_c^{(n_l+1)}(\ell', m, \mu, \nu) \,.
$$

(D.59)

Employing a gluon mass the associated expression for $Z_{\mathscr{S}_c}^{(1)}$ can be read off from Eq. (D.55) and is given by (expanded in η and ϵ)

$$
Z_{\mathscr{S}_c}^{(1)}(\ell, \mu, \nu) = 4 C_F \left\{ \delta(\ell) \left[\frac{1}{\eta} \left(\frac{1}{\epsilon} - \ln \frac{\Lambda^2}{\mu^2} + \mathcal{O}(\epsilon) \right) - \frac{1}{\epsilon^2} \right] + \frac{\nu}{\mu^2} \mathcal{L}_0 \left(\frac{\ell \nu}{\mu^2} \right) \frac{1}{\epsilon} \right\} \,.
$$

(D.60)

The counterterm $Z_{\mathscr{S}_c}^{(2,h)}$ absorbs all divergences and is given by[2]

$$
\begin{aligned}
Z_{\mathscr{S}_c}^{(2,h)}(\ell, m, \mu, \nu) &= C_F \left\{ \delta(\ell) \left[\frac{1}{\eta} \left(\frac{8}{3\epsilon^2} - \frac{40}{9\epsilon} - \frac{16}{3} L_m \ln \frac{\Lambda^2}{\mu^2} + \frac{8}{3} L_m^2 + \frac{80}{9} L_m + \frac{224}{27} + \mathcal{O}(\epsilon) \right) \right. \right. \\
&\quad \left. \left. - \frac{4}{\epsilon^3} + \frac{20}{9\epsilon^2} + \frac{1}{\epsilon} \left(\frac{112}{27} - \frac{2\pi^2}{9} \right) \right] + \frac{\nu}{\mu^2} \mathcal{L}_0 \left(\frac{\ell \nu}{\mu^2} \right) \left[\frac{8}{3\epsilon^2} - \frac{40}{9\epsilon} \right] \right\} \,.
\end{aligned}
$$

(D.61)

Using Eqs. (D.57), (D.60) and (D.61) in Eq. (D.58) we obtain the full result for the renormalized csoft function at two loops in Eq. (C.32).

---

[2] The anomalous dimension for the csoft function $\mathcal{S}_c$ can be obtained from the ratio of $Z_{\mathscr{S}_c}^{(n_l+1)}$ and $Z_{\mathscr{S}_c}^{(n_l)}$, upon which the IR sensitivity cancels.

Appendix E

Massive quark effects in DY at fixed order

The factorization formulae in the Secs. 2.1 and 2.2 contain together all information about the singular massive quark corrections to the differential cross sections in QCD at fixed order (for any given hierarchy between the mass and $q_T/\mathcal{T}$). Here we provide the results at $\mathcal{O}(\alpha_s^2)$ for Drell-Yan for both primary and secondary corrections. We write for each of these contributions ($e = q_T^2, \mathcal{T}$)

$$\frac{\mathrm{d}\sigma}{\mathrm{d}e\,\mathrm{d}Q^2\,\mathrm{d}Y}(e, Q, m, x_a, x_b) = \sum_{i,j=q,\bar{q},g} \int \frac{\mathrm{d}z_a}{z_a} \frac{\mathrm{d}z_b}{z_b} \frac{\mathrm{d}\hat{\sigma}_{ij}}{\mathrm{d}e\,\mathrm{d}Q^2\,\mathrm{d}Y}(e, Q, m, z_a, z_b, \mu)\, f_i\Big(\frac{x_a}{z_a}, \mu\Big)\, f_j\Big(\frac{x_b}{z_b}, \mu\Big),$$

(E.1)

and expand the partonic result in the n_l-flavor scheme for α_s as

$$\frac{\mathrm{d}\hat{\sigma}_{ij}}{\mathrm{d}e\,\mathrm{d}Q^2\,\mathrm{d}Y} = \frac{\mathrm{d}\hat{\sigma}_{ij}^{(0)}}{\mathrm{d}Q^2\,\mathrm{d}Y}\,\delta(q_T^2) + \frac{\alpha_s^{(n_l)}(\mu)}{4\pi} \frac{\mathrm{d}\hat{\sigma}_{ij}^{(1)}}{\mathrm{d}e\,\mathrm{d}Q^2\,\mathrm{d}Y}$$

$$+ \left(\frac{\alpha_s^{(n_l)}(\mu)}{4\pi}\right)^2 \left[T_F n_l \frac{\mathrm{d}\hat{\sigma}_{ij}^{(2,l)}}{\mathrm{d}e\,\mathrm{d}Q^2\,\mathrm{d}Y} + T_F \frac{\mathrm{d}\hat{\sigma}_{ij}^{(2,h)}}{\mathrm{d}e\,\mathrm{d}Q^2\,\mathrm{d}Y} + \dots \right] + \mathcal{O}(\alpha_s^3), \qquad \text{(E.2)}$$

where $\mathrm{d}\sigma_{q\bar{q}}^{(0)}/(\mathrm{d}Q^2\mathrm{d}Y)$ denotes the Born cross section for the corresponding Drell-Yan process $q\bar{q} \to Z/\gamma^* \to \ell\bar{\ell}$. In this context $\mathrm{d}\sigma_{Q\bar{Q}}^{(0)}/(\mathrm{d}Q^2\mathrm{d}Y)$ indicates the Born cross section for a massless quark q with the same charge and isospin as the heavy quark Q.

E.1 Fixed-order result for the q_T spectrum

The singular fixed-order corrections for the q_T-spectrum (i.e. for $q_T \ll Q$) at $\mathcal{O}(\alpha_s^2 C_F T_F)$ consist of the virtual (full QCD) contributions encoded in Eqs. (C.2) and (C.3) and the secondary collinear and soft real radiation corrections contained in Eqs. (C.15) and (C.30). Setting common scales $\mu = \mu_H = \mu_B = \mu_S$ and $\nu = \nu_B = \nu_S$ yields for the corrections to virtual photon production

$$\frac{\mathrm{d}\hat{\sigma}_{q\bar{q}}^{(2,h)}}{\mathrm{d}q_T^2\,\mathrm{d}Q^2\,\mathrm{d}Y} = \frac{\mathrm{d}\hat{\sigma}_{q\bar{q}}^{(0)}}{\mathrm{d}Q^2\,\mathrm{d}Y}\, C_F \Bigg\{ h_{\mathrm{virt}}\Big(\frac{m^2}{Q^2}\Big)\, \delta(q_T^2)\, \delta(1-z_a)\, \delta(1-z_b)$$

$$+ \frac{1}{q_T^2}\, b_{\mathrm{real}}^{q_T}\Big(\frac{m^2}{q_T^2}, z_a, \frac{\nu}{\omega_a}\Big)\, \delta(1-z_b) + \frac{1}{q_T^2}\, b_{\mathrm{real}}^{q_T}\Big(\frac{m^2}{q_T^2}, z_b, \frac{\nu}{\omega_b}\Big)\, \delta(1-z_a)$$

$$+ \frac{1}{q_T^2}\, s_{\mathrm{real}}^{q_T}\Big(\frac{m^2}{q_T^2}, \frac{\nu}{m}\Big)\, \delta(1-z_a)\, \delta(1-z_b) + \mathcal{O}\Big(\frac{q_T}{Q}\Big) \Bigg\},$$

(E.3)

where $h_{\rm virt}$, $b_{\rm real}^{q_T}$ and $s_{\rm real}^{q_T}$ are given in Eqs. (C.2), (D.22) and (D.45). For Z-boson production one has to include in addition the anomalous axial current correction in Eq. (C.3) as contribution to the $\delta(q_T^2)$-term (which gives in conjunction with the isospin partner a μ-independent result). Writing out the nontrivial terms in the spectrum explicitly we get

$$
\begin{aligned}
\frac{\mathrm{d}\hat{\sigma}_{q\bar{q}}^{(2,h)}}{\mathrm{d}q_T^2\,\mathrm{d}Q^2\,\mathrm{d}Y}(q_T^2, Q, m, z_a, z_b) &= \frac{\mathrm{d}\hat{\sigma}_{q\bar{q}}^{(0)}}{\mathrm{d}Q^2\,\mathrm{d}Y}\,\theta(z_a)\,\theta(z_b)\,C_F\Bigg\{ h_{\rm virt}\Big(\frac{m^2}{Q^2}\Big)\,\delta(q_T^2)\,\delta(1-z_a)\,\delta(1-z_b) \\
&+ \frac{\delta(1-z_b)}{q_T^2}\bigg[\Big(-\frac{80}{9}+\frac{64}{3}\hat{m}^2+\frac{16}{3}(1-2\hat{m}^2)\ln\frac{c+1}{c-1}\Big)\Big(\mathcal{L}_0(1-z_a)+\delta(1-z_a)\ln\frac{Q}{m}\Big) \\
&\quad + \theta(1-z_a)\Big(\frac{8}{3d_a(1-z_a)}\big[1+z_a^2+2\hat{m}^2z_a(1+z_a^2)+4\hat{m}^4z_a^2(-5+6z_a-5z_a^2)\big]\ln\frac{d_a+1}{d_a-1} \\
&\quad - \frac{16c(1-2\hat{m}^2)}{3(1-z_a)}\ln\frac{c+1}{c-1}+\frac{16}{9}+\frac{64}{9}z_a+\frac{16}{3}\hat{m}^2(-4+z_a-5z_a^2)\Big) \\
&\quad + \delta(1-z_a)\Big(\frac{8}{3}c(1-2\hat{m}^2)\Big[\mathrm{Li}_2\Big(\frac{(c-1)^2}{(c+1)^2}\Big)+2\ln\frac{c+1}{c-1}\ln\frac{\hat{m}(c+1)}{2c}-\frac{\pi^2}{6}\Big] \\
&\quad + \frac{8}{9}c(5-16\hat{m}^2)\ln\frac{c+1}{c-1}+\frac{64}{9}\hat{m}^2\Big)\bigg] \\
&+ \frac{\delta(1-z_a)}{q_T^2}\Big[(z_a\leftrightarrow z_b)\Big]+\mathcal{O}\Big(\frac{q_T}{Q}\Big)\Bigg\},
\end{aligned}
\tag{E.4}
$$

where

$$
\hat{m}=\frac{m}{q_T}, \quad c=\sqrt{1+4\hat{m}^2}, \quad d_a=\sqrt{1+4\hat{m}^2 z_a}.
\tag{E.5}
$$

The singular fixed-order corrections for the q_T spectrum at $\mathcal{O}(\alpha_s^2 T_F^2)$ consist of the primary collinear real radiation corrections in Eq. (C.13) for both beam directions,

$$
\begin{aligned}
\frac{\mathrm{d}\hat{\sigma}_{gg}^{(2,h)}}{\mathrm{d}q_T^2\,\mathrm{d}Q^2\,\mathrm{d}Y}(q_T^2, Q, m, z_a, z_b) &= 2\,\frac{\mathrm{d}\hat{\sigma}_{Q\bar{Q}}^{(0)}}{\mathrm{d}Q^2\,\mathrm{d}Y}\times\frac{\pi}{T_F}\int\mathrm{d}^2 p_T\,\mathcal{I}_{Qg}^{(1)}(\vec{q}_T-\vec{p}_T, m, z_a)\,\mathcal{I}_{Qg}^{(1)}(\vec{p}_T, m, z_b) \\
&= \frac{\mathrm{d}\hat{\sigma}_{Q\bar{Q}}^{(0)}}{\mathrm{d}Q^2\,\mathrm{d}Y}\,\theta(z_a)\,\theta(z_b)\,\theta(1-z_a)\,\theta(1-z_b)\frac{8T_F}{q_T^2 c^4}\Bigg\{ 2(1-z_a-z_b+2z_az_b)(z_a+z_b-2z_az_b) \\
&+ 8\hat{m}^2[z_a(1-z_a)+z_b(1-z_b)-3z_az_b(1-z_a-z_b+z_az_b)]-16\hat{m}^4 z_az_b(1-z_a-z_b+z_az_b) \\
&+ \frac{1}{c}\ln\Big(\frac{1+c+2\hat{m}^2(2+c)+2\hat{m}^4}{2\hat{m}^4}\Big)\Big[(1-2z_a+2z_a^2)(1-2z_b+2z_b^2) \\
&\quad + 2\hat{m}^2\Big(4-7z_a(1-z_a)-7z_b(1-z_b)+12z_az_b(1-z_a-z_b+z_az_b)\Big) \\
&\quad + 8\hat{m}^4\Big(2-3z_a(1-z_a)-3z_b(1-z_b)+6z_az_b(1-z_a-z_b+z_az_b)\Big) \\
&\quad + 16\hat{m}^6 z_az_b(1-z_a)(1-z_b)\Big]+\mathcal{O}\Big(\frac{q_T}{Q}\Big)\Bigg\}.
\end{aligned}
\tag{E.6}
$$

Depending on the hierarchy between m and q_T and Q some of the contributions in Eqs. (E.4) and (E.6) are power-suppressed and therefore only appear via nonsingular corrections in the factorization formula for the associated parametric regime in Sec. 2.1. Note also that virtual corrections are reshuffled among the components of the factorization theorem, which are in addition evaluated with α_s in different flavor number schemes. This essentially allows for a consistent factorization and the resummation of logarithms at higher orders.

E.2 Fixed-order result for the beam thrust spectrum

The singular fixed-order corrections for the $\mathcal{T}$ spectrum (i.e. for $\mathcal{T} \ll Q$) at $\mathcal{O}(\alpha_s^2 C_F T_F)$ consist of the virtual (full QCD) contributions encoded in Eqs. (C.2) and (C.3) and the secondary collinear and soft real radiation corrections contained in Eqs. (C.20) and (C.34). Setting common scales $\mu = \mu_H = \mu_B = \mu_S$ yields for the corrections to virtual photon production

$$
\frac{d\hat{\sigma}_{q\bar{q}}^{(2,h)}}{d\mathcal{T}\,dQ^2\,dY} = \frac{d\hat{\sigma}_{q\bar{q}}^{(0)}}{dQ^2\,dY}\, C_F \left\{ h_{\text{virt}}\left(\frac{m^2}{Q^2}\right) \delta(\mathcal{T})\,\delta(1 - z_a)\,\delta(1 - z_b) \right.
$$

$$
+ \frac{1}{\mathcal{T}}\, b_{\text{real}}^{\mathcal{T}}\left(\frac{m^2}{\omega_a \mathcal{T}}, z_a\right) \delta(1 - z_b) + \frac{1}{\mathcal{T}}\, b_{\text{real}}^{\mathcal{T}}\left(\frac{m^2}{\omega_b \mathcal{T}}, z_b\right) \delta(1 - z_a)
$$

$$
\left. + \frac{1}{\mathcal{T}}\, s_{\text{real}}^{\mathcal{T}}\left(\frac{m^2}{\mathcal{T}^2}\right) \delta(1 - z_a)\,\delta(1 - z_b) + \mathcal{O}\left(\frac{\mathcal{T}}{Q}\right) \right\}, \tag{E.7}
$$

where h_{virt} and $b_{\text{real}}^{\mathcal{T}}$ are given in Eqs. (C.2) and (D.29), respectively, and $s_{\text{real}}^{\mathcal{T}}$ is given implicitly by the nondistributive terms in Eq. (C.34). Again, for Z-boson production the anomalous axial current correction in Eq. (C.3) has to be included in the $\delta(\mathcal{T})$ term. Writing out the nontrivial terms in the spectrum we get

$$
\frac{d\hat{\sigma}_{q\bar{q}}^{(2,h)}}{d\mathcal{T}\,dQ^2\,dY}(\mathcal{T}, Q, m, z_a, z_b) = \frac{d\hat{\sigma}_{q\bar{q}}^{(0)}}{dQ^2\,dY}\,\theta(z_a)\,\theta(z_b)\, C_F \left\{ \delta(\mathcal{T})\,\delta(1 - z_a)\,\delta(1 - z_b)\, h_{\text{virt}}\left(\frac{m^2}{Q^2}\right) \right.
$$

$$
+ \frac{\delta(1 - z_b)}{\mathcal{T}} \left[\frac{\theta(v_a)}{1 - z_a} \left(-\frac{16}{9} v_a \left[4 - 3z_a + 4z_a^2 + \frac{z_a(11 - 21z_a + 29z_a^2 - 15z_a^3)}{1 - z_a} \hat{m}_a^2 \right] \right. \right.
$$

$$
\left. - \frac{8}{3u_a}\left[1 + z_a^2 - 2\hat{m}_a^2 z_a(1 + z_a^2) - 4\hat{m}_a^4 z_a^2(2 - 3z_a + 5z_a^2) \right] \ln\frac{u_a - v_a}{u_a + v_a} \right)
$$

$$
+ \delta(1 - z_a)\left(\theta(\mathcal{T} - 2m)\left[\frac{32}{3}\,\text{Li}_2\left(\frac{w - 1}{w + 1}\right) + \frac{8}{3}\ln^2\frac{1 - w}{1 + w} - \frac{32}{3}\ln\frac{1 - w}{1 + w}\ln\hat{m}_{\mathcal{T}} \right. \right.
$$

$$
\left. \left. \left. - \frac{80}{9}\ln\frac{1 - w}{1 + w} - w\left(\frac{448}{27} + \frac{128}{27}\hat{m}_{\mathcal{T}}^2\right) + \frac{8\pi^2}{9}\right] + \frac{\mathcal{T}\,\Delta S_{\tau,m}(\mathcal{T}, m)}{2} \right) \right]
$$

$$
\left. + \frac{\delta(1 - z_a)}{\mathcal{T}}\left[(z_a, \omega_a \leftrightarrow z_b, \omega_b) \right] + \mathcal{O}\left(\frac{\mathcal{T}}{Q}\right) \right\}, \tag{E.8}
$$

where

$$
\hat{m}_a = \frac{m}{\sqrt{\omega_a \mathcal{T}}}, \quad \hat{m}_{\mathcal{T}} = \frac{m}{\mathcal{T}}, \quad u_a = \sqrt{1 - 4\hat{m}_a z_a}, \quad v_a = \sqrt{1 - \frac{4\hat{m}_a^2 z_a}{1 - z_a}}, \quad w = \sqrt{1 - 4\hat{m}_{\mathcal{T}}^2}. \tag{E.9}
$$

The singular fixed-order corrections for the $\mathcal{T}$ spectrum at $\mathcal{O}(\alpha_s^2 T_F^2)$ consist of the collinear real

radiation corrections in Eq. (C.19) for both beam directions,

$$
\frac{d\hat{\sigma}_{gg}^{(2,h)}}{d\mathcal{T}\,dQ^2\,dY}(\mathcal{T},Q,m,z_a,z_b) = 2\,\frac{d\sigma_{Q\bar{Q}}^{(0)}}{dQ^2\,dY} \times \frac{Q^2}{T_F} \int d\mathcal{T}'\,\mathcal{I}_{Qg}^{(1)}(\omega_a(\mathcal{T}-\mathcal{T}'),m,z_a)\,\mathcal{I}_{Qg}^{(1)}(\omega_b\mathcal{T}',m,z_b)
$$

$$
= \frac{d\sigma_{Q\bar{Q}}^{(0)}}{dQ^2\,dY}\,\theta(z_a)\,\theta(z_b)\,\theta\!\left(\mathcal{T} - \frac{m^2 z_a}{\omega_a(1-z_a)} - \frac{m^2 z_b}{\omega_b(1-z_b)}\right)\frac{8T_F}{\mathcal{T}}
$$

$$
\times \left\{\frac{2}{(1-z_a-\hat{m}_a^2 z_a)(1-z_b-\hat{m}_b^2 z_b)}\left[(1-z_a)(1-z_b) - \hat{m}_a^2 z_a(1-z_b) - \hat{m}_b^2 z_b(1-z_a)\right]\right.
$$

$$
\times \left[(1-z_a-z_b+2z_a z_b)(z_a+z_b-2z_a z_b) - \hat{m}_a^2 z_a^2(1-2z_b)^2 - \hat{m}_b^2 z_b^2(1-2z_a)^2 - 4\hat{m}_a^2 \hat{m}_b^2 z_a^2 z_b^2\right]
$$

$$
+ \left(\ln\frac{1-z_a-\hat{m}_a^2 z_a}{z_a \hat{m}_a^2} + \ln\frac{1-z_b-\hat{m}_b^2 z_b}{z_b \hat{m}_b^2}\right)\left[(1-2z_a+2z_a^2)(1-2z_b+2z_b^2)\right.
$$

$$
\left.\left. + 2\hat{m}_a^2 z_a^2(1-2z_b+2z_b^2) + 2\hat{m}_b^2 z_b^2(1-2z_a+2z_a^2) + 8\hat{m}_a^2 \hat{m}_b^2 z_a^2 z_b^2\right]\right\}. \tag{E.10}
$$

Depending on the hierarchy between m and $\mathcal{T}$ and Q some of the contributions in Eqs. (E.8) and (E.10) are power-suppressed and therefore only appear via nonsingular corrections in the factorization formula for the associated parametric regime in Sec. 2.1.

Appendix F

The diagram $gg \to Z^* \to \bar{\ell}\ell$
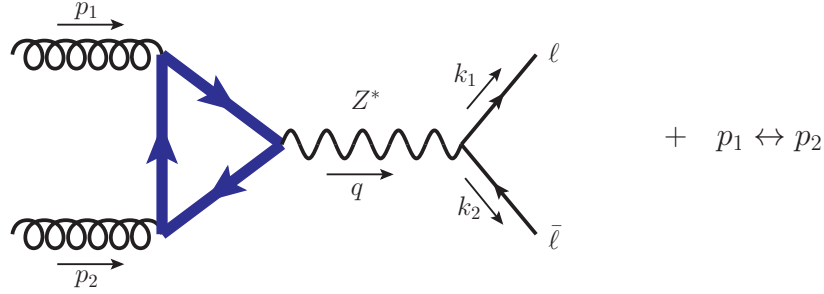

Figure F.1: Feynman diagram for $gg \to Z^* \to \bar{\ell}\ell$ at leading order in the strong and the electroweak coupling. There is a second diagram that results from crossing the incoming gluon lines.

When discussing the massive quark effects in Drell-Yan in chapter 2, we ignored the gluon initiated subprocess shown in Fig. F.1. In principle this diagram would lead to massive quark corrections to the cross section at $\mathcal{O}(\alpha_s^2)$, but it turns out that it vanishes for on-shell Z-boson production due to the Landau-Yang theorem [48, 49], and also for off-shell Z-bosons it is strongly suppressed, as we will now discuss. In fact both statements do not rely on the mass of the quark in the loop, and therefore apply to massive as well as massless quarks.

The amplitude for the diagram in Fig. F.1 is

$$\mathcal{M}(gg \to Z^* \to \bar{\ell}\ell) = \epsilon^\mu(p_1, \lambda_1)\epsilon^\nu(p_2, \lambda_2)\Gamma^{VVA}_{\mu\nu\rho} \frac{i\left(-g^{\rho\sigma} + \frac{q^\rho q^\sigma}{m_Z^2}\right)}{q^2 - m_Z^2 + im_Z\Gamma} L_\sigma(k_1, k_2)\,, \tag{F.1}$$

where we are not showing color indices and the leptonic tensor is defined as

$$L_\sigma(k_1, k_2) = \frac{-ie}{\cos\theta_W \sin\theta_W} \bar{u}(k_1)\gamma_\sigma(g_V + g_A\gamma_5)v(k_2)\,, \tag{F.2}$$

with the vector and axial-vector couplings

$$g_V = \frac{T_\ell^3}{2} - Q_\ell \sin^2\theta_W\,, \qquad g_A = -\frac{T_\ell^3}{2}\,, \tag{F.3}$$

where T_ℓ^3 and Q_ℓ are the third component of weak isospin and electric charge of the produced lepton, respectively. The on-shell conditions for the external particles and four-momentum conservation gives

$$q = p_1 + p_2 = k_1 + k_2\,, \qquad p_1^2 = p_2^2 = 0\,, \qquad k_1^2 = k_2^2 = m_\ell^2\,. \tag{F.4}$$

213

The factor $\Gamma_{\mu\nu\rho}^{VVA}$ stands for the quark loop (including the diagram with inversed momentum flow in the loop when crossing the gluon lines), coupled to the bosons via two vector couplings for the gluons and an axial-vector coupling to the Z-boson. The corresponding contribution with three vector couplings $\Gamma_{\mu\nu\rho}^{VVV}$ vanishes identically due to Furry's theorem, which implies that there are no contributions from virtual photons.

As a next step we split the the tensor structure of the propagator in an "on-shell" part and a purely longitudinal term

$$
\begin{aligned}
\left(-g^{\rho\sigma} + \frac{q^\rho q^\sigma}{m_Z^2}\right) &= \left(-g^{\rho\sigma} + \frac{q^\rho q^\sigma}{q^2}\right) + \frac{(q^2 - m_Z^2)q^\rho q^\sigma}{q^2 m_Z^2} \\
&= \sum_{\lambda_3} \epsilon_Q^{*\rho}(q,\lambda_3)\epsilon_Q^\sigma(q,\lambda_3) + \frac{(q^2 - m_Z^2)q^\rho q^\sigma}{q^2 m_Z^2} \,.
\end{aligned}
\tag{F.5}
$$

In the last line the ϵ_Q are polarization vectors of a fictive on-shell spin-1 particle with momentum q and mass $Q = \sqrt{q^2}$. When plugging this back into the expression for the full amplitude in Eq. (F.1), we find a term that is proportional to the amplitude for the process of two gluons going to this fictive spin-1 particle with mass Q, let us denote it as Z_Q

$$
\epsilon^\mu(p_1,\lambda_1)\epsilon^\nu(p_2,\lambda_2)\Gamma_{\mu\nu\rho}^{VVA}\epsilon_Q^{*\rho}(q,\lambda_3) \sim \mathcal{M}(gg \to Z_Q) = 0 \,.
\tag{F.6}
$$

This amplitude vanishes due to the Landau-Yang theorem. The Landau-Yang theorem of QED states that no spin-1 particle can decay to two photons. When replacing the photons by gluons[1] and reversing the process, it tells us that two on-shell gluons cannot produce a spin-1 particle. Thus the amplitude for two external gluons going to the fictive Z_Q particle $\mathcal{M}(gg \to Z_Q)$ has to vanish.

Therefore only the second term in the second line of Eq. (F.5) contributes, and when using this together with the relation

$$
q^\sigma L_\sigma(k_1, k_2) = \frac{-2im_\ell g_A}{\cos\theta_W \sin\theta_W} \left[\bar{u}(k_1)\gamma_5 v(k_2)\right],
\tag{F.7}
$$

the result for the full amplitude is

$$
\mathcal{M}(gg \to Z^* \to \bar{\ell}\ell) = \frac{2m_\ell e g_A(q^2 - m_Z^2)}{\cos\theta_W \sin\theta_W \, q^2 m_Z^2 (q^2 - m_Z^2 + im_Z\Gamma)} \epsilon^\mu(p_1,\lambda_1)\epsilon^\nu(p_2,\lambda_2)q^\rho\Gamma_{\mu\nu\rho}^{VVA}[\bar{u}(k_1)\gamma_5 v(k_2)] \,.
\tag{F.8}
$$

We first note that this is proportional to $(q^2 - m_Z^2)$, which is exactly the statement of the Landau-Yang theorem that we applied above, that the amplitude vanishes for on-shell Z-bosons. We therefore have to consider this diagram only for off-shell Z-bosons, but also in this case the amplitude is strongly suppressed with respect to other diagrams, because it is proportional to the lepton mass m_ℓ. Thus this diagram will lead only to corrections to the cross section that are of order $\mathcal{O}(m_\ell^2/Q^2)$, which we can safely neglect in our analysis.

---

[1]The Landau-Yang theorem can be violated in QCD, but it still holds for color-singlet states like the Z-boson [224,225].

Appendix G

Jet and soft functions in SCET and bHQET with a $p_\perp$ cut at $\mathcal{O}(\alpha_s)$

G.1 Unreleased soft function for thrust

In this section we provide details on the calculation of the unreleased thrust soft function $S_{\mathrm{ur}}^{(\tau)}$ at $\mathcal{O}(\alpha_s)$. The unreleased soft function describes large angle soft radiation originating *from below* the $p_\perp$ cut Q_0. We carry out the calculation using the dressed gluon propagator of Eq. (8.18) which is suitable to obtain the soft function in Borel space (accounting for fermion bubble resummation to all orders). From this we can easily identify the $\mathcal{O}(\Lambda_{\mathrm{QCD}})$ renormalon pole located at $u = 1/2$. To obtain the usual one-loop result one can take the limit $u \to 0$ in the end and multiply back the factor $(\alpha_s \beta_0)/(4\pi)$ effectively removed by the dressed gluon propagator in this limit. We note that at $\mathcal{O}(\alpha_s)$ all integrations can be readily carried out in 4 dimensions because the unreleased radiation does not result in any ultraviolet divergences. However, in contrast to the calculations without any $p_\perp$ cut we also have to consider the contributions from the virtual diagrams, because the scale Q_0 constitutes an additional scale such that the virtual diagrams may lead to finite contributions. Interestingly, as we show below, the virtual diagrams lead to vanishing results even for finite Q_0.

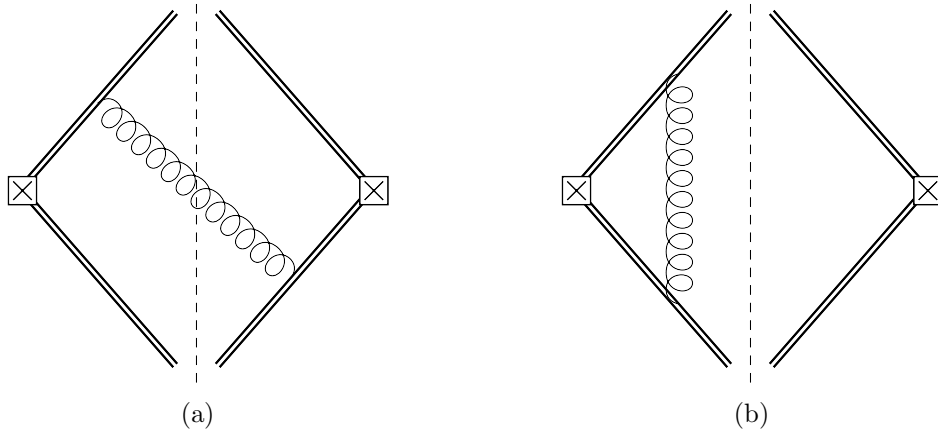The Borel space contribution from the real radiation diagrams (including the mirror diagram) shown

(a)   (b)

Figure G.1: Diagrams relevant for computation of the partonic soft function at $\mathcal{O}(\alpha_s)$.

in Fig. G.1a reads

$$B\Big[S_{\mathrm{ur}}^{(\tau,\mathrm{real})}(k,Q_0)\Big] = \frac{4C_F}{\beta_0}\big(\mu^2 e^{-c}\big)^u \theta(k) \int \frac{dq^+ dq^-}{q^+ (q^-)^{1+\alpha}}$$
$$\times \Big(\theta(q^- - q^+)\delta(k - q^+) + \theta(q^+ - q^-)\delta(k - q^-)\Big)$$
$$\times \frac{1}{\pi}\,\mathrm{Im}\Bigg[\int_0^{Q_0^2} dq_\perp^2 \,\frac{1}{\big(q_\perp^2 - (q^+ q^- + i0)\big)^{1+u}}\Bigg]\,, \tag{G.1}$$

with $c = 5/3$ in the $\overline{\mathrm{MS}}$ renormalization scheme for the strong coupling. In Eq. (G.1) we introduced the rapidity regulator α on the q^- light-cone component. This is regulator is useful because the upper bound for the transverse momentum integration leads to intermediate $1/\alpha$ rapidity divergences, which, however, cancel when summing the contributions from the two hemispheres (defined by the contributions associated to the two θ step functions). So, overall there are no rapidity divergences in the $\mathcal{O}(\alpha_s)$ thrust soft function with an upper $p_\perp$ cutoff. Doing the trivial delta function integrations gives

$$\frac{4C_F}{\beta_0}\big(\mu^2 e^{-c}\big)^u \frac{\theta(k)}{k} \int_k^\infty \frac{dq}{q}\big(q^{-\alpha} + k^{-\alpha}\big) \times \frac{1}{\pi}\,\mathrm{Im}\Bigg[\int_0^{Q_0^2} dq_\perp^2 \,\frac{1}{\big(q_\perp^2 - (qk + i0)\big)^{1+u}}\Bigg]\,. \tag{G.2}$$

Next we can calculate the $q_\perp$ integral and take the imaginary part employing the relation

$$\frac{1}{\pi}\,\mathrm{Im}\Bigg[\int_0^{Q_0^2} dq_\perp^2 \,\frac{1}{\big(q_\perp^2 - (qk + i0)\big)^{1+u}}\Bigg] = \frac{1}{u\pi}\,\mathrm{Im}\Big[(-qk - i0)^{-u} - (Q_0^2 - qk - i0)^{-u}\Big]$$
$$= \frac{1}{\Gamma(1-u)\Gamma(1+u)}\Big((qk)^{-u} - \theta(qk - Q_0^2)(qk - Q_0^2)^{-u}\Big)\,, \tag{G.3}$$

where in the last line we have used the fact that $qk > 0$. This leaves us with the sum of three integrals

$$\frac{4C_F}{\beta_0}\frac{\big(\mu^2 e^{-c}\big)^u}{\Gamma(1-u)\Gamma(1+u)}\frac{1}{k^{1+u}}\Bigg[2\int_k^\infty \frac{dq}{q^{1+u}} - 2\,\theta(k - Q_0)\int_k^\infty \frac{dq}{q}\big(q - \frac{Q_0^2}{k}\big)^{-u}$$
$$- \theta(Q_0 - k)\int_{\frac{Q_0^2}{k}}^\infty \frac{dq}{q}\big(q - \frac{Q_0^2}{k}\big)^{-u}\big(q^{-\alpha} + k^{-\alpha}\big)\Bigg] \tag{G.4}$$
$$= \frac{2C_F}{\beta_0}\frac{\big(\mu^2 e^{-c}\big)^u}{\Gamma(1-u)\Gamma(1+u)}\Bigg[\frac{2}{u\,k^{1+2u}} - \theta(k - Q_0)\frac{2\,Q_0^{-2u}}{k}\mathrm{B}\Big[\frac{Q_0^2}{k^2}; u, 1-u\Big]$$
$$- \theta(Q_0 - k)Q_0^{-2u-\alpha}\Gamma(1-u)\Big(\frac{Q_0^\alpha \Gamma(u)}{k^{1+\alpha}} + \frac{Q_0^{-\alpha}\Gamma(u+\alpha)}{\Gamma(1+\alpha)\,k^{1-\alpha}}\Big)\Bigg]\,,$$

where we have already taken the limit $\alpha \to 0$ in the first two terms since they are finite for $\alpha \to 0$, and $\mathrm{B}[z; a, b]$ is the incomplete beta function. For the third term the $\alpha \to 0$ limit has to be taken more carefully, using

$$\frac{Q_0^{\pm\alpha}}{k^{1\pm\alpha}} = \mp\frac{1}{\alpha}\delta(k) + \frac{1}{Q_0}\Big[\frac{\theta(k/Q_0)}{k/Q_0}\Big]_+ + \mathcal{O}(\alpha)\,. \tag{G.5}$$

With this we finally arive at

$$B\Big[S_{\mathrm{ur}}^{(\tau)}(k,Q_0)\Big] = B\Big[S_{\mathrm{ur}}^{(\tau,\mathrm{real})}(k,Q_0)\Big]$$
$$= \frac{8C_F}{\beta_0}\frac{\big(\frac{\mu^2 e^{-c}}{Q_0^2}\big)^u}{\Gamma(1-u)\Gamma(1+u)}\Bigg[\frac{Q_0^{2u}}{u\,k^{1+2u}} - \theta(k - Q_0)\frac{1}{k}\mathrm{B}\Big[\frac{Q_0^2}{k^2}, u, 1-u\Big] \tag{G.6}$$
$$- \theta(Q_0 - k)\Gamma(u)\Gamma(1-u)\Big(\delta(k)\frac{\mathrm{H}_{u-1}}{2} + \frac{1}{Q_0}\Big[\frac{\theta(k/Q_0)}{k/Q_0}\Big]_+\Big)\Bigg]\,,$$

where $H_n = \psi(n+1) + \gamma_E$ is the harmonic number function and $B[z; a, b]$ the incomplete Beta function. As already discussed before, there are no rapidity divergences in the thrust soft function and all $\frac{1}{\alpha}$ poles cancel in the final result. Since the virtual diagrams turn out to vanish (see below), this represents already the full result for the unreleased thrust soft function.

To identify the leading renormalon pole we Laurent expand Eq. (G.6) around $u = 1/2$. Using the relation

$$\frac{\mu^{2u}}{k^{1+2u}} = \frac{\mu}{2(u - \frac{1}{2})} \delta'(k) + \mathcal{O}\left((u - \frac{1}{2})^0\right),$$ (G.7)

we find the pole contribution

$$B\left[S_{\text{ur}}^{(\tau)}(k, Q_0)\right]\left(u \approx \frac{1}{2}\right) = \frac{16 C_F \mathrm{e}^{-\frac{c}{2}}}{\pi \beta_0} \frac{\mu}{u - \frac{1}{2}} \delta'(k).$$ (G.8)

To obtain the $\mathcal{O}(\alpha_s)$ unreleased soft function one has to take the limit $u \to 0$ of Eq. (G.6) and include back again the factor $(\alpha_s \beta_0)/(4\pi)$. The result is

$$S_{\text{ur}}^{(\tau)}(k, Q_0) = \frac{\alpha_s C_F}{4\pi} 16\, \theta(Q_0 - k)\left\{-\frac{1}{Q_0}\left[\frac{\theta(\tilde{k}) \ln \tilde{k}}{\tilde{k}}\right]_+\right\},$$ (G.9)

with $\tilde{k} = k/Q_0$.

We will now show that the virtual contributions to unreleased soft function vanish even in the presence of a $p_\perp$ cut. The Borel space contribution from the sum of the virtual diagrams shown in Fig. G.1b reads

$$B\left[S_{\text{ur}}^{(\tau,\text{virt})}(k, Q_0)\right] = \frac{i\,64\,C_F \pi^2}{\beta_0}\left(\mu^2 \mathrm{e}^{-c}\right)^u \delta(k) \int \frac{\mathrm{d}^4 q}{(2\pi)^4} \frac{\theta(Q_0 - q_\perp)}{(-q^2)^{1+u}(n \cdot q)(\bar{n} \cdot q)^{1+\alpha}},$$ (G.10)

where we have again introduced the α regulator and used $n^2 = \bar{n}^2 = 0$ and $n \cdot \bar{n} = 2$. This integral is most conveniently solved by using Feynman parameters of the form

$$\frac{1}{a^\alpha b^\beta c^\gamma} = \frac{\Gamma(\alpha + \beta + \gamma)}{\Gamma(\alpha)\Gamma(\beta)\Gamma(\gamma)} \int_0^\infty \mathrm{d}\lambda_1 \mathrm{d}\lambda_2 \frac{\lambda_1^{\beta-1}\lambda_2^{\gamma-1}}{(a + \lambda_1 b + \lambda_2 c)^{\alpha+\beta+\gamma}},$$ (G.11)

such that one finds

$$\frac{-i\,64\,C_F}{\beta_0}\left(\mu^2 \mathrm{e}^{-c}\right)^u \frac{\Gamma(3 + u + \alpha)}{\Gamma(1 + u)\Gamma(1 + \alpha)}(-1)^{u+\alpha}\delta(k)$$
$$\times \int_0^\infty \mathrm{d}\lambda_1\, \mathrm{d}\lambda_2\, \lambda_2^\alpha \int \frac{\mathrm{d}^4 q}{(2\pi)^4} \frac{\theta(Q_0 - q_\perp)}{(q^2 - \lambda_1\lambda_2)^{3+u+\alpha}}.$$ (G.12)

The q integral is solved by using Eq. (I.6) and leads to

$$B\left[S_{\text{ur}}^{(\text{virt})}(k, Q_0)\right] = \frac{-4C_F}{\beta_0}\left(\mu^2 \mathrm{e}^{-c}\right)^u \frac{\Gamma(1 + u + \alpha)}{\Gamma(1 + u)\Gamma(1 + \alpha)}\delta(k)$$
$$\times \int_0^\infty \mathrm{d}\lambda_2\, \lambda_2^\alpha \int_0^\infty \mathrm{d}\lambda_1\left((\lambda_1\lambda_2)^{-1-u-\alpha} - (Q_0^2 + \lambda_1\lambda_2)^{-1-u-\alpha}\right)$$
$$= \frac{4C_F}{\beta_0}\left(\frac{\mu^2 \mathrm{e}^{-c}}{Q_0^2}\right)^u \frac{\Gamma(u + \alpha)}{\Gamma(1 + u)\Gamma(1 + \alpha)}\delta(k)\, Q_0^{-2\alpha} \int_0^\infty \mathrm{d}\lambda_2\, \lambda_2^{-1+\alpha}$$
$$= 0.$$ (G.13)

The integral is scaleless and thus vanishes. Thus virtual diagrams do not contribute to the unreleased soft function at $\mathcal{O}(\alpha_s)$.

G.2   Unreleased soft function for angularities and C-parameter

It is straightforward to determine soft functions for other event shape variables using the method described in Sec. G.1. In the following we provide the corresponding results for the angularities τ_α and the C-parameter for future use.

For the angularities the measurement function shown in the second line of Eq. (G.1) for thrust reads

$$\theta(q^- - q^+)\delta\Big(k - (q^+)^{1-\frac{a}{2}}(q^-)^{\frac{a}{2}}\Big) \; + \; \big[\, q^- \leftrightarrow q^+ \,\big]. \tag{G.14}$$

and the resulting unreleased soft function at $\mathcal{O}(\alpha_s)$ has the form

$$S_{\mathrm{ur}}^{(\tau_a)}(k, Q_0) = \frac{\alpha_s(Q_0)C_F}{4\pi} \frac{16\,\theta(Q_0 - k)}{1 - a}\left\{ -\frac{1}{Q_0}\Big[\frac{\theta(\tilde{k})\ln\tilde{k}}{\tilde{k}}\Big]_+ \right\}. \tag{G.15}$$

The pole of the Borel transform at $u = 1/2$ reads

$$B\Big[S_{\mathrm{ur}}^{(\tau_a)}(k, Q_0)\Big]\Big(u \approx \frac{1}{2}\Big) = \frac{16C_F e^{-\frac{c}{2}}}{\pi\beta_0(1 - a)}\frac{\mu}{u - \frac{1}{2}}\,\delta'(k), \tag{G.16}$$

and the first moment has the form

$$\int \mathrm{d}k\, k\, S_{\mathrm{ur}}^{(\tau_a)}(k, Q_0) = \frac{\alpha_s(Q_0)C_F}{4\pi} \frac{16\,Q_0}{1 - a}. \tag{G.17}$$

For the C-parameter the measurement function shown in the second line of Eq. (G.1) for thrust reads

$$\delta\Big(k - \frac{q^- q^+}{q^- + q^+}\Big) \tag{G.18}$$

and the resulting unreleased soft function at $\mathcal{O}(\alpha_s)$ has the form $[w(z) = (1 - 4/z)^{1/2}]$

$$S_{\mathrm{ur}}^{(C)}(k, Q_0) = \frac{\alpha_s(Q_0)C_F}{4\pi} 16\,\theta\Big(\frac{Q_0}{2} - k\Big)\left\{ -\frac{1}{Q_0}\Big[\frac{\theta(\tilde{k})\ln\tilde{k}}{\tilde{k}}\Big]_+ + \frac{\pi^2}{24}\delta(k) + \frac{\ln\Big(\frac{1 + w(1/\tilde{k}^2)}{2}\Big)}{k} \right\}. \tag{G.19}$$

The pole of the Borel transform at $u = 1/2$ reads

$$B\Big[S_{\mathrm{ur}}^{(C)}(k, Q_0)\Big]\Big(u \approx \frac{1}{2}\Big) = \frac{4C_F e^{-\frac{c}{2}}}{\beta_0}\frac{\mu}{u - \frac{1}{2}}\,\delta'(k). \tag{G.20}$$

and the first moment has the form

$$\int \mathrm{d}\ell\, \ell\, S_{\mathrm{ur}}^{(C)}(\ell, Q_0) = \frac{\alpha_s(Q_0)C_F}{4\pi} 4\pi Q_0. \tag{G.21}$$

For all results we have $c = 5/3$ in the $\overline{\mathrm{MS}}$ scheme and $\tilde{k} \equiv k/Q_0$.

G.3   Unreleased bHQET jet function

In this section we calculate the unreleased bHQET jet function at $\mathcal{O}(\alpha_s)$. The unreleased bHQET jet function arises from ultra-collinear radiation off the massive quark coming *from below* the $p_\perp$ cut Q_0. As for the unreleased soft function we carry out the calculation using the dressed gluon propagator of Eq. (8.18), which is suitable to obtain the Borel transform accounting for fermion bubble resummation to all orders and to obtain the usual $\mathcal{O}(\alpha_s)$ result from the limit $u \to 0$ and
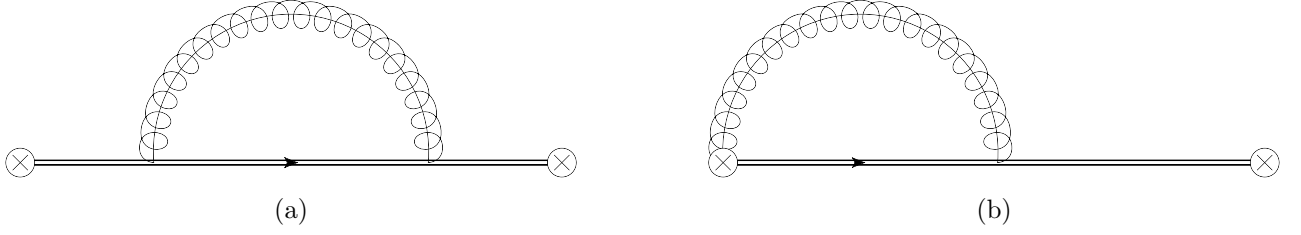
Figure G.2: Diagrams relevant for computation of the bHQET jet function at $\mathcal{O}(\alpha_s)$.

accounting for the additional factor $(\alpha_s \beta_0)/(4\pi)$. All integrals can again be carried out in 4 dimensions since in the presence of the $p_\perp$ cut they are ultraviolet finite. In contrast to the calculation for the soft function, there are no rapidity divergences at intermediate steps of the calculation. We note that in the following we determine the $\mathcal{O}(\alpha_s)$ corrections to the unreleased bHQET jet function matrix element $\mathcal{J}_{B,\mathrm{ur}}^{(\tau)}(\hat{s}, Q_0)$ with and $\hat{s} = \hat{s} + i0$ following the conventions from Ref. [19]. The actual unreleased bHQET jet function $J_{B,\mathrm{ur}}(\hat{s}, Q_0)$ appearing in the factorization theorem of Eq. (7.25) is then obtained by taking the imaginary part:

$$J_{B,\mathrm{ur}}^{(\tau)}(\hat{s}, Q_0) \;=\; \mathrm{Im}\Big[\mathcal{J}_{B,\mathrm{ur}}^{(\tau)}(\hat{s} + i0, Q_0)\Big] . \tag{G.22}$$

The self energy diagram Fig. G.2a in Borel space reads (already including a factor two because the jet function in the factorization theorem Eq. (7.25) accounts for both hemispheres)

$$B\Big[\mathcal{J}_{B,\mathrm{ur}}^{(a)}(\hat{s}, Q_0)\Big] = \frac{i\,64\pi\,C_F}{m\hat{s}^2\beta_0}\big(\mu^2 e^{-c}\big)^u \theta(\hat{s}) \int \frac{\mathrm{d}^4 q}{(2\pi)^4} \frac{\theta(Q_0 - q_\perp)}{(-q^2)^{1+u}(-v\cdot q - \frac{\hat{s}}{2})} , \tag{G.23}$$

with $v^2 = 1$ and $c = 5/3$ in the $\overline{\mathrm{MS}}$ renormalization scheme. The integral is evaluated in 4 dimensions because in the unreleased contributions there are no divergences that need to be regularized by dimensional regularization. It can be calculated by using Feynman paramters of the form

$$\frac{1}{a^\alpha b^\beta} = \frac{\Gamma(\alpha + \beta)}{\Gamma(\alpha)\Gamma(\beta)} \int_0^\infty \mathrm{d}\lambda \frac{\lambda^{\beta - 1}}{(a + \lambda b)^{\alpha + \beta}} , \tag{G.24}$$

such that

$$B\Big[\mathcal{J}_{B,\mathrm{ur}}^{(a)}(\hat{s}, Q_0)\Big] = \frac{i\,64\pi\,C_F}{m\hat{s}^2\beta_0}\big(\mu^2 e^{-c}\big)^u (1+u)(-1)^u \theta(\hat{s})$$
$$\times \int_0^\infty \mathrm{d}\lambda \int \frac{\mathrm{d}^4 q}{(2\pi)^4} \frac{\theta(Q_0 - q_\perp)}{\big(q^2 - \frac{\lambda}{2}(\frac{\lambda}{2} - \hat{s})\big)^{2+u}} . \tag{G.25}$$

The q integral is solved by using Eq. (I.6) and leads to (after doing the additional substitution $\lambda \to 2Q_0 \lambda$ and $\tilde{s} = \hat{s}/Q_0$)

$$B\Big[\mathcal{J}_{B,\mathrm{ur}}^{(a)}(\hat{s}, Q_0)\Big] = \frac{-8C_F Q_0}{m\hat{s}^2\pi\beta_0}\Big(\frac{\mu^2 e^{-c}}{Q_0^2}\Big)^u \theta(\hat{s}) \frac{1}{u} \int_0^\infty \mathrm{d}\lambda \Big[\big(\lambda(\lambda - \tilde{s})\big)^{-u} - \big(1 + \lambda(\lambda - \tilde{s})\big)^{-u}\Big] . \tag{G.26}$$

Let us first look at the on-shell (os) self-energy contribution of this diagram. Due to the cutoff Q_0 it does not vanish and is therefore relevant for the mass renormalization scheme. It is obtained by setting $\hat{s} \to 0$ under the integral. This yields

$$B\Big[\mathcal{J}_{B,\mathrm{ur}}^{(a,\mathrm{os})}(\hat{s}, Q_0)\Big] = \frac{-8C_F Q_0}{m\hat{s}^2\pi\beta_0}\Big(\frac{\mu^2 e^{-c}}{Q_0^2}\Big)^u \theta(\hat{s}) \frac{1}{u} \int_0^\infty \mathrm{d}\lambda \Big[\lambda^{-2u} - (1 + \lambda^2)^{-u}\Big]$$
$$= \frac{4C_F Q_0}{m\hat{s}^2\pi\beta_0}\Big(\frac{\mu^2 e^{-c}}{Q_0^2}\Big)^u \theta(\hat{s}) \frac{\sqrt{\pi}\,\Gamma\big(u - \frac{1}{2}\big)}{\Gamma(1 + u)} . \tag{G.27}$$

219

The first term under the integral in the first line is scaleless and can be dropped. To identify the leading renormalon pole we expand Eq. (G.27) for $u \to 1/2$ to obtain

$$B\left[\mathcal{J}^{(a,\text{os})}_{B,\text{ur}}(\hat{s}, Q_0)\right]\left(u \approx \frac{1}{2}\right) = \frac{8C_F e^{-\frac{c}{2}}}{m\hat{s}^2 \pi \beta_0} \theta(\hat{s}) \frac{\mu}{u - \frac{1}{2}} . \tag{G.28}$$

To get the one-loop result one has to take the limit $u \to 0$ of Eq. (G.27) and include again the factor $(\alpha_s \beta_0)/(4\pi)$:

$$\mathcal{J}^{(a,\text{os})}_{B,\text{ur}}(\hat{s}, Q_0) = -\frac{1}{m} \frac{\alpha_s C_F}{4\pi} \frac{\theta(\hat{s})}{\pi \hat{s}^2} 8\pi Q_0 . \tag{G.29}$$

To get the result of the integral in Eq. (G.26) for finite $\hat{s}$ we first note that this does not give a pole for $u \to 1/2$. This can be seen by setting $u = 1/2$ and investigating the behavior of the integrand for small and large values of λ:

$$\lambda^{-\frac{1}{2}} \quad \text{for} \quad \lambda \to 0 , \tag{G.30}$$

$$\lambda^{-3} \quad \text{for} \quad \lambda \to \infty . \tag{G.31}$$

This implies that the integral converges and that there is no renormalon pole at $u = 1/2$ in the off-shell case. To get the corresponding one-loop result we take the limit $u \to 0$ and multiply back the factor $(\alpha_s \beta_0)/(4\pi)$ and get $[w(z) = (1 - 4/z)^{1/2}]$

$$\mathcal{J}^{(a)}_{B,\text{ur}}(\hat{s}, Q_0) = \frac{1}{m} \frac{\alpha_s C_F}{4\pi} \frac{\theta(\hat{s})}{\pi \hat{s}^2} 8Q_0 \int_0^\infty d\lambda \, \ln\left(\frac{\lambda(\lambda - \tilde{s})}{1 + \lambda(\lambda - \tilde{s})}\right) \tag{G.32}$$

$$= \frac{1}{m} \frac{\alpha_s C_F}{4\pi} \frac{\theta(\hat{s})}{\pi \hat{s}} 8 \left[\theta(2Q_0 - \hat{s})\left(-\frac{w\left(\frac{16}{\tilde{s}^2}\right)\left(2\text{Tan}^{-1}\left(\frac{\tilde{s}}{2w\left(\frac{16}{\tilde{s}^2}\right)}\right) + \pi\right)}{\tilde{s}} + \ln(-\tilde{s})\right)\right.$$

$$\left. + \theta(\hat{s} - 2Q_0)\left(i\pi(w(\tilde{s}^2) - 1) + \ln\tilde{s} - \frac{w(\tilde{s}^2)}{2} \ln\left(\frac{1 + w(\tilde{s}^2)}{1 - w(\tilde{s}^2)}\right)\right)\right] .$$

The diagram in Fig. G.2b in Borel space reads (including a factor two to account for both hemispheres and a factor two for the mirror diagram)

$$B\left[\mathcal{J}^{(b)}_{B,\text{ur}}(\hat{s}, Q_0)\right] = \frac{-i\,64\pi\,C_F}{m\hat{s}\beta_0}\left(\mu^2 e^{-c}\right)^u \theta(\hat{s}) \frac{Q}{m} \tag{G.33}$$

$$\times \int \frac{d^4q}{(2\pi)^4}\left[\frac{\theta(Q_0 - q_\perp)}{(-q^2)^{1+u}(-v \cdot q - \frac{\hat{s}}{2})(-n \cdot q)} - \frac{\theta(Q_0 - q_\perp)}{(-q^2)^{1+u}(-\frac{Q}{2m}\bar{n} \cdot q - \frac{\hat{s}}{2})(-n \cdot q)}\right] ,$$

with $v^2 = 1$, $n^2 = \bar{n}^2 = 0$, $n \cdot \bar{n} = 2$ and $n \cdot v = Q/m$. Again the prescription $\hat{s} = \hat{s} + i0$ is implied. The second term under the integral is the 0-bin that needs to be subratcted to avoid a double counting between the soft and the collinear regions. We can again use Feynman parameters of the form Eq. (G.11) to obtain

$$B\left[\mathcal{J}^{(b)}_{B,\text{ur}}(\hat{s}, Q_0)\right] = \frac{i\,64\pi\,C_F}{m\hat{s}\beta_0}\left(\mu^2 e^{-c}\right)^u \frac{(-1)^u \Gamma(3 + u)}{\Gamma(1 + u)} \theta(\hat{s}) \frac{Q}{m} \tag{G.34}$$

$$\times \int_0^\infty d\lambda_1 d\lambda_2 \int \frac{d^4q}{(2\pi)^4}\left[\frac{\theta(Q_0 - q_\perp)}{\left(q^2 - \frac{\lambda_1}{2}\left(\frac{\lambda_1}{2} + \frac{Q\lambda_2}{m} - \hat{s}\right)\right)^{3+u}} - \frac{\theta(Q_0 - q_\perp)}{\left(q^2 - \frac{\lambda_1}{2}\left(\frac{Q\lambda_2}{m} - \hat{s}\right)\right)^{3+u}}\right] .$$

The q integral is solved by using Eq. (I.6) and leads to (after doing the additional substitution $\lambda_1 \to 2Q_0\lambda_1$, $\lambda_2 \to Q_0 m\lambda_2/Q$ and $\tilde{s} = \hat{s}/Q_0$)

$$
B\left[\mathcal{J}_{B,\mathrm{ur}}^{(b)}(\hat{s},Q_0)\right] = \frac{8\,C_F}{m\hat{s}\pi\beta_0}\left(\frac{\mu^2 \mathrm{e}^{-c}}{Q_0^2}\right)^u \theta(\hat{s})
$$

$$
\times \int_0^\infty \mathrm{d}\lambda_1\mathrm{d}\lambda_2 \left[\left(\lambda_1(\lambda_1+\lambda_2-\hat{s})\right)^{-1-u} - \left(1+\lambda_1(\lambda_1+\lambda_2-\hat{s})\right)^{-1-u}\right.
$$

$$
\left. - \left(\lambda_1(\lambda_2-\hat{s})\right)^{-1-u} + \left(1+\lambda_1(\lambda_2-\hat{s})\right)^{-1-u}\right]
$$

$$
= \frac{8\,C_F}{m\hat{s}\pi\beta_0}\left(\frac{\mu^2 \mathrm{e}^{-c}}{Q_0^2}\right)^u \theta(\hat{s}) \frac{1}{u} \int_0^\infty \frac{\mathrm{d}\lambda_1}{\lambda_1}\left[\left(\lambda_1(\lambda_1-\hat{s})\right)^{-u} - \left(1+\lambda_1(\lambda_1-\hat{s})\right)^{-u}\right.
$$

$$
\left. - \left(-\lambda_1\hat{s}\right)^{-u} + \left(1-\lambda_1\hat{s}\right)^{-u}\right]. \tag{G.35}
$$

We note that the integral does not lead to a pole at $u = 1/2$, because the λ integral is finite. This can be seen by investigating the behavior of the integrand for the small and larger λ:

$$
\lambda^{-\frac{1}{2}} \quad \text{for} \quad \lambda \to 0\,, \tag{G.36}
$$

$$
\lambda^{-\frac{3}{2}} \quad \text{for} \quad \lambda \to \infty\,. \tag{G.37}
$$

To get the one-loop result we take the limit $u \to 0$ and multiply back the factor $(\alpha_s\beta_0)/(4\pi)$ to obtain $[w(z) = (1-4/z)^{1/2}]$

$$
\mathcal{J}_{B,\mathrm{ur}}^{(b)}(\hat{s},Q_0) = -\frac{1}{m}\frac{\alpha_s C_F}{4\pi}\frac{\theta(\hat{s})}{\pi\hat{s}}8\int_0^\infty \frac{\mathrm{d}\lambda_1}{\lambda_1} \ln\left(\frac{-(\lambda_1-\hat{s})(1-\lambda_1\hat{s})}{\hat{s}\left(1+\lambda_1(\lambda_1-\hat{s})\right)}\right) \tag{G.38}
$$

$$
= \frac{1}{m}\frac{\alpha_s C_F}{4\pi}\frac{\theta(\hat{s})}{\pi\hat{s}}8\left[\theta(2Q_0-\hat{s})\left(-\ln^2(-\tilde{s}) - \frac{\pi^2}{4} - \left(\mathrm{Tan}^{-1}\left(\frac{\tilde{s}}{2w(\frac{16}{\tilde{s}^2})}\right)+\pi\right)\mathrm{Tan}^{-1}\left(\frac{\tilde{s}}{2w(\frac{16}{\tilde{s}^2})}\right)\right)\right.
$$

$$
\left. + \theta(\hat{s}-2Q_0)\left(i\pi\left(2\ln\tilde{s} - \ln\left(\frac{1+w(\tilde{s}^2)}{1-w(\tilde{s}^2)}\right)\right) - \ln\left(\frac{1+w(\tilde{s}^2)}{2}\right)\ln\left(\frac{1-w(\tilde{s}^2)}{2}\right)\right)\right].
$$

The complete sum of all off-shell $\mathcal{O}(\alpha_s)$ corrections, defined as the sum of all contributions for finite $\hat{s}$ minus the on-shell diagram of Eq. (G.29), reads

$$
\mathcal{J}_{B,\mathrm{ur}}^{(\mathrm{off})}(\hat{s},Q_0) = \mathcal{J}_{B,\mathrm{ur}}^{(a)}(\hat{s},Q_0) + \mathcal{J}_{B,\mathrm{ur}}^{(b)}(\hat{s},Q_0) - \mathcal{J}_{B,\mathrm{ur}}^{(a,\mathrm{os})}(\hat{s},Q_0)
$$

$$
= \frac{1}{m}\frac{\alpha_s C_F}{4\pi}\frac{1}{\pi\hat{s}}\left\{\theta(2Q_0-\hat{s})\left[-8\ln^2(-\tilde{s}) + 8\ln(-\tilde{s}) + \frac{8\pi(1-w(\frac{16}{\tilde{s}^2}))}{\tilde{s}}\right.\right.
$$

$$
\left. - \frac{16w(\frac{16}{\tilde{s}^2})\mathrm{Tan}^{-1}\left(\frac{\tilde{s}}{2w(\frac{16}{\tilde{s}^2})}\right)}{\tilde{s}} - 8\mathrm{Tan}^{-1}\left(\frac{\tilde{s}}{2w(\frac{16}{\tilde{s}^2})}\right)\left(\mathrm{Tan}^{-1}\left(\frac{\tilde{s}}{2w(\frac{16}{\tilde{s}^2})}\right)+\pi\right) - 2\pi^2\right]
$$

$$
+ \theta(\hat{s}-2Q_0)\left[i\pi\left(8w(\tilde{s}^2) - 8 + 16\ln\tilde{s} - 8\ln\left(\frac{1+w(\tilde{s}^2)}{1-w(\tilde{s}^2)}\right)\right) + 8\ln\tilde{s}\right.
$$

$$
\left.\left. - 4w(\tilde{s}^2)\ln\left(\frac{1+w(\tilde{s}^2)}{1-w(\tilde{s}^2)}\right) - 8\ln\left(\frac{1-w(\tilde{s}^2)}{2}\right)\ln\left(\frac{1+w(\tilde{s}^2)}{2}\right) + \frac{8\pi}{\tilde{s}}\right]\right\}, \tag{G.39}
$$

and the corresponding Borel space result at the pole at $u = 1/2$ has the form

$$
B\left[\mathcal{J}_{B,\mathrm{ur}}^{(\mathrm{off})}(\hat{s},Q_0)\right]\left(u \approx \frac{1}{2}\right) = \frac{-8C_F\mathrm{e}^{-\frac{c}{2}}}{m\hat{s}^2\pi\beta_0}\theta(\hat{s})\frac{\mu}{u-\frac{1}{2}}\,. \tag{G.40}
$$

To obtain the $\mathcal{O}(\alpha_s)$ results for the bHQET jet function we take the imaginary part of Eqs. (G.29) and (G.39) following Eq. (G.22). Writing the jet function as a sum of the on-shell (os) self-energy contribution and the remaining off-shell contributions (off)

$$J_{B,\mathrm{ur}}^{(\tau)}(\hat{s}, Q_0) = J_{B,\mathrm{ur}}^{(\mathrm{os})}(\hat{s}, Q_0) + J_{B,\mathrm{ur}}^{(\mathrm{off})}(\hat{s}, Q_0) \tag{G.41}$$

we obtain $[w(z) = (1 - 4/z)^{1/2}, \tilde{s} = \hat{s}/Q_0]$

$$J_{B,\mathrm{ur}}^{(\mathrm{os})}(\hat{s}, Q_0) = \frac{1}{m}\frac{\alpha_s C_F}{4\pi}\left(-8\pi Q_0\,\delta'(\hat{s})\right), \tag{G.42}$$

$$J_{B,\mathrm{ur}}^{(\mathrm{off})}(\hat{s}, Q_0) = \frac{1}{m}\frac{\alpha_s C_F}{4\pi}\left\{2\left(4 - \frac{\pi^2}{3}\right)\delta(\hat{s})\right. \tag{G.43}$$

$$+ \theta(2Q_0 - \hat{s})\left(-\frac{8}{Q_0}\left[\frac{\theta(\tilde{s})}{\tilde{s}}\right]_+ + \frac{16}{Q_0}\left[\frac{\theta(\tilde{s})\ln\tilde{s}}{\tilde{s}}\right]_+\right)$$

$$+ \left. \theta(\hat{s} - 2Q_0)\frac{8}{\hat{s}}\left[\left(w(\tilde{s}^2) - 1\right) - \left(\ln\left(\frac{1 + w(\tilde{s}^2)}{1 - w(\tilde{s}^2)}\right) - 2\ln\tilde{s}\right)\right]\right\}.$$

The corresponding Borel space result at the pole at $u = 1/2$ are obtained by taking the imaginary parts of Eqs. (G.28) and (G.40) giving

$$B\left[J_{B,\mathrm{ur}}^{(\mathrm{os})}(\hat{s}, Q_0)\right]\left(u \approx \frac{1}{2}\right) = \frac{8C_F e^{-\frac{c}{2}}}{m\beta_0}\frac{\mu}{u - \frac{1}{2}}\delta'(\hat{s}), \tag{G.44}$$

$$B\left[J_{B,\mathrm{ur}}^{(\mathrm{off})}(\hat{s}, Q_0)\right]\left(u \approx \frac{1}{2}\right) = \frac{-8C_F e^{-\frac{c}{2}}}{m\beta_0}\frac{\mu}{u - \frac{1}{2}}\delta'(\hat{s}). \tag{G.45}$$

G.4 Unreleased SCET jet function

The calculation for the unreleased SCET thrust jet function for massless quark production can be carried out in close analogy to Sec. G.3. The full result (accounting for the contributions arising from two hemispheres, which leads to a different factor of 2 compared to the single hemisphere jet function that was used in the first part of the thesis) at $\mathcal{O}(\alpha_s)$ reads $[s' = s/Q_0^2, w(z) = (1 - 4/z)^{1/2}]$

$$J_{\mathrm{ur}}^{(\tau)}(s, Q_0) = \frac{\alpha_s(Q_0)C_F}{4\pi}\left\{\left(12 - \frac{4\pi^2}{3}\right)\delta(s) + \theta(4Q_0^2 - s)\left(-\frac{6}{Q_0^2}\left[\frac{\theta(s')}{s'}\right]_+ + \frac{8}{Q_0^2}\left[\frac{\theta(s')\ln s'}{s'}\right]_+\right)\right.$$

$$+ \left. \theta(s - 4Q_0^2)\frac{1}{s}\left[6(w(s') - 1) - 8\left(\ln\left(\frac{1 + w(s')}{1 - w(s')}\right) - \ln s'\right)\right]\right\}. \tag{G.46}$$

For future reference we also provide some useful intermediate results the SCET jet function in Feynman gauge. The self-energy diagrams yields

$$\frac{\alpha_s(\mu)C_F}{4\pi}\left\{-\delta(s) + \frac{1}{\mu^2}\left[\frac{\theta(s/\mu^2)}{s/\mu^2}\right]_+\right\} \tag{G.47}$$

without any cut and

$$\frac{\alpha_s(Q_0)C_F}{4\pi}\left\{-2\delta(s) + \theta(4Q_0^2 - s)\frac{1}{Q_0^2}\left[\frac{\theta(s/Q_0^2)}{s/Q_0^2}\right]_+ + \frac{\theta(s - 4Q_0^2)}{s}\left(1 - w(s/Q_0^2)\right)\right\} \tag{G.48}$$

for the unreleased contribution. The Wilson-line diagrams (containing the Eikonal propagator) yield

$$\frac{\alpha_s(\mu)C_F}{4\pi}\left\{\left(4 - \frac{\pi^2}{2}\right)\delta(s) - \frac{2}{\mu^2}\left[\frac{\theta(s/\mu^2)}{s/\mu^2}\right]_+ + \frac{2}{\mu^2}\left[\frac{\theta(s/\mu^2)\ln s/\mu^2}{s/\mu^2}\right]_+\right\} \tag{G.49}$$

without any cut and

$$
\frac{\alpha_s(Q_0)C_F}{4\pi}\left\{\left(4-\frac{\pi^2}{3}\right)\delta(s)+\theta(4Q_0^2-s)\left(-\frac{2}{Q_0^2}\left[\frac{\theta(s/Q_0^2)}{s/Q_0^2}\right]_++\frac{2}{Q_0^2}\left[\frac{\theta(s/Q_0^2)\ln s/Q_0^2}{s/Q_0^2}\right]_+\right)\right.
$$
$$
\left.+\theta(s-4Q_0^2)\frac{2}{s}\left[w(s/Q_0^2)-1+\ln\frac{s}{Q_0^2}-\ln\left(\frac{1+w(s/Q_0^2)}{1-w(s/Q_0^2)}\right)\right]\right\} \qquad \text{(G.50)}
$$

for the unreleased contribution.

Appendix H

Unreleased contributions with an angular cut

In this section we present the calculation for the unreleased contributions (i.e. the contributions coming from below the shower cut Q_0) at $\mathcal{O}(\alpha_s)$ with an additional constraint on the angle of the emitted gluon. The results for the shower cut dependence of the fitted top quark mass from $m_{b_j\ell}$ and m_{b_jW} (see Sec. 9.6) as function of the angular cut are compared to the Herwig 7 event generator in Sec. H.4. These results were not contained in Ref. [3].

The angle θ under which a gluon with four momentum q^μ is emitted from the quark can be written in terms of its light-cone components as

$$\cos\theta = \frac{q^3}{q^0} = \frac{q^- - q^+}{q^- + q^+} \, . \tag{H.1}$$

The constraint that the gluon has to be emitted with an angle smaller than some maximum jet opening angle R is then given by

$$q^- > q^+ x^2 \, , \qquad \text{with} \quad x = \sqrt{\frac{1 + \cos R}{1 - \cos R}} = \cot\left(\frac{R}{2}\right) \, . \tag{H.2}$$

For $R = \pi/2$ we get back the full hemisphere $q^- > q^+$.

H.1 Unreleased soft function with an angular cut

To calculate the unreleased (i.e. $q_\perp < Q_0$) soft function with the additional constraint $\theta < R$ we start from Eq. (G.1). Because we are only interested in the one-loop contribution we can set $u = 0$ and include again the factor $(\alpha_s\beta_0)/(4\pi)$. We are only looking at radiation in one hemisphere $q^- > q^+$ and calculate only contributions for $k > 0$ such that we can drop the α-regulator.

$$S_{\text{ur}}^{(\tau,\text{real})}(k, Q_0, R) = \frac{\alpha_s C_F}{\pi}\theta(k)\int \frac{\mathrm{d}q^-\mathrm{d}q^+}{q^-q^+}\theta(q^- - q^+x^2)\delta(k - q^+)\frac{1}{\pi}\mathrm{Im}\Big[\int_0^{Q_0^2} \mathrm{d}q_\perp^2 \frac{1}{q_\perp^2 - q^-q^+ - i0}\Big] \, , \tag{H.3}$$

where the theta function $\theta(q^- - q^+)$ restricting the radiation to one hemisphere was replaced by $\theta(q^- - q^+x^2)$ to now restrict it inside the cone with opening angle R. After doing the $q_\perp$ integral and taking the imaginary part

$$\frac{1}{\pi}\mathrm{Im}\Big[\int_0^{Q_0^2} \mathrm{d}q_\perp^2 \frac{1}{q_\perp^2 - q^-q^+ - i0}\Big] = \theta(q^-q^+)\theta(Q_0^2 - q^-q^+) \, , \tag{H.4}$$

and doing the trivial q^+ integration we get

$$
\begin{aligned}
S_{\mathrm{ur}}^{(\tau,\mathrm{real})}(k,Q_0,R) &= \frac{\alpha_s C_F}{\pi}\frac{\theta(k)}{k}\int\frac{\mathrm{d}q^-}{q^-}\,\theta(q^- - kx^2)\theta\Big(\frac{Q_0^2}{k} - q^-\Big) \\
&= \frac{\alpha_s C_F}{4\pi}\theta\Big(\frac{Q_0}{x} - k\Big)\Big(-\frac{8}{k}\ln\frac{kx}{Q_0}\Big).
\end{aligned} \tag{H.5}
$$

For $R = \pi/2$ we recover our result from Eq. (G.9) (note the additional factor of 1/2 because we are only considering one hemisphere here).

The first moment of the unreleased soft function with an angular cut R is

$$
\begin{aligned}
\int \mathrm{d}k\, k\, S_{\mathrm{ur}}^{(\tau,\mathrm{real})}(k,Q_0,R) &= \frac{\alpha_s C_F}{4\pi}\,Q_0 8\tan\Big(\frac{R}{2}\Big) \\
&= \frac{\alpha_s C_F}{4\pi}\,Q_0\big(4R + \mathcal{O}(R^3)\big).
\end{aligned} \tag{H.6}
$$

H.2 Unreleased bHQET jet function with an angular cut

To calculate the unreleased bHQET jet function with an angular cut we have to recalculate the unreleased contributions to the diagrams in Fig. G.2 with the additional constraint of Eq. (H.2) on the momentum of the radiated gluon. Since this cut only affects the real radiation, i.e. $\hat{s} > 0$, the calculation becomes easier when taking the imaginary part (see Eq. (G.22)) prior to doing the integrals by replacing each of the propagators in the integral by its on-shell condition

$$
\frac{i}{k^2 + i0} \to 2\pi\delta(k^2)\theta(k^0). \tag{H.7}
$$

The unreleased contributions to the self-energy diagram in Fig. G.2a with an angular cut are

$$
\begin{aligned}
J_{B,\mathrm{ur}}^{(a,\mathrm{real})}(\hat{s},Q_0,R) &= \frac{-4\alpha_s C_F}{m\hat{s}^2}\int\frac{\mathrm{d}^4 q}{(2\pi)^4}\,2\pi\delta(q^2)\theta(q^0)\,2\pi\delta\Big(v\cdot q - \frac{\hat{s}}{2}\Big)\theta(Q_0^2 - q_\perp^2)\theta(q^0\cos R - q^3) \\
&= -\frac{1}{m}\frac{\alpha_s C_F}{4\pi}\frac{4}{\hat{s}^2}\int \mathrm{d}q^-\mathrm{d}q^+\mathrm{d}q_\perp^2\,\theta(q_\perp^2)\theta(q^-)\delta(q^+q^- - q_\perp^2)\delta\Big(\frac{Q}{2m}q^+ + \frac{m}{2Q}q^- - \frac{\hat{s}}{2}\Big) \\
&\qquad\qquad\qquad \times \theta(Q_0^2 - q_\perp^2)\theta(q^- - x^2 q^+),
\end{aligned} \tag{H.8}
$$

where the last two theta-functions restrain the radiation of the gluon into the unreleased region and within the jet cone with x defined in Eq. (H.2). After doing the trivial q^+ and $q_\perp$ integrations using the delta-functions and a simple rescaling $q^- \to \frac{Q}{m}q^-$ one arrives at

$$
J_{B,\mathrm{ur}}^{(a,\mathrm{real})}(\hat{s},Q_0,R) = -\frac{1}{m}\frac{\alpha_s C_F}{4\pi}\frac{4}{\hat{s}^2}\int_0^\infty \mathrm{d}q^-\,\theta(\hat{s} - q^-)\theta(Q_0^2 - \hat{s}q^- + (q^-)^2)\theta\Big(q^- - \frac{\hat{s}y}{1+y^2}\Big), \tag{H.9}
$$

where we introduced the variable

$$
y = \frac{m}{Q}\cot\Big(\frac{R}{2}\Big). \tag{H.10}
$$

This integral is solved to $[w(z) = (1-z^2)^{1/2},\ \tilde{s} = \hat{s}/Q_0]$

$$
\begin{aligned}
J_{B,\mathrm{ur}}^{(a,\mathrm{real})}(\hat{s},Q_0,R) = \frac{1}{m}\frac{\alpha_s C_F}{4\pi}\frac{4}{\hat{s}}\Bigg\{ &\theta\Big(\frac{Q_0(1+y^2)}{y} - \hat{s}\Big)\frac{-1}{1+y^2} + \theta\Big(\hat{s} - \frac{Q_0(1+y^2)}{y}\Big)\frac{1}{2}\Big(w\Big(\frac{2}{\tilde{s}}\Big) - 1\Big) \\
&+ \theta(1-y)\theta(\hat{s} - 2Q_0)\theta\Big(\frac{Q_0(1+y^2)}{y} - \hat{s}\Big)w\Big(\frac{2}{\tilde{s}}\Big)\Bigg\}.
\end{aligned} \tag{H.11}
$$

The contribution from real radiation to the second diagram in Fig. G.2b (also including the mirror diagram but again with a missing factor of 2 with respect to the previous sections because we only consider one hemisphere) is

$$
\begin{aligned}
J_{B,\mathrm{ur}}^{(b,\mathrm{real})}(\hat{s}, Q_0, R) =& \frac{4Q\alpha_s C_F}{m^2\hat{s}} \int \frac{\mathrm{d}^4 q}{(2\pi)^4} \frac{1}{q^-} 2\pi\delta(q^2)\theta(q^0) \, 2\pi\delta\big(v\cdot q - \frac{\hat{s}}{2}\big)\theta(Q_0^2 - q_\perp^2)\theta(q^0\cos R - q^3) \\
& - \text{zero-bin} \\
=& \frac{Q}{m^2} \frac{\alpha_s C_F}{4\pi} \frac{2}{\hat{s}} \int \mathrm{d}q^- \mathrm{d}q^+ \mathrm{d}q_\perp^2 \frac{1}{q^-}\theta(q_\perp^2)\theta(q^-)\delta(q^+ q^- - q_\perp^2) \\
& \times \left[\delta\big(\frac{Q}{2m}q^+ + \frac{m}{2Q}q^- - \frac{\hat{s}}{2}\big) - \delta\big(\frac{Q}{2m}q^+ - \frac{\hat{s}}{2}\big) \right]\theta(Q_0^2 - q_\perp^2)\theta(q^- - x^2 q^+)\,,
\end{aligned}
$$
(H.12)

where the last two theta-functions restrain the radiation of the gluon into the unreleased region and within the jet cone with x defined in Eq. (H.2). After doing the trivial q^+ and $q_\perp$ integrations using the delta-functions and a simple rescaling $q^- \to \frac{Q}{m}q^-$ one arrives at

$$
J_{B,\mathrm{ur}}^{(b,\mathrm{real})}(\hat{s}, Q_0, R) = \frac{1}{m} \frac{\alpha_s C_F}{4\pi} \frac{4}{\hat{s}} \int_0^\infty \frac{\mathrm{d}q^-}{q^-} \left[\theta(\hat{s} - q^-)\theta(Q_0^2 - \hat{s}q^- + (q^-)^2)\theta\big(q^- - \frac{\hat{s}y}{1+y^2}\big) \right.
$$
$$
\left. - \theta(Q_0^2 - \hat{s}q^-)\theta(q^- - \hat{s}y^2) \right]\,,
$$
(H.13)

This integral is solved to

$$
\begin{aligned}
J_{B,\mathrm{ur}}^{(b,\mathrm{real})}(\hat{s}, Q_0, R) =& \frac{1}{m} \frac{\alpha_s C_F}{4\pi} \frac{4}{\hat{s}} \left\{ \theta\big(\frac{Q_0(1+y^2)}{y} - \hat{s}\big) \ln\big(\frac{1+y^2}{y^2}\big) \right. \\
& + \theta\big(\hat{s} - \frac{Q_0(1+y^2)}{y}\big) \ln\big(\frac{2}{1 + w(\frac{2}{\tilde{s}})}\big) + \theta\big(\frac{Q_0}{y} - \hat{s}\big) 2\ln\big(\frac{\hat{s}y}{Q_0}\big) \\
& \left. + \theta(1-y)\theta\big(\frac{Q_0(1+y^2)}{y} - \hat{s}\big)\theta(\hat{s} - 2Q_0) \ln\big(\frac{1 - w(\frac{2}{\tilde{s}})}{1 + w(\frac{2}{\tilde{s}})}\big) \right\}\,.
\end{aligned}
$$
(H.14)

Adding up all diagrams the unreleased bHQET jet function with an angular cut R for $\hat{s} > 0$ is $[w(z) = (1 - z^2)^{1/2}, \tilde{s} = \hat{s}/Q_0]$.

$$
\begin{aligned}
J_{B,\mathrm{ur}}^{(\mathrm{real})}(\hat{s}, Q_0, R) =& \frac{1}{m} \frac{\alpha_s C_F}{4\pi} \frac{4}{\hat{s}} \left\{ \theta\big(\frac{Q_0}{y} - \hat{s}\big) \left[2\ln\tilde{s} + \ln(1+y^2) - \frac{1}{1+y^2} \right] \right. \\
& + \theta\big(\hat{s} - \frac{Q_0}{y}\big)\theta\big(\frac{Q_0(1+y^2)}{y} - \hat{s}\big)\left[\ln\big(\frac{1+y^2}{y^2}\big) - \frac{1}{1+y^2} \right] \\
& + \theta\big(\hat{s} - \frac{Q_0(1+y^2)}{y}\big)\left[\ln\big(\frac{2}{1 + w(\frac{2}{\tilde{s}})}\big) + \frac{1}{2}\big(w(\frac{2}{\tilde{s}}) - 1\big) \right] \\
& \left. + \theta(1-y)\theta(\hat{s} - 2Q_0)\theta\big(\frac{Q_0(1+y^2)}{y} - \hat{s}\big) \left[w(\frac{2}{\tilde{s}}) - \ln\big(\frac{1 + w(\frac{2}{\tilde{s}})}{1 - w(\frac{2}{\tilde{s}})}\big) \right] \right\}\,,
\end{aligned}
$$
(H.15)

with y defined in Eq. (H.10).

The first moment of the unreleased bHQET jet function with an angular cut R is

$$
\int \mathrm{d}\hat{s} \, \hat{s} \, m J_{B,\mathrm{ur}}^{(\mathrm{real})}(\hat{s}, Q_0, R) = \frac{\alpha_s C_F}{4\pi}(-4Q_0\pi)\left[1 - \frac{2}{\pi}\tan^{-1}\big(\frac{m}{Q}\cot\big(\frac{R}{2}\big)\big) \right]\,.
$$
(H.16)

For $R = \pi$ or in the limit of infinite boost $m/Q \to 0$ we exactly recover our result in Eq. (8.26) for the real radiation terms, i.e. the terms without the δ'-distribution (note the additional factor of $1/2$ because we are considering only one hemisphere jet function here). For $R = \pi/2$ we do so up to terms suppressed by m/Q.

The result can be expanded to simplify to

$$\int \mathrm{d}\hat{s}\, \hat{s}\, m J_{B,\mathrm{ur}}^{(\mathrm{real})}(\hat{s}, Q_0, R) = \frac{\alpha_s C_F}{4\pi}(-4Q_0\pi)\Big[1 - \frac{2}{\pi} \tan^{-1}\Big(\frac{2m}{QR}\Big) + \mathcal{O}\Big(\frac{mR}{Q}\Big)\Big]. \tag{H.17}$$

For $R \ll \frac{m}{Q}$ we find a linear dependence on R

$$\int \mathrm{d}\hat{s}\, \hat{s}\, m J_{B,\mathrm{ur}}^{(\mathrm{real})}(\hat{s}, Q_0, R) = \frac{\alpha_s C_F}{4\pi}Q_0\Big(-\frac{4Q}{m}R + \mathcal{O}\Big(\frac{Q^3 R^3}{m^3}\Big)\Big). \tag{H.18}$$

Comparing the first moment with Eq. (H.6) we see that

$$\int \mathrm{d}\hat{s}\, \hat{s}\, m J_{B,\mathrm{ur}}^{(\mathrm{real})}(\hat{s}, Q_0, R) = -\frac{Q}{m}\int \mathrm{d}k\, k\, S_{\mathrm{ur}}^{(\tau,\mathrm{real})}(k, Q_0, R) + \mathcal{O}\Big(\frac{Q^3 R^3}{m^3}\Big), \tag{H.19}$$

which implies a cancellation of the leading contributions to the cutoff induced peak shift from soft and ultra-collinear radiation for small jet radii R.

H.3 Coherent branching with an angular cut

To calculate the unreleased contributions in coherent branching with a constraint on the angle of the gluon emission $\theta < R$, we start from Eq. (8.6), with and additional factor of $1/2$ because we are only looking at one hemisphere. The light-cone components of the gluon momentum after the first emission can be expressed in terms of the variables of coherent branching as

$$q^- = Q(1-z) + \mathcal{O}\Big(\frac{m^2}{Q^2}\Big),$$
$$q^+ = \frac{q_\perp^2}{Q(1-z)^2} + \mathcal{O}\Big(\frac{m^2}{Q^2}\Big), \tag{H.20}$$

where we have neglected terms that are quadratic in the mass because we are only interested in the term linear in the mass that gives the leading contribution to the peak shift. With these relations the angular constraint in Eq. (H.2) can be expressed as

$$z < 1 - \frac{q_\perp x}{Q}. \tag{H.21}$$

For $R = \pi/2$ we recover again the integration limit $z < 1 - q_\perp/Q$ as it is already present in Eq. (8.6). For $R < \pi/2$ we can distinguish two cases for the resulting integration limits on $q_\perp$ and z

$$\text{for } R > 2\cot^{-1}\Big(\frac{Q}{Q_0}\Big) \sim \frac{2Q_0}{Q}: \qquad 0 < q_\perp < Q_0\,,\ 0 < z < 1 - \frac{q_\perp x}{Q}$$
$$\text{for } R < 2\cot^{-1}\Big(\frac{Q}{Q_0}\Big) \sim \frac{2Q_0}{Q}: \qquad 0 < q_\perp < \frac{Q}{x}\,,\ 0 < z < 1 - \frac{q_\perp x}{Q} \tag{H.22}$$

The latter one is relevant only for unrealistically small $R \lesssim Q_0/Q$, and furthermore these contributions can be shown to scale like Q_0^2 and are therefore neglected. Expanding the exponential function

keeping only terms linear in ν and changing the integration variable $q_\perp^2 \to q^2 - m^2(1-z)^2$ we get $[v = \sqrt{1 + \frac{m^2 x^2}{Q^2}}]$

$$
\begin{aligned}
\mathcal{I}(\nu, Q, m, Q_0, R) &= -\frac{\nu}{Q^2} \int_0^{Q_0^2} \mathrm{d}q_\perp^2 \int_0^{1-\frac{q_\perp x}{Q}} \mathrm{d}z\, P_{QQ}\Big[\alpha_s\big(q_\perp^2 + m^2(1-z)^2\big), z, \frac{m^2(1-z)^2}{q_\perp^2 + m^2(1-z)^2}\Big] \\
&= -\frac{2\nu}{Q^2} \left\{ \int_0^{Q_0 v} \mathrm{d}q\, q \int_{1-\frac{q}{m}}^{1-\frac{qx}{Qv}} \mathrm{d}z\, P_{QQ}\Big[\alpha_s(q), z, \frac{m^2(1-z)^2}{q^2}\Big] \right. \\
&\qquad\qquad \left. + \int_{Q_0 v}^{m} \mathrm{d}q\, q \int_{1-\frac{q}{m}}^{1-\sqrt{\frac{q^2-Q_0^2}{m^2}}} \mathrm{d}z\, P_{QQ}\Big[\alpha_s(q), z, \frac{m^2(1-z)^2}{q^2}\Big] \right\} \\
&= -\frac{2 C_F \nu}{\pi Q^2} \left\{ \Big[\frac{Qv}{x} + m\Big(\frac{mx}{Qv} - 2\Big)\Big] \int_0^{Q_0 v} \mathrm{d}q\, \alpha_s(q) \right. \\
&\qquad\qquad \left. + m \int_{Q_0 v}^{m} \mathrm{d}q\, \alpha_s(q) \frac{\big(q - \sqrt{q^2 - Q_0^2}\big)^2}{q\sqrt{q^2 - Q_0^2}} \right\}, \qquad \text{(H.23)}
\end{aligned}
$$

dropping terms of order Q_0/m and m/Q. Keeping only terms linear in Q_0 we can extend the upper limit of the second integral to infinity, which leads to the result

$$
\mathcal{I}(\nu, Q, m, Q_0, R) = -\left\{ 8\frac{Q_0}{Q}\tan\Big(\frac{R}{2}\Big) - 4\pi\frac{Q_0 m}{Q^2}\Big[1 - \frac{2}{\pi}\tan^{-1}\Big(\frac{m}{Q}\cot\Big(\frac{R}{2}\Big)\Big)\Big] \right\} \frac{C_F \alpha_s(\tilde{Q}_0)}{4\pi}\, \nu\,, \quad \text{(H.24)}
$$

in perfect agreement with Eqs. (H.6) and (H.16). In the presence of the angular cut the scale of the strong coupling is changed from Q_0 to

$$
\tilde{Q}_0 = Q_0 \sqrt{1 + \frac{m^2}{Q^2}\cot^2\Big(\frac{R}{2}\Big)} \approx Q_0 \frac{2m}{QR}\Big[1 + \mathcal{O}\Big(\frac{Q^3 R^3}{m^3}\Big)\Big]. \qquad \text{(H.25)}
$$

In the limit of the full hemisphere $R = \pi/2$ (and multiplying a factor of 2 for accounting for both hemispheres) we recover the result of Eq. (8.8).

H.4 Comparison with MC runs

In the previous sections we have calculated how the shower cut dependent unreleased contributions of a top quark jet are affected by an additional constraint on the momentum of the radiated gluon. The constraint was that the gluon has to be emitted with an angle with respect to the top quark smaller than some jet radius R. Under the assumption that the jet axis is aligned with the direction of the original top quark, this corresponds to the condition that any gluon radiated from that top must fulfill in order to get clustered into that jet when applying the Cambridge-Aachen-type jet algorithms defined with the distance measures in Eq. (9.4) with $p = 0$. Since we now know how the cutoff dependence of these contributions depends itself on the jet radius R, we can use this to argue how the cutoff dependence of the mass fitted from b-jet+lepton and b-jet+W spectra, as described in Sec. 9.6, should depend on R. This is, however, *not* a real derivation, since we are still using the factorization setup valid for the decay insensitive thrust observable. An actual calculation of how the choice of the jet radius affects the cutoff dependence of the b-jet+lepton/W would require a factorization theorem designed specifically for those observables, which is still missing today. But if we assume that at least the part of that factorization theorem related to the top quark will have a similar form consisting of a bHQET jet function and a soft function of Wilson line along the direction of the top quark momentum, we can try to make some conclusions about the dependence on the

production stage shower. This means we consider only variations in the shower cutoff for radiation off the top quark before its decay, but leave the cutoff on radiation from the bottom quark fixed. Furthermore we are assuming that the b-jet axis is aligned with the direction of the top quark, which is a good approximation only for very large boosts.

The conclusions presented here should thus rather be seen as an educated guess, and even though the analytic calculations agree very well with the results obtained from actual MC runs as shown below, one should be cautious as this might still be only coincidence.

Assuming that the dependence on the production stage shower cut of the mass parameter fitted from b-jet+lepton/W spectra can be estimated from the cutoff dependence of the coherent branching top jet function with an angular cut in Eq. (H.24) (or likewise from the soft and jet functions in Eqs. (H.6) and (H.16)), we find from the cutoff induced shift in the distributions that the relation between the fitted mass for two different cutoffs is

$$
m_{t,\mathrm{fit}}^R(Q_0) = m_{t,\mathrm{fit}}^R(Q_0') - \left\{ 4\frac{Q}{m_t}\tan\left(\frac{R}{2}\right) - 2\pi\left[1 - \frac{2}{\pi}\tan^{-1}\left(\frac{m_t}{Q}\cot\left(\frac{R}{2}\right)\right)\right]\right\}
$$
$$
\times \int_{Q_0'}^{Q_0} \mathrm{d}R' \, \frac{C_F\alpha_s\left(R'\sqrt{1 + \frac{m_t^2}{Q^2}\cot^2\left(\frac{R}{2}\right)}\right)}{4\pi} \,. \quad \text{(H.26)}
$$

We can now compare this with the results from fitting the mass $m_{t,\mathrm{fit}}$ from the invariant mass spectrum of the b-jet-lepton and the b-jet-W invariant as in Sec. 9.6. In Fig. H.1 we show the mass values obtained from runs with different Q_0 fitted to reference runs with $Q_0 = 1.5$ GeV, while the decay stage cut $Q_{0,b}$ is held fixed at $Q_{0,b} = 1.5$ GeV. Otherwise we use the same settings and parameters as in Sec. 9.6. The results are shown for different values of the angular cut $0.25 < R < 1.5$. The dashed gray line is the prediction of the dependence of the fitted mass on the production shower cut Q_0 in Eq.(H.26), with $m_{t,\mathrm{fit}}^R(Q_0' = 1.5\,\mathrm{GeV}) = 173$ GeV.

We see a very good agreement over the full range of tested values of R, reaching from the limit of $R \sim m_t/Q$, where we see the cancellation of the cutoff induced shifts from soft and ultra-collinear radiation leading to a cutoff independent result for the fitted mass, to $R \sim \pi/2$ where Eq. (H.26) reduces to Eq. (9.5). But it should be emphasized once more that this is no theoretically sound derivation and no proof that the dependence on the production stage shower cut of those observables can really be computed in this simply way.
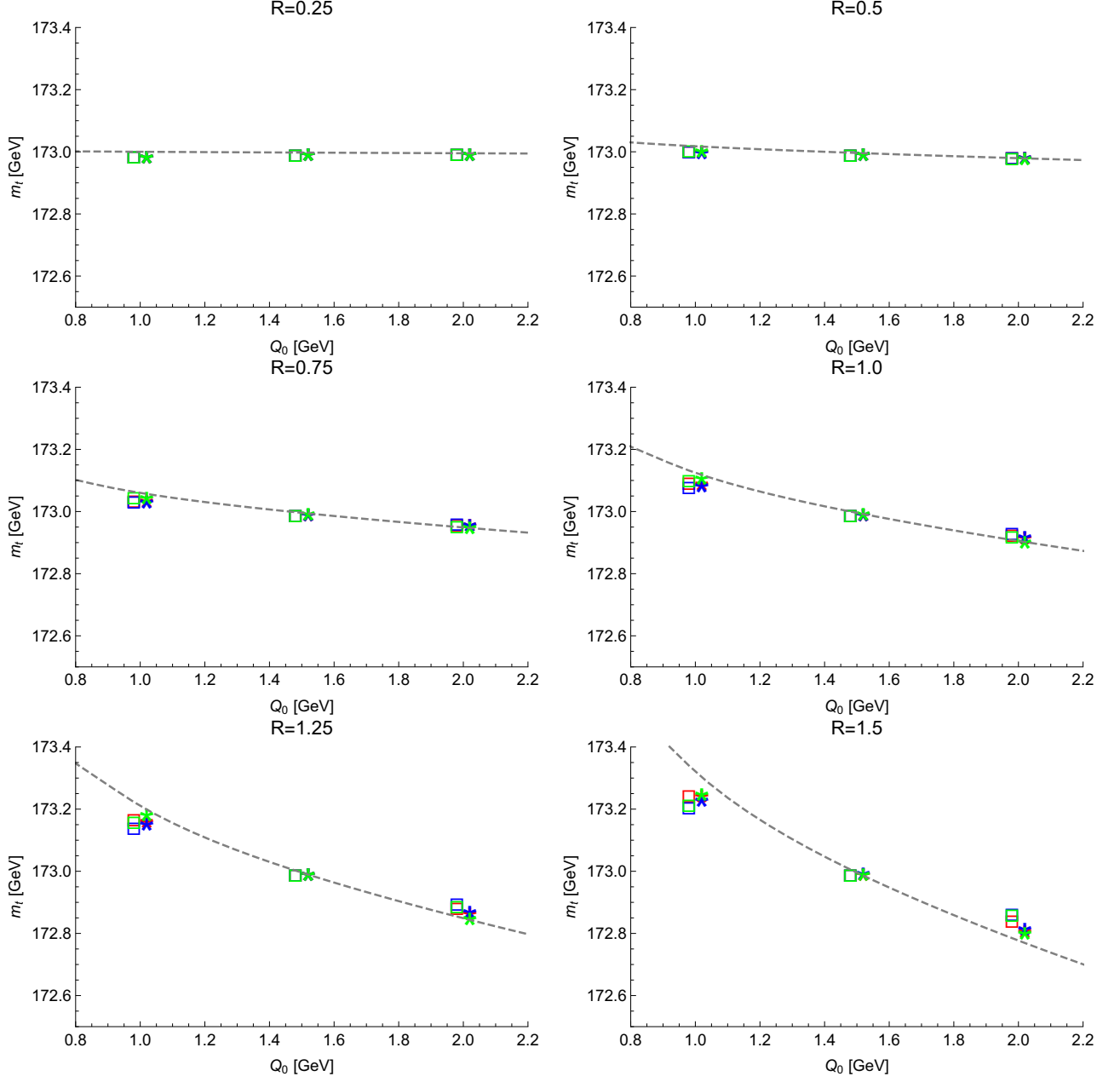
Figure H.1: Fitted top quark mass as a function of the production state shower cut Q_0 for $Q = 700$ GeV and a fixed decay stage shower cut $Q_{0,b} = 1.5$ GeV, obtained from the $m_{b_j\ell}$ endpoint (stars) and the m_{b_jW} resonance region (triangles) using the k_t-type algorithm (green), the Cambridge-Aachen-type algorithm (blue) and the anti-k_t-type algorithm (red) for b-jet clustering. The dashed line corresponds to Eq. (H.26).

Appendix I

Integrals in d-dimensions with $p_\perp$ cut

For the calculation of the jet and soft functions with and without a $q_\perp$-cut we need to solve d-dimensional integrals of the form

$$\int \frac{\mathrm{d}^d q}{(2\pi)^d} \frac{f_{Q_0}(q_\perp)}{(q^2 + \Delta)^n} \,, \tag{I.1}$$

for the cases $f_{Q_0}(q_\perp) = 1$ (no cut), $f_{Q_0}(q_\perp) = \theta(q_\perp - Q_0)$ (only above cut) and $f_{Q_0}(q_\perp) = \theta(Q_0 - q_\perp)$ (unreleased). After a Wick-rotation and doing the energy and angular integrals that are not affected by the cutoff, one arrives at

$$\frac{2i(-1)^n}{(4\pi)^{\frac{d}{2}}(n-1)\Gamma\left(\frac{d}{2}-1\right)} \int_0^\infty \mathrm{d}q_\perp \, f_{Q_0}(q_\perp) \frac{q_\perp^{d-3}}{(q_\perp^2 - \Delta)^{n-1}} \,. \tag{I.2}$$

This can be solved for the three different cases and gives

$$\int \frac{\mathrm{d}^d q}{(2\pi)^d} \frac{1}{(q^2 + \Delta)^n} = \frac{i(-1)^n \, \Gamma\left(n - \frac{d}{2}\right)}{(4\pi)^{\frac{d}{2}} \Gamma(n)} (-\Delta)^{\frac{d}{2}-n} \,, \tag{I.3}$$

$$\int \frac{\mathrm{d}^d q}{(2\pi)^d} \frac{\theta(q_\perp - Q_0)}{(q^2 + \Delta)^n} = \frac{i(-1)^n \, \mathrm{B}\left(\frac{\Delta}{Q_0^2}, n - \frac{d}{2}, 2 - n\right)}{(4\pi)^{\frac{d}{2}} (n-1)\Gamma\left(\frac{d}{2}-1\right)} (\Delta)^{\frac{d}{2}-n} \,, \tag{I.4}$$

$$\int \frac{\mathrm{d}^d q}{(2\pi)^d} \frac{\theta(Q_0 - q_\perp)}{(q^2 + \Delta)^n} = \frac{i(-1)^n \, {}_2\mathrm{F}_1\left(\frac{d}{2} - 1, n - 1, \frac{d}{2}, \frac{Q_0^2}{\Delta}\right)}{(4\pi)^{\frac{d}{2}} (n-1)\Gamma\left(\frac{d}{2}\right)} (Q_0^2)^{\frac{d}{2}-1} (-\Delta)^{1-n} \tag{I.5}$$

$$\xrightarrow[d\to 4]{} \frac{i(-1)^n}{16\pi^2 (n-1)(n-2)} \left((-\Delta)^{2-n} - (Q_0^2 - \Delta)^{2-n}\right) \,, \tag{I.6}$$

where in the last line we took the limit $d \to 4$ since there are no divergences in the unreleased contributions that need to be regularized by dimensional regularization.

Appendix J

Plus distributions

The standard plus distribution for some dimensionless function $g(x)$ is defined as

$$[\theta(x)g(x)]_+ = \lim_{\beta \to 0} \frac{\mathrm{d}}{\mathrm{d}x} \left[\theta(x - \beta)G(x)\right] \qquad \text{with} \qquad G(x) = \int_1^x \mathrm{d}x' \, g(x') \,. \tag{J.1}$$

The special case used in this thesis is

$$\mathcal{L}_n(x) = \left[\frac{\theta(x)\ln^n x}{x}\right]_+ \,, \tag{J.2}$$

such that

$$\int_0^\Delta \mathrm{d}x \, \mathcal{L}_n(x) = \frac{\ln^{n+1}\Delta}{n+1} \,. \tag{J.3}$$

The 2-dimensional plus distributions that appear in the TMD beam and soft functions are defined as

$$\mathcal{L}_n(\vec{p}_T, \mu) = \frac{1}{\pi\mu^2}\mathcal{L}_n\left(\frac{|\vec{p}_T|^2}{\mu^2}\right) \,, \tag{J.4}$$

such that

$$\int_{|\vec{p}_T| < \Delta} \mathrm{d}^2\vec{p}_T \, \mathcal{L}_n(\vec{p}_T, \mu) = \frac{\ln^{n+1}\left(\frac{\Delta^2}{\mu^2}\right)}{n+1} \,. \tag{J.5}$$

For the Fourier transform we use the convention

$$\tilde{f}(\vec{b}) = \int \mathrm{d}^2\vec{p}_T \, \mathrm{e}^{i\vec{b}\cdot\vec{p}_T} f(\vec{p}_T) \,. \tag{J.6}$$

The Fourier transforms of the 2-dimensional distributions required here are

$$
\begin{aligned}
\delta^{(2)}(\vec{p}_T) &\longleftrightarrow 1 \,, \\
\mathcal{L}_0(\vec{p}_T, \mu) &\longleftrightarrow -L_b \,, \\
\mathcal{L}_1(\vec{p}_T, \mu) &\longleftrightarrow \frac{L_b^2}{2} \,, \\
\mathcal{L}_2(\vec{p}_T, \mu) &\longleftrightarrow -\frac{1}{4}\left(L_b^3 + 4\zeta_3\right) \,,
\end{aligned}
\tag{J.7}
$$

with L_b defined in Eq. (2.67).

Appendix K

Simulation settings for Herwig 7

In this appendix we document the changes relative to the default settings in Herwig version 7.1.2 [226] with which these studies have been carried out. All of the results are parton level simulations, with special settings to make contact with the analytic approach and are not advocated to be used in a full simulation. All simulation is based on the default `LEP-Matchbox.in` input file, which is prepared to generate both leading order and next-to-leading order matched simulations.

K.1   Common settings

In all of the simulations we consider, we use light quarks u, d, s, c, b by setting their nominal mass to zero, and their consitutent masses, as well as the gluon's constituent mass to be effectively zero,

```
set /Herwig/Particles/x:NominalMass 0*GeV
set /Herwig/Particles/x:ConstituentMass 0.00001*GeV
set /Herwig/Particles/g:ConstituentMass 0.000021*GeV
```

where `x = u,d,s,c,b`. We also switch off QED initial state radiation,

```
set /Herwig/Particles/e+:PDF /Herwig/Partons/NoPDF
set /Herwig/Particles/e-:PDF /Herwig/Partons/NoPDF
```

and do consider the kinematic reconstruction option employed in earlier Herwig versions,

```
set /Herwig/Shower/ShowerHandler:ReconstructionOption CutOff
```

We always consider parton level results

```
read Matchbox/PQCDLevel.in
```

The parton shower cutoff is changed via

```
set /Herwig/Shower/QtoQGSudakov:pTmin X*GeV
set /Herwig/Shower/GtoGGSudakov:pTmin X*GeV
set /Herwig/Shower/GtoQQbarSudakov:pTmin X*GeV
```

where `X`=Q_0/GeV. If gluon branchings are desired to be switched off, we use

```
cd /Herwig/Shower
do SplittingGenerator:DeleteFinalSplitting g->g,g; GtoGGSudakov
do SplittingGenerator:DeleteFinalSplitting g->x,xbar; GtoQQbarSudakov
```

where x again runs over the different quark flavors. We always switch off $g \to t\bar{t}$ branchings by an according statement. If additionally we qant to quantify the remaining impact of angular ordering, we choose

```
cd /Herwig/Shower
set QtoQGSplitFn:AngularOrdered No
set GtoGGSplitFn:AngularOrdered No
set QtoQGSplitFn:ScaleChoice pT
set GtoGGSplitFn:ScaleChoice pT
```

As far as the calculation of the production process is concerned, we either use the leading order, subtractive or multiplicative matched simulation,

```
read Matchbox/MCatLO-DefaultShower.in
read Matchbox/MCatNLO-DefaultShower.in
read Matchbox/Powheg-DefaultShower.in
```

respectively. The MATCHBOX build-in matrix elements for $e^+e^- \to$ jets at leading and next-to-leading order are employed in our simulation. Unless stated otherwise, matrix elment corrections are switched off,

```
set /Herwig/Shower/ShowerHandler:HardEmission None
```

K.2 Massless case

In the massless case we generate two-jet events using light flavours only

```
set Factory:OrderInAlphaS 0
set Factory:OrderInAlphaEW 2
do Factory:Process e+ e- -> j j
```

No other special settings are applied.

K.3 Massive case

In the massive case, we produce top quark pairs on-shell,

```
read Matchbox/OnShellTopProduction.in
set Factory:OrderInAlphaS 0
set Factory:OrderInAlphaEW 2
do Factory:Process e+ e- -> t tbar
```

We exclusively select leptonic decays,

```
do /Herwig/Particles/t:SelectDecayModes t->nu_mu,mu+,b; t->nu_e,e+,b;
do /Herwig/Particles/tbar:SelectDecayModes tbar->nu_mubar,mu-,bbar; \
 tbar->nu_ebar,e-,bbar;
```

If an independent cutoff on the top quark shower is desired, we use

```
cd /Herwig/Shower
do SplittingGenerator:DeleteFinalSplitting t->t,g; QtoQGSudakov
cp QtoQGSudakov TtoTGSudakov
do SplittingGenerator:AddFinalSplitting t->t,g; TtoTGSudakov
set /Herwig/Shower/TtoTGSudakov:pTmin X*GeV
```

Bibliography

[1] P. Pietrulewicz, D. Samitz, A. Spiering, and F. J. Tackmann, "Factorization and Resummation for Massive Quark Effects in Exclusive Drell-Yan," *JHEP* **08** (2017) 114, `arXiv:1703.09702 [hep-ph]`.

[2] A. H. Hoang, P. Pietrulewicz, and D. Samitz, "Variable Flavor Number Scheme for Final State Jets in DIS," *Phys. Rev.* **D93** no. 3, (2016) 034034, `arXiv:1508.04323 [hep-ph]`.

[3] A. H. Hoang, S. Plätzer, and D. Samitz, "On the Cutoff Dependence of the Quark Mass Parameter in Angular Ordered Parton Showers," *JHEP* **10** (2018) 200, `arXiv:1807.06617 [hep-ph]`.

[4] M. Aivazis, F. I. Olness, and W.-K. Tung, "Leptoproduction of heavy quarks. 1. General formalism and kinematics of charged current and neutral current production processes," *Phys. Rev.* **D50** (1994) 3085–3101, `arXiv:hep-ph/9312318 [hep-ph]`.

[5] M. Aivazis, J. C. Collins, F. I. Olness, and W.-K. Tung, "Leptoproduction of heavy quarks. 2. A Unified QCD formulation of charged and neutral current processes from fixed target to collider energies," *Phys. Rev.* **D50** (1994) 3102–3118, `arXiv:hep-ph/9312319 [hep-ph]`.

[6] R. Thorne and R. Roberts, "An Ordered analysis of heavy flavor production in deep inelastic scattering," *Phys.Rev.* **D57** (1998) 6871–6898, `arXiv:hep-ph/9709442 [hep-ph]`.

[7] S. Kretzer and I. Schienbein, "Heavy quark initiated contributions to deep inelastic structure functions," *Phys.Rev.* **D58** (1998) 094035, `arXiv:hep-ph/9805233 [hep-ph]`.

[8] J. C. Collins, "Hard scattering factorization with heavy quarks: A General treatment," *Phys.Rev.* **D58** (1998) 094002, `arXiv:hep-ph/9806259 [hep-ph]`.

[9] S. Forte, E. Laenen, P. Nason, and J. Rojo, "Heavy quarks in deep-inelastic scattering," *Nucl. Phys.* **B834** (2010) 116–162, `arXiv:1001.2312 [hep-ph]`.

[10] M. Bonvini, A. S. Papanastasiou, and F. J. Tackmann, "Resummation and matching of b-quark mass effects in $b\bar{b}H$ production," *JHEP* **11** (2015) 196, `arXiv:1508.03288 [hep-ph]`.

[11] S. Gritschacher, A. H. Hoang, I. Jemos, and P. Pietrulewicz, "Secondary Heavy Quark Production in Jets through Mass Modes," *Phys.Rev.* **D88** (2013) 034021, `arXiv:1302.4743 [hep-ph]`.

[12] P. Pietrulewicz, S. Gritschacher, A. H. Hoang, I. Jemos, and V. Mateu, "Variable Flavor Number Scheme for Final State Jets in Thrust," *Phys.Rev.* **D90** no. 11, (2014) 114001, `arXiv:1405.4860 [hep-ph]`.

[13] I. W. Stewart, F. J. Tackmann, and W. J. Waalewijn, "Factorization at the LHC: From PDFs to Initial State Jets," *Phys.Rev.* **D81** (2010) 094035, `arXiv:0910.0467 [hep-ph]`.

[14] C. W. Bauer, S. Fleming, and M. E. Luke, "Summing Sudakov logarithms in $B \to X_s\gamma$ in effective field theory," *Phys. Rev.* **D63** (2000) 014006, `arXiv:hep-ph/0005275 [hep-ph]`.

[15] C. W. Bauer, S. Fleming, D. Pirjol, and I. W. Stewart, "An Effective field theory for collinear and soft gluons: Heavy to light decays," *Phys. Rev.* **D63** (2001) 114020, `arXiv:hep-ph/0011336 [hep-ph]`.

[16] C. W. Bauer and I. W. Stewart, "Invariant operators in collinear effective theory," *Phys.Lett.* **B516** (2001) 134–142, `arXiv:hep-ph/0107001 [hep-ph]`.

[17] C. W. Bauer, D. Pirjol, and I. W. Stewart, "Soft collinear factorization in effective field theory," *Phys. Rev.* **D65** (2002) 054022, `arXiv:hep-ph/0109045 [hep-ph]`.

[18] S. Fleming, A. H. Hoang, S. Mantry, and I. W. Stewart, "Jets from massive unstable particles: Top-mass determination," *Phys. Rev.* **D77** (2008) 074010, `arXiv:hep-ph/0703207 [hep-ph]`.

[19] S. Fleming, A. H. Hoang, S. Mantry, and I. W. Stewart, "Top Jets in the Peak Region: Factorization Analysis with NLL Resummation," *Phys. Rev.* **D77** (2008) 114003, `arXiv:0711.2079 [hep-ph]`.

[20] P. Pietrulewicz, "Variable Flavor Scheme for Final State Jets", *doctoral thesis* (2014), University of Vienna, `http://othes.univie.ac.at/34439/`.

[21] **ATLAS** Collaboration, G. Aad *et al.*, "Measurement of the Transverse Momentum Distribution of W Bosons in pp Collisions at $\sqrt{s} = 7$ TeV with the ATLAS Detector," *Phys. Rev.* **D85** (2012) 012005, `arXiv:1108.6308 [hep-ex]`.

[22] **CMS** Collaboration, S. Chatrchyan *et al.*, "Measurement of the Rapidity and Transverse Momentum Distributions of Z Bosons in pp Collisions at $\sqrt{s} = 7$ TeV," *Phys. Rev.* **D85** (2012) 032002, `arXiv:1110.4973 [hep-ex]`.

[23] **ATLAS** Collaboration, G. Aad *et al.*, "Measurement of the Z/γ^* boson transverse momentum distribution in pp collisions at $\sqrt{s} = 7$ TeV with the ATLAS detector," *JHEP* **09** (2014) 145, `arXiv:1406.3660 [hep-ex]`.

[24] **CMS** Collaboration, V. Khachatryan *et al.*, "Measurement of the Z boson differential cross section in transverse momentum and rapidity in proton–proton collisions at 8 TeV," *Phys. Lett.* **B749** (2015) 187–209, `arXiv:1504.03511 [hep-ex]`.

[25] **ATLAS** Collaboration, G. Aad *et al.*, "Measurement of the transverse momentum and ϕ_η^* distributions of Drell–Yan lepton pairs in proton–proton collisions at $\sqrt{s} = 8$ TeV with the ATLAS detector," *Eur. Phys. J.* **C76** no. 5, (2016) 291, `arXiv:1512.02192 [hep-ex]`.

[26] **CMS** Collaboration, V. Khachatryan *et al.*, "Measurement of the transverse momentum spectra of weak vector bosons produced in proton-proton collisions at $\sqrt{s} = 8$ TeV," *JHEP* **02** (2017) 096, `arXiv:1606.05864 [hep-ex]`.

[27] V. Buge, C. Jung, G. Quast, A. Ghezzi, M. Malberti, and T. Tabarelli de Fatis, "Prospects for the precision measurement of the W mass with the CMS detector at the LHC," *J. Phys.* **G34** (2007) N193–N220.

[28] **ATLAS** Collaboration, N. Besson, M. Boonekamp, E. Klinkby, S. Mehlhase, and T. Petersen, "Re-evaluation of the LHC potential for the measurement of Mw," *Eur. Phys. J.* **C57** (2008) 627–651, `arXiv:0805.2093 [hep-ex]`.

[29] **CMS** Collaboration, "W-like measurement of the Z boson mass using dimuon events collected in pp collisions at $\sqrt{s} = 7$ TeV,". CMS-PAS-SMP-14-007 (2016).

[30] **ATLAS** Collaboration, G. Aad *et al.*, "Studies of theoretical uncertainties on the measurement of the mass of the W boson at the LHC,". ATL-PHYS-PUB-2014-015.

[31] **ATLAS** Collaboration, M. Aaboud *et al.*, "Measurement of the W-boson mass in pp collisions at $\sqrt{s} = 7$ TeV with the ATLAS detector," *Eur. Phys. J. C* **78** no. 2, (2018) 110, `arXiv:1701.07240 [hep-ex]`. [Erratum: Eur.Phys.J.C 78, 898 (2018)].

[32] J. C. Collins and D. E. Soper, "Back-To-Back Jets in QCD," *Nucl. Phys.* **B193** (1981) 381. [Erratum: Nucl. Phys.B213,545(1983)].

[33] J. C. Collins and D. E. Soper, "Back-To-Back Jets: Fourier Transform from B to K-Transverse," *Nucl. Phys.* **B197** (1982) 446–476.

[34] J. C. Collins, D. E. Soper, and G. F. Sterman, "Transverse Momentum Distribution in Drell-Yan Pair and W and Z Boson Production," *Nucl. Phys.* **B250** (1985) 199.

[35] C. Balazs and C. P. Yuan, "Soft gluon effects on lepton pairs at hadron colliders," *Phys. Rev.* **D56** (1997) 5558–5583, `arXiv:hep-ph/9704258 [hep-ph]`.

[36] C. Balazs and C. P. Yuan, "Higgs boson production at the LHC with soft gluon effects," *Phys. Lett.* **B478** (2000) 192–198, `arXiv:hep-ph/0001103 [hep-ph]`.

[37] G. Bozzi, S. Catani, G. Ferrera, D. de Florian, and M. Grazzini, "Production of Drell-Yan lepton pairs in hadron collisions: Transverse-momentum resummation at next-to-next-to-leading logarithmic accuracy," *Phys. Lett.* **B696** (2011) 207–213, `arXiv:1007.2351 [hep-ph]`.

[38] D. de Florian, G. Ferrera, M. Grazzini, and D. Tommasini, "Transverse-momentum resummation: Higgs boson production at the Tevatron and the LHC," *JHEP* **11** (2011) 064, `arXiv:1109.2109 [hep-ph]`.

[39] T. Becher and M. Neubert, "Drell-Yan production at small q_T, transverse parton distributions and the collinear anomaly," *Eur.Phys.J.* **C71** (2011) 1665, `arXiv:1007.4005 [hep-ph]`.

[40] J.-Y. Chiu, A. Jain, D. Neill, and I. Z. Rothstein, "The Rapidity Renormalization Group," *Phys.Rev.Lett.* **108** (2012) 151601, `arXiv:1104.0881 [hep-ph]`.

[41] J.-Y. Chiu, A. Jain, D. Neill, and I. Z. Rothstein, "A Formalism for the Systematic Treatment of Rapidity Logarithms in Quantum Field Theory," *JHEP* **1205** (2012) 084, `arXiv:1202.0814 [hep-ph]`.

[42] M. G. Echevarria, A. Idilbi, and I. Scimemi, "Factorization Theorem For Drell-Yan At Low q_T And Transverse Momentum Distributions On-The-Light-Cone," *JHEP* **07** (2012) 002, `arXiv:1111.4996 [hep-ph]`.

[43] I. W. Stewart, F. J. Tackmann, and W. J. Waalewijn, "The Beam Thrust Cross Section for Drell-Yan at NNLL Order," *Phys. Rev. Lett.* **106** (2011) 032001, `arXiv:1005.4060 [hep-ph]`.

[44] C. F. Berger, C. Marcantonini, I. W. Stewart, F. J. Tackmann, and W. J. Waalewijn, "Higgs Production with a Central Jet Veto at NNLL+NNLO," *JHEP* **04** (2011) 092, `arXiv:1012.4480 [hep-ph]`.

[45] P. M. Nadolsky, N. Kidonakis, F. I. Olness, and C. P. Yuan, "Resummation of transverse momentum and mass logarithms in DIS heavy quark production," *Phys. Rev.* **D67** (2003) 074015, `arXiv:hep-ph/0210082 [hep-ph]`.

[46] S. Berge, P. M. Nadolsky, and F. I. Olness, "Heavy-flavor effects in soft gluon resummation for electroweak boson production at hadron colliders," *Phys. Rev.* **D73** (2006) 013002, `arXiv:hep-ph/0509023 [hep-ph]`.

[47] A. Belyaev, P. M. Nadolsky, and C. P. Yuan, "Transverse momentum resummation for Higgs boson produced via b anti-b fusion at hadron colliders," *JHEP* **04** (2006) 004, `arXiv:hep-ph/0509100 [hep-ph]`.

[48] L. Landau, "On the angular momentum of a system of two photons," *Dokl. Akad. Nauk SSSR* **60** no. 2, (1948) 207–209.

[49] C.-N. Yang, "Selection Rules for the Dematerialization of a Particle Into Two Photons," *Phys. Rev.* **77** (1950) 242–245.

[50] J. C. Collins and D. E. Soper, "Parton Distribution and Decay Functions," *Nucl. Phys.* **B194** (1982) 445–492.

[51] J. Collins, "New definition of TMD parton densities," *Int. J. Mod. Phys. Conf. Ser.* **4** (2011) 85–96, `arXiv:1107.4123 [hep-ph]`.

[52] I. O. Cherednikov and N. G. Stefanis, "Renormalization, Wilson lines, and transverse-momentum dependent parton distribution functions," *Phys. Rev. D* **77** (2008) 094001, `arXiv:0710.1955 [hep-ph]`.

[53] B. Pasquini, S. Cazzaniga, and S. Boffi, "Transverse momentum dependent parton distributions in a light-cone quark model," *Phys. Rev. D* **78** (2008) 034025, `arXiv:0806.2298 [hep-ph]`.

[54] S. Catani, L. Cieri, D. de Florian, G. Ferrera, and M. Grazzini, "Vector boson production at hadron colliders: hard-collinear coefficients at the NNLO," *Eur. Phys. J.* **C72** (2012) 2195, `arXiv:1209.0158 [hep-ph]`.

[55] T. Gehrmann, T. Lubbert, and L. L. Yang, "Transverse parton distribution functions at next-to-next-to-leading order: the quark-to-quark case," *Phys. Rev. Lett.* **109** (2012) 242003, `arXiv:1209.0682 [hep-ph]`.

[56] T. Gehrmann, T. Luebbert, and L. L. Yang, "Calculation of the transverse parton distribution functions at next-to-next-to-leading order," *JHEP* **06** (2014) 155, `arXiv:1403.6451 [hep-ph]`.

[57] T. Lübbert, J. Oredsson, and M. Stahlhofen, "Rapidity renormalized TMD soft and beam functions at two loops," *JHEP* **03** (2016) 168, `arXiv:1602.01829 [hep-ph]`.

[58] Y. Li, D. Neill, and H. X. Zhu, "An exponential regulator for rapidity divergences," *Nucl. Phys. B* **960** (2020) 115193, `arXiv:1604.00392 [hep-ph]`.

[59] Y. Li and H. X. Zhu, "Bootstrapping Rapidity Anomalous Dimensions for Transverse-Momentum Resummation," *Phys. Rev. Lett.* **118** no. 2, (2017) 022004, `arXiv:1604.01404 [hep-ph]`.

[60] A. A. Vladimirov, "Soft-/rapidity- anomalous dimensions correspondence," *Phys. Rev. Lett.* **118** no. 6, (2017) 062001, `arXiv:1610.05791 [hep-ph]`.

[61] T. Becher and T. Neumann, "Fiducial q_T resummation of color-singlet processes at N³LL+NNLO," *JHEP* **03** (2021) 199, `arXiv:2009.11437 [hep-ph]`.

[62] W. Bizon, A. Gehrmann-De Ridder, T. Gehrmann, N. Glover, A. Huss, P. F. Monni, E. Re, L. Rottoli, and D. M. Walker, "The transverse momentum spectrum of weak gauge bosons at N^{3}LL + NNLO," *Eur. Phys. J. C* **79** no. 10, (2019) 868, `arXiv:1905.05171 [hep-ph]`.

[63] S. Camarda, L. Cieri, and G. Ferrera, "Drell-Yan lepton-pair production: q_T resummation at N^{3}LL accuracy and fiducial cross sections at N^{3}LO," `arXiv:2103.04974 [hep-ph]`.

[64] M. A. Ebert, J. K. L. Michel, I. W. Stewart, and F. J. Tackmann, "Drell-Yan q_T resummation of fiducial power corrections at N^{3}LL," *JHEP* **04** (2021) 102, `arXiv:2006.11382 [hep-ph]`.

[65] M. A. Ebert and F. J. Tackmann, "Resummation of Transverse Momentum Distributions in Distribution Space," *JHEP* **02** (2017) 110, `arXiv:1611.08610 [hep-ph]`.

[66] P. F. Monni, E. Re, and P. Torrielli, "Higgs Transverse-Momentum Resummation in Direct Space," *Phys. Rev. Lett.* **116** no. 24, (2016) 242001, `arXiv:1604.02191 [hep-ph]`.

[67] B. A. Kniehl and J. H. Kuhn, "QCD Corrections to the Z Decay Rate," *Nucl. Phys.* **B329** (1990) 547–573.

[68] R. J. Gonsalves, C.-M. Hung, and J. Pawlowski, "Heavy quark triangle diagram contributions to Z boson production in hadron collisions," *Phys. Rev.* **D46** (1992) 4930–4942.

[69] W. Bernreuther, R. Bonciani, T. Gehrmann, R. Heinesch, T. Leineweber, and E. Remiddi, "Two-loop QCD corrections to the heavy quark form-factors: Anomaly contributions," *Nucl. Phys.* **B723** (2005) 91–116, `arXiv:hep-ph/0504190 [hep-ph]`.

[70] A. H. Hoang, A. Pathak, P. Pietrulewicz, and I. W. Stewart, "Hard Matching for Boosted Tops at Two Loops," *JHEP* **12** (2015) 059, `arXiv:1508.04137 [hep-ph]`.

[71] A. H. Hoang, C. Lepenik, and M. Stahlhofen, "Two-Loop Massive Quark Jet Functions in SCET," *JHEP* **08** (2019) 112, `arXiv:1904.12839 [hep-ph]`.

[72] L. A. Harland-Lang, A. D. Martin, P. Motylinski, and R. S. Thorne, "Parton distributions in the LHC era: MMHT 2014 PDFs," *Eur. Phys. J.* **C75** no. 5, (2015) 204, `arXiv:1412.3989 [hep-ph]`.

[73] I. Z. Rothstein and I. W. Stewart, "An Effective Field Theory for Forward Scattering and Factorization Violation," *JHEP* **08** (2016) 025, `arXiv:1601.04695 [hep-ph]`.

[74] J. R. Gaunt, "Glauber Gluons and Multiple Parton Interactions," *JHEP* **1407** (2014) 110, `arXiv:1405.2080 [hep-ph]`.

[75] M. Zeng, "Drell-Yan process with jet vetoes: breaking of generalized factorization," *JHEP* **10** (2015) 189, `arXiv:1507.01652 [hep-ph]`.

[76] S. Alioli, C. W. Bauer, C. J. Berggren, A. Hornig, F. J. Tackmann, C. K. Vermilion, J. R. Walsh, and S. Zuberi, "Combining Higher-Order Resummation with Multiple NLO Calculations and Parton Showers in GENEVA," *JHEP* **09** (2013) 120, `arXiv:1211.7049 [hep-ph]`.

[77] S. Alioli, C. W. Bauer, C. Berggren, F. J. Tackmann, and J. R. Walsh, "Drell-Yan production at NNLL'+NNLO matched to parton showers," *Phys. Rev.* **D92** no. 9, (2015) 094020, `arXiv:1508.01475 [hep-ph]`.

[78] S. Alioli, C. W. Bauer, S. Guns, and F. J. Tackmann, "Underlying event sensitive observables in Drell-Yan production using GENEVA," *Eur. Phys. J.* **C76** no. 11, (2016) 614, `arXiv:1605.07192 [hep-ph]`.

[79] T. Sjostrand and M. van Zijl, "A Multiple Interaction Model for the Event Structure in Hadron Collisions," *Phys. Rev.* **D36** (1987) 2019.

[80] T. Sjostrand and P. Z. Skands, "Multiple interactions and the structure of beam remnants," *JHEP* **03** (2004) 053, `arXiv:hep-ph/0402078 [hep-ph]`.

[81] T. Sjostrand and P. Z. Skands, "Transverse-momentum-ordered showers and interleaved multiple interactions," *Eur. Phys. J.* **C39** (2005) 129–154, `arXiv:hep-ph/0408302 [hep-ph]`.

[82] D. Kang, O. Z. Labun, and C. Lee, "Equality of hemisphere soft functions for e^+e^-, DIS and pp collisions at $\mathcal{O}(\alpha_s^2)$," *Phys. Lett.* **B748** (2015) 45–54, `arXiv:1504.04006 [hep-ph]`.

[83] R. Kelley, M. D. Schwartz, R. M. Schabinger, and H. X. Zhu, "The two-loop hemisphere soft function," *Phys. Rev.* **D84** (2011) 045022, `arXiv:1105.3676 [hep-ph]`.

[84] P. F. Monni, T. Gehrmann, and G. Luisoni, "Two-Loop Soft Corrections and Resummation of the Thrust Distribution in the Dijet Region," *JHEP* **1108** (2011) 010, `arXiv:1105.4560 [hep-ph]`.

[85] I. W. Stewart, F. J. Tackmann, and W. J. Waalewijn, "The Quark Beam Function at NNLL," *JHEP* **1009** (2010) 005, `arXiv:1002.2213 [hep-ph]`.

[86] J. R. Gaunt, M. Stahlhofen, and F. J. Tackmann, "The Quark Beam Function at Two Loops," *JHEP* **04** (2014) 113, `arXiv:1401.5478 [hep-ph]`.

[87] J. Gaunt, M. Stahlhofen, and F. J. Tackmann, "The Gluon Beam Function at Two Loops," *JHEP* **08** (2014) 020, `arXiv:1405.1044 [hep-ph]`.

[88] A. V. Manohar and I. W. Stewart, "The Zero-Bin and Mode Factorization in Quantum Field Theory," *Phys. Rev.* **D76** (2007) 074002, `arXiv:hep-ph/0605001 [hep-ph]`.

[89] C. W. Bauer, F. J. Tackmann, J. R. Walsh, and S. Zuberi, "Factorization and Resummation for Dijet Invariant Mass Spectra," *Phys.Rev.* **D85** (2012) 074006, `arXiv:1106.6047 [hep-ph]`.

[90] M. Procura, W. J. Waalewijn, and L. Zeune, "Resummation of Double-Differential Cross Sections and Fully-Unintegrated Parton Distribution Functions," *JHEP* **1502** (2015) 117, `arXiv:1410.6483 [hep-ph]`.

[91] A. J. Larkoski, I. Moult, and D. Neill, "Non-Global Logarithms, Factorization, and the Soft Substructure of Jets," *JHEP* **09** (2015) 143, `arXiv:1501.04596 [hep-ph]`.

[92] P. Pietrulewicz, F. J. Tackmann, and W. J. Waalewijn, "Factorization and Resummation for Generic Hierarchies between Jets," *JHEP* **08** (2016) 002, `arXiv:1601.05088 [hep-ph]`.

[93] C. Lee and G. F. Sterman, "Momentum Flow Correlations from Event Shapes: Factorized Soft Gluons and Soft-Collinear Effective Theory," *Phys. Rev.* **D75** (2007) 014022, `arXiv:hep-ph/0611061 [hep-ph]`.

[94] A. Idilbi and T. Mehen, "On the equivalence of soft and zero-bin subtractions," *Phys. Rev.* **D75** (2007) 114017, `arXiv:hep-ph/0702022 [HEP-PH]`.

[95] S. Gritschacher, A. Hoang, I. Jemos, and P. Pietrulewicz, "Two loop soft function for secondary massive quarks," *Phys.Rev.* **D89** (2014) 014035, `arXiv:1309.6251 [hep-ph]`.

[96] A. V. Manohar, "Deep inelastic scattering as $x \to 1$ using soft collinear effective theory," *Phys.Rev.* **D68** (2003) 114019, `arXiv:hep-ph/0309176 [hep-ph]`.

[97] T. Becher, M. Neubert, and B. D. Pecjak, "Factorization and Momentum-Space Resummation in Deep-Inelastic Scattering," *JHEP* **0701** (2007) 076, arXiv:hep-ph/0607228 [hep-ph].

[98] J. Chay and C. Kim, "Deep inelastic scattering near the endpoint in soft-collinear effective theory," *Phys.Rev.* **D75** (2007) 016003, arXiv:hep-ph/0511066 [hep-ph].

[99] A. Idilbi, X.-d. Ji, and F. Yuan, "Resummation of threshold logarithms in effective field theory for DIS, Drell-Yan and Higgs production," *Nucl.Phys.* **B753** (2006) 42–68, arXiv:hep-ph/0605068 [hep-ph].

[100] P.-y. Chen, A. Idilbi, and X.-d. Ji, "QCD Factorization for Deep-Inelastic Scattering At Large Bjorken $x_B \sim 1 - \mathcal{O}(\Lambda_{\text{QCD}}/Q)$," *Nucl.Phys.* **B763** (2007) 183–197, arXiv:hep-ph/0607003 [hep-ph].

[101] S. Fleming and O. Z. Labun, "Rapidity Divergences and Deep Inelastic Scattering in the Endpoint Region," *Phys. Rev.* **D91** no. 9, (2015) 094011, arXiv:1210.1508 [hep-ph].

[102] F. Olness and I. Schienbein, "Heavy Quarks: Lessons Learned from HERA and Tevatron," *Nucl.Phys.Proc.Suppl.* **191** (2009) 44–53, arXiv:0812.3371 [hep-ph].

[103] J. Chay and C. Kim, "Proper factorization theorems in high-energy scattering near the endpoint," *JHEP* **1309** (2013) 126, arXiv:1303.1637 [hep-ph].

[104] T. Becher and G. Bell, "Analytic Regularization in Soft-Collinear Effective Theory," *Phys. Lett.* **B713** (2012) 41–46, arXiv:1112.3907 [hep-ph].

[105] J. C. Collins, F. Wilczek, and A. Zee, "Low-Energy Manifestations of Heavy Particles: Application to the Neutral Current," *Phys.Rev.* **D18** (1978) 242.

[106] A. Hoang, M. Jezabek, J. H. Kuhn, and T. Teubner, "Radiation of heavy quarks," *Phys.Lett.* **B338** (1994) 330–335, arXiv:hep-ph/9407338 [hep-ph].

[107] A. Hoang, J. H. Kuhn, and T. Teubner, "Radiation of light fermions in heavy fermion production," *Nucl. Phys.* **B452** (1995) 173–187, arXiv:hep-ph/9505262 [hep-ph].

[108] **CMS** Collaboration, V. Khachatryan *et al.*, "Measurement of the top quark mass using proton-proton data at $\sqrt{(s)} = 7$ and 8 TeV," *Phys. Rev.* **D93** no. 7, (2016) 072004, arXiv:1509.04044 [hep-ex].

[109] **ATLAS** Collaboration, M. Aaboud *et al.*, "Measurement of the top quark mass in the $t\bar{t} \to$ lepton+jets channel from $\sqrt{s} = 8$ TeV ATLAS data and combination with previous results," *Eur. Phys. J. C* **79** no. 4, (2019) 290, arXiv:1810.01772 [hep-ex].

[110] **CDF, D0** Collaboration, T. E. W. Group, "Combination of CDF and D0 results on the mass of the top quark using up to 9.7 fb^{-1} at the Tevatron," arXiv:1407.2682 [hep-ex].

[111] J. Bellm, G. Nail, S. Plätzer, P. Schichtel, and A. Siódmok, "Parton Shower Uncertainties with Herwig 7: Benchmarks at Leading Order," *Eur. Phys. J.* **C76** no. 12, (2016) 665, arXiv:1605.01338 [hep-ph].

[112] J. R. Andersen *et al.*, "Les Houches 2017: Physics at TeV Colliders Standard Model Working Group Report," in *10th Les Houches Workshop on Physics at TeV Colliders (PhysTeV 2017) Les Houches, France, June 5-23, 2017.* 2018. arXiv:1803.07977 [hep-ph]. http://inspirehep.net/record/1663483/files/1803.07977.pdf.

[113] M. Dasgupta, F. A. Dreyer, K. Hamilton, P. F. Monni, and G. P. Salam, "Logarithmic accuracy of parton showers: a fixed-order study," *JHEP* **09** (2018) 033, arXiv:1805.09327 [hep-ph]. [Erratum: JHEP 03, 083 (2020)].

[114] H. Baer, T. Barklow, K. Fujii, Y. Gao, A. Hoang, S. Kanemura, J. List, H. E. Logan, A. Nomerotski, M. Perelstein, *et al.*, "The International Linear Collider Technical Design Report - Volume 2: Physics," `arXiv:1306.6352 [hep-ph]`.

[115] D. Asner, A. Hoang, Y. Kiyo, R. Pöschl, Y. Sumino, and M. Vos, "Top quark precision physics at the International Linear Collider," in *Proceedings, 2013 Community Summer Study on the Future of U.S. Particle Physics: Snowmass on the Mississippi (CSS2013): Minneapolis, MN, USA, July 29-August 6, 2013*. 2013. `arXiv:1307.8265 [hep-ex]`. `http://inspirehep.net/record/1245485/files/arXiv:1307.8265.pdf`.

[116] M. Vos *et al.*, "Top physics at high-energy lepton colliders," `arXiv:1604.08122 [hep-ex]`.

[117] A. Jain, I. Scimemi, and I. W. Stewart, "Two-loop Jet-Function and Jet-Mass for Top Quarks," *Phys. Rev.* **D77** (2008) 094008, `arXiv:0801.0743 [hep-ph]`.

[118] M. Butenschoen, B. Dehnadi, A. H. Hoang, V. Mateu, M. Preisser, and I. W. Stewart, "Top Quark Mass Calibration for Monte Carlo Event Generators," *Phys. Rev. Lett.* **117** no. 23, (2016) 232001, `arXiv:1608.01318 [hep-ph]`.

[119] A. H. Hoang *et al.*, "Top - anti-top pair production close to threshold: Synopsis of recent NNLO results," *Eur. Phys. J.direct* **2** no. 1, (2000) 3, `arXiv:hep-ph/0001286 [hep-ph]`.

[120] A. H. Hoang and I. W. Stewart, "Top Mass Measurements from Jets and the Tevatron Top-Quark Mass," *Nucl. Phys. Proc. Suppl.* **185** (2008) 220–226, `arXiv:0808.0222 [hep-ph]`.

[121] A. H. Hoang, "The Top Mass: Interpretation and Theoretical Uncertainties," in *7th International Workshop on Top Quark Physics (TOP2014) Cannes, France, September 28-October 3, 2014*. 2014. `arXiv:1412.3649 [hep-ph]`. `http://inspirehep.net/record/1333866/files/arXiv:1412.3649.pdf`.

[122] M. Neubert, "Heavy quark symmetry," *Phys. Rept.* **245** (1994) 259–396, `arXiv:hep-ph/9306320 [hep-ph]`.

[123] A. V. Manohar and M. B. Wise, "Heavy quark physics," *Camb. Monogr. Part. Phys. Nucl. Phys. Cosmol.* **10** (2000) 1–191.

[124] A. H. Hoang, A. Jain, I. Scimemi, and I. W. Stewart, "Infrared Renormalization Group Flow for Heavy Quark Masses," *Phys. Rev. Lett.* **101** (2008) 151602, `arXiv:0803.4214 [hep-ph]`.

[125] A. H. Hoang, A. Jain, C. Lepenik, V. Mateu, M. Preisser, I. Scimemi, and I. W. Stewart, "The MSR mass and the $\mathcal{O}\left(\Lambda_{\text{QCD}}\right)$ renormalon sum rule," *JHEP* **04** (2018) 003, `arXiv:1704.01580 [hep-ph]`.

[126] P. Nason, "The Top Mass in Hadronic Collisions," 2017. `arXiv:1712.02796 [hep-ph]`. `http://inspirehep.net/record/1642228/files/arXiv:1712.02796.pdf`.

[127] T. Sjöstrand, S. Ask, J. R. Christiansen, R. Corke, N. Desai, P. Ilten, S. Mrenna, S. Prestel, C. O. Rasmussen, and P. Z. Skands, "An Introduction to PYTHIA 8.2," *Comput. Phys. Commun.* **191** (2015) 159–177, `arXiv:1410.3012 [hep-ph]`.

[128] P. Skands, S. Carrazza, and J. Rojo, "Tuning PYTHIA 8.1: the Monash 2013 Tune," *Eur. Phys. J.* **C74** no. 8, (2014) 3024, `arXiv:1404.5630 [hep-ph]`.

[129] A. H. Hoang, S. Mantry, A. Pathak, and I. W. Stewart, "Extracting a Short Distance Top Mass with Light Grooming," *Phys. Rev. D* **100** no. 7, (2019) 074021, `arXiv:1708.02586 [hep-ph]`.

[130] M. Dasgupta, A. Fregoso, S. Marzani, and G. P. Salam, "Towards an understanding of jet substructure," *JHEP* **09** (2013) 029, `arXiv:1307.0007 [hep-ph]`.

[131] A. J. Larkoski, S. Marzani, G. Soyez, and J. Thaler, "Soft Drop," *JHEP* **05** (2014) 146, `arXiv:1402.2657 [hep-ph]`.

[132] J. Kieseler, K. Lipka, and S.-O. Moch, "Calibration of the Top-Quark Monte Carlo Mass," *Phys. Rev. Lett.* **116** no. 16, (2016) 162001, `arXiv:1511.00841 [hep-ph]`.

[133] **CMS** Collaboration, J. H. Kim, "Alternative methods for top quark mass measurements at the CMS," *EPJ Web Conf.* **141** (2017) 08006.

[134] **ATLAS, CMS** Collaboration, M. Vos, "Top-quark mass measurements at the LHC: alternative methods," *PoS* **TOP2015** (2016) 035, `arXiv:1602.00428 [hep-ex]`.

[135] S. Adomeit, "Top-quark mass measurements: Alternative techniques (LHC + Tevatron)," in *Proceedings, 7th International Workshop on Top Quark Physics (TOP2014): Cannes, France, September 28-October 3, 2014.* 2014. `arXiv:1411.7917 [hep-ex]`. `http://inspirehep.net/record/1331406/files/arXiv:1411.7917.pdf`.

[136] G. Corcella, R. Franceschini, and D. Kim, "Fragmentation Uncertainties in Hadronic Observables for Top-quark Mass Measurements," *Nucl. Phys.* **B929** (2018) 485–526, `arXiv:1712.05801 [hep-ph]`.

[137] K. Agashe, R. Franceschini, D. Kim, and M. Schulze, "Top quark mass determination from the energy peaks of b-jets and B-hadrons at NLO QCD," *Eur. Phys. J.* **C76** no. 11, (2016) 636, `arXiv:1603.03445 [hep-ph]`.

[138] S. Biswas, K. Melnikov, and M. Schulze, "Next-to-leading order QCD effects and the top quark mass measurements at the LHC," *JHEP* **08** (2010) 048, `arXiv:1006.0910 [hep-ph]`.

[139] C. G. Lester and D. J. Summers, "Measuring masses of semiinvisibly decaying particles pair produced at hadron colliders," *Phys. Lett.* **B463** (1999) 99–103, `arXiv:hep-ph/9906349 [hep-ph]`.

[140] K. T. Matchev and M. Park, "A General method for determining the masses of semi-invisibly decaying particles at hadron colliders," *Phys. Rev. Lett.* **107** (2011) 061801, `arXiv:0910.1584 [hep-ph]`.

[141] **CMS** Collaboration, "Mass determination in the $t\bar{t}$ system with kinematic endpoints," Tech. Rep. CMS-PAS-TOP-11-027, CERN, Geneva, 2012. `http://cds.cern.ch/record/1478421`.

[142] **CMS** Collaboration, A. M. Sirunyan *et al.*, "Measurement of the top quark mass in the dileptonic $t\bar{t}$ decay channel using the mass observables $M_{b\ell}$, M_{T2}, and $M_{b\ell\nu}$ in pp collisions at $\sqrt{s} = 8$ TeV," *Phys. Rev.* **D96** no. 3, (2017) 032002, `arXiv:1704.06142 [hep-ex]`.

[143] G. Heinrich, A. Maier, R. Nisius, J. Schlenk, M. Schulze, L. Scyboz, and J. Winter, "NLO and off-shell effects in top quark mass determinations," *JHEP* **07** (2018) 129, `arXiv:1709.08615 [hep-ph]`.

[144] T. Gleisberg, S. Hoeche, F. Krauss, M. Schonherr, S. Schumann, F. Siegert, and J. Winter, "Event generation with SHERPA 1.1," *JHEP* **02** (2009) 007, `arXiv:0811.4622 [hep-ph]`.

[145] S. Ferrario Ravasio, T. Ježo, P. Nason, and C. Oleari, "A theoretical study of top-mass measurements at the LHC using NLO+PS generators of increasing accuracy," *Eur. Phys. J. C* **78** no. 6, (2018) 458, `arXiv:1906.09166 [hep-ph]`. [Addendum: Eur.Phys.J.C 79, 859 (2019)].

[146] S. Frixione, P. Nason, and C. Oleari, "Matching NLO QCD computations with Parton Shower simulations: the POWHEG method," *JHEP* **11** (2007) 070, `arXiv:0709.2092 [hep-ph]`.

[147] S. Alioli, P. Nason, C. Oleari, and E. Re, "A general framework for implementing NLO calculations in shower Monte Carlo programs: the POWHEG BOX," *JHEP* **06** (2010) 043, `arXiv:1002.2581 [hep-ph]`.

[148] S. Frixione, P. Nason, and G. Ridolfi, "A Positive-weight next-to-leading-order Monte Carlo for heavy flavour hadroproduction," *JHEP* **09** (2007) 126, `arXiv:0707.3088 [hep-ph]`.

[149] J. M. Campbell, R. K. Ellis, P. Nason, and E. Re, "Top-Pair Production and Decay at NLO Matched with Parton Showers," *JHEP* **04** (2015) 114, `arXiv:1412.1828 [hep-ph]`.

[150] T. Jezo, J. M. Lindert, P. Nason, C. Oleari, and S. Pozzorini, "An NLO+PS generator for $t\bar{t}$ and Wt production and decay including non-resonant and interference effects," *Eur. Phys. J.* **C76** no. 12, (2016) 691, `arXiv:1607.04538 [hep-ph]`.

[151] J. Bellm *et al.*, "Herwig 7.0/Herwig++ 3.0 release note," *Eur. Phys. J.* **C76** no. 4, (2016) 196, `arXiv:1512.01178 [hep-ph]`.

[152] J. Bellm *et al.*, "Herwig 7.1 Release Note," `arXiv:1705.06919 [hep-ph]`.

[153] S. Frixione and A. Mitov, "Determination of the top quark mass from leptonic observables," *JHEP* **09** (2014) 012, `arXiv:1407.2763 [hep-ph]`.

[154] Y. L. Dokshitzer, V. A. Khoze, and S. I. Troian, "Particle spectra in light and heavy quark jets," *J. Phys.* **G17** (1991) 1481–1492.

[155] Y. L. Dokshitzer, V. A. Khoze, and S. I. Troian, "On specific QCD properties of heavy quark fragmentation ('dead cone')," *J. Phys.* **G17** (1991) 1602–1604.

[156] F. Maltoni, M. Selvaggi, and J. Thaler, "Exposing the dead cone effect with jet substructure techniques," *Phys. Rev.* **D94** no. 5, (2016) 054015, `arXiv:1606.03449 [hep-ph]`.

[157] G. Marchesini and B. R. Webber, "Simulation of QCD Jets Including Soft Gluon Interference," *Nucl. Phys.* **B238** (1984) 1–29.

[158] G. Marchesini and B. R. Webber, "Monte Carlo Simulation of General Hard Processes with Coherent QCD Radiation," *Nucl. Phys.* **B310** (1988) 461–526.

[159] S. Catani, B. R. Webber, and G. Marchesini, "QCD coherent branching and semiinclusive processes at large x," *Nucl. Phys.* **B349** (1991) 635–654.

[160] S. Gieseke, P. Stephens, and B. Webber, "New formalism for QCD parton showers," *JHEP* **12** (2003) 045, `arXiv:hep-ph/0310083 [hep-ph]`.

[161] F. Krauss and G. Rodrigo, "Resummed jet rates for e+ e- annihilation into massive quarks," *Phys. Lett.* **B576** (2003) 135–142, `arXiv:hep-ph/0303038 [hep-ph]`.

[162] G. Rodrigo and F. Krauss, "Resummed jet rates for heavy quark production in e^+e^- annihilation," *Eur. Phys. J.* **C33** no. S1, (2004) S457–S459, `arXiv:hep-ph/0309325 [hep-ph]`.

[163] S. Catani, L. Trentadue, G. Turnock, and B. R. Webber, "Resummation of large logarithms in e+ e- event shape distributions," *Nucl. Phys.* **B407** (1993) 3–42.

[164] R. Abbate, M. Fickinger, A. H. Hoang, V. Mateu, and I. W. Stewart, "Thrust at N³LL with Power Corrections and a Precision Global Fit for $\alpha_s(M_Z)$," *Phys. Rev.* **D83** (2011) 074021, `arXiv:1006.3080 [hep-ph]`.

[165] E. Farhi, "A QCD Test for Jets," *Phys. Rev. Lett.* **39** (1977) 1587–1588.

[166] I. W. Stewart, F. J. Tackmann, and W. J. Waalewijn, "N-Jettiness: An Inclusive Event Shape to Veto Jets," *Phys. Rev. Lett.* **105** (2010) 092002, `arXiv:1004.2489 [hep-ph]`.

[167] S. Catani and L. Trentadue, "Resummation of the QCD Perturbative Series for Hard Processes," *Nucl. Phys.* **B327** (1989) 323–352.

[168] G. P. Korchemsky and G. F. Sterman, "Power corrections to event shapes and factorization," *Nucl. Phys.* **B555** (1999) 335–351, `arXiv:hep-ph/9902341 [hep-ph]`.

[169] C. F. Berger, T. Kucs, and G. F. Sterman, "Event shape / energy flow correlations," *Phys. Rev.* **D68** (2003) 014012, `arXiv:hep-ph/0303051 [hep-ph]`.

[170] R. A. Davison and B. R. Webber, "Non-Perturbative Contribution to the Thrust Distribution in e+ e- Annihilation," *Eur. Phys. J.* **C59** (2009) 13–25, `arXiv:0809.3326 [hep-ph]`.

[171] M. D. Schwartz, "Resummation and NLO matching of event shapes with effective field theory," *Phys. Rev.* **D77** (2008) 014026, `arXiv:0709.2709 [hep-ph]`.

[172] T. Becher and M. D. Schwartz, "A precise determination of α_s from LEP thrust data using effective field theory," *JHEP* **07** (2008) 034, `arXiv:0803.0342 [hep-ph]`.

[173] L. G. Almeida, S. D. Ellis, C. Lee, G. Sterman, I. Sung, and J. R. Walsh, "Comparing and counting logs in direct and effective methods of QCD resummation," *JHEP* **04** (2014) 174, `arXiv:1401.4460 [hep-ph]`.

[174] A. H. Hoang and I. W. Stewart, "Designing gapped soft functions for jet production," *Phys. Lett.* **B660** (2008) 483–493, `arXiv:0709.3519 [hep-ph]`.

[175] M. Bähr *et al.*, "Herwig++ Physics and Manual," *Eur. Phys. J.* **C58** (2008) 639–707, `arXiv:0803.0883 [hep-ph]`.

[176] J. C. Collins and D. E. Soper, "The Two Particle Inclusive Cross-section in e^+e^- Annihilation at PETRA, PEP and LEP Energies," *Nucl. Phys.* **B284** (1987) 253–270.

[177] S. Plätzer and S. Gieseke, "Coherent Parton Showers with Local Recoils," *JHEP* **01** (2011) 024, `arXiv:0909.5593 [hep-ph]`.

[178] D. Reichelt, P. Richardson, and A. Siodmok, "Improving the Simulation of Quark and Gluon Jets with Herwig 7," *Eur. Phys. J.* **C77** no. 12, (2017) 876, `arXiv:1708.01491 [hep-ph]`.

[179] B. R. Webber, "A QCD Model for Jet Fragmentation Including Soft Gluon Interference," *Nucl. Phys.* **B238** (1984) 492–528.

[180] H. Contopanagos, E. Laenen, and G. F. Sterman, "Sudakov factorization and resummation," *Nucl. Phys.* **B484** (1997) 303–330, `arXiv:hep-ph/9604313 [hep-ph]`.

[181] M. Beneke, "Large order perturbation theory for a physical quantity," *Nucl. Phys.* **B405** (1993) 424–450.

[182] P. Ball, M. Beneke, and V. M. Braun, "Resummation of (beta0 alpha-s)**n corrections in QCD: Techniques and applications to the tau hadronic width and the heavy quark pole mass," *Nucl. Phys.* **B452** (1995) 563–625, `arXiv:hep-ph/9502300 [hep-ph]`.

[183] M. Beneke, "More on ambiguities in the pole mass," *Phys. Lett.* **B344** (1995) 341–347, `arXiv:hep-ph/9408380 [hep-ph]`.

[184] M. Beneke and V. M. Braun, "Heavy quark effective theory beyond perturbation theory: Renormalons, the pole mass and the residual mass term," *Nucl. Phys.* **B426** (1994) 301–343, `arXiv:hep-ph/9402364 [hep-ph]`.

[185] A. H. Hoang and S. Kluth, "Hemisphere Soft Function at $\mathcal{O}(\alpha_s^2)$ for Dijet Production in e^+e^- Annihilation," `arXiv:0806.3852 [hep-ph]`.

[186] A. H. Hoang, C. Lepenik, and M. Preisser, "On the Light Massive Flavor Dependence of the Large Order Asymptotic Behavior and the Ambiguity of the Pole Mass," *JHEP* **09** (2017) 099, `arXiv:1706.08526 [hep-ph]`.

[187] K. Hamilton and P. Richardson, "A Simulation of QCD radiation in top quark decays," *JHEP* **02** (2007) 069, `arXiv:hep-ph/0612236 [hep-ph]`.

[188] A. Buckley, J. Butterworth, L. Lonnblad, D. Grellscheid, H. Hoeth, J. Monk, H. Schulz, and F. Siegert, "Rivet user manual," *Comput. Phys. Commun.* **184** (2013) 2803–2819, `arXiv:1003.0694 [hep-ph]`.

[189] R. Baumeister and S. Weinzierl, "Cutoff dependence of the thrust peak position in the dipole shower," *Eur. Phys. J. C* **80** no. 9, (2020) 843, `arXiv:2004.01657 [hep-ph]`.

[190] Z. Nagy and D. E. Soper, "A New parton shower algorithm: Shower evolution, matching at leading and next-to-leading order level," in *Ringberg Workshop on New Trends in HERA Physics 2005*, pp. 101–123. 1, 2006. `arXiv:hep-ph/0601021`.

[191] Z. Nagy and D. E. Soper, "Matching parton showers to NLO computations," *JHEP* **10** (2005) 024, `arXiv:hep-ph/0503053`.

[192] S. Plätzer and S. Gieseke, "Dipole Showers and Automated NLO Matching in Herwig++," *Eur. Phys. J.* **C72** (2012) 2187, `arXiv:1109.6256 [hep-ph]`.

[193] M. Cacciari, G. P. Salam, and G. Soyez, "FastJet User Manual," *Eur. Phys. J.* **C72** (2012) 1896, `arXiv:1111.6097 [hep-ph]`.

[194] S. Frixione and B. R. Webber, "Matching NLO QCD computations and parton shower simulations," *JHEP* **06** (2002) 029, `arXiv:hep-ph/0204244 [hep-ph]`.

[195] S. Hoeche, F. Krauss, M. Schonherr, and F. Siegert, "A critical appraisal of NLO+PS matching methods," *JHEP* **09** (2012) 049, `arXiv:1111.1220 [hep-ph]`.

[196] P. Nason and B. Webber, "Next-to-Leading-Order Event Generators," *Ann. Rev. Nucl. Part. Sci.* **62** (2012) 187–213, `arXiv:1202.1251 [hep-ph]`.

[197] M. Beneke, P. Marquard, P. Nason, and M. Steinhauser, "On the ultimate uncertainty of the top quark pole mass," *Phys. Lett.* **B775** (2017) 63–70, `arXiv:1605.03609 [hep-ph]`.

[198] **CMS** Collaboration, "Projected improvement of the accuracy of top-quark mass measurements at the upgraded LHC," Tech. Rep. CMS-PAS-FTR-13-017, CERN, Geneva, 2013. `http://cds.cern.ch/record/1605627`.

[199] **CMS** Collaboration, "ECFA 2016: Prospects for selected standard model measurements with the CMS experiment at the High-Luminosity LHC," Tech. Rep. CMS-PAS-FTR-16-006, CERN, Geneva, 2017. `http://cds.cern.ch/record/2262606`.

[200] A. H. Hoang, Z. Ligeti, and A. V. Manohar, "B decay and the Upsilon mass," *Phys. Rev. Lett.* **82** (1999) 277–280, `arXiv:hep-ph/9809423 [hep-ph]`.

[201] A. H. Hoang, Z. Ligeti, and A. V. Manohar, "B decays in the upsilon expansion," *Phys. Rev.* **D59** (1999) 074017, `arXiv:hep-ph/9811239 [hep-ph]`.

[202] A. H. Hoang, "1S and $\overline{\text{MS}}$ bottom quark masses from Upsilon sum rules," *Phys. Rev.* **D61** (2000) 034005, `arXiv:hep-ph/9905550 [hep-ph]`.

[203] M. Beneke, "A Quark mass definition adequate for threshold problems," *Phys. Lett.* **B434** (1998) 115–125, `arXiv:hep-ph/9804241 [hep-ph]`.

[204] A. H. Hoang, C. Lepenik, and V. Mateu, "REvolver: Automated running and matching of couplings and masses in QCD," `arXiv:2102.01085 [hep-ph]`.

[205] T. Matsuura and W. van Neerven, "Second Order Logarithmic Corrections to the Drell-Yan Cross-section," *Z.Phys.* **C38** (1988) 623.

[206] M. G. Echevarria, I. Scimemi, and A. Vladimirov, "Unpolarized Transverse Momentum Dependent Parton Distribution and Fragmentation Functions at next-to-next-to-leading order," *JHEP* **09** (2016) 004, `arXiv:1604.07869 [hep-ph]`.

[207] A. Vogt, S. Moch, and J. Vermaseren, "The Three-loop splitting functions in QCD: The Singlet case," *Nucl.Phys.* **B691** (2004) 129–181, `arXiv:hep-ph/0404111 [hep-ph]`.

[208] S. Moch, J. Vermaseren, and A. Vogt, "The Three loop splitting functions in QCD: The Nonsinglet case," *Nucl.Phys.* **B688** (2004) 101–134, `arXiv:hep-ph/0403192 [hep-ph]`.

[209] S. Moch, B. Ruijl, T. Ueda, J. A. M. Vermaseren, and A. Vogt, "Four-Loop Non-Singlet Splitting Functions in the Planar Limit and Beyond," *JHEP* **10** (2017) 041, `arXiv:1707.08315 [hep-ph]`.

[210] T. Becher and M. Neubert, "Toward a NNLO calculation of the $\bar{B} \to X_s \gamma$ decay rate with a cut on photon energy. II. Two-loop result for the jet function," *Phys. Lett.* **B637** (2006) 251–259, `arXiv:hep-ph/0603140 [hep-ph]`.

[211] R. Brüser, Z. L. Liu, and M. Stahlhofen, "Three-Loop Quark Jet Function," *Phys. Rev. Lett.* **121** no. 7, (2018) 072003, `arXiv:1804.09722 [hep-ph]`.

[212] B. A. Kniehl, "Two Loop QED Vertex Correction From Virtual Heavy Fermions," *Phys.Lett.* **B237** (1990) 127.

[213] A. Hoang, "Applications of two loop calculations in the standard model and its minimal supersymmetric extension", *doctoral thesis* (1996), Karlsruhe Institute of Technology, `https://publikationen.bibliothek.kit.edu/4396`.

[214] S. Catani, S. Dittmaier, and Z. Trocsanyi, "One loop singular behavior of QCD and SUSY QCD amplitudes with massive partons," *Phys. Lett.* **B500** (2001) 149–160, `arXiv:hep-ph/0011222 [hep-ph]`.

[215] Z.-B. Kang, F. Ringer, and I. Vitev, "Effective field theory approach to open heavy flavor production in heavy-ion collisions," *JHEP* **03** (2017) 146, `arXiv:1610.02043 [hep-ph]`.

[216] C. W. Bauer and E. Mereghetti, "Heavy Quark Fragmenting Jet Functions," *JHEP* **04** (2014) 051, `arXiv:1312.5605 [hep-ph]`.

[217] M. Buza, Y. Matiounine, J. Smith, and W. L. van Neerven, "Charm electroproduction viewed in the variable flavor number scheme versus fixed order perturbation theory," *Eur. Phys. J.* **C1** (1998) 301–320, `arXiv:hep-ph/9612398 [hep-ph]`.

[218] J. Ablinger, A. Behring, J. Blümlein, A. De Freitas, A. von Manteuffel, and C. Schneider, "The 3-loop pure singlet heavy flavor contributions to the structure function $F_2(x, Q^2)$ and the anomalous dimension," *Nucl. Phys.* **B890** (2014) 48–151, arXiv:1409.1135 [hep-ph].

[219] J. Ablinger, A. Behring, J. Blümlein, A. De Freitas, A. Hasselhuhn, *et al.*, "The 3-Loop Non-Singlet Heavy Flavor Contributions and Anomalous Dimensions for the Structure Function $F_2(x, Q^2)$ and Transversity," *Nucl.Phys.* **B886** (2014) 733–823, arXiv:1406.4654 [hep-ph].

[220] J. Ablinger, J. Blümlein, A. De Freitas, A. Hasselhuhn, A. von Manteuffel, M. Round, C. Schneider, and F. Wissbrock, "The Transition Matrix Element $A_{gq}(N)$ of the Variable Flavor Number Scheme at $\mathcal{O}(\alpha_s^3)$," *Nucl. Phys.* **B882** (2014) 263–288, arXiv:1402.0359 [hep-ph].

[221] I. Z. Rothstein, "Factorization, power corrections, and the pion form-factor," *Phys. Rev.* **D70** (2004) 054024, arXiv:hep-ph/0301240 [hep-ph].

[222] A. K. Leibovich, Z. Ligeti, and M. B. Wise, "Comment on quark masses in SCET," *Phys. Lett.* **B564** (2003) 231–234, arXiv:hep-ph/0303099 [hep-ph].

[223] A. Jain, M. Procura, and W. J. Waalewijn, "Fully-Unintegrated Parton Distribution and Fragmentation Functions at Perturbative k_T," *JHEP* **04** (2012) 132, arXiv:1110.0839 [hep-ph].

[224] W. Beenakker, R. Kleiss, and G. Lustermans, "No Landau-Yang in QCD," arXiv:1508.07115 [hep-ph].

[225] M. Cacciari, L. Del Debbio, J. R. Espinosa, A. D. Polosa, and M. Testa, "A note on the fate of the Landau–Yang theorem in non-Abelian gauge theories," *Phys. Lett.* **B753** (2016) 476–481, arXiv:1509.07853 [hep-ph].

[226] "The Herwig Event Generator http://herwig.hepforge.org," 2018.